

**15<sup>th</sup> Symposium on  
High-Performance Marine Vehicles**

**HIPER'23**

**Bernried, 18-20 September 2023**

**15<sup>th</sup> Symposium on  
High-Performance Marine Vehicles**

# **HIPER'23**

**Bernried, 18-20 September 2023**

Edited by Volker Bertram

**15<sup>th</sup> Symposium on High-Performance Marine Vehicles**, Bernried, 18-20 September 2023

## Sponsored by



<https://www.dnv.com/maritime/maritime-academy/index.html>



[www.numeca.de](http://www.numeca.de)

# SIEMENS

[www.siemens.com](http://www.siemens.com)



[www.hempel.com](http://www.hempel.com)



[www.jotun.com](http://www.jotun.com)



[www.hoppe-marine.com](http://www.hoppe-marine.com)



[www.idealship.de](http://www.idealship.de)



**HASYTEC.COM**  
hanseatic system technologies

[www.hasytec.com](http://www.hasytec.com)

## Media Partners

# HANSA

INTERNATIONAL MARITIME JOURNAL

<https://hansa-online.de/>



<https://www.rina.org.uk/>



# Index

Volker Bertram	6
<i>Future Ships and Shipping – Green &amp; Smart</i>	
Thomas Hildebrandt, Sven Albert, Stefano Carugno, Günther Migeotte, Stefan Harries, Heinrich von Zadow	19
<i>Hydrodynamic Optimization of an E-Powered Catamaran in Early Design</i>	
Xavier Mayorga, Jan Kelling, Matti Früchtenicht	32
<i>AI-Enhanced Ultrasonic Biofouling Protection</i>	
Henrique Gaspar, Volker Bertram, Tracy Plowman	41
<i>Hic Rhodus, Hic Salta: ChatGPT and other A.I. Tools for Maritime Applications</i>	
Volker Bertram	53
<i>A Snapshot of Evolving Innovative Antifouling Options</i>	
Rodrigo Perez Fernández	62
<i>Engineering Marine Digital Twins with Sustainability</i>	
Matteo Barsotti	75
<i>Manual vs Automatic Data Collection for Energy Efficiency Management: The Old Debate</i>	
Arnau Carrera Viñas, Thomas Vonach	80
<i>Autonomous Robotic In-Water Hull Inspection for Fouling and Structural Condition</i>	
Kostas Belibassakis, Dimitris Liarokapis, Anders Öster	86
<i>A Novel Energy Saving Device for Ferry Ships in Waves based on Flapping Thrusters</i>	
Richard Marioth, Tobias Wesnigk	101
<i>The MCN Guideline: An Overview of Measures Improving Ship Efficiency in the Context of IMO and EU Emission Regulations</i>	
Claus Schreiner, Dorothea Stübing, Volker Föste, Volkmar Stenzel, Jochen Marzi	108
<i>Use of the Building Principle of the Dolphin's Skin to Reduce Hydrodynamic Drag on Ship Hulls - Recent Achievements</i>	
Heikki Hansen, Karsten Hochkirch, Uwe Hollenbach, Volker Bertram	116
<i>Where Wind Power Makes Business Sense for Bulk Carriers</i>	
Florian Gerland, Kyrillos Atallah, Thomas Schomberg	127
<i>Larabicus - Development of an Autonomous and Energy Autarkic In-transit Hull Cleaning Robot using Hydrodynamic Optimization based on CFD</i>	
Uwe Altenbach	135
<i>CII Optimized Ship Operation for Ships with Refrigerated Cargo</i>	
Fabian Pinkert	141
<i>Biofuel Compatibility: Testing Matrix and Case Reports</i>	
David Pang, Nishant Dhyani	155
<i>Complying EEXI, EEOI &amp; CII from Owner's Perspective</i>	
Prateek Gupta, Sverre Steen, Bingjie Guo, Hans Anton Tvette	166
<i>Reliable Hull Performance Analysis using Vessel Technical Index</i>	
Simon Hauschulz, Stefan Harries	181
<i>Reduced-Order Modelling for the Preliminary Design of Propellers</i>	

Christian Emmersberger, Stefan Krüger <i>A Tool to Predict Route-Specific Energy Consumption for Ships with Battery-Supported Propulsion</i>	189
Panagiotis Manias, Dominic Hudson, Damon Teagle, Stephen Turnock <i>Fuel Cell Performance Evaluation under Ship Motions</i>	203
Ivana Melillo, Angela Craciun, Kenneth Widell, Alexandra Widelund, Arno Dubois, Jan Kelling, Yildiz Williams, Mia Elg, Veronica Asta <i>Towards Zero-Emission Cruise Shipping</i>	218
Annika Sandberg, Mia Elg, Bogdan Molchanov, Arun Krishnan, Ville Wejberg <i>Development in CII Performance of a Bulk Carrier, Transitioning from Today's State of the Art to Net-Zero Design</i>	234
Erik van Ballegooijen <i>Smart ShaPoLi Solution for EEXI Compliance</i>	248
Emir Ejder, Frederik Hammer Berthelsen <i>Learnings from a Biofuel Trial</i>	259
Helle Vines Ertsås, Morten Sten Johansen <i>Combine and Conquer for Smart Hull Management</i>	265
Philippos Sfiris, Yigit Kemal Demirel, Andrea Farkas, Sofia Pagoni <i>A Case Study: Combined Effect of a Silicone-Based Low Friction Coating and a Weld Seam Fairing Solution</i>	273
Elisabeth Banken, Vincent E. Schneider, Johannes Oeffner <i>Biomimetics for Maritime Applications – En Route to Decarbonization until 2050</i>	285
Stavros Kontos, Da-Qing Li, Chiara Wielgosz, Laura Marimon Giovannetti, Frederik Gerhardt, Sofia Werner, Ville Paakkari <i>Comparison of Full-scale Flettner Rotor Performance Prediction Methods with Sea Trial Data</i>	299
Sven-Eric Salecker, Jakob Lohse <i>AI-enabled Democratizing of CFD Data for Decarbonization of Shipping</i>	322
Ivan Stojanovic <i>Methanol as a Marine Fuel: Techno-Economic Considerations</i>	332
Michael Stein <i>Applying Fouling Detection with ROV and AI and Big Data Analysis for EEXI/CII Fleet Optimization</i>	343
Kenneth Goh <i>Techno-economic Vessel Design Method for Assessing Alternative Fuels &amp; Power Architectures</i>	355
List of authors	
Call for Papers for next HIPER	

# Future Ships and Shipping – Green & Smart

Volker Bertram, DNV, Hamburg/Germany, [volker.bertram@dnv.com](mailto:volker.bertram@dnv.com)

## Abstract

*The paper discusses key trends in ship designs and ship operation and attempts to extrapolate into the future. The two key trends are decarbonizing shipping and digital transformation. Decarbonizing shipping involves low/no-carbon fuels, wind assisted ship propulsion and smart hull management including friction-reducing technology. Proliferation of sensors, data processing and communication will enable smarter ship operation. Improved situation awareness will have benefits for energy efficiency and smart maintenance schemes. The unmanned ship will remain an exception, but remote supervision and operation will reduce workload and crew sizes on board, and autonomous systems of various degrees of autonomy and scope will be found on most ships.*

## 1. Introduction

In the 1970s book “Ships and Shipping of Tomorrow” by Schönknecht *et al.* (1973), wonderful artistic visions predicted a future of nuclear-powered submarines transporting crude oil, giant hydrofoils bringing people around the world and streamlined catamarans carrying containers at speeds of up to 35 knots across the Atlantic. There have been assorted other bold and fascinating visions for future ships in the course of time, Fig.1. And while some predictions have proven to be correct, at least in some aspects, many more have been completely wrong.



Fig.1: (Artist) visions of ships of the future as imagined in the 1930s (left) and 1980s (right)

As Nobel laureate Niels Bohr put it so aptly: Prediction is very difficult, especially about the future. Six years after my previous attempt to speculate on ships and shipping of the future, Bertram (2017), it may be time to check and correct some of the trend analyses. It is a challenging, but fun endeavor. And if it gets me nowhere, I'll go there proud.

And “future” in the context of this paper means a time horizon of 30 years. I am better at engineering extrapolations than at writing science fiction novels. The hope and ambition is still that the predictions are closer to truth 30 years from now than those that I found in blogs and tech gizmo journalism.

## 2. “Green” ships of tomorrow

Broadly speaking, ships of the future will evolve naturally in line with economic trends, legal constraints, and advancing technological possibilities. And the over-arching trends of green shipping, in particular decarbonizing shipping, and digital transformation with all its facets are the leitmotifs in the individual expected developments discussed below.

## 2.1. Ship hulls

Public perception, including that of the wider maritime community, is distorted by media reporting of eye-catching designs and concepts. If you google images of “future ships”, half are cruise ships and half are navy ships, neither representing the majority of the world’s fleet now or in 30 years.

Future concepts for atypical “air transporters” with negligible payload (navy ships, megayachts, ferries, cruise vessels) often feature multihull design, Fig.2. But such unconventional hull shapes will remain unconventional, the rare exemption and not the rule for future design shapes.

The world’s fleet is and will continue to be much more mundane and pragmatic. Shipping of the future will still mean mainly dry bulk, liquid bulk, and general, mostly containerized cargo.

The long-term economic and ecological pressure for energy efficiency will inevitably lead to lower ship speeds. At the same time, smarter design processes will optimize hull shapes for more realistic operational scenarios, considering variations of operational conditions (speed, load) and ambient conditions (sea state), *Bertram and Campana (2020)*. As a result, bulbous bows are likely to shrink or even disappear, and we may see a return to straight stems on many cargo ships, as indicated by some concept designs already, such as the “Diamond 2” bulk carrier, Fig.3, *Lovstad and Bertram (2022)*, or the NCL container feeder shown in Fig.5.

The quest for transport efficiency (reducing fuel bill and emissions alike) will favor lower ship speeds. Ships are likely to become wider and shorter with propellers having fewer blades. Propulsion improving devices (PIDs), <https://glomeep.imo.org/technology/propulsion-improving-devices-pids/>, may become standard.



Fig.2: Multihull design concept for future warship (left) and cruise vessel (right)



Fig.3: Diamond 2 bulk carrier design with straight stem at bow

Most likely, ship hulls will continue to be made of steel, simply because steel is cheap, strong, and easy to recycle. Better coatings and inspection programs will compensate for steel's main shortcoming, namely, corrosion. Intelligent condition monitoring schemes will provide the appropriate technologies to extend the average life-span of steel structures while reducing (if not avoiding completely) the risk of structural failure. Composites, including metal foam sandwiches, Fig.4, *Longva et al. (2014)*, *Hipke (2022)*, will be limited mainly to weight-sensitive niche applications, such as high-speed craft (HSC), navy vessels, or cruise vessel superstructures. An increasingly important hurdle to wider uptake of composites is the problematic recyclability of many composite materials.



Fig.4: Steel-aluminium foam-steel sandwiches, *Hipke (2022)*

## 2.2. Fuels and machinery

The broader trend towards cleaner fuels combined with lower design speeds will affect maritime propulsion profoundly. Heavy fuel oil (HFO) reigned supreme as the standard fuel for shipping for decades, but IMO regulation curbing Sulphur emissions to air effectively ended this reign in 2020. No single fuel solution will obtain a similarly dominant position; instead we will see a mix of various fuel options on the market, with varying uptake over time, *DNV (2021)*. Various likely contenders include, *Bertram (2021a)*, *Brynolf et al. (2022)*:

- LNG (Liquified Natural Gas) is likely to play a major role for the next two decades, but will fade out as a fossil fuel with a still significant carbon footprint. LNG is an important bridging technology, as (natural) gas as a fuel has been key to developing technologies (e.g. dual-fuel diesel engines) and regulations which pave the way for other low-carbon/no-carbon fuels.
- Biofuels, with minimum changes to machinery and crew training. Long-term, maritime biofuels may be based on algae and offshore production akin to fish farming.
- Methanol, as a fuel with similarly few changes for machinery and crew. The key here is ramping up production and bunkering infrastructure worldwide for clean Methanol (not employing fossil fuels in the production). Methanol is already the widely established as ship fuel for short sea shipping in the North Sea and Baltic Sea, e.g. as for a container feeder project of NCL for 2024, Fig.5, <https://www.ncl.no/campaigns/sea-change/>.
- Ammonia, as a convenient way to store hydrogen. Large-scale production facilities exist worldwide for Ammonia as cargo (fertilizer), but facilities for clean and cost-effective production have yet to evolve.
- Hydrogen (liquid LH2) is less likely to gain significant market shares in blue shipping due to the difficulties and costs in storage and transport.
- Nuclear fuels are unlikely to gain significant market shares, due to technical and political hurdles. It is more likely that nuclear power is used on land to produce synthetic fuels such as Methanol and Ammonia.





Fig.5: Prototype of future feeder ship using Methanol as fuel, source: NCL (2022)

Most larger, “blue-shipping” cargo ships will continue to rely on diesel engine technology, but with evolving technology using dual-fuel diesel engines in a transition phase of 1-2 decades. The much cleaner fuels will make some of periphery of traditional main engines obsolete, such as separators and filters. Overall, cleaner fuel and the more robust set-up of the engine room together with smarter condition-based maintenance schemes will reduce the workload of the engine department.

In addition, we will see the rise of e-power on ships, mostly in the form of fuel cells and batteries, Figs.5 and 6, *Van Biert and Visser (2022)*, *Coraddu et al. (2022)*, mostly on short sea shipping, as already envisioned by *Rohde and Sames (2012)*, or just for on-board electricity supply on blue shipping. The highly efficient fuel cells will supply a constant base load; batteries will supply power for short-term peaks and fast reaction.



Fig.6: All-battery powered ferry “Ellen” (4.3 MWh), 2019



Fig.7: 23 MW fuel cell installation planned for 2027 on “Europa Seaways”, source: Knud E. Hansen

### 2.3. Energy efficiency through low-friction hulls

Up until the 2020s, antifouling strategies (for energy efficiency reasons, but also to prevent the spread of invasive species) have been based almost exclusively on antifouling (biocide) coatings. The paradigm is likely to shift towards more sustainable technologies, *Bertram (2020)*, including:

- Mechanically repellent surfaces – e.g., nano-coatings with microscopic surface structures, making adhesion difficult, similar to anti-graffiti coatings on houses.
- Frequent proactive cleaning (grooming) of ship hulls using in-water cleaning robots, *Bertram (2022)*, Fig.8. These robots are becoming increasingly affordable and available.
- Ultra-sonic protection is at present a complementary technology for regions with limited or difficult access. Full-hull protection is currently feasible for boats, but envisioned also for large ocean-going ships, Fig.9, *Kelling (2021)*.

These measures are widely expected to save ~10% of the fuel consumption (averaged over 5-year docking intervals), as hull performance is kept rather level with the new regimes.



Fig.8: Hull Skater robot for proactive cleaning, [www.jotun.com](http://www.jotun.com)

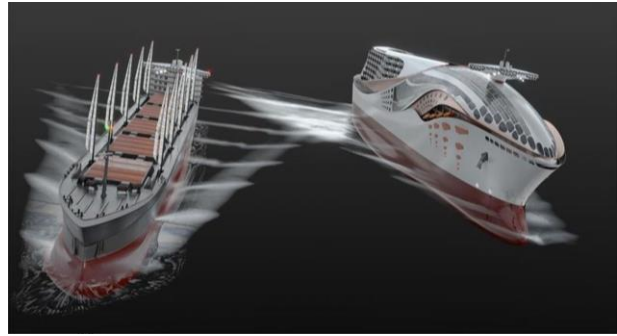


Fig.9: Vision for full ultrasonic hull protection, <https://www.projectchek.eu/>

Air lubrication, Fig.10, has been progressing significantly in industry perception and take-up within less than a decade, from *Silberschmidt et al. (2016)* to *Connolly (2022)*. As the general trends towards lower speeds and wider ships play in favor of air lubrication technology, we can expect more such installations in the years to come. Net savings of 5-10% on shaft power have been proven in third-party performance monitoring, *Camilleri et al. (2022)*.



Fig.10: Air lubrication system, <https://www.silverstream-tech.com/>

## 2.4. Wind-assisted ship propulsion (WASP)

The general trend towards lower ship speeds favors also the business cases of wind-assisted ship propulsion (WASP). For commercial shipping, only robust and highly automated systems make sense. There is a multitude of concepts, including Flettner rotors, Fig.11, rigid sails, and kites, *Hollenbach et al. (2020)*, *Hochkirch and Bertram (2021)*, *Thies and Fakiolas (2022)*. Energy saving potential and associated business cases of WASP systems can be improved by smart routing systems considering the specifics of WASP ships with tacking courses. Future engine configurations with electric propulsion also benefit WASP installations, as power take-in from WASP systems is limited on conventional propulsion ships with diesel engines and fixed-pitch propellers, *Thies and Fakiolas (2022)*.



Fig.11: Tiltable Flettner rotors on bulk carriers, source: Berge Bulk



Fig.12: Vision of cargo ship with many rigid sails, source: <https://www.vplp.fr/en/shipping/>



Time is on the side of WASP systems, and a continuation of the exponential growth in take-up seen in recent years may be extrapolated over the next decade at least. Many of the artist visions showing large cargo ships with several WASP systems installed, Fig.12, may well become reality within the next 10 years.

### 3. Smart ships of tomorrow

#### 3.1. Sensors and IoT

Falling costs for sensors, computing power, and satellite communications make it a safe prediction that ships of the future will be “smart”, i.e., they will be equipped with various embedded data processing. Today’s leading-edge ships, Fig.13, will be tomorrow’s standard fare. The vision is having sensors literally “everywhere”, in the hull, main engine, auxiliary machinery, and even small equipment items, *Etienne and Romano (2016)*. And they will have the computing power to process most data directly (Edge computing), escalating resulting information and insight selectively when needed. “Today’s mobile phones have the processing power of desktop computers 10 years ago. In 2020, mobile phones will have the power of today’s PCs. Cheap and small distributed sensors will have the abilities of today’s mobile phones, and so on,” *Longva et al. (2014)*.

The Internet of Things (IoT) is turning from vision to reality in our time. The ubiquitous interface problems between thousands of native data formats of assorted original equipment manufacturers are gradually overcome through industry standards, a sometimes still reluctant opening due to customer pressure and smart data adapters, sometimes dubbed as Intelligent Internet of Things (IIoT), *Danese and Vannas (2020)*.



Fig13: Modern ship with extensive sensor network (2017), source: Maersk



Future ships will have more complex energy systems, *Baldi and Elg (2022)*, typically featuring a mix of diesel engines, electrical systems with fuel cells and batteries, and WASP systems. There will be smart software support to manage these complex machinery systems optimally, both in design and in operation. In modern parlance, we will have Digital Twins of the machinery and propulsion system, data-fueled by the ubiquitous sensors, and smart thanks to simple expert systems or agents driving the decision support with well-established expert rules. DNV's COSSMOS (Complex Ship Systems Modelling and Simulation) is such a software, modeling complex ship machinery systems, Fig.14, *Kakalis et al. (2014)*, *Georgopoulou et al. (2021)*, which is increasingly attractive with higher complexity of these systems.

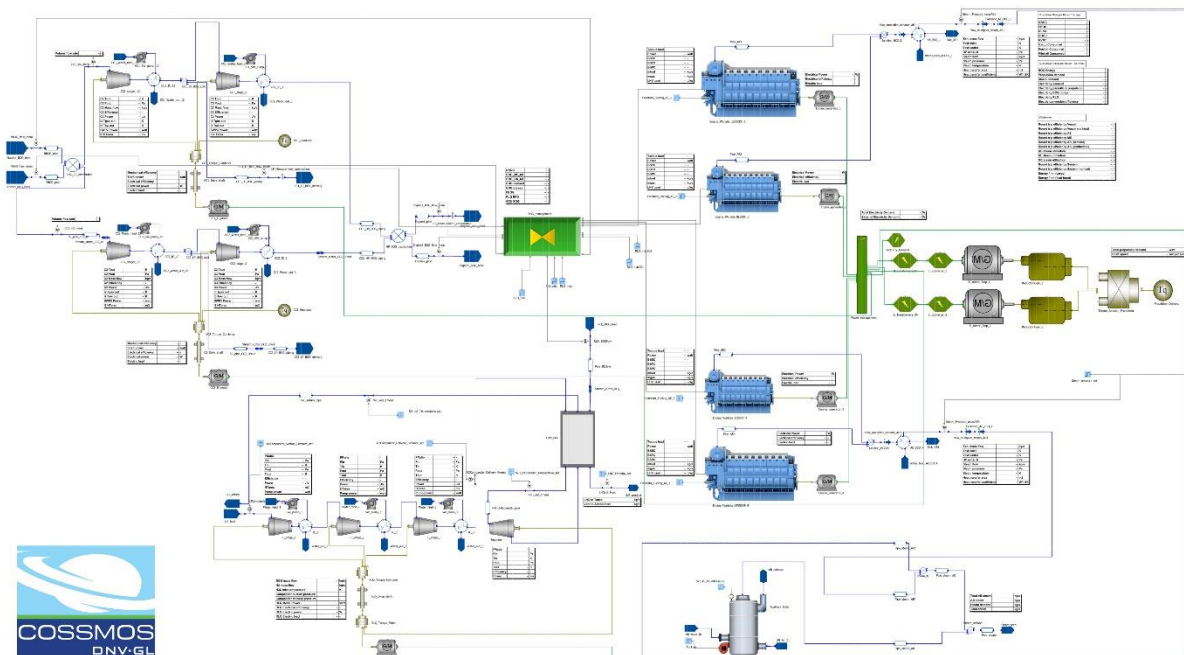


Fig.14: COSSMOS model of energy providers and consumers for next-generation LNG carrier

The wealth of data coming from onboard sensors and external sources can be used to build Digital Twins for assorted applications, often combining Artificial Intelligence/Machine Learning (black-box models) and First-Principle simulations (white-box models). For example, hull performance monitoring has become a lot more mature and widely adopted by best business practice operators in shipping, as seen in the HullPIC conference series, [www.hullpic.info](http://www.hullpic.info). Performance monitoring is an important flanking measure to accelerate the adoption of green technologies such as WASP in the industry, as it adds transparency and supports the assessment of business cases: “[G]reen technologies further complicate[] the problem as their nonlinear behaviour [...] prevents the true savings they offer from being fully understood or compared”, *Camilleri et al. (2022)*.



Fig.15: Bluebottle drone, <https://ocius.com.au>



Fig.16: Drone view with automatic object detection

Besides onboard sensors, ships of the future will have access to a mix of external sources to complement information for enhanced situation awareness:

- Satellites will offer exponentially growing bandwidth, *Laag et al. (2015)*, improving among others AIS (and thus traffic) information for more efficient port and traffic planning, *Hüffmeier et al. (2020)*, MetOcean data, etc.
- Swarms of smart, low-cost drones may furnish “satellite of the seas” in the future, as indicated by the energy autonomous Bluebottle drones with solar sails, Fig.15, <https://ocius.com.au/>
- Aerial drones may become so cheap that they may become a common sight in ports and above certain vessels, giving live CCTV-like bird-view images for increased situation awareness, Fig.16, *Mancarella et al. (2022)*

### 3.2. Smart maintenance and repair

Several ICT technologies, [https://en.wikipedia.org/wiki/Information\\_and\\_communications\\_technology](https://en.wikipedia.org/wiki/Information_and_communications_technology), contribute to easier maintenance of future ships.

Performance monitoring, discussed above for energy efficiency, will also enable predictive maintenance in most cases, reducing unplanned ad-hoc maintenance work by the ship’s crew. Condition-based maintenance systems may diagnose eventual problems at an early stage and support the fixing of the problem, e.g. by ordering spare parts, preparing 3D printing, or guiding repair by ordinary persons using embedded expert systems. Along with reduced workload in the engine room due to cleaner fuels, this will allow further reductions in minimum crew sizes.

Remote inspection schemes will become standard, whether they are based on permanent on-board cameras, *Mavi et al. (2021)*, aerial drones, Fig.17, *Stensrud et al. (2022)*, or underwater drones, Fig.18, *Guere and Gambini (2021)*. In any case, machine vision based on Artificial Intelligence will be used to detect occurrence and degree of deficiencies.



Fig.17: Ship hull inspection drone (DNV)



Fig.18: In-water inspection drone (Blueye Robotics)

Drones may also be used to deliver required parts to remote areas, such as ships, as demonstrated in 2016 by Maersk. However, often, delivery will no longer be needed. Instead, 3D printing (a.k.a. additive manufacturing) may generate required parts, mainly in the supply industry and on ships, *Bergsma et al. (2016)*, *Junghans and Babu Govindaraj (2022)*:

- Maersk and the US Navy are reported to test 3D printing of spare parts on board their vessels. Generally, spare parts seem to be a prime application of 3D printing in shipping, Fig.19.
- Model basins explore the possibility of using 3D printing for models in towing tanks, *Hentschel (2019)*. Propeller manufacturers report that full-scale propeller 3D printing is at least feasible, Fig.20.

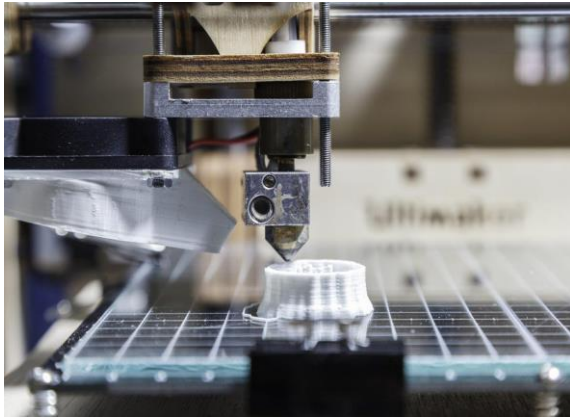


Fig.19: 3D printing of spare part



Fig.20: 3D printed propeller, source: Naval Group

Unavoidable repair onboard ships, as well as advanced maintenance, will be facilitated by Augmented Reality (AR), *Matsuo (2018)*, *Petersen (2020)*, allowing intuitive instructions making highly specialized expertise obsolete. While current Augmented Reality applications in the maritime industry are largely based on tablets, Fig.21, within a decade head-mounted devices (successors of the current Microsoft HoloLens) will become standard, allowing hands-free operation, Fig.22. Instructions will be either coming from embedded expert systems or live via headphones from shore-based experts. In sum, the maintenance friendly ship of the future will support further reductions in crewing.



Fig.21: Current AR application on ships (NMRI)

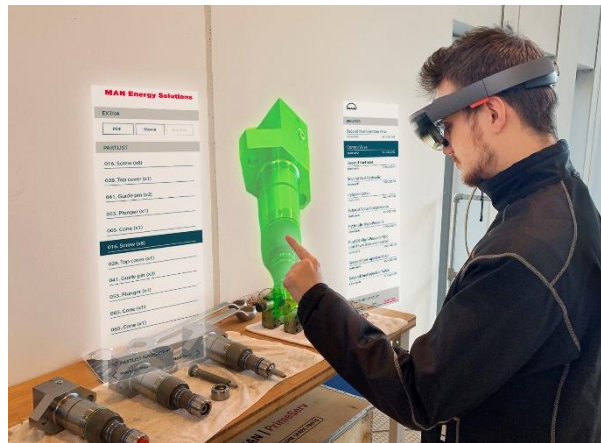


Fig.22: Future AR hands-free operation (MAN)

### 3.3. Remote control and autonomous systems

The vision of unmanned intercontinental cargo shipping will remain largely a vision in my lifetime, as legal and economic hurdles stand in the way of these visions becoming rapidly reality, *Bertram (2016)*. Even if main machinery systems will need less maintenance and repair, the multitude of other systems on board will make crew-based maintenance strategies more attractive than alternative options, *Eriksen (2021)*. However, autonomous technology will progress both in scope and capability of systems. Many developments will mirror trends in the automotive industry: we have smart cars (automatic brake systems if pedestrians are crossing; valet parking; self-monitoring tire pressure; ability to drive autonomously on highways, etc.) and we have driverless cars (most notably the Google driverless car, <https://en.wikipedia.org/wiki/Waymo>).

For selected applications, we will have unmanned, autonomous ships (e.g. short-distance ferries or dedicated short-sea cargo shipping like the 'MV Yara Birkeland', Fig.23, [https://en.wikipedia.org/wiki/MV\\_Yara\\_Birkeland](https://en.wikipedia.org/wiki/MV_Yara_Birkeland)), and remote-controlled ships (e.g. tugboats and fire-fighting vessels), Fig.24.



For ships, we will have low-crew smart ships (with automatic collision avoidance, Fig.25; automatic berthing; self-monitoring for hull, engine, and cargo; ability to sail autonomously for limited time in certain conditions, etc.),



Fig.25: MV Yara Birkeland for short sea shipping with unmanned operation expected in 2024



Fig.24: Unmanned, remote-control tug (Riviera)

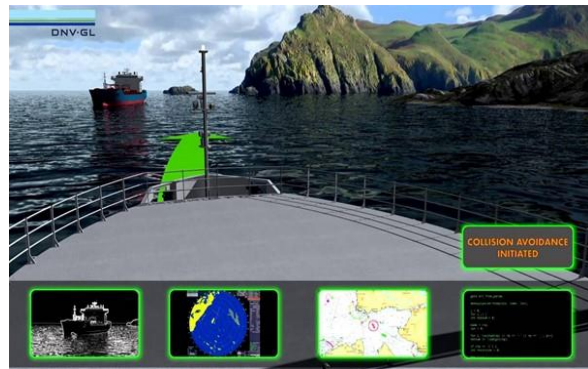


Fig.25: Autonomous collision avoidance system

#### 4. Conclusions

The future of shipping is driven by engineers, not artist visions. Realistic predictions may be disappointingly sober for the general public, but serve as a useful roadmap for engineers. The more you know, the more you appreciate the progress made in recent years and the ingenious solutions made to work by my fellow engineers. The future is smart and green – thanks to them.

#### Acknowledgments

This paper is the result of countless contributions to the COMPIT and HIPER conferences, where over the years I have seen the arrival and application of new technologies. The papers, but perhaps even more the discussions, have shaped my view of our industry and the assorted developments for future ships and future shipping. For this insight, I am very grateful. If I have overlooked key publications in my already long list of publications, I beg your indulgence.

## References

- BALDI, F.; ELG, M. (2022), *Overall system integration: synergies and interactions*, Sustainable Energy Systems on Ships (Eds. F. Baldi et al.), Elsevier, pp.233-302
- BERGSMA, J.M.; ZALM, M.v.d.; PRUYN, J.F.J. (2016), *3D-printing and the maritime construction sector*, 10<sup>th</sup> HIPER Conf., Cortona, pp.428-442, [http://data.hiper-conf.info/Hiper2016\\_cortona.pdf](http://data.hiper-conf.info/Hiper2016_cortona.pdf)
- BERTRAM, V. (2016), *Unmanned & Autonomous Shipping – A Technology Review*, 10<sup>th</sup> HIPER Conf., Cortona, pp.10-24, [http://data.hiper-conf.info/Hiper2016\\_cortona.pdf](http://data.hiper-conf.info/Hiper2016_cortona.pdf)
- BERTRAM, V. (2017), *Future of Shipbuilding and Shipping - A Technology Vision*, 16<sup>th</sup> COMPIT Conf., Cardiff, pp.17-30, [http://data.hiper-conf.info/compit2017\\_cardiff.pdf](http://data.hiper-conf.info/compit2017_cardiff.pdf)
- BERTRAM, V. (2020), *Options for the Post-Biocide Era of Antifouling*, 12<sup>th</sup> HIPER Symp., Cortona, pp.51-56, [http://data.hiper-conf.info/Hiper2020\\_Cortona.pdf](http://data.hiper-conf.info/Hiper2020_Cortona.pdf)
- BERTRAM, V. (2021a), *Fuel options for decarbonizing shipping*, 13<sup>th</sup> HIPER Symp., Tullamore, pp.12-20, [http://data.hiper-conf.info/Hiper2021\\_Tullamore.pdf](http://data.hiper-conf.info/Hiper2021_Tullamore.pdf)
- BERTRAM, V. (2022), *Review of Robotic In-Water Hull Cleaning*, 3<sup>rd</sup> PortPIC Conf., Hamburg, pp.3-11, [http://data.hullpic.info/PortPIC2022\\_Hamburg.pdf](http://data.hullpic.info/PortPIC2022_Hamburg.pdf)
- BERTRAM, V.; CAMPANA, E.F. (2020), *Ship Hull Optimization – An Attempt to Determine Position and Course of the State of the Art*, 19<sup>th</sup> COMPIT Conf., Pontignano, pp.271-279, [http://data.hiper-conf.info/compit2020\\_pontignano.pdf](http://data.hiper-conf.info/compit2020_pontignano.pdf)
- BRYNOLF, S.; GRAHN, M.; HANSSON, J.; KORBERG, A.D.; MALMGREN, E. (2022), *Sustainable fuels for shipping - Novel Technologies for Low Carbon Shipping*, Sustainable Energy Systems on Ships (Eds. F. Baldi et al.), Elsevier, pp.403-430
- CAMILLERI, J.; CONNOLLY, D.; SOBEY, A.; HUDSON, D. (2022), *Quantifying the Effect of Green Technologies on Ship Performance using Operational Data – Design of Experiments and Data Collection*, 14<sup>th</sup> HIPER Symp., Cortona, pp.176-190, [http://data.hiper-conf.info/Hiper2022\\_Cortona.pdf](http://data.hiper-conf.info/Hiper2022_Cortona.pdf)
- CONNOLLY, D. (2022), *Status of Air Lubrication Technology*, 14<sup>th</sup> HIPER Symp., Cortona, pp.295-302, [http://data.hiper-conf.info/Hiper2022\\_Cortona.pdf](http://data.hiper-conf.info/Hiper2022_Cortona.pdf)
- CORADDU, A.; GIL, A.; AKHMETOV, B.; YANG, L.Z.; ROMAGNOLI, A.; RITARI, A.; HUOTARI, J.; TAMMI, K. (2022), *Energy storage on ships*, Sustainable Energy Systems on Ships (Eds. F. Baldi et al.), Elsevier, pp.197-232
- DANESE, N.; VANNAS, A. (2020), *Intelligent Industrial Internet of Things & Services (IIoT&S): An Innovative, Plug & Play, High-ROI Approach for The Extended Enterprise*, 12<sup>th</sup> HIPER Symp., Cortona, pp.359-375, [http://data.hiper-conf.info/Hiper2020\\_Cortona.pdf](http://data.hiper-conf.info/Hiper2020_Cortona.pdf)
- DNV (2021), *Energy Transition Outlook 2021 - Maritime Forecast To 2050*, 5<sup>th</sup> Ed., DNV, Høvik, <https://eto.dnv.com/2021/maritime-forecast-2050/about>
- ERIKSEN, S. (2021), *Autonomous ships from the perspective of operation and maintenance*, PhD thesis, SDU, Svendborg, <https://simac.dk/media/3093/stig-eriksen-autonomous-ships-from-the-perspective-of-operation-and-maintenance.pdf>

- ETIENNE, M.; ROMANO, A. (2016), *The Internet of Things for smarter, safer, connected ships*, 10<sup>th</sup> HIPER Conf., Cortona, pp.164-171, [http://data.hiper-conf.info/Hiper2016\\_cortona.pdf](http://data.hiper-conf.info/Hiper2016_cortona.pdf)
- GEORGOPOULOU, C.; KOUKOULOPOULOS, L.; DIMOPOULOS, G.; OVRUM, E.; NIKOLOPOULOS, L.; BOUGIOURIS, K. (2021), *Model-Based Assessment of a Fuel Cell Driven Very Large Crude Carrier Concept*, 13<sup>th</sup> HIPER Symp., Tullamore, pp.209-217, [http://data.hiper-conf.info/Hiper2021\\_Tullamore.pdf](http://data.hiper-conf.info/Hiper2021_Tullamore.pdf)
- GUERE, S.; GAMBINI, N. (2021), *Notilo Cloud AI Platform for Hull Condition Reporting*, 13<sup>th</sup> HIPER Symp., Tullamore, pp.62-70, [http://data.hiper-conf.info/Hiper2021\\_Tullamore.pdf](http://data.hiper-conf.info/Hiper2021_Tullamore.pdf)
- HENTSCHEL, W.R. (2019), *Design and construction of a propeller open water testing apparatus and testing of a stereolithography 3D printed model propeller*, MIT, <https://hdl.handle.net/1721.1/122139>
- HIPKE, T. (2022), *Metal Foams – Ready for Shipbuilding?*, 14<sup>th</sup> HIPER Symp., Cortona, pp.90-95, [http://data.hiper-conf.info/Hiper2022\\_Cortona.pdf](http://data.hiper-conf.info/Hiper2022_Cortona.pdf)
- HOCHKIRCH, K.; BERTRAM, V. (2021), *Wind-assisted propulsion: Economic and ecological considerations*, Maritime Technology & Research 4/3, <https://so04.tci-thaijo.org/index.php/MTR/article/view/254498/173271>
- HÜFFMEIER, J.; SIWE, U.; PSARROS, G.; SÁNCHEZ-HERES, L. (2020), *Smart Tanker Shipping supported by STM BALT SAFE*, 8<sup>th</sup> Transport Arena Conf., Helsinki, [https://stm-stmvalidation.s3.eu-west-1.amazonaws.com/uploads/20200325075227/TRA2020\\_SmartShippingsupportedbySTMBaltSafe\\_Final.pdf](https://stm-stmvalidation.s3.eu-west-1.amazonaws.com/uploads/20200325075227/TRA2020_SmartShippingsupportedbySTMBaltSafe_Final.pdf)
- HOLLENBACH, U. HANSEN, H.; HYMPENDAHL, O.; RECHE, M.; RUIZ CARRIO, E. (2020), *Wind Assisted Propulsion Systems as Key to Ultra Energy Efficient Ships*, 12<sup>th</sup> HIPER Symp., Cortona, pp.278-276, [http://data.hiper-conf.info/Hiper2020\\_Cortona.pdf](http://data.hiper-conf.info/Hiper2020_Cortona.pdf)
- JUNGHANS, E.; BABU GOVINDARAJ (2022), *Additive Manufacturing enters the maritime mainstream*, DNV Maritime Impact, DNV, Høvik, <https://www.dnv.com/expert-story/maritime-impact/Additive-Manufacturing-enters-the-maritime-mainstream.html>
- KAKALIS, N.M.P.; GEORGIOS G. DIMOPOULOS, G.G.; STEFANATOS, I.C. (2014), *A Novel Framework for Dynamic Modelling of Integrated Machinery Systems*, 13<sup>th</sup> COMPIT Conf., Redworth, pp.137-149, [http://data.hiper-conf.info/compit2014\\_redworth.pdf](http://data.hiper-conf.info/compit2014_redworth.pdf)
- KELLING, J. (2021), *EU Project CHEK – Ultrasonic Antifouling and other Measures to Meet the CII Challenge*, 13<sup>th</sup> HIPER Symp., Tullamore, pp.132-139, [http://data.hiper-conf.info/Hiper2021\\_Tullamore.pdf](http://data.hiper-conf.info/Hiper2021_Tullamore.pdf)
- LAAG, S.; VARTDAL, B.J.; KNUTSEN, K.E. (2015), *Ship Connectivity*, DNV, Høvik, [https://www.dnv.com/Images/DNV%20GL%20-%20Ship%20Connectivity\\_tcm8-56026.pdf](https://www.dnv.com/Images/DNV%20GL%20-%20Ship%20Connectivity_tcm8-56026.pdf)
- LONGVA, T.; HOLMVANG, P.; GUTTORMSEN, V.J. (2014), *The Future of Shipping*, Whitepaper, DNV, Høvik, <https://www.dnv.com/publications/the-future-of-shipping-april-2014--14230>
- LOVSTAD, M.; BERTRAM, V. (2022), *The Decarbonizing Quest for Future Bulk Carriers*, 14<sup>th</sup> HIPER Symp., Cortona, pp.6-19, [http://data.hiper-conf.info/Hiper2022\\_Cortona.pdf](http://data.hiper-conf.info/Hiper2022_Cortona.pdf)
- MANCARELLA, L.; CALABRESE, F.; CATALDO, M.; SERAFINO, G.; PAIANO, L.; CARLINO, L.; CIRIGLIANO, A.; LEONARDI, N.; SANSEBASTIANO, E.; SEBASTIANI, L. (2022), *A Novel Integrated Multi-System Approach for Situational Awareness in Maritime Environment*, 21<sup>st</sup> COMPIT Conf., Pontignano, pp.387-402, [http://data.hiper-conf.info/compit2022\\_pontignano.pdf](http://data.hiper-conf.info/compit2022_pontignano.pdf)

- MATSUO, K. (2018), *Technology Mega Trends That Will Change Shipbuilding*, 17<sup>th</sup> COMPIT Conf., Pavone, pp.153-162, [http://data.hiper-conf.info/compit2018\\_pavone.pdf](http://data.hiper-conf.info/compit2018_pavone.pdf)
- MAVI, A.; KAUR, G.; KAUR, N. (2012), *Paint defect detection using a machine vision system – A review*, Int. J. Research in Management & Technology 2/3, pp.334-337, <http://www.ircst.org/ijrmt/papers/vol2no32012/11vol2no3.pdf>
- PETERSEN, P.D. (2020), *Enhancing the Quality and Reliability of Maintenance Operations using Mixed Reality*, 19<sup>th</sup> COMPIT Conf., Pontignano, pp.271-279, [http://data.hiper-conf.info/compit2020\\_pontignano.pdf](http://data.hiper-conf.info/compit2020_pontignano.pdf)
- ROHDE, F.; SAMES, P. (2012), *Conceptual Design of a Zero-Emission Open-Top Container Feeder*, 8<sup>th</sup> HIPER Symp., Duisburg, pp.207-215, [http://data.hiper-conf.info/Hiper2012\\_Duisburg.pdf](http://data.hiper-conf.info/Hiper2012_Duisburg.pdf)
- SCHÖNKNECHT, R.; LÜSCH, R.; SCHELZEL, M.; OBENAU, H. (1973), *Schiffe und Schifffahrt von Morgen*, VEB Verlag Technik Berlin, translated (1983) as *Ships and shipping of tomorrow*, MacGregor Publ.
- SILBERSCHMIDT, N.; TASKER, D.; PAPPAS, T.; JOHANNESSEN, J. (2016), *Silverstream system – Air-lubrication performance verification and design development*, 10<sup>th</sup> HIPER Conf., Cortona, pp.236-246, [http://data.hiper-conf.info/Hiper2016\\_cortona.pdf](http://data.hiper-conf.info/Hiper2016_cortona.pdf)
- STENSRUD, E.; KLAUSEN, K. (2022), *Another Step towards Remote Inspections of Maritime Vessels using Tailored Inspection Drones Instrumented with Computer Vision*, 21<sup>st</sup> COMPIT Conf., Pontignano, pp.212-220, [http://data.hiper-conf.info/compit2022\\_pontignano.pdf](http://data.hiper-conf.info/compit2022_pontignano.pdf)
- THIES, F.; FAKIOLAS, K. (2022), *Wind Propulsion*, Sustainable Energy Systems on Ships (Eds. F. Baldi et al.), Elsevier, pp.353-402
- VAN BIER, L.; VISSER, K. (2020), *Fuel cells systems for sustainable ships*, Sustainable Energy Systems on Ships (Eds. F. Baldi et al.), Elsevier, pp.81-122



# Hydrodynamic Optimization of an E-Powered Catamaran in Early Design

**Thomas Hildebrandt**, NUMECA Ingenieurbüro, Altdorf/Germany, [thomas.hildebrandt@numeca.de](mailto:thomas.hildebrandt@numeca.de)

**Sven Albert**, NUMECA Ingenieurbüro, Altdorf/Germany, [sven.albert@numeca.de](mailto:sven.albert@numeca.de)

**Stefano Carugno**, Gloss Design, Pescara/Italy, [stefcar@glossdesign.it](mailto:stefcar@glossdesign.it)

**Günther Migeotte**, Icarus Marine, Cape Town/South Africa, [gunther@icarusmarine.com](mailto:gunther@icarusmarine.com)

**Stefan Harries**, Friendship Systems, Potsdam/Germany, [harries@friendship-systems.com](mailto:harries@friendship-systems.com)

**Heinrich von Zadow**, Friendship Systems, Potsdam/Germany, [von.zadow@friendship-systems.com](mailto:von.zadow@friendship-systems.com)

## Abstract

*The paper presents a design study for a crew transfer vessel undertaken in the early design stage. The vessel is designed as a catamaran with electric propulsion to meet port requirements. Striving for small battery weight, the key design mission was to reduce resistance as far as possible to improve performance and range of the vessel. For this purpose, a parametric modeling and hydrodynamic optimization campaign was conducted. A parametric model for the hull was set up in CAESES. Resistance predictions. Power requirements were calculated using CFD with FINE/Marine using a simplified propulsor model. The optimization was accelerated using surrogate models for a coarse optimization search, before employing high-fidelity models for the final search. Potential for further improvement in design details is discussed.*

## 1. Introduction – Design task

The maritime industry steadily gains momentum in introducing new ways of providing boats and ships with clean(er) energy. For more than a century the main source of energy for shipping came first in form of coal, then in form of fuel oils, and more recently increasingly in the form of LNG (Liquefied Natural Gas). The IMO (International Maritime Organisation) targets for decarbonization of shipping will lead to fundamental changes in ship fuels and energy converters in the next three decades. The transformation process has already started.

For usual deep-sea shipping, i.e. long-distance, high-deadweight shipping, the most likely scenarios are based on diesel engines and fuel cells, using alternative fuels with low carbon footprint, such as biofuels, methanol, LNG, and ammonia, *Bertram (2021)*. For short sea shipping, more and more projects consider purely electric propulsion, using fuel cell or battery technology, *Hoedemaker (2022)*. Ferries for relatively short distances have turned out to be good candidates for early adaptation of such e-propulsion. They allow full charging of batteries during the nights when in port and intermediate recharging of batteries when (un)loading, *Jokinen et al. (2021)*.

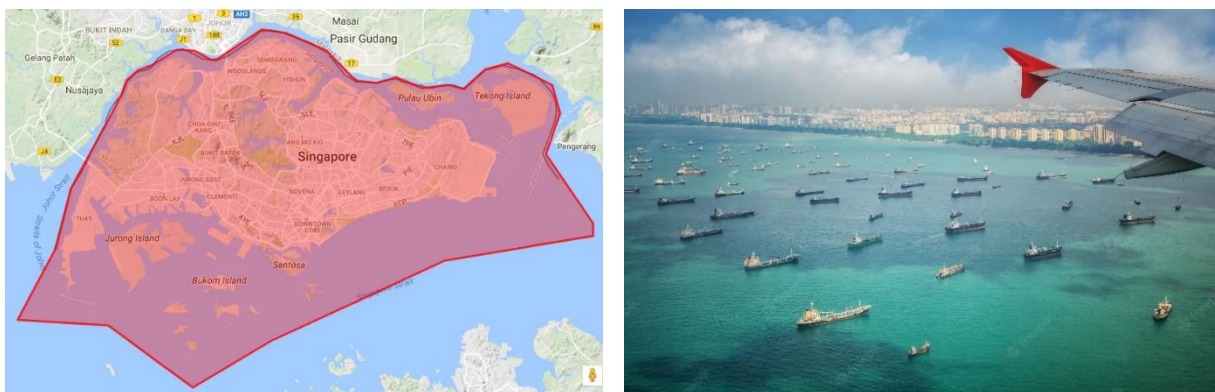


Fig.1: Port of Singapore

The project presented in this paper focuses on the hydrodynamics of a small crew transfer vessel for the port of Singapore, Fig.1. Singapore Port is a major international crew change hub for ships and its port authority is seeking to electrify all harbour craft. The particular focus of this project was on effi-



cient outer port limits (OPL) crew transfer. The new design had to be fully electrical, and its performance was to exceed those of existing conventional craft in service, in terms of speed and range, with in combination with high battery weight poses a considerable design challenge.

Normally, such a small ferry project would not undergo a thorough hydrodynamic optimization campaign. However, the high price and weight of batteries justified the extra design effort in this project, as it did in several other for applications of simulation-driven design (SDD) to electrically powered small craft in our experience, *Albert et al. (2020, 2021)*.

Gloss Design and Icarus Marine as small craft design specialists assumed the leading role as designers, while FRIENDSHIP SYSTEMS and NUMECA Ingenieurbüro contributed their expertise of geometric modeling and numerical flow simulation, respectively. Fig.2 shows the general arrangement of the base design.

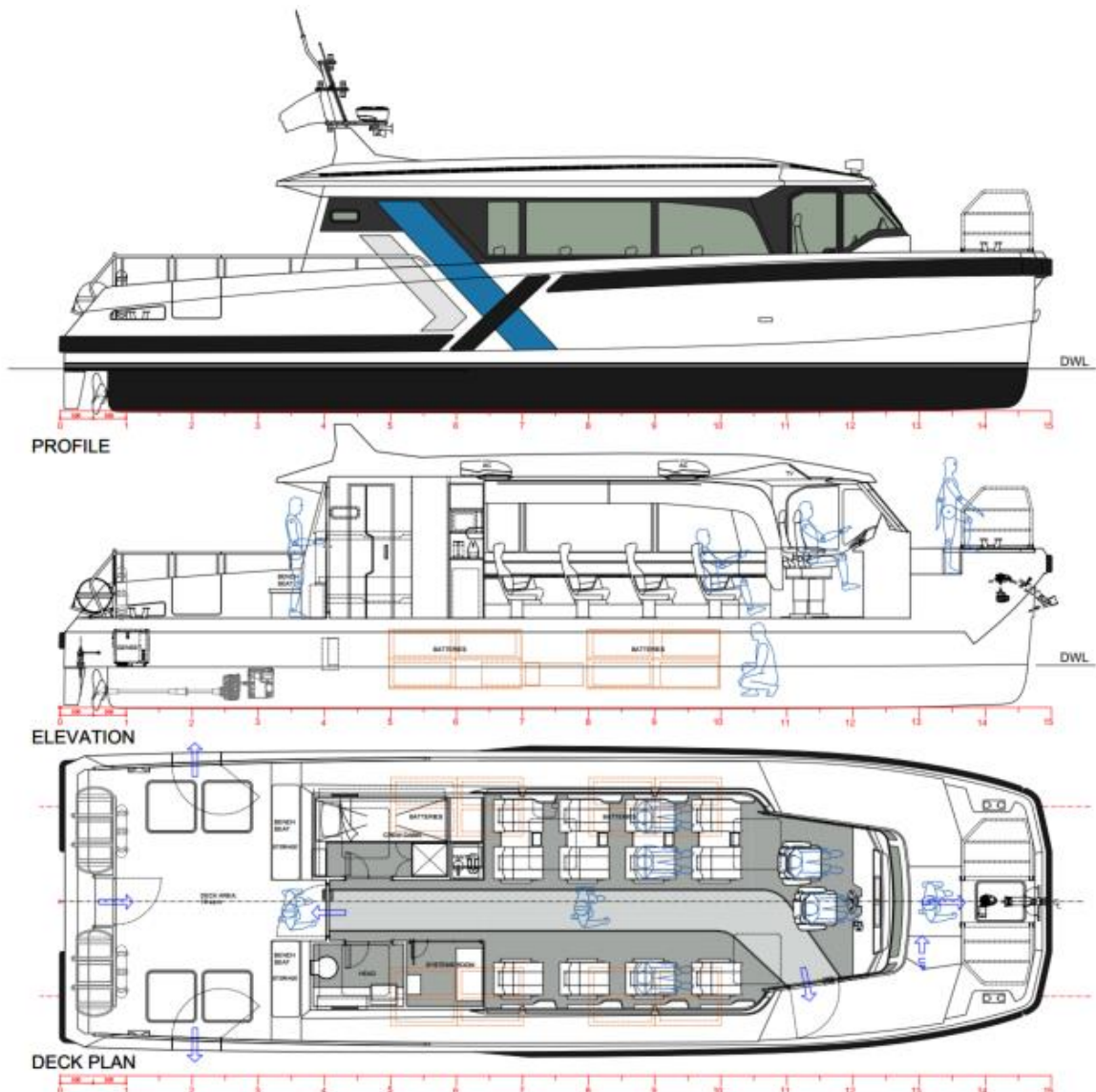


Fig.2: General arrangement of base design

The base design is a catamaran, Fig.3. The chosen canoe stern design, Fig.4, features generally very low resistance compared to conventional hulls, with low appendage drag as there are no exposed shafts or brackets.



Fig.3: Artist vision of design



Fig.4: Canoe stern design

## 2. Partially parametric modelling

Parametric modeling for the design and optimization of ship hulls, propellers, appendages, etc. is by now widely accepted and applied in both academia and industry. To balance intelligently a meaningful range of shape variations and a small enough set of free variables to control them, different approaches of parametric modeling have been developed; see *Harries (2020)* for an overview.

In SDD these Computer Aided Design approaches (CAD) are typically subdivided into fully parametric and partially parametric modeling. While fully parametric modeling (FPM) is more powerful with regard to the scope and the precision of achievable modifications, partially parametric modeling (PPM) is easier and faster to set up and handle. For this project, a PPM model was set up in the CAESES framework of FRIENDSHIP SYSTEMS, <https://www.caeses.com>. CAESES is a flexible CAD modeler for fast and robust design studies. Integrated capabilities for process automation and shape optimization make it an all-in-one design system for simulation engineers.

### 2.1. BRep morphing

In a first approach, a PPM model based on radial basis functions (RBFs) was used. RBFs offer a very intuitive set-up of defining modifications on a base design and can be considered a morphing approach in its broader sense. (Note that quite frequently the term morphing is used for most partially parametric modeling approaches.) In CAESES two RBF techniques are available: A discrete approach for interactively changing point data (trimeshes) and a continuous approach for changing mathematically closed geometries represented by B-splines (BReps), *Harries and Abt (2021)*. For the catamaran optimization presented here, the continuous BReps approach was chosen since it allows the design team a fine-tuned modification of various regions that are likely to influence the hydrodynamic performance positively. For details of the RBF approach in CAESES, see *Albert et al. (2021)*.

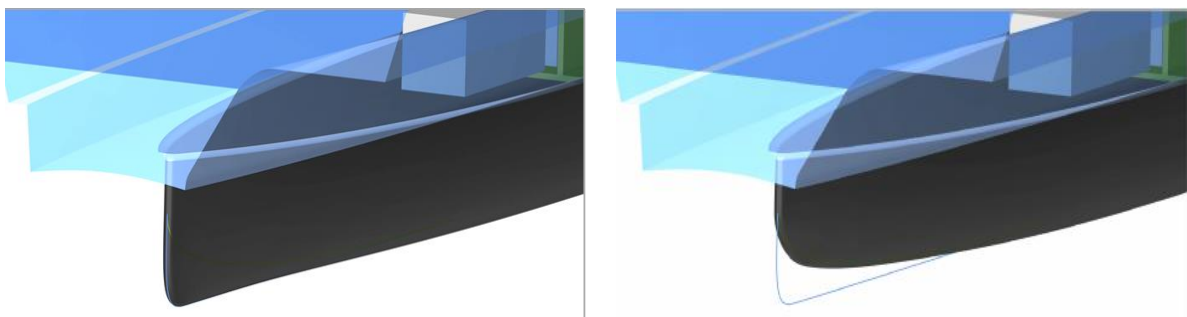


Fig.5: Push stern in as parametric variation example

Variations in the stern were particularly effective in adjusting transom immersion, trim, anti-ventilation, propeller inflow, and pressure recovery, all affecting the resistance respectively the power requirements. The tunnel height was an important parameter to ensure enough room for the propeller

at lower transom heights. Pushing the stern in, Fig.5, was surprisingly effective, but cannot be overdone because the propeller shaft still needs to fit. Asymmetry was also found to be very important due to a very bad combination of speed and demi-hull spacing in the base design. Maximum asymmetry allowed to get reduce the unfavorable wave interference significantly, but it was tricky to still fit the batteries, Fig.6.

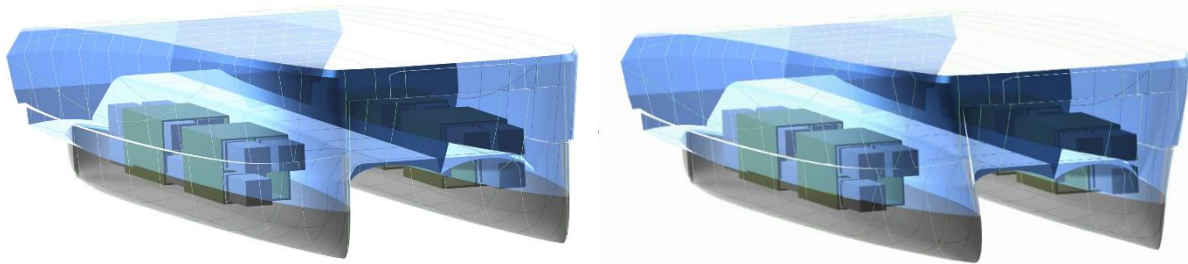


Fig.6: Asymmetry as parametric variation example

## 2.2. Free Form Deformation

The second technique that was used is Free Form Deformation. Here, based on an existing baseline design, the modification of the shape (and not the shape itself) is defined parametrically. Transformations of the control points of the B-spline volume are easy to set up and control, but give very good results (both in terms of surface quality and resistance reduction). The “taper aftbody” shown in Fig.7 was responsible for more than 40% of the total resistance reduction in the optimization. In the “taper forebody” modification, it was again important to allow enough space for the batteries at large asymmetries and gentle waterline entry, Fig.8.

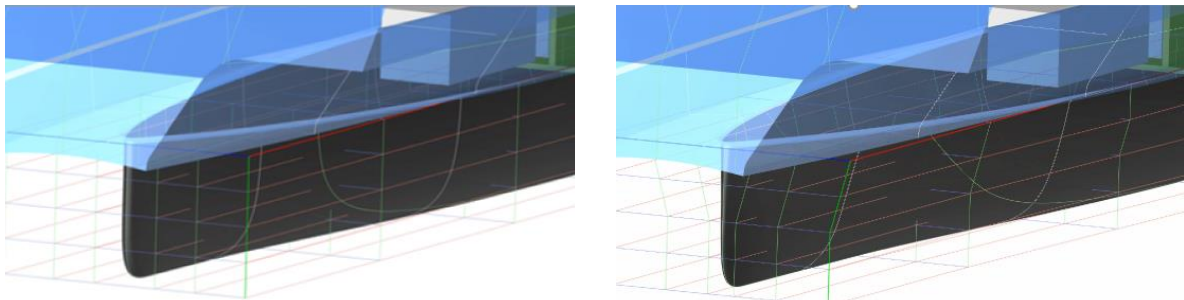


Fig.7: Taper aftbody modification in Free Form Deformation

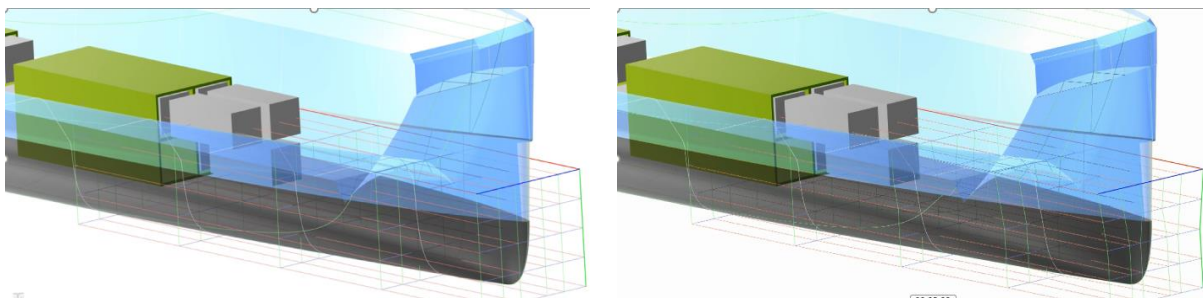


Fig.8: Taper forebody modification in Free Form Deformation

## 2.3. Lackenby transformation

The last transformation applied to the model before sending it to the CFD analysis was a Lackenby transformation, shifting sections in longitudinal direction, <https://www.caeses.com/blog/2016/ship-hull-optimization-generalized-lackenby/>. In a way, Lackenby transformations are the “holy grail” of transformations for the naval architect.



Whatever we have done to the model so far, with this single transformation we can simultaneously set 100% accurate displacement and LCB (either fixed, or within user-defined limits) and simultaneously (even independently) shift the mid frame (our free design variable in this step). As a result, we will only generate feasible designs (from a hydrostatics' point of view) with maximum shape variations.

A few more words on the hydrostatics - Batteries make up a large portion of the deadweight of a battery-electric vessel. They are also quite large and need to be fitted into the narrow demi-hulls, preferably very low for stability reasons. In search of the optimum shape, we must shift the batteries longitudinally within the permissible limits. This changes the LCG (longitudinal center of gravity), but the Lackenby transformations can ensure a corresponding LCB. We can shift the batteries to generate a few more mm of clearance in critical areas. We found that even with just a few mm of clearance for the batteries, we were able to achieve large variations in shape, Fig.9, which in turn facilitated significant improvements in hydrodynamics.

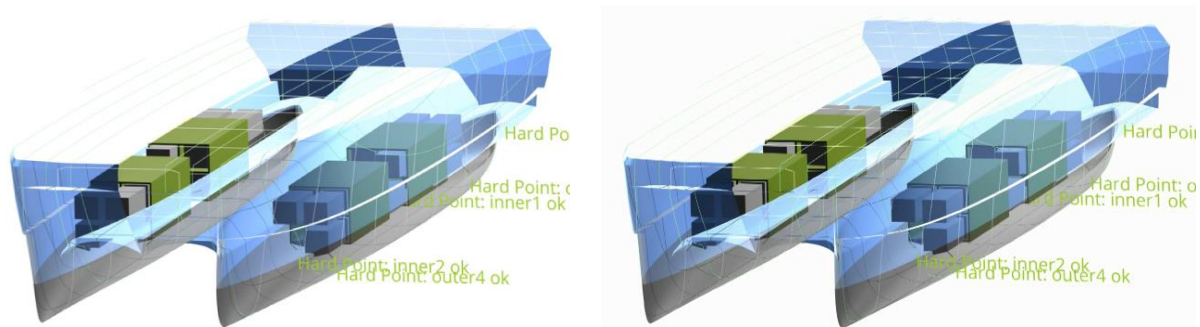


Fig.9: Variations in battery positions to shift LCG and LCB

### 3. CFD evaluation for base design

NUMECA's FINE™/Marine package was used for the viscous CFD calculations, utilizing a volume-of-fluid (VOF) method for free surface capturing, *Queutey and Visonneau (2007)*. The numerical representation and accuracy of the time-dependent free surface is strongly affected by the spatial discretization in the grid, especially perpendicular to the air-water-interface. FINE™/Marine features an adaptive grid refinement (AGR) technique, which can create or remove mesh cells during solver runtime, triggered by various physical phenomena. The current location of the free surface acts as the sensor and the mesh is refined until a user-specified threshold in terms of the cell size is achieved. This procedure is called in certain intervals and ensures an ideal grid at all locations and at all time steps. Such an approach does not require any pre-refined mesh zones where the user would need to anticipate important phenomena in the flow field beforehand, e.g. wave patterns and regions of breaking waves. During an optimization with variable geometry and for two different displacements, which on their own strongly affect the location of the free surface. An AGR thus reduces the necessary CPU time for each variant investigated.

The typical starting point for any optimization campaign is a detailed analysis of the baseline, the set-up of a smooth workflow and the investigation of possible numerical sensitivities like boundary conditions and grid resolution. The aim of the project was a reduction of total resistance for the wetted hull, including the lower parts of the freeboard. The superstructure was not taken into account. This is a valid approach since, especially for low operating speeds, air drag is rather small and even in rough weather the variation of the hull should have only negligible effect on the flow about the superstructure. The cat was supposed to run straight ahead in calm seas, solving for sinkage and trim for the two displacement conditions using an integrated body-motion solver, *Leroyer and Visonneau (2005)*.

The flow was simulated at full-scale for only one speed, 12 kn, and one displacement condition, 19.5 t (fully loaded). Such a simulation can be handled fully automatically using the C-Wizard in FINE™/Marine, which provides meshing templates for various densities as well as the full solver set-

up. However, for more flexibility, we used our own set-up in Python. In conjunction with the stable yet flexible STL file export from CAESES® the Python set-up ensures a smooth workflow. For the set-up of a suitable flow domain and the exchange of data between CAESES® and FINE™/Marine via STL files, see *Albert et al. (2016)* for details. Importantly, within CAESES the topology of the flow domain along with the colors and name tags assigned to various parts of the domain (e.g. inner hull, outer hull, spray rail, deck, transom etc.) stay unaltered during any variation. Hence, when exporting them in a multi-body STL file, FINE/Marine can readily handle any new variant without manual interaction.

The propeller was modelled by an actuator disk, enhanced with an open-water characteristics of the design propeller, Fig.10. Such a model gives similarly good results for global resistance and propulsion cases as using meshed propellers, but at a fraction of the computational costs.

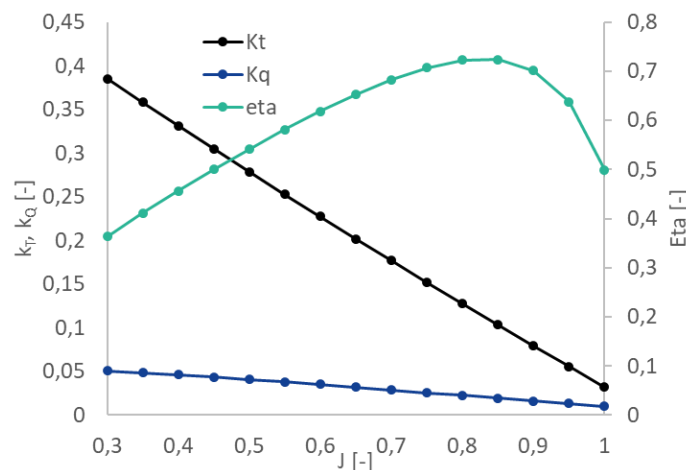


Fig.10: Open-water characteristics of propeller

The CFD mesh was generated using HEXPRESS, exploiting port-starboard symmetry. Based on our experience, we decided that a mesh with 610000 cells and a  $y^+ \approx 80$  would suffice to capture all important flow patterns for reliable resistance values. This can be considered a “competitive” numerical set-up that should allow many design variations in a short timeframe (3.5 h on two cores), fairly balancing computational effort and accuracy.

## 4. Optimisation campaign

### 4.1. Overview

The next step was the assembly of the optimization chain as illustrated in Fig.7(a). The optimization tool employed was NUMECA FINE™/Design3D, which controls all the sub-processes like geometry variation and export, meshing, solver runs and data collection in the post-processor. A Python API ensures a flexible and easy to use access to the various tools and exchange of data. The optimization loop itself is based on a surrogate model. The approach is shown in Fig.7(b). It starts with the generation of a database from a sampling of the design space via a Design-of-Experiment (DoE). It aims at a maximum scattering of the samples within the bounds of the free variables with as few designs as possible. Here, 13 free variables were used and 10 designs created in a Sobol sequence. The displacement is kept constant, and LCB = LCG for all designs. No hard points were violated.

From this discrete set of data points, bringing together geometry and performance, a surrogate model is built which offers a continuous description that is cheap and fast to evaluate. An evolutionary algorithm then calls this surrogate model thousands of times to generate new candidates in the design loop. The algorithm mimics evolutionary processes with selection of strong traits in a design with respect to the performance and to the constraints over several generations.

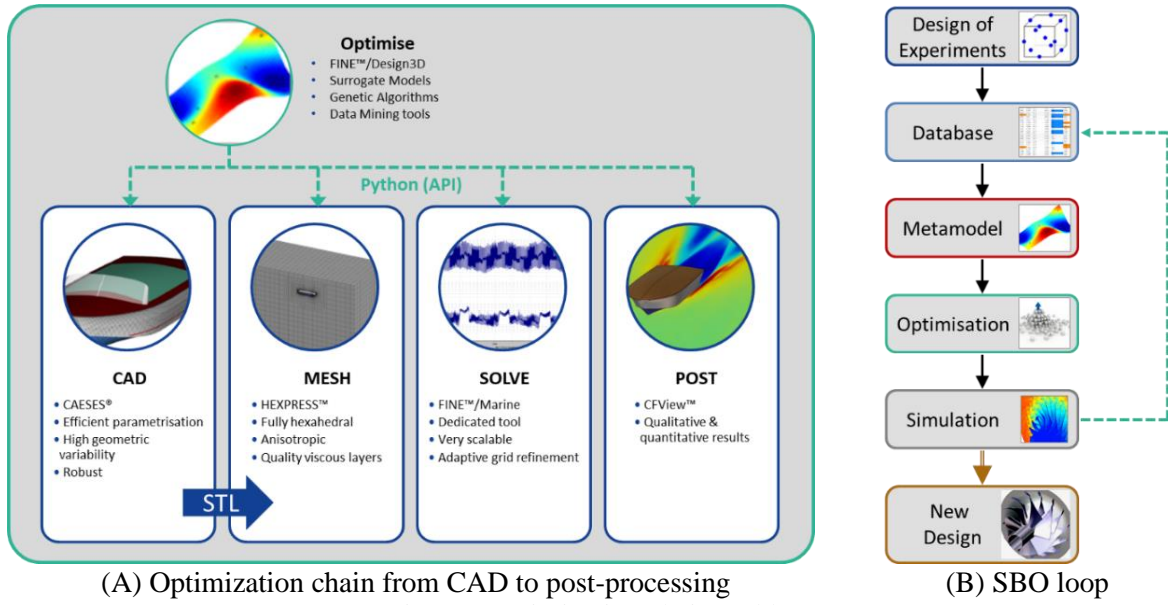


Fig.11 : Optimization chain and loop

Weak samples tend to become extinguished while methods like mutation help to keep a large diversity from one population to the next. In the end such an optimizer yields a high probability of finding optimum solutions, even globally, especially in comparison to local strategies such as a gradient method. Since the actual search is performed on the surrogate model the number of variants can be very high without using any tangible computer resources. When a new and promising candidate is identified it is evaluated by means of (substantially more expensive) CFD simulations, using the optimization chain. The results are subsequently appended to enrich the database and to provide an even better surrogate model. The process is then re-started until convergence.

#### 4.2. Design-of-Experiment (DoE)

Prior to starting the DoE to create the actual database, a few checks for plausibility of parameter ranges and stability of the meshing and workflow templates were made. Naturally, the bounds of the free variables constitute a crucial input to any optimization: It is desirable to have sufficient geometric variability, while as few variants as possible should be unusable. The latter can appear quite easily if the chosen parametrization is not well-suited for the design task or if extreme parameter combinations lead to designs that any engineer would readily reject. Moreover, any failure in the optimization chain should be handled correctly by the optimizer. Machine issues or plain technical issues like licensing must be identified so that the optimizer does not neglect any region in the design space which could be of interest. In addition, physical phenomena like excessive drag or strong unsteadiness in resistance values should also be monitored. For this purpose, the time series for total resistance for each variant was evaluated for the last 30% of simulation time, delivering both a mean value as objective and a standard deviation for quality checks.

Results of the DoE, i.e., the database run, are displayed in Fig.12, giving the mean total resistance values and the shaft power values. The baseline is shown in the center, indicated via a large blue cross, while the points give the performance of the 39 DoE samples. The overall scattering of the resistance is quite large, and there is only little clustering of the designs, which indicate a nice sampling even with the relatively few samples. As can be seen, there are variants that perform far worse but also quite a bit better than the baseline design. The database sampling gets already a good improvement, but the subsequent optimizing achieved almost 10% in shaft power.

A surrogate-based optimization relies heavily on the quality of the prediction. If a surrogate model does not predict new and unknown variants with a certain accuracy or fails to capture trends correctly, there is no chance for any optimizer to find good solutions, at least within a reasonable timeframe.

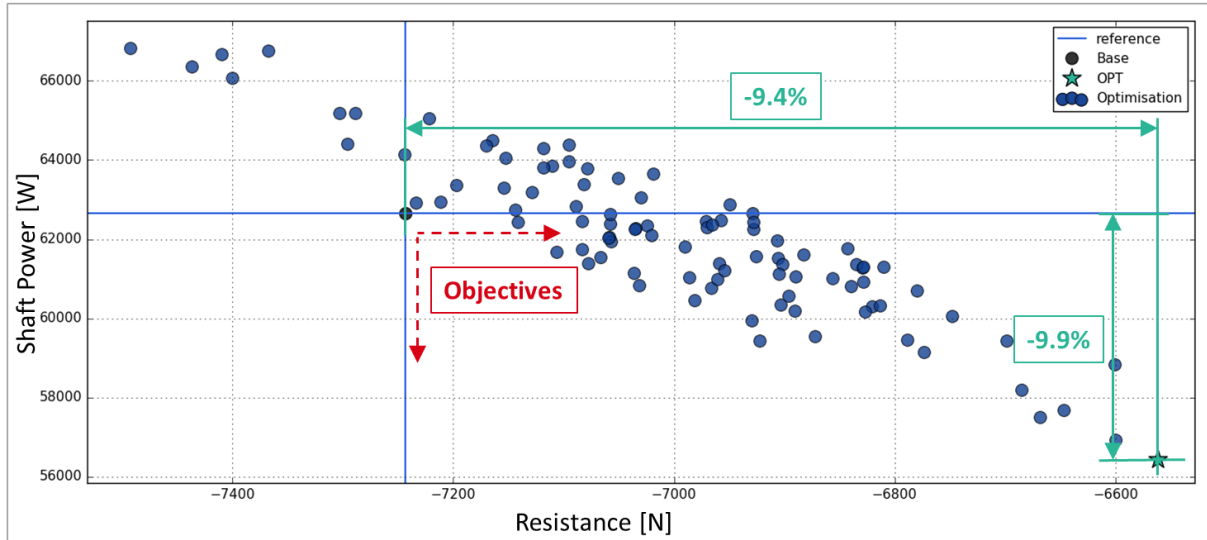


Fig.12: Shaft power over total resistance for 12 kn and 19.5 t displacement

One way to quantify the accuracy is the “leave-one-out analysis”, which calculates the correlation and, hence, the surrogate quality of a given set of data without the need for an additional set of evaluation samples. Such an analysis is depicted in Fig.13. The correlation in this case is relatively poor compared to other projects in our experience, very likely due to the limited number of samples in limited time and some issues encountered in the CAESES process control.

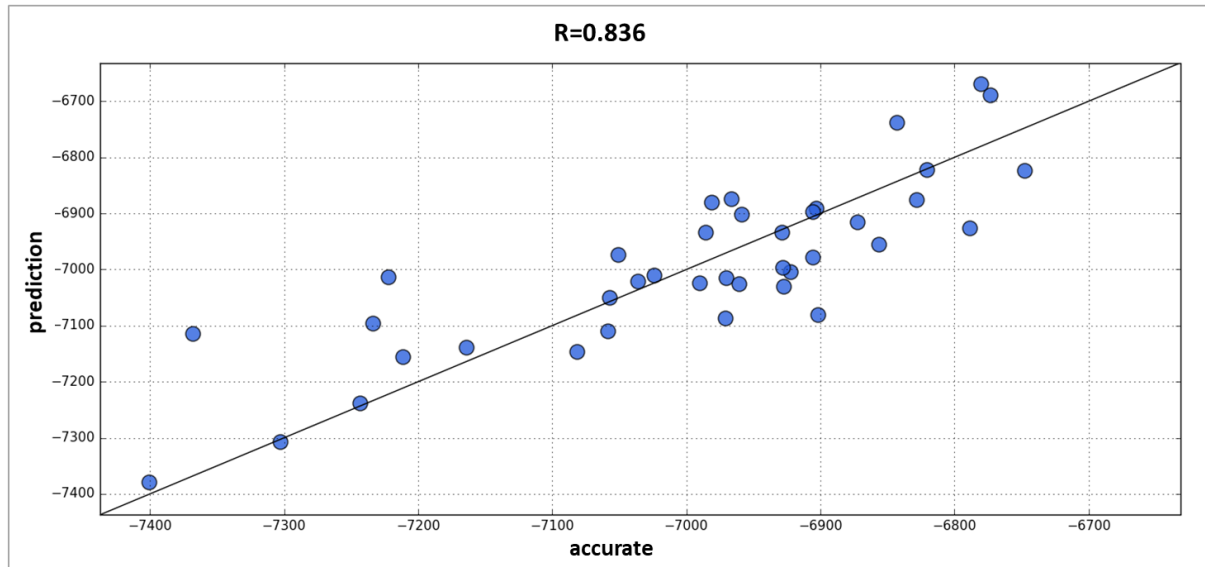


Fig.13: Correlation between surrogate model prediction and CFD values

Still, the achieved “optimum” represents a significant progress in the design, albeit for one operating point (design point). The next phase was to reveal how much room for improvement there was left to exploit and whether an improved design good be achieved for a range of operating points.

#### 4. Next design iteration

Figs.14-16 show CFD results from the first optimization campaign with the relatively coarse CFD mesh. Flow details indicating further improvement potential include:

- Bow spray still hits the tunnel in the optimized version, Fig.14.
- Ventilation at the stern still occurs in the optimized version, Fig.15.



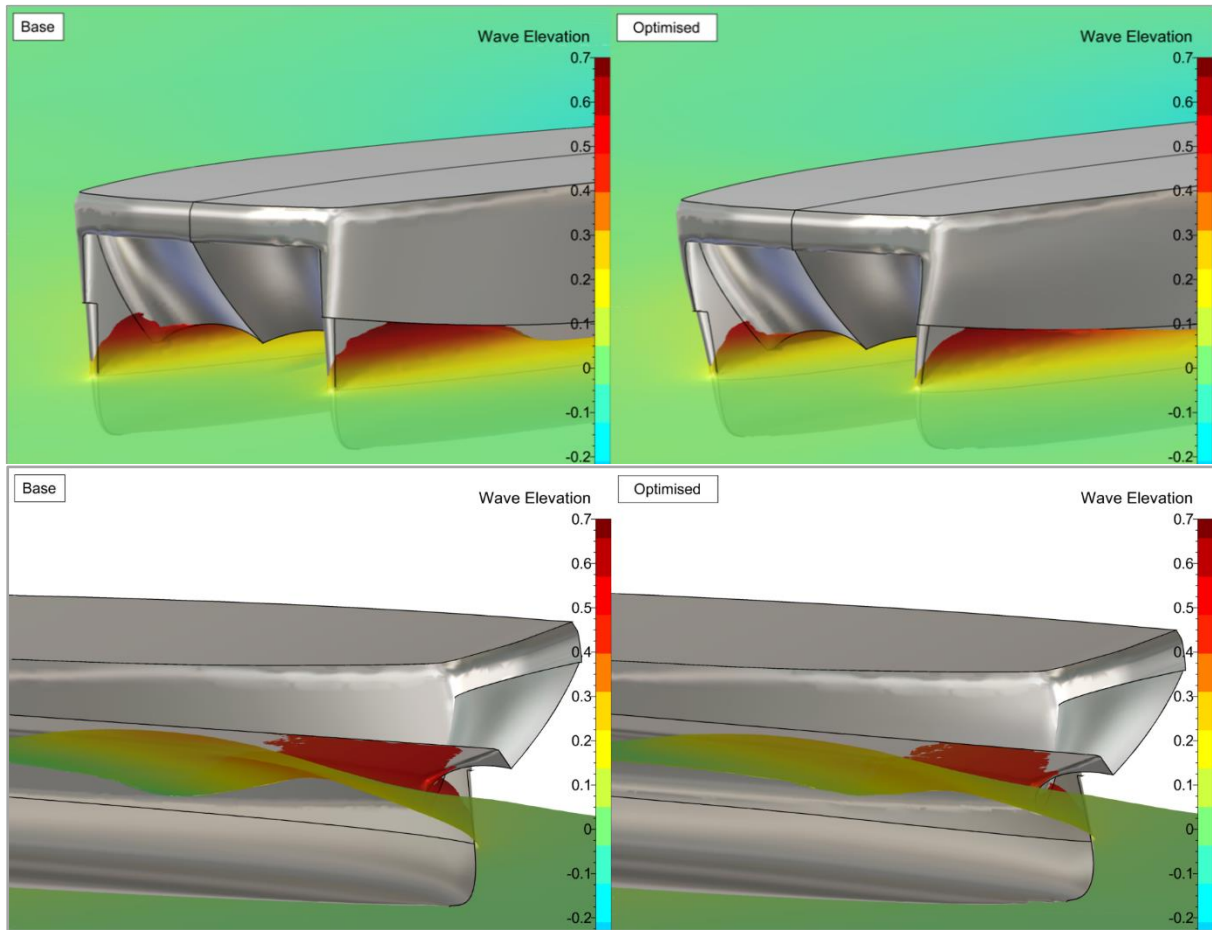


Fig.14: Bow spray hits tunnel in both Base and Opt design (12 kn, 19.5 t)

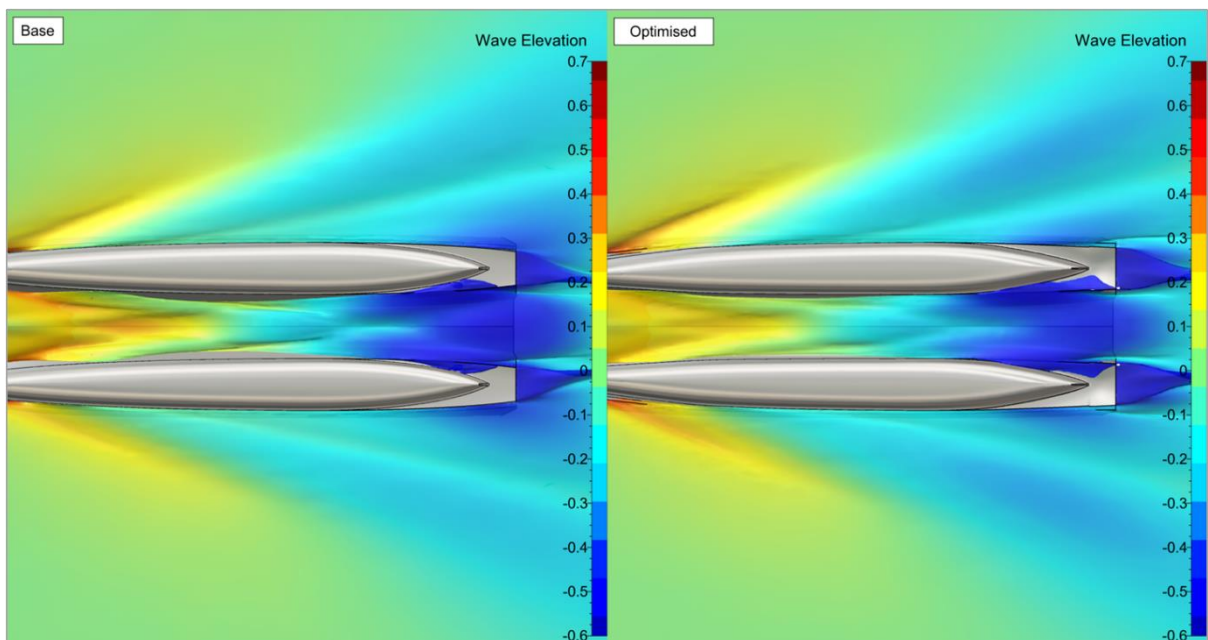


Fig.15: Ventilation in both Base and Opt design (12 kn, 19.5 t)

One lesson learnt in this project was that designer experience can also be misleading in some cases. The flat bottom above the propeller was intended to prevent ventilation, according to literature, but the simulation proved that wrong in this case, Fig.15.



The experienced small-craft designers in our team, Stefano Carugno and Günther Migeotte, now tried to improve the design based on their experience, but unaware of parameter sensitivity. Key modifications were:

- Implement an inner spray rail, Fig.16
- Move tunnel upwards, Fig.16
- Move tunnel backwards
- Slightly modify the stern (the sensitive part!), Fig.17

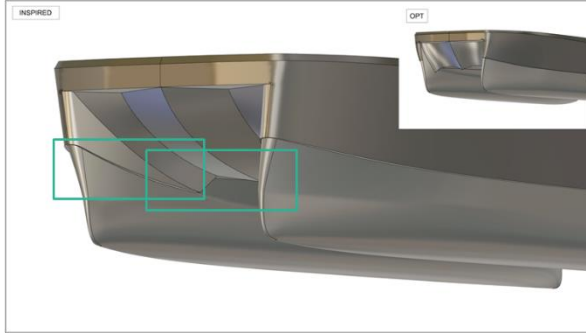


Fig.16: Designer modifications at bow

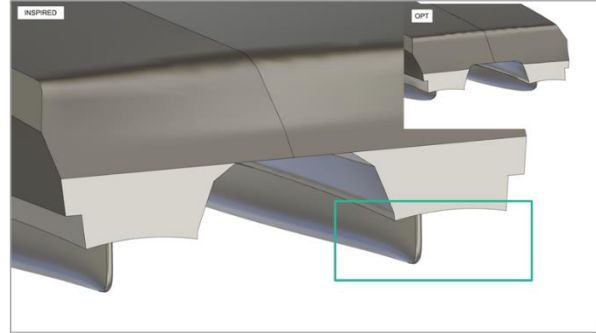


Fig.17: Designer modifications at stern

Base design (“base”), design optimized for 12 kn (“opt”) and human designer modified design (“insp”) were then assessed with high-fidelity CFD simulations, 2.3 million cells and  $y^+ \approx 50$ . This time, a matrix of operational conditions was assessed, with 4 speeds (8, 10, 12, and 14 kn) and 2 loading conditions (17.5 t and 19.5 t). Meshing was done in FIDELITY, using the family tree option, Fig.18. The “family tree” allows very similar grids for a family of similar designs, accelerating meshing and making results well comparable.

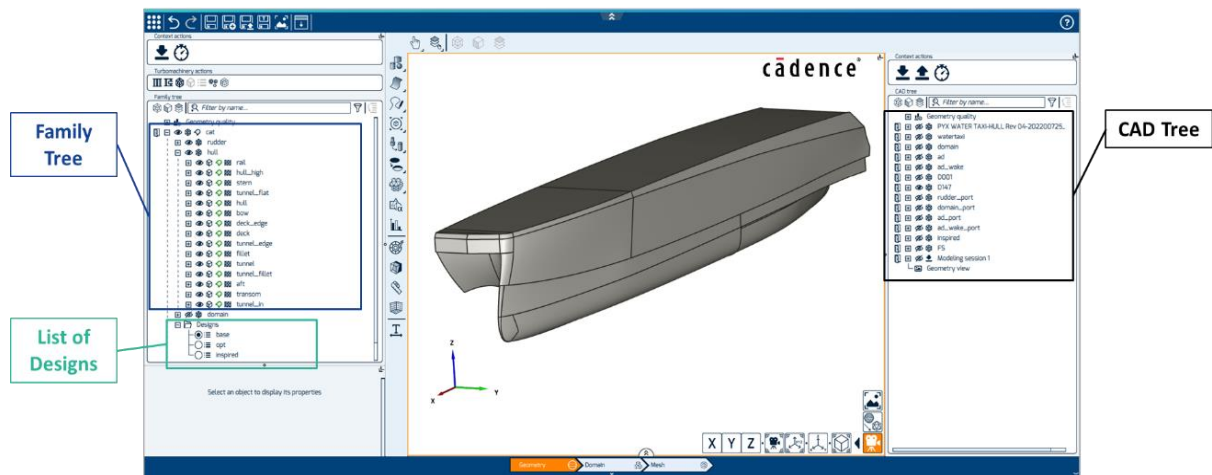


Fig.18: Meshing in FIDELITY

Figs.19 to 22 show mesh details in CFVIEW after simulation, i.e. with the AGR free-surface modifications on the original FIDELITY mesh. Separation zones were also meshed in FIDELITY (although that could have been left to AGR as well). The local clustering in Fig.22 is also from the AGR algorithm, as we have spray there.

Fig.23 shows the results for 17.5 t displacement. Results for 19.5 t were similar in general characteristics and conclusions. Compared to the base design, the “opt” design showed improvements over the speed range, except for 10 kn (start of the hump in the resistance curve at Froude number  $F_n = 0.43$ ). There is a higher uncertainty about the data at this speed due to a very strong unsteadiness in the flow observed in the simulations. The “insp” design lost some of the improvements of the “opt” design.

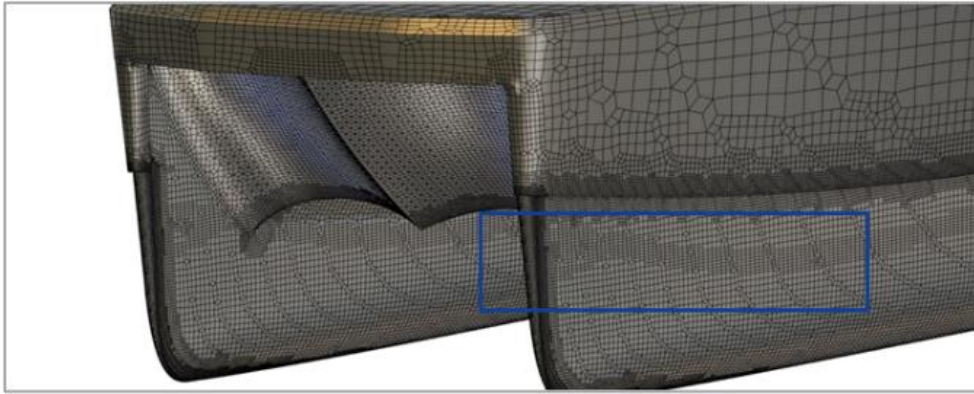


Fig.19: Mesh at bow, blue box: AGR

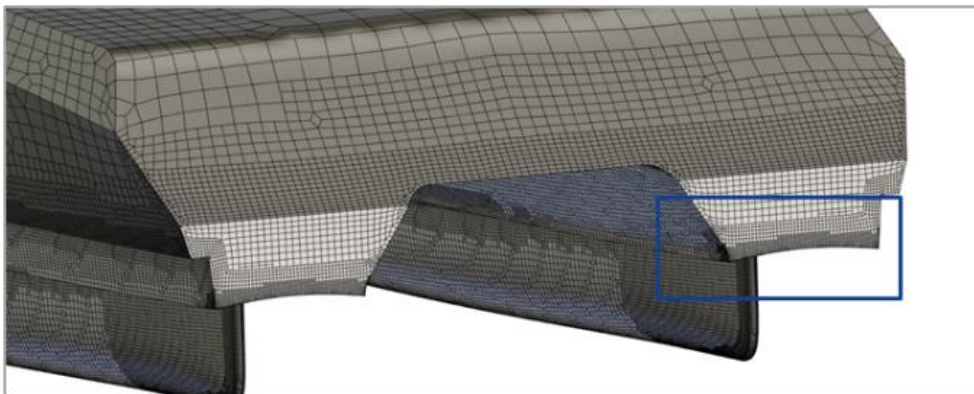


Fig.20: Mesh at stern, blue box: separation zone

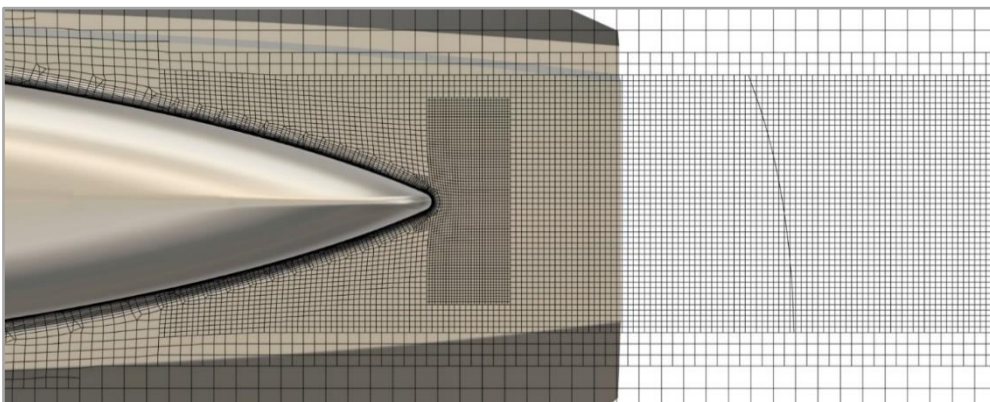


Fig.21: Cut view actuator disc including inflow and outflow

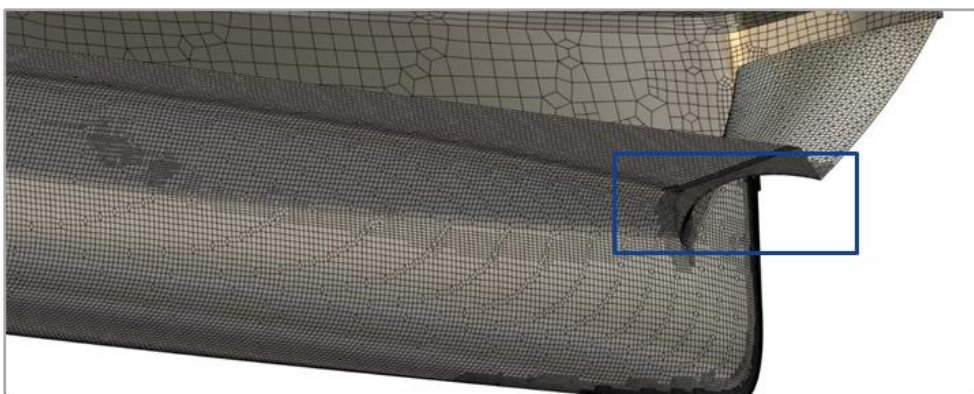


Fig.22: Tunnel edge, blue box: separation zone

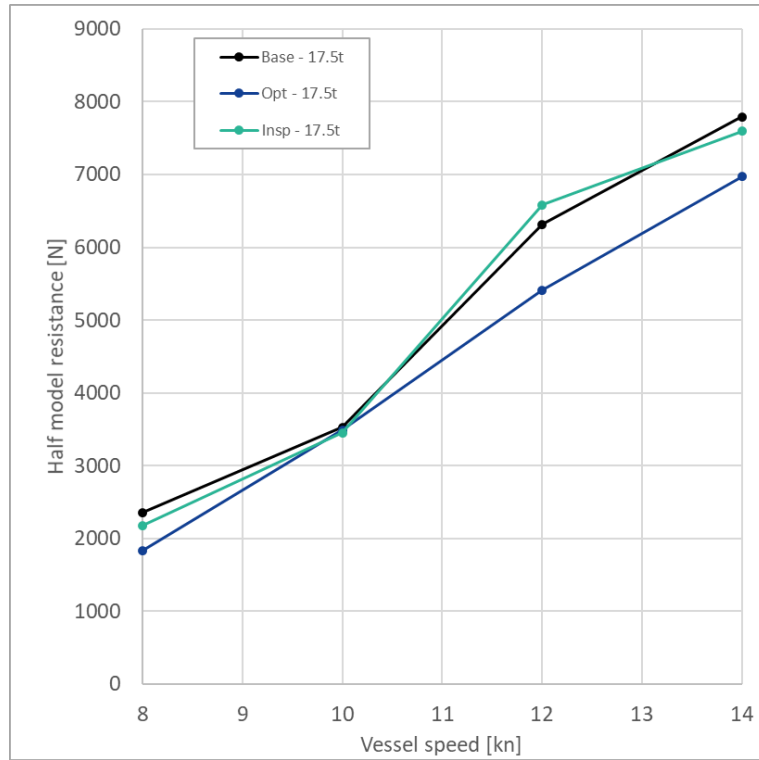


Fig.23: Resistance at 17.5 kn

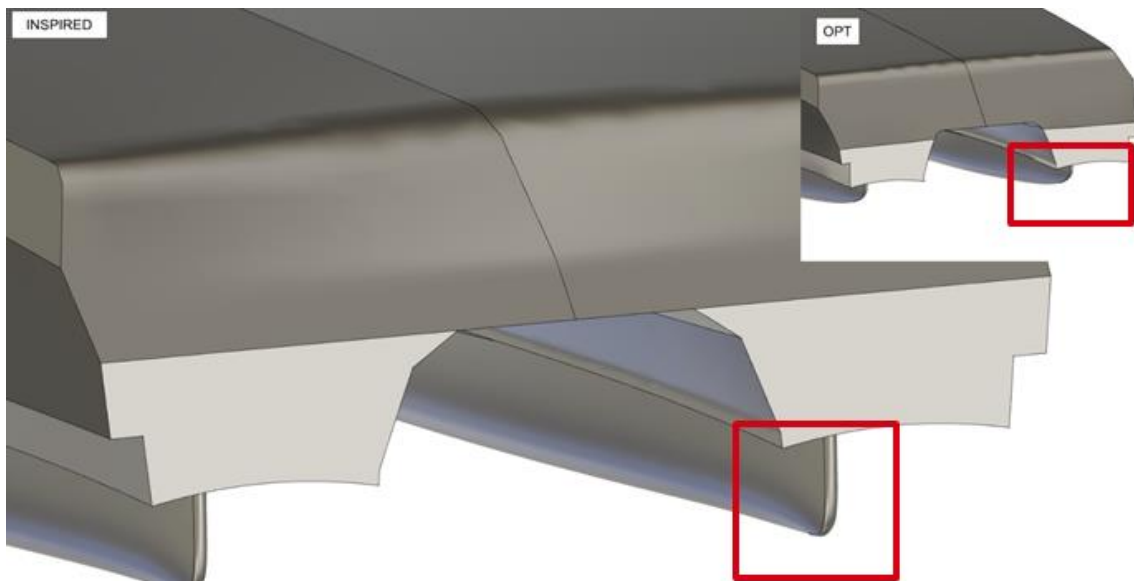


Fig.24: Push stern in details for “opt” and “insp” contributing significantly to resistance difference

Small design changes have a big impact in this case. The importance of the push stern in parameter was revealed already in the DoE phase, and confirmed in this concrete comparison. This episode is a reminder of the importance of data mining, and that design parameter elucidation is a powerful tool that should not be ignored.

## 5. Conclusions

- A design for an electrically powered catamaran vessel was improved in a very early design stage, resulting in -10% power consumption.
- The partially parametric modelling was very time efficient for design variations, once it had been created.

- Such a design study has only modest hardware requirements: CFD simulations and optimization on 80 samples were run over a weekend on a 32-cores machine.
- The DoE phase offered important insights into critical parts of the hull which affect overall power consumption above proportion.

The project brought four companies together, two from a traditional naval architecture culture, two from a CFD simulation culture. We experienced some “frictional” losses in communication between the two cultures. Lessons learnt on the human factor side were:

- Naval architects: Do not touch an optimized design.
- CFD engineers: Tell the naval architects what you know (in a language they can understand)

## Acknowledgments

We are grateful for the support of many colleagues in this project, and to Volker Bertram for his guidance in writing this paper.

## References

ALBERT, S.; HARRIES, S.; HILDEBRANDT, T.; REYER, M. (2016), *Hydrodynamic Optimization of a Power Boat in the Cloud*, 10<sup>th</sup> HIPER Symp., Cortona, pp.458-472, [http://data.hiper-conf.info/Hiper2016\\_Cortona.pdf](http://data.hiper-conf.info/Hiper2016_Cortona.pdf)

ALBERT, S.; CORRÊA, R.; HILDEBRANDT, T., HARRIES, S. (2020), *An Electrified RIVA Powerboat – Optimised*, 12<sup>th</sup> HIPER Symp., Cortona, pp.264-277, [http://data.hiper-conf.info/Hiper2020\\_Cortona.pdf](http://data.hiper-conf.info/Hiper2020_Cortona.pdf)

ALBERT, A.; HILDEBRANDT, T.; HARRIES, S.; BERGMANN, E.; KOVACIC, M. (2021), *Hydrodynamic Optimization of a Small Electric Catamaran Ferry*, 13<sup>th</sup> HIPER Symp., Tullamore, pp.106-120, [http://data.hiper-conf.info/Hiper2021\\_Tullamore.pdf](http://data.hiper-conf.info/Hiper2021_Tullamore.pdf)

BERTRAM, V. (2021), *Fuel Options for Decarbonizing Shipping*, 13<sup>th</sup> HIPER Symp., Tullamore, pp.12-20, [http://data.hiper-conf.info/Hiper2021\\_Tullamore.pdf](http://data.hiper-conf.info/Hiper2021_Tullamore.pdf)

HARRIES, S. (2020), *Practical Shape Optimization Using CFD: State-Of-The-Art in Industry and Selected Trends*, 19<sup>th</sup> COMPIT Conf., Pontignano, pp.196-222, [http://data.hiper-conf.info/compit2020\\_pontignano.pdf](http://data.hiper-conf.info/compit2020_pontignano.pdf)

HARRIES, S.; ABT, C. (2021), *Integration of Tools for Application Case Studies, A Holistic Approach to Ship Design – Vol. 2: Optimisation of Ship Design and Operation for Life Cycle*, Springer

HOEDEMAEKER, S.t.C. (2022), *Current Status of Maritime Batteries and Future Outlook*, 14<sup>th</sup> HIPER Symp., Cortona, pp.124-135, [http://data.hiper-conf.info/Hiper2022\\_Cortona.pdf](http://data.hiper-conf.info/Hiper2022_Cortona.pdf)

JOKINEN, M.; BROGLIA, R.; GATCHELL, S.; AUBERT, A.; GUNAWAN, R.; SCHELLENBERGER, G.; HARRIES, S.; VON ZADOW, H. (2021), *Double ended Ferry, A Holistic Approach to Ship Design – Vol. 2: Optimisation of Ship Design and Operation for Life Cycle*, Springer

LEROYER, A.; VISONNEAU, M. (2005), *Numerical methods for RANSE simulations of a self-propelled fish-like body*, J. Fluid & Structures, 20/3, pp.975-991

QUEUTEY, P.; VISONNEAU, M. (2007), *An interface capturing method for free-surface hydrodynamic flows*, Computers & Fluids, 36/9, pp.1481-1510



# AI-Enhanced Ultrasonic Biofouling Protection

**Xavier Mayorga**, HASYTEC electronics, Kiel/Germany, [x.mayorga@hasytec.com](mailto:x.mayorga@hasytec.com)

**Jan Kelling**, HASYTEC electronics, Kiel/Germany, [j.kelling@hasytec.com](mailto:j.kelling@hasytec.com)

**Matti Früchtenicht**, HASYTEC electronics, Kiel/Germany, [m.fruechtenicht@hasytec.com](mailto:m.fruechtenicht@hasytec.com)

## Abstract

*This paper describes further developments to make ultrasonic transducers more effective and efficient in biofilm prevention. Artificial Intelligence (AI) technology is used to match transducer parameter setting to biofilm prevention. Each transducer is AI-enabled to adapt its parameter settings (frequency and intensity level) to optimize effectiveness in biofilm protection.*

## 1. Introduction

IMO, [www.imo.org](http://www.imo.org), has the ambition to halve GHG emissions by 2050 and to completely decarbonize shipping “as soon as possible” within this century. The initial IMO Greenhouse Gas strategy will be revised this year (2023), including a revision of these goals, but the changes are unlikely to take the pressure off the shipping industry. Instead, IMO is likely to urge member states to accelerate their efforts to accelerate decarbonizing of shipping.

IMO is following a two-tier approach to implement decarbonization measures, focusing first on short-term energy efficiency improving measures, before embarking on more comprehensive medium-term and long-term measures that will include alternative low-carbon/no-carbon fuels, see for example *Bertram (2021)*, *Løvstad and Bertram (2022)*.

Current measures addressing GHG emissions include three mandatory requirements:

- The Energy Efficiency Design Index (EEDI) for newbuildings mandating successive improvement in design performance of 30% compared to the average of ships built 1999-2009.
- The Ship Energy Efficiency Management Plan (SEEMP) for all ships above 400 GT in operation, making a continuous energy efficiency improvement management plan mandatory, although not stating explicit requirements to content, scope and implementation.
- The Fuel Oil Consumption Data Collection System (DCS) mandating annual reporting of CO<sub>2</sub> emissions for all ships above 5000 GT.

At MEPC 76, in 2021, three additional measures were adopted, affecting all existing cargo and cruise ships after 2023:

- The Energy Efficiency Design Index for Existing Ships (EEXI), essentially making requirements equivalent to EEDI Phase 2 or 3 mandatory to all existing ships.
- A mandatory Carbon Intensity Indicator (CII) and rating scheme for all cargo and cruise ships above 5000 GT. Poor CII ratings will lead to mandatory requirements for corrective action plans to improve the CII. The criteria for CII ratings will get progressively stricter by 1% per year for 2020-2022, followed by 2% per year for 2023-2026.
- SEEMP requirements were made stricter (Enhanced SEEMP) to include mandatory content, such as an implementation plan on how to achieve the CII targets.

These new requirements for existing ships will increase the focus on energy efficiency measures both in design/retrofit and operation. For most ships, the CII will be more critical than the EEXI, as discussed by *Løvstad and Bertram (2022)* for bulk carriers.

For the operational measures affecting directly the CII, improved hull management is widely seen as one of the most important measures, with potential gains in the order of magnitude of 10%.

## 2. EU R&D Project CHEK

The R&D project CHEK (deCarbonising sHipping by Enabling Key technology symbiosis on real vessel concept designs), <https://www.projectchek.eu/>, has as a goal to reduce CO<sub>2</sub> emissions in global shipping. The focus is on the combined application of advanced key technologies in shipbuilding. The project is described in more detail in Appendix I.

The CHEK project proposes to reach zero-emission shipping by disrupting the way ships are designed and operated today. The project will illustrate concrete measures in the context of two bespoke vessel designs, Fig.1:

- Kamsarmax bulk carrier with significant contributions from a wind-assisted propulsion system (WASP)
- hydrogen powered cruise ship with focus on decarbonizing hotel load



Fig.1: Application cases: Bulk carrier and cruise ship, source: Wärtsilä

The investigated vessel designs are equipped with an interdisciplinary combination of innovative technologies working in symbiosis to:

- reduce greenhouse gas emissions by 99%
- achieve at least 50% energy savings
- reduce black carbon emissions by over 95%.

The innovative energy-saving technologies include the use of wind assisted propulsion systems, batteries, heat recovery, hydrogen as fuel, air lubrication, and intelligent ultrasonic anti-fouling.

Rather than “stacking” novel technologies onto existing vessel designs, the consortium is proposing to develop a unique Future-Proof Vessel (FPV) Design Platform to ensure maximised symbiosis between the novel technologies proposed and taking into consideration the vessels’ real operational profiles (rather than just sea-trial performance). The FPV Platform will also serve as a basis for replicating the CHEK approach towards other vessel types such as tankers, container ships, general cargo ships and ferries. These jointly cover over 93% of the global shipping tonnage and are responsible for 85% of global GHG emissions from shipping.

In order to achieve real-world impact and the decarbonisation of the global shipping fleet, the consortium is analysing framework conditions influencing long-distance shipping today (including infrastructure availability) and to ensure the proposed vessel designs can and will be deployed in reality. A Foresight Exercise will simulate the deployment of the CHEK innovations on the global shipping fleet with the aim of reaching the IMO's goal of halving shipping emissions by 2050 and contributing to turning Europe into the first carbon-neutral continent by 2050 (as stipulated by the European Green Deal).

The effectiveness and saving potential of the considered options depend on various factors, including ship types and associated typical operational patterns. Fig.2 gives the selected measures for the bulk carrier, Fig.3 for the cruise vessel within the CHEK project.

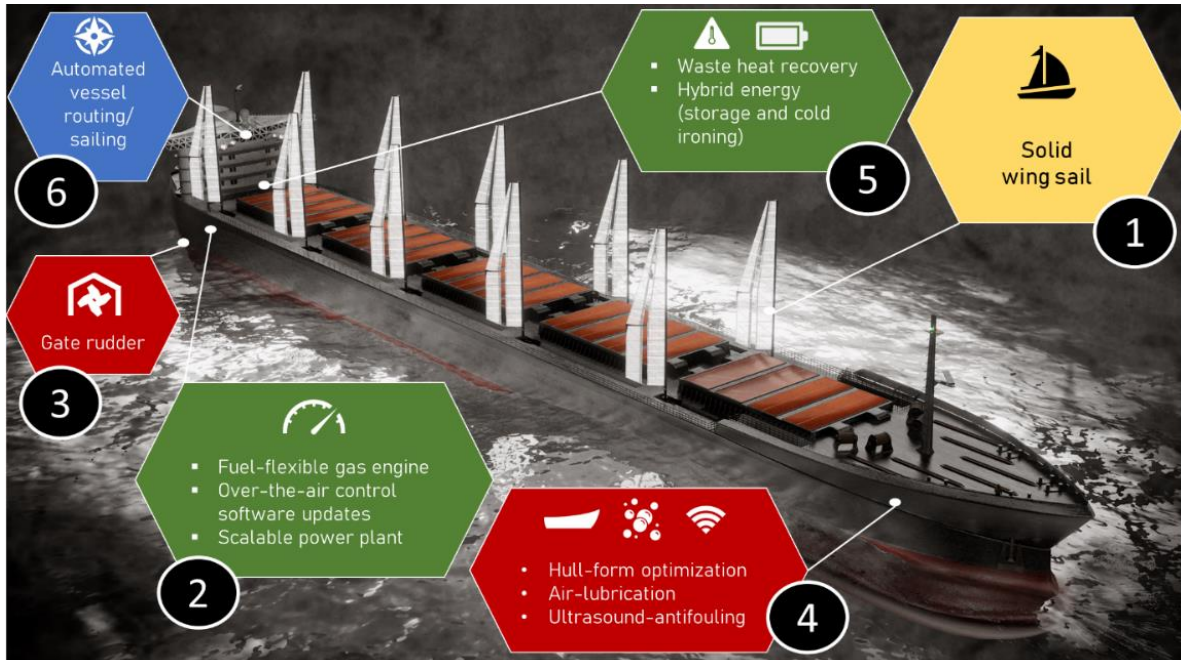


Fig.2: Emission saving technologies envisioned for bulk carrier

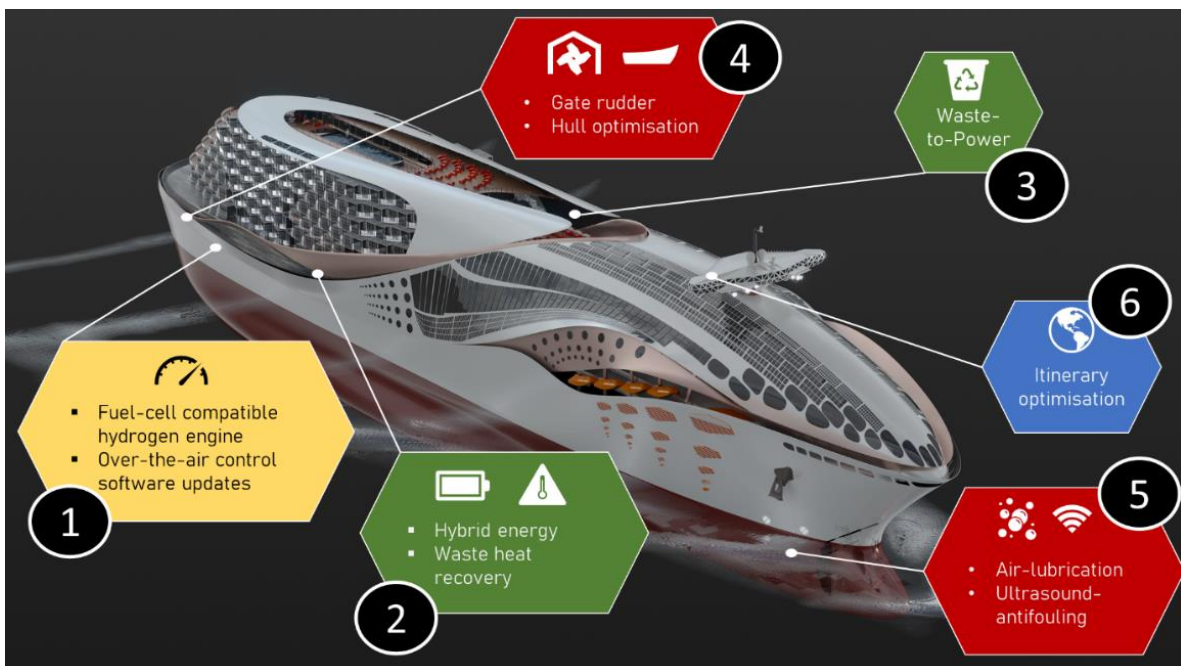


Fig.3: Emission saving technologies envisioned for cruise vessel

Figs.4 and 5 compare the expected CO<sub>2</sub> emissions to a baseline design, where the bars are normalized to 100% for the baseline design, for bulk carrier and cruise vessel, respectively. The selected measures lead to an expected decrease in CO<sub>2</sub> emissions of 40% for the bulk carrier and 50% for the cruise vessel. A significant contribution comes from drag reduction technology, including ultrasonic protection against biofouling. The approach will be elaborated in more detail in the following chapter.

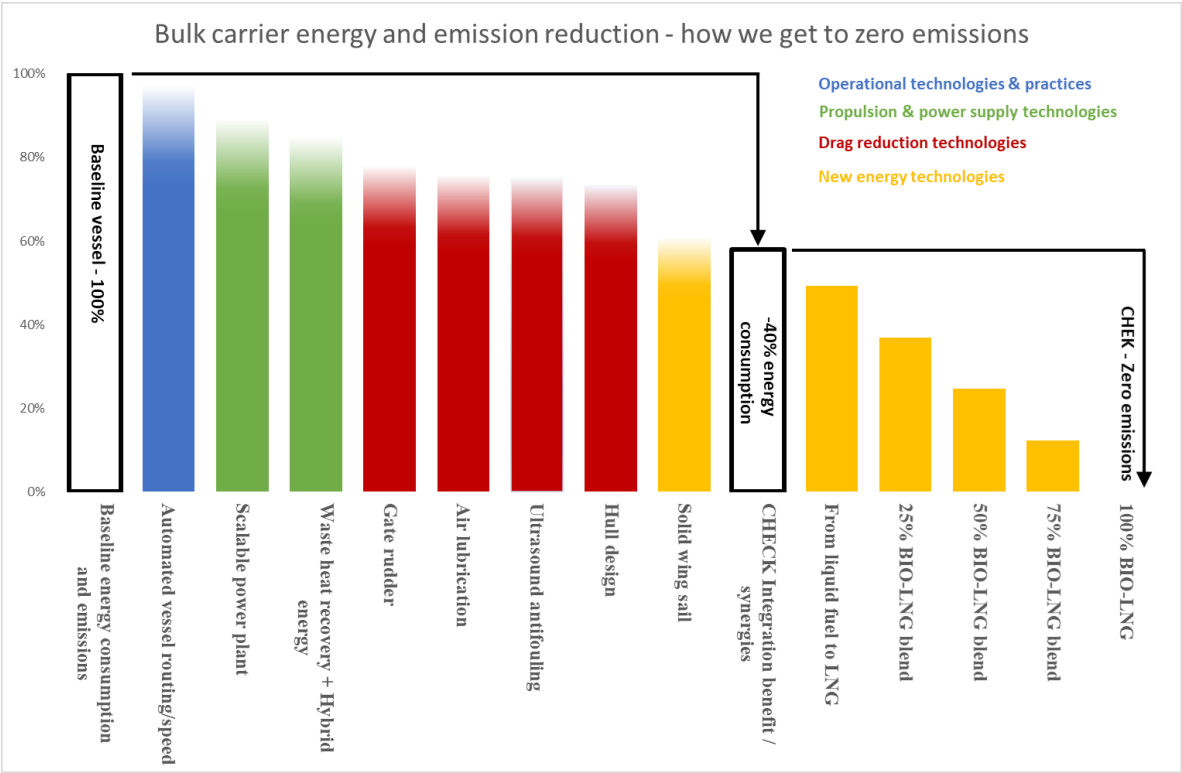


Fig.4: Expected emissions compared to baseline design for bulk carrier

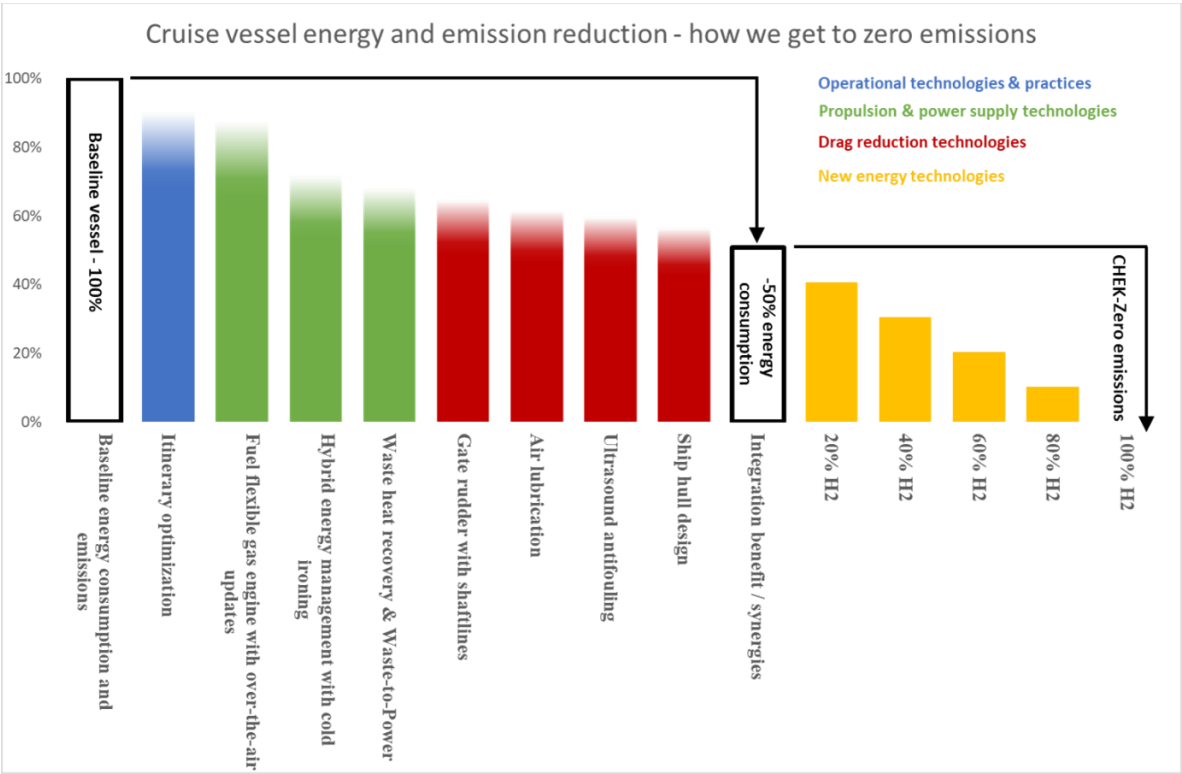


Fig.5: Expected emissions compared to baseline design for cruise vessel



### 3. Intelligent Dynamic Biofilm Protection in CHEK

In relation to the AFS (Anti-Fouling Systems) convention, *IMO (2001)*, the EU Regulation No. 528/2012 details restrictions on the marketing and use of biocide containing products. As an example, almost no copper-based active substances will get permission to be used in the future. This leaves essentially two options:

- taking the risk of using less effective antifouling systems with associated higher costs for maintenance and repair as well as higher fuel expenses
- looking for alternatives to replace the traditionally used antifouling systems

Ultrasonic systems are such an alternative and are increasingly adopted by various segments of shipping. Ideally, such ultrasonic systems inhibit the chain of fouling development at the beginning, namely the biofilm. Biofilm is formed when bacteria adhere to a solid surface, Fig.6. It is a prerequisite for later, more developed and harmful fouling stages, *Kelling (2017)*. Addressing biofouling already at the biofilm stage avoids numerous issues with macrofouling, such as the complete capture of removed fouling in cleaning operations to avoid the spread of Aquatic Invasive Species.

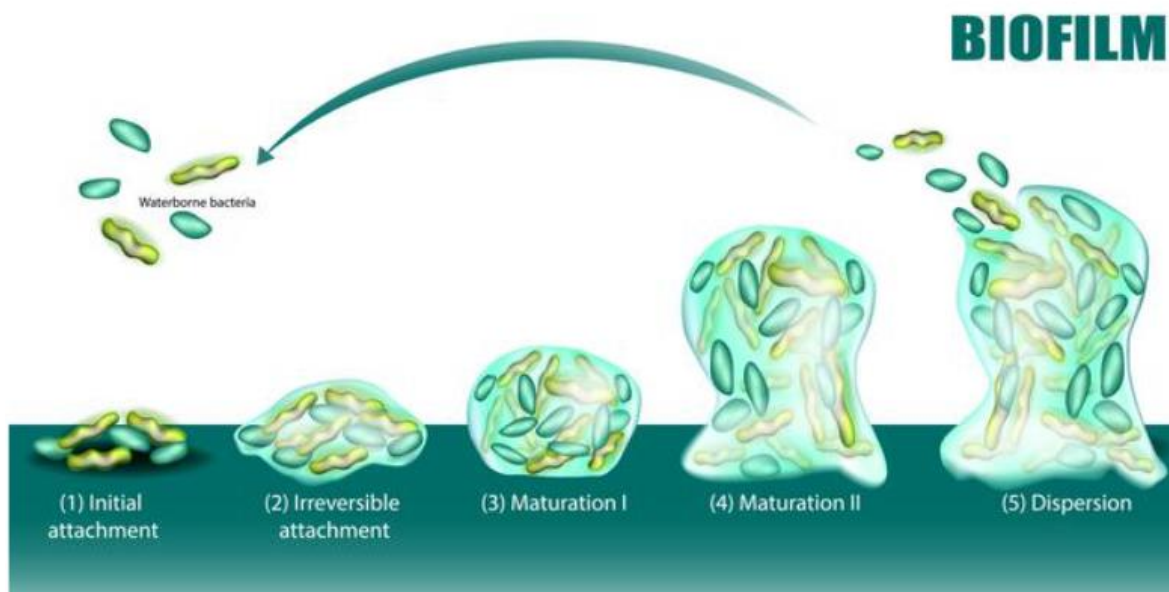


Fig.6: Biofilm formation

Older ultrasound methods followed the idea of getting rid of hard growth which had already attached. Using hard cavitation, this might work in certain situations but may also damage the vessel's steel or coating itself. Consequently, this approach was not accepted by the market. Low-powered ultrasound (avoiding cavitation) destroys the cell structures in biofilm and thus the prerequisite for higher stages of fouling, such as algae, barnacles, and shells.

Ultrasonic antifouling solutions are also 100% effective at zero speed, e.g. in longer stays in port or at mooring. Ultrasonic antifouling solutions have enjoyed exponentially growing market acceptance in shipping over the last decade. For details on the technology, see e.g. *Kelling (2017)*, *Kelling and Mayorga (2020)*.

So far, ultrasonic biofouling protection has been used predominantly for:

- niche areas (such as sea chests, bow thrusters, etc.)
- internal equipment (heat exchangers, pipes, etc.)
- propellers

The technology has also been successful applied to smaller vessels, such as yachts, tugs, and workboats, where access to the bottom is relatively easy and up to 30 transducers suffice to cover complete hull area immersed in water. Fig.7 shows exemplarily the effectiveness for a workboat, *Kelling (2017)*.



Fig.7: Tugboat without (top) and with (bottom) ultrasonic antifouling protection

Within the CHEK project, the full hull protection shall be scaled up to large commercial ships, both for hull and internal equipment. A key enabler in this context is increased effectiveness harnessing the power of Artificial Intelligence (AI).

Dynamic Biofilm Protection Intelligent® (DBPi) is the next generation of the award-winning Dynamic Biofilm Protection® of HASYTEC, *Kelling and Mayorga (2020)*. DBPi prevents marine growth, biofouling and biocorrosion on all liquid carrying surfaces even more efficiently, following the current and future demands of the shipping industry.



Fig.8: Transducers



Fig.9: Modular control unit

The underlying process is unique, and the first time AI has been applied to ultrasonic biofouling protection. Each single transducer, Fig.8, measures its own environment at the installation spot, considering all influencing ambient parameters, such as temperature, material and thickness of substrate material attached to, viscosity and temperature of water. Using Artificial Intelligence (namely a trained Artificial Neural Net), the optimum combination of frequency and intensity level is then set by the modular control unit, Fig.9. Each transducer adapts itself to the permanently changing conditions, based on the measured parameters.

The integrated USB port allows easy installation of software updates. In addition, all relevant data of the system can be analyzed, driving further development of the DBPi keeping pace with the latest state of the art during the lifetime of the ship. The new hardware design provides the opportunity to upgrade each system to up to 8 transducers, with a maximum cable length of 50 m to each system.

DBPi is the first ultrasonic antifouling technology with type approval by a classification society (Lloyd's Register).

#### **4. Outlook**

The CHEK project started in June 2021 and has a planned duration of 36 months. During this time, concept designs will be developed, and performance monitoring will validate expected energy savings of installed devices. The DBPi technology will be installed on various ships, the CHEK project ship type candidates and other customer projects ships. In parallel, work continues on the AI technology inside.

Project progress and insight gained, with particular focus on the ultrasonic antifouling technology, will be disseminated in suitable conferences like this one.

#### **Acknowledgements**

The CHEK project has received funding from the European Union's Horizon 2020 research and innovation program under grant agreement No 955286.

We are grateful to Volker Bertram for supplying text material on Artificial Intelligence techniques.

#### **References**

BERTRAM, V. (2021), *Fuel Options for Decarbonizing Shipping*, 13<sup>th</sup> HIPER Symp., Tullamore, pp.12-20, [http://data.hiper-conf.info/Hiper2021\\_Tullamore.pdf](http://data.hiper-conf.info/Hiper2021_Tullamore.pdf)

IMO (2001), *International Convention on the Control of Harmful Anti-Fouling Systems on Ships*, Int. Mar. Org., London

KELLING, J.; MAYORGA, X. (2020), *Dynamic Biofouling Protection*, 5<sup>th</sup> HullPIC Conf., Hamburg, pp.184-187, [http://data.hullpic.info/HullPIC2020\\_Hamburg.pdf](http://data.hullpic.info/HullPIC2020_Hamburg.pdf)

KELLING, J.; (2017), *Ultrasonic Technology for Biocide-Free Antifouling*, 11<sup>th</sup> HIPER Symp., Zevenwacht, pp.70-76, [http://data.hiper-conf.info/Hiper2017\\_Zevenwacht.pdf](http://data.hiper-conf.info/Hiper2017_Zevenwacht.pdf)

LØVSTAD, M.; BERTRAM, V. (2022), *The Decarbonizing Quest for Future Bulk Carriers*, 14<sup>th</sup> HIPER Symp., Cortona, pp.6-19, [http://data.hiper-conf.info/Hiper2022\\_Cortona.pdf](http://data.hiper-conf.info/Hiper2022_Cortona.pdf)

SILBERSCHMIDT, N.; TASKER, D.; PAPPAS, T.; JOHANNESSON, J. (2016), *Silverstream® System – Air Lubrication Performance Verification and Design Development*, 10<sup>th</sup> HIPER Symp., Cortona, pp.236-246, [http://data.hiper-conf.info/Hiper2016\\_Cortona.pdf](http://data.hiper-conf.info/Hiper2016_Cortona.pdf)

## Appendix I: CHEK project

The CHEK project is supported by the European Union with a total of 10 million Euro from the Horizon 2020 funding program, <https://ec.europa.eu/programmes/horizon2020/en/home>. The Horizon 2020 program is the biggest EU research & innovation program ever, with nearly € 80 billion of funding over 7 years. Its aim is combining European research and innovation to achieve excellent science, industrial leadership and tackling societal challenges. The CHEK project partners are:

- University of Vaasa (UV), <http://www.uwasa.fi/>, is a business-oriented, multidisciplinary, and international university.
- Wärtsilä, [www.wartsila.com](http://www.wartsila.com), is a provider of ship machinery, propulsion and manoeuvring solutions, supplying engines and generating sets, reduction gears, propulsion equipment, control systems, and sealing solutions for all types of vessels and offshore applications.
- Cargill Ocean Transportation, <https://www.cargill.com/transportation/cargill-ocean-transportation>, is a freight-trading business that provides bulk shipping services to customers across the globe.
- MSC Cruises, [www.msccruises.com](http://www.msccruises.com), is a global cruise line, which is part of the Cruises Division of MSC Group, the privately held Swiss-based shipping and logistics conglomerate.
- Lloyd's Register EMEA (LR), [www.lr.org](http://www.lr.org), is part of the Lloyd's Register Group, a global independent risk management and safety assurance organisation that works to enhance safety and improve the performance of assets and systems at sea, on land and in the air.
- World Maritime University (WMU), [www.wmu.se](http://www.wmu.se), was established in 1983 by the International Maritime Organization (IMO).
- Silverstream Technologies, <https://www.silverstream-tech.com/>, was established in 2010 and the company specialises in Air Lubrication Technology, Silberschmidt et al. (2016), which is designed to reduce the frictional impact between the flat bottom of the ship hull and water.
- HASYTEC Electronics GmbH, <https://www.hasytec.de/>, is market leader in ultrasound based antifouling technology.
- Deltamarin, <https://deltamarin.com/>, is a ship engineering and design company.
- Climeon AB, <https://climeon.com/>, has well proven technology to convert waste heat to clean power.
- BAR Technologies, <https://www.bartechnologies.uk/>, have used its in-house tool ShipSEAT to design and optimise their own patented and trademarked wind propulsion system called WindWings, <https://www.bartechnologies.uk/project/windwings/>.

The project aims to combine a variety of innovative technologies to achieve its goals of significant increase (>50%) of energy efficiency and virtual elimination (>99%) of greenhouse gases, Fig. I.1:

- New energy technologies
  - Fixed wing sails
  - Fuel-cell ready hydrogen engine
- Operational technologies and practices
  - Automated vessel routing/sailing
  - Cruise vessel itinerary optimization
- Propulsion/Power supply technologies
  - Fuel-flexible gas engine incl. over-the-air software updates
  - Scalable power plant
  - Hybrid energy management
  - Waste heat recovery
  - Waste-to-power
- Drag reduction technologies
  - Gate rudder
  - Air lubrication
  - Ultrasound antifouling
  - Ship hull optimization



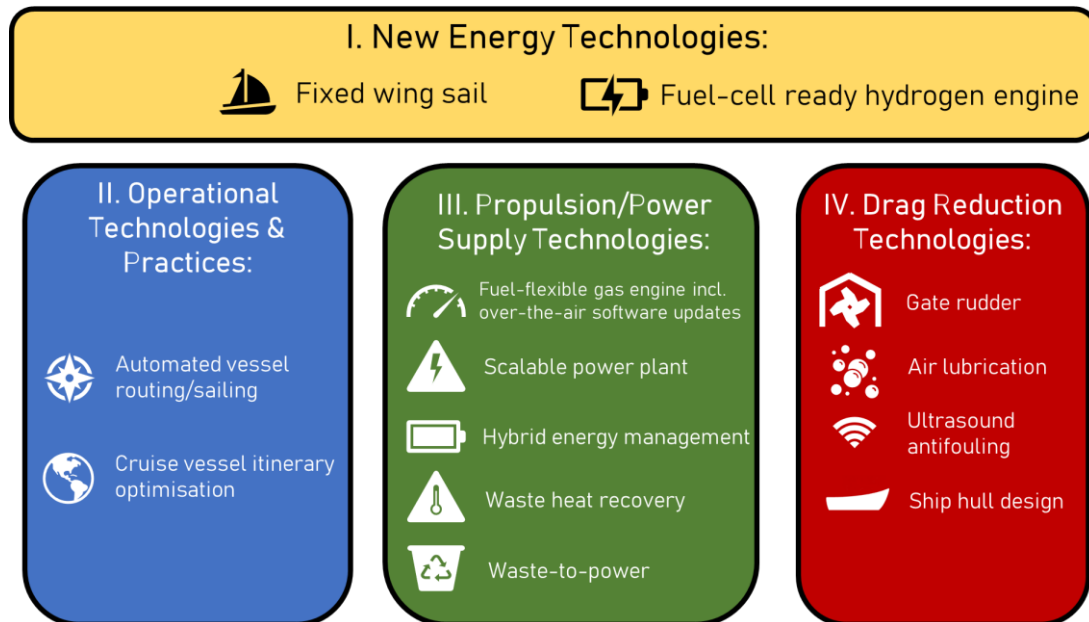


Fig.I.1: Technological synergy for emission savings

# Hic Rhodus, Hic Salta: ChatGPT and other A.I. Tools for Maritime Applications

**Henrique Gaspar**, NTNU, Alesund/Norway, [henrique.gaspar@ntnu.no](mailto:henrique.gaspar@ntnu.no)

**Volker Bertram**, DNV, Hamburg/Germany, [volker.bertram@dnv.com](mailto:volker.bertram@dnv.com)

**Tracy Plowman**, DNV, Hamburg/Germany, [Tracy.plowman@dnv.com](mailto:Tracy.plowman@dnv.com)

## Abstract

*ChatGPT and other artificial intelligence (AI) tools are subject to controversial and very active debate. Both opponents and aficionados of AI technology assign extraordinary power to the tools, both in language processing (writing), symbolic processing (coding), and graphics processing (creation of images or visual presentations). We investigated here ChatGPT, Dall-E 2, Docebo Shape, and Piggy for maritime applications, where we deem the test cases simple to moderately difficult. Contrary to common perception and our own expectations, we found the tools' performance soberingly poor. ChatGPT gave convincingly sounding, but wrong answers, and was generally not concise, requiring significant human postprocessing to give useful texts. Dall-E 2 gave drawings worthy of a child. Docebo Shape's PowerPoint suggestions were nonsense. In summary, it feels and behaves as pseudoscience.*

## 1. Introduction

Artificial Intelligence or “AI” is a term often used, yet little understood. The technology is both overestimated and underused. The blind faith in AI is reminiscent of the 1970s' misconception of computers and software: the computer says so and therefore it must be true.

There is no coherent definition of what “Artificial Intelligence” is, [https://en.wikipedia.org/wiki/Artificial\\_intelligence](https://en.wikipedia.org/wiki/Artificial_intelligence). In its broadest sense, AI is concerned with the investigation and simulation of human intelligence with the ambition to replicate the processes in machines. A not exhaustive list of sub-branches of AI encompasses:

- machine learning
- knowledge-based systems
- machine vision
- natural language processing / gesture processing
- ...

Machine learning is the most prominent AI application, and frequently “using AI” means “using machine learning” these days. For better context and understanding, it is useful to recall that “machine learning” builds models and produces results based on empirical knowledge, and if underlying data bases are sparse or biased, or if the software attempts extrapolation beyond the scope of the data base, errors occur. *Bertram (2018)* reviewed AI applications in the maritime context with focus on the first three items in above list, concluding that AI techniques can be put to good use for maritime applications, but cautioning against just using new tools without understanding their fundamental working principles and resulting limitations. In similar vein, *Colle and Morobé (2022)* warn against an ignorant use of machine learning, in the context of ship performance monitoring.

We will focus here on the fourth item of above list, namely natural language processing, and discuss in passing also more symbolic processing, e.g., for images, applied to maritime topics with a focus on graduate training and naval architecture. The reasons for this narrow focus are our own interests and expertise, as well as an awareness that many AI tools are challenged when applied to highly specialized domains where there are fewer textbooks and openly available documentation. Besides the by now widely known ChatGPT, we also tested Dall-E 2 (for graphics), Docebo Shape (for presentations), and Piggy (for short text trainings and quizzes).

## 2. ChatGPT for maritime applications

### 2.1. Introduction to ChatGPT

ChatGPT (Chat Generative Pre-trained Transformer), <https://en.wikipedia.org/wiki/ChatGPT>, is an AI-based chatbot, that has caused furore since its launch in November 2022, and concern, particularly in academic and educational circles. We tested only ChatGPT, and not its more recent competitor Google Bard, <https://en.wikipedia.org/wiki/LaMDA#Bard>, or Bing Chat (aka Bing AI), [https://en.wikipedia.org/wiki/Microsoft\\_Bing](https://en.wikipedia.org/wiki/Microsoft_Bing), but suspect that limitations are similar, as basic approaches are similar.

But maybe it is best to let ChatGPT introduce itself (based on a ChatGPT sessions in February and August 2023):

Question: “What is ChatGPT?”

Answer: “ChatGPT is an advanced language model created by OpenAI, specifically based on the GPT-3.5 architecture. It enables natural and contextually relevant text generation, allowing it to engage in human-like conversations, answer questions, offer explanations, and perform a variety of language-related tasks, making it a versatile tool for applications ranging from customer support to content creation and beyond.”

ChatGPT is not Google, and it is based on AI, i.e., on experience, trained on vast amounts of text files taken from the internet, but not using real-time access to internet sites. ChatGPT was ignorant about itself one month after the launch. But chat with follow-up questions and ChatGPT will generally improve its response:

Question: “Who are you?”

Answer: “I am an AI language model developed by OpenAI. I was trained on a large corpus of text data and designed to respond to user inputs in a conversational manner. My primary purpose is to assist users in generating human-like text based on the prompts given to me, and to answer questions to the best of my abilities.”

Apart from the repetition, the answer is a good explanation of what ChatGPT is and can do. It also hints at its limitations. ChatGPT is intended to create texts, where it draws on its training, but cannot specifically search ad hoc outside its inherent knowledge base.

### 2.2. Concerns in Academia

ChatGPT’s ability to create human-like texts has raised concerns within the educational community. Within seconds, ChatGPT can create some text to a given assignment, and with several follow-up questions, the text can be modified and made unique, passing state-of-the-art plagiarism tests. Some universities in many countries, including France, Japan, China, Sweden, and the UK have banned the use of chatbots like ChatGPT to write assignments such as essay, reports, and theses. Other universities condone the use of ChatGPT and do not see its use as academic misconduct. The different attitudes may be rooted in different academic cultures. E.g., the University of Glasgow is exploring the use of ChatGPT as a learning tool for its students.

Using ChatGPT for academic writing is of particular concern in the so-called “soft sciences”, [https://en.wikipedia.org/wiki/Hard\\_and\\_soft\\_science](https://en.wikipedia.org/wiki/Hard_and_soft_science), where texts play a big role in examinations (“write an essay of 2000 words on the concept of ...”) and academic achievement is based on producing texts. Incidentally, these are also academic curricula where plagiarism and ghost-writing have been traditional issues of strong concern. In engineering, the concerns are not (yet) as pressing, as mathematical derivations and simulation software coding and application are seen as the predominant intellectual achievements.

The use of software as such in academic tasks is by now widely accepted, and even expected:

- Literature research via search machines and academic databases (Google, ResearchGate, etc.), [https://en.wikipedia.org/wiki/List\\_of\\_academic\\_databases\\_and\\_search\\_engines](https://en.wikipedia.org/wiki/List_of_academic_databases_and_search_engines)
- Checking grammar and spelling in writing texts, e.g. in Word or TeXidote for LaTeX documents
- Referencing via databases
- Translating texts from one language to another (typically between native language and English), e.g. by [www.deepl.com](http://www.deepl.com) or [www.reverso.com](http://www.reverso.com).
- Layout with desktop publishing software (with embedded intelligence on making suggestions for suitable layout), with automatic management of tables of content, tables of figures, etc.
- Statistical analyses and charts generated by spreadsheet tools such as Excel.

ChatGPT is the new kid on the block – and we have yet to decide whether it is just another tool to support research and publishing, or whether it is disrupting our examination and grading traditions, possibly even threatening jobs. To get some decision support, we decided to put ChatGPT to the test with some application cases coming from marine engineering.

### 2.3. Application tests for ChatGPT

ChatGPT is in the news, even the mainstream media and national television news. It is described as “revolutionizing the internet”: “The tool responds to your queries in chat format and can answer simple questions as well as write complex texts such as papers and essays” [translated from German]. ChatGPT is “capable of understanding questions and answering them in natural language with unprecedented quality”. These are just some ad hoc quotes from the first two pages of 766,000,000 on Google [10.6.2023].

We decided in early 2023 to explore how ChatGPT would perform in our domain, namely naval architecture. Near-mythical achievements in other fields were difficult to judge. “Hic Rhodus, hic salta!”, [https://en.wikipedia.org/wiki/Hic\\_Rhodus,\\_hic\\_salta](https://en.wikipedia.org/wiki/Hic_Rhodus,_hic_salta). And maybe ChatGPT would save us a lot of time in our own work, e.g. in writing conference papers like this one. We approached the “stress test” for ChatGPT as we might have done with a student in an oral exam, asking successively more detailed questions. We would then see how far we would get before ChatGPT reached its limits.

#### 2.3.1. Explain how to compute initial ship stability (GM)

The first question concerns the basics of ship stability, a question any naval architect at bachelor level or ship master should be able to answer without hesitation:

Question: “[Please] explain the stability of a boat:  $GM = KB + BM - KG$ ”

Answer [omitting repetitions]: “The equation states that the metacentric height of a boat (GM) is equal to the distance between the center of buoyancy and the center of gravity (KB), plus the beam of the boat (BM), minus the distance between the keel and the center of gravity (KG). This equation helps calculate the stability of a boat, and a higher metacentric height generally indicates a more stable boat.”

We underlined the key error in the answer. Were you an amateur boat builder and to follow above computation of initial stability, it might have catastrophic consequences. Your boat may capsize after launching. Similarly, if you were a student of naval architecture and gave this response in an exam, you would fail the exam. ChatGPT was off to a bad start, as we thought this was the easiest of our questions.

#### 2.3.2. Explain added mass in heave motion

Our next question would be typical in an exam for a graduate student in naval architecture, on a fundamental concept in potential flow theory for ship seakeeping, *Bertram (2000)*.



Question: “What is added mass, in hydrodynamics?”

Answer [omitting repetitions]: “In hydrodynamics, added mass is the inertia a body gains when it is submerged in a fluid. It is a property of the fluid that causes an increase in the effective mass of a submerged object, which can affect the motion and stability of the object. The added mass coefficient is a dimensionless number that describes the added mass relative to the mass of the object itself. It is typically determined experimentally, and can vary depending on the shape and size of the object and the properties of the fluid.”

The answer is typical for ChatGPT in our experience. It consists of several lines, using suitable jargon, and no errors in grammar or spelling. Only an expert in the field would pick out the shortcomings. Added mass is typically determined in potential-flow computations (and for some simple geometries analytically). As an examiner, we would drill deeper with follow-up questions, since the answer omits the important dependency on motion frequency in seakeeping applications. We may also ask what “properties of the fluid” affected added mass. But this answer was fairly good, and in an exam the student would have now given a positive impression. Next we would increase the level of detail, asking for some details omitted in the initial response and see how good the coding skills of the graduate student are.

### 2.3.3. Write a code to compute heave motion

We omit here an intermediate question explaining heave motion of a barge (= simple hexahedron) described previously in *Gaspar and Bertram (2023)*. The answer was of similar quality as for added mass, a bit wordy, not quite right (e.g. describing ships being equipped with bilge keels to dampen heave motion while bilge keels have only small damping effect on heave), but fairly good. We moved on to:

Question: “How to code heave for a rectangular barge of  $L = 100$ ,  $B = 20$ ,  $D = 10$ , in water?”

Answer: [see Appendix 1 for detailed long answer with Python source code]

At first glance, the answer might impress. ChatGPT answered in correct jargon, grammar and spelling, and there were no formal mistakes in the Python code. ChatGPT is indeed fluent in several languages, including English and Python.

Closer inspection by an expert reveals some shortcomings, though:

1. ChatGPT sets added mass proportional to velocity  $v$ . In heave motion, damping would be proportional to  $v$ , added mass proportional to acceleration. This is a serious error. It indicates a lack of understanding of the added mass concept, and our initially more positive impression worsens.
2. ChatGPT uses a constant added mass of 50% of half the physical mass. In reality, added mass is frequency dependent. ChatGPT does point out that the “the hydrodynamic forces acting on the barge can be more complex depending on the velocity, the frequency of the waves”.

### 2.3.4. Conclusion on ChatGPT’s responses – AI as Pseudoscience

ChatGPT disappointed us. As an advisor or source of information, ChatGPT is very dangerous, as most users would not see through the façade of jargon and code, and just take the advice and move on based on false information.

As ghost-writer for exam papers, ChatGPT is not concise enough, and requires too much editing. The quality of the writing is shallow and repetitive. Students may get a passing grade, but not a good grade. If you want to cheat the system, it is probably more efficient to just copy and paste from sources in the web and rephrase. For us, writing a paper directly ourselves with occasional resorting to other tools like Google, Wikipedia, or DeepL leads to better results. As a writing aid, ChatGPT did not write usable text and did not create usable lists of references. The texts produced needed so much reworking that

any time savings as compared to writing yourself disappeared. ChatGPT proved to be of some use only when asked to simplify or shorten existing texts and proposing structures for a book. (See *Gaspar and Bertram (2023)* for a discussion on DeepL and ChatGPT as writing aids.)

In conclusion, analysing the results from the chat in the topic of maritime technology feels similar as listening to a charlatan trying to convince their audience on buying the elixir of life, a seller pushing you a software that will solve all your problems at the design office / engineering / yard / operations; or in smaller scale, as student that just decorated the textbook without assimilating it, and repeat sentences based on matching words, and gets caught when we clarify that B from BM is not the breadth of the vessel.

The “science” is not there, just speculation and repetition. Pseudoscience. It cleverly mimics the appearance of science, the appearance of intelligent, without being so. As correctly pointed out by Chomsky *et al.* (2023), (true) intelligence should investigate cause and consequence rather than just speculate and *is demonstrated in the ability to think and express improbable but insightful things*.

Our findings were confirmed by a blog from the tool’s vendor, <https://openai.com/blog/chatgpt>, on key limitations of ChatGPT:

- “ChatGPT sometimes writes plausible-sounding but incorrect or nonsensical answers. [...]”
- The model is often excessively verbose and overuses certain phrases [...].”

Adding the pseudoscience argument (<https://en.wikipedia.org/wiki/Pseudoscience>), we found that it:

- Produces contradictory, exaggerated or unfalsifiable claims
- High reliance on confirmation bias
- Lack of openness on the source of information
- Absence of systematic practices when developing hypotheses

### 3. Dall-E 2 for maritime applications

While ChatGPT deals with text, another AI application from the same company OpenAI, Dall-E 2, claims to be capable of returning images, not just alphanumeric information (prose texts, poetry, programming code, formulas, etc.). For example, <https://www.dallewizard.com/prompts/van-gogh> advertises an application, where you can prompt the tool to paint a specified object in the style of Vincent Van Gogh, Fig.1.



Fig.1: Dall-E 2 response to prompts for Van Gogh style fisherman (left) and avocado toast (right)

### 3.1. Stability curve (GZ curve)

As with ChatGPT, we started with a simple test case from ship stability, namely drawing a ship stability curve (aka GZ curve), as explained e.g. in <https://www.marineinsight.com/naval-architecture/ship-stability-understanding-curves-static-stability/>. The tool responded very quickly with a perfect sin curve, plotted over  $x$  rather than heel angle, Fig.2 (left).

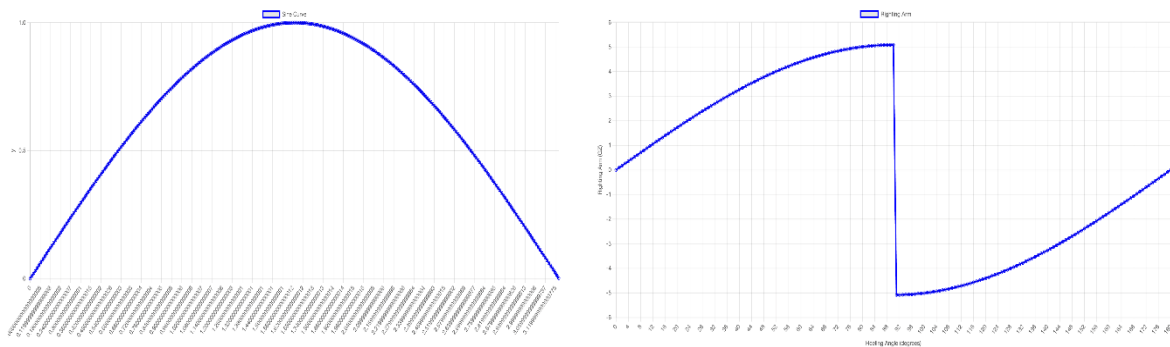


Fig.2: Initial response for GZ-curve (left) and correction after chat (right)

After 20 minutes of chat, trying to prompt Dall-E 2 into plotting a simple GZ curve, it still did not reach an acceptable result. Results were variation of the sin curve or broken graphs with labeling that looked like letters having been hacked up. Fig.2 (right) show an example after pointing out in the chat that the barge would capsize at  $90^\circ$ .

### 3.2. General arrangement plan (GAP) for a frigate

The next test case was more challenging: “Can you make a general arrangement drawing of a frigate ship” resulted in the drawing shown in Fig.3. The interpretation is subject to attitude and expectation to AI. Were Dall-E 2 our child, say 8 years old, we would probably be proud and point out correct details such as superstructures, gun turrets, and helideck. As it is not our child, we notice wrong ratio of length-to-draft, no sonar dome or bulbous bow, no propeller, no internal compartmentation, and wrong arrangement of some of the equipment. The image would probably not even pass as a first sketch for a conceptual design, leave alone a general arrangement plan.

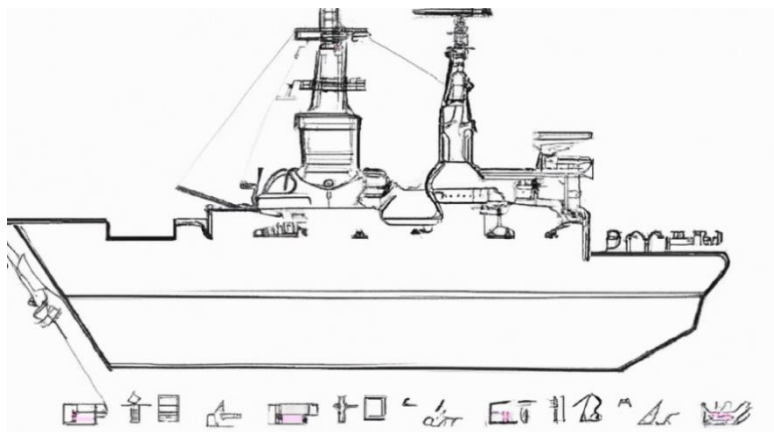


Fig.3: Dall-E 2 response to the request of a general arrangement plan for a frigate

### 3.3. Conclusion for Dall-E 2

Dall-E 2 raised high hopes looking at the Van Gogh paintings. For technical drawings in naval architecture, it failed. Both for the simple static stability curve and the challenging general arrangement plan, Dall-E 2 failed to convince even after investing significant time in chatting further.

## 4. Docebo Shape for presentations

Developing presentations (such as for a conference) and trainings based on presentations or e-learning frameworks generally takes a lot more time than outsiders suspect, *Bertram and Plowman (2019)*. And time is money, especially in industry, where hourly rates for skilled staff are typically 150-250 €/h. Against this backdrop, DNV management stumbled across an advertisement: “Get AI-based learning content in minutes - Content can make or break your learning programs. Let Shape’s AI do the heavy lifting.”, <https://www.docebo.com/products/shape/>.

### 4.1. “Train the Trainer” test case

As many of DNV’s training topics are highly specialized, we decided on a rather simple test case beyond the narrow domain of ship technology, namely DNV’s “Train the Trainer” course aimed at giving an initial training for ship technology experts with no previous pedagogical experience. We had course material based on PowerPoint, but we were curious what AI would make of it. Maybe we would see new ideas that our human development experts had not thought of. The start was easy. After trial registration, the upload of the original file was fast, and within a minute, as promised, we had the suggested online content for a training. But the result was largely useless, sometimes amusingly so, as the AI software just picked up keywords and assigned images that matched the keywords, but out of context: In introducing the trainers for the course, which hold post-graduate degrees in pedagogy, an image for a fitness trainer was selected, Fig.3 (left). Or for training workshops, an industrial workshop with a worker welding was chosen as visual aid, Fig.3 (centre). The verb “train” was visualized with an image of a train.

Text was chopped into fragments and reassembled, adding apparently random text snippets to form new sentences, which were often nonsensical, Fig.3 (right). For example, “Bernhard Löbermann has a master [degree] in teaching. He has developed trainings in maritime applications for specific purposes.” was converted into “Bernhil Loesbermann has a Masters in Teaching for Specific Purposes”. (Typos were introduced by Docebo Shape.)



Fig.3: Images are selected based on keywords without context resulting in “nonsense”

### 4.2. Conclusion for Docebo Shape

For the specific application we tested, the AI-based software created useless and often nonsensical material. We looked at other AI tools to create trainings and presentation “within minutes” and they fell similarly short of the marketing promises, *Gaspar and Bertram (2023)*.

## 5. Piggy for online teaching with text and quizzes

Piggy is a “visual, creative, and interactive mobile documents creator”, <https://piggy.to/>. Its website states that it is intended to “create social stories, presentations, and quizzes”, designed for use on mobile phones. We decided to test it similarly as ChatGPT on themes of naval architecture.

### 5.1. Story and quiz on “ship stability”

Just entering “ship stability” and a “story” button, Piggy created 8 pages of similarly sized chunks of text on ship stability, in correct grammar and spelling, with concise text and suitable image material.



The suggested text covers key aspects of ship stability, including metacentric height GM, free surfaces, dynamic stability, trim, [dynamic] stability correcting measures such as anti-roll tanks. It fared better than ChatGPT or Docebo Shape in that respect, but the content contained several grave errors, including wrong explanations of metacentric height and free-surface effects, Fig.4 (from left to right):

- The starting page is OK, the extended title is suitably chosen.
- “A ship’s stability is maintained when the centre of buoyancy [...] coincides with the centre of gravity [...]”. The stable floatation condition is such that centre of buoyancy and centre of gravity are vertically aligned, i.e. have the same x and y coordinates, but generally not the same z coordinate.
- Free-surface effects do not refer to liquids (dynamically) entering or leaving tanks. They describe the reduced stability as liquids in partially filled tanks (statically) shift to the side of ship heel.
- The text on the effect of loading conditions on ship stability is correct and acceptable for a very brief, very high-level 8-page text on ship stability.

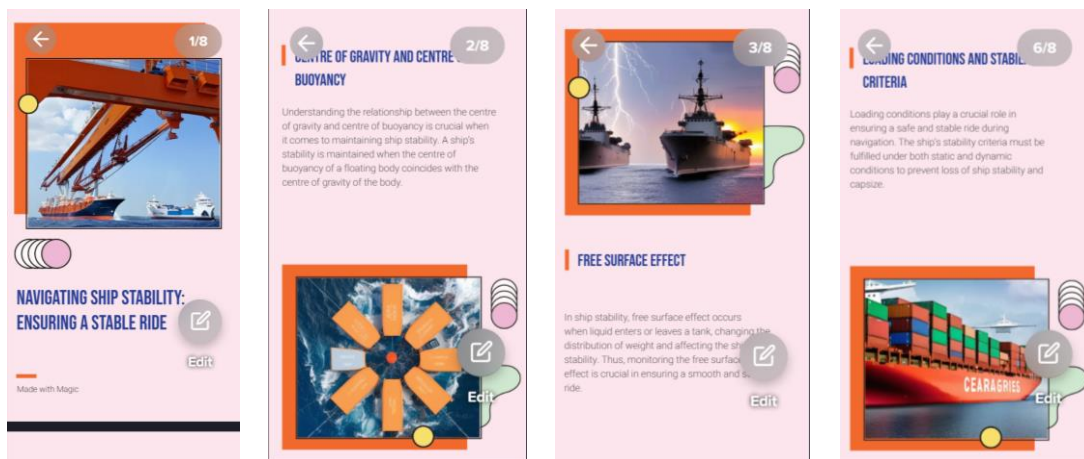


Fig.4: Sample pages for ship stability story from Piggy

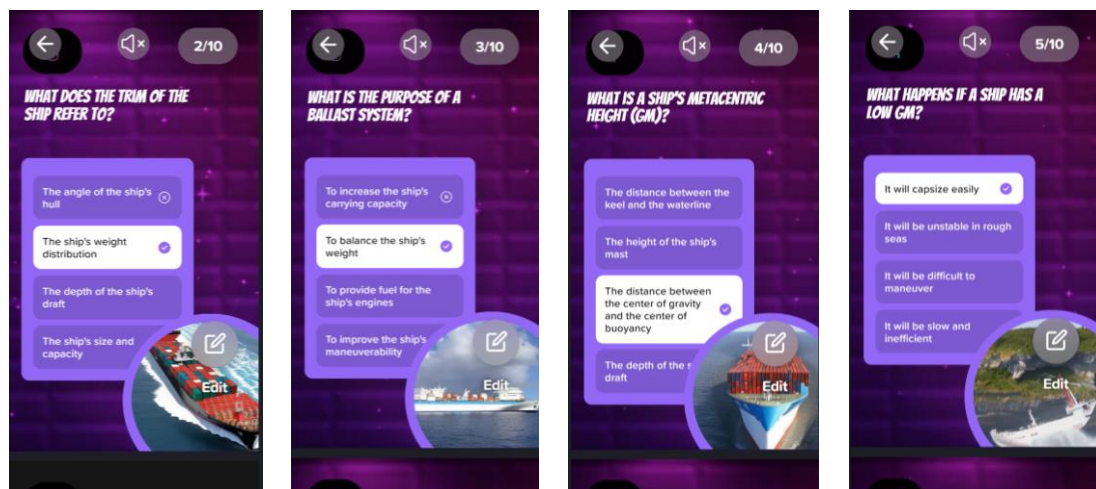


Fig.5: Sample pages for ship stability quiz from Piggy

We then asked Piggy to create a quiz on “ship stability”. Some of the quiz questions were OK, some wrong or nonsense, Fig.5 (from left to right):

- The trim refers rather to an angle of the hull (first choice) than the ship’s weight distribution (second choice, given as the correct answer).
- The purpose of ballast tanks is certainly not to balance the ship’s weight.

- The effect of low GM is given correctly as ship “will capsize easily”, but “ship gets unstable in rough sea” is arguably also possible, and ship will be difficult to manoeuvre or be slow and inefficient can be easily ruled out in a quiz on stability.
- The metacentric height GM is not the distance between centre of buoyancy and centre of gravity.

## 5.2. Story and quiz on “GZ curve”

The response to story and quiz on “GZ curve” as input was worse, as expected. Piggy realized that the topic refers to ship stability, the text was again structured into similarly sized text bites. Story and quiz were correct in grammar and spelling, but on the subject matter the text contained assorted errors, e.g. stating that the GZ curve depends on the waterline length.

## 5.3. Story and quiz on “added mass in ship hydrodynamics”

The response was significantly better than for ChatGPT, but contained a serious error saying that added mass was related to velocity rather than acceleration. Not surprisingly, Piggy didn’t find suitable image material for such a specialized topic.

## 5.4. Conclusion on Piggy

The texts created by Piggy were concise, well structured, and formally correct, but contained serious errors in definitions and descriptions. With increasing level of specialization, the results deteriorated. Piggy may be a good tool for party games or ice breakers in training, but otherwise failed to convince.

## 6. Different perceptions in the community

We started our analysis without preconceived notions of what the results would be. Our investigation was not about bad-mouthing a product or a technology, nor singing marketing praises. Ideally, we would have discovered in the process a tool that would make our work easier, getting better papers or presentations in shorter time.

When we first shared our findings in May 2023, *Gaspar and Bertram (2023)*, we were surprised by the ensuing passionate discussion. The continuing discussion prompted us to review our initial assessment, run further test cases, and look at the experience of colleagues challenging our testing approach or our conclusions. In some cases, this resulted in rephrasing our testing objective, our findings in the individual test cases, and our conclusions in hopefully clearer language.

Asking other colleagues for input on ChatGPT, impressions varied, depending on how specialized the topic was. A professor teaching introduction to mechatronics at NTNU was worried, as the tool could pass his exams effortlessly, including preparing the Arduino code that he requests from his students. Similarly worried was the colleague teaching basics of Python and data-handling. A colleague from hydrodynamics, on the other hand, shared our impression that ChatGPT did not “understand” (or better express) more specific concepts. To clarify this, we asked ChatGPT:

Question: Why do you understand some concepts well, such as data handling, but are poor in specific concepts, such as ship design and stability?

Answer: One of the reasons that OpenAI's understanding of specific concepts may vary is due to the size of the sample used to train the AI. OpenAI's models are trained on a massive amount of text data from the internet, and the quality and relevance of the information included in the training data can have a big impact on the model's ability to understand and generate text about a specific topic. In the case of ship design, it's possible that there was less relevant and high-quality text data included in the training data compared to other topics, such as data handling. As a result, the model may have a weaker understanding of ship design compared to data handling. It's also worth noting that the OpenAI models have a very large capacity, meaning they can learn a wide variety of

information, but the accuracy of their outputs can still be influenced by the quality and relevance of the training data they were exposed to.

In the following, we answer to some recurrent arguments in our discussion with colleagues:

- “The prompting questions were misleading.”  
Wrong. Our questions were neither leading nor misleading, but short and clear. What is misleading or unclear about “explain the stability of a boat:  $GM = KB + BM - KG$ ”?
- “With the right prompting, ChatGPT would give the right answer.”  
Partly true. ChatGPT tends to agree with the prompting. Sometimes ChatGPT can be nudged to give the correct answer in a chat. However, if one already knows the correct answer, what is the point in prompting it long enough until it gives the right answer? It should never give wrong answers as in our test cases. Unfortunately, most Artificial Intelligence tools are not intelligent enough to know their limits and respond with an intelligent answer like “I don’t know.” With Dall-E 2, we ran out of patience as 20 minutes of chatting did not move the tool into producing an acceptable response.
- “ChatGPT is not meant for your applications. It works very well for my knowledge domain (e.g. mechanical engineering) or my application (e.g. setting formulas in LaTeX or programming an application programming interface (API))”  
Partly true. We only investigated maritime applications. The specialized nature of naval architecture with fewer online texts to train on explains to some extent the relatively poor performance for our test cases. For an application like data driven design, which is used extensively in other engineering domains, ChatGPT performed better, *Gaspar and Bertram (2023)*. ChatGPT speaks many languages, including human languages like German, Portuguese, and programming languages Python and LaTeX, without making formal mistakes. We never contested that.
- “ChatGPT is still learning, getting ever more powerful and knowledgeable.”  
True. We only investigated and concluded on the current capabilities of ChatGPT. Note, however, that suitable texts on initial stability and GZ curves were available online at the time ChatGPT was initially trained. Maybe, in the future, there will be customized bots trained on our domain or even the complete IP (intellectual property) of a company like DNV, to create useful, rather standard texts within that domain or company. But such speculation brings us to another déjà vu of the 1970s: The next release will fix all bugs and be able to do everything that you require...
- “You are just biased against Artificial Intelligence.”  
False. We have applied machine learning and knowledge-based systems with success to assorted maritime applications, concluding repeatedly that “AI techniques can be put to good use for maritime applications”, e.g. *Bertram (2013, 2018)*. We may have started with different expectations, but were open to adapt our assessment in the light of the obtained test results.

## 7. Conclusions

We investigated here ChatGPT, Dall-E 2, Docebo Shape, and Piggy for maritime applications, assessing their current capabilities. The results were falling short of our expectations for all three tools, with often wrong and sometimes ridiculous responses to our prompts.

A fundamental criticism of all AI tools investigated is that they are not intelligent enough to know their limits and return useless or sometimes dangerously misleading response rather than stating “I don’t know”. This reflects the same dangerous as any other pseudoscience, and therefore its results should be treated as such.

*Chomsky et al. (2023)* reach an even harsher conclusion, pointing out the lack of cognition. “[ChatGPT’s] deepest flaw is the absence of the most critical capacity of any intelligence: to say not only what is the case, what was the case and what will be the case - that’s description and prediction -

but also what is not the case and what could and could not be the case (...) The crux of machine learning is description and prediction; it does not posit any causal mechanisms or physical laws. Of course, any human-style explanation is not necessarily correct; we are fallible. But this is part of what it means to think: To be right, it must be possible to be wrong.”

There is hope, however, as pointed out by Karl Popper (<https://blogs.scientificamerican.com/doing-good-science/drawing-the-line-between-science-and-pseudo-science/>), as some sciences developed from pseudoscience (such as chemistry from alchemy), and it may be possible that, a future AI is able to redeem itself, incorporating elements of science, such as testing, and refutability. The history of science (and consequently maritime technology) is full of false claims, similar as the ones given by ChatGPT, and it is our duty, we humans that do science, to locate and remove these false claims. When the AI from the future, almighty, be able to do the same, to check if its answers are scientific or pseudoscience, to prove or refute it, without the human on the background, then we can jump to the “intelligent” level. Until then, we will keep asking the prompt to jump here the same way as in Rhodes.

## Acknowledgements

We are grateful for colleagues sharing success and failure stories on using AI-based tools discussed here. We thank Bernhard Löbermann (DNV) for testing Docebo Shape and sharing his experience and slides; Bjørnar Krukhaug (DNV) for contributing on Piggy; Øivind Kjerstad, Yasuo Ichinose, and Stein Ove Erikstad at NTNU, for sharing their views on ChatGPT. Special thanks go to ChatGPT for entertaining us for hours and writing most of this paper, even if we mostly discarded its suggested texts in the end.

## References

BERTRAM, V., *A survey on knowledge-based systems for ship design and ship operation*, Int. J. Intelligent Engineering Informatics 2/1, pp.71-90, 2013

BERTRAM, V. (2018), *Demystify Artificial Intelligence for Maritime Applications*, 17<sup>th</sup> COMPIT Conf., Pavone, pp.22-35, [http://data.hiper-conf.info/compit2018\\_pavone.pdf](http://data.hiper-conf.info/compit2018_pavone.pdf)

BERTRAM, V. (2000), *Practical Ship Hydrodynamics*, Butterworth & Heinemann

BERTRAM, V.; PLOWMAN, T. (2019), *A Hitchhiker’s Guide to the Galaxy of Maritime e-Learning*, 18<sup>th</sup> COMPIT Conf., Tullamore, pp.7-23, [http://data.hiper-conf.info/compit2019\\_tullamore.pdf](http://data.hiper-conf.info/compit2019_tullamore.pdf)

CHOMSKY, N; ROBERTS, I.; WATUMULL, J. (2023). *The False Promise of ChatGPT*, Guest Essay, The New York Times, <https://www.nytimes.com/2023/03/08/opinion/noam-chomsky-chatgpt-ai.html>

COLLE, C.; MOROBÉ, C. (2022), *Saving AI from its Own Hype: Getting Real about the Benefits and Challenges of Machine Learning for Ship Performance Modelling Aimed at Operational Optimizations*, 7<sup>th</sup> HullPIC Conf., Tullamore, pp.198-206, [http://data.hullpic.info/HullPIC2022\\_Tullamore.pdf](http://data.hullpic.info/HullPIC2022_Tullamore.pdf)

GASPAR, H.; BERTRAM, V. (2023), *The Use of ChatGPT and Similar AI in Marine Engineering: Limitations and Opportunities*, 24<sup>th</sup> COMPIT Conf., Drübeck, pp.73-83, [http://data.hiper-conf.info/compit2023\\_drubeck.pdf](http://data.hiper-conf.info/compit2023_drubeck.pdf)



## Appendix 1: ChatGPT response on code to compute heave motion of barge

Question: “How to code heave for a rectangular barge of  $L = 100$ ,  $B = 20$ ,  $D = 10$ , in water?”

Answer:

Coding the heave motion of a rectangular barge in water would involve a few steps. Here is an example of one approach you could take using the Python programming language:

Import the necessary libraries, such as NumPy for mathematical calculations and SciPy for solving differential equations:

```
import numpy as np
from scipy.integrate import odeint
```

Define the dimensions of the barge ( $L$ ,  $B$ ,  $D$ ) and any other relevant properties, such as the mass of the barge, the density of the water, and the added mass coefficient:

Copy code

```
L = 100
B = 20
D = 10
mass = 1000
density = 1000
added_mass_coefficient = 0.5
```

Define a function that describes the heave motion of the barge. This function should take in the current state of the barge (position and velocity) and return the derivative of the state (acceleration). The equation of motion for the heave motion can be modeled as  $ma = -mg + F_h$  where  $m$  is the mass of the barge,  $a$  is the acceleration,  $g$  is the acceleration due to gravity, and  $F_h$  is the hydrodynamic force acting on the barge.

```
def heave_motion(state, t):
    x, v = state
    Fh = added_mass_coefficient * density * L * B * D * v
    a = (-mass*9.81 + Fh) / mass
    return [v, a]
```

Use the odeint function from the SciPy library to integrate the differential equation and solve for the position and velocity of the barge over time:

```
t = np.linspace(0, 10, 100)
initial_state = [0, 0]
state = odeint(heave_motion, initial_state, t)
```

The state variable contains the position and velocity of the barge over time. The first column will be the position and the second one the velocity. You can visualize the results with a plot or print them out to check the results.

Please note this is a simple example and the hydrodynamic forces acting on the barge can be more complex depending on the velocity, the frequency of the waves, the draft of the barge, etc. Therefore, the real-world application would be more complex than this example.

# A Snapshot of Evolving Innovative Antifouling Options

Volker Bertram, DNV, Hamburg/Germany, [volker.bertram@dnv.com](mailto:volker.bertram@dnv.com)

## Abstract

*This paper surveys recent developments for biocide-free antifouling solutions. On the coating side, nano-coatings including graphene-based coatings, coatings with passive air lubrication, and biocide-free SPC (self-polishing copolymers) are covered. Active protection systems based on ultrasonic or ultraviolet radiation have progressed significantly in recent years. Robotic cleaning shows rapid growth in technological and business maturity, enabling hard coatings as a viable option to replace the current standard solution of biocide-containing SPC coatings.*

## 1. Antifouling as an ecological and economic necessity

### 1.1. A problem as old as shipping

Fouling has been a headache for shipping since ancient times, *Bertram and Yebra (2017), Doran (2019), Bertram (2020)*. Over the centuries, human ingenuity has come up with various countermeasures to prevent or reduce fouling, lumped here collectively under the term “antifouling”.

The most widely adopted antifouling solution in modern shipping has been antifouling SPC (self-polishing copolymers) paints, where the coating matrix containing the biocides dissolved slowly in water, Fig.1. The release of biocides and paint particles (microplastics) is significantly accelerated under abrasive forces as experienced in hull cleaning with brushes. IMO has banned two biocides for antifouling coatings on ship hulls so far, namely TBT (tributyltin) since 2003 and Cybutryne since 2023. Further substances are under scrutiny, resulting in regional bans and proposals to add them to the list of antifouling substances banned by IMO.

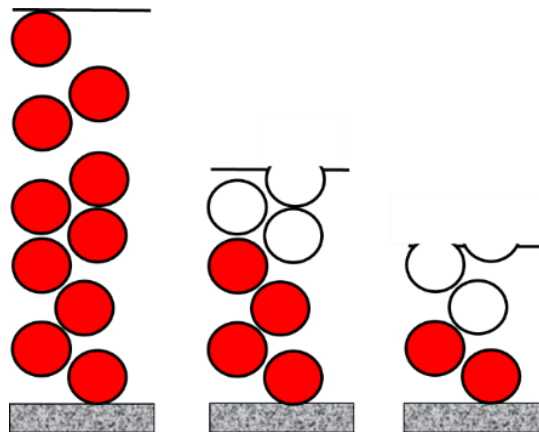


Fig.1: Principle of SPC with biocides (red) and leached layer (empty circles)

Biocidal antifouling coatings have fueled also a debate on in-water cleaning of ships. Over the past decade, more and more port authorities have banned in-water cleaning in their ports. This is partly due to the fear that aquatic invasive species may be released and spread uncontrollably threatening the local ecosystem, but another concern is that the cleaning will release biocides and microplastics which will settle and contaminate the soil.

As such, biocidal antifouling paints are now widely seen as a bridging technology. But what could be on the other side of the bridge? World shipping moves slowly, but steadily towards sustainable shipping. Leaching copper and micro-plastics (the dissolved ingredients of today’s standard SPC coatings) into the world oceans is not sustainable. *Dafforn et al. (2011)* argue “that the way forward is to phase-out metals and organic biocides from [antifouling] paints and to adopt non-toxic alternatives.

[...] However, we call for caution in the time-frame for making these changes.” There is no shortage of ideas, but the road from concept to deployment is often a long one. This is especially true for antifouling, where a product’s success and effectiveness are generally measured over at least five years, the standard interval for ships to be drydocked for cleaning and new coating.

We cannot simply abolish biocidal SPCs, as antifouling measures for ships are both an ecological and economic necessity.

## 1.2. Key role of antifouling for energy efficiency in ship operation

Marine growth can decrease ship performance drastically, resulting in a 30-50% increase of fuel consumption (and associated emissions) compared to a smooth hull, Fig.2. The effect of even light slime is with up to 20% fuel increase larger than widely thought, *GIA (2023)*. *CSC (2011)* estimates the financial impact of fouling to 30 billion USD per year for the world fleet, and the contribution to man-made CO<sub>2</sub> emissions to 0.3%.

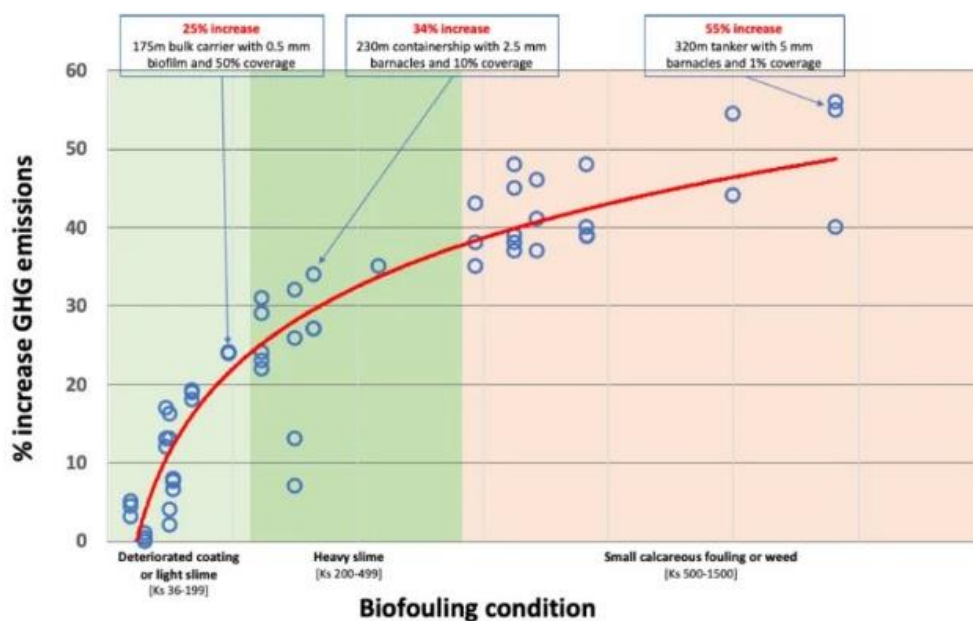


Fig.2: Effect of biofouling on fuel consumption and CO<sub>2</sub> emissions, *GIA (2023)*

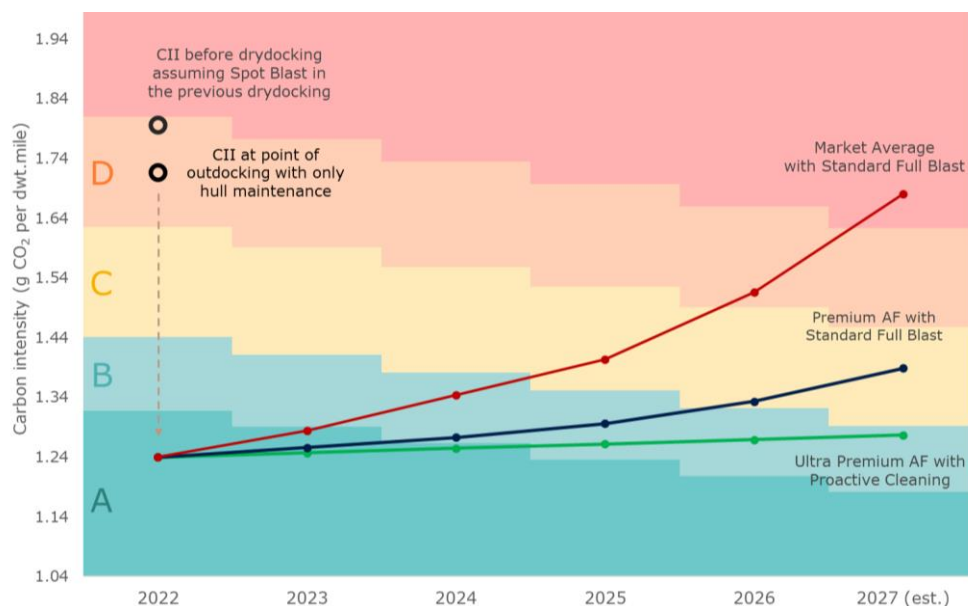


Fig.3: Projected CII development of different coating and cleaning options, source: Jotun

Progressing fouling can deteriorate a ship's CII (Carbon Intensity Indicator) rating from an A to an E within 5 years, Fig.3, *Tan et al. (2022)*. On the other hand, optimum coating and cleaning strategies can maintain hull performance largely, with a deterioration from A to B within five years, mainly due to the increasingly stricter thresholds on the CII rating, Fig.3. Despite the significantly higher CAPEX, the resultant lower OPEX for fuel make ultra premium coatings often a convincing business case.

### 1.3. Biofouling management to prevent transport of aquatic invasive species

After IMO's ballast water management convention went into force in 2017, hull fouling has become the main contributor for the spread of aquatic invasive species. For energy efficiency, the key focus lies on the large surfaces, such as ships sides. For prevention of invasive species, the key focus lies on niche areas which are hard to clean. Besides IMO's 2011 Guidelines for the Control and Management of Ships' Biofouling to Minimize the Transfer of Invasive Aquatic Species, revised in 2023, various organisations have recently proposed guidelines for the cleaning of hulls, such as Jotun, *Oftedahl and Enström (2020)*, and BIMCO, *Sørensen (2020)*, *BIMCO (2021)*.

## 2. New developments in coating technology

### 2.1. Nano-coatings

'Nano-coatings' use bio-inspired microscopic surface structures (e.g. shark skin, lotus effect) to make adhesion difficult for organisms, Fig.4. Nano-coatings are expected to have better long-term performance than low-surface energy foul-release coatings ('silicone paints') which degrade as the silicone film weathers, *Bertram and Yebra (2017)*. Several nano-coating products are already on the market, Fig.4. Stolt Tankers announced in 2023 that 25 of their tankers will have their propellers coated with graphene-based nano-coating, Fig.5.



Fig.4: Nano-coating structure (left) and demonstrating non-stick effect (right), source: Ultra Ever Dry

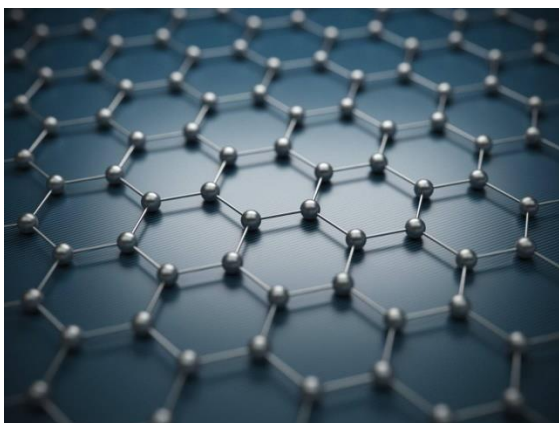


Fig.5: Graphene (left) is the base for the nano-coating on propellers of Stolt Tankers (right)



## 2.2. Biocide-free SPCs

Nippon Paint Marine has developed an innovative biocide-free SPC antifouling paint for ships. Here the slowly dissolving coating with a special micro-structure apparently prevents adhesion of fouling as the marine organisms do not recognize the coating as a surface: “when marine life finds the micro-domain surface, they are confused and hesitate to try to adhere there because they do not recognise the microdomain surface as a place where they can easily develop,” *Yamashita (2022)*.

## 2.3. Passive air lubrication

The AIRCOAT (AIR-induced friction reducing ship COATing) project, <https://aircoat.eu/>, has developed foils with a surface structure mimicking floating ferns (*Salvinia*), which trap a fine film of air, Fig.6, *Oeffner et al. (2020)*, *Walheim et al. (2022)*. In 2021, field tests showed that the foils work at least in the short terms, but more time is needed to assess the long-term performance in practical applications.

While the focus here is on reducing resistance through passive air lubrication, note that *Silberschmidt et al. (2016)* report that active air lubrication may substitute antifouling coatings, as apparently the change between water and air saturated water inhibits marine growth on the ship bottom.



Fig.6: Floating fern (left) inspired the passive air-trapping foil (right) in the AIRCOAT project

## 3. Ultra-X protection methods

### 3.1. Ultrasonic technology

Ultrasonic vibrations cause very high accelerations, which destroy cell structures of fouling. A strong point of ultrasonic protection is that it offers biocide-free protection for ships even at zero speed. The technology has progressed from research to industrial applications. More recently, ‘intelligent’ dynamic biofilm protection has been developed, where Artificial Intelligence sets the optimum parameters for each transducer based on assorted sensor information, Fig.7, *Mayorga et al. (2023)*.



Fig.7: DBPI from Hasytec

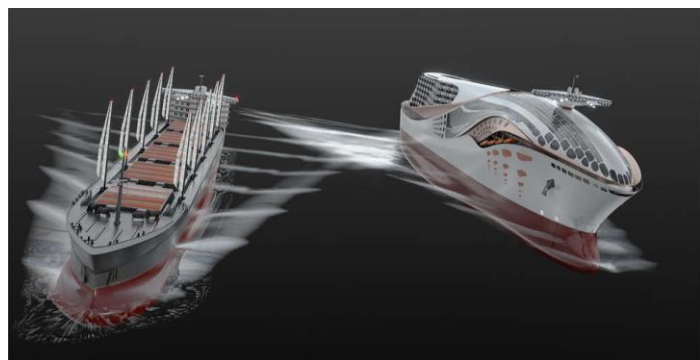


Fig.8: CHEK cases for full hull ultrasonic protection

The technology is by now widely adopted for niche areas on ships, such as sea chests, bow thrusters, heat exchangers, and propellers. Current protective range of ultrasonic transducers is ~6-8m. For a cargo-ship, this would mean hundreds of transducers to protect the full in-water hull. The CHEK project, <https://www.projectchek.eu/>, Kelling (2021), investigates the feasibility of doing just this, with a bulk carrier and a cruise ship as application cases, Fig.8.

### 3.2. Ultraviolet technology

Ultraviolet (UV) radiation is widely used in ballast water treatment. It has been proposed for hull anti-fouling decades ago, Benson et al. (1973). The rapid attenuation of UV radiation and relatively high initial and operational costs has made this option rather unattractive for external antifouling applications. This may change now. AkzoNobel, Philips, and since 2023 also Damen Shipyards, have developed a novel fouling prevention solution, based on the generation of UV light by LEDs embedded in a transparent layer, Fig.9 (left), *Salters et al. (2022)*. The LEDs form thin tiles, relatively light-weight and thin. The tiles are 100% watertight and powered via wireless power transfer, thus substantially reducing any chance of electrical shorts. The technology is in the prototype stage, Fig.9 (right).

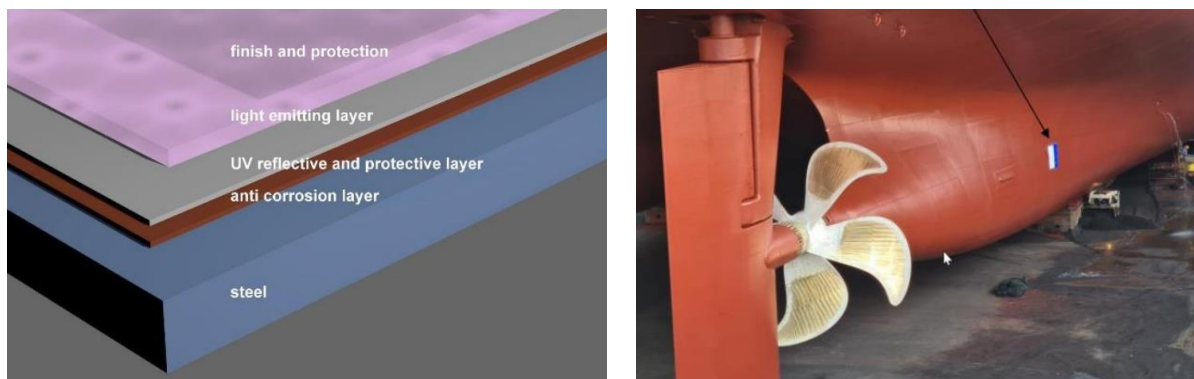


Fig.9: Principle of UVC LED foil application (left) and tile installation on LNG carrier (right)

## 4. Robotic cleaning and inspection

### 4.1. Proactive cleaning (grooming)



Fig.10: Effect of proactive cleaning, GIA (2022)

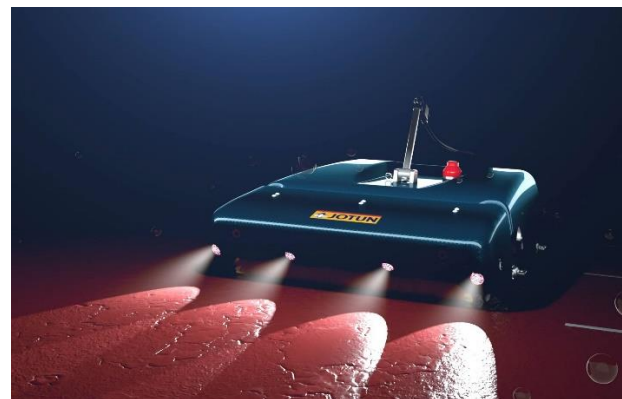


Fig.11: Hull Skater robot, source: Jotun

Proactive cleaning (a.k.a. grooming) has been increasingly advocated as a key measure to reduce fuel consumption and the CII in service. Such frequent, soft cleaning at biofilm stage keeps hull performance degradation in check, resulting in significant in-between docking fuel savings, Fig.10.

For effective proactive cleaning, cleaning technology and coating technology should be matched. Jotun's Hull Skating Solution is a prime example for this, *Oftedahl and Enström (2020)*, combining a high-performance, abrasion-resistant coating allowing frequent cleaning without coating erosion;

performance monitoring based on ISO 19030 for decision support on when to clean; hull inspection and cleaning of biofilm by the Hull Skater robot, Fig.11, and performance-based contracts and service guarantees.

#### 4.2. Smarter robots learn new tricks

Robotic hull cleaning has enjoyed exponential growth, moving from first research in the 1980s to mature industry services offered by various service providers, *Bertram (2021)*. The state of the art of in-water robotic cleaning and inspection continues to evolve in various aspects:

- Automatic identification and quantification of fouling using machine vision, e.g. *Guéré and Gambini (2021)*. Continuing development aims at aligning various machine vision system to use a common scale for rating of fouling on images.
- Laser scanning hull surfaces with resolution of 0.01 mm (= 10 microns) on crawling robots and 0.5 mm on free-floating robots, Fig.11, *Paranhos (2020)*. This resolution would allow quantification of macrofouling.
- Team-capable autonomous robots as the HSR robots of Armach Technology, Fig.12, *Lander (2022)*. Team capable robots can clean ship hulls in shorter time, parallelizing the work. A large cargo ship can then be cleaned during one regular port stay.

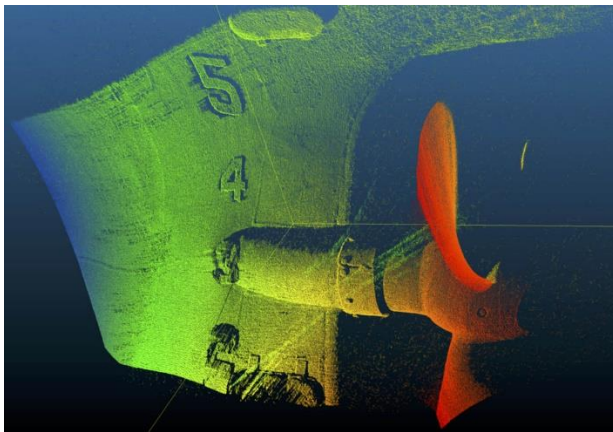


Fig.12: In-water scan from floating robot, source: Kraken Robotics



Fig.11: Team-capable HRS robots, source: Armach Robotics

#### 4.3. In-transit cleaning

In-transit cleaning would resolve some current issues with in-water cleaning in ports, such as requirements for collection and disposal of removed fouling and paint particles and availability of cleaning services. In Norway, Shipshave pioneered in-transit cleaning of hulls with its ITCH system, *Freyer and Eide (2021)*, a semi-autonomous system for cleaning ship sides with a tethered robot that swipes up and down, using ship hydrodynamic forces for up-and-down motion and adhesion to hull. Ships ends, bottom, and niche areas cannot be cleaned by the ITCH.

Israeli startup NakAI Robotics has developed an autonomous in-transit robotic system to remove biofilm while the ship is in transit, *Nice and Aharony (2023)*. The robot self-deploys from the side of the ship, Fig.13 (left). It then autonomously moves over the hull, Fig.13 (right), using hydrodynamic forces for adhesion and UV light and soft brushes for cleaning, deemed soft enough to avoid abrasion of SPC coatings. The robot does not operate near the propeller, near the bow, or in niche areas. First prototype testing on a cargo ship was performed in 2021. Further developments shall fit the robot with class-approved inspection sensors. The robot may then be used for steel structure survey, cleaning, and fouling condition documentation.



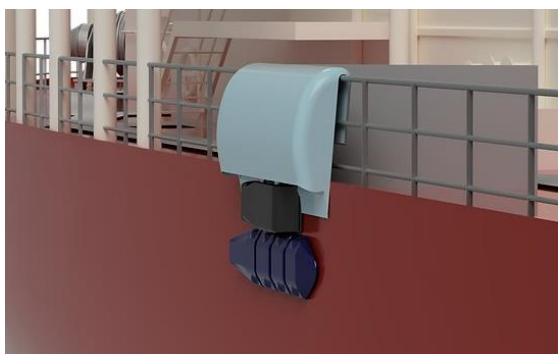


Fig.13: NakAI robot for in-transit cleaning, <https://www.nakairobotics.com/>

Gerland *et al.* (2023) describe a German development for autonomous in-transit hull cleaning: Larabicus, a robotic ‘cleaning fish’, Fig.14, continuously cleans the ship's hull, removing the biofilm and thus inhibiting higher fouling stages. The Larabicus robot is agile enough to bypass attachments such as bilge keels, galvanic anodes, or openings for ballast water tanks. The concept has been tested so far only under laboratory conditions. A first pilot project on a ship in operation are envisioned for Q4 2024.



Fig.14: Larabicus robot for in-transit cleaning

## 5. Conclusion

Where there is a problem, there is a solution. New challenges for the shipping industry, such as increasingly strict CII requirements for operational energy efficiency and wider application of biofouling management requirements, are answered by innovative solutions. Ingenuity and entrepreneurship thrive, and established big players are kept on their toes by start-ups challenging the status quo.

The progress towards more efficient and more sustainable hull management solutions in the last five years is impressive and encouraging.

## References

BERTRAM, V. (2020), *Options for the Post-Biocide Era of Antifouling*, 12<sup>th</sup> HIPER Symp., Cortona, pp.51-56, [http://data.hiper-conf.info/Hiper2020\\_Cortona.pdf](http://data.hiper-conf.info/Hiper2020_Cortona.pdf)

BERTRAM, V. (2021), *Robotic Hull Cleaning – State of the Art and Roadmap*, 13<sup>th</sup> HIPER Symp., Tullamore, pp.37-44, [http://data.hiper-conf.info/Hiper2021\\_Tullamore.pdf](http://data.hiper-conf.info/Hiper2021_Tullamore.pdf)

BERTRAM, V.; YEBRA, D.M. (2017), *Past, Present and Prospects of Maritime Antifouling*, 11<sup>th</sup> HIPER Symp., Zevenwacht, pp.32-43, [http://data.hiper-conf.info/Hiper2017\\_Zevenwacht.pdf](http://data.hiper-conf.info/Hiper2017_Zevenwacht.pdf)



BIMCO (2021), *Industry Standard on In-Water Cleaning with Capture*, BIMCO, <https://www.bimco.org/-/media/bimco/ships-ports-and-voyage-planning/environment-protection/biofouling/2021-industry-standard-in-water-cleaning-final.ashx>

CSC (2011), *A transparent and reliable hull and propeller performance standard*, Clean Shipping Coalition submission to MEPC 63/4/8, Int. Mar. Org., London, <https://bellona.no/assets/sites/3/2015/06/fil MEPC 63-4-8 - A transparent and reliable hull and propeller performance standard CSC1.pdf>

DAFFORN, K.A.; LEWIS, J.A., JOHNSTON, E.L. (2011), *Antifouling strategies: History and regulation, ecological impacts and mitigation*, Marine Pollution Bulletin 62/3, pp.453-465

DORAN, S. (2019), *A Short History of Hull Cleaning and Where Do We Go Now*, 4<sup>th</sup> HullPIC Conf., Gubbio, pp.97-102, [http://data.hullpic.info/HullPIC2019\\_gubbio.pdf](http://data.hullpic.info/HullPIC2019_gubbio.pdf)

FREYER, R.; EIDE, E. (2021), *In-Transit Cleaning of Hulls*, 2<sup>nd</sup> PortPIC Conf., Pontignano, pp.72-76, [http://data.hullpic.info/PortPIC2021\\_Pontignano.pdf](http://data.hullpic.info/PortPIC2021_Pontignano.pdf)

GERLAND, F.; ATALLAH, K., SCHOMBERG, T. (2023), *Larabicus the autonomous in transit cleaning system*, 15<sup>th</sup> HIPER Symp., Bernried, pp.127-134, [http://data.hiper-conf.info/Hiper2023\\_gerlandBernried.pdf](http://data.hiper-conf.info/Hiper2023_gerlandBernried.pdf)

GIA (2022), *Analysing the Impact of Marine Biofouling on the Energy Efficiency of Ships and the GHG Abatement Potential of Biofouling Management Measures*, GloFouling Partnerships Project Coordination Unit, Int. Maritime Org., London, [https://www.glofouling.imo.org/\\_files/ugd/34a7be02bd986766d44728b85228c3ec9b95ee.pdf](https://www.glofouling.imo.org/_files/ugd/34a7be02bd986766d44728b85228c3ec9b95ee.pdf)

GUERE, S.; GAMBINI, N. (2021), *Notilo Cloud AI Platform for Hull Condition Reporting*, 13<sup>th</sup> HIPER Symp., Tullamore, pp.62-70, [http://data.hiper-conf.info/Hiper2021\\_Tullamore.pdf](http://data.hiper-conf.info/Hiper2021_Tullamore.pdf)

KELLING, J. (2021), *EU Project CHEK – Ultrasonic Antifouling and other Measures to Meet the CII Challenge*, 13<sup>th</sup> HIPER Symp., Tullamore, pp.132-139, [http://data.hiper-conf.info/Hiper2021\\_Tullamore.pdf](http://data.hiper-conf.info/Hiper2021_Tullamore.pdf)

LANDER, K. (2022), *Frequent and Habitual: How Autonomous Robots Can Make Routine Grooming and Inspection Accessible*, 3<sup>rd</sup> PortPIC Conf., Hamburg, pp.119-123, [http://data.hullpic.info/PortPIC2022\\_Hamburg.pdf](http://data.hullpic.info/PortPIC2022_Hamburg.pdf)

MAYORGA, X.; KELLING, J.; FRÜCHTENICHT, M. (2023), *AI-Enhanced Ultrasonic Biofouling Protection*, 15<sup>th</sup> HIPER Symp., Bernried, pp.32-40, [http://data.hiper-conf.info/Hiper2023\\_Bernried.pdf](http://data.hiper-conf.info/Hiper2023_Bernried.pdf)

NICE, M.; AHARONY, Z. (2023), *Developing a Novel Fully Autonomous In-Transit Hull Grooming Platform*, 4<sup>th</sup> PortPIC Conf., Pontignano, pp.49-55, [http://data.hullpic.info/PortPIC2023\\_Pontignano.pdf](http://data.hullpic.info/PortPIC2023_Pontignano.pdf)

OEFFNER, J.; HAGEMEISTER, N.; JAHN, C.; BRETSCHNEIDER, H.; SCHMALE, J. (2020), *Reducing friction with passive air lubrication: Initial experimental results and the numerical validation concept of AIRCOAT*, 12<sup>th</sup> HIPER Conf., Cortona, [http://data.hiper-conf.info/Hiper2020\\_Cortona.pdf](http://data.hiper-conf.info/Hiper2020_Cortona.pdf)

OFTEDAHL, G.A.; ENSTRÖM, A. (2020), *Proactive Cleaning and the Jotun Hull Skating Solution*, 1<sup>st</sup> PortPIC Conf., Hamburg, pp.66-78, [http://data.hullpic.info/PortPIC2020\\_Hamburg.pdf](http://data.hullpic.info/PortPIC2020_Hamburg.pdf)

- PARANHOS, P.M. (2020), *3D Laser Inspection of Ship Hulls*, 1<sup>st</sup> PortPIC Conf., Hamburg, pp.14-22, [http://data.hullpic.info/PortPIC2020\\_Hamburg.pdf](http://data.hullpic.info/PortPIC2020_Hamburg.pdf)
- SALTERS, B.; WIJNEN, M.; REYNOLDS, K. (2022), *UVC Anti-Fouling Solution – Design, Experiments and Results of Next Generation Samples*, 14<sup>th</sup> HIPER Symp., Cortona, pp.211-220, [http://data.hiper-conf.info/Hiper2022\\_Cortona.pdf](http://data.hiper-conf.info/Hiper2022_Cortona.pdf)
- SILBERSCHMIDT, N.; TASKER, D.; PAPPAS, T.; JOHANNESSEN, J. (2016), *Silverstream system – Air lubrication performance verification and design development*, 10<sup>th</sup> HIPER Conf., Cortona, pp.236-246, [http://data.hiper-conf.info/Hiper2016\\_Cortona.pdf](http://data.hiper-conf.info/Hiper2016_Cortona.pdf)
- SØRENSEN, A.F. (2020), *Industry Standard for In-water Cleaning with Capture*, 1<sup>st</sup> PortPIC Conf., Hamburg, pp.79-82, [http://data.hullpic.info/PortPIC2020\\_Hamburg.pdf](http://data.hullpic.info/PortPIC2020_Hamburg.pdf)
- TAN, K.K.; PAERELI, S.; BRINK, A. (2022), *Impact of hull coating on EEXI and CII*, 7<sup>th</sup> HullPIC Conf., Tullamore, pp.190-197, [http://data.hullpic.info/HullPIC2022\\_Tullamore.pdf](http://data.hullpic.info/HullPIC2022_Tullamore.pdf)
- WALHEIM, S.; SCHIMMEL, T.; BARCZEWSKI, M.; SPEICHERMANN-JÄGEL, L.; DROLL, R.; DULLENKOPF-BECK, S.; OEFFNER, J.; WEISHEIT, J.; MINOR, J.C.; BELTRI, M. (2021), *Passive Air Lubrication: Demonstrating a Research Vessel Coated with a Hull of Air*, 13<sup>th</sup> HIPER Symp., Tullamore, pp.203-208, [http://data.hiper-conf.info/Hiper2021\\_Tullamore.pdf](http://data.hiper-conf.info/Hiper2021_Tullamore.pdf)
- YAMASHITA, A. (2022), *Biocide-Free Antifouling Paint / Possible and Effective*, 3<sup>rd</sup> PortPIC Conf., Hamburg, pp.90-99, [http://data.hullpic.info/PortPIC2022\\_Hamburg.pdf](http://data.hullpic.info/PortPIC2022_Hamburg.pdf)

# Engineering Marine Digital Twins with Sustainability

Rodrigo Perez Fernández, Siemens Digital Industries Software, Madrid/Spain,  
[rodrigo.fernandez@siemens.com](mailto:rodrigo.fernandez@siemens.com)

## Abstract

*This paper presents how our Industry will achieve more with less by combining the real and digital world. The comprehensive Digital Twin plays a key role to improve environmental compatibility of technology. It collects data across the entire lifecycle of a product, from the initial concept to production and use. Our future technologies make it possible to understand this data and use finite resources more efficiently. This is how we strive to make industry more sustainable. Up to 80% of all product-related environmental impacts are determined during the product design phase.*

## 1. A paper title explanation

The title of this paper, Engineering Marine Digital Twins with Sustainability, refers to the application of Digital Twin technology in the maritime industry with a specific focus on sustainability. A Digital Twin is a virtual replica of a physical asset or system that enables real-time monitoring, analysis, and optimization.

In the context of the maritime sector, engineering marine Digital Twins with sustainability involves creating virtual representations of ships, vessels, or maritime infrastructure to enhance their operational efficiency, reduce environmental impact, and promote sustainable practices. This approach combines data analytics, simulation, and advanced modelling techniques to support decision-making processes and improve overall performance. By utilizing Digital Twin technology, various aspects of maritime operations can be analysed and optimized for sustainability, Walker (2013). This includes factors such as energy consumption, emissions reduction, fuel efficiency, maintenance planning, and resource allocation. Digital Twins provide a holistic view of the asset's performance, allowing for data-driven insights and predictive analytics to identify areas for improvement and implement sustainable measures.

The integration of sustainability into engineering marine Digital Twins can lead to several benefits, Aouad et al. (2019), Baldauf et al. (2020), Huang et al. (2021), Lu et al. (2020). It enables the identification of energy-saving opportunities, optimization of operational processes, and better utilization of resources. By simulating different scenarios and evaluating their environmental impact, stakeholders can make informed decisions to minimize the carbon footprint of maritime operations.

The Digital World strives to ensure the environmental compatibility of products, focusing on reducing material consumption throughout their entire life cycle while maximizing the use and value of all components and materials. Its goal is to decouple economic activity from the release of climate-damaging gases and substances into the environment and the use of finite resources. Digital Twins play a crucial role in considering ecological factors during product planning and design, as this phase accounts for up to 80% of their life-cycle environmental impact. By developing components and parts that don't become waste, all design options are evaluated in advance to enhance the sustainability of products and associated processes along their entire value chains, including resource procurement, precursor, and final product production, as well as logistics and transportation processes.

Digital Twin technology serves as an anchor for the Circular Economy, where resources are processed in a loop without generating waste, promoting sustainable development by preserving, enhancing, or restoring the value of materials. Currently, only 7.2% of materials are preserved for further use, while the majority is disposed of or incinerated as waste. This highlights the importance of assessing products using transparent and comprehensive data-based accounting methods, effectively addressing their negative environmental impacts during the planning and design phase.

To ensure transparency for market participants and stakeholders, reporting is based on *Environmental, Social, and Governance* (ESG) criteria. These criteria facilitate decision-making by considering how investments and companies can improve their impact on climate change, water and land use, biodiversity, substance emissions, and the Circular Economy. Aligning corporate activities with the ambition of the Paris Agreement to limit global warming to 1.5° C is crucial, as it enables the preservation of our natural resources and existence.

The shipbuilding industry faces significant challenges due to its direct environmental impact on ship construction, maintenance, and repair. While not directly responsible for the environmental impact of ship operation and final recycling, shipbuilding plays a vital role in improving the industry's environmental performance. Increasing efforts in this regard are essential as the industry's environmental impact becomes more prominent in the public domain. Although ships offer advantages in terms of energy efficiency in transporting goods, greenhouse gas emissions from this sector are projected to rise significantly in the coming years. The industry also faces environmental concerns related to the discharge of hazardous contaminants into waterways, marine ecosystems, and food chains. The industry's open-air working environments and waterfront locations can elevate the risks of environmental damage by providing direct pathways for pollutants to reach air, soil, and water.

Overall, there is insufficient information available to paint a comprehensive picture of the shipbuilding industry's environmental impact, highlighting the need for greater environmental focus and transparency. Many shipbuilding and ship recycling activities take place in countries with lax health, safety, and environmental regulations and enforcement, exacerbating the issue.

While shipbuilding is not directly responsible for the environmental concerns associated with ship use and final recycling, it can play a more significant role as an integral part through a life-cycle approach to ships. By accepting environmental responsibilities, the shipbuilding industry can demonstrate its commitment to governments and the public. Failing to do so may lead to the industry losing control over these issues and being subjected to potentially harsh measures that could harm the industry.

This paper examines the progress made in the field of Digital Twins and digitalization, focusing on successful business cases in shipbuilding construction, maintenance and repair, and the environmental impacts of shipping, ship dismantling, and recycling. Its aim is to contribute to sustainability efforts in these areas, *Mostafa et al. (2017)*.

Furthermore, engineering marine Digital Twins with sustainability can facilitate compliance with environmental regulations and standards. It allows for the continuous monitoring and reporting of environmental indicators, ensuring adherence to sustainable practices and enhancing transparency.

In summary, engineering marine Digital Twins with sustainability combines advanced digital technologies with the principles of sustainability to optimize maritime operations, reduce environmental impact, and promote responsible resource management in the maritime industry.

## **2. Construction, maintenance, and repair**

Shipbuilding, ship maintenance, and ship repair are key areas in the maritime industry where sustainability practices are increasingly being implemented. These activities have a significant impact on the environmental and social aspects of the industry and focusing on sustainability in these areas is crucial for the long-term well-being of the sector.

Shipbuilding plays a crucial role in ensuring the sustainability of the maritime industry and reducing its environmental impact. Several key factors and practices contribute to increasing sustainability in shipbuilding, like employing advanced design tools and simulations which could help optimize the hull form and propulsion system, leading to better fuel efficiency and reduced emissions. For example, Computational Fluid Dynamics (CFD) and other modelling techniques enable shipbuilders to identify and implement energy-saving features.



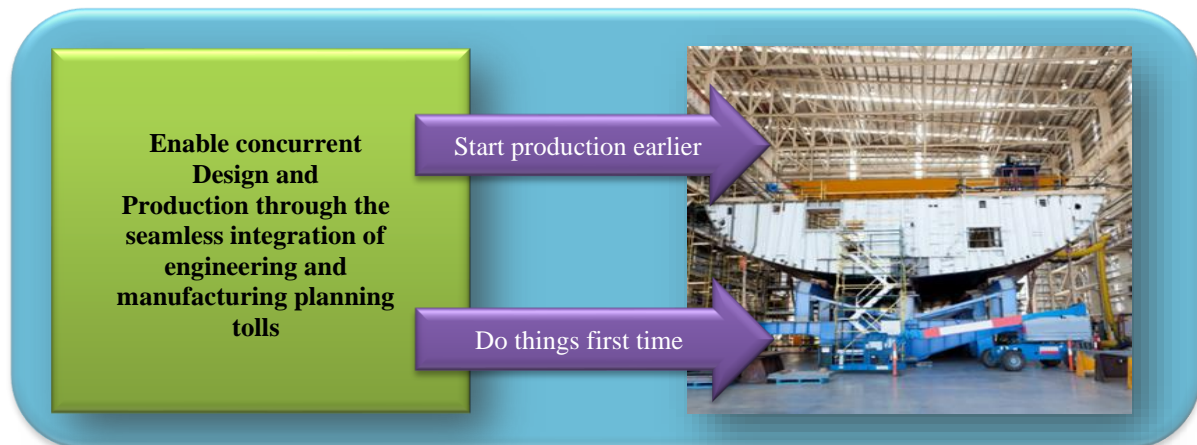


Fig.1: Key Factors and practices that increase sustainability

Enabling concurrent design and production in shipbuilding and other manufacturing industries requires the seamless integration of engineering and manufacturing planning tools as presented in Fig.1. This integration allows for real-time collaboration, data sharing, and efficient communication between different teams involved in the design and production processes. Some strategies to achieve this goal are Digital Twin technology, Product Data Management (PDM) and Product Lifecycle Management (PLM) Systems, collaborative software platforms, Building Information Modelling (BIM), integrated CAD/CAM Systems, real-time simulation and visualization, agile project management, cross-functional teams, standardization of data formats and communication protocols and training and skill development.

- **Shipbuilding:** Sustainable shipbuilding involves integrating environmentally friendly design principles and technologies into the construction process. This includes using energy-efficient materials, implementing waste reduction strategies, and incorporating renewable energy sources. By prioritizing sustainable practices from the outset, shipbuilders can reduce emissions, minimize waste generation, and enhance the overall environmental performance of ships, *DNV GL (2014)*.

To optimize building strategy and de-risk manufacturing schedule delays, simulation of the production process can be a powerful tool (like the conception shown in Fig.2). Simulations allow shipbuilders to model and analyse the manufacturing process in a virtual environment before actual production begins, *LR (2015)*.

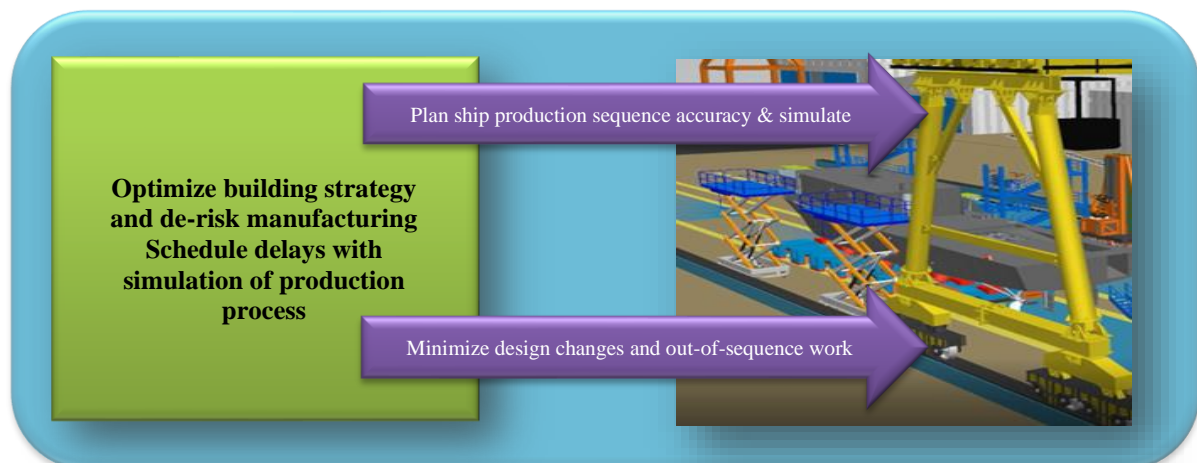


Fig.2: Environmentally friendly design principles

- **Ship Maintenance:** Regular maintenance is essential for ensuring the safe and efficient operation of ships. Sustainable ship maintenance involves adopting environmentally responsible practices

such as proper waste management, utilizing eco-friendly cleaning products, and employing efficient energy management systems as elucidated in Fig.3. Additionally, implementing condition-based maintenance strategies and optimizing the use of resources can contribute to the sustainability of ship operations.



Fig.3: Sustainable ship maintenance environmentally responsible practices

- **Ship Repair:** Sustainable ship repair focuses on minimizing the environmental impact of repair activities while ensuring vessel safety and functionality (as it is enlightened in *figure 4*). This includes using eco-friendly repair materials, employing efficient repair techniques, and complying with relevant environmental regulations. Proper waste disposal, recycling of materials, and reducing energy consumption during repair processes are also essential elements of sustainable ship repair practices.



Fig.4: Digital Twin maintenance sustainable benefits

Overall, embracing sustainability in shipbuilding, ship maintenance, and ship repair is vital for reducing the industry's ecological footprint, conserving resources, and promoting a cleaner and more responsible

maritime sector. It requires collaboration among shipbuilders, shipowners, operators, and regulatory bodies to prioritize sustainable practices and drive positive change throughout the entire life cycle of a ship.

## 2.1 Metal working operations

Shipbuilding requires a wide range of metalworking operations to create hull & internal structure, piping, machinery, and other essential parts of a vessel. Here are some common metalworking operations in shipbuilding:

- **Cutting:** Cutting operations involve the removal of excess material from metal sheets, plates, or profiles. Techniques such as shearing, sawing, plasma cutting, or laser cutting are used to achieve precise dimensions and shapes required for ship components.
- **Welding:** Welding is a crucial process in shipbuilding that involves joining metal parts together using heat and pressure. Different welding techniques, including arc welding, gas welding, and resistance welding, are employed to create strong and durable connections between metal components.
- **Forming and bending:** Shipbuilders utilize various techniques to shape metal sheets and profiles into desired forms. These include rolling, bending, stamping, and press brake operations. Forming and bending operations help create curved and contoured sections of the ship's structure.
- **Machining:** Machining operations involve the use of machine tools to shape metal components with high precision. Operations such as drilling, milling, turning, and grinding are performed to create holes, threads, smooth surfaces, and precise dimensions in ship components.
- **Surface treatment:** Surface treatment operations are performed to protect metal components from corrosion, improve their appearance, and enhance their performance. These operations include cleaning, priming, painting, galvanizing, and applying protective coatings to the metal surfaces.
- **Assembly:** Assembly operations involve joining various metal components together to construct the ship's structure. This includes fitting, bolting, riveting, and fastening metal parts to create the hull, superstructure, compartments, and other sections of the vessel.
- **Inspection and quality control:** Throughout the metalworking operations in shipbuilding, inspections and quality control measures are essential to ensure that components meet specified standards and requirements. Non-destructive testing methods, visual inspections, and dimensional checks are performed to verify the integrity and quality of the metalwork.

These metalworking operations, along with other specialized processes, contribute to the construction of ships that are structurally sound, durable, and capable of withstanding the demanding conditions of the marine environment. Skilled metalworkers, in collaboration with engineers and naval architects, play a crucial role in executing these operations to achieve the desired shipbuilding outcomes.

## 2.2 Surface treatment

Integrated material management into the Digital Twin, it is necessary to add enhancements to integrated material management include the ability to assign materials to parts under an assembly, providing a more complete view of materials used. These leverages new capabilities in the Digital Twin to support more holistic materials data management with an integration to CAD. Support for coatings and surface treatments allows you to understand changes to material properties and provide better traceability back to source materials, *Tsamis et al. (2020)*.

Digital Twins, when integrated with material management systems, can play a vital role in making better sustainability choices in shipbuilding and other industries, *Ölçer et al. (2020)*, *Patil et al. (2018)*.

By leveraging Digital Twins integrated with material management systems, manufacturers can make informed decisions (through a mobile device as idealistically represented in Fig.5), reduce their environmental footprint, and contribute to a more sustainable future in the shipbuilding industry and beyond.



Fig.5: Digital Twins integrated material management for better sustainability choices

Users can leverage compound materials to support coatings that are applied to materials and understand impacts on mass calculations and compliance.

### 2.3 Ship maintenance and repair

The new service and maintenance model, bringing the Digital Twin to sea shipping in choppy waters. A ship in the dock or in the berth is like a void property on the rental market: it costs a lot of money (crew, stores, insurance, mortgage, etc.) yet it brings no revenue. As the US Navy Rear Admiral Grace Hopper (1906-1992) said once: “A ship in harbor is safe, but that’s not what ships are built for.”

As the economic slowdown continues to impact the already overcrowded shipping industry, ship owners and operators are looking to maximize profit margins by lowering operational costs and improving vessel availability. At the same time, the rise of Information and Communication Technology (ICT) is bringing data collection, exchange, and analysis to an unprecedented level, opening new horizons for shipping companies and shipbuilders alike. So how can the marine industry capitalize on this sea of newly available data to reduce operational costs and increase vessel availability?

Transitioning to a service-oriented business model, overcapacity in the shipping market means increased competition in the newbuild market and shrinking orderbooks for most shipyards. As a result, shipbuilders and marine suppliers have been looking to diversify their revenue streams by offering service and maintenance, until now typically performed by specialized ship repair yards, and in some instance, leasing packages as part of a portfolio traditionally focused on production and sales. This more continuous, less risky source of revenue has become increasingly important for many yards and suppliers, especially in the naval and yachting segments.

This moves from product-only to a product-and-service business model makes sense for many reasons. First, having built the vessel, shipyards have all design and equipment details on hand for easy reference. Second, shipyards already have a relationship with the vessel owner/operator.

The need for a new maintenance model. As ships become more digital and highly technological, the number of cables and complex components onboard increases. Without a significant way to effectively coordinate maintenance schedules for all onboard systems, a vessel may be out of service for unnecessary periods of time, with a direct impact on profitability for ship owners and operators. Shipyards must find a way to optimize service and maintenance operations. In order to fulfil this new way of interaction between shipyards and ship owners, a new scalable maintenance model is required.



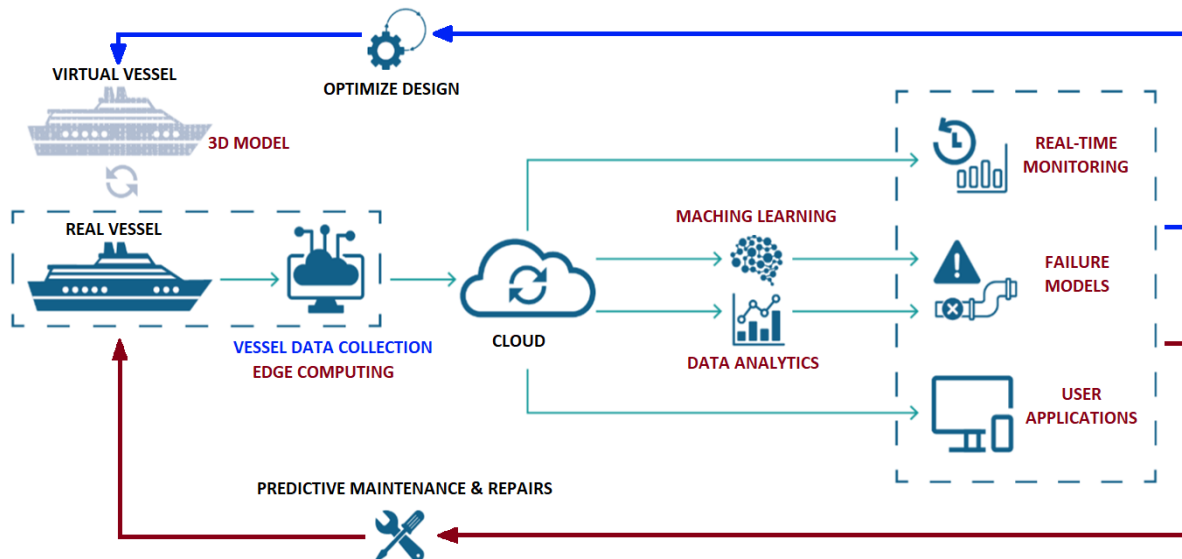


Fig.6: Leveraging Digital Twins with real data diagram

Key developments in ICT and digitalization technologies enable shipowners/operators and shipyards to adopt a fully integrated approach to ship service and maintenance. This approach, Fig.6, relies on implementing a service data collection and management system that links to the comprehensive Digital Twin as the single source of truth for all vessel performance and service needs. It facilitates shipyards' transition to a greener industry.

### 3. Shipbuilding and related environmental impacts of shipping

Shipbuilding and shipping have significant environmental impacts that arise throughout the lifecycle of a vessel. Here are some key points regarding shipbuilding and related environmental impacts of shipping:

- **Greenhouse Gas Emissions:** The shipping industry is a substantial contributor to the global greenhouse gas emissions. Vessels mainly emit carbon dioxide (CO<sub>2</sub>), which is a key contributor to climate change. Other greenhouse gases radiated by ships include sulphur oxide (SO<sub>x</sub>) and nitrous oxide (N<sub>2</sub>O). The shipbuilding process also produces CO<sub>2</sub> emissions due to energy-intensive manufacturing processes.
- **Air Pollution:** Ships emanate pollutants that can have undesirable effects on air quality. Together with greenhouse gases, marine artifacts release nitrogen oxides (NO<sub>x</sub>), sulphur dioxide (SO<sub>2</sub>) and particulate matter (PM). These emissions can contribute to acid rain, formation of smog and respiratory problems.
- **Ballast Water Discharge:** Ballast water is essential for ship stability and is often taken on board in one location and discharged in another. However, ballast water can carry non-native species, resulting in the introduction of invasive marine organisms into new ecosystems, which can harm biodiversity and disrupt local ecosystems.
- **Noise Pollution:** Shipping activities generate significant underwater noise, which can disturb marine life, particularly marine mammals that rely on sound for communication and navigation. This noise pollution can interfere with feeding, mating, and migration patterns, impacting marine ecosystems.
- **Fuel Consumption and Efficiency:** The fuel consumption of ships is substantial, particularly in larger vessels. High fuel consumption not only leads to higher emissions but also contributes to resource depletion and energy inefficiency. Improving fuel efficiency through technological advancements and operational measures can reduce environmental impacts.
- **Waste Generation:** Shipbuilding and ship operations generate various forms of waste, including sewage, solid waste, and hazardous materials. Improper disposal or inadequate waste management practices can result in marine pollution, threatening marine ecosystems and wildlife.

- **Ship Recycling:** Ship disposal and recycling can have significant environmental and health impacts if not carried out properly. Improper shipbreaking practices can result in pollution, worker safety hazards, and the release of hazardous materials into the environment. Sustainable ship recycling practices aim to minimize environmental and social impacts.

To mitigate these environmental impacts, the shipping industry is increasingly adopting measures such as adopting cleaner fuels, implementing energy-efficient technologies, optimizing operational practices, and complying with international regulations like the International Maritime Organization's (IMO) regulations on emissions and ballast water management.

It is essential for shipbuilders, shipowners, and the maritime industry to prioritize sustainability, embrace eco-friendly technologies, and promote responsible practices throughout the entire lifecycle of ships to minimize environmental impacts and work towards a more sustainable shipping industry.

### 3.1 Reducing environmental impacts due to propulsion

Reducing environmental impacts due to propulsion, and generation of energy consumption, in the shipping industry requires a combination of technological advancements, operational practices, and regulatory measures. Here are some strategies that can help minimize the environmental footprint of propulsion in shipping:

- **Alternative Fuels:** Transitioning from conventional fossil fuels to cleaner alternative fuels is a critical step towards reducing greenhouse gas emissions. Low-sulphur marine fuels, biodiesel, Liquefied Natural Gas (LNG), and biofuels are some of the viable options that produce fewer harmful emissions compared to traditional heavy fuel oils.
  - **Energy Efficiency Technologies:** Investing in energy-efficient propulsion technologies is one of the most effective ways to reduce environmental impacts. Advancements in engine design, such as high-pressure and electronically controlled fuel injection systems, waste heat recovery systems, and advanced propulsion systems, can significantly improve fuel efficiency and decrease emissions.
- Wind-Assisted Propulsion:** Implementing wind-assisted propulsion systems, like wind sails or rotors, can harness the power of the wind to supplement engine power. This approach can substantially reduce fuel consumption and emissions, especially during favourable wind conditions. Leverage single simulation for hydrodynamic and aerodynamic to directly compare the efficiency of Wind Assisted Ship Propulsion (WASP) devices and to determine the potential power saving. For example, making a simulation we can compare different solution like the above example, exposed in Fig.7, where two solid sails reduced the power consumption 24% in comparison with the second Flettner rotor that is reduced 14%.

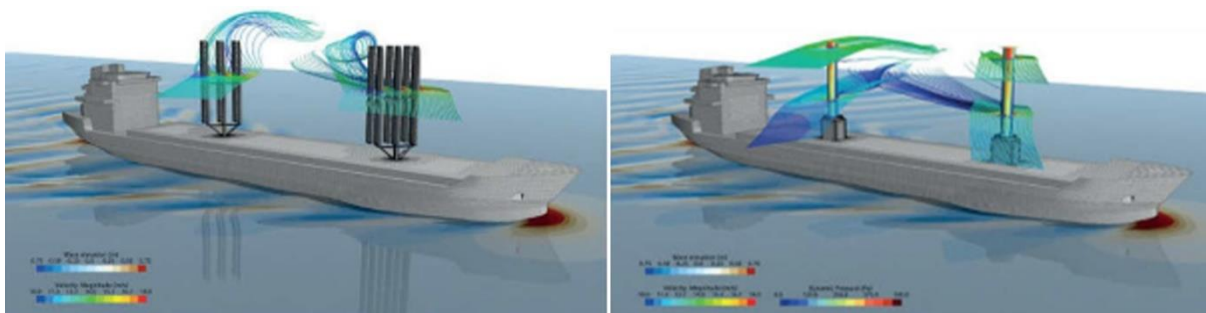


Fig.7: Digital Twins supporting a better wind-assisted propulsion

- **Hybrid Propulsion Systems:** Combining traditional fossil fuel engines with electric or battery-based propulsion systems allows ships to operate more efficiently. Hybrid solutions can be particularly effective during low-speed operations or in ports, where engines can be partially or fully shut down, leading to emissions reduction.

- **Slow Steaming:** Operating vessels at reduced speeds, known as “slow steaming”, can significantly cut fuel consumption and emissions. While this approach may lead to longer transit times, it offers considerable environmental benefits and has been adopted by some shipping companies voluntarily.
- **Hull Design Optimization:** Advancements in hull design, such as air lubrication systems, hull coatings, and streamlined shapes, can reduce drag, and improve fuel efficiency, and combine with other technologies, can facilitate the fuel consumption as consume in a software like in Fig.8.

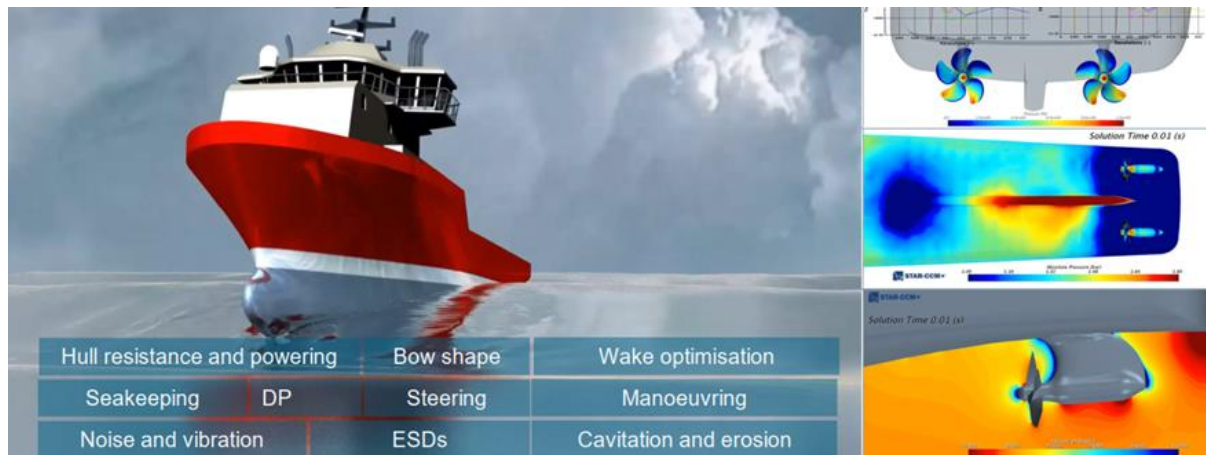


Fig.8: Digital Twins supporting and optimizing new technologies

- **Anti-Fouling Measures:** Applying environmentally friendly anti-fouling coatings to ship hulls helps prevent the growth of marine organisms, which can increase fuel consumption and emissions.
- **Cold Ironing:** Encouraging ports to provide shore power facilities, also known as "cold ironing" or shore-to-ship power, enables ships to turn off their engines while docked and use onshore electricity. This eliminates port-related emissions and improves air quality.
- **Regular Maintenance and Retrofits:** Ensuring that ships undergo regular maintenance and implementing retrofitting projects to upgrade older vessels with modern, eco-friendly technologies can lead to substantial efficiency gains.
- **Regulatory Compliance:** Governments and international organizations play a vital role in setting and enforcing stringent environmental regulations for the shipping industry. Adherence to regulations like the International Convention for the Prevention of Pollution (MARPOL) helps to limit pollutant discharges and emissions.
- **Research and Innovation:** Continued research and development in propulsion technologies, including zero-emission options like hydrogen fuel cells or ammonia-based systems, can pave the way for a more sustainable future for shipping.

By adopting a combination of these strategies and promoting sustainable practices, the shipping industry can reduce its environmental impacts significantly and contribute to global efforts to combat climate change and preserve marine ecosystems.

### 3.2 How reduce the environmental impacts during the ship design

European Commission Proposal for Directive on Eco-design requirements for Energy-Using products states “80% of a product’s sustainability impact is determined in its design phase”.

The new ship designs must handle the current market demands:

- Net Zero commitments and regulations.
- Capital flowing toward sustainability.
- Resource scarcity and the transition to the circular economy.
- Customers are demanding it.

Design engineers can no longer design products by only looking at performance, cost, and quality. To design more sustainable products, they need to look at their processes through the lens of sustainability:

- **Flexible and reliable:** the products of tomorrow need to easily be upgradable and repairable and adaptable to extend their life. The longer you can keep a product in use, the better.
- **Resource efficiency:** Our products need to be designed to deliver greater value while using fewer materials, water, and chemicals, not only in their use phases but also during the manufacturing and maintenance phase.
- **Decarbonized:** meaning design products to produce less CO<sub>2</sub> across the lifecycle. This can be achieved through energy efficiency, electrification, fuel efficiency, resource efficiency etc.
- **Circular:** Reuse and recovery of materials and parts need to become integral to the design process, not seen as a bonus.
- **Innovative:** leveraging new materials, carbon-free technologies, and new production methods such as additive manufacturing.
- **Energy efficient:** It means using less energy in the manufacturing of the product as well as its usage and maintenance. This is of course also the most cost-effective way to decarbonize.

#### 4. Ship dismantling and recycling

Ship dismantling and recycling, also known as shipbreaking, is the process of dismantling and recycling decommissioned or end-of-life ships. It involves the dismantling and disposal of ships in an environmentally and socially responsible manner. Here are some key points regarding ship dismantling and recycling:

- **Ship Recycling Process:** Ship recycling typically involves several stages. Initially, the ship is prepared for recycling by removing hazardous materials such as asbestos, PCBs, and other toxic substances. Then, the shipbreaking process begins, which includes the mechanical cutting and dismantling of the vessel. Various equipment and machinery are used to dismantle and separate different materials, such as steel, non-ferrous metals, and other recyclable components.
- **Environmental and Social Challenges:** Shipbreaking can present environmental and social challenges if not carried out responsibly. Improper shipbreaking practices can lead to pollution, marine ecosystem damage, and risks to human health and safety. Toxic substances can be released into the environment if not handled properly, and workers may be exposed to hazardous conditions. These challenges highlight the importance of promoting safe and environmentally sound ship recycling practices.
- **Certification and Standards:** Various certification schemes and standards have been developed to promote responsible ship recycling practices. These include the Hong Kong Convention, the EU Ship Recycling Regulation, and industry initiatives such as the Responsible Ship Recycling Standards (RSRS) and the Ship Recycling Transparency Initiative (SRTI). These frameworks aim to ensure transparency, accountability, and the adoption of sustainable practices in the ship recycling industry.
- **Reasons for Ship Dismantling:** Ships are dismantled and recycled for several reasons, including age, obsolescence, damage, or the end of their operational life. Ship dismantling allows for the recovery and reuse of valuable materials and components, reduces the environmental impact of abandoned vessels, and ensures safe disposal of hazardous materials.
- **International Regulations:** To address the environmental and social concerns associated with ship dismantling, international regulations have been established. IMO adopted the Hong Kong International Convention for the Safe and Environmentally Sound Recycling of Ships in 2009. The convention aims to ensure that ships are recycled in an environmentally and socially responsible manner. However, it has yet to enter into force.
- **Sustainable Ship Recycling:** Sustainable ship recycling practices prioritize the protection of the environment, worker safety, and the proper handling of hazardous materials. This includes the safe disposal of toxic substances, proper management of waste and by-products, and the implementation of occupational health and safety measures. Sustainable ship recycling also emphasizes the



recycling and reuse of materials and components to reduce resource consumption and promote circular economy principles.

Efforts are ongoing to improve ship recycling practices globally, promote worker safety, and protect the environment. The aim is to establish a more sustainable and responsible approach to ship dismantling and recycling, mitigating the environmental and social impacts associated with the end-of-life phase of ships.

#### 4.1 Environmental impact

It is important to focus on how to create a sustainable concept connected to sustainability requirements. It is key to capture the new requirements related to sustainability and evaluate them across every stage of the product lifecycle.

The application requirements management provides an enterprise with a systematic and repeatable solution for defining, capturing, engineering, managing, and leveraging sustainability requirements. It allows you to continuously verify conformance to these requirements throughout the product lifecycle, therefore facilitating requirements-driven design.

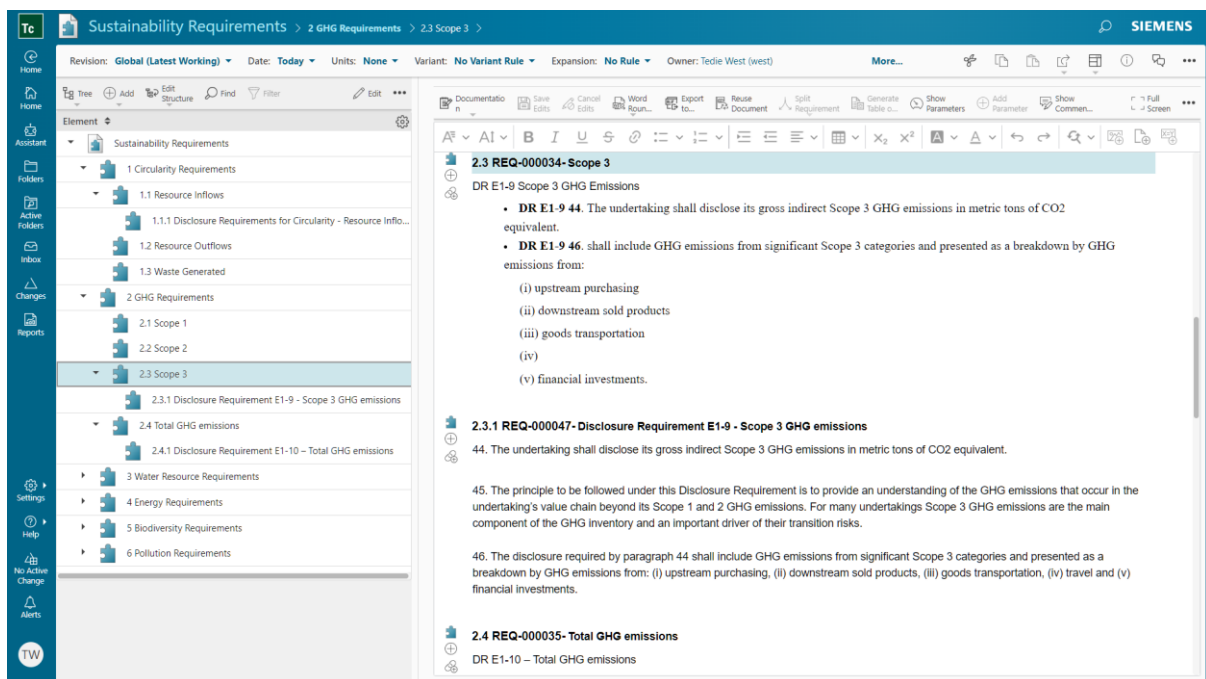


Fig.9: Sustainability requirements tool driving eco-design

Many designers struggle to make trade-offs between driving down Carbon Dioxide Equivalent (CO<sub>2</sub>e) emissions, reducing costs and addressing product performance demands all at once. It requires linking cost and CO<sub>2</sub> equivalent emissions along the value chain to identify the drivers and dependencies.

The Carbon Footprint Calculator software, enables organizations to measure, simulate and track their product carbon footprint early in the design phase. This approach capitalizes on the transparency and optimization that bottom-up target costing provides. It allows companies to calculate product carbon footprints in the same detailed way so they can set eco-design strategies such as: design for resource efficiency or design for recycling using an approach that integrates all aspects from product planning, development, and design process through the entire product lifecycle.

Manufacturer can use a bottom-up approach to roll up cost and CO<sub>2</sub>e emissions along the value chain, as each material, manufacturing, and overhead resource comes with both a financial cost and a CO<sub>2</sub>e emission cost. As an example of a product which it is possible to calculate the direct costs (material,

labour, equipment, tooling, energy consumption, and yield along the manufacturing process) with indirect cost (overheads, administration, and onetime cost allocations), it is worth it to highlight the TcPCM, a Siemens Product Costing tool, Fig.9. For the carbon footprint TcPCM follows the same bottom-up analysis workflow, aggregating all relevant emission factors of the product along the value chain. That means gathering data on the full set of emissions corresponding to direct costs, including for upstream activities for purchased goods, energy consumption, transportation, direct manufacturing labour, equipment, and tooling. It also means gathering data on the emissions associated with the indirect costs embedded in the product, such as for overheads.

Manufacturer can do all sorts of scenario analyses in the product-design phase, looking at the different levers to evaluate trade-offs. For instance, they can see what happens when it switches between plant locations, mix of energy resources, and logistics costs. It can compare the effects of switching to higher-efficiency production equipment with those of optimizing design by swapping materials or thinning out a component. The provided transparency gives component manufacturer a new level of flexibility. And it's present not just at the initial design or redesign phases but also when there's a need to change to suppliers that follow more sustainable practices or make any change at any point in the value chain.

## **5. Conclusions**

The concept of Engineering Marine Digital Twins with Sustainability offers a promising approach to address environmental challenges in the marine industry. By leveraging digital technologies, such as Digital Twins, throughout the engineering and design process, it becomes possible to integrate sustainability considerations from the very beginning.

The use of Digital Twins permits reduction of waste, optimization of material consumption and maximization of component and material value. This approach aims to decouple economic activity from climate-damaging emissions and the depletion of finite resources.

Furthermore, Engineering Marine Digital Twins align with the principles of the Circular Economy, where resources are utilized in a closed-loop system to minimize waste and promote sustainable development. By preserving, enhancing, or restoring the value of materials, the marine industry can contribute to a more sustainable and responsible approach.

Transparency and comprehensive data play a crucial role in assessing and addressing the environmental impacts of products. ESG criteria provide a framework for evaluating and improving the industry's impact on climate change, water and land use, biodiversity, and the Circular Economy. These criteria enable informed decision-making and help align corporate activities with global sustainability goals, such as those outlined in the Paris Agreement.

While the direct environmental impact of shipbuilding, maintenance, and repair poses challenges, the industry has an opportunity to improve its environmental performance. By implementing sustainable practices and embracing a life-cycle approach to ships, the industry can demonstrate its commitment to environmental responsibility and contribute to a cleaner and more sustainable future.

In summary, Engineering Marine Digital Twins with Sustainability represents a proactive and holistic approach to address environmental impacts in the marine industry. Through the integration of digital technologies, sustainability considerations can be embedded into engineering and design processes, enabling the industry to minimize its ecological footprint, optimize resource utilization, and foster a more sustainable and resilient maritime sector.

## References

- AOUAD, T.; SUCCAR, B.; KASSEM, M. (2019), *Sustainable Digital Twin: A Conceptual Framework*, Advanced Engineering Informatics
- BALDAUF, M.; FISCHER, M.; WALDECK, B. (2020), *Towards a Sustainable Maritime Industry: Energy Management and Efficiency Optimization Through Digital Twin Technology*, Energies
- DNV GL (2014), *The Future of Shipping*, DNV, Høvik
- HUANG, F.; CUI, W.; MORRISON, J.R. (2021), *Digital Twins in Marine Science: Applications and Challenges*, Frontiers in Marine Science
- LR (2015), *Global Marine Technology Trends 2030*, Lloyd's Register, Qinetiq, University of Southampton, Southampton
- LU, M.; WANG, X.; YU, Y. (2020), *Digital Twins and Simulation Technologies for Sustainable Built Environment*, Advanced Engineering Informatics
- MOSTAFA, S.; SUCCAR, B.; KASSEM, M. (2017), *Towards a Comprehensive Digital Twin for Sustainable Construction Project Management*, Procedia Engineering
- ÖLÇER, A.I.; YAYINLI, N.O.; ŞAHİN, M.N. (2020), *Twin Ships: An Application of Digital Twin Concept in the Design and Operation of Ships*, Int. Congress of Maritime Technological Innovations and Research
- PATIL, S.P.; MODAK, J.P.; PATIL, S.P. (2018), *Digital Twin: The Backbone for Industry 4.0 and Industrial IoT*, Procedia Computer Science
- TSAMIS, C.; DIMOPOULOS, G.; KYRITSIS, D. (2020), *Digital Twins for Energy Efficiency in Maritime Systems*, Energies
- WALKER, S. (2013), *The Handbook of Design for Sustainability*, Bloomsbury Academic

# Manual vs Automatic Data Collection for Energy Efficiency Management: The Old Debate

Matteo Barsotti, Oceanly, Genova/Italy, [matteo.barsotti@theoceanly.com](mailto:matteo.barsotti@theoceanly.com)

## Abstract

*Manual or Automatic? This a question that a shipowner or ship manager makes to himself many times in recent years. It's a topic that holds immense significance in the maritime industry, especially when we consider the crucial role data plays in performance monitoring, emissions control, condition-based maintenance, optimization, and energy efficiency. Let's then dive in and discuss the benefits of both data gathering, and how we can bring them together to ensure accurate and reliable data gathering. By bridging the gap between these reporting, we can pave the way for a more efficient, environmentally conscious, and prosperous maritime industry.*

## 1. Introduction

In the recent years there were many new regulations from IMO, European Union, and other regulatory entities with the aim of the decarbonization; EU MRV data collection, the IMO- DCS data collection, the HFO 3,5% ban, the CII introduction and then the new EU ETS that is now approaching.

But also “the best is yet to come” with the new Fuel EU Maritime Fit for 55 regulations from 2025 the global GHG emission for shipping companies including the Well-to-tank emission and the net-zero GHG emission by or around 2050 just agreed in the last MEPC 80 held in July.

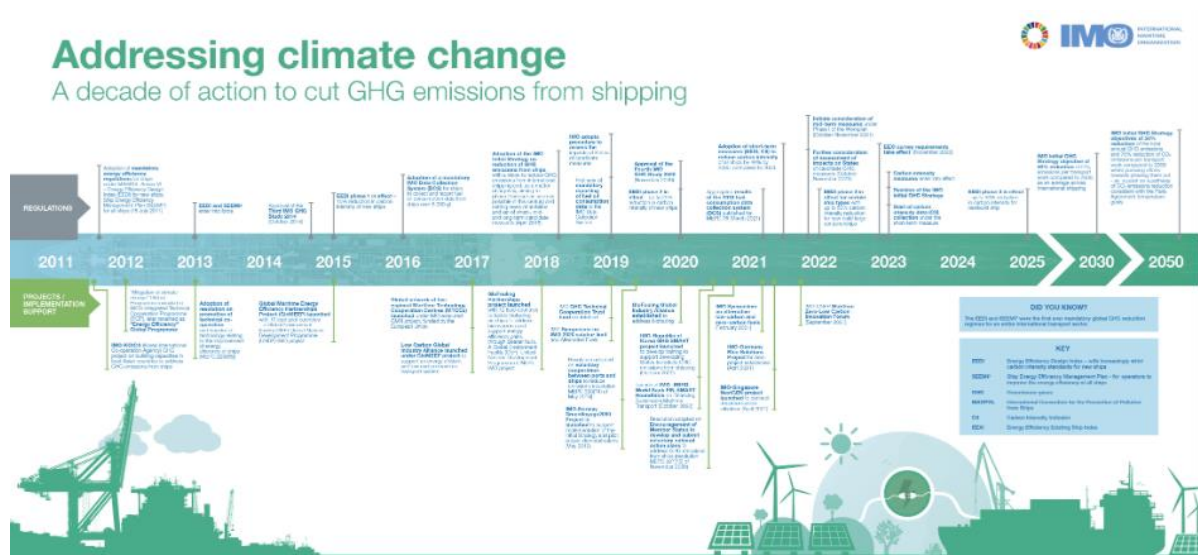


Fig.1: IMO timeline for decarbonization

All these new regulations have one big prerequisite, receiving good data from the ship in the fleet, that's why it is extremely important to discuss about how the data are collected. It has also to be said that till today the data reported and specifically emission reported were just compliance but from tomorrow emission will be money with the entrance into force of EU ETS. So here we are to dive in the old debate of this industry, Manual or Automatic? As we will see below both can have pros or cons but none of them alone can provide the correct assurance that what is recorded is correct. From 2017 to 2022 the reporting of the emission was just for compliance with MRV regulation and then for IMO-DCS but, apart from spot checks on the data by Verifier and Recognized Organization the content of the emission reports were not very considered in the shipping company. I think we all remember the first EU MRV report with those impossible data extracted from the Thetis database.



For sure the so-called Sustainability put attention on the Emission in general but still the general feeling was not to worry too much. A very big step forward has been done with EEXI and CII because these put pressure on the shipowner because with these regulations the non-compliance means ship not commercially attractive because of its performance. But still there was room for not to worry because for EEXI there is an escape plan, EPL or SHAPOLI and the CII is a 3-year plan so some ships can still survive, and this of course just help to post-pone big decisions.

Now the time has come, with the upcoming EU-ETS regulation that will enter into force next year, every emission reported is money. So, it is time to check the reporting process and assure that what will be reported is the truth.

## 2.Manual Reporting

This traditional approach has been the backbone of the maritime industry for years, enabling ship operators to closely monitor and report essential information.

Despite the growing prominence of automated systems, manual reporting still holds relevance in certain contexts. Manual data collection allows for more personalized observations, as crew members can report on specific incidents or conditions that may not be captured by automated sensors. This human element can provide valuable insights and context, especially in situations where subjective judgment is required. With manual reporting, operators can detect anomalies, identify maintenance needs, and make real-time decisions based on their intimate knowledge of the ship.

Moreover, manual reporting can be more accessible and cost-effective for smaller vessels or those with limited resources. It eliminates the need for substantial technology investments and complex installations. Additionally, manual reporting can foster crew engagement and awareness of the ship's performance, encouraging a culture of responsible energy consumption and environmental stewardship.

DATA POINT	VALUE	STANDARD UNIT
<b>General</b>		
Position	HHMMSS.SS,III,II,a,yyyy.yy,a (UTC, Latitude, N or S, Longitude, E or W)	
Time	yyyy-mm-ddThh:mm:ssZ	
Vessel Name	Text (Translated from ASCII)	
IMO Number	XXXXXXXX (Seven Digits, Translated from ASCII)	
Ship Type	Text (Select from prescribed list)	
Voyage Number	Text (Manual Input)	
Leg	HHMMSS.SS,III,II,a,yyyy.yy,a,XXX (as with Position above, plus Three digit Waypoint ID)	
Remarks	Text (Manual Input)	
<b>Port and Route Information</b>		
Departure Port	XX XXX (UN/LOCODE Designation)	
Departure Time	yyyy-mm-ddThh:mm:ssZ	
Destination Port	XX XXX (UN/LOCODE Designation)	
ETA PBP	yyyy-mm-ddThh:mm:ssZ	
ETA Berth	yyyy-mm-ddThh:mm:ssZ	
ETA VTS	yyyy-mm-ddThh:mm:ssZ	
Distance to next waypoint NM	NM	
Distance to next waypoint km	km	
Distance to destination port NM	NM	
Distance to destination port km	km	
Projected Speed kn	kn	
Projected Speed km/h	km/h	
Voyage Time	hrs	
<b>Speed and Distance</b>		
Boiler Electricity Consumption	kWh	
Generator Production	kWh	
Draft	m	
Draft Fore	m	
Draft Aft	m	
DWT	t	
Heading	°	
CP / Order Speed	kn	
Observed Distance NM	NM	
Observed Distance km	km	
RPM	r/min	
Slip %	%	
Engine Distance NM	NM (Calculated from RPM multiplied by propeller pitch)	
Engine Distance km	km (Calculated from RPM multiplied by propeller pitch)	
Speed Over Ground kn	kn	
Speed Over Ground km/h	km/h	
Speed Over Water kn	kn	

Fig.2: Standardised Vessel Dataset (SVD) for noon reports

In 2023 Smart Maritime Network with its Standardised Vessel Dataset (SVD) tried to standardize the reporting and not spread the exact same data in twenty different ways and this could be a real improvement in the industry so every party can use the same data using the same language.

Reporting in general is more and more required by many parties even inside the same companies and this may lead to several reports to be prepared and sent by the ships; this could lead to error in reporting because of repetitive actions and minor or big differences.

Apart from the accuracy perspective, it is also to be said that commercially speaking, the TCP calculation are all based on manual reporting, so still such reporting cannot be completely abandoned in any case. Nevertheless, manual reporting has its drawbacks. It heavily relies on human compliance, which may lead to inconsistent and delayed data collection. Crew members are susceptible to human error, and the process can be time-consuming and labour-intensive, diverting their focus from other critical tasks.

### 3. Automatic Reporting

Automatic data reporting has emerged as a powerful tool in this era of technological advancements. By leveraging sensors, data loggers, and real-time monitoring systems, automatic reporting offers unparalleled accuracy, efficiency, and timeliness. It empowers ship operators to detect performance inefficiencies, optimize voyage planning, and proactively address maintenance requirements. The data-driven insights obtained through automation enable operators to maximize fuel efficiency, reduce emissions, and enhance overall operational efficiency.

With automated systems, data can be collected in real-time, ensuring up-to-date information for analysis and decision-making. This real-time data empowers us to identify issues promptly and take immediate corrective actions, ultimately leading to improved performance, reduced emissions, and enhanced energy efficiency.

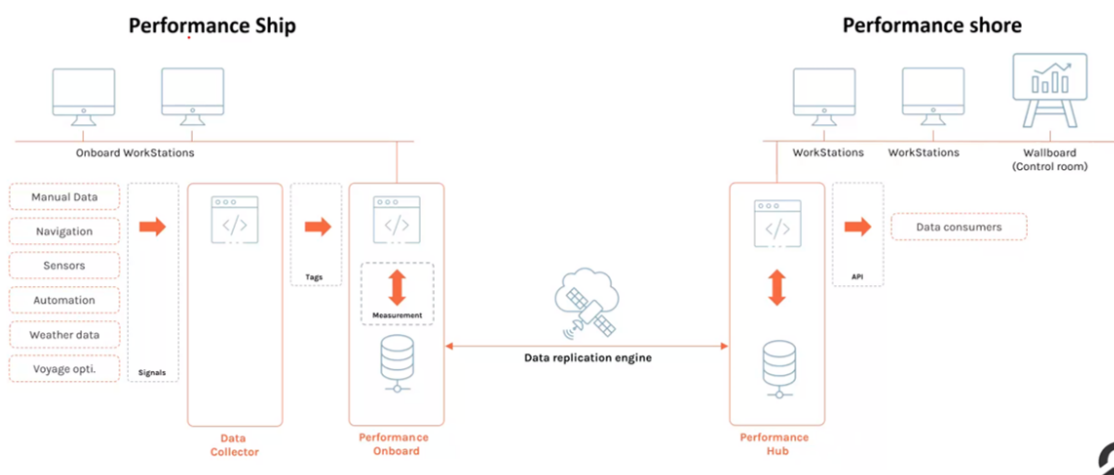


Fig.3: Data synchronization between ship and shore

Furthermore, automation minimizes human error and eliminates the need for manual data entry, reducing the risk of inaccuracies and inconsistencies. By leveraging sensor technologies, monitoring equipment, and data analytics tools, we can obtain comprehensive insights into ship operations, enabling us to optimize maintenance schedules and mitigate potential failures. This not only enhances safety but also maximizes the vessel's lifespan and reduces downtime.

However, automatic data collection does have its limitations. It requires significant investment in advanced technologies and infrastructure. Some ships, especially older ones, may not be equipped with the necessary sensors and systems, making it challenging to implement fully automated data

collection and reporting. Additionally, maintenance and calibration of these systems can be complex and time-consuming, demanding specialized expertise.

Nevertheless, the actual framework of the MRV, both for EU and UK, still rely on inputs from the ship to identify Port of Calls, voyage to drydock, cargo operation outside port area and many other peculiar conditions that is impossible to manage automatically.

#### **4. The Hybrid solution**

Now, you may be wondering: Can these seemingly opposing approaches coexist? Absolutely! In fact, the key lies in finding harmony between manual and automatic reporting. Rather than viewing them as adversaries, we should embrace them as complementary forces. Automated systems can collect real-time data on performance, emissions, and maintenance indicators, while crew members can contribute their observations through standardized manual reporting. Manual reporting provides essential contextual knowledge and human expertise that automated systems may lack. It serves as a vital check and balance, ensuring that the data obtained through automation aligns with the realities on board; in this era of rapid technological advancements, let us not forget the value of human expertise and experience.

The marriage of manual and automatic reporting ensures that we have reliable information at our disposal, allowing us to meet regulatory requirements effectively. This fusion allows for a comprehensive dataset that provides accurate insights while incorporating human judgment and situational context.

To ensure the effectiveness of such a system, it is imperative to provide crew members with adequate training and clear guidelines for manual reporting. This will help standardize the data collection process, minimize errors, and ensure consistency across vessels and fleets. Furthermore, regular audits and checks should be conducted to verify the accuracy and reliability of the data, guaranteeing compliance with regulatory requirements.

This marriage is possible if:

- 1) Manual Reports can be fed with the automatic data and then leave the crew the burthen to just check the correctness of the data. Each field is capable to:
  - a. Recall a specific value in a specific datetime.
  - b. Integrate a specific value since the previous report (i.e., the sum of the Main Engine Flowmeter consumption)
  - c. Integrate a specific value since the beginning of the leg (i.e., average speed in the voyage leg)
- 2) Every field of the report can be configured to have a plausibility check but also to copy from previous report because this helps the crew to not insert the same values in all the reports.
- 3) The office system should also highlight any deficiencies in the sensors but also in the reporting using Alerting otherwise we still have a manual reporting but onshore by operators.

Not only the reporting method should be hybrid but also the receiving system should; a complete and competitive system should have the possibility to support, Automatic, Manual and Hybrid reporting to have a consistent and a standard reporting inside the same company because the company could have new ship but also old ones where implementing an automatic data collection could be very unworthy.

Noon Report

Date (Local Time)  Elapsed time since last report  [Fetch cluster data](#)

Notes  
Test

General and Movement Present Weather at Noon Average Past Weather Sailing Conditions Schedule (ordered speed and fuel mode) ROB and Consumption Cargo Tanks GCU / Boiler Spray / Sub-Cooler

Voyage Number  Voyage Leg Number  Voyage Type

Latitude  Longitude  Course over Ground  Speed over Ground [kn]  Max 50

Port of arrival

ETA  Distance to Go [nm]  Required

Daily Distance Made Good [nm]  Daily Distance GPS [nm]  Daily Distance Speed Log [nm]  Daily Distance Engine [nm]  Distance for Safe Condition [nm]  Distance in ICE [nm]

Fig.4: Hybrid reporting

## 5. Conclusion

So, it is important to understand that the manual versus automatic data reporting debate is not an "either-or" situation. It's an opportunity for collaboration and integration. Both methods have their strengths, and by bringing them together, we unlock a powerful synergy. Technology enables us to gather data efficiently, while manual reporting offers the human touch necessary for validation and cross-verification. By embracing both approaches, we can navigate the challenges posed by performance monitoring, emissions control, condition-based maintenance, optimization, and energy efficiency more effectively.

Together, let us forge a path towards a more sustainable and responsible maritime industry, where manual and automatic reporting work hand in hand to drive progress and chart a course towards a brighter future.

## References

<https://smartmaritimenetwork.com/standardised-vessel-dataset-for-noon-reports/>

IMO (2023) *IMO's work to cut GHG emissions from ships*, Int. Mar. Org., London

# Autonomous Robotic In-Water Hull Inspection for Fouling and Structural Condition

Arnau Carrera Viñas, subdron, Lauterach/Austria, [arnau.carrera@subdron.com](mailto:arnau.carrera@subdron.com)

Thomas Vonach, subdron, Lauterach/Austria, [thomas.vonach@subdron.com](mailto:thomas.vonach@subdron.com)

## Abstract

*This paper shows the capabilities of fully autonomous data collection with minimized user interaction in confined environments, plus the use-case specific automatized data processing and labeling. Subdron's proprietary technology for highly accurate subsea positioning in confined environments allows generating 3D reconstructions of any structure at a unique level of accuracy even in zero visibility. This creates added value for port authorities in monitoring underwater assets and applying predictive maintenance on it. For ship owners, it provides the possibility to monitor the status of the hull and receive accurate information about the fouling status: a 3D map of biofouling – exact position and quantity of it. This service offered by subdron, will significantly increase quality of the hull monitoring process, that will be executed in shorter time and at lower cost.*

## 1. Robotic in-water inspection

The increasing demand for remotely conducted in-water surveys (IWS) requires sophisticated automated concepts. Subdron GmbH, [www.subdron.com](http://www.subdron.com), has initiated 'Robotics as a Service' applications that can support infrastructure monitoring in ports and on waterways, offshore structures, and ships, Fig.1, Vonach and Carrera Viñas (2023). Subdron specialises in the development of navigation algorithms, autonomous underwater vehicle (AUV) navigation in the object-relative range, and the collection and evaluation of inspection data. The idea was to develop an AUV as an application-related overall system suitable also for in-water ship hull surveys, both for structural integrity and extent of biofouling. The latter has received increasing attention in the maritime community due to the focus on ship hull management, especially in the context of proactive hull cleaning.

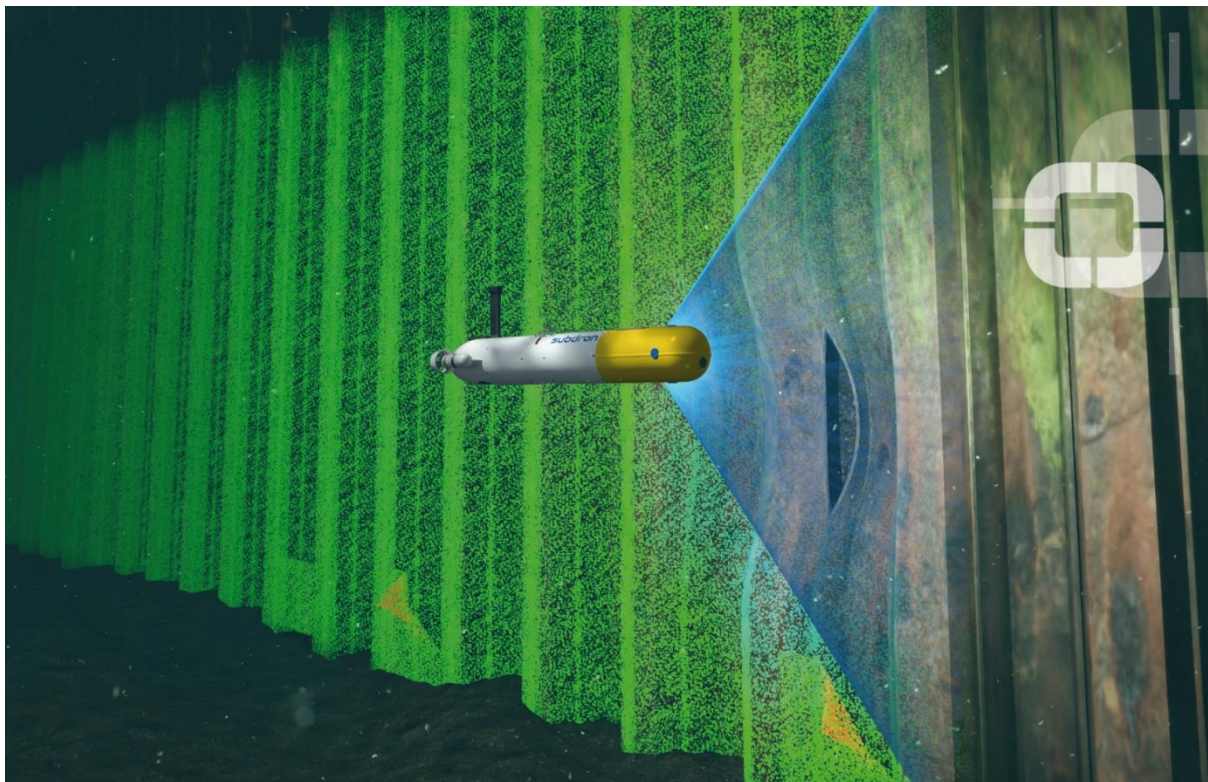


Fig.1: Subdron in-water scanning



The use of proprietary relative object navigation (RON) allows dispensing with cost-intensive external positioning systems. Currently, subdron is in the process of offering the mission expertise it has accumulated over the past years as a project related service. The resulting advantage for port authorities and diving companies is that technology and underwater robotics expertise are available exactly when and where they are needed, without having to develop their own technologies. This also eliminates the clients' need for specialists who need to be continuously trained and retained within the company.

Robotic in-water inspection of ships is in increasing demand for assorted applications:

- In-water surveys (IWS) – scanning ships for structural integrity, for regular surveys and post-damage surveys as required by classification societies (Under water inspections in lieu of drydock (UWILD)), e.g. *Banken et al. (2022)*, *Caponi (2022)*
- Geometry digitalization – scanning to obtain the hull and propeller geometry which may be required for retrofits or simulations to obtain hydrodynamic knowledge bases for trim optimization or performance monitoring, e.g. *Paranhos (2020)*, *Bertram and Harries (2022)*
- Biofouling documentation – before and after cleaning events, screening for biofouling, e.g. *Guéré and Gambini (2021)*, *Doran (2022)*, *Caponi (2023)*, *Lander (2023)*
- Security - scanning of ship hulls regarding smuggled goods or other unwanted foreign objects. The same applies to the increasing demand for remotely conducted in-water surveys (IWS) for hull inspections to comply with classification regulations, e.g. *Stein (2018)*, *Stein and Parviainen (2020)*.

Traditionally, divers have been used for in-water inspection tasks, often performing their analysis under great time and cost pressure in sometimes murky visibility in the sediment-laden waters of inland ports. Remotely operated vehicles (ROVs) are now increasingly used for these tasks, but only qualified pilots can perform the measurements. They depend on sight – so optimal positioning is also a challenge. In the future, these tasks will be ideal areas of application for specially equipped AUVs.

Using a third-party provider like subdron, the technology and underwater robotics expertise are available exactly when and where they are needed, without having to develop in-house expertise and staff for only occasionally required services.

## **2. Autonomy for Underwater Robotics**

With the goal of autonomously collecting and processing underwater survey data, subdron GmbH has been putting the idea of 'Robotics as a Service' into practice. A complete system developed by subdron can move stably, safely, and autonomously in the object-relative range of 1-2 m using proprietary navigation algorithms. Navigating in very confined environments is also possible.

Specific environmental perception sensor technology integrated into the vehicle generates and processes data that is directly incorporated into the navigation algorithm. This is the core of subdron's proprietary relative object navigation (RON). RON can ensure that the vehicle always moves in the desired position and orientation to the object. The imaging sensor system is aligned in an ideal position and orientation to ensure the best possible data acquisition. This, in turn, results in every analysed structural area being imaged at the same resolution.

Thus, even demanding inspection tasks can be undertaken and evaluated with a high level of detail. Field tests of the systems were performed at the subdron test facility on Lake Constance, and in the ports of Hamburg and Bremerhaven, Fig.2, before commercial investigations for various port and shipping stakeholders have been conducted.



Fig.2: Vehicle after mission completion of customs ship hull inspection in the Port of Hamburg

### 3. High-Performance Underwater Carrier Vehicle

The carrier vehicle is the Sparus II AUV from IQUA Robotics, <https://iquarobotics.com/>, with software and hardware modified by subdron GmbH, Fig.3. It is a torpedo-shaped vehicle with mission-specific payload range and efficient hydrodynamics for long autonomous operation time. The hovering AUV is designed to operate in open water, has a length of 160 cm, a fuselage diameter of 23 cm and a weight of 52 kg in air. This makes it small, light, and manoeuvrable. With a speed of up to 3 kn and an operating time of 8-10 h, even extensive missions can be planned. An open software architecture based on a robot operating system (ROS) is used for mission programming, *Carreras et al. (2015)*.



Fig.3: Sparus II AUV carrier vehicle

For navigation on the water surface, the AUV uses a GPS antenna to determine its position. Underwater navigation uses an inertial navigation system (INS) to determine the AUV's acceleration and angular velocity in three-dimensional space. A downward-looking doppler velocity log (DVL) coordinates the exact direction of travel and speed over ground.

Classic sensor technology is also used for this AUV. A pressure sensor reports the current depth of the AUV. For open water operations, an ultra-short baseline (USBL) system is available to position the submerged AUV and maintain communication. However, due to frequency (multipathing, etc.), the USBL has limited use in a harbour area. All data acquired here is used to validate the position data during post-processing of the point clouds.

For bathymetry and side-scan applications, a 260 KHz multibeam echosounder (MBES), a 1.1 MHz side-scan sonar, and a 2.25 MHz MBES are available as a separate payload with full functionality. Depending on the environmental conditions, the AUV can be equipped with additional technologies such as cameras or lasers.

For maximum resolution, the optimum distance between the vehicle and the object to be measured is 1.5-2.5 m. If greater area performance is desired, this distance can be increased. However, greater area performance will result in lower resolution. Before a mission begins, the sensors of the entire system are calibrated to provide precise measurement results for up to one day. Should the mission require it, recalibration can be carried out quickly. With a resolution of 1 cm, the measurement accuracy is excellent for resolving even small structures.

Depending on mission requirements and desired data quality, subdrone can survey 1-2 km of a harbour wall or a complete ship hull within 8-12 h on a single battery charge. At present, usually 2-3 subdrone staff members are deployed to enter mission parameters (e.g. scan length and depth) into the system. Current R&D aims at developing capabilities to perform a mission with a "non-robotics expert" and an assistant on site.

#### **4. Processing Algorithm providing Data Format**

Depending on customer's requirements, the acquired data can be prepared and transferred as a point cloud in xyz or by common processing programs. For this purpose, after completion of the mission, the data pass through a specially developed processing algorithm in which the fan data are correlated with the navigation data and thus geo-referenced.

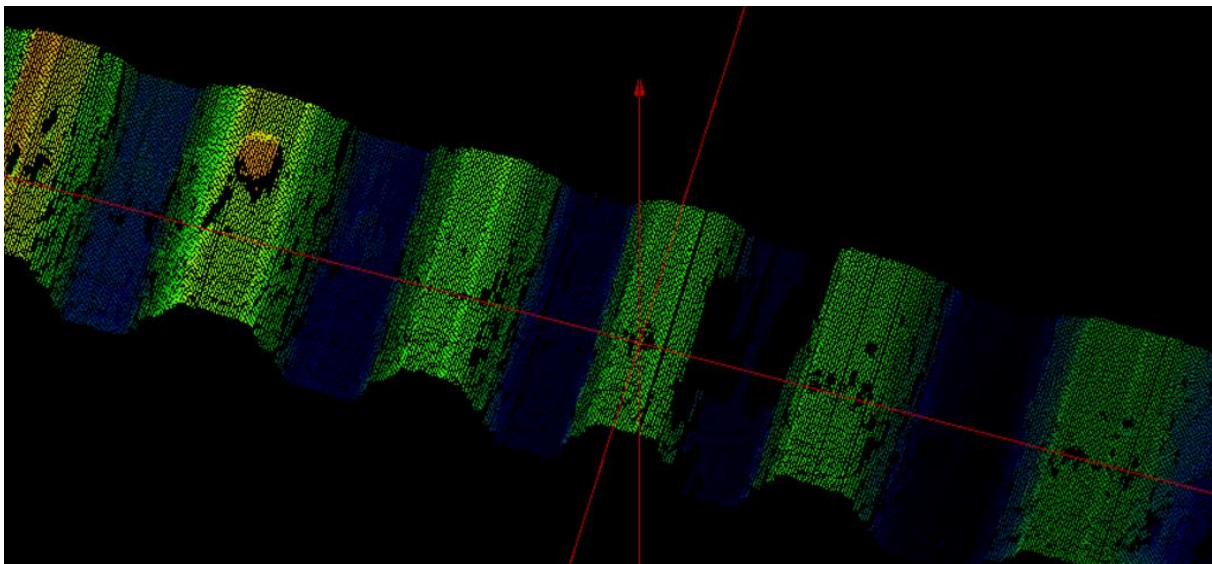


Fig.3: Raw data of sheet pile wall scan. The left section shows a concrete block as a test object. Dimensions of the concrete block: 20x20cm



With a density of 10000 measurement points per  $\text{m}^2$  ( $= 1$  measurement point per  $\text{cm}^2$ ), the subdron technology delivers a high resolution that is currently higher by a factor of 100 than that of the multibeam installed on board the survey vessel ‘Seeadler’ in 2016 with a maximum point density of 100-120 measurement points per  $\text{m}^2$  at the container quay in the lower area, *Döscher* (2019). With the current resolution, even small deformations can be detected. Once the AUV has undertaken its mission and the processing has been completed, clients receive data in the desired format.

Fig.4 shows results of a sheet pile wall survey, resulting in a high-resolution 3D point cloud with approximately 10000 measurement points per  $\text{m}^2$  and no irregularities.

## 5. Ship Hull Inspection

The fact that the high-resolution imaging of a system developed by subdron is also suitable for scanning ships’ hulls was demonstrated in the Port of Hamburg, Fig.5. Herer the hull was scanned for attached objects (as applicable in port security investigations against smuggling or terrorist activities, or navy applications).

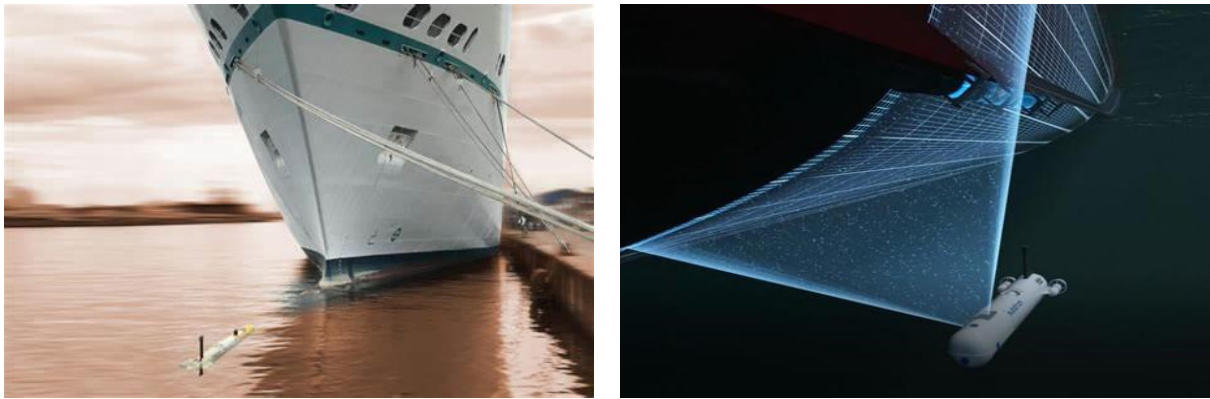


Fig.5: In-port underwater hull screening

In the sediment-laden waters of the port, with a visibility of 30-50 cm, a foreign object measuring  $55 \times 35 \times 15 \text{ cm}$  was detected that had been attached to the hull of a 20 m-long customs ship. In the section of the point cloud, the 3D reconstruction of the foreign object on the hull can be clearly seen by orange-coloured dots, Fig.5. Disregarding the mission setup, the acquisition time for this scan from ferrying to recovery of the AUV was approximately half an hour.

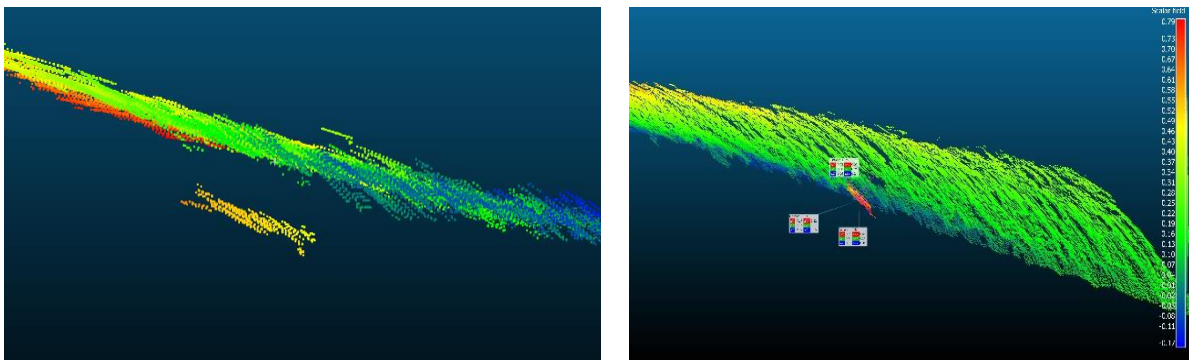


Fig.6: Overview of foreign object on the hull (left) and close-up (right)

This test under the customs vessel provided valuable insights for further development of stable navigation under large commercial vessels. These will be applied during in-water surveys for biofouling inspections. Likewise, such inspections are envisaged for out-of-tour damage inspections after groundings or damage due to mooring manoeuvres.

## 6. Conclusions

In port operations, the service package of subdron GmbH has already proven to be a useful support for survey tasks that can be realised quickly. Future 'Robotics as a Service' applications include a much wider range of inspections of offshore structures and ships for biofouling management and structural integrity.

## References

- BERTRAM, V.; HARRIES, S. (2022), *Re-Creating 3D Ship Geometries as Maps for Inspection and Reporting*, 3<sup>rd</sup> PortPIC Conf., Hamburg, pp.12-18
- GUÉRÉ, S.; GAMBINI, N. (2021), *Hull Reports at Scale - Notilo Cloud AI Platform*, 2<sup>nd</sup> PortPIC Conf., Pontignano, pp.11-19
- PARANHOS, P.M. (2020), *3D Laser Inspection of Ship Hulls*, 1<sup>st</sup> PortPIC Conf., Hamburg, pp.14-22
- BANKEN, E.; SCHNEIDER, V.E.; OEFFNER, J., SCHIPPERS, M. (2022), *Remote Ship Hull Inspection using a Robotic Crawler*, 3<sup>rd</sup> PortPIC Conf., Hamburg, pp.23-33
- CAPONI, R. (2022), *Replacing Dry-Dock or UWILD Hull Inspections with ROV Visual Inspections*, 3<sup>rd</sup> PortPIC Conf., Hamburg, pp.34-45
- CAPONI, R. (2023), *How Robotics Can Contribute to Greater Fuel and Maintenance Efficiency with More Frequent Monitoring Schedules*, 4<sup>th</sup> PortPIC Conf., Pontignano, pp.44-48
- DÖSCHER, T. (2019), *Multibeam-Vermessung von Spundwänden – Möglichkeiten und Grenzen anhand von Untersuchungen in Bremerhaven*, Hydrographische Nachrichten 113, <https://henry.baw.de/server/api/core/bitstreams/fa92e3de-bedd-4914-811a-9382218fa0cd/content>
- DORAN, S. (2022), *Evolving Inspection and Cleaning Technology*, 3<sup>rd</sup> PortPIC Conf., Hamburg, pp.19-22
- LANDER, K. (2023), *A Smarter Approach to Maintenance and Inspection*, 4<sup>th</sup> PortPIC Conf., Pontignano, pp.32-37
- STEIN, M. (2018), *Integrating unmanned vehicles in port security operations: An introductory analysis and first applicable frameworks*, Ocean Yearbook Online 32(1), pp.556-583
- STEIN, M.; PARVIAINEN, H. (2020), *Remote Vessel Inspections with an ROV using Livestreaming*, 1<sup>st</sup> PortPIC Conf., Hamburg, pp.55-65
- VONACH, T.; CARRERA VIÑAS, A. (2023), *Fully Autonomous Port Asset and Ship Hull Inspection for Structural Integrity and Biofouling Management*, 4<sup>th</sup> PortPIC Conf, Pontignano, pp.56-62



# A Novel Energy Saving Device for Ferry Ships in Waves based on Flapping Thrusters

Kostas Belibassakis, Nat. Techn. Univ. Athens, Athens/Greece, [kbel@fluid.mech.ntua.gr](mailto:kbel@fluid.mech.ntua.gr)

Dimitris Liarokapis, Nat. Techn. Univ. Athens, Athens/Greece, [dliaro@central.ntua.gr](mailto:dliaro@central.ntua.gr)

Anders Öster, Wärtsilä, Helsinki/Finland, [anders.oster@wartsila.com](mailto:anders.oster@wartsila.com)

## Abstract

*Flapping-foil thrusters arranged at the bow of the ship are examined for extraction of energy from wave motions by direct conversion to thrust, offering also dynamic stability and reduction of added wave resistance. In the framework of H2020 Seatech project the above innovation, operating both in dynamic mode and in static mode as T-foil configuration is examined, aiming at an increase in fuel efficiency and radical emission reductions. Results from the development and testing of tank-scale models of the considered biomimetic system and its performance in waves in the case of a ferry ship are presented. The experiments provide useful data for the calculation of the combined performance with the propulsion system, and establish design requirements and methodologies to extend predictions to full scale.*

## 1. Introduction

In the current period the International Maritime Organization (IMO 2023) has revised the strategy for substantial greenhouse gas (GHG) and fuel consumption reduction from the international shipping industry. Among various ambition levels the new strategy includes reducing emissions and consumption per transport work, targeting at least to 40% reduction by 2030, as compared to the 2008 levels, and continuing efforts in the next years. Noting that a significant part of the power demand for ship propulsion in moderate and higher sea-states is due to ship operation in waves, leading to powering requirements and increased fuel consumption compared to calm water conditions, flapping-foil thrusters arranged at the bow of the ship are examined for augmenting ship propulsion in waves by extraction of energy from ship motions by direct conversion to thrust, offering also dynamic stability, reduction of added wave resistance and enhancement of propulsion efficiency.

The EU H2020 SeaTech project (<https://seatech2020.eu/>) is developing two symbiotic ship engine and propulsion innovations, that when combined, will lead to a significant increase of fuel efficiency and radical emission reductions. The innovations will be characterized by high retrofitability, maintainability and operational cost savings. The ship engine innovation is based on optimally controlled DF engine leading to substantial emission reductions. The propulsion innovation consists of a dynamic wing arranged at the bow ship, operating as an unsteady flapping thruster, which converts wave induced ship motions (wave energy) into a net additional thrust force (augmented propulsion) and contributes to the reduction of added wave resistance. As the ship undergoes moderate or higher-amplitude oscillatory motions due to waves, in real sea conditions the ship motions could be exploited for providing the foil heaving motion free of cost, especially if the foil is located at the bow, as studied by various authors; see, e.g., *Belibassakis and Politis (2013)*, *Bøckmann and Steen (2016)*, *Bowker et al. (2020)*, *Rozhdestvensky and Htet (2021)*. In the framework of H2020 Seatech project the above innovation is examined for a ferry ship hull both theoretically and experimentally, operating in dynamic mode, *Belibassakis et al. (2022)*, and in static mode, *Ntouras et al. (2022)*. In the above studies, the bow foil includes two vertical struts for better support of the whole configuration and accurate transmission of the controllable pitching foil oscillatory motion. In this work, results from the development and testing of the considered biomimetic system and its performance in waves are presented. The experiments provide useful data for the calculation of the combined performance with the propulsion system, and establish design requirements and methodologies to extend predictions to full scale. Aiming at the further reduction of wave resistance of the device a T-foil configuration is also examined aiming at an increase of the system efficiency.

## 2. Ship model for towing tank experiments at NTUA tank

A ferry ship model, with length  $L_{BP} = 3.3$  m and main dimensions:  $L_{BP}/B = 7.67$ ,  $B/T=3.3$  and block coefficients  $C_b = 0.45$ ,  $C_{wl} = 0.7$ ,  $C_m = 0.82$ , was designed and constructed for testing at the NTUA towing tank, Fig.1.



Fig.1: NTUA tank-scale hull model of  $L/B = 7.67$  used for tests

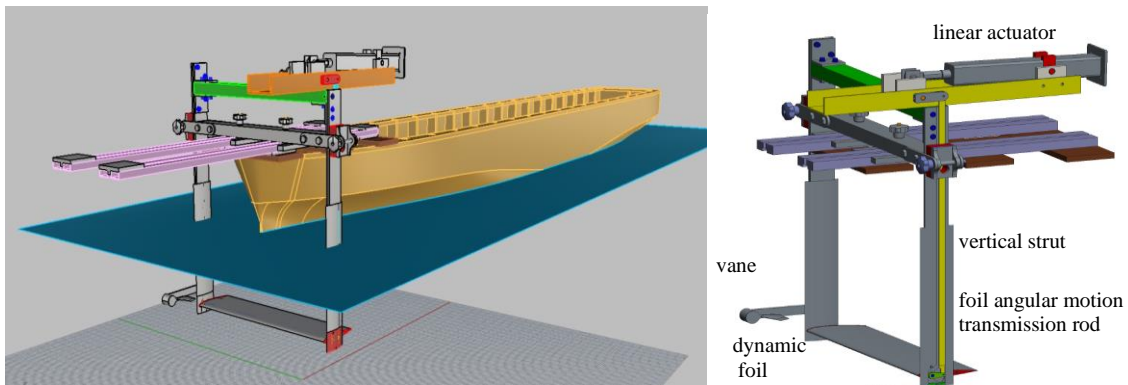


Fig.2: General arrangement of the NTUA tank scale model with the dynamic-wing arranged at the bow, for testing at NTUA tank

### 2.1. Model development

The model was made out of wood, polished and painted and prepared for testing at two selected drafts  $B/T=3.18$  and  $B/T=3.44$ . The foil is constructed by PVC polished and painted. The foil has rectangular planform shape, the section is NACA0012 and its aspect ratio is 4. The dynamic wing system is designed to be arranged at the bow of the ship, Fig.2. For the operation and powering of the flapping thruster a servomotor coupled to linear actuator is used. The pivot axis of the wing is located at its hydrodynamic center, and the power required for the dynamic pitching of the foil is found to be negligible compared with the effective horsepower associated with the resistance of the ship model. The angular oscillatory motion of the flapping foil is transmitted by means of two rods arranged inside the vertical struts that are used to support the system, Fig.2. The configuration ensures that the motion is transmitted very accurately, as instructed by the control system. Using the above model a series of experiments concerning calm water resistance at the two drafts have been performed. In particular, the model is tested without and with the operation of a biomimetic dynamic wing at the bow, and tests in harmonic and irregular waves are performed, and the responses including motions and total wave resistance are measured. In the next subsection the control system for the dynamic wing is briefly discussed and subsequently, indicative results are presented demonstrating the performance of the examined system.

### 2.2. Dynamic wing control system

The Control System (CS) of the self-pitching motion of the dynamic wing is based on the reading of the angle of attack of the flow in front of the dynamic wing, using the angle of attack meter (vane) which is shown in Fig.3.

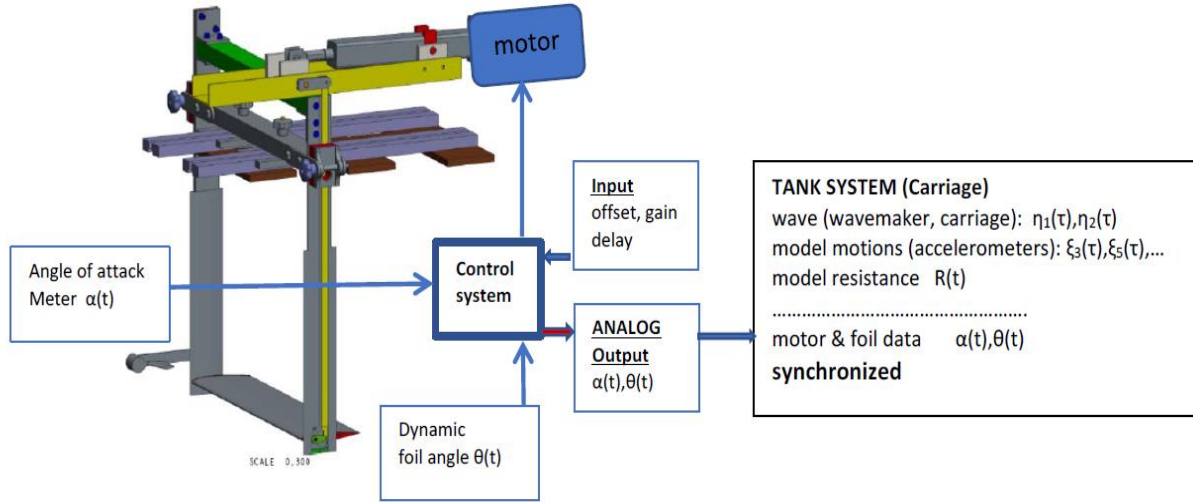


Fig.3: Basic workflow of the control system for the NTUA tank-scale model.

The signal was directed to a fully adjustable PID controller that continuously calculated the difference between a desired setpoint (SP) and the measured process variable (PV) and applied a correction based on proportional, integral and derivative terms (denoted  $P$ ,  $I$ , and  $D$  respectively).

The control system is depicted in Fig.3 and accepts the following input data (O=offset, G=gain, D=delay), and performs the following functions:

- The foil angle is measured by using a potentiometer providing input  $\theta(t)$  to the CS.
- The CS send signal pulses to the motor of the linear actuator to accurately position the crankshaft by oscillating the vertical rods and transmitting the angular motion  $\theta(t)$  to the foil which is set equal to:  $\theta(t) = Ga(t - D) + O$ .

The output is synchronized with the towing tank acquisition system, providing simultaneous records of the following data for given tank carriage speed (model speed):

- wave elevation from wavemaker and near the tank carriage (near the vessel):  $\eta_1(t)$ ,  $\eta_2(t)$
- ship model motions (heave and pitch of the hull from tank accelerometers):  $\xi_3(t)$ ,  $\xi_5(t)$
- the model resistance in the presence of waves with the dynamic foil in operation:  $R(t)$
- the angle of attack  $\alpha(t)$  and the foil angle  $\theta(t)$

The input signal from the angle of attack meter (vane) was low pass filtered as follows:

- 0 - 6 Hz, Gain = 1 / ripple 2.75 dB
- 18 - 104 Hz, Gain = 0 / Actual attenuation -43 dB.

The sampling rate was set to 208 Hz.

The CS is a custom design board based on an ST microelectronics STM32F429 ARM mcu, running at 168 MHz. The firmware is based on FreeRTOS real time operating system. The control board provides the following functions:

- Analog input for the AoA sensor. Oversampled at 2048 Hz and low pass filtered at 6Hz.
- Digital serial output to Animatics/Moog brushless servo motor (actuator).
- 5x12 bits spare analog outputs for monitoring.
- 3x12 bits spare analog inputs for interfacing auxiliary sensors

- 3D gyroscope and 3D accelerometer.
- 3D magnetometer and pressure sensor.
- GNSS and WiFi / Bluetooth.
- GPRS /2G / 3G.
- CAN Bus interface and uSD card for the data acquisition.

The firmware implements various control and RTK kinematics algorithms such as:

- Quaternion estimation and Euler angles
- Linear acceleration and speed
- Assisted global positioning and real time spectral analysis.

### 3. Towing tank experiments

The design Froude number concerning the ferry-ship model tests is  $F=0.25$  ( $V_s=1.42$  m/s), and only head waves are considered in the towing tank experiments. The measured calm water resistance of the NTUA model at the two drafts without and with the flapping thruster, Fig.4, is presented in Fig.5. The total resistance coefficient  $C_T = R_{tot} / (0.5\rho S V^2)$  is plotted against the Froude number  $F = V / \sqrt{gL_{BP}}$ .

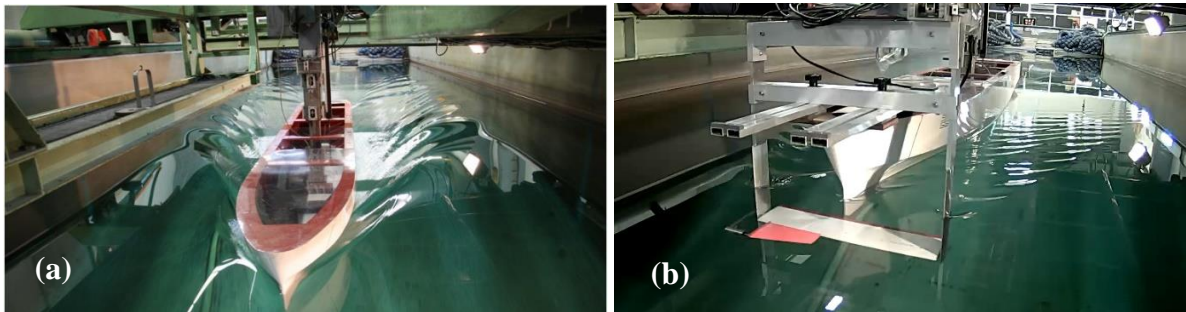


Fig.4: Tank tests of the NTUA hull model in calm water: (a) without the dynamic wing, and (b) with the flapping thruster, and determination of calm-water resistance

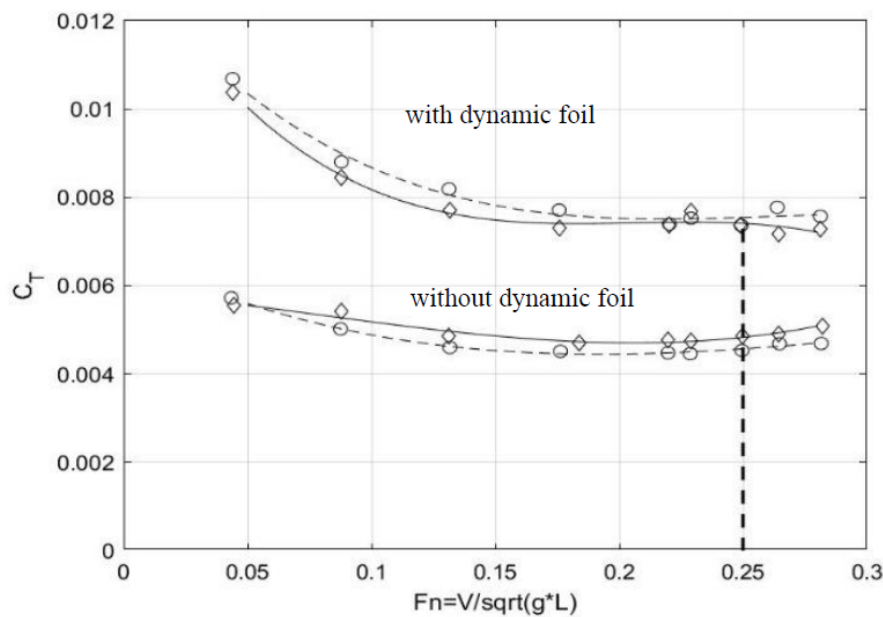


Fig.5: Resistance characteristics of the system without and with the dynamic foil at the bow of the ferry ship model. Dashed lines are for the model draft  $T=0.125$  m and solid lines are for model draft  $T=0.135$  m.



The increase of the resistance coefficient is almost constant for a range of ship speeds. Further experimental study has revealed that the above increase of resistance by the foil and support configuration is almost equally split to the foil and each of the two vertical skegs contributions, which is also confirmed by CFD analysis, *Ntouras et al. (2022)*. In particular the two vertical skegs resistance is both due to wave-making and frictional resistance components while the foil being submerged at a depth below the waterline contributes mainly to friction and viscous pressure resistance.

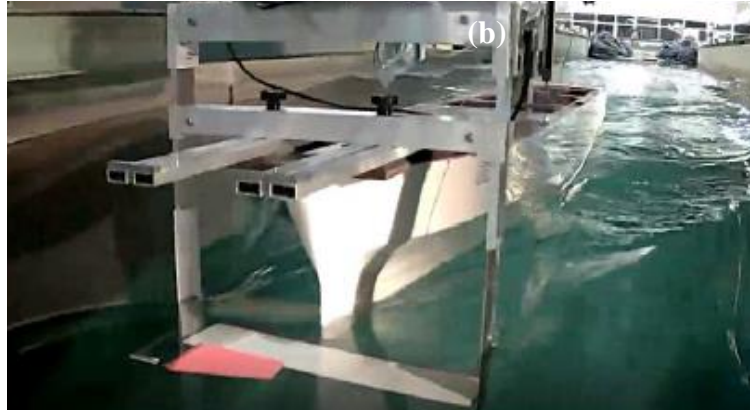


Fig.6: Tank tests of the hull model in head waves with the flapping thruster operating at the bow, and determination of motions and total resistance

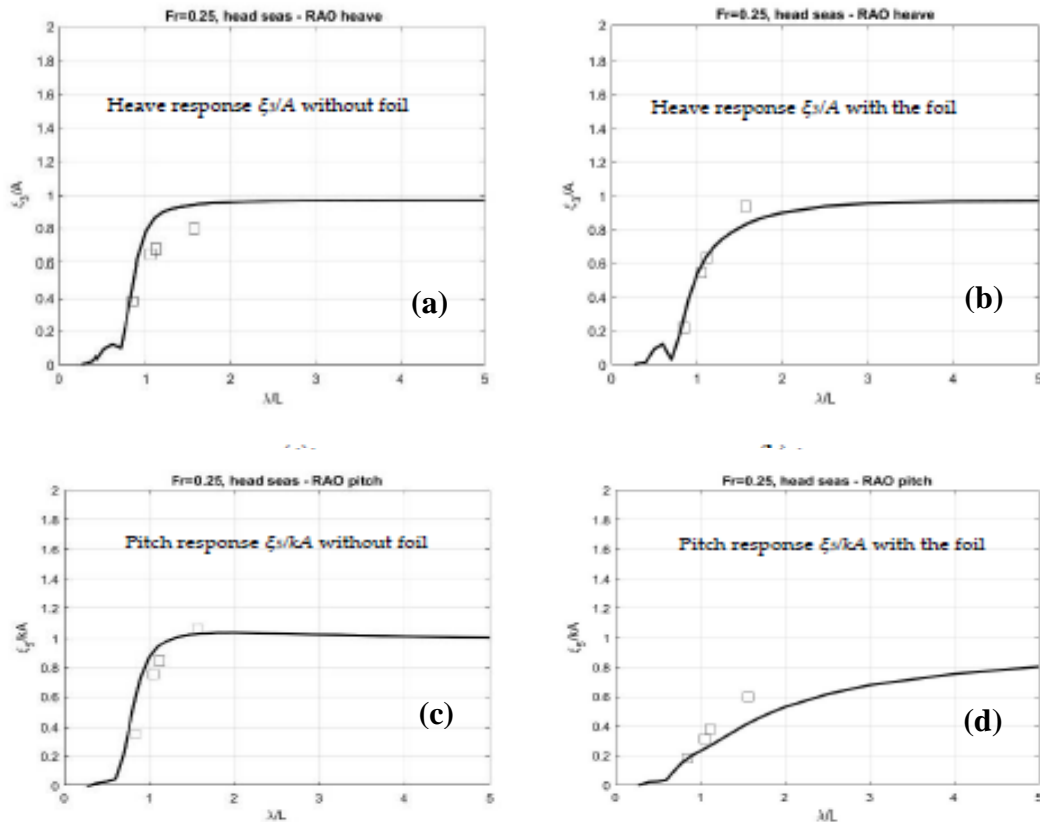


Fig.7: Tank tests of the hull model in head waves, and determination of motions (a,b) heave responses, (c,d) pitch responses without and with the flapping thruster at the bow. Model predictions are presented by using lines and experimental data by using symbols.

Tank tests of the hull model in waves are then performed for various conditions, Fig.6. Measured data concerning the ship motion responses with and without the operation of the dynamic wing in head waves are presented in Fig.7, for Froude number  $F=0.25$ , and the smaller draft of the ship.



In Fig.7, the predictions obtained by the numerical models developed are also plotted using solid lines presenting very good agreement. The operation of the foil leads to significant reduction of ship hull motion responses, and particularly concerning the pitching motion of the system, in a range of frequencies around the resonance, which is equivalent to reduction of added wave resistance and an overall increase of propulsion performance in waves.

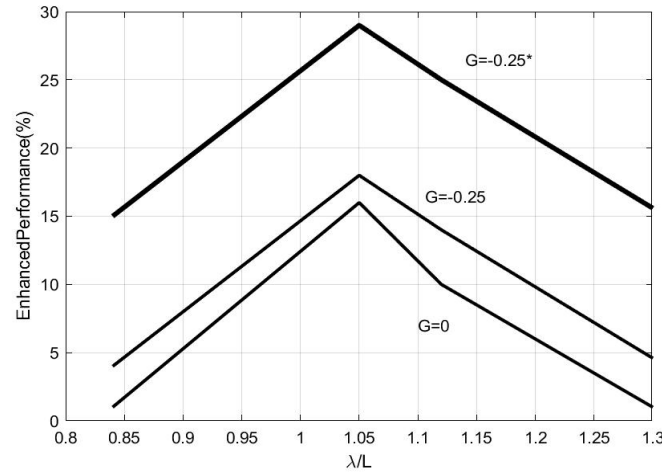


Fig.8: Performance enhancement due to dynamic foil operation at the bow of the NTUA Ferry ship model for  $F=0.25$  and various values of the gain parameter ( $G$ ).

Finally, the total resistance is measured with and without the flapping thruster at the bow, and the performance enhancement is presented in Fig.8, also for  $F=0.25$  and various values of the gain parameter ( $G$ ). The performance enhancement is defined as the ratio of total resistance with the operation of the dynamic foil in waves compared to the resistance of the model without the foil at the same speed and in the same wave conditions. It is derived that for an extended frequency band around the resonance of the system the performance enhancement ranges from 15-30% depending on the selection of the gain parameter of the control system. The larger performance (indicated in Fig.8 by using an asterisk) is achieved if the penalty due to resistance increase by the vane is eliminated. More details concerning the design and analysis of the system as well as the performance prediction of the system are available in *Belibassakis et al. (2022)* and *Ntouras et al. (2022)*.

#### 4. Further testing using a large-scale model at sea

Based on the towing tank experiments an extension of the previous research is performed using a large-scale model tested in real sea conditions, *Belibassakis (2023)*. The hull of the large model is geometrically similar to the tank model and its length is  $L = 10$  m. A wooden frame and a reinforced structure procedure were used. The hull construction of the NTUA large-scale model has been completed in the workshop of the Laboratory of Ship and Marine Hydrodynamics of NTUA, and was coated with waterproof protection and painted, Fig.9.



Fig.9: Completed NTUA large model of length 10 m and standard propulsion system at the stern using electric outboard engines for standard propulsion of the large-scale model

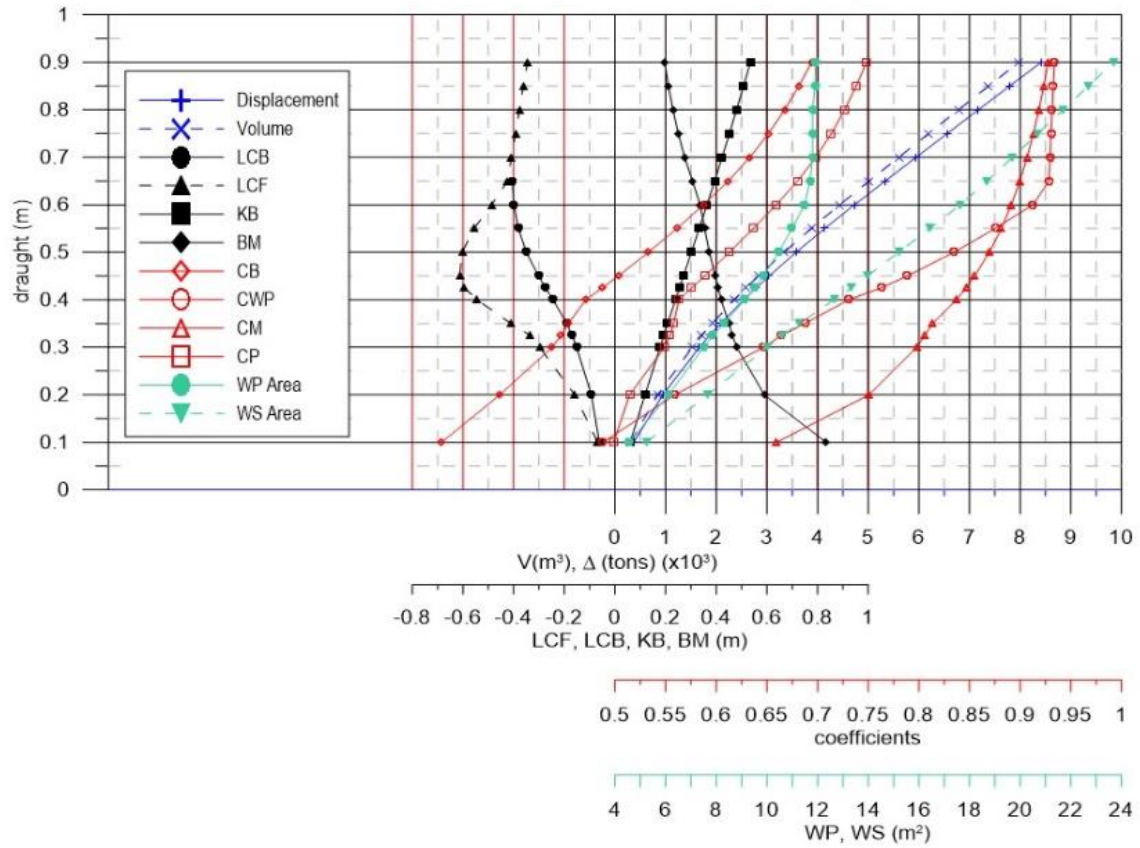


Fig.10: Hydrostatic diagram of the NTUA large-scale model (displacement is shown for salt water with specific gravity parameter  $\gamma = 1.025 \text{ t/m}^3$ )

The full length of the large-scale model with the propulsion system at the stern and the dynamic wing at the bow ranges from  $L = 10.5 \text{ m}$  to  $11.0 \text{ m}$ , the breadth of the ship is  $B = 1.30 \text{ m}$  and the freeboard height is  $0.65 \text{ m}$ . The draft of the model used in the tests at sea was  $T = 0.44 \text{ m}$ , and the freeboard height was  $0.65 \text{ m}$ . The hydrostatic data are presented in Fig.10. After the completion of the construction, fiberglass insulation and painting the model was tested for waterproof protection and stability requirements.



Fig.11: The self-propelled NTUA large-scale model docked at jetty of Olympic Marine SA premises

Two outboard electric motors (each with nominal power 4 kW) were used fully capable for the propulsion of the large model in above travelling speeds ( $V_s = 2.5\text{-}3\text{ m/s}$ ), offering excellent maneuverability characteristics, Fig.9. Load cells were arranged in order to measure the thrust of propellers, and the thrust and lift of the dynamic foil, which was arranged at the bow at a distance 0.3 m below the keel. It has orthogonal planform, with chord  $c = 0.35\text{ m}$ , span  $s = 1.75\text{ m}$ , and NACA 0012 sections. The same control system as in the tank tests was used to control the self-pitching motion of the dynamic wing operating in waves. In addition, the power consumption for the propellers was simultaneously measured in order to verify the enhancement of the performance offered by the dynamic wing during tests at sea. In the tests, the model track was monitored via an IMU Inertial measurement unit, while the dynamic responses of the model were measured via a 6-dof system, consisting of 7 accelerometers and 3D-gyro.

The model was transferred from the NTUA-LMSH workshop to the test site served by the marina of Olympic Marine S.A. in Lavrion area near Athens/Greece, Fig.11. Representative tests without the bow dynamic foil are presented in Fig.12. Then, the model was extracted out of the water and transferred in the shelter of Olympic Marine SA in order to install the dynamic wing at the bow, activate and test the functionality of the system. Subsequently, the NTUA ship model was again deployed and the corresponding tests with the operation of the dynamic wing were carried out in realistic conditions at the sea. Representative consecutive time snapshots during a run are presented in Fig.13.



Fig.12: Instances of tests of NTUA large-scale model in wave conditions at sea, without the foil



Fig.13: Instances of tests of NTUA large-scale model in wave conditions at sea, with the operation of the dynamic foil at the bow

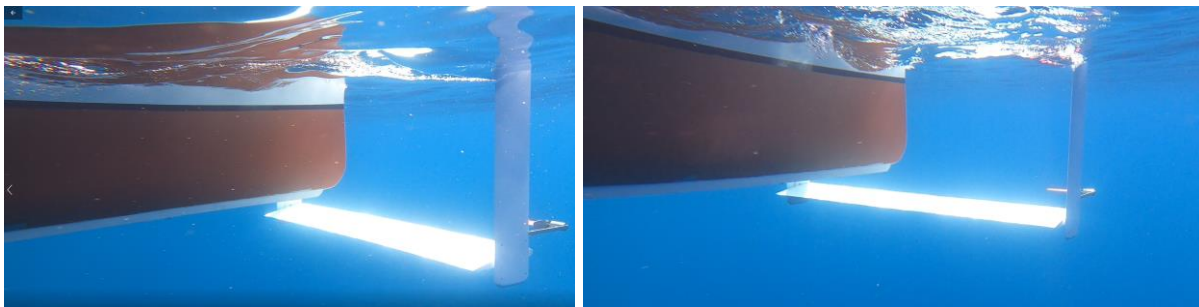


Fig.14: Underwater shots of the dynamic wing operating at the bow of the large NTUA ship model

In this case also underwater shots of the dynamic wing operating under the bow of the NTUA large-scale model were taken, and the foil at two instances is shown in Fig.14. Note that in these pictures the vane measuring the angle of attack of the flow affected by ship speed and motions in waves, as well as the wave flow, which was then used by the control system in order to instruct the self-pitching motion of the dynamic wing.

Indicative results concerning the wave conditions during the experiments at sea model speed 5 kn for responses and thrust of the propellers are presented in Fig.15 for the tests without the dynamic wing at the bow, when the recorded significant wave height was  $H_s = 0.13\text{m}$  and peak period  $T_p = 1.9\text{ s}$ . Corresponding results with the operation of the dynamic wing operating at the bow of the large NTUA model, Fig.28, are presented in Fig.16, when the significant wave height was  $H_s = 0.20\text{ m}$ , and peak period  $T_p = 1.9\text{ s}$ . In both cases the relative direction of waves with the route(s) of the model was  $\beta = 210^\circ$ , corresponding to bow-quartering waves, and the recorded speed of the model was 5.1 kn.

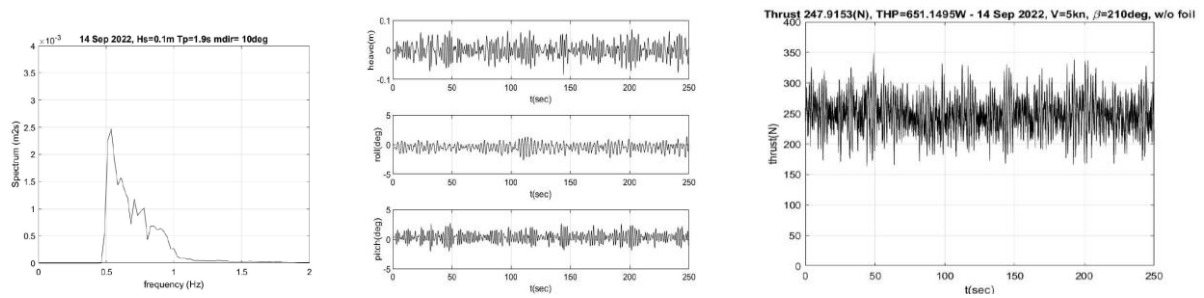


Fig.15: Wave conditions and measured data during tests at sea without the foil at the bow. (a) Wave spectrum (b) Recorded responses. (c) Thrust from engine propellers.

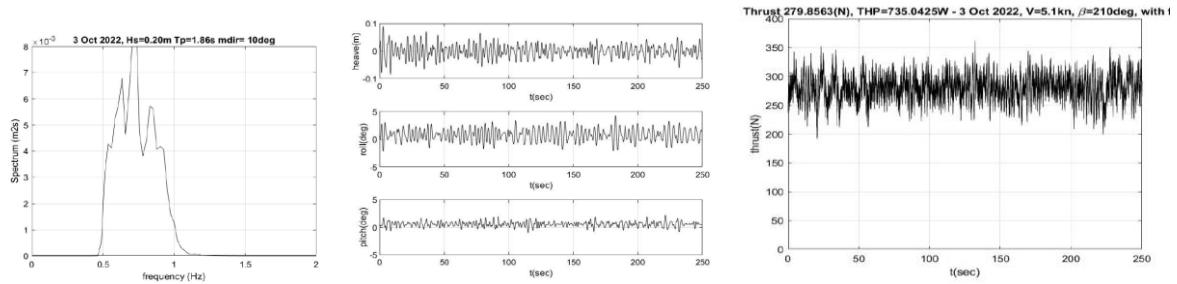


Fig.16: Wave conditions and measured data during tests at sea with the dynamic foil operating at the bow. (a) Wave spectrum (b) Recorded responses. (c) Thrust from engine propellers.

As shown in the above figures, the mean thrust of the propellers in the case with the foil was recorded to be 280 N, increased by 16% with respect to the corresponding value that was 241 N without the foil, which corresponds to an increase of the Thrust Horse Power by 13%. In this case the dynamic set-up and measured responses of the foil are presented in Fig.17, where it is seen that the foil contributed to a thrust equal to 28 N, confirming its operation in fish propulsion mode producing extra positive thrust. However, the significant wave height during the tests with the foil was increased by 55% compared to the corresponding value in the tests without the foil. In order to take into account the above effect, the calculated added wave resistance was found to contribute an extra  $\delta\text{THP} = 50\text{ W}$  for the model speeds  $V_s = 5\text{ kn}$  and value when the significant wave height is increased to  $H_s = 0.2\text{ m}$ , as compared to  $H_s = 0.13\text{ m}$ . Taking this into account it is derived that in the tested condition the foil compensates the increase of resistance due to its presence and support system (vertical skegs) while it offers significant dynamic stabilization in waves, as listed in Table I.

As previously mentioned, a double skeg system was used providing a rigid support of the whole configuration for the tests in waves at sea, ensuring accurate transmission of the self-pitching motion to the dynamic foil as instructed by the control system. The use of the relatively large vertical skegs at



the model-scale level led to an increase of wave resistance of the whole hull and foil system, especially for moderate and higher values of the Froude numbers, due to the increased wave resistance component and the fact that the struts cut the free surface. In full-scale applications, the area of the supporting vertical skeg system could be reduced, either by using smaller skeg chord or by designing a single (instead of double) supporting skeg system. In that case a new estimation is possible by considering only 50% of the additional THP due to the vertical skegs. The latter is estimated from data collected with the same ferry ship and foil model at smaller scale in the NTUA towing tank and if subtracted it offers as extra  $\delta$ THP gain of 55 W for the model speed of  $V_s = 5$  kn.

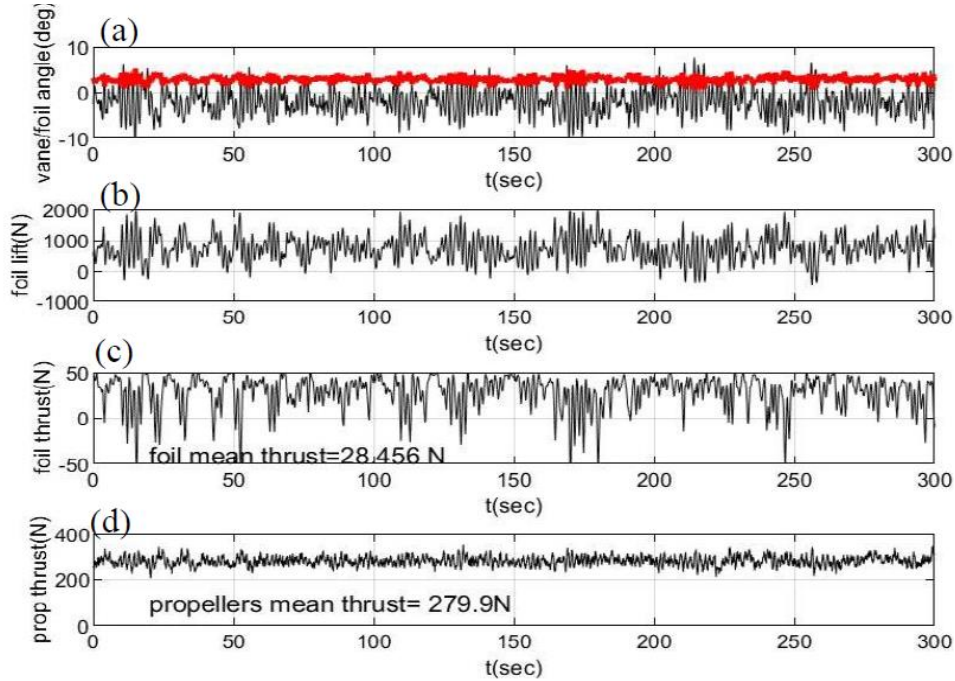


Fig.17: Dynamic foil data at vessel speed 5.1 kn and wave conditions: significant wave height was  $H_s = 0.20$  m, and peak period  $T_p = 1.9$  s and mean wave direction  $\beta = 210^\circ$ . (a) Vane reading and foil angle. (b) Foil lift and (c) Foil thrust (d) Propellers thrust.

Table I: THP (W) of the outboard engine propellers for the large ferry model at various vessel speeds and in head-quartering waves ( $\beta = 210^\circ$ )

	Wave condition	$V_s=4\text{kn}$	$V_s=5\text{kn}$	$V_s=6\text{kn}$
no foil	$H_s=0.10\text{m}$ , $T_p=1.9\text{s}$	366	651	1184
with foil	$H_s=0.20\text{m}$ , $T_p=1.9\text{s}$	380	735	1282
Change (%)		3.1%	12.9%	12.8%
no foil prediction	$H_s=0.20\text{m}$ , $T_p=1.9\text{s}$	$366+41=407$	$651+50=701$	$1184+54=1227$
with foil	$H_s=0.20\text{m}$ , $T_p=1.9\text{s}$	380	735	1282
Improvement(%)		18%	-4.8%	-4.4%
with foil and smaller 50% skeg	$H_s=0.20\text{m}$ , $T_p=1.9\text{s}$	330	685	1232
Improvement(%)		19%	2.4%	0.4%

With this new estimation of THP for waves of  $H_s = 0.2$  m the dynamic foil is expected to provide an improvement of the propulsive performance in the considered wave conditions ranging from to 2.4% for the design speed corresponding to  $F = 0.25$ . and increases to 19% for a lower speed corresponding to Froude number  $F = 0.2$ , and the performance enhancement offered by the dynamic foil is expected to become even greater as the wave height further increases and for head waves, Table I.



## 5. Further testing of the system in T-foil configuration

*Ntouras et al. (2022)* studied the dynamic wing in static mode, but with a pre-selected inclination for studying its effects on ship trim-control in calm water and in waves, as well as on ship resistance, using both computational tools and experimental data. Although the bow wing is considered static with respect to the ship, an important part of our study concerns the case when a ship oscillates in waves and, thus, the wing also operates in dynamic mode due to ship heave and pitch responses. It is shown that a reduction in the total resistance of the system of the order of 5% if the effects of skegs supporting the foil in the water in front of the ship bow can be minimized, and also an improved performance of the system due to a significant decrease in added resistance in the waves of the studied configuration of the order of 12–34% compared to the bare hull, with the larger values achieved near the resonance conditions. Based on the above results a series of further tests are performed by using the same ferry ship model in the towing tank and a T-foil configuration at the bow, as presented in Fig.18, which is used to eliminate the vertical skegs resistance. The foil has a span of 0.5 m and a backward sweep angle of  $12^\circ$ , and is placed at a submergence depth  $d = 0.27$  m below the waterline. The model is tested in calm water and in harmonic and irregular head waves, for the same draft and Froude number ( $F = 0.25$ ). In order to study also the trim control the inclination of the foil is statically controlled and set-up at a selected fixed value, Fig.19.



Fig.18: The NTUA ferry ship model with a T-foil arrangement at the bow



Fig.19: Tank tests of the NTUA ferry ship model with a T-foil at the bow in calm water

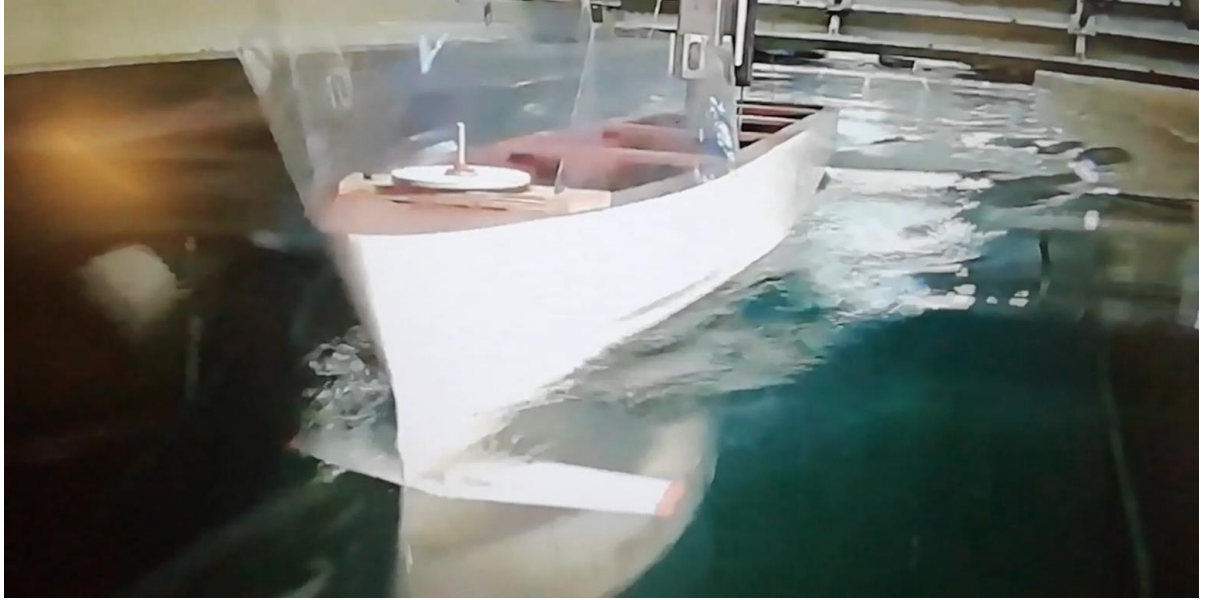


Fig.20: Tank tests of the NTUA ferry ship model with a T-foil at the bow in waves

The experiments were conducted at one draft ( $T = 0.135$  m), two speeds ( $V = 1.2$  m/s,  $V = 1.42$  m/s) corresponding to Froude numbers  $F = 0.21$  and  $F = 0.25$  at even keel condition. The model was tested at harmonic waves of frequency  $f = 0.55$  Hz,  $0.67$  Hz and  $0.75$  Hz corresponding to non-dimensional wavelength ratio  $\lambda/L = 1.56, 1.06, 0.84$ , respectively, and wave height of  $0.06$  m. Also two irregular waves were used in the tests characterized by the spectral parameters:  $H_s = 0.06$  m and  $T_p = 1.35$  s and  $H_s = 0.07$  m and  $T_p = 1.5$  s. Selected results concerning the enhancement of the thrust performance measured at the reduction of total resistance in waves with respect to the corresponding value without the foil are provided in Table II. Similarly as before, we observe significant performance enhancement near the resonance conditions as the ones observed with the operation of the dynamic foil, Fig.8, which becomes of the order of 3.5- 6.5% for the two ship speeds in irregular waves.

Table II: Performance enhancement (%) due to T-foil at the bow of the NTUA Ferry ship model for  $F = 0.21$  and  $0.25$  in regular and irregular head waves.

Harmonic waves $\lambda/L$	Foil nose up $2.3^\circ$		Foil at $0^\circ$	
	$F = 0.21$	$F = 0.25$	$F = 0.21$	$F = 0.25$
1.56	12.3	8.3	15.1	11.8
1.06	38.4	30.3	40.7	32.1
0.84	29.6	6.7	-30.5	9.5
Irregular waves $H_s=0.07$ m and $T_p=1.5$ s	3.5	6.5	4.3	4.7

## 6. Combined performance based on climatological data

The above analysis facilitates the simulation of ship dynamics and the combined performance of the ship propulsion system with the flapping thruster for a variety of sea states covering the climatology of a ship route area for the considered vessel, and can be used to derive useful information and data concerning the life-cycle analysis of the device. As an example, we consider a prototype ferry ship with the same geometry as the NTUA model with length  $L = 150$  m. In order to provide predictions of the examined ship, engine and flapping thruster system in waves, a ship route scenario in the North Sea is considered, and a representative point ( $55.05^\circ$  N,  $6.5^\circ$  E) in the southern-central North Sea sub-region characterized by dense marine traffic was selected for the calculations, *Belibassakis (2022)*. For the above location, using data from MetOcean View a bivariate model of significant wave height and peak period based on the lognormal distribution is derived for the probability density of wave parameters at the specific point. On the basis of the calculated results the expected improvement by the operation of the wave thruster for various sea states represented by values of the significant wave

height is calculated and shown in Fig.7, in the case of the short-sea ferry for head seas  $\beta = 180^\circ$ , and ship speeds  $V_s = 15$  kn, 17 kn and the service speed  $V_s = 19$  kn, for the given location in the North Sea. The standard propulsion system of the ferry ship in this example consists of two main engines with MCR 5000kW at 112RPM (propeller revolutions). The effect of waves is shown on the SHP-propeller RPM diagram of Fig.21 by using color representing the significant wave height. A dashed line is used to indicate the performance of the standard propulsion system in calm water. Increase of energy consumption above this limit is due to weather conditions without the presence of the dynamic foil. Decrease below the dashed line is due to the improvement of performance offered by the dynamic foil operating at the bow of the ship, in complementarity of the ship engines and propulsion system. A cyan line is used to indicate the value of significant wave height equal to 5m after which the dynamic foil should be retracted out of the water for safety.

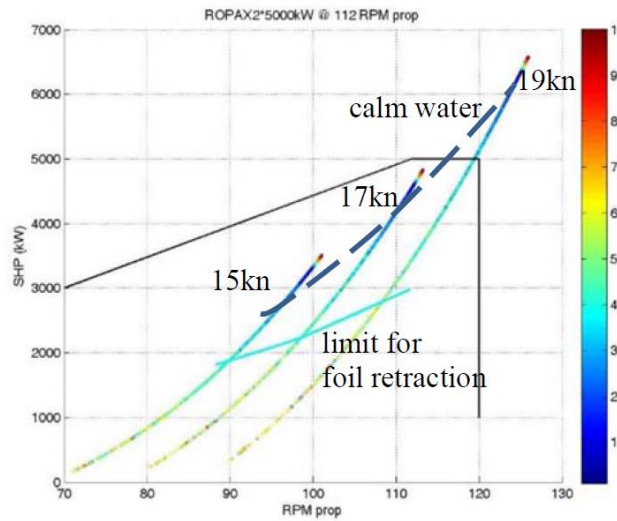


Fig.21: Simulation of the performance of ferry ship engine, in complementarity with biomimetic flapping thruster for head seas ( $\beta = 180^\circ$ ) and ship speeds  $V_s = 15$  kn, 17 kn and the design speed 19 kn. The significant wave height is shown by using color.

Significant savings can be achieved for moderate wave conditions, Fig.21. However, the life-long average of the performance enhancement is expected to be smaller due to possible mismatch between the peak of the population of the wave conditions depending on ship route climatology and the domain of good-performance of the present system, which is strongly dependent on the resonance characteristics of the combined system, that could be further improved by optimal design.

## 7. Conclusions

Flapping-foil thrusters arranged at the bow of the ship are examined for extraction of energy from wave motions by direct conversion to thrust, offering also dynamic stability and reduction of added wave resistance. In the framework of H2020 Seatech project the above innovation, combined with standard propulsion system based on optimally controlled Dual Fuel engine, is examined, aiming at an increase in fuel efficiency and radical emission reductions. Results from the development and laboratory testing of tank-scale models of the considered biomimetic system and its performance in waves are presented. Additional results from the design and development of large-scale model tested at sea are also presented.

The results of the examined model scale tests show that the dynamic wing technology provides a significant reduction in propulsive power required to maintain a constant speed of the ship in waves, offering also enhancement of stability due to the drop of responses. An average pitch and heave reduction of 30% and 15%, respectively, is demonstrated, and a reduction of delivered power of up to 30% for regular head waves near the resonance are reported in the case of the ferry ship model with an actively controlled flapping thruster.



Subsequently the demonstration of the dynamic wing technology in wave conditions at real sea using a manned large-scale, ferry ship model of 10m length with the same hull geometry as the tank scale model and selected results obtained are described in detail. The large ship model is equipped with an autonomous propulsion system and was deployed in coastal area near Athens, Greece where the experiments took place, supported by the premises of Olympic Marine S.A. Standard hydrodynamic tests are performed, including measurements of resistance and propulsion, seakeeping and maneuvering tests. For the seakeeping and propulsion tests in waves the sea conditions at the coastal-sea area were monitored using portable directional wave buoy.

The overall performances in waves with and without the dynamic wing operating at the bow were recorded and the energy gains are evaluated. Also, the dynamic stabilization of the ship due to the reduction of its responses with the foil operating at the bow and the corresponding reduction of added wave resistance is presented based on measured data. The experiments provide useful data for the calculation of the combined performance of the actively controlled foil thruster with the propulsion system, and establish design requirements and methodologies to extend predictions to full scale. The results based on the data collected will be exploited to update the developed numerical simulation models for full scale powering, consumption and emission predictions, LCCA and derivation of KPIs for various ship types. Also, the present results will support the design of full-size wing including strength, fatigue and service-life considerations, as well as actuation and mechanical wing-retractability system for calm and heavy weather conditions, respectively.

## Acknowledgements

The present work has been supported by Seatech H2020 project received funding from the European Union's Horizon 2020 research and innovation program under the grant agreement No 857840. The opinions expressed in this document reflect only the author's view and in no way reflect the European Commission's opinions. The European Commission is not responsible for any use that may be made of the information it contains. We wish also to acknowledge the director Prof. G. Grigoropoulos and the personnel of the Laboratory of Ship and Marine Hydrodynamics of National Technical University of Athens for their participation and assistance at various stages of the project. In particular, the valuable contributions by Mr J. Trahanas and Mr G. Milonas are greatly acknowledged.

## References

- BELIBASSAKIS, K.A. (2022), *Combined performance of biomimetic ship propulsion system in waves with ship engine and application to short-sea shipping*, Int. Conf. Trends in Maritime Technology and Engineering 1, pp.301-308
- BELIBASSAKIS, K.A. (2023), *Augmenting ship propulsion in waves by flapping-foil thrusters*, 8<sup>th</sup> SNAME Int. Symp. on Ship Operations, Management and Economics, Athens
- BELIBASSAKIS, K.; FILIPPAS, E. (2022), *A dynamical system for the combined performance of innovative biomimetic thruster with standard propulsion system in waves*, 41<sup>st</sup> Int. Conf. Ocean, Offshore and Arctic Engineering, Hamburg
- BELIBASSAKIS, K.A.; POLITIS, G.K. (2013), *Hydrodynamic performance of flapping wings for augmenting ship propulsion in waves*, Ocean Engineering 72, pp.227-240
- BELIBASSAKIS, K.A.; FILIPPAS, E. (2015), *Ship propulsion in waves by actively controlled flapping foils*, Applied Ocean Research 52, pp.1–11
- BELIBASSAKIS, K.A.; FILIPPAS, E.; PAPADAKIS, G. (2022), *Numerical and Experimental Investigation of the Performance of Dynamic Wing for Augmenting Ship Propulsion in Head and Quartering Seas*, J. Marine Science and Engineering 1024



- BØCKMANN, E.; STEEN, S. (2016), *Model test and simulation of a ship with wavefoils*, Applied Ocean Research 57, pp.8–18
- BOWKER, J.A.; TAN, M.D.; TOWNSEND, N.C. (2020), *Forward Speed Prediction of a Free-Running Wave-Propelled Boat*, IEEE J. Oceanic Engineering 46(2), pp.402–413
- BOWKER, J.A.; TOWNSEND, N.C. (2022), *Evaluation of bow foils on ship delivered power in waves using model tests*, Appl. Ocean Research 123
- FILIPPAS, E.; PAPADAKIS, G.; BELIBASSAKIS, K.A. (2020), *Free-Surface Effects on the Performance of Flapping-Foil Thruster for Augmenting Ship Propulsion in Waves*, J. Marine Science & Engineering 8(5), pp.357
- IMO (2023), *Revised strategy to reduce greenhouse gas emissions from international shipping*, Int. Mar. Org., London, <https://www.imo.org/en/MediaCentre/PressBriefings/pages/Revised-GHG-reduction-strategy-for-global-shipping-adopted-.aspx>
- NTOURAS, D.; PAPADAKIS, G.; BELIBASSAKIS, K.A. (2022), *Ship Bow Wings with Application to Trim and Resistance Control in Calm Water and in Waves*, J. Mar. Sci. Eng. 10(4), pp.492
- ROZHDESTVENSKY, K.; HTET, Z.M. (2021), *A Mathematical Model of a Ship with Wings Propelled by Waves*, J. Marine Science and Application 20, pp.595–620
- TRIAANTAFYLLOU, M.S.; TRIAANTAFYLLOU, G.S.; YUE, D.K.P. (2000), *Hydrodynamics of fishlike swimming*, Annual Review of Fluid Mechanics 32, pp.33–53
- WU, X; ZHANG, X. ; TIAN, X. ; LI, X. ; Lu, W. (2020), *A review on fluid dynamics of flapping foils*, Ocean Eng. 195

# The MCN Guideline: An Overview of Measures Improving Ship Efficiency in the Context of IMO and EU Emission Regulations

Richard Marioth, Idealship, Itzehoe/Germany, [rm@idealship.de](mailto:rm@idealship.de)

Tobias Wesnigk, MCN, Kiel/Germany, [tobias.wesnigk@maritimes-cluster.de](mailto:tobias.wesnigk@maritimes-cluster.de)

## Abstract

*This paper presents an introduction to the so-called MCN Guideline, which first version was published in September 2022 as an handbook and knowledge-base to cope with the increasing number of requirements related to the EEDI, EEXI, CII and the upcoming EU ETS regulations. The Guideline provides an overview of technical solutions as well as maintenance and operational measures that can be considered to improve fuel efficiency of ships and reduce their greenhouse gas emissions. Furthermore, focus was given analysing and comparing the future of marine fuels. The advantages that Carbon neutral or carbon-free fuels offer are highlighted, without hiding the associated disadvantages. A revised version of the MCN guideline will be published in autumn 2023. This paper provides an overview about the guideline and what will be added soon.*

## 1. Introduction

Shipping and in particular the technical aspects of shipping are strongly represented by the members of the Maritime Cluster Northern Germany (MCN). Among them are companies with a long tradition and a high level of expertise as maritime suppliers or ship designers, working on the further technical development of ship-related technologies in international projects. In order to align and team-up these different players, the establishment of the MCN Expert Group Ship Efficiency in 2014 was a clear consequence for the increased demand for such kind of forum. Such concentrated expertise is also very important in the pursuit of the ambitious goals formulated and demanded by the authorities for more environmentally friendly (“green”) shipping, flanked by the voluntary commitment announced by the shipping companies.

To assist shipowners and other stakeholders in the process of improving the efficiency of the existing fleet in light of the new EEXI and CII rules, this MCN Expert Group has developed a guideline covering various technical aspects of increasing efficiency and decarbonization, Fig.1, MCN (2022).

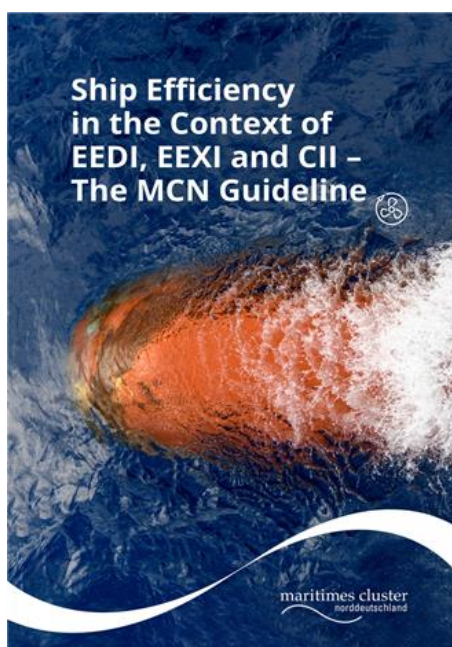


Fig.1: Ship Efficiency Guideline – document cover

The guideline contains a brief overview of the general regulatory framework in the shipping industry, including the evolution of efficiency-related regulations. The main focus was put on the two options how shipping companies can decarbonize:

- changing the primary energy source to a less carbon or carbon neutral/carbon free fuel, and
- becoming more energy efficient

Starting with the first version in September 2022, the guideline is intended to be “open-ended”. This means that there will be updates in certain intervals. The first update will follow in late fall 2023. This paper gives an overview about the two main chapters and the planned update.

## 2. Green-shipping, the choice of an adequate fuel

The guideline provides an overview of possible types of marine fuels with a particular focus on the so-called future fuels like Methanol or Ammonia. Brief descriptions provide detailed information for each of the fuels, while a comparison matrix highlights the differences in many aspects.

A first approach to reducing or even eliminating fossil CO<sub>2</sub> emissions is to choose an adequate fuel. Liquefied Natural Gas (LNG), for example, has been considered a good solution for emitting less carbon dioxide and sulphur oxides than heavy fuel oil or marine diesel. Some ships therefore were converted or equipped with auxiliary tanks for LNG so that so-called dual-fuel engines could burn both natural gas and diesel-based fuels. However, due to the stricter regulations, operating on natural gas alone does no longer provide the desired emission savings. Focus has shifted towards decarbonization, and this means that the perception has changed and a variety of "new" fuels, are being considered as possible candidates for ship propulsion, depending on the vessel's tasks, operation areas as well as the worldwide availability.

With these diverse "new" fuels, there are new requirements, e.g., in production and bunkering possibilities, and furthermore in the handling of gaseous and pressurized fuels or e.g., their cryogenic/liquefied storage. Also, on the engine side with regard to optimal combustion in the main engine or the auxiliary aggregates, there are still much needs to be done to ensure safe and reliable ship operation required from the maker's side.

Apart from that the crew of a ship operating with such fuels will need training about handling and possible dangers emanating from these new fuels. The current education programs of universities where one can become a marine engineer do not yet cover all these new requirements.

Table I: Assessment matrix marine fuels

Fuel Type	Effect on												
	GHG	EED/EECI	CII	Availability of Combustion Engines	Space required/ tanks & machinery & components/ Payload	Bunker availability of Fuels	Ships Endurance (Range)	Retrofit (from DO)	Bunkering procedure	Storage/ Storage on Board	Legislation / issues *	IMO Goals 2050	Reputation / Image
HFO	--	--	--	++	+	++	++	+	+	+	++	--	--
MDO	--	-	-	++	++	++	++	0	++	++	++	--	--
LNG	+	+	+	+	-	-/0	-	-	0	-	++	0/+	0
LPG	-/0	--	--	-	-	+	-	-	+	0	++	-	0
Methanol	0/+	+	+	+	-	+	0	-	++	0	+	0	+
Ethanol	-/0	0/+	0	+	0	-/0	0/+	-	++	0	+	-	+
Bio Fuel Oil (FAME)	-/0	-	-	++	++	++	++	0	++	++	++	--	--
Ammonia, cooled	++	++	++	-	-	-	-	--	0	--	--	++	-
Ammonia, pressurized	++	++	++	-	-	-	-	--	0	--	--	++	-
Hydrogen, liquid (LH <sub>2</sub> )	++	++	++	--	--	--	--	--	--	--	--	++	++
Hydrogen, gaseous (GH <sub>2</sub> )	++	++	++	--	--	-	--	--	--	--	--	++	++

\*classification/legislation rules available

The following fuels were considered and compared in the guideline document:

- Traditional fuels: HFO, MDO, LNG
- “New fuels”: LPG, methanol, ethanol, biofuel oil (FAME), ammonia cooled and ammonia pressurized; liquid hydrogen liquid (LH<sub>2</sub>) and gaseous hydrogen (GH<sub>2</sub>).

For each of the fuels considered, material properties, components, characteristics, and handling were summarized and examined an overview of the outcome is shown in Table I.

The following aspects are considered for each fuel in this comparison:

- GHG: Tank-to-wake (TtW) CO<sub>2</sub> emissions from fossil fuels and well-to tank (WtK) value.
- EEDI/EEXI: The fuel specific conversion factor (CF) in EEDI/EEXI calculation is considered.
- CII: Also considered through fuel conversion factor.
- Availability of combustion engines: For the time being, the combustion engine remains the standard energy converter onboard. It is essential that the fuel type can be used practically.
- Required space for tanks / machinery & components / pay load
- Calorific value per volume [MJ/l] and calorific value per mass [MJ/kg] are criteria for ship design. All alternative fuels have lower calorific values as the MDO reference.
- Bunker availability: The transport industry requires a good network of refilling locations.
- Ship’s endurance (range): Lower calorific values mean that more tank volume is needed.
- Retrofit (from DO) available/possible: Possibility of retrofitting existing main engines.
- Bunker procedure: Local constraints and restrictions could limit the flexibility and bunker location.
- Onboard storage/handling: Increased risks and physical properties like pressure, temperature, flammability and toxicity require additional safety precautions.
- Legislation/Issues: It is assessed whether guidelines exist how to use each substance as fuel.
- IMO Goals 2050: Is the fuel compliant to the GHG Strategy that envisages a carbon neutral transportation by 2050.
- Reputation/Image: The image of shipping brands will be enhanced in the eyes of customers if they offer alternative shipping strategies to minimize their carbon footprint.

A more detailed description of the above points can be found in the MCN Guideline. The document contains also two pages for each fuel type in the appendix. These pages include a general description of the fuel, specific physical and chemical characteristics and some action instructions for the crew.

### 3. Technical Solutions for a better Ship Efficiency

The second major element of the MCN guideline is an overview of technologies available for energy efficiency improvement of a vessel. When Naval Architects consider ship efficiency, the first decisive moment is obviously the ship design and all related optimisation steps before the vessel is built for new vessels. Computerization and simulations have helped to improve to optimise the vessels within the last decade and some design elements, like improved propellers are also available for a refit. Besides the design, there are resistance increasing influences like hull fouling, propeller/rudder fouling, additional wave resistance and many other operational impacts. New or additional technologies/components or digital systems can be installed on board to overcome some of these challenges or even add some pulling force power, like modern Sailing Technologies do. An example of digital technologies like Hull Performance Monitoring solutions is shown in Fig.2.

Because of fouling over time, the vessel loses performance (speed drop at same power). After a certain level of performance loss, a hull cleaning is recommended/initiated. Nevertheless, overall hull-performance drops over several years so a complete renewal of the antifouling including hull-blasting is mandatory.



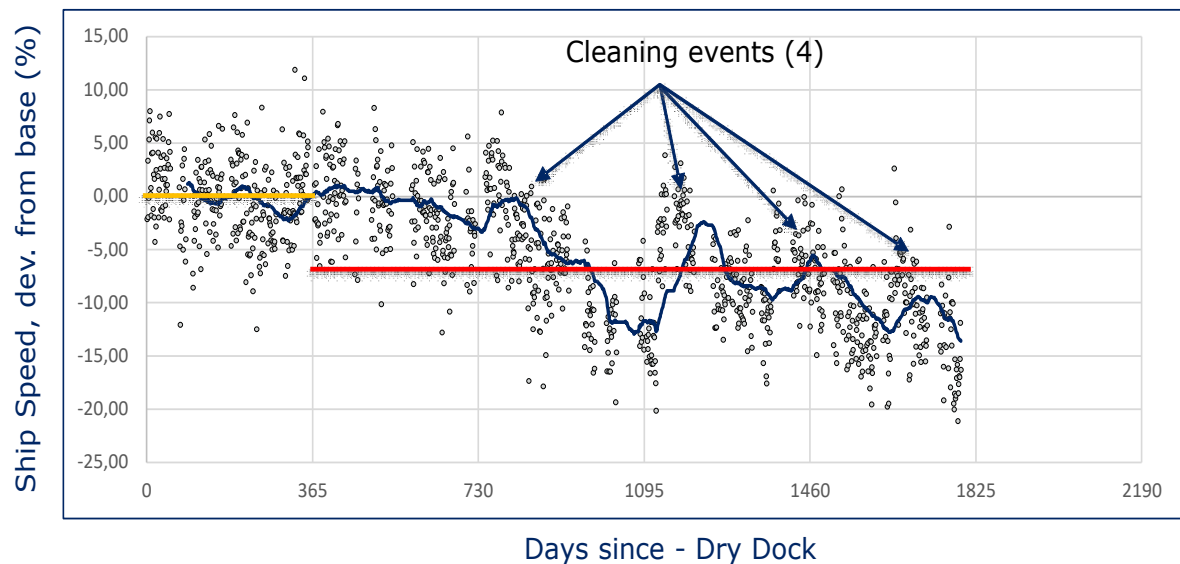


Fig.1: Example of changes in hull performance as per ISO 19030-2 on reactively cleaned

The guideline document aims to present a holistic overview of the available technology measures to improve ship efficiency. This is done through an evaluation matrix where in total 17 criteria are analysed and compared for all technologies. This technology matrix does not claim to be exhaustive, but covers already in its first version about 24 retrofit technologies. This way, the guideline is a valuable addition to other ESD technology overviews like the IMO Greenvoyage 2050 project, <https://greenvoyage2050.imo.org/technology-groups/>. Fig.3 shows a fraction of the MCN technology matrix.

Technology	Ship type / size	CAPEX			Energy savings		
		New build	Refit	Remark	Propulsion	Aux.	Remark
Biofilm protection based on Ultrasound Technology	any ship	low	-	depending on ship size and area to be protected; example - shaft propeller: 15-20T€; pod drive: 20T€ per drive; bow thruster: 0-15 T €; freshwater generator: 10-15 T€	low-medium	very low	biofilm protection on rudder, propp, hull, cooling systems, fresh water systems ...
Change from HFO to green Methanol	any ship	high	"high"	depending on conversion concept (approx 4.5 Mio. € for 8-10 MW main engine retrofit incl. fuel supply system & tank coating	+100%	+100%	depending on fuel pricing and CO <sub>2</sub> tax
Dynamic Draught and Floating Monitoring	Length > 80m	50 KUSD	50 kUSD	-	none	-	-
Energy Saving Device: Becker Mewis Duct® (MD)	Tankers Bulk Carrier Heavy-Lift MPP	80-300k USD plus Design Package	80-300k USD	depending on aft ship design, propeller diameter, and quantity	high	-	depending on hull design / wakefield

Fig.2: Fraction of the matrix "Assessment Matrix Ship Efficiency"

Typically, the technologies were added through a cooperation between the MCN Expert Group Ship Efficiency and technology suppliers. This way, important aspects about each product can be given by the technology provider whereas the expert group tries to ensure that a certain comparability between the technologies remain. A general challenge in the filling of the matrix is the fact that many aspects depend on the individual ship, hence the most rating criteria are judged qualitatively through ranges (very low, low, medium, high, very high). Furthermore, the option is given at every rating criteria to leave a remark with additional information.

Table II gives an overview of all evaluation criteria with definitions.

Table II: Criteria of evaluation matrix with definitions

	Abbreviations	Short definition
<b>Effects on</b>	CAPEX	Capital expenditures for system itself, installation, setting-to-work and training
	Energy savings	Saving of energy. Costs (fuel costs).
	ROI	Duration after the savings are equal or higher than the investment (including CAPEX and OPEX)
	Operational effort	All extra handling or effort required for the technology (e.g. crew training/time)
	GHG	Gases that causes the greenhouse effect
	EEDI / EEXI	Defined by IMO. Indicating how much CO <sub>2</sub> per cargo ton and nautical mile is used (new built regulation)
	CII	Regulation by IMO for 2023. Indicates a ship's performance level on emitting carbon dioxides based on measurements.
	Cargo Capacity	The cargo capacity measured in tons or volumetric space (or lane meters or passengers).
<b>Application range</b>	Speed	The ship's speed range at which a specific technology can be used or is well-effective.
	Ops hours	The operating hours per year - how long a technology can be used or is effective.
	Sailing area	The area in which a technology can be used or will usually be used (examples: Global, Only ECA, close to shore)
	Ship size / type	How ship size and type limit the application of a certain technology.
	Other dependencies	Other aspects (boundary conditions) that have to be considered for application or availability of a certain technology.
<b>Influence on</b>	Pay load	The cargo capacity measured in tons or volumetric space (or lane meters or passengers).
	Installed power	The influence on the installed power on board
	Space	The influence on the available space on board
	Ship handling	The influence on the ship handling, (e.g. bunkering efforts, fuel swap at ECA, fuel heat & cleaning, safety aspects, etc.)

Apart from the matrix structure itself a valuable addition of the MCN guideline is the CAPEX indication for retrofit given in kUSD. Of course, this is just a first indication which will be dependent on several additional factors. This cost indication could only be done with the support of the suppliers, who are contacted by the MCN team before the next version of the guideline is released.

Below is a list of technologies available in the assessment matrix of MCN Guideline 2022:

- Biofilm protection based on ultrasound technology
- Change from HFO to green Methanol
- Dynamic Draught and Floating Monitoring
- Energy Saving Device / Propeller Duct
- Roll damping solution
- Full blasting of the hull before paint application
- High Performance Antifouling Solutions
- Hybrid Power System
- Marine ORC waste heat recovery - transferring waste heat into sustainable electricity
- Numerical Wave Tank

- Onboard measurement - Common condition-based efficiency assistance
- Onboard measurements - Fuel performance assessments to fulfil energy efficiency regulations
- Onboard measurements - Hull and propeller performance management
- Onboard measurements - the electronic record book
- Operational measure: Robotic hull cleaning with capture
- Proactive hull cleaning without capture
- Propeller Fin Cap
- Propeller Retrofit
- Reduction of parasitic losses on 4-Stroke-Medium-Speed Diesel Engine
- Shaft Generator
- Variable Speed DC Drive and Distribution System
- Weather Routing
- Wind assisted Propulsion with Flettner-Rotor
- Wind Assisted Propulsion – Suction Wing

Apart from the assessment matrix, every technology is explained in more detail by “one page” descriptions in the appendix of the document. This way it’s easier to understand and identify reasonable solutions or combinations of solutions to improve vessel’s efficiency and achieve a clear reduction of fuel oil consumption and related greenhouse gas emissions.

#### **4. Upcoming MCN Guideline 2023**

As written above the guideline is intended to be “open-ended”. Starting with the first version in September 2022, an update will follow in late fall 2023. One main element is that the MCN Expert Group Ship Efficiency decided to split the Assessment Matrix Ship Efficiency into three main categories:

- Matrix 1 – Operational measures:  
These are mostly digital assistance solutions like Weather Routing and so on.
- Matrix 2 – Periodical measures  
All kinds of hull, rudder and propeller maintenance measures, which need to be done within certain intervals like Hull Cleaning or paint application.
- Matrix 3 – Technical retrofits  
Technical add-ons and/or retrofit solutions like Propeller Retrofit, Wind Assistance Devices or installations concerning the electricity grid of a vessel.

Apart from that the MCN Expert Group Ship Efficiency team had met with several stakeholders and the following valuable technologies will be added to the guideline in 2023:

- Air Lubrication
- Bow-Windshield / Wind-Deflector
- Gate-Rudder
- Lightweight Construction
- Variable-Speed Drives (Pump and Fan Application)
- Wing-Sails and Kite-Sails

In addition to these updates a chapter on the EU Emissions Trading Scheme (EU ETS) was added, which includes the main aspects and a description of the legal framework.

Another chapter “New training requirements” will be added to the guideline. It’s obviously that all those new and fast changing regulations, technologies and fuels, especially the handling and the risks

of these diverse fuels, require training of the crew. The guideline aims to supply initial guidance for shipping companies in this field as well.

## **5. Where to get the document and how to contribute**

The mission of the Maritime Cluster Northern Germany is to promote, facilitate and consolidate collaboration within the maritime industry. This includes supporting the maritime industry with their efforts in the field of decarbonization. With these motivations the MCN guideline is published free of charge and it can be received by e-mail upon request from [ines.jahnke@maritimes-cluster.de](mailto:ines.jahnke@maritimes-cluster.de)

Distribution was chosen like this by MCN to be able to automatically send a new release of the guideline when available.

The Guideline will be revised in regular intervals by the team of MCN along with its Expert Group Ship Efficiency. The group welcomes further contributions and additions to the guideline. Kindly contact Mrs. Jahnke if you have any questions to this.

## **6. Conclusions**

In order to give an overview of the underlying regulations and to present possible measures for decarbonization and improving ship efficiency, the “Ship Efficiency in the Context of EEDI, EEXI and CII - The MCN Guideline” has been compiled with the help of many authors and their valuable contributions. Care has been taken to ensure that the proposed technological improvements have been implemented at least in prototype form and that experience has first been gained at sea.

The document was created with the idea of providing an overview which helps ship operators, ship owners, shipbuilders, engineers, and many other stakeholders to ecologically improve ship development and operation. Improving ship efficiency will also help to comply to current and future regulations of the IMO in the sense of a sustainable shipping.

## **Acknowledgements**

MCN wants to thank all its authors for their commitment, knowledge and time that they put pro bono and without remuneration into creating this guideline.

## **References**

MCN (2022), *Ship Efficiency in the Context of EEDI, EEXI and CII – the MCN Guideline*, Maritime Cluster North Germany, Kiel



# Use of the Building Principle of the Dolphin's Skin to Reduce Hydrodynamic Drag on Ship Hulls - Recent Achievements

Claus Schreiner, Dorothea Stübing, Volker Föste, Volkmar Stenzel,  
Fraunhofer Institute for Manufacturing Technology and Advanced Materials IFAM  
Bremen/Germany, [Claus.Schreiner@ifam.fraunhofer.de](mailto:Claus.Schreiner@ifam.fraunhofer.de)

Jochen Marzi, Hamburgische Schiffbau Versuchsanstalt, Hamburg/Germany [marzi@hsva.de](mailto:marzi@hsva.de)

## Abstract

*This paper presents the achievements of a joint research project with the aim, to investigate an industrially feasible approach to drag-reducing surfaces inspired by the skin structure of dolphins. Former investigations have proven a drag-reducing effect of compliant coatings, which are able to maintain the flow laminar along the ship hull significantly longer than rigid surfaces. The main challenge is to find materials and application processes that are executable for industrial utilization of the drag-reducing effect.*

## 1. Introduction

It has been known for decades that the dolphin is able to keep the flow laminar along its fast-moving body and thus glide through the water extremely energy-efficiently. The special skin structure, consisting of the dermis and the underlying layer of fat ("blubber"), was held responsible for this early on. Since the 1950s there has been evidence that a compliant surface inspired by dolphin skin texture is able to significantly reduce the drag between a solid surface and a fluid, *Kramer (1957)*. The reason for this effect is a prolonged laminar flow along the body. However, the promising results obtained at that time in the USA could not be reproduced and transferred to a technical application for many decades.

From 2014 to 2017, the research project "FLIPPER", *Schrader (2016)*, carried out by Fraunhofer IFAM, the HSVA and other partners, was able to show for the first time that the flow on a ship model with a suitable coating structure in the flow channel of the HSVA was kept laminar and an associated reduction in flow resistance of 6% could be achieved, *Schrader (2019)*. The coating materials and processes examined and used there were selected with the aim of achieving an optimal result for the model test. An industrial applicability of the concept was not intended. This is where the NeWS project (FKZ 13XP5167A, funded by the German Federal Ministry of Education and Research) comes in, with the aim of developing an industrially applicable coating concept with the function of maintaining the laminar flow and the associated reduction in fuel consumption.

## 2. Key findings

In terms of the NeWS project, the previously used FLIPPER coating materials – silicone rubber as blubber, polyethylene foil as dermis – needed to be replaced by more common, more economic and easier-to-use/easier-to-apply coating systems while maintaining the materials' properties (storage modulus  $E$ , damping factor  $\tan \delta$ ) that proved successful. In addition, an antifouling solution needed to be implemented in the coating system to permit real environment applicability. With the materials selected and after cross-check with partner HSVA responsible for the hydrodynamic calculations and testing, several demonstrators (50 by 200 cm each) were coated and tested in HSVA's Hydrodynamics and Cavitation Tunnel (HYKAT). The demonstrator design, construction and calculation/simulation were also performed at HSVA.

### 2.1. Coating materials

In the FLIPPER project, a blend of two-component RTV silicones in different layer thicknesses were used as compliant blubber. The rigid dermis was formed by low-density polyethylene foil (LDPE)

which virtually wrapped (and thus held together) the whole demonstrator model, as the adhesion between both layers is extremely low. Thus, for practical purposes and durability reasons, a well adhering dermis on top of the blubber was highly desired.

Therefore, polyurethane gels were considered as blubber: such materials are rather economic, commercially available (Technogel® grades) and can simply be overcoated by polyurethane topcoats of various material properties.

From the FLIPPER project it is known that a suitable blubber material is characterized by a storage modulus  $E$  in the range of 50 to 100 kPa for an effective mitigation of the Tollmien-Schlichting (TS) waves while  $\tan \delta$  must be as low as possible (approx. around 0.05) to prevent the formation of flow-induced surface instability (FISI) waves. As both values need to be determined at a frequency of 300 Hz (= frequency of the most relevant wave to damp), dynamic mechanical analysis (DMA) was used employing time-temperature superposition (TTS).

It was found that the storage moduli of the PU gels at 300 Hz – dependent on the type tested (BTG 130 with a Shore 000-value of 60, BTG S 135 with Shore 000 35 and BTG S 120 with Shore 000 20) – were quite in the desired range (200 – 700 kPa), whereas  $\tan \delta$  values turned out far too high, Fig.1.

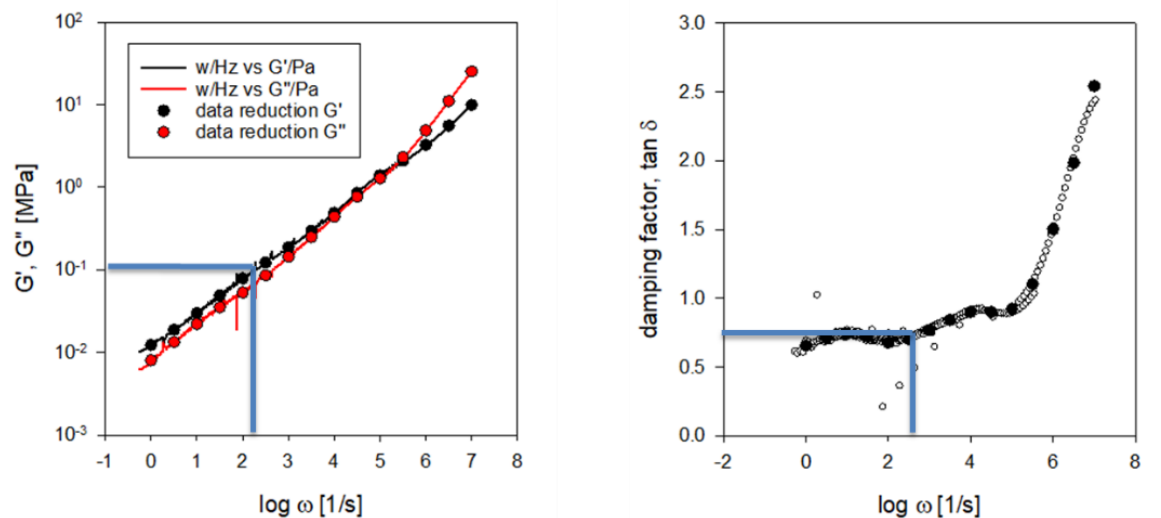


Fig.1: DMA (ARES) results for BTG S 120:  $E = 300$  kPa,  $\tan \delta = 0.7$

With  $\tan \delta$  at 0.7, a PU gel-based blubber would most likely cause FISI waves, and therefore the PU path was not followed further. Instead, like in the FLIPPER project, the focus was set on silicone rubber as blubber material. Here, tile-like concept of pre-fabricated silicone “cushions” covered by LDPE foil was evaluated, Fig.2.

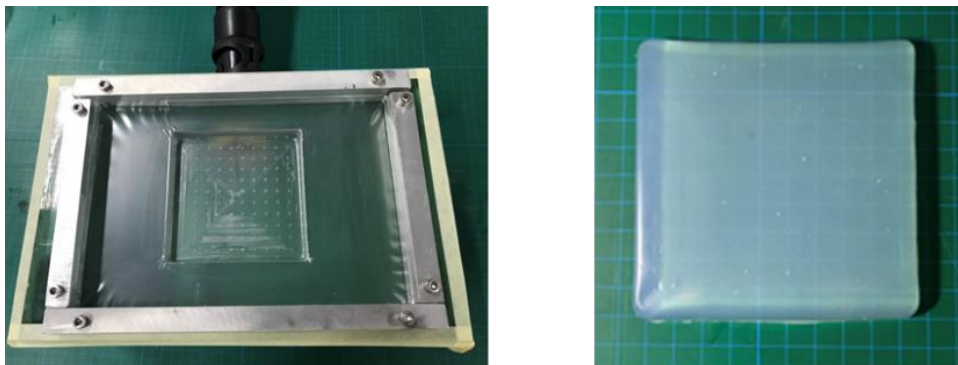


Fig.2: Approaches for silicone tile fabrication; left: mould with LDPE foil, right: silicone cushion covered by PE foil

However, as the adhesion of PE foil on silicone rubber was inadequate and overcoating of PE (see 2.2. Antifouling properties) is challenging even after activation with atmospheric plasma, examinations on dermis modification were conducted.

From HSVA calculations it was evident that in fact the storage modulus of the dermis is not too critical as long as the damping of the material is low, Fig.3. Therefore, a silicone-based dermis was considered: here, the compatibility to the blubber as well as to the fouling control topcoat (which is also silicone-based) should be best.

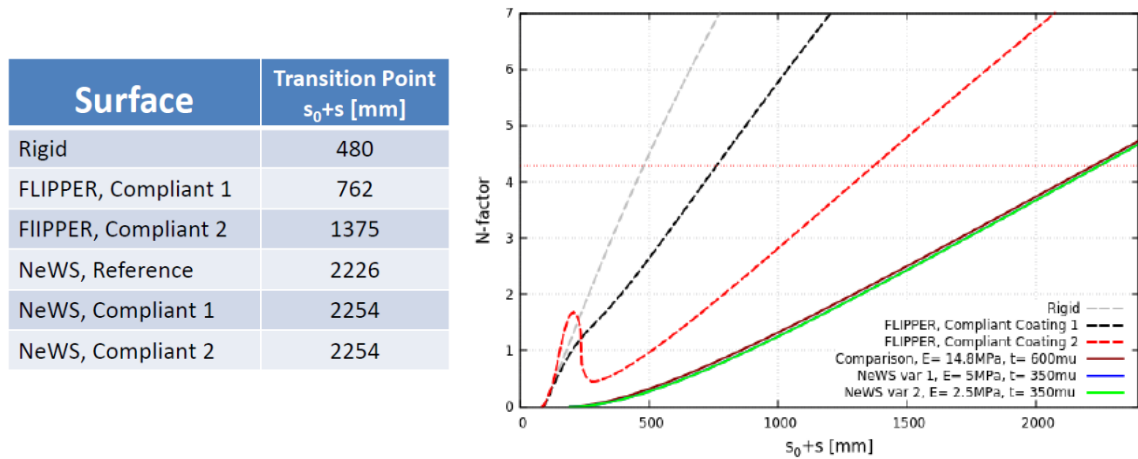


Fig.3: Growth curves: with the FLIPPER approaches (Compliant 1 and 2) the transition point is shifted from 480 (rigid wall) to 762 and 1375 mm, respectively. With a storage modulus of 14.8 MPa (NeWS, Reference), 5 (NeWS, Compliant 1) and 2.5 MPa (NeWS, Compliant 2), the transition points are shifted to approx. 2.2 m, rather independent on E.

As given in Fig.3, a storage modulus for dermis + fouling release coating of ~2.5 MPa should be sufficient to achieve a significant shift in laminar-turbulent transition. Therefore, experiments on enforcing silicone rubber with functional filler materials were conducted.

Two sorts of fillers were tested at various concentrations. In the best cases, storage moduli of 9 MPa with damping factors still below 0.1 were achieved, Fig.4.

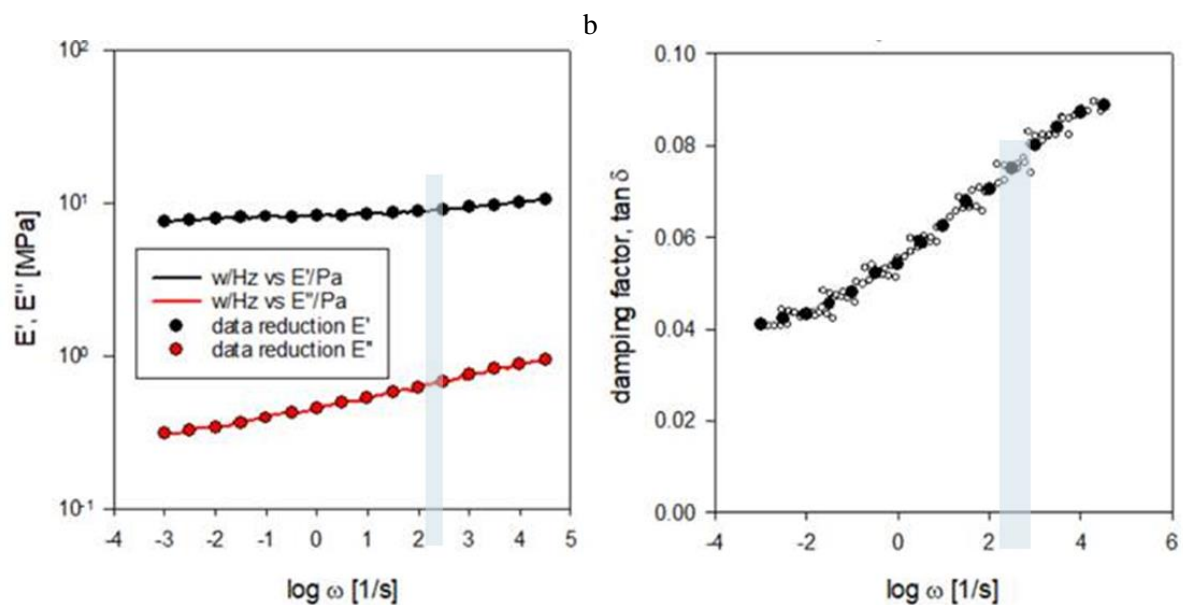


Fig.4: DMA (Tension) results for silicone equipped with 25% filler B:  $E = 9$  MPa,  $\tan \delta = 0.075$  (at the relevant frequency of 300 Hz)

All the data obtained made clear that a successful approach for demonstration would foresee the following build up, Fig.5: the silicone blubber is fixed to the aluminum plates by use of a two-component silicone adhesive. As dermis material, a reinforced silicone film is wrapping the blubber, and in the end the silicone-based fouling-release coating is applied on top.

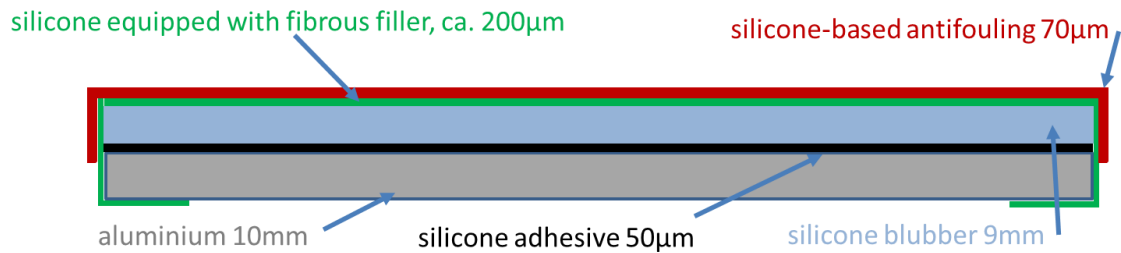


Fig.5: Build up designated for the demonstrator fabrication

## 2.2. Antifouling properties

For the implementation of antifouling properties, the use of a commercially available, biocide-free fouling release coating on the dermis was foreseen. As initially LDPE foil was intended as dermis, ensuring adequate adhesion on the polymer foil was challenging. Different methods – the perforation with numerous small holes in the dermis to bridge between both silicones or by treatment with atmospheric plasma – were examined. In the end, none of these proved adequately promising.

However, after replacing the dermis by a fibre-enforced silicone film of good compatibility with the antifouling topcoat, the inter-system adhesion seemed sufficient for the HYKAT tests.







Fig.6: Static immersion testing of compliant coatings. a) panel before static immersion, b) after 5 months (October 2022), c) after 11 months (March 2023) when the experiment was terminated by assessing the ease of biofouling removal: d) cleaned panel

The fouling control performance of the compliant coating system was tested by static immersion on the island of Helgoland, German Bight, North Sea. A test panel with different compliant coating build ups was prepared: i) Si-blubber + LDPE dermis corresponding to the original FLIPPER set-up, Fig.6a, four dark squares right hand side, ii) Si-blubber + LDPE dermis overcoated by the commercial fouling release coating (FRC), Fig.6a, four squares in the centre, and iii) the Si-blubber material directly overcoated by the FRC, Fig.6a, four squares left hand side. Thus, it was tested whether the compliant material has an intrinsic fouling control property and, in comparison, the performance of the system in combination with an FRC was assessed. The biofouling development on the test panel was monitored for about 11 months from beginning of May 2022, Fig.6b, to the end of March 2023, Fig.6c. At the end of this testing period, the cleaning behaviour of the materials was assessed by gentle cleaning with a soft sponge, Fig.6d). Evidently, the compliant coating set-up did not show any intrinsic biofouling control behaviour. These test areas were covered with heavy biofouling consisting mainly of red, green, and brown algae, ascidians, and blue mussels. The areas overcoated by the FRC on the other hand were only covered by microalgae. Nevertheless, all biofouling could be removed relatively easily by means of the soft sponge, even the heavily fouled LDPE surfaces could be cleaned in this way, Fig.6d. However, adhesion issues of the FLIPPER set up plus FRC could be observed after prolonged immersion (~11 months). Here, delamination of the FRC from the LDPE foil occurred corroborating the initial observation that even plasma activation of the LDPE surface is not sufficient to provide adequate and durable adhesion between the two layers. No such delamination occurred on the samples where the silicone blubber was directly overcoated by the FRC.



### 2.3. Demonstration

The demonstrator panels to be tested at HSVA were fabricated as follows: at first, a reinforced silicone film was cast by blade technique. After full cure, a frame defining the correct dimension as well as thickness of the silicone build up was put around the film. Then, the form was filled with the blubber silicone mixture, Fig.7.



Fig.7: left: casting of the reinforced silicone film; middle: free silicone dermis; right: frame set up on the silicone dermis, ready to be filled up with blubber material

After full cure of the blubber, the demonstrator part was deformed and, by the use of a two-component silicone adhesive, attached to the aluminium plate, Fig.8.



Fig.8: Silicone build up attached to one aluminium demonstrator panel

Two of such cushions were attached to each plate, and finally, the antifouling topcoat was applied. At HSVA, the plates were mounted on the demonstration unit which was then tested in the Hydrodynamics and Cavitation Tunnel (HYKAT), Fig.9, in comparison to a hard surface (= aluminium plates covered with a common 2K-PU coating material).



Fig.9: Full demonstrator prior to mounting in the HYKAT channel

The total drag of the demonstrator setup consists of a pressure- and a friction-related part. Due to identical geometry, the pressure-related part is equal for the rigid reference as well as for the compliant coatings. As only the coated aluminium plates were exchanged between reference and experimental testing, the rest of the demonstrator build up remained unchanged. Therefore, the differences detected concerning friction resistance can fully be attributed to the coatings (hard vs. compliant).

The results obtained are given in Fig.10.

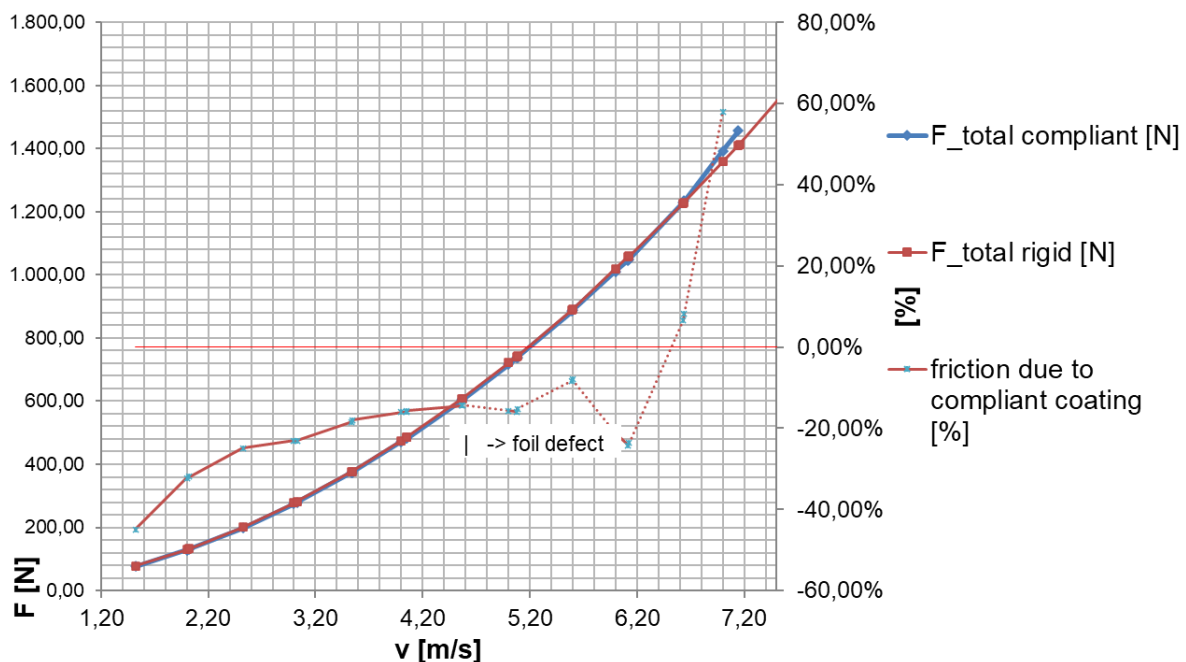


Fig.10: Results of the HYKAT experiments: ~14% reduction in friction due to the compliant vs. the rigid surface up to flow speeds of 5.5 m/s

The reason why the positive trend of friction reduction was only maintained up to flow speeds of 5.5 m/s must be seen in delamination issues at the rear end of the coated plates, Fig.11. Unfortunately, the desired positive pressure gradient across the whole demonstrator build up was not achieved in that specific area (which equals a suction force of ~200 N) which in the end led to adhesive failure of the coating system.

However, it could well be demonstrated that the materials selected show high potential for the use as compliant ship hull coatings.

As the friction-reducing effect could by now be shown reliably in terms of two projects – FLIPPER and NeWS – it can be considered highly interesting to test, as a next step, the coating setup in a more realistic environment; getting the chance to coat a real ship with the technology developed would surely bring the approach a further step forward.

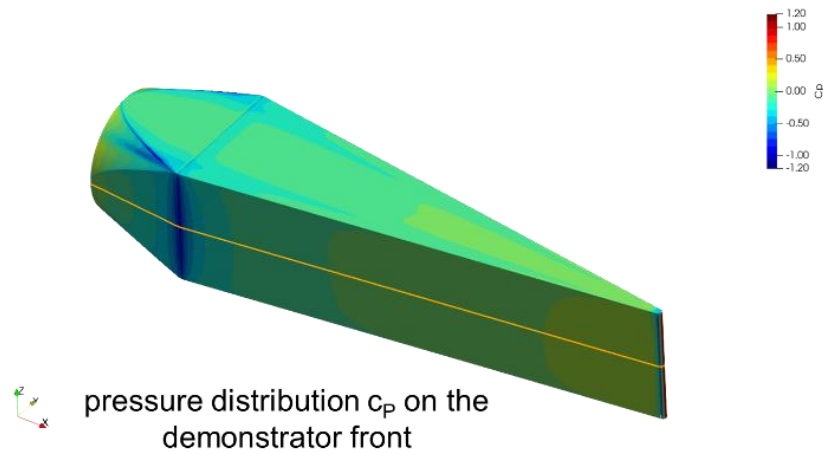


Fig.11: Negative pressure at the rear end of the coated plates which caused delamination issues during the HYKAT experiment

### Acknowledgements

The Project NeWS was funded by the German Federal Ministry of Education and Research under the reference number 13XP5167A. The authors would also like to thank the Fassmer Group for providing an internship and the willingness to discuss the project results.

### References

- KRAMER, M.O. (1957), *Boundary layer stabilization by distributed damping*, J. Aeronaut. Sci., 24(6), pp.459-460
- SCHRADER, L.-U. (2016), *Drag reduction for ships: Drawing inspiration from dolphins*, 10<sup>th</sup> Symp. High-Performance Marine Vehicles (HIPER), pp.187-192
- SCHRADER, L.-U. (2019), *Passive drag reduction via bionic hull coatings*, J. Ship Res. 63(03), pp.206-218

# Where Wind Power Makes Business Sense for Bulk Carriers

**Heikki Hansen**, DNV, Hamburg/Germany, [heikki.hansen@dnv.com](mailto:heikki.hansen@dnv.com)  
**Karsten Hochkirch**, DNV, Hamburg/Germany, [karsten.hochkirch@dnv.com](mailto:karsten.hochkirch@dnv.com)  
**Uwe Hollenbach**, DNV, Hamburg/Germany, [uwe.hollenbach@dnv.com](mailto:uwe.hollenbach@dnv.com)  
**Volker Bertram**, DNV, Hamburg/Germany, [volker.bertram@dnv.com](mailto:volker.bertram@dnv.com)

## Abstract

*Rising fuel prices, environmental pressures, and regulations (EEXI and CII) are starting to drive the decarbonisation of shipping. Consequently, wind propulsion is revitalized to help reduce CO<sub>2</sub> emissions. But under which scenarios does wind propulsion make business sense? For the example of a Capesize bulk carrier, the economic viability of installing a wind-assisted propulsion system (WAPS) is assessed by studying the impact of several parameters: WAPS savings, WAPS cost, routes, vessel speed, fuel price and charter rate. Variation of these parameters shows how they drive the business case and how the investment risk can be minimized.*

## 1. Introduction

The maritime industry stands at a critical juncture, where the pursuit of environmental sustainability converges with the imperatives of economic viability. As the sector seeks innovative solutions to reduce its carbon footprint and align with global emission reduction goals, wind-assisted propulsion systems have emerged as a compelling avenue. These systems harness wind energy to augment traditional propulsion methods, offering the promise of reduced fuel consumption, lowered operational costs, and decreased greenhouse gas emissions. However, the successful integration of wind-assisted propulsion systems hinges on careful economic considerations.

While the environmental benefits are clear, it is imperative to analyse the financial feasibility, investment costs, and long-term returns associated with these technologies. This paper delves into the relationship between wind-assisted propulsion systems and economic factors, exploring how these systems can be not only environmentally advantageous but also economically prudent choices for the maritime industry's sustainable evolution.

For the example of a Capesize bulk carrier, the economic viability of installing a wind-assisted propulsion system (WAPS) is assessed. The performance of a typical Capesize bulk carrier with and without a WAPS is conducted utilizing DNV'S Performance Prediction Program for wind-assisted cargo ships. The power reduction due to the WAPS is then assessed on different routes representing trading areas around the world. The impact of several parameters on the economic viability is investigated for the different routes to show what drives the business case and investment risk.

## 2. Performance prediction for WAPS on Capesize bulk carrier

This study is conducted for a Capesize bulk carrier. The principal particular of the typical Capesize bulk carrier used here are shown in Table I.

Table I: Principal particulars of Capesize bulk carrier

Length (O.A.)	292 m	Cargo-hold capacity (grain)	200,000 m <sup>3</sup>
Length (B.P.)	284 m	Gross tonnage	93,000
Breadth	45 m	Net tonnage	60,000
Draft (scantling)	18.2 m	Main engine MCR	15,500 kW
Deadweight	180,000 MT	Service speed	14.5 kn

Saving from a WAPS not only depend on the installed system but also on the vessel characteristics. It is therefore important not to look at a WAPS by itself but in combination with a specific vessel. A



performance prediction for the vessel without and with a WAPS is conducted to calculate the power reduction from the WAPS.

DNV's Performance Prediction Program (PPP) for wind-assisted cargo ships is employed, which utilizes DNV's modular 6 DoF (degrees of freedom) performance prediction workbench FS-Equilibrium. It is a fast and easy tool able to reasonably accurately predict the performance of any commercial ship equipped with WAPS such as rotor sails, suction sails, rigid wing sails and Dyna rigs. The tool works with only the ship main particulars and general dimensions as input data and is based on semi-empirical methods and a WAPS aerodynamic database created from published data on lift and drag coefficients. All WAPS data can be interpolated to scale to different sizes and configurations. Vessel or WAPS specify input data can also be used to increase the accuracy of the prediction. All forces are modelled as separate force components so that it is easily possible to combine input data from different sources and fidelity levels. For details on the PPP refer to *Reche-Vilanova et al. (2021)* and *Hollenbach et al. (2020)*.

For this study the vessel hydrodynamics and aerodynamics are modelled in 4 DoF (surge, sway, roll, yaw). The external forces acting on the vessel are modelled by force modules, Table II.

Table II: External forces acting on the vessel

Force type	Data source
Righting moment	GM from stability book
Hull resistance	Resistance from model tests
Hull side force	Approach by <i>Schenzle (1985)</i> for sailing ships without long fin keels
Propeller thrust	Propeller open water curves for Wageningen B-Series propeller with same principal particulars
Rudder side force and drag	Semi-empirical model based on low aspect ratio foils
Superstructure and hull windage	Standard coefficients available for bulk carriers
WAPS (rotor sails)	Aero coefficients and required operating power from WAPS published data

Rotor sails (Flettner rotors) are selected for this study because they are currently the most mature and most widely used WAPS. This study could equally well be conducted with another WAPS. The power reduction achieved by the WAPS is varied in this study to show certain trends and the choice of rotor sails is only exemplary. The principal particulars of the rotor sails use for this study are shown in Table III.

Table III: Principal particulars of the rotor sails

Number of units (base configuration)	4	
Rotor sail height	35	m
Rotor sail diameter	5	m
Maximum rotation speed	180	rpm

The force equilibrium in 4 DoF is found for constant ship speed. The free variable in surge is the propeller RPM. The other free variables are leeway, heel and rudder angle.

For each operating condition with WAPS, an optimization algorithm is utilized to find the rotation speed that results in the minimum net propulsion power (power delivered to propeller + power required to operate WAPS). In this study interaction of the different rotors is not considered and the rotation speed of all rotors is the same.

The true wind speed and angle (TWS and TWA) are defined at a height of 10 m. The apparent wind speed and angle (AWS and AWA) are calculated at the respective centre of area of the force component (i.e. WAPS and superstructure).

The wind gradient is modelled with the power law and exponent of 0.11 (1/9).

The WAPS savings are calculated as the difference in propulsion power of the vessel with and without WAPS. The savings are presented as a power reduction in kilo watts. The power reduction is the most relevant parameter to assess the WAPS performance and commercial viability. When specifying percentage savings, one must be extremely careful to understand how the reference power is defined (draft, sea margin, added wind and wave resistance). These factors have much less influence when specifying the power reduction in kilo watts directly.

Fig.1 shows the power reduction for the vessels with 4 rotor sails as a function of true wind angle (TWA) for three true wind speeds (TWS) and two ship speeds (Vs).

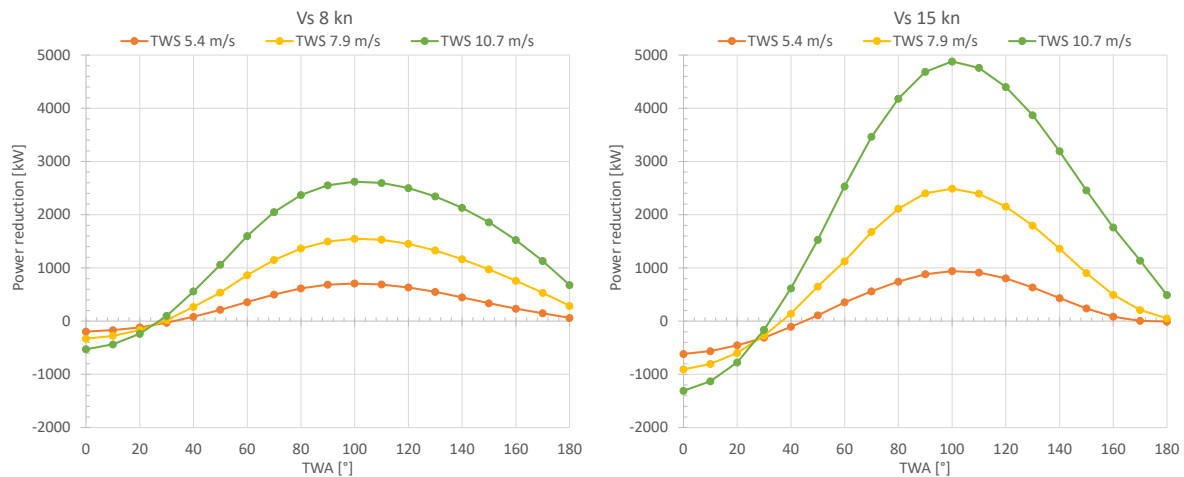


Fig.1: Power reduction for vessel with 4 rotor sails

It is assumed that the rotor sails are not tiltable during ocean passages. The vessel with WAPS therefore has additional windage when the WAPS is not in use. In Fig.1 the additional windage caused by the WAPS can be seen for small TWA. The rotors are only turned off at 0° TWA. Already at 10° TWA it is more beneficial to have the rotors rotate at relatively small RPM. Although the rotors do not produce a forward thrust, the resistance (along the ship centreline) is less than with the system turned off.

The power reduction from a WAPS is strongly dependent on the true wind speed and the ship speed as these define the apparent wind speed (AWS) and apparent wind angle (AWA) experienced by the WAPS. Fig.2 shows the AWS at the height of the centre of area (CoA) of the rotors. The AWS changes more significantly with TWA as the ship speed (Vs) gets larger.

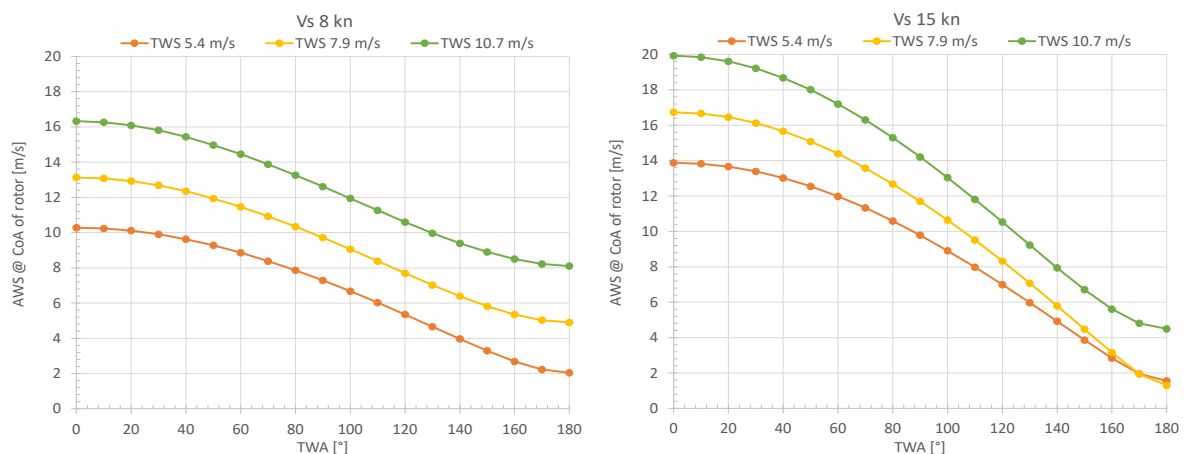


Fig.2: Apparent wind speed (AWS) at the CoA of the rotors

Fig.3 shows the AWA at the height of the centre of area (CoA) of the rotors. For a ship speed of 8 kn, the AWA is not fundamentally different for the different TWS. For a ship speed of 15 kn, the AWA is significantly different for the lowest TWS. The AWA is never larger than  $55^\circ$ .

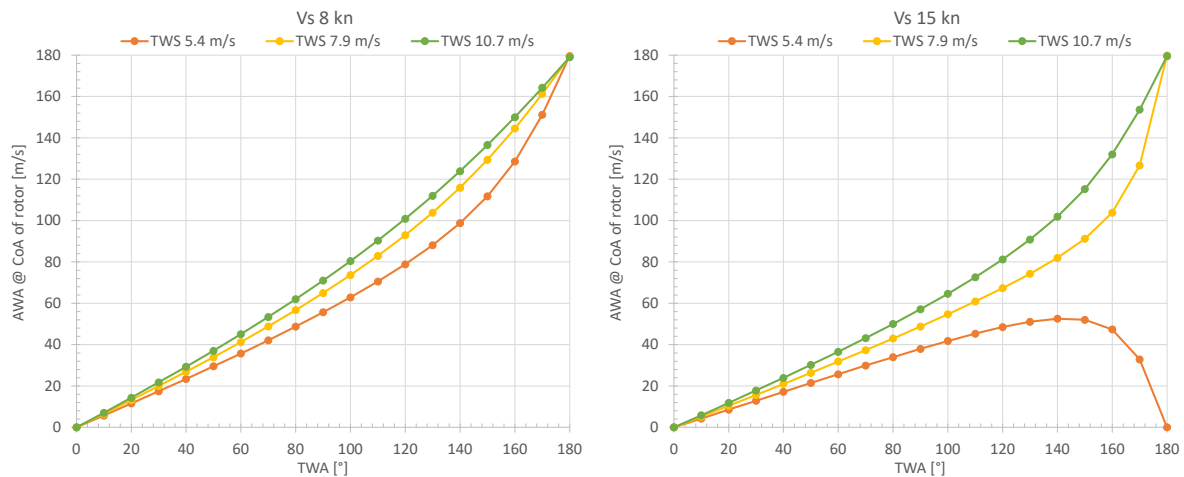


Fig.3: Apparent wind angle (AWA) at the CoA of the rotors

### 3. Assessment of WAPS savings on different routes

The WAPS savings calculated in the previous section need to be applied to vessel routes to obtain realistic savings. The operating condition of the vessel and the environmental conditions are relevant. For vessel or fleet specific investigations this can be done accurately with hindsight operational and weather data. Many past voyages should be investigated to determine statistically relevant weather conditions. Route optimization can also be conducted on past voyages to illustrate the achievable savings more realistically since a vessel with WAPS should sail a different route optimized for WAPS usage.

For this study a more generic approach is employed to look at different routes. Three fictive routes of 10,000 nm round trip are defined in different parts of the world. For each route a representative average wind speed is used depending on the area as shown in Table IV.

Table IV: Definition of routes

Route	Average wind speed	Wind direction	Length (round trip)
Topical	5.4 m/s	Evenly distributed	10,000 nm
North Sea	7.9 m/s	Evenly distributed	10,000 nm
Nordic Ocean	10.7 m/s	Evenly distributed	10,000 nm

It is assumed that the wind direction on each route is evenly distributed. The WAPS power reduction calculated in the previous section are averaged over the whole TWA range and Fig.4 shows the resulting WAPS power reduction as a function of ship speed for the three different wind speeds representing the different routes. For the tropical route (TWS 5.4 m/s) the power reduction does not change significantly with ship speed. For the routes with more wind, the power reduction increases with ship speed. In higher TWS, the WAPS operating conditions where high lift results in maximum drive force dominate also for higher ship speeds. Higher ship speed increases the AWS so that more drive force is generated. The power reduction increases.

Each route is a return trip of 10,000 nm. On the outbound leg the vessel operates at scantling draft and on the return leg in ballast draft. It is assumed that the auxiliary engines run at 50% load and the resulting fuel consumption of 5.5 t/d is included in the total consumption. Fig.5 shows the resulting change in fuel consumption or CO<sub>2</sub> emission for the North Sea route as a function of vessel speed. At the reference speed of 15 kn without WAPS, the CO<sub>2</sub> emissions are 7,101 t. The significant reduction

in fuel consumption due to speed reduction can be seen. The reduction due to the WAPS is between 6-20% of the total fuel consumption including auxiliary engine consumption.

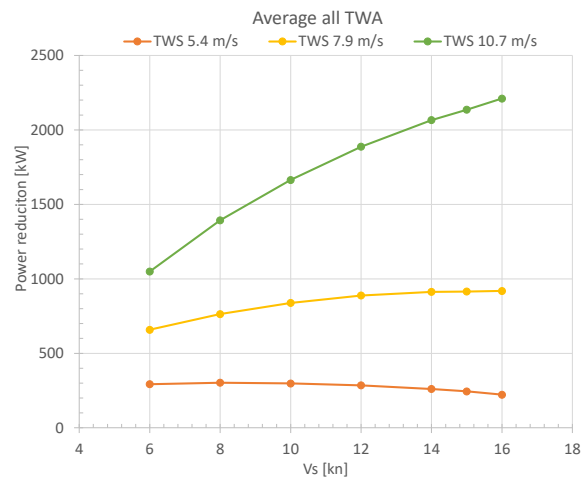


Fig.4: WAPS power reduction on different routes

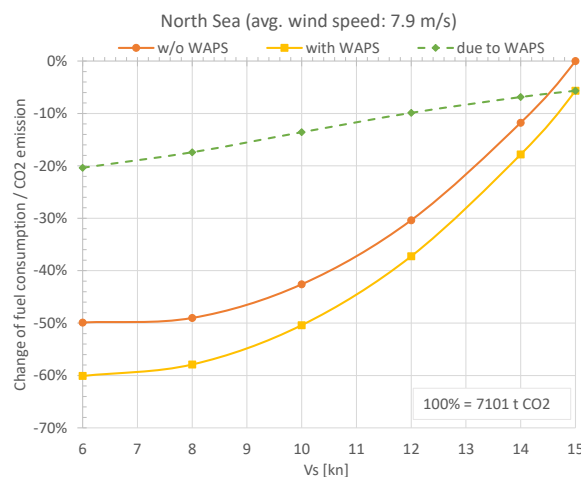


Fig.5: Change in fuel consumption or CO<sub>2</sub> emission on North Sea route

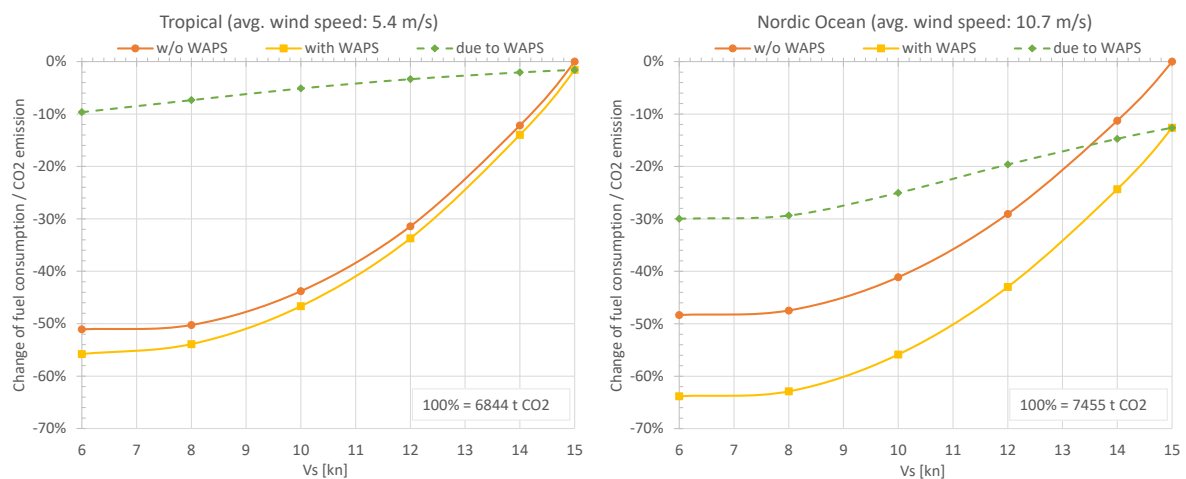


Fig.6: Change in fuel consumption or CO<sub>2</sub> emission on Tropical and Nordic Ocean route

Fig.6 shows the change in fuel consumption or CO<sub>2</sub> emission for two other routes. For the Tropical route the WAPS savings are between 2-10% depending on the ship speed. The savings on the Nordic Ocean route are between 13-30%. For the lowest ship speed of 6 kn, the WAPS can reduce the



propulsion power by 100% (ship is full sailing) in certain conditions. On the Nordic Ocean route the average propulsion power reduction across all true wind angles is 45% at 6 kn ship speed. This results in the total fuel consumption reduction of 30% shown in Fig.6 due to the auxiliary engine consumption.

#### 4. Economic assessment of WAPS

For the economic assessment of the WAPS the following parameters are added in the calculations. The daily charter rate for is taken as 15,000 USD/d. The installation cost of the four rotor sails is assumed to be 4 x 750,000 USD and a yearly maintenance of 2.3% of the initial investment is required. Depreciation is set at 10 years and capital is subject to 5% interest rate. The case study assumes a round trip of 10,000 nm and considers 60% sailing time (220 days/year) of the vessel. The price for very low-sulphur fuel oil is taken as 600 USD/t for this study. Although not yet implemented for shipping, discussions on trading schemes for emissions are ongoing and, at least for the EU, it seems likely that shipping will be included in the ETS. This would mean extra costs for using fossil fuel and currently a ton of CO<sub>2</sub> is traded at ~90 €/t (~ 100 USD/t). Table V summarizes these assumptions.

Table V: Economic assumptions

Charter rate of conventional powered vessel	15,000	USD/d
Capital cost of WAPS installation	4 x 750,000	USD
Maintenance cost of WAPS system	2.3	% pa
Depreciation period	10	years
Interest rate	5	% pa
Auxiliary fuel consumption	5.5	t/d
Fuel price	600	USD/t
CO <sub>2</sub> emission trading	100	USD/t
Costs for port call	50,000	USD/trip

Fig.7 shows the resulting change in total cost for the North Sea route. The optimum is at a ship speed of about 9-10 kn. The total cost can be reduced by 25-30% by reducing the ship speed from 15 kn. The relative increase of costs for very low speeds is mainly a result of the charter costs which are applicable daily and the anti-proportional increase with the reduction of ship speed. The same applies to costs for powering the auxiliary engines. Fig.8 illustrates this by showing the split up of the total trip costs for different speeds for the WAPS supported vessel on the North Sea route. Fig.7 also shows that the WAPS reduces the total cost by 2-3%.

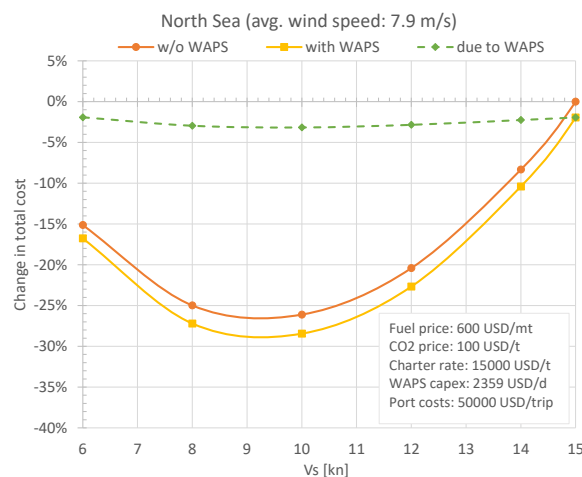


Fig.7: Change in total cost on North Sea route

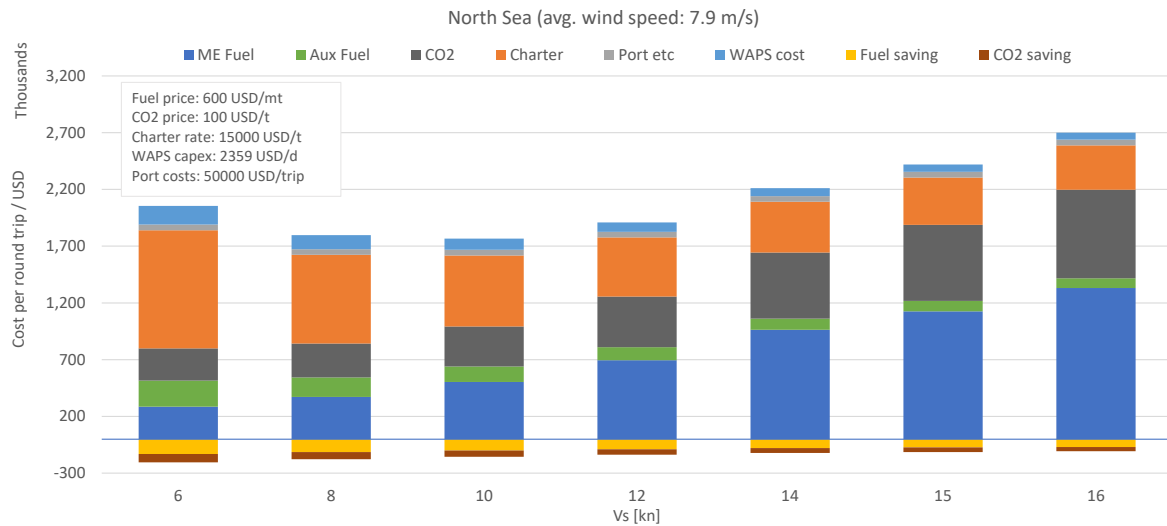


Fig.8: Cost split up for different ship speeds on North Sea route

Fig.9 shows the change in total cost for the two other routes. For the Tropical route the total cost with the WAPS is higher for all ship speeds. This means that the fuel savings are not large enough to cover the WAPS costs. In the Nordic Ocean the WAPS reduces total cost by around 10%.

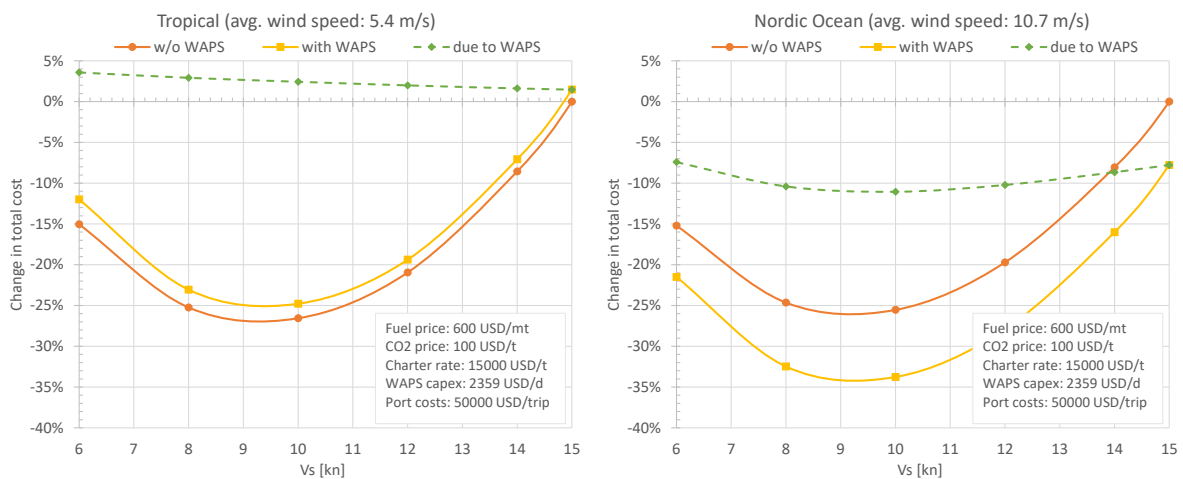


Fig.9: Change in total cost on Tropical and Nordic Ocean route

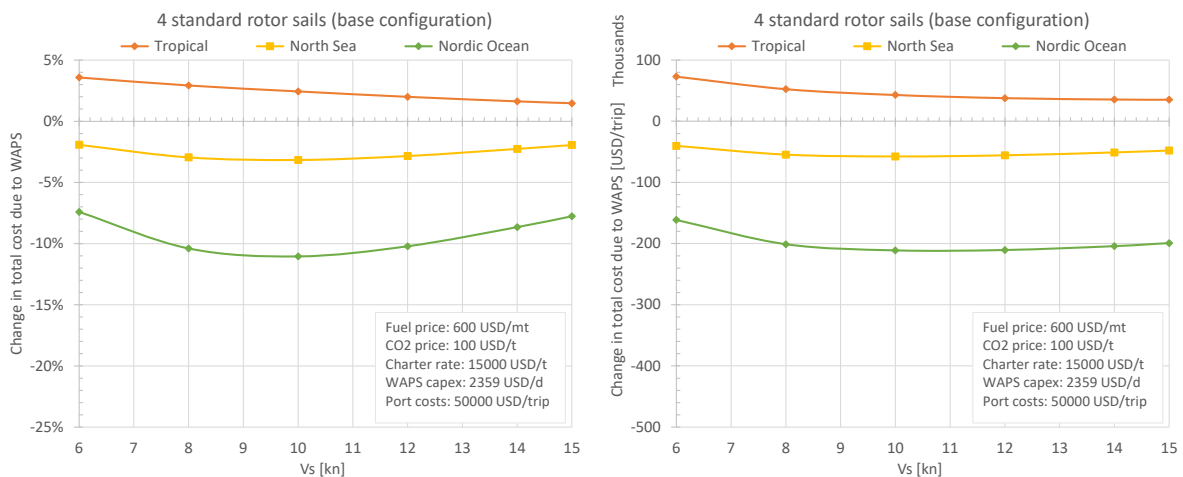


Fig.10: Change in total cost due to WAPS in percent and in USD/trip

Fig.10 shows the change in total cost for all three routes together as percentage change and as absolute change in USD per trip. The WAPS increases the cost of a trip on the Tropical route by around 50,000 USD. On the North Sea and Nordic Ocean routes, the trip cost reduces by around 50,000 USD and 200,000 USD respectively.

## 5. Impact assessment of economic factors on WAPS cost savings

For the economic assessment it is also important to understand the impact of different parameters on the total operating cost when installing a WAPS. For an investment decision the absolute cost in USD is usually more relevant than the percentage cost change. When considering the absolute cost, expenditures not directly related to the WAPS are not relevant. The charter rate, port costs and auxiliary fuel consumption are not relevant. These factors influence the relative total cost change but not the absolute cost change. Factors in this study directly related to the WAPS economic performance are the fuel price (and CO<sub>2</sub> price), the WAPS cost per unit, the number of installed units and the efficiency of the WAPS system (reduction of power).

Fig.11 shows the total change in cost due to the WAPS when the fuel price is 1,200 USD/t instead of 600 USD/t. The reference results for 600 USD/t are presented and discussed in the previous section and shown in Fig.10. Fig.11 shows that with double the fuel price the WAPS system on the Tropical route is about cost neutral compared to the 50,000 USD/trip extra cost before. For the other two routes the cost reduction increases significantly. On the Nordic Ocean route the cost reduction is now around 400,000 USD/trip compared to 200,000 USD/trip before. An increase in fuel price increases the cost reduction. But a doubling of the fuel price is required to make the WAPS profitable on the Tropical route. On the other hand, the WAPS on the North Sea route is still economical down to a fuel price of around 300 USD/t.

Fig.12 shows the total change in cost due to the WAPS when the installation and maintenance costs are halved. It is assumed that the same system costs half the price. The number of units and the performance of the system remain the same. The results can be compared to the reference case in Fig.10 as before. With the half price system, the Tropical route is about cost neutral. For the other routes the cost reduction increases. The trends are similar to the increased fuel price case, Fig.11, but the increase in cost reduction is not as high.

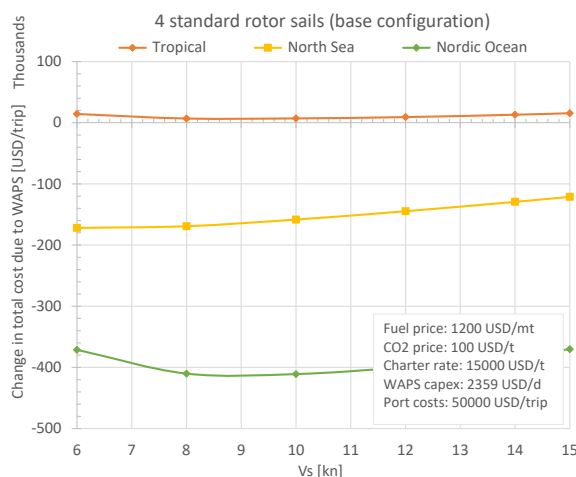


Fig.11: Change in total cost due to WAPS:  
2 x fuel price

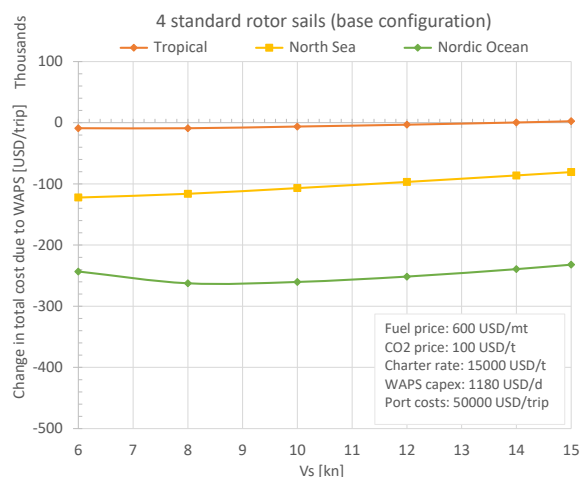


Fig.12: Change in total cost due to WAPS:  
0.5 x WAPS cost

Fig.13 looks at the effect of installing 5 instead of 4 rotor sails. A performance prediction with 5 rotor sails is conducted and the WAPS power reduction values presented in Fig.4 are updated in the calculations. The performance prediction results in an average increase in power reduction of 21.2% for the operating conditions shown in Fig.4. Linear scaling of the power reduction from 4 to 5 rotors

would result in an increase by 25%. As expected, the increase in power reduction is relatively close to linear but some nonlinear effects reduce the savings by 4 percentage points. This is caused by changes in leeway, rudder angle and propeller efficiency. At ship speed of 6 kn and 8 kn the vessel can fully sail in certain conditions. In such cases the rotor RPM are reduced to maintain the constant speed. This also contributes to the nonlinear effect when moving from 4 to 5 rotors. The installation and maintenance costs are increased proportionally for the additional unit.

Fig.13 shows that increasing the number of rotors increases the cost reduction on the North Sea and Nordic Ocean routes. However, on the Tropical route the increase in cost also gets higher. Installing more units for the Tropical route would be counterproductive.

Fig.14 shows the effect of installing more efficient rotor sails. It is assumed that the installation and maintenance costs remain the same. A performance prediction is conducted with a different rotor sail aerodynamic model, which has a higher lift to drag ratio at small lift coefficients. This makes the rotor sails better in close hauled conditions. The performance prediction shows an average increase in power reduction of 45.8% for the operating conditions shown in Fig.4. With this improvement in power reduction, the WAPS is cost neutral on the Tropical route for higher ship speeds. At slower speeds there is still on cost increase of up to 50,000 USD/trip at 6 kn ship speed. On the North Sea and Nordic Ocean routes the cost reduction increases to 200,000 USD/trip and 300,000 USD/trip respectively for the higher ship speeds. At higher ships speeds to apparent wind angles are generally smaller and a more efficient sail makes a bigger difference.

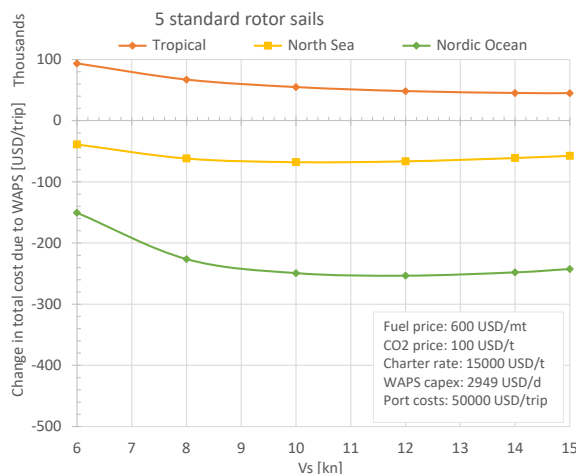


Fig.13: Change in total cost due to WAPS:  
5 standard rotor sails

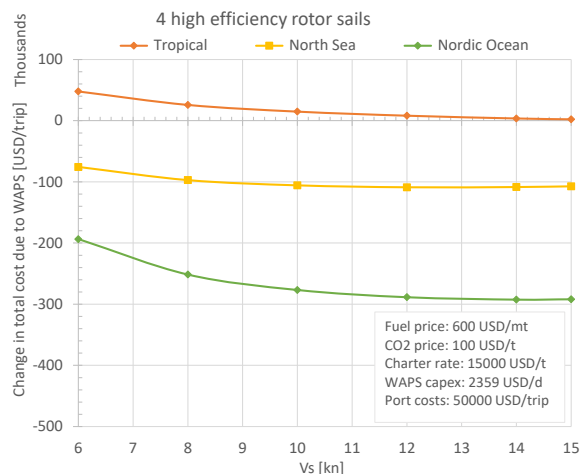


Fig.14: Change in total cost due to WAPS:  
4 high efficiency rotor sails

Fig.15 shows the total cost reduction for rotor sails that are fully tiltable to the deck during ocean passages when not in use. A performance prediction is run with reduced windage of the tilted rotor sails when not in used. The standard aerodynamic model is utilized, and it is assumed that the installation and maintenance cost remain the same. The performance prediction results in an average increase in power reduction of 10.2% for the operating conditions shown in Fig.4.

Fig.16 shows the total cost reduction due to the rotor sails being tiltable. The savings effect of tilting the rotor sails increases with ship speed. At higher ship speeds the apparent wind angle gets smaller for most conditions and there are more conditions where the WAPS is not used. In these conditions the apparent wind speed increases with ship speeds as well. On the Tropical route the cost reduces on average by around 7,000 USD/trip. An installation and maintenance cost increase for the tiltable rotor sails of around 7% would offset the cost reduction. On the North Sea and Nordic Ocean routes the cost reduces on average by around 10,000 USD/trip and 13,000 USD/trip. An installation and maintenance cost increase for the tiltable rotor sails of around 10% and 14% would offset the cost reduction on these two routes respectively.

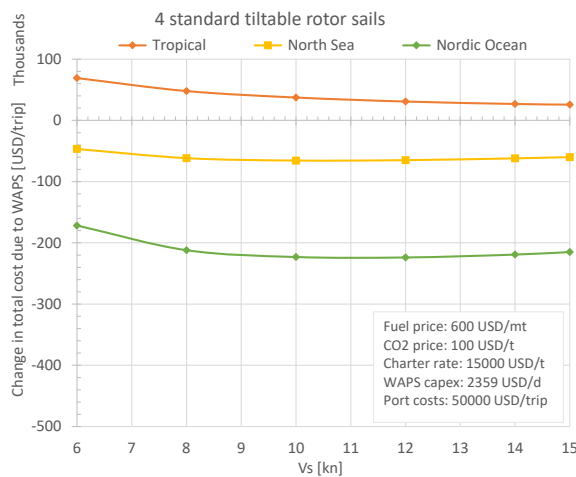


Fig.15: Change in total cost due to WAPS:  
4 standard tiltable rotor sails

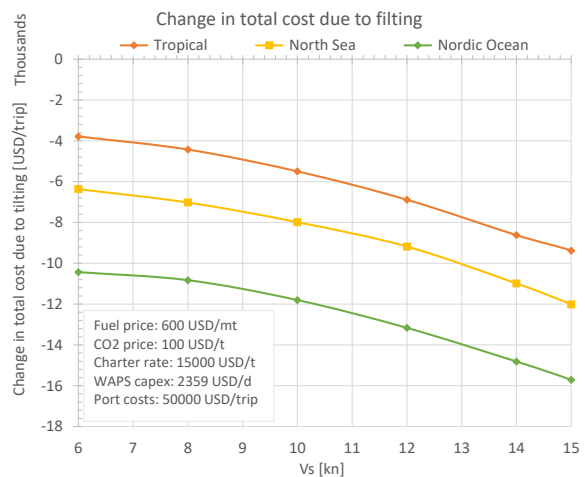


Fig.16: Change in total cost due to tilting of 4  
standard rotors when not in use

## 6. Conclusions

The WAPS power reduction is assessed for a Capesize bulk carrier utilizing 4 DoF performance predictions. Based on the performance predictions, the effect on the total operating cost is evaluated for three fictive routes describing the average wind conditions expected in different parts of the world.

The most important factor for the economic viability of the WAPS is the route, i.e. the average wind speed. On the North Sea and the Nordic Ocean routes with average wind speeds of 7.9 m/s and 10.7 m/s the WAPS leads to a cost reduction. All the investigated parameter changes increase the cost reduction; increase of fuel price, reduced WAPS cost, installation of an additional rotor sail, more efficient rotor sails and tiltable rotor sails. The WAPS on the North Sea route is still economical down to a fuel price of around 300 USD/t.

On the Tropical route with an average wind speed of 5.4 m/s the WAPS leads to an increase in total cost. The fuel and CO<sub>2</sub> savings are less than the installation and maintenance costs. The fuel price needs to double to 1,200 USD/t or the WAPS cost needs to half to make the system economic on this route. Installation of an additional rotor sail increases the total cost further. Even high efficiency rotor sails that achieve almost 50% more power reduction do not make the WAPS economical for speeds below 14 kn. Only at the higher ship speeds the WAPS becomes cost neutral.

Tiltable rotor sails are more economical if the installation and maintenance cost does not increase more than 7-14 % depending on the route.

The study highlights that the wind conditions are the most important factor determining the economic viability of a WAPS. The operating profile of a vessel and the weather routing potential should therefore be investigated in detail when considering a WAPS. If a system is economical on the operating profile, increasing the number of units should increase the savings. Cost and efficiency of the WAPS is also important. It should be investigated after the vessel operating profile is assessed and optimized.

## References

HOLLENBACH, U.; HANSEN, H.; HYMPENDAHL, O.; RECHE, M.; RUIZ CARRIO, E. (2020), *Wind Assisted Propulsion Systems as Key to Ultra Energy Efficient Ships*, 12<sup>th</sup> HIPER Conf., Cortona, [http://data.hiper-conf.info/Hiper2020\\_Cortona.pdf](http://data.hiper-conf.info/Hiper2020_Cortona.pdf), pp. 543-561



RECHE-VILANOVA, M.; HANSEN, H.; BINGHAM, H.B. (2021), *Performance Prediction Program for Wind-Assisted Cargo Ships*, J. Sailing Technology 6 (01), pp.91-117

SCHENZLE, P. (1985), *Estimation of Wind Assistance Potential*, J. Wind Engineering and Industrial Aerodynamics 20, pp. 97-110

# Larabicus - Development of an Autonomous and Energy Autarkic In-transit Hull Cleaning Robot using Hydrodynamic Optimization based on CFD

Florian Gerland, University of Kassel, Kassel/Germany, [florian.gerland@larabicus.com](mailto:florian.gerland@larabicus.com)

Kyrillos Atallah, University of Kassel, Kassel/Germany

Thomas Schomberg, University of Kassel, Kassel/Germany, [thomas.schomberg@larabicus.com](mailto:thomas.schomberg@larabicus.com)

## Abstract

*After only a few days in the water, a thin slime layer of micro-organisms forms on the ship's hull, which drastically increases the fuel consumption. After weeks and months, higher organisms can settle on the surface, further increasing the flow resistance and spreading invasive aquatic species. Larabicus, a "robotic-cleaning-fish", continuously cleans the ship's hull, keeping the hull free of any slime layer and thereby also preventing colonization by macroscopic organisms. Until now, ships have at best been cleaned in water at intervals of six months. Unlike alternatives already available on the market, Larabicus can stay and move autarkically on the hull even and especially while the ship is in transit. This is possible mainly due to its hydrodynamic shape and its innovative propulsion system which allows the robot to harvest its energy from the water flowing around the ship. By not using holding devices such as lines, the robot is maneuverable enough to bypass attachments such as bilge keels, galvanic anodes, or openings for ballast water tanks and can thus keep the hull clean. A new way of keeping the ship hulls clean while in transit will be presented in this paper.*

## 1. Introduction

The latest technical developments in the maritime shipping industry are essentially driven by sharply tightened environmental and safety requirements. These are significantly increasing the urge to modernize the fleet. In 2023, the International Maritime Organization (IMO) has adopted its strategy for reducing greenhouse gas emissions from ships. Compared to the reference year 2008, it targets a reduction in absolute GHG emissions of 30% by 2030 and net-zero GHG emissions by or around 2050, *IMO (2023)*. As a first step towards this goal, the IMO Marine Environment Committee (MEPC) decided in November 2020 to implement a series of short-term technical and operational measures to increase the energy efficiency of ships. This includes the introduction of a ship-specific energy efficiency index for ship operation, including a classification into energy efficiency classes, which provide information on the climate efficiency of a ship and are to be documented and reviewed as part of the ship's energy efficiency management plan.

The new regulations apply since January 1, 2023 to all ships of 5,000 GT or larger, *BMWK (2021)*, which account for 90% of CO<sub>2</sub> emissions, *EU (2023)*. Furthermore, the EU Commission is planning to oblige maritime shipping to participate in EU emissions trading as of 2024. Step by step, certificates will have to be purchased for 45% of the emissions and from 2026 for 100%. In addition to obligations to reduce emissions, the legal framework for the introduction of invasive species will be tightened. As of June 2022, Australia currently has the world's strictest measures in place to prevent invasive species. Ships entering Australian territorial waters must either demonstrate effective bio-fouling management or, alternatively, the last cleaning of the ship must have taken place no longer than 30 days ago. In addition to Australia, New Zealand and the USA have also implemented regulations. In the next five years, further regulations are planned in Canada, England, Norway, the Baltic Sea, Spain, and France. The multitude of different requirements poses a considerable challenge for ship operators. The IMO is working internationally to standardize them, *IMO (2022a)*.

For container ships and general cargo vessels, we are seeing a current trend toward larger ships with increased cargo capacities, which can exert additional price pressure on smaller ships in particular. In addition to alternative fuels, a reduction in sailing speed (slow steaming) can make a significant contribution to energy savings, which, however, results in a significant reduction in freight capacity. The United Nations assumes that the future environmental protection regulations will have a significant

impact on the freight rate and its price fluctuations, *UN (2022)*. In addition, the IMO states that maintaining a smooth and clean hull, free from biological fouling, is of utmost importance in optimizing the energy efficiency of ships, *IMO (2022b)*. Current coatings can delay fouling, but not prevent it. In its biofouling guidelines, the IMO therefore explicitly recommends the removal of microfouling by gentle in-water cleaning. This substantially preserves the effect of the antifouling coating, prevents the growth of macrofouling and thus additionally reduces the risk of invasive species.

The international merchant fleet causes about 3% of global greenhouse gas emissions. Per ship, a 30% reduction in greenhouse gas emissions is potentially to be achieved compared to the standard use of antifouling coatings. If the world merchant fleet were to be kept permanently free of fouling rather than only inadequately cleaned, as is currently the case, this would reduce greenhouse gas emissions from international shipping by about 19% per year, *Swain et al. (2022)*. This corresponds to a reduction in global greenhouse gas emissions of 0.57%, which is roughly 1/3 of the total GHG emissions of the Federal Republic of Germany, *Statista (2022)*.

## 2. Potential of In-Transit Cleaning

When asked about the main challenges to complying with biofouling regulations, 58% of respondents said there was not enough cleaning opportunities available, according to a survey among ship operators conducted by the IMO in 2022. In addition, 61% of respondents indicated that in-water cleaning is not possible due to regulations in their respective ports or countries, *IMO (2022a)*.

A highly promising approach to addressing the problems faced by shipowners lies in in-transit cleaning. If the ship is cleaned on the open sea, the risk of spreading invasive species is minimized. At the same time, the initial slime layer that tends to form during mooring is removed at the earliest possible stage. Furthermore, there is no dependence on cleaning facilities in the respective ports and there is no downtime of the ship.



Fig.1: Prototype of the Larabicus robot

Larabicus, a "robotic cleaner fish," Fig.1, continuously cleans the vessel's hull, keeping it free of any slime layer and thereby also preventing colonization by larger organisms. Unlike alternatives already available on the market, Larabicus is able to stay and move on the hull even and especially while the ship is underway. This is possible primarily due to its hydrodynamic shape and its patented SuSa-Drive (Subsea Sailing Drive) propulsion system. The SuSa-Drive is in concept a sailing drive, which allows the robot to harvest its propulsion energy from the water flowing around the ship. By combining these technologies, the robot can operate autonomously underwater for a long time without having to charge its batteries. By avoiding tethers such as ropes, the robot is maneuverable enough to bypass attachments such as bilge keels, galvanic anodes, or openings for ballast water tanks, despite the large current forces - and can thus keep the hull clean.

### 3. CFD optimization of the robot propulsion system

The propulsion system is of fundamental importance for this robot because it provides a secure energy supply so that the wireless operation of the robot is possible at all. With pure battery operation, the uninterrupted operating time would drop sharply. An economically viable operation of the system for the ship operators would be questionable without such a propulsion system.

In order to design the propulsion system, numerical simulations and experimental investigations were conducted. The numerical investigations have allowed to design the shape, size, position, and number of the drive wings. The result demonstrated that by arranging two symmetrical wing sections of different lengths (comparable to landing flaps on airplanes), an optimal efficiency for each module can be achieved.

#### 3.1. Numerical modeling

For the optimization of the propulsion wing configuration, various degrees of freedom (e.g. angle of attack and distances between the hydrofoils) and their interaction have to be investigated. Therefore, an overset mesh is used in the numerical investigation of the propulsion system, which reduces the re-meshing effort. The numerical geometry model consists of several components, Fig.2:

1. background mesh (red)
2. mesh of the support profile (green).

The generation of the hydrofoil mesh is performed using the programming language Python in ANSYS SpaceClaim as shown in Fig.3. The background mesh is a simple geometry; therefore it is constructed directly in SpaceClaim. For clarity, only one profile is shown in Fig.2. However, the principle can easily be extended to multi-wing configurations.

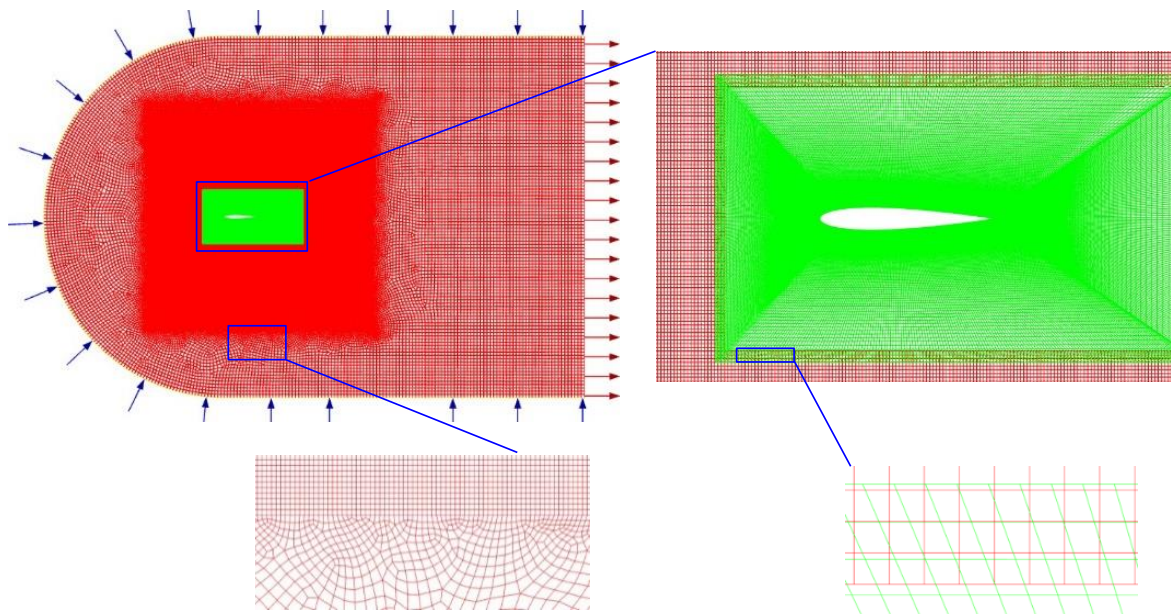


Fig.2: Overset mesh of the configuration

The subgrid components are meshed separately. Then, each component is embedded into the background mesh. Interpolation is performed in the overlapping regions, Fig.2. Initial and boundary conditions are assigned to the background mesh. Blue arrows represent the inlet (inflow boundary) and red arrows represent the outlet (outflow boundary). As can be seen in the left part of Fig.2, the background mesh consists of two domains. A finer mesh is generated in the smaller region, where the background mesh in the overset region has the same mesh size as the support mesh. Unlike the background mesh, non-equidistant meshes are generated in the hydrofoil mesh in order to be able to



resolve the boundary layer. For this purpose, an estimate for the dimensionless boundary layer thickness  $y^+$  must be determined.

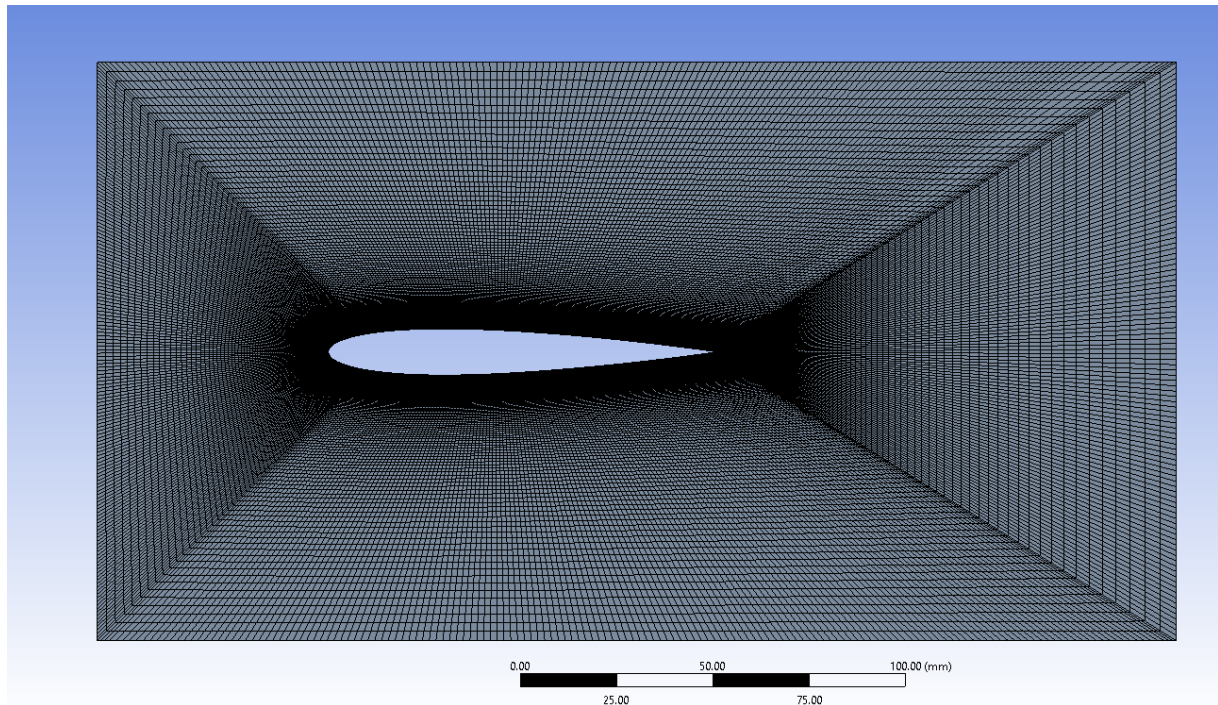


Fig.3: Finite Volume Mesh around the near field of the hydrofoil

A common approach for the numerical modeling of turbulent flow processes is RANS (Reynolds Averaged Navier-Stokes Simulation), where transport equations with statistical averaged terms of the flow variables are solved. The large- and small-scale turbulent fluctuations are not calculated, but their influence on the flow process is captured by a turbulence model. Examples of turbulence models are K- $\omega$  SST, K- $\omega$ - $\gamma$  SST (known as  $\gamma$  model), and K- $\omega$ - $\gamma$ - $Re_\theta$  (known as  $\gamma$ - $Re_\theta$  model).

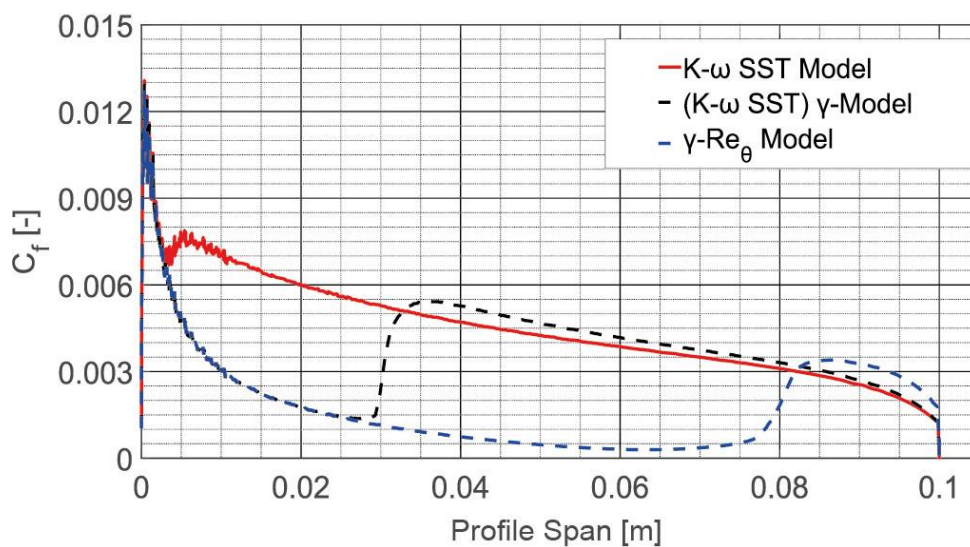


Fig.2: Friction coefficient along profile span

The Reynolds number of the flow at the propulsive wing is  $Re = 1E+06$  at typical cruising speeds of ships. Thus, it is larger than the critical Reynolds number ( $Re = 1E+05$ ), so in principle a viscous turbulence model (K- $\omega$  SST,  $\gamma$  model or  $\gamma$ - $Re_\theta$  model) should be applied. The specific choice of an appropriate physical model depends on the laminar-turbulent transition of the boundary layer. This tran-



sition does not occur randomly but depends on the flow velocity and the profile shape and pitch. Fig.4 shows the variation of the friction coefficient  $C_f$  along the span of a symmetrical exemplary airfoil with no pitch. It can be seen that the widely used fully turbulent  $K-\omega$  SST model cannot capture the turbulent transition. Also, the  $K-\omega-\gamma$  model, which is supposed to model the transition process at least rudimentarily, cannot predict the transition point with sufficient accuracy. The reason is that even with this model, the critical Reynolds number  $Re_{\theta c}$  is not being calculated. Therefore, this model also does not determine the laminar-turbulent transition with sufficient accuracy. The four-equation model  $K-\omega-\gamma-Re_{\theta}$ , on the other hand, correctly determines the laminar-turbulent transition in the rear portion of the airfoil. Since the initial laminar region cannot be neglected, the resource-intensive four-equation model ( $K-\omega-\gamma-Re_{\theta}$ ) is used for further investigations.

### 3.2. Optimization

The possibilities for arranging the profiles on the robot are hardly limited. At the same time, depending on the arrangement, various interactions occur between the profiles, which may be constructive or destructive. In order to efficiently identify an optimal configuration of the profiles, an advanced optimization algorithm is applied in the following to control the numerical investigations. The algorithms flowchart is given in Fig.5.

First, the set of input parameters called the design candidate (DC) is determined by Design of Experiments (DoE), and the configuration of the numerical experiments is performed based on probability theory and statistics. In the present study, the samples are generated according to the Latin Hypercube Sampling (LHS) algorithm.

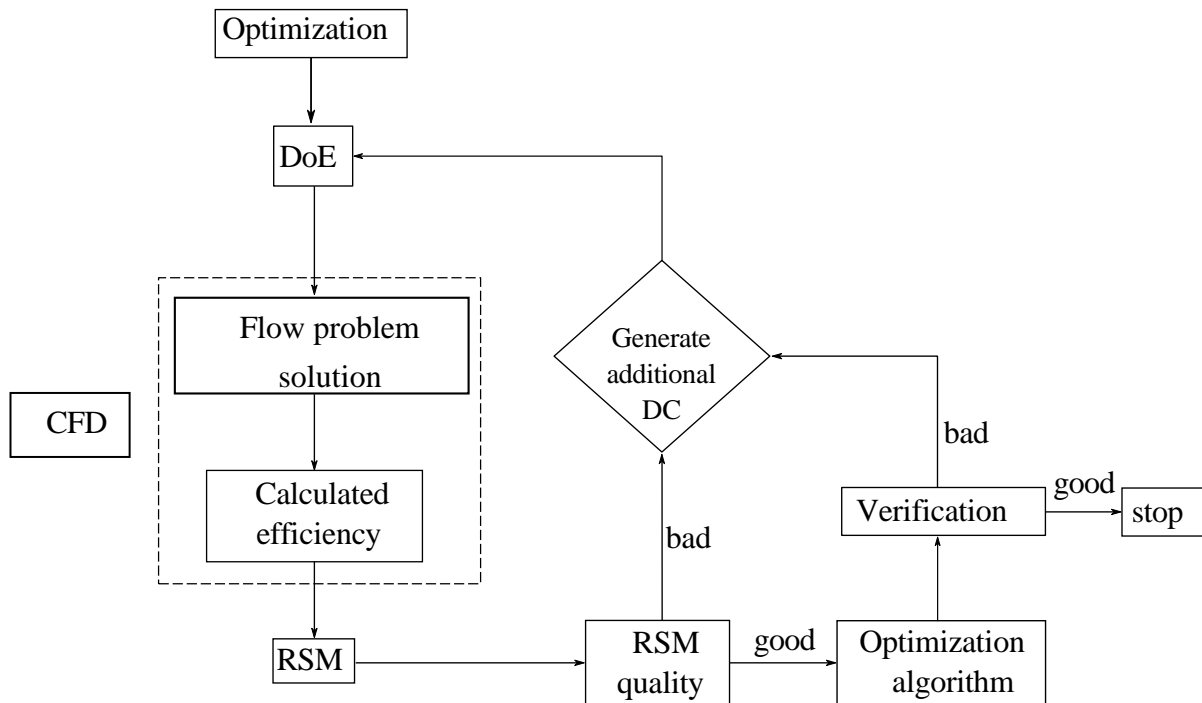


Fig.3: Optimization process flowchart

In the Latin Hypercube sampling procedure, the samples are uniformly distributed over the design space. The design candidates are randomly distributed in a square grid over the entire design space. This ensures complete coverage of the range of each variable's values over the sample space, *Kleijnen (2008)*. Fifteen samples were picked to start with. Based on this, a response surface is modeled in the second step in order to predict the behavior of the system based on statistics. Here, the interpolation is done according to the Kriging model, which can determine more precise global maxima compared to the standard model (quadratic model), *Sakata et al. (2007)*. In order to increase the quality and accuracy of the response surface, 15 refinement points are additionally generated and verified, whereby

the maximum tolerable relative error is set to 5%. The response surface modeling is considered converged at the eleventh refinement point, where the relative error is 4.6%, which is smaller than the maximum permissible error.

The goal of the optimization is to find a global maximum of the propulsion wing performance. The MOGA optimization algorithm (Multi-Objective Genetic Algorithm) and the screening optimization algorithm are suitable for this purpose. Compared to screening, MOGA is an iterative Multi-Objective Genetic Algorithm that provides more accurate results.

After the first iteration, each population is passed through until the maximum number of samples (=150) is reached. MOGA converges as soon as the maximum allowable Pareto percentage is reached. This process is visualized in Fig.6.

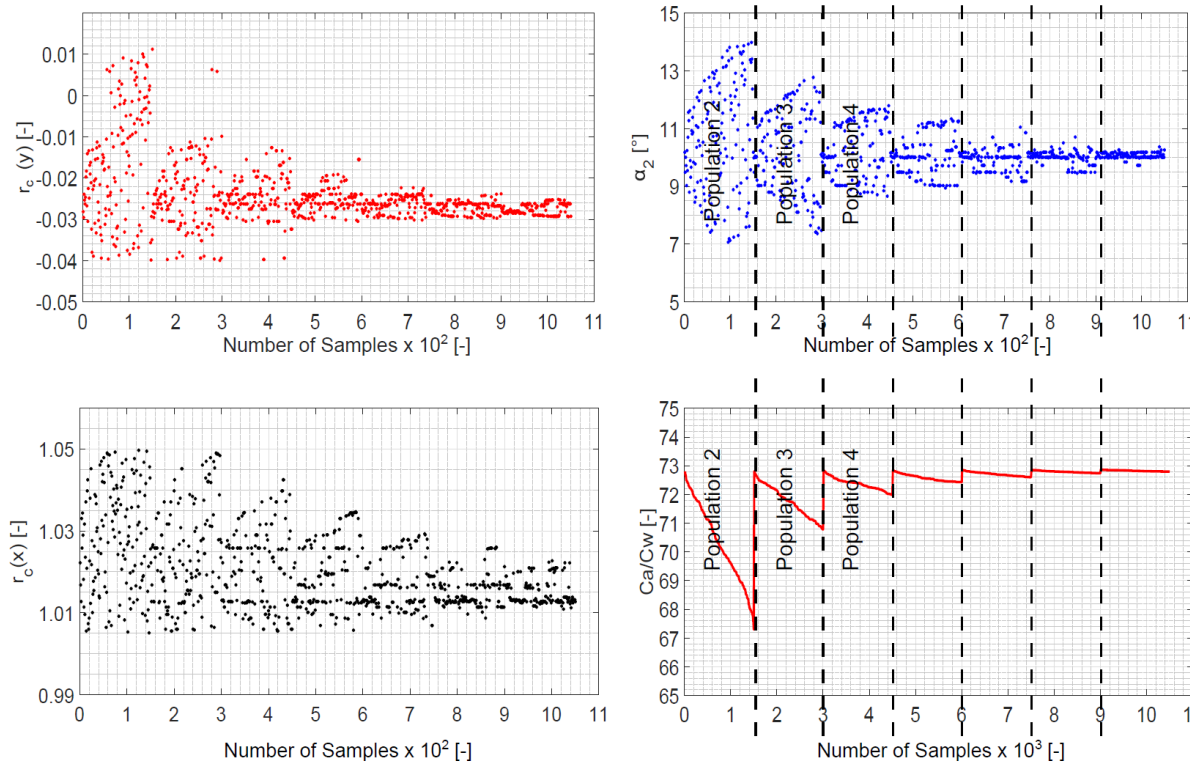


Fig.4: Development of the design candidates parameters during the optimization process

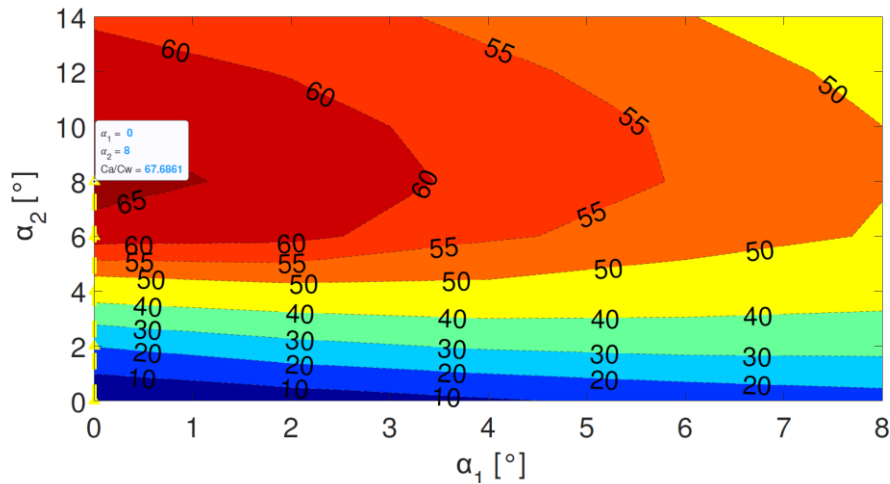


Fig.5: Efficiency over the angles of attack  $\alpha_1$  and  $\alpha_2$

An example of the efficiency over the angles of attack  $\alpha_1$  and  $\alpha_2$ , keeping all other design parameters unchanged is presented in Fig.7.

Although the efficiency shows some dependence on the angle of attack  $\alpha_1$ , the dependence on the angle of attack  $\alpha_2$  is much more pronounced. At an angle of attack  $\alpha_2 \geq 5^\circ$  and  $\alpha_1 = 0^\circ$ , the values of the efficiencies increase significantly. The propulsion system reaches its optimum efficiency at the angle of attack combination  $\{0^\circ; 8^\circ\}$ , where the efficiency is  $C_a/C_w = 67.69$ . With this efficiency, the two profiles ordered in series show an efficiency increase of 14.14% compared to the single profile configuration.

### 3.3. Analysis of the flow

Fig.8 presents the velocity profiles and the pressure coefficients in comparison of two configurations with different profile length ratio of  $r_c = 1$  and  $r_c = 2/3$ . Decreasing the dimensionless profile length ratio  $r_c$  increases the flow velocity at the suction side of the rear profile, which in turn decreases the suction pressure at the profile nose ( $C_p = -1.4$ ). For the front profile, on the other hand, the differences between the two configurations are negligible. Consequently, decreasing the dimensionless profile aspect ratio  $r_c$  exhibits a positive impact on the efficiency of the propulsion system. Reducing the dimensionless profile length ratio  $r_c$  decreases the drag coefficient as well.

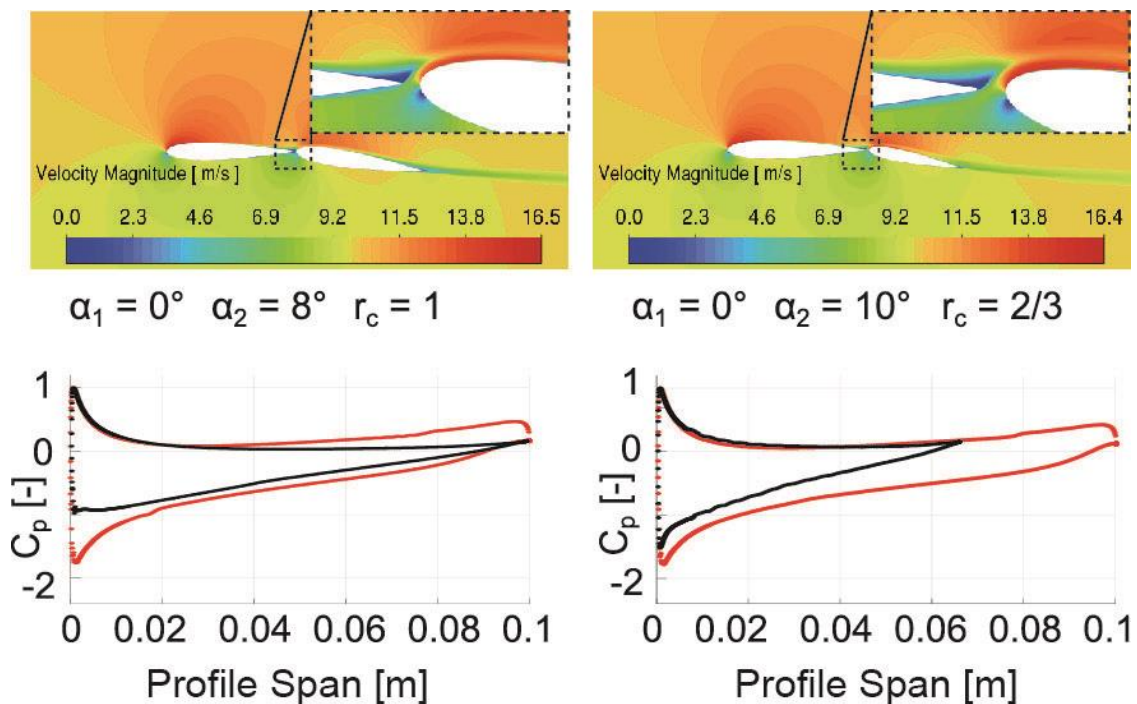


Fig.6: Velocity field (top) and the pressure coefficient (bottom) of two design candidates with different profile length ratio  $r_c$

### 4. Conclusion

The propulsion system has been identified as a particularly important component for the autarkic operation of the hull cleaning robot. Its mechanical principle of operation is similar to that of a sailing ship. In order to identify a favorable design for the system, numerical simulations of the flow were carried out on a large number of profile configurations. Using modern design optimization tools, it was possible to identify an optimum from the possible configuration space in which the airfoil efficiency is maximized. In the present work, the hydrodynamic properties of the studied configurations were considered in order to design configurations with the highest possible lift coefficient and the lowest possible drag coefficient. One possible solution to achieve this was to arrange the profiles in a row so that a constructive interaction occurs.

## Acknowledgements

Larabicus is funded by the German Federal Ministry for Economics and Climate Action and the European Social Fund as part of the EXIST program.

## References

BMWK (2021), *Siebter Bericht der Bundesregierung über die Entwicklung und Zukunftsperspektiven der maritimen Wirtschaft in Deutschland*, German Government, Berlin, <https://www.bmwk.de/Redaktion/DE/Downloads/B/bericht-der-bundesregierung-ueber-die-entwicklung-und-zukunftsperspektiven-der-maritimen-wirtschaft-in-deutschland.pdf>

EU (2023), *Reduzierung der Emissionen im Luft- und Schiffsverkehr: EU-Maßnahmen erklärt*, European Parliament, <https://www.europarl.europa.eu/news/de/headlines/society/20220610STO32720/reduzierung-der-emissionen-im-luft-und-schiffsverkehr-eu-massnahmen-erklart>

IMO (2022a), *Compilation and Comparative Analysis of Existing and Emerging Regulations, Standards and Practices Related to Ships' Biofouling Management*, GEF-UNDP-IMO GloFouling Partnerships Project and GIA for Marine Biosafety, Int. Mar. Org., London

IMO (2022b), *Analysing the Impact of Marine Biofouling on the Energy Efficiency of Ships and the GHG Abatement Potential of Biofouling Management Measures*, GEF-UNDP-IMO GloFouling Partnerships Project and GIA for Marine Biosafety, Int. Mar. Org., London

IMO (2023), *2023 IMO Strategy on Reduction of GHG Emissions from Ships*, IMO Res. MEPC.377(80) (Annex1), Int. Mar. Org., London

KLEIJNEN, J.P.C. (2008), *Design and analysis of simulation experiments*, International Series in Operations Research & Management Science 111, Springer

SAKATA, S.; ASHIDA, F.; ZAKO, M. (2007), *Hybrid approximation algorithm with Kriging and quadratic polynomial-based approach for approximate optimization*, Int. J. Numer. Methods Eng. 70/6, pp.631–654

STATISTA (2022), *CO2-Emissionen: Größte Länder nach Anteil am weltweiten CO2-Ausstoß im Jahr 2021*, Statista, <https://de.statista.com/statistik/daten/studie/179260/umfrage/die-zehn-groessten-CO2-emittenten-weltweit/>

SWAIN, G.; ERDOGAN, C.; FOY, L.; GARDNER H.; HARPER, M.; HEARIN, J. HUNSUCKER, K.Z.; HUNSUCKER, J.T. LIEBERMAN, K.; NANNEY, M.; RALSTON, E.; STEPHENS, A. TRIBOU, M.; WALKER, B.; WASSICK, A. (2022), *Proactive In-Water Ship Hull Grooming as a Method to Reduce the Environmental Footprint of Ships*, Front. Mar. Sci., 8, <https://www.frontiersin.org/articles/10.3389/fmars.2021.808549>

UN (2022), *Review of Maritime Transport*, United Nations, New York

# CII Optimized Ship Operation for Ships with Refrigerated Cargo

Uwe Altenbach, Hoppe Marine, Hamburg/Germany, [u.altenbach@hoppe-marine.com](mailto:u.altenbach@hoppe-marine.com)

## Abstract

*The MEPC Res. 355 (78) describes the application of correction factors in the determination of the carbon intensity indicator (CII), with the intention to substitute energy-intensive cargo such as frozen food products and liquified gases from CII calculation. This paper addresses the technical prerequisites and challenges in the transport of refrigerated goods by using the examples of container ships and gas tankers. Following this, the possible energy-saving measures and their leverage effect are analysed, taking into account the respective type of ship.*

## 1. Important Milestones of IMO Greenhouse Gas Strategy Regulatory Framework in a nutshell

With the global drive for decarbonization the shipping industry is facing the challenge to comply with more stringent regulations related to greenhouse gas emissions (GHG). At the 80<sup>th</sup> session of the Marine Environment Protection Committee the previous in 2018 released targets have been tightened significantly. While the former regulation has defined a greenhouse gas reduction by 50% of 2050 compared with the level of 2008, [MEPC 304 \(72\) \(imo.org\)](#), the latest amendment, [MEPC 377 \(80\) \(imo.org\)](#), calls for a reduction relative to 2008 of:

- 20% and striving for 30% by 2030
- 70% and striving for 80% by 2040
- 0% by 2050

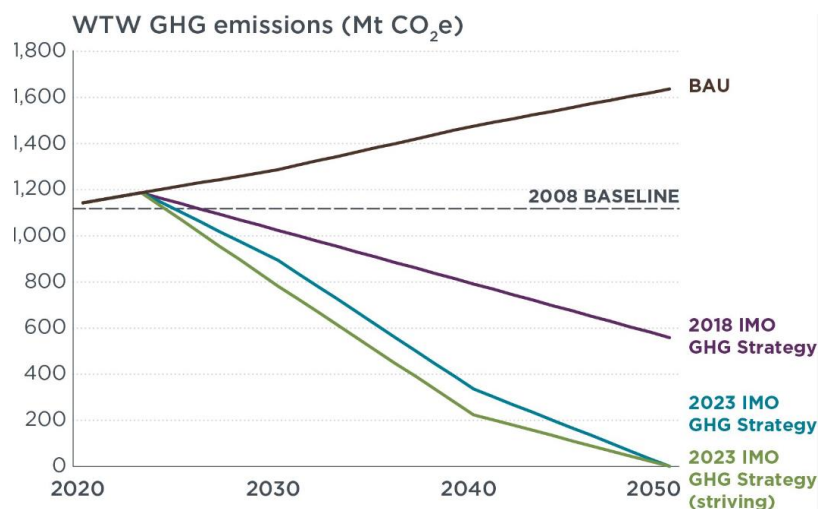


Fig.1: Well-to-wake GHG emissions pathways implied by the revised (2023) strategy compared to the initial (2018) strategy, the emissions in 2008, and business-as-usual (BAU) emissions, source: Comer and Carvalho (2023)

Most important milestones for the implementation of GHG targets in the past were the introduction of the Energy Efficiency Design Index (EEDI), and the Ship Energy Efficiency Management Plan (SEEMP) resolved in 2011, [MEPC.203 \(62\) \(imo.org\)](#), and entered into force on 1<sup>st</sup> of January 2013. This was followed by the introduction of Energy Efficiency Existing Ship Index (EEXI), [EEXI and CII \(imo.org\)](#), resolved in 2018 and set into force on 1<sup>st</sup> of November 2022. EEDI and EEXI are measures of the energy efficiency of the design of a vessel and technology on board, and do not indicate how the vessel is being operated. These indicators just represent the expected CO<sub>2</sub> emissions per cargo ton and mile based on the vessel's engine power, cargo capacity and speed.



## 2. CII – Carbon Intensity Indicator

Different from the previously mentioned measures, an assessment of the operational carbon intensity of ships was considered for the first time in MEPC Resolution 339 (76) in June 2021 by introducing the Carbon Intensity Rating (CII). The first year of the attained annual operational CII verification will be 2024 for the operation in calendar year 2023. Fuel consumption data, which is mandatory to be reported for vessels of 5,000 GT analogue to the IMO Data Collection System (DCS), [IMO Data Collection System \(DCS\)](#), since beginning of 2019 shall serve the data basis this.

The data is evaluated in an assessment and depending on the specific type of the vessel, an environmental rating of the CO<sub>2</sub> emissions according to grades A (major superior) to D (minor inferior) is assigned. The thresholds for classification will become increasingly stringent over time until 2030.

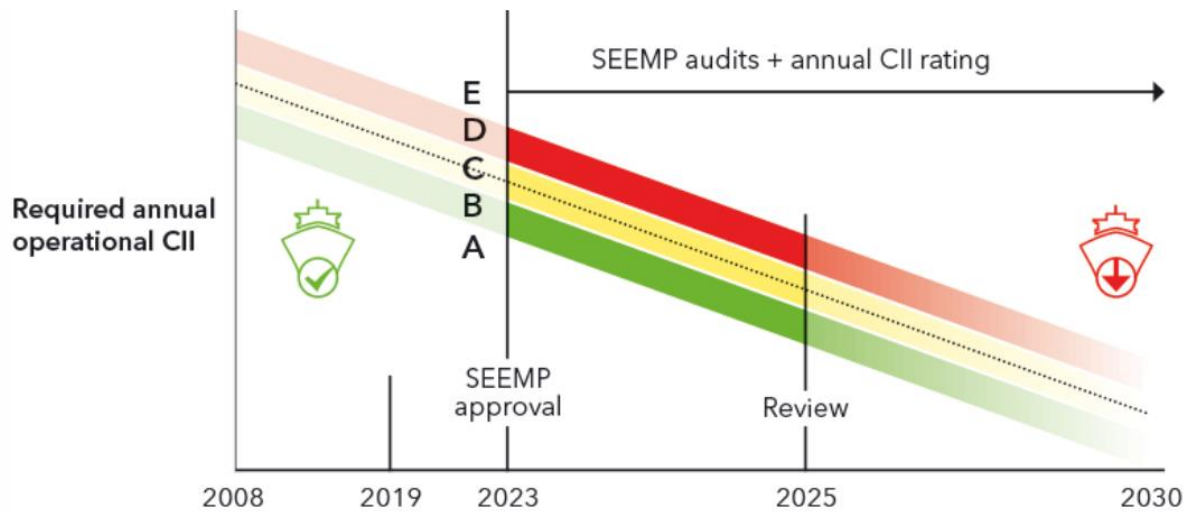


Fig.2: Required annual operational CII, [CII - Carbon Intensity Indicator - DNV](#)

The attained annual operational CII (Grams CO<sub>2</sub> per cargo capacity and nautical mile) and the related environmental rating (A to E), [MEPC 354 78 \(imo.org\)](#), will be noted on the DCS Statement of Compliance (SoC) and must be kept on board for five years and must be kept on board for a compulsory five years. Poorly rated vessels, this includes a D-rating for three consecutive years, or a one-time E-rating will result in the submission of a corrective action plan before the SoC can be issued. The corrective action plan should consist of an analysis of why the required CII was not achieved and include a revised implementation plan.

## 3. CII – Carbon Intensity Indicator, Application of Correction Factors and Voyage Adjustments

The formula for calculating the attained CII was extended within the framework of MEPC 35 (78) incorporating correction factors and voyage adjustments. This means that for certain ship types and operations a “correction” to the CII may be given, either by removing a certain period of the vessels operation or by reducing the CII according to criteria explained below. Required annual operational CII, [MEPC 354 78 \(imo.org\)](#):

$$CII_{Ship} \triangleq \frac{\sum CF_j \cdot \{FC_j - (FC_{voyage,j} + TF_j + (0.75 - 0.03_{yt}) \cdot (FC_{electrical,j} + FC_{boiler,j} + FC_{others,j}))\}}{fi \cdot fm \cdot fc \cdot fi_{vse} \cdot Capacity \cdot (D_t - D_x)} \quad (1)$$

The motivation for introducing these corrections in the CII calculation mainly relates to the exclusion of competitive disadvantages due to energy-intensive cargo, special, energy-intensive ship operation due to short routes and cargo handling exclusively using onboard energy supply (e.g. generators and boilers). The corrections applied in the formula above can be divided into three sections:

- a. Voyage Adjustments –  $FC_{Voyage,j}$ :
  - Securing the safety of a ship or saving life at sea (applicable for all vessels)
  - Sailing in ice conditions (applicable for ice-classed vessels)
- b. Correction Factors:
  - $AF_{TankerSTS}$  – oil tankers engaged in STS voyages
  - $AF_{TankerShuttle}$  – shuttle tankers equipped with dynamic positioning
  - $FC_{electrical}$  – cargo-related electrical consumers (reefers, refrigeration plants, el. pumps)
  - $FC_{boiler}$  – cargo-related fuel mass for boilers (heating, steam pumps)
  - $FC_{others}$  – fuel mass for e.g. for pumps driven by combustion engines
- c. Correction factors adopted from EEDI and EEXI calculation:
  - $f_i$  – capacity correction factor for ice-classed ships
  - $f_m$  – ships having ice classes IA Super and IA
  - $f_c$  – cubic capacity correction factors for chemical tankers
  - $f_{i,VSE}$  – correction factor for ship-specific voluntary structural enhancement

While the items mentioned under a. result from environmental and weather conditions, section c. considers exclusively fix factors derived from the EEDI/EEXI calculation considering the design characteristics of the ship. The subsequent consideration shall focus on the correction factors mentioned under c.  $FC_{electrical}$ ,  $FC_{boiler}$ , and  $FC_{others}$ .

The IMO assumes that the total fuel quantity of the ship is recorded for the calculation of the CII. This includes main engines, auxiliary engines, gas turbines, boilers and for each type of fuel oil consumed, regardless of whether a ship is sailing or at anchor. For the collection of consumption data itself, different methods are specified:

- a. Bunker delivery note (BDN)
- b. Bunker fuel oil monitoring
- c. Flow meters (according to vessels data collection plan)
- d. LNG / alternative fuel tank monitoring

The determination of the CII based on a. - bunker delivery note only, although satisfying the basic requirements, is the least sophisticated method, on the one hand due to inaccuracies of the bunker procedure itself, on the other hand this method does not allow to focus on fuel oil consumption on a certain leg of a route and the aforementioned CII correction factors can only be taken into account to a very limited extent. At present, a substitute value for energy consumption is only envisaged for refrigerated containers if these are operated with on-board energy. Otherwise, it is crucial to install suitable and reliable measuring systems and sensors for automated data acquisition and storage in order to differentiate between the various energy consumers on board being able to deduct cargo related energy from the CII-calculation. Examples include the energy-intensive transport of liquefied gases due to the cooling and liquefaction plants installed on board. Tankers, especially heavy oil tankers, can deduct energy required for cargo heating and transport, e.g. for steam-driven pumps, from the CII calculation. Additional electrical consumers related to cargo handling may be calculated with an approximation of the Specific Fuel Consumption. SFOC in g/kWh associated with the relevant source of electrical power as per the EEDI/EEXI Technical File or NOx Technical File. In the case of ships without a Technical File, a default value of 175 g/kWh for 2 stroke engines and 200 g/kWh for 4 stroke engines shall be applied.

#### 4. Market impact - vessels affected

The CII rating in general will in future affect ship owner and charterer in the same manner, not least impending penalties and rising fuel prices will force and motivate to monitor and optimize the vessels operation. Focussing on IMO's approach to deducting cargo-related energy consumption a 36% share

could benefit from applying that. The potential reduction strongly depends on the respective operating profile of the ship and the cargo to be transported. The greatest saving is considered on gas tankers, trading on short distances, due to extensive energy consumption for required pressure reduction during the first days on sailing after loading the vessel.

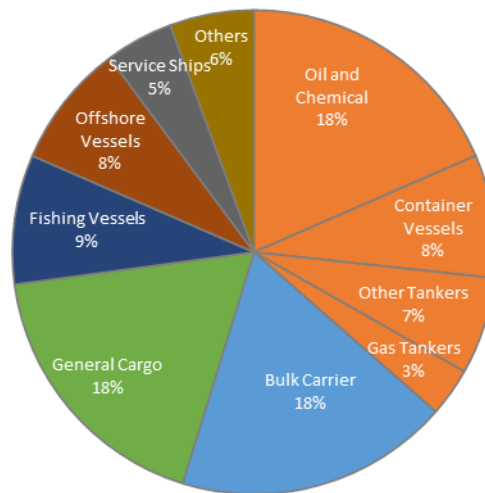


Fig.3: World Merchant Fleet Distribution, [equasis.org](http://equasis.org)

## 5. Technical Requirements for On-board Energy Monitoring

As already stated in chapter 3, the IMO authorises the vessel operator within the regulatory framework of SEEMP Part II to submit a vessels Data Collection Plan, in which is specifies how individual energy mass flows relevant for CII calculation in the form of fuel or electrical power shall be monitored and recorded, [MEPC 346 78 \(imo.org\)](https://www.imo.org/en/About/Pages/MEPC-346-78.aspx). Also self-diagnostic algorithms, maintenance and device-calibration intervals must be defined within this document.

The system itself must consist of at least of an iPC for data acquisition, fuel flow meters for main engine, auxiliary engine and boiler as well as electric power meters for generator and cargo related switchboards, e.g. for reefer containers or handling/conditioning units on oil or gas tankers. Navigation data (vessels position, speed, rudder angle, wind speed, etc.) can be read out and transmitted from the wheelhouse via interface.

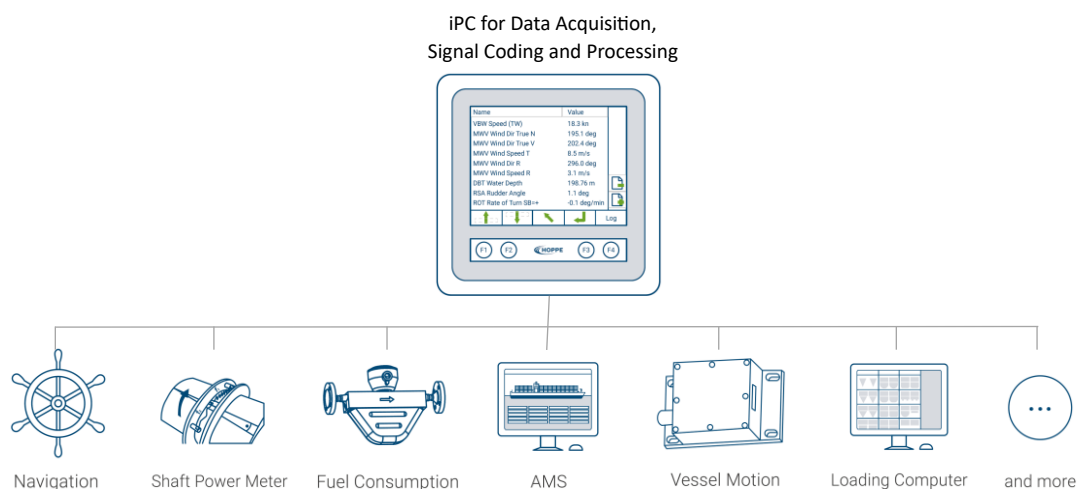


Fig.4: System Requirements for CII-related energy data acquisition and vessel optimization

Optionally, the system can also be equipped with further components such as draught measurement (dynamic trim), shaft power meter (plausibility check of the fuel consumption of the main engines

depending on the engine condition or hull condition), loading computer, etc., which enhance the database in its capability as instrument for holistic ship optimisation.

## 6. Added Value through digitalisation and MIIOT

The connection of a Vessels Performance Monitoring System – even if only focused on CII-relevant data - is predestined for digital connection technologies, not least to generate transparency of the vessels status on both, crews and owners / ship operators perspective. Hand in hand, ship and fleet operations can be sustainably optimised from an operational and strategic point of view in terms of costs and greenhouse gas emissions.

- **Ship to Shore infrastructure:** A vessel performance monitoring system in its function as a data logger or IoT device offers the possibility to build a proper (stable, low bandwidth, cyber-secure, etc.) ship-to-shore infrastructure. It will be possible to monitor all essential parameters of the performance monitoring system and connect additional data sources without major effort. With the data collected and stored in the cloud, it will be possible to analyze and evaluate the data over a long period of time. With the high-quality data stored over a long period of time, it is in turn possible to improve the performance of the vessel and investigate minor and major issues.

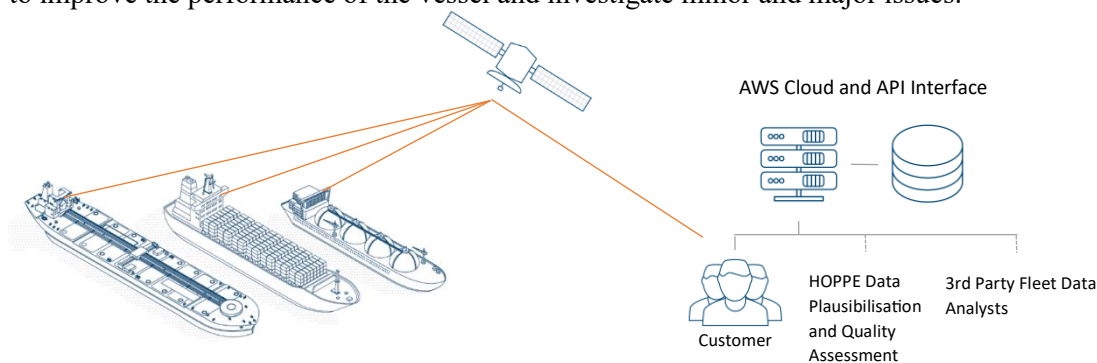


Fig.5: Ship to Shore Data Highway

- **Data sharing and collaboration:** Modern cloud solutions allow easy integration between suppliers, ship-owners, charters etc. Web Application programming interfaces (APIs) have been adopted within the industry. Testing and identifying the benefit of a new application on a set of high-quality high-frequency data has never been as easy as it is today. Decision support tools for hull-cleaning, weather routing, engine maintenance are much easier to integrate nowadays. Barriers for collaboration can be reduced and time for integration is lowered.
- **Remote Updates and support:** With the establishment of a permanent ship-to-shore connection remote updates and services will be available. A reduction of service attendances and improvement of mean time to recovery has been identified within remote-enabled systems within Hoppe products. In additional travel requirements are reduced, helping to reduce the general carbon footprint. Future outlook: Integration of self-diagnostic algorithms to empower the system avoiding downtimes by forwarding health data to crew and ship management (predictive maintenance).

## 7. Conclusion

The decarbonisation targets set by the IMO for the reduction of greenhouse gases are progressing rapidly, as can be seen from the conclusions of the 80th MEPC meeting in early July 2023. The resulting measures concern both the short-term optimisation of ship operations and the long-term technical design of ships, propulsion units and energy resources used.

With the mandatory introduction of CII monitoring based on fuel consumption data, the acquisition of the energy demand of the individual consumers on board the ship is at least mandatory when considering deductible energy expenditures caused by cargo handling and thermal conditioning (cooling / heating) that can be deducted from over-all energy requirement of the vessel's operation.

The technical environment such as data acquisition / processing unit, sensors and interfaces to the offers even more - namely the data basis for a holistic optimisation of the ship's operation and, last but not least, increases transparency for efficiency and health state of the vessel's technical infrastructure. As a result, a sustainable and cost-efficient fleet operation can be realized with these Performance Monitoring Systems in a straightforward way, with joint cooperation by digital connection between vessels technical management and crew.

## References

COMER, B.; CARVALHO, F. (2023), *IMO's Newly Revised GHG Strategy: What It Means for Shipping and the Paris Agreement*, Int. Council on Clean Transportation, <https://theicct.org/marine-imo-updated-ghg-strategy-jul23/#:~:text=In%20the%20first%20scheduled%20revision,by%202030%20and%2070%25%20and>



# Biofuel Compatibility: Testing Matrix and Case Reports

Fabian Pinkert, FVTR GmbH, Rostock/Germany, [fabian.pinkert@fvtr.de](mailto:fabian.pinkert@fvtr.de)

## Abstract

*The paper delves into the challenges of assessing biofuels for marine applications, a response to environmental regulations and emissions reduction needs. Grounded in FVTR's testing matrix, the study spans lab to full-engine evaluations. Case reports examine fuels like hydrogenated vegetable oil (HVO) and oxymethylenether (OME), revealing combustion behaviors, emissions, and compatibility. The potential of refined waste oil (RWO) and cashew nut shell liquid (CNSL) as biofuel sources is explored. The research underscores the pivotal role of comprehensive assessment and collaboration in driving maritime industry transition to sustainable feedstocks, aligning with stricter regulations and green energy goals.*

## 1. Introduction

Since about two years, we have seen a steadily increasing interest of our customers in testing of biofuels for marine application. These customers are interested in the reduction of CO<sub>2</sub> emissions from these fuels in order to protect the world climate and prepare for changes in legislation in the recent past and in the near future. FVTR and its close partner the University of Rostock have been dealing with these kinds of fuels for a long time and are keen to support and advise in this task.

Already in the late 90s and up until now a high effort was made at our site to test many kinds of fuels from different biomass feedstocks mainly in public funded projects, supported by FNR, UFOP and other institutions. Leading with Biodiesel or FAME (Fatty Acid Methyl Esther) and subsidized by the German and other European governments, these fuels were eagerly adopted into road traffic. For marine applications however there was no legislative incentive and prices as well as handling efforts were significantly less attractive compared to fossil fuels.

Recently however a new wave of interest has arisen in these fuels from the marine industry. The robust fuel systems of marine engines enable the use of production bottoms and waste products that could not be used in mobile applications previously. As entirely new feedstocks are being tapped, the quality requirements, fuel formulation and handling procedures need to be adapted in order to allow the fuel to be drop-in capable. The identification of obstacles in the fuel path from tank to wake is the specialty of the research center for combustion engines and thermodynamics Rostock - FVTR. We have developed a test matrix in order to individually assess each fuel as each fuel has to be evaluated on a case-by-case basis.

### 1.1. Legislative Background

The increased interest in biofuels that we are currently experiencing is mainly motivated by the need to gain experiences with ways to reduce greenhouse gas emissions in preparation for upcoming changes in legislation.

Of these new legislative instruments, the newest and most stringent is the Fuel EU Maritim regulation enforcing a reduction of GHG emission from on-board energy consumption by a fixed percentage. The law aims specifically for the substitution of conventional maritime fuels or the use of carbon capture technologies. It is well conceivable that the 2 % and 6 % caps that come into effect until 2025 and 2030 will be reached mainly by the used of drop-in fuels as it presents a fast and easy way to reduce the carbon footprint. Drop-in capable E-fuels like Fischer-Tropsch fuel, OME or blue LNG will not be available in sufficient quantities and will be applied preferably in other transport sectors, so biofuel is the most likely option in shipping. Later stages of the regulation with significantly larger caps of up to 80% will have to be dealt with using other alternative fuels like methanol and ammonia that require

significant changes to the ship and engine. Failure to comply with the regulation will be penalized with about 59 €/GJ of non-compliant energy use with progressive penalties after consecutive years, *DNV (2023)*.

A rather soft measure is the Carbon Intensity Index (CII) which serves to monitor the ships Carbon Emissions by categorizing ships into efficiency groups from A to E. Getting the mark E or the mark D for 3 years in a row forces the ship operator to devise a plan for improving the rating. One of the possibilities for improving the rating is the use of carbon neutral fuels like biofuel.

Lastly the European Emission Trade System which will be applied fully to marine transport by 2026 aims to motivate the saving of greenhouse gases financially. While some industries are dealt free allowances, the shipping sector will have to auction their emission certificates on the European trading platform. The cost of certificates is therefore determined by the market and will cause a price advantage of carbon neutral fuels, *Kolos (2022)*. A B30 VLSFO for example will gain a price advantage of 5% at the current CO<sub>2</sub> price of 60 €/t and VLSFO price of 600 \$/mt. It is very likely that the CO<sub>2</sub> price will increase over the coming years although it is hard to predict at which rate. At a value of 150 €/t the advantage for B30 will be 12% and at a value of 300 €/t it further increases to 18%.

## 2. Biofuel Testing Matrix

Building on the experience gained in public projects and specific customer requests we were able to compile a comprehensive testing matrix to prove the compatibility of newly developed fuels and in particular biofuels with existing state of the art engine hardware. These tests range from laboratory tests over component tests to full engine test runs and vary in its scope from straight forward practical orientation to a more academic focus. This is visualized in the flow diagram in Fig.1.

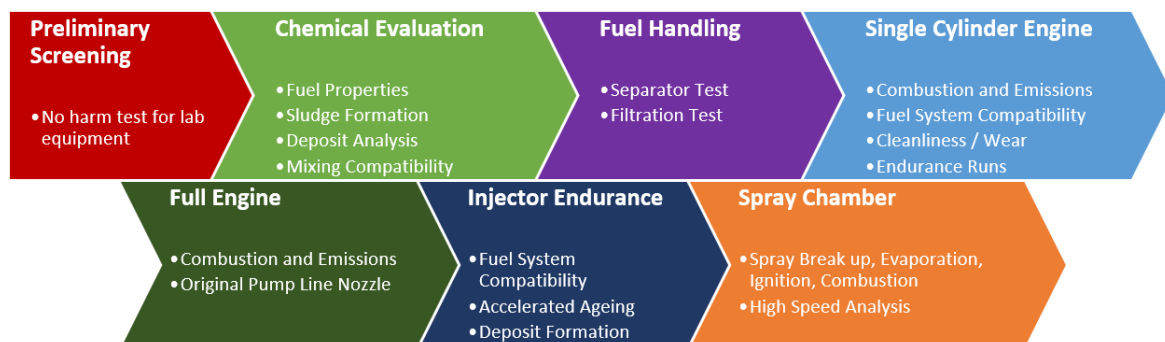


Fig.1: Overview of the complete workflow for testing an unknown biofuel

### 2.1 Chemistry Lab

A special feature of the Rostock University's Chair of reciprocating machines and internal combustion engines (ger. abbr.: LKV), and at the same time an excellent prerequisite for working on current topics in the field of fuel and lubricant development and analysis, is the LKV's own state-of-the-art Laboratory for Fuel and Lubricant Research, which is an integral part of many research projects. In addition to the analysis of fuels and lubricants in accordance with standards, the main focus of the work is on: Development and evaluation of alternative fuels, the effectiveness of fuel and lubricant additives as well as the damage assessment of engine components and the corresponding cause research. Due to the large number of research projects already completed, the working group has very specialized know-how regarding biofuels, marine fuels, blends and fuel-lubricant interactions. In the last ten years, the laboratory has developed into a recognized competence centre for the analysis of biogenic fuels.

### 2.2 Separator and fuel handling bench

The Separator test bench was created to answer a customer's request for reproducible and also realistic determination of a fuels sludge formation tendency. Other uses of the test bench include the

determination of interaction between water and the fuel within the separator and the determination of the filter plugging potential. The test bench is a good representation of an onboard fuel handling system and features the following main components:

- Tilted barrel representing a settling tank
- Elwa electric fuel heater
- Krohne Coriolis for exact measurement of separator flowrate
- Alpha Laval MIB 503 manual separator
- Boll Filter with different mesh sizes

Furthermore, the testing procedure is chosen to represent the stressing and ageing of a fuel on board by including phases of heating, settling and stirring. Boundary conditions of the procedure can be set very accurately though the use of an electric heater and the Coriolis flow rate measurement.

The manual separator used in the setup has a slightly lower rotational speed compared to large automatic separators, which is compensated by a lower feed rate and therefore a longer retention time in the centrifuge. This is outweighed however, by the manual emptying of the bowl and therefore very accurate determination of the sludge content.

### **2.3 Injector durability bench**

The injector durability bench is used to test the long-term impact of critical fuels on the injection hardware – pumps, filters and injectors. The bench allows the operation of marine and heavy-duty common rail injectors. By using rugged equipment and heating of the system to a maximum of 135°C the rig is fully compatible to residual fuels up to RMG 380 and equivalent. The rig allows multiple configurations to test a Bosch LE Injector that is also used on our single cylinder engine or a larger L'Orange prototype medium speed diesel injector. Other configurations for testing non common rail solenoid valves and marine hardware have also been realized in the past.

Scenarios tested using this setup include:

- Formation of internal diesel injector deposit
- Polymerization of fuel in the injector nozzle
- Wear and abrasion of nozzle, needle and pilot valve

### **2.4 High pressure high temperature combustion chamber**

For investigation of the injection and ignition behaviour of the test fuels, a high-temperature / high-pressure injection chamber located at Rostock University is used. The chamber can be operated with temperatures up to 850 K and pressures up to 90 bar and thus produces conditions similar to large diesel engines. It is possible to use nitrogen as scavenging gas for visualization of the injection event and the subsequent mixture formation or to operate the chamber with air for reactive conditions and the investigation of ignition and combustion. The large 300 mm window enables investigation of the complete spray pattern of common injection nozzles in large diesel engines.

To conduct research of injection and mixture formation a schlieren-scatter light method is used, simultaneously collecting information about the liquid and evaporated phase of the fuel in a hot inert environment. At reactive conditions, high speed color images are taken of the glowing soot using a bayer masked CMOS camera. The data is evaluated using a two-color method based on a method by Schmidradler in order to calculate the temperature of the glowing soot particles as well as a measure of the soot volume fraction.

Additionally, a photo diode and photo multiplier with appropriate optical filters are mounted in front of the chamber to detect the integral soot incandescence and OH-chemiluminescence. To minimize the impact of shot-to-shot deviations, the results of 15 injections are averaged.

## 2.5 Single cylinder research engine

A single-cylinder research engine (1VDS18/15CR) is used for investigation of fuel impact on engine performance, combustion and emission. The layout and size of the engine is representative for a maritime medium speed engine. The Common-Rail injection system and freely adjustable charge air and back pressure offer a high flexibility. Engine specifications are summarized in Table I.

Table I: Engine specification of single-cylinder research engine

Unit	Value
Engine ID	1 VDS 18/15 CR
Charging system	Externally charged
Engine type	4-stroke
Stroke / mm	180
Bore / mm	150
Compression ratio	13 (15, 16)
Rated power / kW	80
Max. cyl. pressure / bar	170
BMEP / bar	20
Rated speed / min <sup>-1</sup>	1500
Fuel injection system	Common Rail, HFO capable

The test bed is equipped with state-of-the-art pressure-trace indication system and exhaust analysis (O<sub>2</sub>, CO<sub>2</sub>, CO, NO<sub>x</sub> (NO + NO<sub>2</sub>), SO<sub>2</sub>, HC, FSN). Engine tests are performed at steady-state operation points at rated engine speed and varying engines loads, rail pressures and injection timing (start of energization, SOE).

## 2.6 Six-cylinder full engine

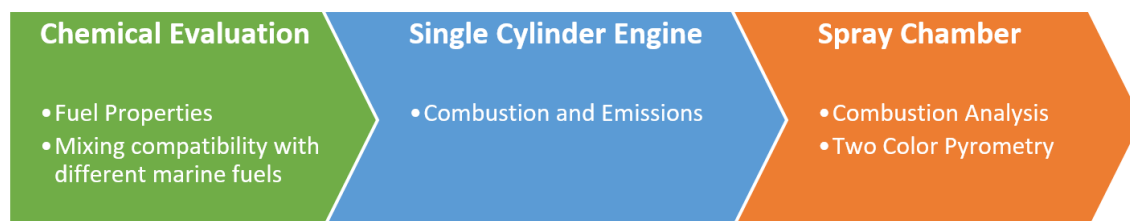
The final step of the fuel evaluation is a test on our full engine, a medium-speed marine research diesel engine. It's based on a Caterpillar MaK 6M20 engine block and power unit and coupled to an electric load unit, which can be tuned to allow engine operation in generator as well as in propeller mode. Apart from the injection system, which can be converted to a common rail system developed in house with support by L'Orange, all other components such as valve timing or turbocharger setup, for example, are identical to the serial production engine. Table II give an overview of the engine's technical data. Combustion in all cylinders is evaluated using high speed pressure indication. Exhaust gas measuring equipment is installed to acquire the exhaust gas component concentrations and the filter smoke number (O<sub>2</sub>, CO<sub>2</sub>, CO, NO<sub>x</sub> (NO + NO<sub>2</sub>), SO<sub>2</sub>, HC, FSN).

Table II: Engine specification of six cylinder full engine

Unit	Value
Name	Caterpillar MaK 6M20
Engine type	Straight six cylinder 4-stroke
Bore / mm	200
Stroke / mm	300
Displacement / l	56.4
Compression ratio	14.8
Rated power / kW	1020
Rated speed / min <sup>-1</sup>	1000
Fuel injection system	Pump-Line-Nozzle or Common Rail

### 3. Case reports of biofuel testing

#### 3.1. Hydrogenated Vegetable Oil – HVO



Hydrogenated vegetable oil, is vegetable oil (triglycerides) which was converted into hydrocarbons by a catalytic reaction with hydrogen (hydrogenation). This fuel was tested in our labs within the public project ISystem4EFuels as a representative of paraffinic drop-in E-fuels that are very much alike to diesel fuel. The hydrogenation changes the properties of the plant oil, making it significantly easier to store and handle in the fuel system. Tests were carried out alongside another E-Fuel, Oxymethylenether (OME, also called Polyoxymethylene dimethyl ether PODE) in varying blend ratios with diesel fuel. As common for public projects, these tests were rather academically motivated and more detailed information can be published.

The fuels were analysed regarding their chemical as well as thermodynamic properties. In Table III the properties of the test fuel samples are summarised. There are three fossil test fuels: highest quality diesel compliant with the European standard for on-road diesel fuels EN 590 (Diesel EN590), a high-quality marine distillate fuel (MDO) compliant with DMA according to ISO 8217 and a marine residual fuel (HFO) which is conform to RMG 380 limits of ISO 8217.

Table III: Properties of fossil fuels and paraffinic fuel

Parameter	Unit	Diesel EN 590	MDO	HFO	HVO (paraff.)
Density	kg/m <sup>3</sup>	837,5	833,9	967,9	780,2
Viscosity at 40°C	mm <sup>2</sup> /s	2,90	3,10	700,0 (360 @ 50°C)	2,95
Heating Value Hu	MJ/kg	42,4	42,9	39,1	43,7
Cetane index	-	51	n. d.	-	92

Table IV: Properties of fuel blends from fossil fuels and paraffinic fuel

Parameter	Unit	HVO 30 Diesel 70	HVO 30 MDO 70	HVO 30 HFO 70
Density	kg/m <sup>3</sup>	818,3	817,9	903,0
Viscosity at 40°C	mm <sup>2</sup> /s	2,88	3,10	49,06
Heating Value Hu	MJ/kg	42,8	43,1	40,5
Cetane index	-	63	65	n. d.

The renewable, paraffinic HVO is a clear and colourless liquid, the EN590 Diesel is clear with a light-yellow colour. The MDO is clear and of brown colour whereas the HFO is black and non-transparent. In the following blending step, the colourless HVO will be used as blend component and the three fossil fuels as base component. During the blending process 30% of HVO will be blended with each base component (V/V).

Table IV summarizes the properties of the blend fuels. Notably, the HVO30/Diesel70 blend approaches the lower limit of Diesel EN590's density range. HVO30/MDO70 blend remains compliant with DMA/DMB distillate fuel norms as per ISO 8217. Blending with HVO significantly lowers HFO's viscosity. HVO30/HFO70 blend now aligns with RMD 80 (ISO 8217).



The color of the blends of Diesel EN590 and MDO with HVO is slightly lighter than the color of the fossil base fuels. The HVO30/HFO70 blend does not differ optically from the HFO base fuel. All three blends of fossil base fuel with 30% HVO could be easily produced without excessive mechanical mixing and without any additives. No deposit formation or phase separation occurred. The blends were then stored at room temperature for several days without any visible generation of deposits. To further test the stability of the blends the samples were stored at a reduced temperature of 5°C over a period of 24 hours.

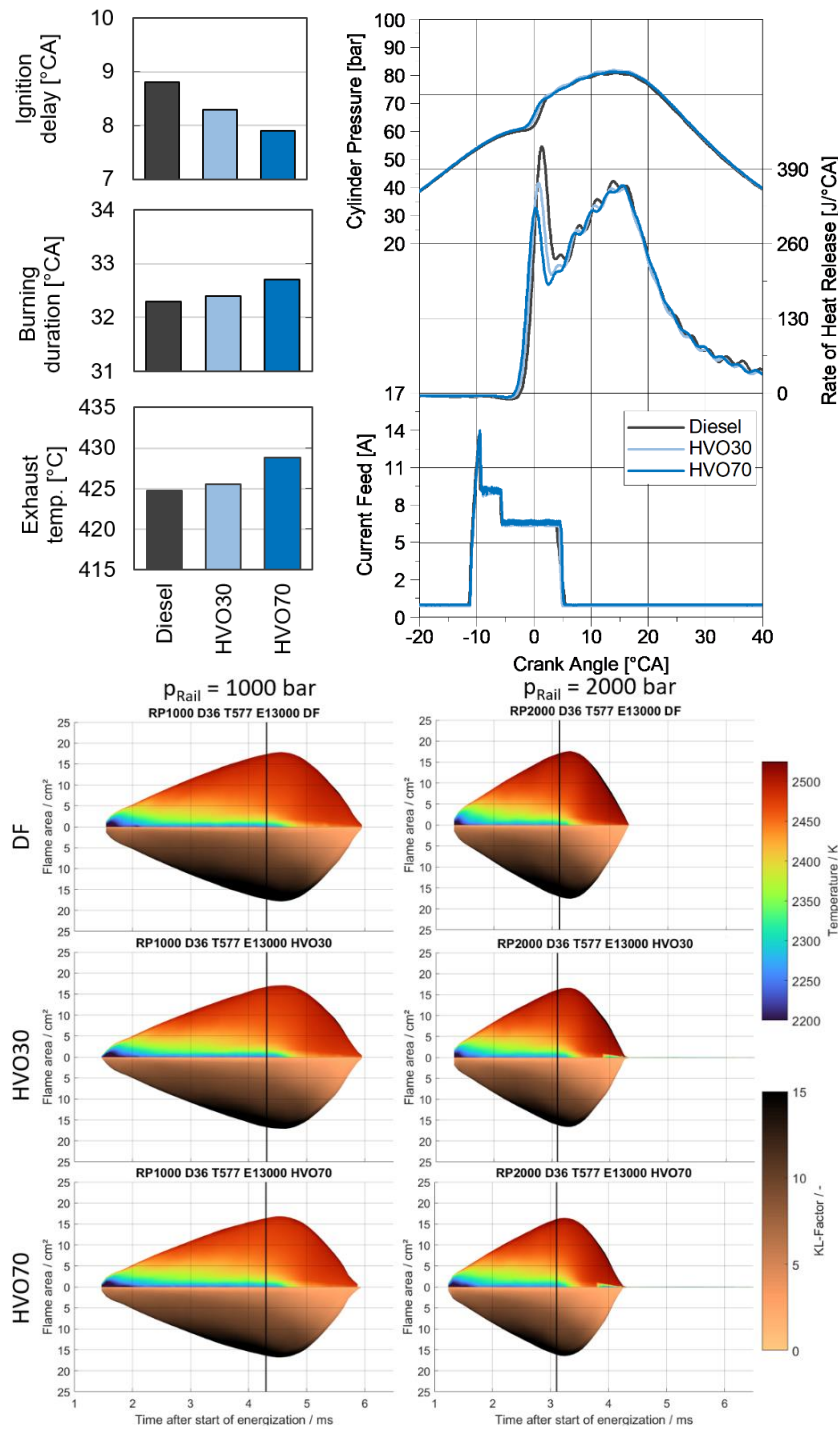


Fig.2: Engine results from single cylinder engine showing the high similarity between paraffinic fuel and diesel fuel (top).

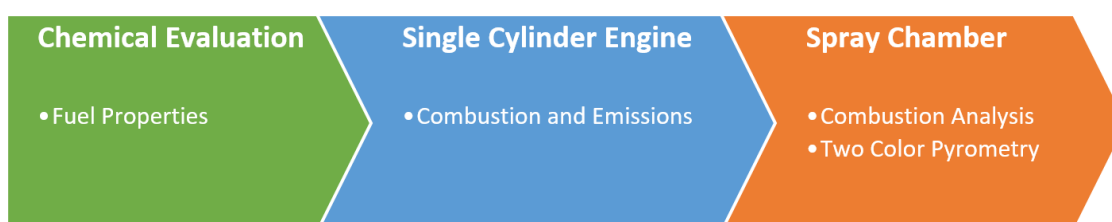
Again, no deposit formation or phase separation could be observed. The blend of HFO with 30% HVO showed a layering with higher viscosity at the bottom of the container. A spot test was carried out and the result confirmed that no chemical mixing instability occurred (no separation of asphaltenes). The photograph in Fig.4 was taken after the storage tests of the samples at room temperature and at 5°C, *Buchholz (2019)*.

Further testing was done on the diesel fuel blend with 30% and 70% HVO using the single cylinder testbed and the injection chamber. HVO turned out to be remarkably similar to diesel fuel in all tests. Its ignition behavior and rate of heat release as measured on the engine is shown in Fig.2. The fuels higher cetane number advances the ignition and thereby lowers the premixed peak. During the diffusion-controlled part of the combustion there is virtually no difference between the fuels. The emission behavior of HVO shows lower soot emissions due to the absence of aromatics/polyaromatics in the paraffinic fuel and a slightly lower boiling end, which improves mixture formation. At the same time, nitrogen oxide emissions were slightly reduced with the same center of gravity.

Fig.2 also shows the results of the combustion analysis on the injection chamber. These flame structure diagrams show the evolution of the flame size as well as the occurrence of temperatures and soot concentrations across the flame. Along with the significantly lower soot concentrations and the earlier start of combustion it can also be seen that the temperatures of the flame are slightly lower for the HVO, which is in accordance with the lower NO<sub>x</sub> emissions seen on the engine. These findings underline how well suited this fuel is for replacing diesel from a combustion point of view. All other characteristics like the lubricity and material compatibility are also very good for use in a standard diesel engine.

The flame structure diagrams (bottom) show the evolution of the flame area (y-axis) and the distribution of soot and temperature (color paving) across the flame over the time (x-axis). Two rail pressures are compared in the left and right column. Diesel Fuel is shown in the top row, blends with HVO are shown in the middle and bottom. HVO has lower soot concentrations apart from this almost no differences between the fuels can be made out.

### 3.2. Oxymethylenether - OME



OME can have different chain lengths and was tested as mixture of 3 to 5 CH<sub>2</sub>O units. In contrast to HVO which originates from vegetable or animal fats and oils, OME is an all-synthetic fuel. It can be synthesized for example from methanol. OME has slightly less advantageous properties compared to HVO. It has some solvent like properties, thereby reducing material compatibility to some elastomers and coatings. The reduced viscosity compared to diesel fuel influences the behavior of the fuel system as for example operational internal leakages of pumps will increase. A noteworthy characteristic is the high level of oxygen within the OME molecules. This can be interpreted as a pre-oxidized molecule. This results in a lowered calorific value of the fuel and a lower equivalence ratio in the flame compared to Diesel Fuel, *Langhorst (2018)*.

In the engine tests the ignition delay was only slightly shorter than diesel fuel but due to the strongly reduced calorific value, the injection duration needed to be increased in order to inject a larger amount of fuel. In the engine tests the center of combustion was kept constant and for this the start of injection was advanced. Despite the later end of injection, the end of combustion is reached earlier compared to

diesel fuel resulting in lowered exhaust temperatures. The fuel oxidizes very quickly and the engine efficiency is increased by about 1 %.

This behavior is also quite impressively demonstrated in the flame structure diagrams. Over the course of the diesel combustion there is an ever increasing deficit of only partially burned fuel. This can be seen from the growing black area in the lower part of the diagrams. These products accumulate in the spray tip resulting in the known shape of a burning diesel plume and in the soot emissions. A reduction of these intermediate products takes place only after the end of injection.

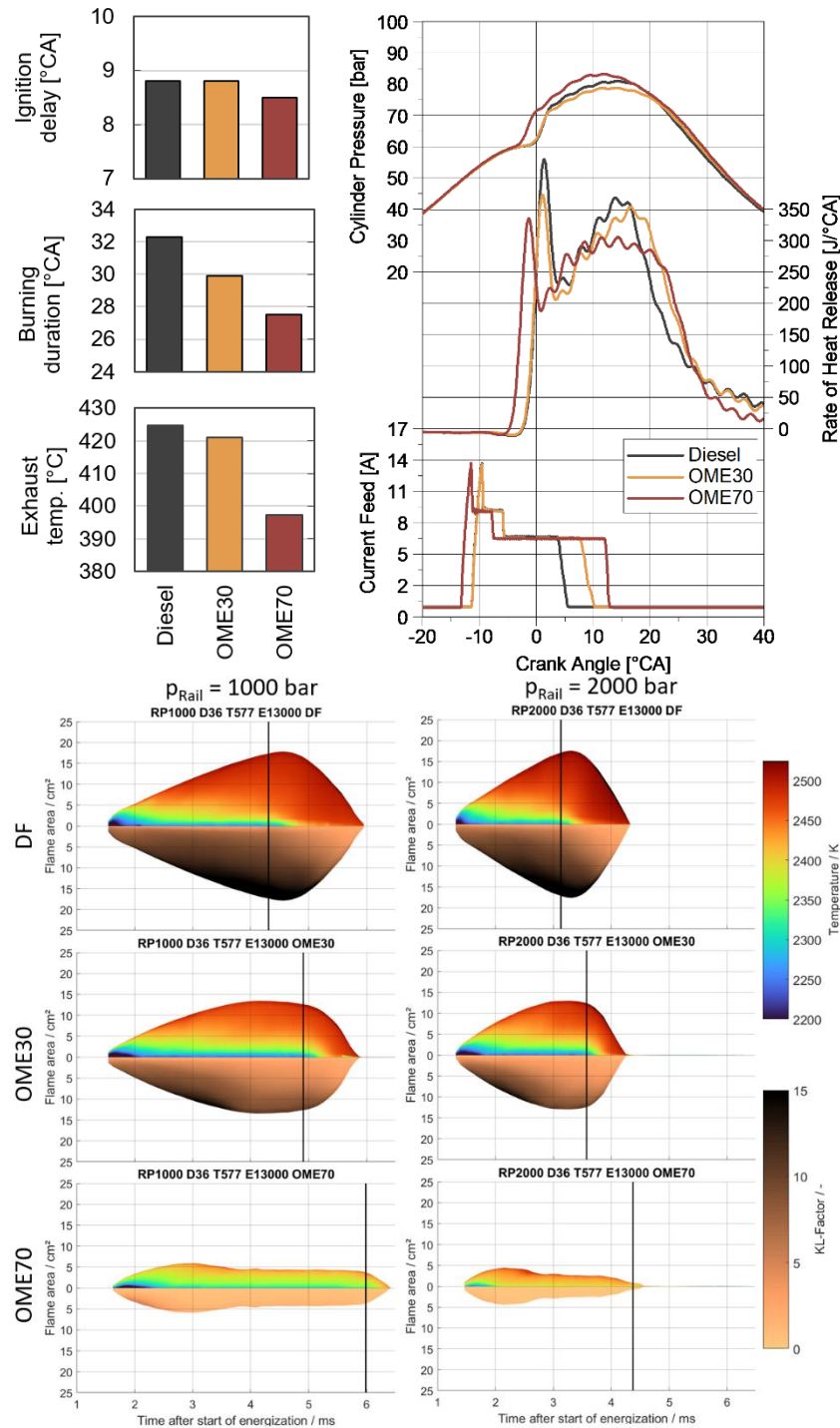
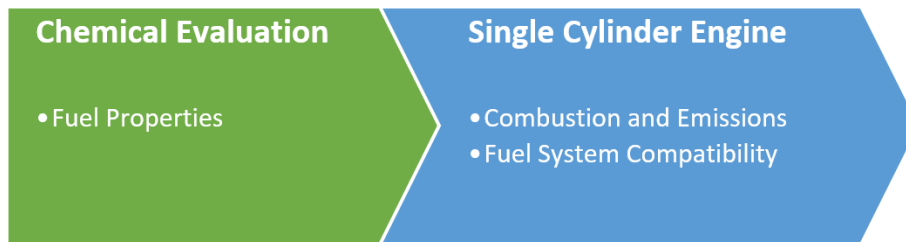


Fig.3: Engine results from single cylinder engine (top) show the influence of the lower calorific value and the higher burning speed of the OME blends.

The flame evolution for the OME30 blend starts similarly but then, once the flame temperature is high enough, the amount of intermediate products and soot is reduced again and reaches steady state. The plume of the flame is shorter and thinner and after the end of the injection the oxidation of the plume takes only about half as long compared to diesel fuel. For the OME70 blend the flame structure is changed again. Now there is virtually no accumulation of intermediate products taking place. The visible flame area is very small. Nonetheless there are some areas with very high temperatures in the flame. The NO<sub>x</sub> emissions are slightly higher compared to diesel fuel. The NO<sub>x</sub> therefore must be produced in these small high-temperature zones at an increased production rate due to the higher level of oxygen available, *Swiderski (2022)*.

The flame structure diagrams (bottom) are arranged like in Fig.2. OME leads to significantly smaller flame area and lower soot concentrations. There is little to no buildup of soot within the tip of the flame, as is typical for the diesel diffusion flame. Furthermore, combustion temperatures are lower due to the lower calorific value and the missing burn out phase.

### 3.3. Refined Waste Oil - RWO



Waste plant oils and animal fats can be sourced from various feedstocks and represents a significant share of the total biofuel potential, *Sekkesæter (2023)*. These fats and oils originate from urban sewage treatment, the food industries as well as restaurant grease traps. They cannot be used as crude oils due to high contamination levels and high acid numbers caused by the high amount of free fatty acids. The product must therefore be processed into a mix of mono-, di- and triglycerides. These are then further blended into the final biofuel product.

The biofuel tested here was provided to us in a customer project. The RWO was blended with low quality FAME, the exact formulation of the test fuel can however not be disclosed. It was tested against an HFO 380 as reference fuel. The RWO was heated to 80°C in order to reach injection viscosity. It was tested on the single cylinder engine for its engine performance and emissions. All engine settings were kept unchanged and therefore portrait the unaltered influence of the fuel change.

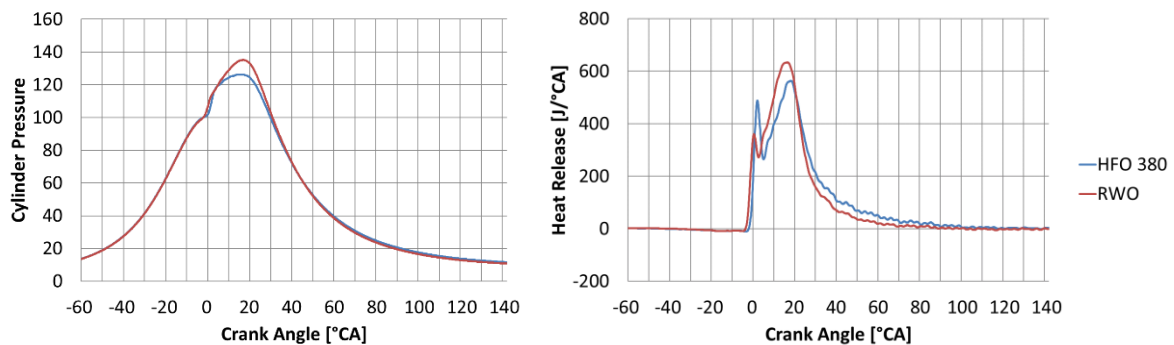


Fig.4: Characterization of combustion process at 100% Load. The biofuel shows improved ignitability and better oxidation behavior during the diffusion combustion compared to the HFO.

As evident from the ignition delay shown in Fig.4 and Table V, the biofuel has a higher cetane number, resulting in a lower premixed peak. During the diffusion phase the biofuel shows significantly improved oxidation behavior. The end of combustion is reached almost 10°CA earlier compared to the HFO. This

increases the engine efficiency. As seen in the emission diagrams in Fig.5 this behavior leads to a higher flame temperature resulting in lower soot emissions as well as an increase in NOx.

In a full engine configuration, the earlier end of combustion lowers the exhaust gas enthalpy which in turn provides less power to the turbocharger. The lowered intake pressure will counteract some of the effects seen on the single cylinder engine. This was confirmed by the fuel manufacturer as NOx emissions were measured in an on-board trial and turned out to be on par with the typical increase experienced from FAME fuels.

Table V: Combustion timings at 100% Load

	$\alpha_5$ [°CA]	$\alpha_{50}$ [°CA]	$\alpha_{90}$ [°CA]
HFO 380	2,5	16,3	47,8
RWO	1	14,4	38,2

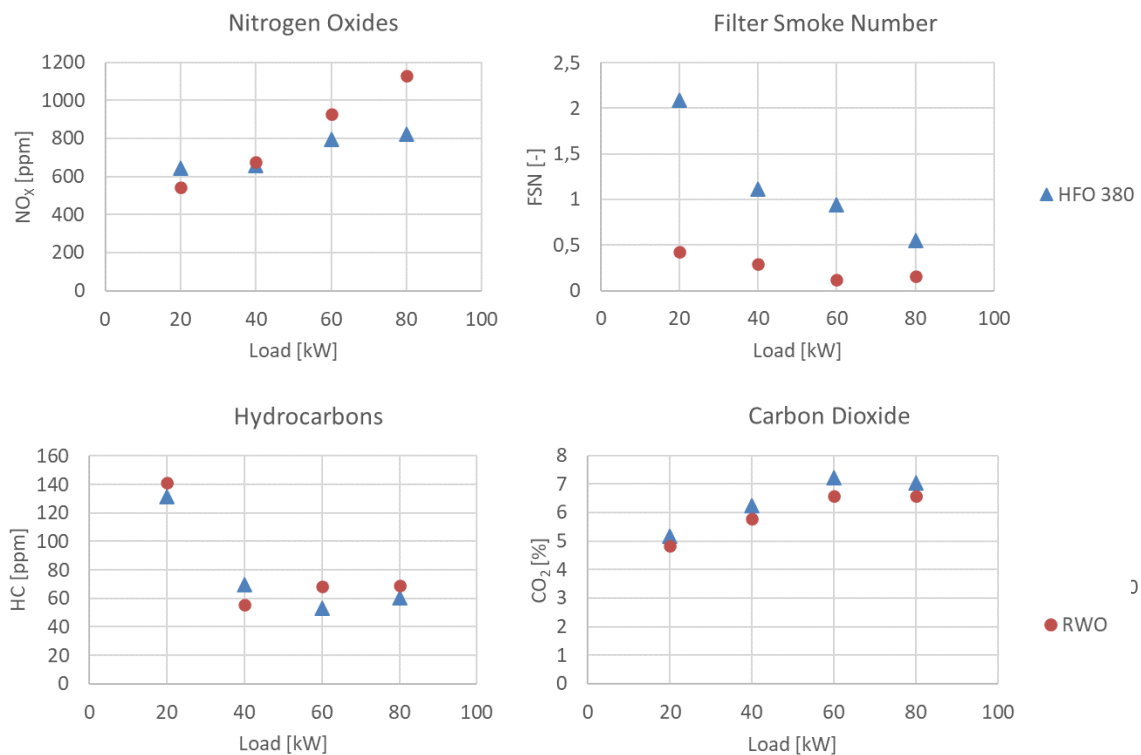
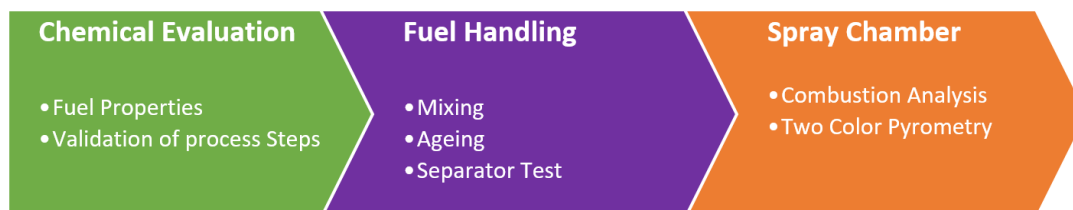


Fig.5: Characterization of the emission behavior at different engine loads, demonstrating the impacts of the improved ignition and oxidation behavior of the biofuel blend.

### 3.4. Fuel Handling Additives



Fuel additives are used to improve many different aspects of biofuels and conventional fuels. Specialty chemicals company Infineum - a joint venture of Shell and ExxonMobil – develops a wide range of additives, some of which are tested at FVTR. In this case an additive designed to improve fuel separator



efficiency and reduce the amount of fuel lost in the form of sludge was tested for its performance against competitor products.

One major origin of sludge is the agglomeration of asphaltenes within a heavy fuel oil. Under certain conditions like ageing, temperature stress or a change of the ratio between paraffins and aromatics in the fuel, asphaltenes will become unstable and produce an increased amount of sludge which in turn can be inhibited by additives. The performance of these additives was tested on the separator test bed, an environment that is very close to a ships fuel system while also being well controlled.

In a defined test method, the test fuels are mixed and heated and left to age, mimicking the fuel supply system onboard a vessel, with bunker, settling tank and day tank. After extraction of the tank bottom the fuel is again stirred and heated and run through the separator in purifier or clarifier configuration at a controlled flow rate. Samples are taken at all process steps and the resulting sludge in the separator bowl is quantitatively and qualitatively rated.

Fig.6 shows images of the sludge bowl for the base fuel as well as the Infineum additive at a concentration of 1000 ppm. The visual amount of sludge is significantly reduced. This is quantitatively visualized in the following diagram. With increasing treat rate the amount of collected sludge is reduced. The additive is effective even at relatively low treat rates of 10 and 100 ppm. As the tests showed, the additive performance scales roughly with the logarithm of the treat rate. The zero treat rate of the base fuel was represented in the logarithmic diagram using a broken x-axis.

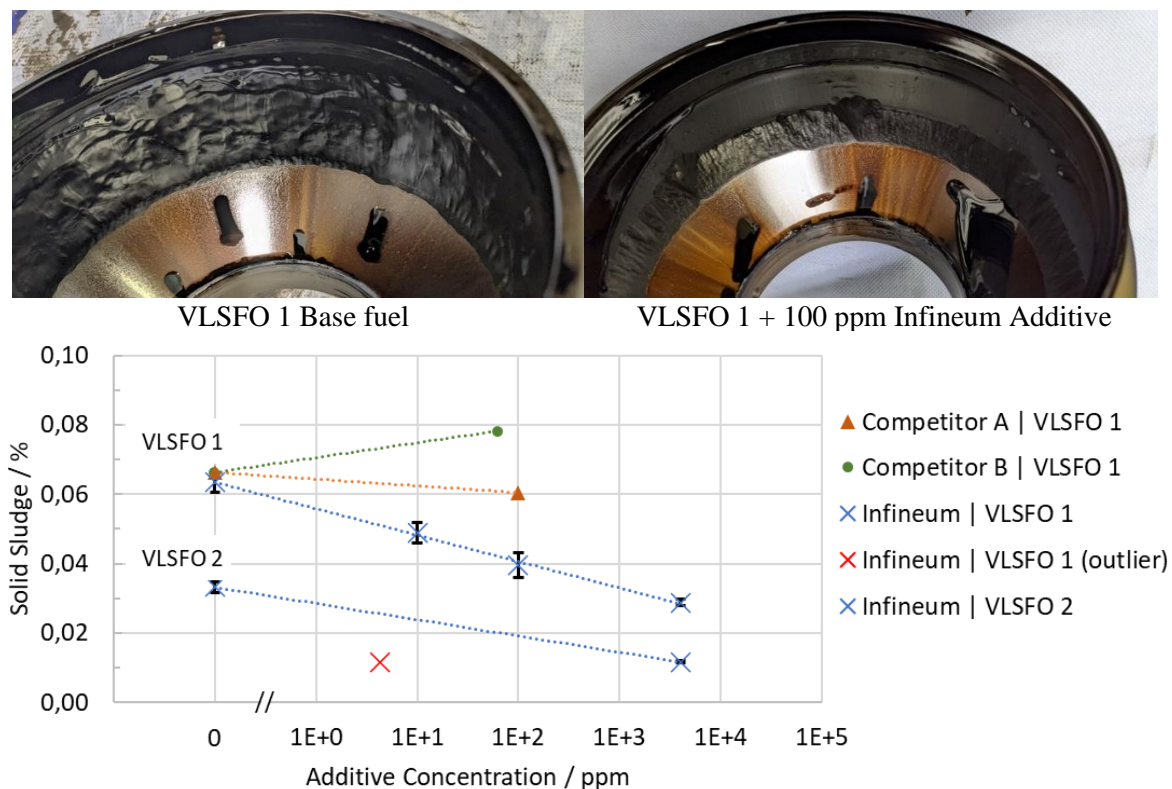
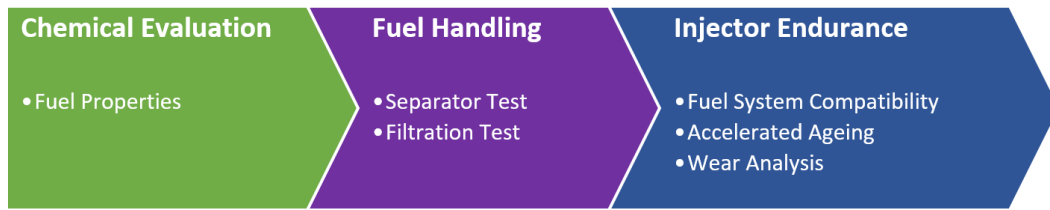


Fig.6: Visual and quantitative representation of collected sludge for two base fuels. The VLSFO 1 with higher sludge potential was also tested against two competitor additives. A min/max band is given for the Infineum test series. An outlier for base fuel 1 was excluded from the data.

The efficacy of the additive at low treat rates was confirmed in field trials. Lab tests like the hot filtration test or the hot spin test were not able to reproduce this behavior. Especially the hot spin test is a very promising procedure to confirm sludge potential and exceeds the classic hot filtration test in its prediction quality. The hot spin test is centrifuge based, which mimics the conditions in a separator. Its failure

to predict the low treat rate efficacy might be caused by the significantly different ratio between sample volume and surface area of lab testing equipment compared to real hardware.

### 3.5. HFO with coal powder



In coal mining, a big environmental impact originates from the waste products, in the form of coal slurries. These waste emulsions of micro-fine hydrocarbons are cleaned and upcycled by the company Arq to produce a very fine coal powder. One of the applications of the Arq powder is to mix it into HFO to produce a waste to energy fuel with lowered CO<sub>2</sub> Emissions compared to the base HFO, *Ahmed (2023)*.

The fuel was tested for its compatibility with marine fuel handling systems and marine common rail pumps and injectors on the injector durability test rig. The fuel was tested for 300 engine hours in an accelerated test while monitoring the operating conditions and fuel mass flow.

The content of Arq powder remained unchanged by the purifier, as chemical analysis showed only a slight reduction of the total sediments. During the test run the injector was able to operate on the test fuel with no apparent change to injection flow rate. Therefore, neither functionally noticeable nor optically visible deterioration was done to the pilot valve, which is the most sensible part of a common rail injector. Microscopic images of the nozzle imprints at start and end of test are shown in Fig.7. The nozzle indeed shows distinct wear marks: The manufacturing marks of the nozzle holes have been smoothed out and the recirculation zone after the spray hole inlet has been slightly washed out. These marks were identified as non-restrictive to the injector functionality and within normal wear levels considering the test time, the use of a heavy fuel oil and the slightly lowered hardness of the injector nozzle used in these tests. No marks were found on the injector needle.

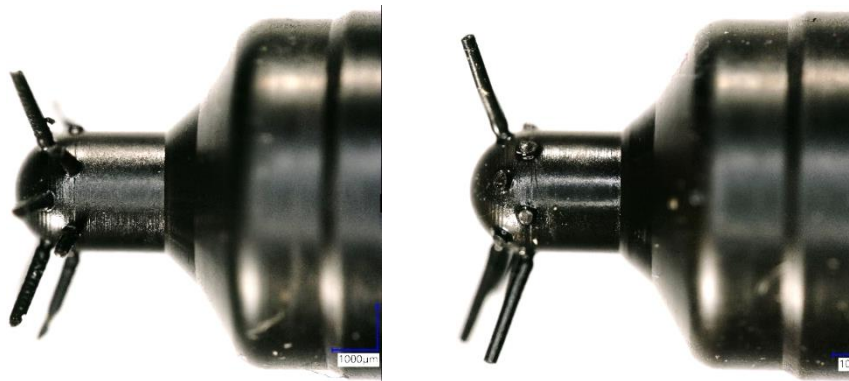
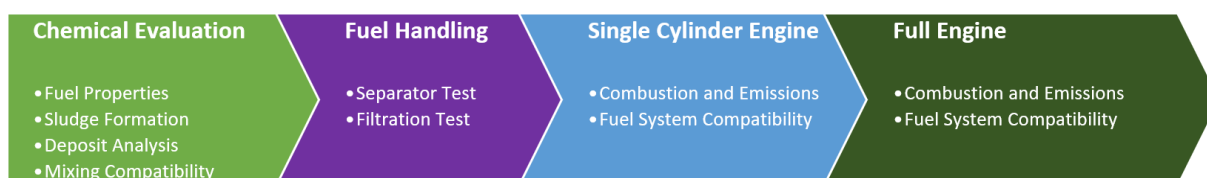


Fig.7: Nozzle imprint at start of test (left) and end of test (right) showing slight wear marks on the nozzle holes which were identified as within normal wear levels.

The fuel was tested for engine performance and emission formation at another lab. Based on these results the fuel could be cleared for an on-board trial for determination of actual engine performance and long-term endurance.

### 3.6. Refined Cashew Nutshell Liquid - CNSL



One of the latest feed stock candidates in the search for new biofuels is cashew nutshell liquid, a brown viscous liquid surrounding the edible cashew nut within the fleshy fruit body. The liquid is a mixture of 70% anacardic acid, 5% cardanol, and 18% cardol. Depending on the feedstock and the production process, these ratios will vary. The liquid is processed to remove impurities and gum. The resulting refined oil can be run in diesel engines. However, it can cause problems during the separation process and in the injector nozzles. The oil can be higher processed to produce fame or pyrolysis oil which should significantly enhance its compatibility in diesel engines, *Kumar (2018)*. This, however, is less economically attractive. In several customer projects efforts were therefore taken at FVTR to use the refined oil as a drop-in fuel. The fame and pyrolysis oil products have not been tested at our labs yet.

In on-board trials, problems were observed with clogging separators using CNSL blends. As reaction to this, lab-tests were conducted on a centrifuge, recreating the interaction between fuel and water in the separator. The CNSL was shown to create a gel with the water. In the separator therefore the fuel itself might lead to normal levels of sludge. However, when run in purifier mode, the CNSL transforms the water seal itself into sludge und thereby clogs the purifier and filters downstream the separator. A remedy to this could not be found to date. Detailed analysis of the sludge showed that all components of the fuel oil are equally present in the gel.

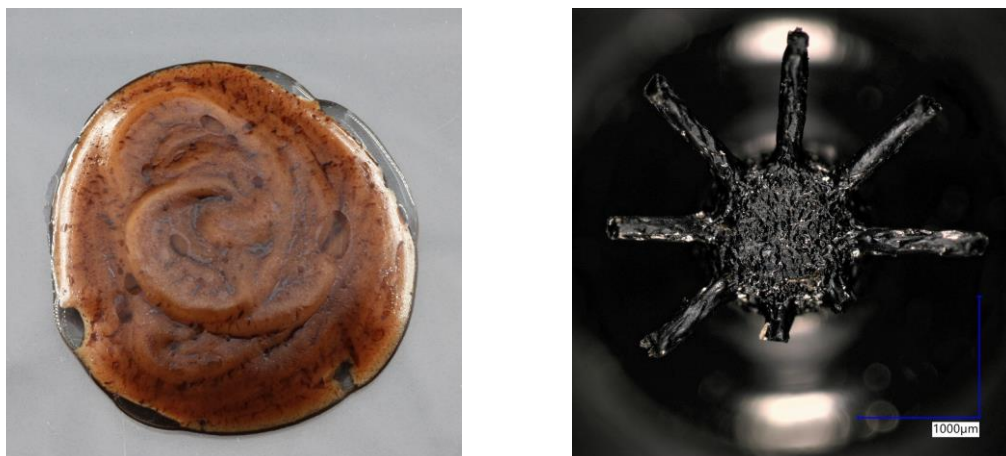


Fig.8: CNSL Sludge created in a Laboratory test by mixing of CNSL with water (left). Injector nozzle imprint of the uncooled common rail nozzle used at the single cylinder test bed, showing high amounts of internal deposits (right).

On the engine, the main problem for CNSL comes from heat stress. At surface temperatures above 200°C the fuel starts to form deposits. These temperatures are reached only within the injection nozzles. In our tests after just a few hours of operation the fuel starts to block the sack hole and the orifices. The injection duration needs to be prolonged to make up for the lower throughput. As an effect of this the center and end of combustion shift to “late”. The exhaust gas temperature rises until the engine power needs to be reduced to maintain safe operation.

When run with cooled nozzles the deposits within the sack hole are reduced significantly. In this case however external deposits build up to form impressive trumpet structures that impede the spray breakup and will also lead to engine problems. Currently, tests are still ongoing aiming to counter these effects by blending, improvement of base fuel quality and additivation.

## 4. Conclusion

Tackling the challenges of the energy transition, many fuel alternatives for marine engines are being developed and have already hit the market. The exploitation of new feedstocks, formulation of fuel blends but also the implementation of new fuels on a ship should be accompanied by fuel and engine experts with hands on experience and state of the art test equipment. In the labs at FVTR and the University of Rostock, a wide variety of fuels and especially biofuels have been analyzed and tested over the last decades, some of which are presented in the present paper.

HVO, a paraffinic biofuel, exhibits remarkable potential as a diesel substitute, showcasing similar combustion characteristics and emission profiles. Its capability to be blended with conventional diesel in varying ratios underscores its versatility and ease of adoption. On the other hand, OME, an all-synthetic fuel, brings its own advantages and challenges. Despite its improved combustion behavior translating to enhanced engine efficiency and reduced emissions, its solvent-like properties and high production cost can make it difficult to implement. Refined waste oil (RWO) and refined cashew nut shell liquid (CNSL) have also been evaluated as potential biofuel sources. RWO, produced from waste plant oils and animal fats, showcases improved combustion characteristics compared to conventional marine fuels. Meanwhile, CNSL presents a promising biofuel candidate, but it needs to go through additional processing steps to produce FAME. When used in a less refined and therefore economically more attractive form, special care needs to be taken in order to make sure the CNSL does not cause deposits within the injection system.

The complexity of biofuel formulation and their interaction with marine systems necessitates advanced testing methodologies and expertise. FVTR's commitment to assessing these fuels in a real-world context has yielded valuable insights into their viability for maritime applications. As the industry grapples with the transition towards sustainable fuels, the role of dedicated research facilities like FVTR becomes increasingly pivotal in bridging the gap between innovation and practical implementation. Through collaboration and continuous testing, the maritime sector can confidently navigate the challenges of adopting new feedstocks and realizing the goal of reduced environmental impact.

## References

- AHMED, R. (2023), *Microfine Carbon blends as fuel for Marine engines*, CIMAC
- BUCHHOLZ, B. (2019), *Potential of Paraffinic Fuels for the Maritime Energy Transition*, CIMAC
- DNV (2023), *The EU Agrees on Well-to-Wake GHG Limits to Energy Used on Board Ships from 2025*, DNV, Hovik, <https://www.dnv.com/news/the-eu-agrees-on-well-to-wake-ghg-limits-to-energy-used-on-board-ships-from-2025-243501>.
- KOLOS, M. (2022), *Carbon Market Survey 2022*, Refinitiv
- KUMAR, S. (2018) *Cashew Nut Shell Liquid as a Fuel for Compression Ignition Engines: A Comprehensive Review*, *Energy & Fuels* 32/7, pp.7237–7244
- LANGHORST, T. (2018), *Investigations on Spark and Corona Ignition of Oxymethylene Ether-1 and Dimethyl Carbonate Blends with Gasoline by High-Speed Evaluation of OH\* Chemiluminescence*, *SAE Int. J. Fuels and Lubricants* 11/1, pp.5–20, <https://doi.org/10.4271/04-11-01-0001>
- SEKKESAETER, Ø. (2023), *Biofuels in shipping*, DNV, Hovik
- SWIDERSKI, E. (2022), *Einfluss von E-Fuels auf Flammen-strukturen und Verbrennungs-prozesse von Großdieselmotoren*, *MTZ - Motortechnische Zeitschrift* 83/5, pp.54–61



# Complying EEXI, EEOI & CII from Owner's Perspective

David Pang, Swire Shipping/Swire Bulk, Singapore, [david.pang@swireshipping.com](mailto:david.pang@swireshipping.com)  
Nishant Dhyani, Swire Shipping /Swire Bulk, Singapore, [nishant.dhyani@swireshipping.com](mailto:nishant.dhyani@swireshipping.com)

## Abstract

*The International Maritime Organization (IMO) enacted the MARPOL Annex VI amendments that went into effect in November 2022. With Energy Efficiency Existing Ship Index (EEXI) and Carbon Intensity Indicator (CII) certification requirements coming into effect on January 1, 2023, it has become crucial for ship owners and operators to comply with the regulations while operating the vessel profitably. When ordering a new ship or purchasing used tonnage on the market, it is crucial for the shipowner to pay close attention to the ship's design parameters. Both Energy Efficiency Design Index (EEDI) and Energy Efficiency Existing Ship Index (EEXI) refer to a vessel's design index. Essentially, the lower the EEDI or EEXI, the lower the fuel consumption, and the lower the emissions. Once the ship has been delivered to the owner/operator, little can be done to enhance its EEDI or EEXI. It is a standard value that appears on the certificates of the classification society of vessel. CII is the form that the ship's genuine emissions take. It could be based on either the 'supply' or 'demand' of the transported cargo. From a legislative standpoint, IMO selected the Annual Efficiency Ratio (AER) that is founded on a 'supply' basis; consequently, the vessel's deadweight (DWT) is utilized in the CII calculation. If the CII were based on 'demand', it would be referred to as the Energy Efficiency Operational Index (EEOI). The International Maritime Organization (IMO) has provided guidance on how to calculate this metric, and many businesses use it as an internal control measure to improve their emission and business performance. With the aid of actual ship data, this paper examines three significant points:*

- 1. The influence of the vessel's design index (EEDI/EEXI) on the CII.*
- 2. The relationship between 'supply' and 'demand' based CII (AER and EEOI).*
- 3. Swire (Swire Shipping & Swire Bulk) approach on addressing these three indexes.*

## 1. Introduction

The AER, or commonly termed as CII, is a performance-based measure that assesses the carbon intensity of a ship's operations. The AER is calculated by dividing the ship's CO<sub>2</sub> emissions by its transport work (measured in tonne-nautical miles). It is expressed as a rating from A to E, with A being the most efficient and E being the least efficient. The indicator is calculated annually and is based on the ship's actual performance over the previous year. The AER is a valuable tool for shipowners and operators to track their carbon footprint progress, while serving as a useful tool for regulators to monitor the overall performance of the shipping industry.

The EEOI is a similar measure to the AER, calculated by dividing the ship's CO<sub>2</sub> emissions by its transport work, instead of using the vessel deadweight throughout. The EEOI is not enforced by the regulators unlike the AER, however, the EEOI is a useful tool for shipowners and operators to compare the efficiency of their ships to other ships of the same type. It is also a useful tool for regulators to assess the overall efficiency of the shipping industry.

The EEXI is a new measure that was adopted by the IMO in 2018. The EEXI is a design-based measure that sets a minimum energy efficiency standard for existing ships. The EEXI is calculated based on the ship's main engine power and its gross tonnage. The EEXI is expressed as a percentage of the EEDI, which is the Energy Efficiency Design Index. The EEXI is a mandatory measure for all existing ships above 400 gross tonnages. Ships that do not meet the EEXI will be required to take measures to reduce their emissions. The EEXI is a significant step forward in the IMO's efforts to reduce the environmental impact of shipping.

While AER is an operational carbon intensity rating that is based on actual emissions and transport work, it sets increasingly stringent annual targets that ships must meet to avoid operational penalties.



The AER rating is influenced by EEXI because ships with more efficient designs have lower baselines and more room for operational modifications. Additionally, actions taken to meet EEXI targets, like engine power limits, directly impact AER performance. However, AER also strongly depends on how vessels are operated, irrespective of design index.

EEOI was introduced earlier than AER and EEXI to monitor operational efficiency and provide a standardized calculation methodology. It tracks fuel consumption per unit of transport work. The relationship between EEOI and AER is complex. Some measures to improve EEOI, like slow steaming and optimized routing, also help comply with AER requirements. However, AER does not account for cargo carried unlike EEOI, so high utilization could negatively affect AER ratings. Companies must balance EEOI and CII carefully through voyage optimization.

Shipping companies are taking a range of actions in response to EEXI, AER, and possibly EEOI. Many have carried out or planned modifications to enhance design efficiency where possible. Such upgrades include propeller modifications, engine power limits, and waste heat recovery systems. Operationally, most companies are starting to optimize speed, routing, and other parameters to maximize efficiency while meeting AER limits. Enhanced data collection and analysis enables smarter decisions around vessel performance. Some firms are also considering early scrapping or retrofits for non-compliant vessels. However, the costs of upgrading ships present challenges, especially in the current financial climate.

This paper provides an examination of the interactions between EEXI, AER, and EEOI for Swire vessels, namely containerships from Swire Shipping and bulk carriers from Swire Bulk based on actual data from the respective vessels. It assesses how EEXI affect the AER and EEOI for the vessels, and the analysis exemplifies the intrinsic relationship between meeting operational AER and EEOI targets. The paper will also discuss how Swire Shipping & Swire Bulk are responding to the new efficiency regulations through upgrades, operational changes, and decision making. The multiple indexes have created a complex compliance landscape that Swire wants to navigate carefully in the coming years.

## **2. Methodology**

The following vessels were selected to provide representation across Swire Shipping and Swire Bulk main ship types and operational profiles. The sample includes 4 bulk carriers from 2 classes, and 5 container ships with capacities ranging from 20,000 DWT to 40,000 DWT. Vessels were chosen across the spectrum of ratings to allow comparison based on design efficiency. The ages of the selected containerships vary between 5 and 10 years to limit the impact of age on efficiency, while the selected bulk carriers are from two different classes, one delivered in 2016 while the other delivered in 2021.

By selecting a diverse sample of vessels, this study aims to draw broadly applicable conclusions regarding the relationships between EEXI, EEOI, and AER. The sample intends to be representative of the Swire global fleet and provide data points across different design efficiencies, ship types, sizes, and ages. Analyzing this mix of vessels will generate insights into how the three indexes interact and influence overall ship efficiency, as the paper will discuss how Swire address some of the metrics in the later part of the paper.

From Table I, except for Containership E, the listed vessels have their attained EEXI lower than the required EEXI. Required EEXI refers to the minimum energy efficiency level that a ship must meet according to regulations adopted by IMO, while setting a baseline for reducing carbon emissions from existing ships. Attained EEXI refers to the actual energy efficiency level achieved by a specific ship. This is calculated by shipowners and then verified by the ship's classification society. To comply with EEXI regulations, a ship's attained EEXI must be equal to or lower than the required EEXI value.

Similarly, The EEDI constant has a direct impact on the EEXI calculation. A higher EEDI constant increases the EEXI value, implying lower energy efficiency. Conversely, a lower EEDI constant reduces the EEXI, improving a ship's efficiency rating. It is crucial for ships to have an attained EEXI lower

than the required EEXI set by IMO's regulations. Having a lower attained EEXI provides more headroom for compliance even if the required EEXI gets tightened in future amendments. It also indicates that the ship has taken concrete steps to improve its energy efficiency and reduce emissions since a lower EEXI signals commitment towards environmentally sustainable operations.

Table I. List of Swire Shipping and Swire Bulk vessels details

Vessel	DWT	EEDI Constant	Required EEXI	Attained EEXI	Attained EEOI 2022	Attained AER 2022
Containership A	30428	174.22	17.5	13	17.14	8.73
Containership B	30401	174.22	17.504	13.1	15.07	6.96
Containership C	30383	174.22	17.506	13.1	34.64	7.96
Containership D	36931	174.22	16.832	10.8	13.65	6.71
Containership E	23305	174.22	18.5	28.6	43.04	16.75
Bulker P1	39777	961.79	4.922	4.611	8.85	6.06
Bulker P2	39790	961.79	4.921	4.582	12.20	5.94
Bulker K1	37440	961.79	5.066	4.62	7.12	4.89
Bulker K2	37440	961.79	5.066	4.61	7.15	4.97

For Containerships A to D and the listed bulkers, these vessels are required to meet stringent conditions before the newbuild phase, such as optimized hull design for maximum hydrodynamic efficiency and repeated modelling of ship's characteristics to achieve optimal attainable EEXI. This is to ensure that the vessels have a buffer for future possible regulatory tightening of EEXI requirements. Besides, these set the vessels up for compliance with upcoming emissions regulations like EEOI and AER. From Table 1, the vessels have attained promising AER and EEOI results in 2022, except for Containership E and Bulk P class. Containership E has a higher attained EEXI value than the required EEXI, which deems her to be inefficient in vessel performance and emissions. Although Bulk P have a good EEXI rating, the seemingly inadequate EEOI and AER values in 2022 are attributed to their sailing and cargo profiles. Nonetheless, the paper will employ actual operational data to substantiate the influence of EEXI on EEOI and AER, as well as to investigate if there can be a masked relationship between EEOI and AER.

### 3. Influence of EEXI on EEOI & AER

#### 3.1. Containerships

In the first part of this paper, the paper will look at the data derived from 2022 for the mentioned vessels, to observe how the EEOI and AER changes in relation to the main parameters of annual vessel operation, namely distance and speed.

In Fig.1, each row is depicted by the respective containership vessels, with the first subplot column showing each daily report the cargo weight parameter against distance, illustrating the EEOI value at the same time. The EEOI values are represented by different colors shown in the color bar, ranging from dark blue to red, with dark blue color preferred as it portrays a lower value of less than 20 gCO<sub>2</sub>/ (tons x nm). The first distinctive observation is that EEOI improves gradually when moving up the y-axis (cargo weight), and it is understandable the vessels will attain better EEOI results by carrying more

cargo weight. In Containership C example, it is also observed that the vessel will have to accept much poorer EEOI values when the cargo weight is below the 5000 mt threshold.

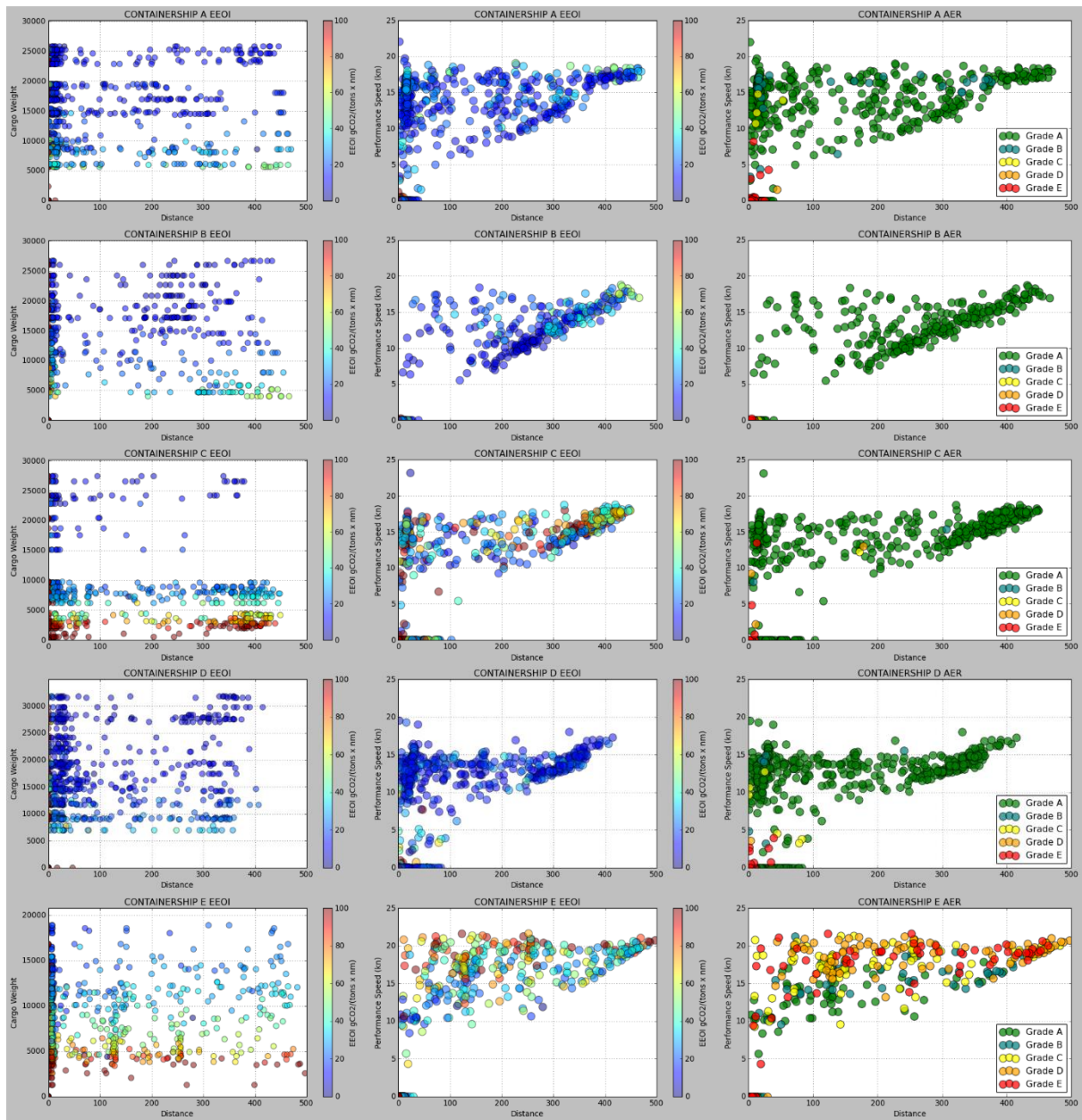


Fig.1: Containerships EEOI and AER

The second subplot column similarly shows the EEOI value of each daily report, albeit plotted in the parameters of speed against distance. The intention of the subplot is to demonstrate the expected upward trend of speed against distance, and to observe if there is any shift of EEOI values when speed increases due to the increment of distance. Nevertheless, there is little correlation between speed/distance with the shown EEOI values, since it is expected that EEOI values may worsen significantly due to the exponential speed-consumption curves as speed increases. The consequence of low cargo weight is again reflected in the Containership C example. However, for Containership E example, a slightly older containership with much poorer EEOI results compared to the other containerships, the EEOI values are similarly scattered across the range like Containership C. Most of the below-par EEOI values may be attributed to the low cargo weight, rather than speed, as substantiated by the first subplot of Containership E.

In the third subplot column, the AER values are depicted in a similar fashion as the second subplot, represented by speed against distance. For Containerships A to D, they are mostly marked by a good rating of A in green. In the Containership C example, the contrast is exemplified with very few sub-par ratings shown, as the graph is encapsulated by mostly green Grade A markers. In contrary, Containership E third subplot illustrates many daily reports attaining rating D or E, especially as the speed increases above 17 knots. This result is not unexpected, since the attained EEXI value (28.6) is much higher than the required EEXI value at 18.5. In comparison, the attained EEXI values of the remaining of the containerships A to D are lower than the required EEXI values, with Containership D achieving the best attained value at 10.8 when the required value is at 16.8. Since EEXI measures the design efficiency of a ship, containerships A to D have the inherent design factors to require less power and fuel to sail at a given speed. With a lower fuel consumption baseline, the ship emits less carbon dioxide for the same transport work, resulting in a lower carbon intensity ratio and subsequently obtaining better AER ratings.

### 3.2. Bulk Carriers

In Fig.2, the representation is similar to Fig.1, the only difference is that the graphs are showing Swire Bulk bulk-carriers instead of containerships from Swire Shipping. For a fair comparison against the containerships, the graphs only depict reports which are laden, while all ballast-related reports have been removed for analysis, explaining why there are distinctively less data points in the plots compared to Fig.1.

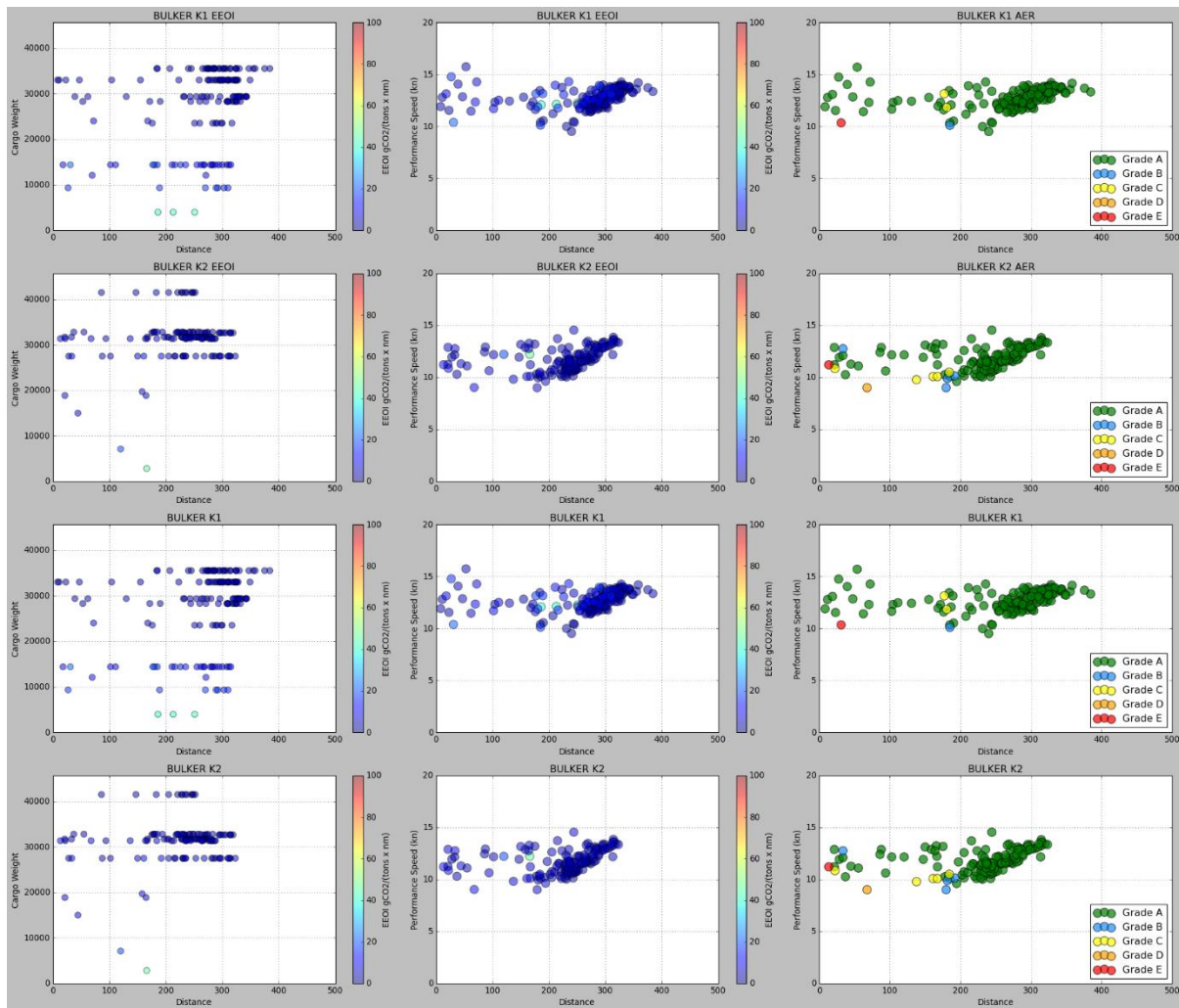


Fig.2: Bulk Carriers EEOI and AER

One observation in the first subplot column is that there are less low-cargo-weight reported in the daily reports, which is attributed to the bulk carrier trade nature to be chartered with more cargo in her voyages.

The first and second subplots columns show that most of the EEOI values are represented in dark blue, which portrays a preferred low value of less than 20 gCO<sub>2</sub>/ (tons x nm). However, it can be noticed that there are several significant points that slightly pales in EEOI in Bulker P2, which are represented in teal blue color. Bulker P2 third subplot further reiterates the poor AER performance of these attained points, which revealed them garnering Grade C or less. An analysis reveals that the poor results of EEOI and AER for Bulker P2 were due to vessel enduring bad weather through the voyage in mid-July off Australia.

Otherwise, the bulkers have attained mostly good results for the EEOI and AER, where bulkers K class are showing more promising results than the bulker P class. From Table 1 EEXI figures, bulkers K class have attained EEXI values approximately 9% lower than the required EEXI target, whereas bulkers P class has attained EEXI values approximately 6% lower than its required benchmark. This imply that the bulkers K class can attain good EEOI and AER results easily, even at high performance speeds, and this is reflected clearly in the second and third subplots columns. Despite bulkers P class having lower attained EEXI values than the required EEXI values, the data reveals a considerable quantity of data points attaining less than desirable targets, especially the vessels having achieved Grade C or less in AER. This has been attributed to mainly bad weather during the voyages, as the bulkers have not fully optimized their planned routes prior to sailing. The contention here is that the bulkers P class are still able to enjoy good EEOI or AER ratings at high sailing speeds, and the number of bad data points can improve considerably if more effort is put into voyage optimization.

#### **4. Relationship between 'Supply' and 'Demand' based CII (AER and EEOI)**

##### **4.1. Containerships**

While the EEOI and AER both measure ship energy efficiency, there will be key differences in their calculation methodology and applicability. This section will analyze the correlations between these two indicators in assessing operational efficiency. Despite their divergent origins, EEOI and AER quantify similar performance dimensions relating to fuel consumption, distance travelled, and the only disparity is the employment of cargo weight carried for EEOI while AER utilizes vessel deadweight throughout.

This analysis will again use monthly data from the vessels in 2022 to explore the theoretical relationship between EEOI and AER scores. It will also outline the relative utility of the two indicators with reference to prominent parameters like distance, speed, cargo weight and port stay percentage. This section aims to link the connections as well as the subtle differences between EEOI and AER, so to provides broader insight into representing and improving ship operational efficiency.

From the graphs in the first subplot column in Fig.3, the monthly results intend to illustrate the relationship between the derived monthly EEOI and AER.

Our hypothesis is that if the EEOI value changes in the subsequent month, there will be an inverse change in the AER value. For example, if EEOI increases from January to February, the AER value would be expected to drop. The reason behind this expectation is that if EEOI increases, the main factor would be a drop in cargo weight given the EEOI calculation. Consequently, less power is required to propel the ship, and this translates into less fuel consumption or less emissions, benefitting the AER.

However, the analysis has shown that there are some deviations from the hypothesis, where AER increases despite increment in EEOI, or vice versa. These are represented by the red markers in the first subplot column. Although the deviations can be possibly explained by differences in parameters such as average speed, amount of port stay, etc., the analysis will also attempt to evaluate the differences from a more theoretical perspective.



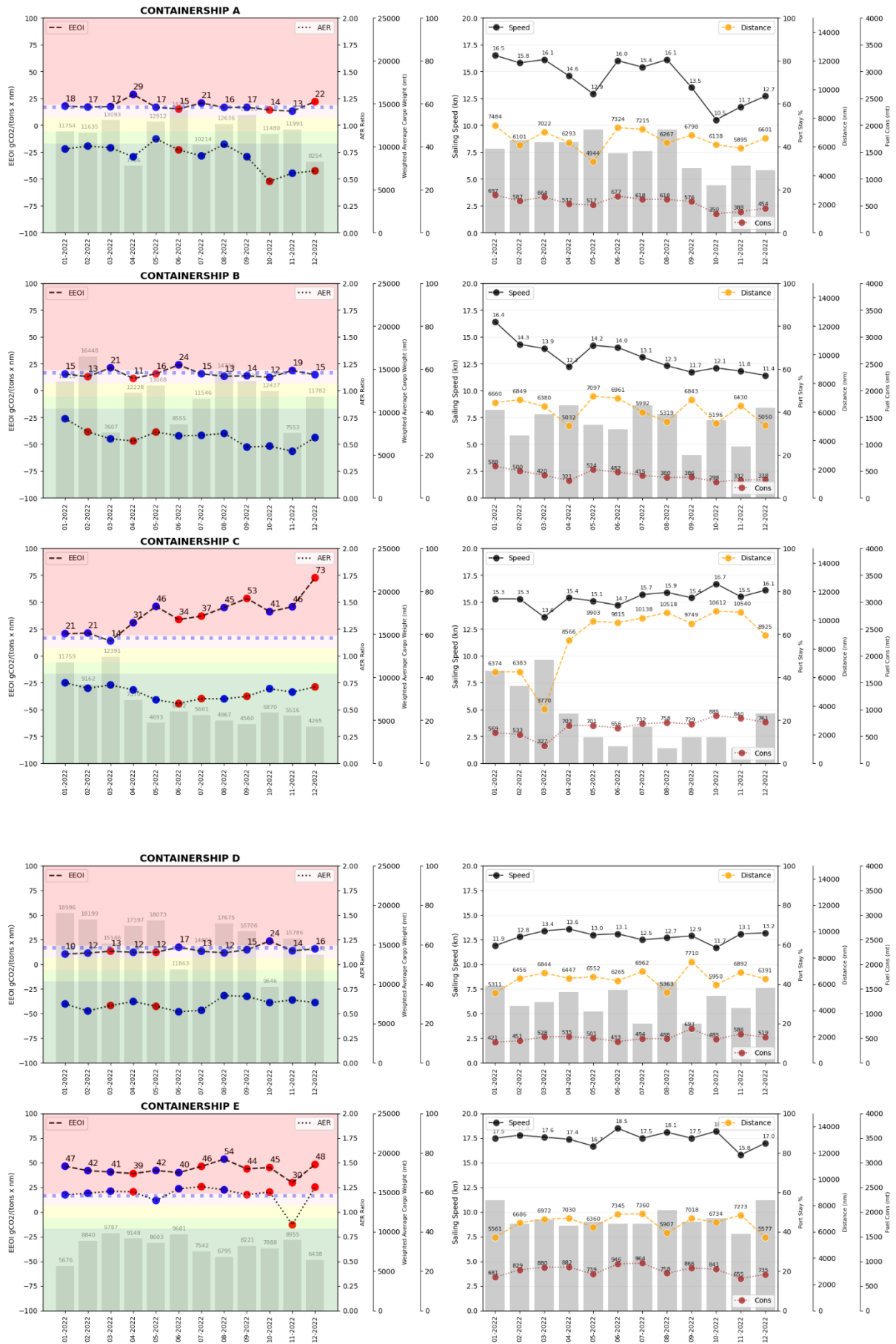


Fig.3: Containerships Relationship between Monthly EEOI and AER

The EEOI calculation is given by Eq. (1):

$$EEOI = \frac{\text{Fuel Consumption} \times \text{Fuel Emission Factors}}{\text{Cargo Weight} \times \text{Distance Travelled}} \quad (1)$$

Alternatively, the equation is similar to (2):

$$EEOI = \frac{1}{\text{Cargo Weight}} \cdot \frac{\text{Fuel Consumption}}{\text{Distance Travelled}} \cdot \text{Fuel Emission Factors} \quad (2)$$

The AER calculation can also be interpreted as follows in (3):

$$AER = \frac{1}{\text{Deadweight}} \cdot \frac{\text{Fuel Consumption}}{\text{Distance Travelled}} \cdot \text{Fuel Emission Factors} \quad (3)$$

From looking at both eq. (2) and eq. (3), the main difference between the two CII indicators is that EEOI considers the actual cargo weight, while AER is only concerned with the deadweight of the vessel, regardless of its ballast or laden condition. Further looking at Eq. (3) outlines that the parameter,  $\frac{1}{\text{Deadweight}}$ , is actually a constant, and  $\frac{\text{Fuel Consumption}}{\text{Distance Travelled}}$  is the only variable in the AER equation. In other words, we can determine the AER performance trend solely by observing the  $\frac{\text{Fuel Consumption}}{\text{Distance Travelled}}$  variable, which foretells the vessel performance. Looking back at Eq. (1), the relationship is easily comprehensible, if  $\frac{\text{Fuel Consumption}}{\text{Distance Travelled}}$  drops, this would mean better vessel performance since less fuel consumed per distance travelled. Instinctively, an increase in  $\frac{1}{\text{Cargo Weight}}$  (less cargo are carried on the vessel) would lead to a drop in  $\frac{\text{Fuel Consumption}}{\text{Distance Travelled}}$  parameter, ceteris paribus.

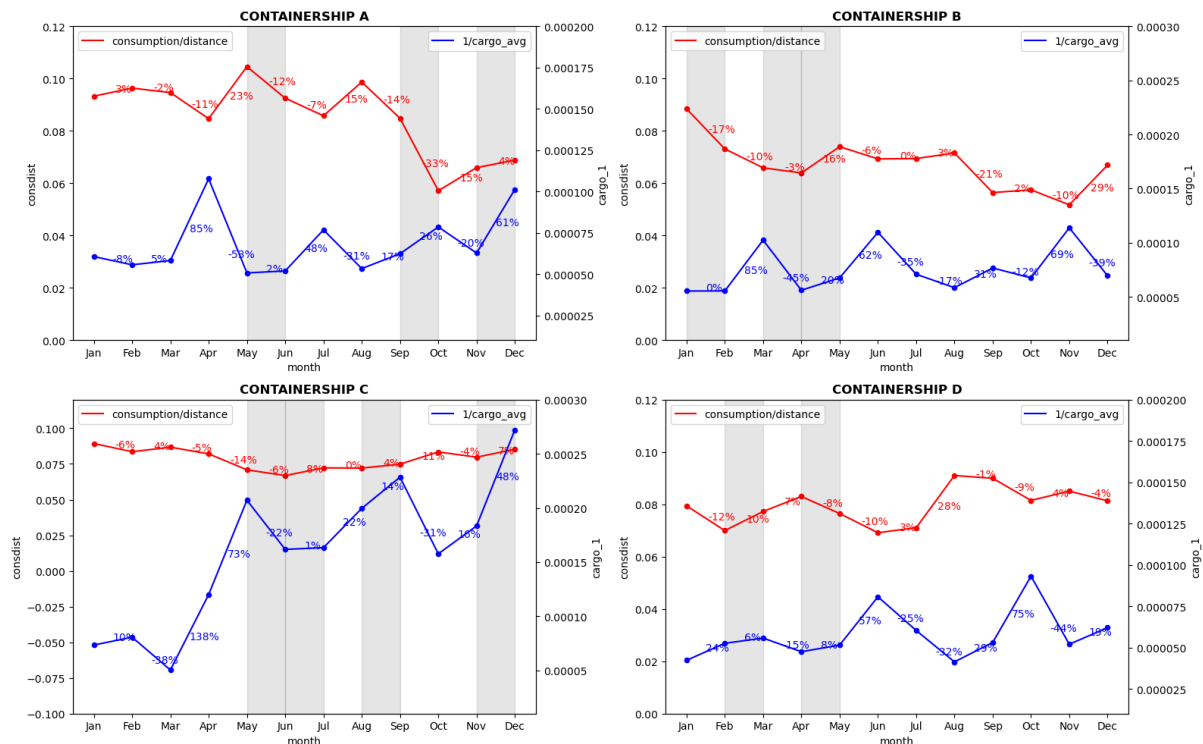


Fig.4: Percentage Change in Monthly EEOI and AER

Hence by only looking at the change in monthly trend from Fig. 3, if  $\frac{\text{Fuel Consumption}}{\text{Distance Travelled}}$  goes down and  $\frac{1}{\text{Cargo Weight}}$  increases, we would expect that AER improves but EEOI deteriorates as there is less cargo

carried. Conversely, if  $\frac{\text{Fuel Consumption}}{\text{Distance Travelled}}$  increases while  $\frac{1}{\text{cargo Weight}}$  decreases (more cargo weight), we will expect that EEOI has improved in the subsequent month while AER has suffered. The percentage changes in the monthly EEOI and AER is then plotted in Fig.4 for better illustration.

To explain the deviations from the hypothesis indicated through the red markers in Fig. 3, the deviated months are being plotted in grey areas in Fig. 4. It can be deduced from the plots that the deviations happen when the absolute of  $\Delta \frac{\text{Fuel Consumption}}{\text{Distance Travelled}}$  in % is more than the absolute of  $\Delta \frac{1}{\text{Cargo Weight}}$  in %. This would indicate that the hypothesized relationship did not materialize as the ship performed worse than expected in terms of performance and was not able to compensate for the change in cargo weight. In Containership A September to October 2022 example, the drop in consumption/distance was more than the drop in cargo weight, resulting in a drop in both the EEOI and AER from Fig. 3. The second subplot in Fig. 3 further substantiate the findings as the average sailing speed has dropped drastically from 13.5 kn to 10.5 kn in Oct 2022.

The other observation made was that the inverse relationship between  $\Delta \frac{\text{Fuel Consumption}}{\text{Distance Travelled}}$  and  $\Delta \frac{1}{\text{Cargo Weight}}$  may be absent, and both  $\Delta$  trends move in the same way, either upwards or downwards. This would infer that the vessel was again not able to compensate the change in performance in terms of consumption/distance to meet the change in cargo. Citing the example of Containership C from Nov to Dec 2022, EEOI was expected to increase due to less cargo in Dec 2022, but AER deteriorated unexpectedly. Both  $\Delta \frac{\text{Fuel Consumption}}{\text{Distance Travelled}}$  and  $\Delta \frac{1}{\text{Cargo Weight}}$  shift upwards, illustrating the vessel was unable to keep performance relative to the drop in cargo weight. This is likely due to a slight increase in average sailing speed in Dec 2022, or the increase in port stay time for the month.

## 4.2. Bulkers

From the diagrams in Fig.5, the bulker results showed less of the relationship between the derived monthly EEOI and AER as hypothesized in 4.1 from the containerships. Fig.5 first subplot column did reveal many more red markers, which indicated that the inverse relationship of both  $\Delta$  trends was not distinguished. Without referring to percentage change plots, we can infer that bulkers are less likely to observe the hypothesized relationship due to the sailing nature, as compared to containerships. Bulkers do not have regulated schedules like the containerships and can spend more than 50% of the time at port. This directly affects the  $\frac{\text{Fuel Consumption}}{\text{Distance Travelled}}$  parameter, or the AER. Because of the unforeseeable trading patterns of bulkers, we are less likely to employ the hypothesis to monitor bulkers EEOI and AER trends.

## 4.3. Conclusion

The hypothesized inverse relationship between the changes in EEOI and AER is evident from the containerships, despite the trend being less significant in the bulkers. While the relationship provides a new and helpful perspective into observing efficiency, Swire also hopes to bring this observation into limelight, so that regulators can regard the complications if EEOI is also considered to be enforced in the future.

Our hypothesis is helpful to monitor if our containerships are unable to comply with the performance expected when there is a change in cargo, especially when the cargo carried is higher than previous month. We would expect that EEOI will drop significantly during such a scenario, but we would also like to ensure that the vessel maintain a healthy sailing profile to keep performance (consumption/distance) within means so that we do not suffer from a drastic increase in AER, especially since AER is regulatory required from 2023.

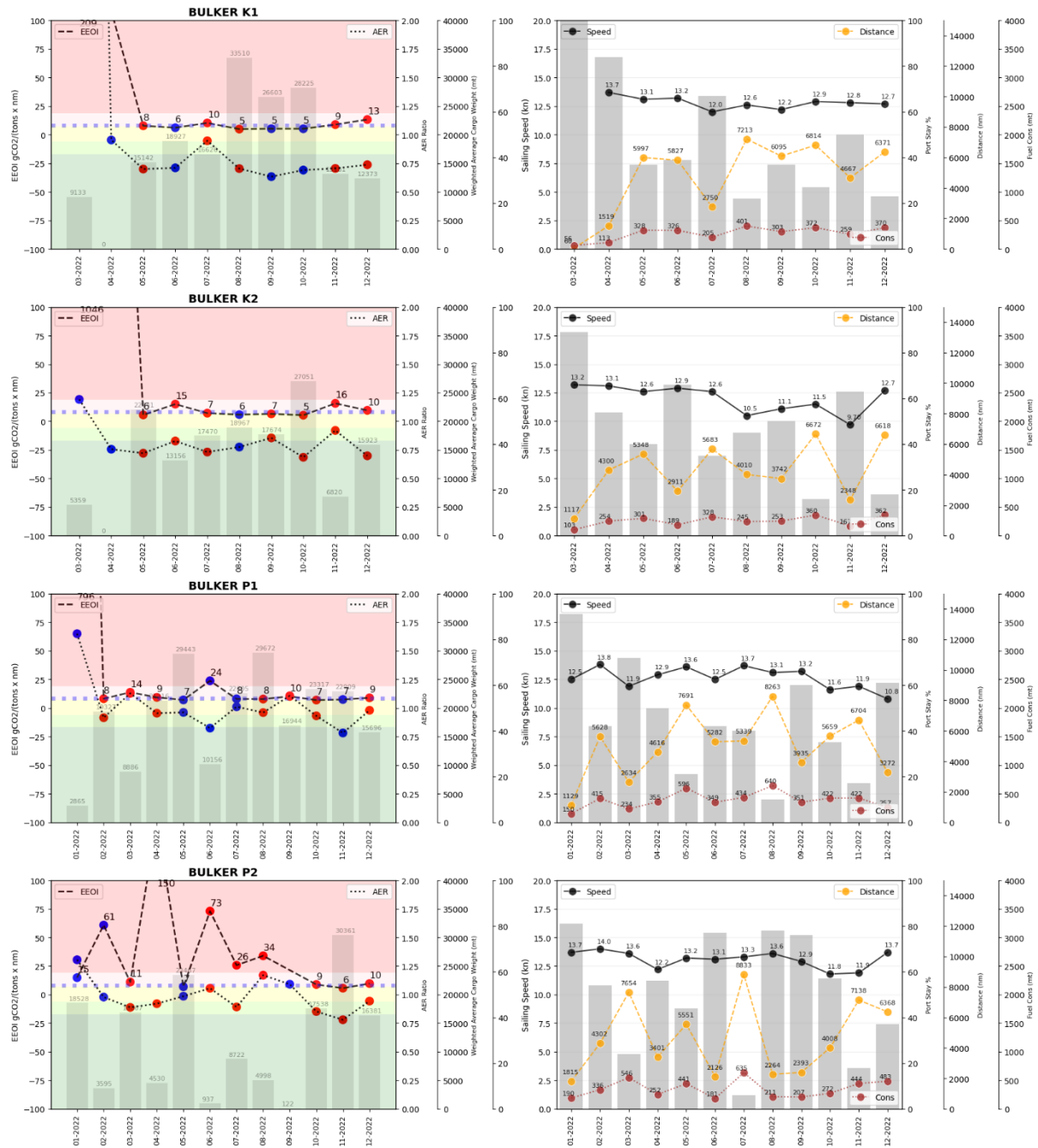


Fig.5: Bulkers Relationship between Monthly EEOI and AER

## 5. Swire Approaches to Address EEXI, EEOI and AER

The AER parameter is mostly related to consumption per distance, and one pragmatic way to improve the AER in the industry is through slow steaming of vessels. *Tezdogan et al. (2016)* assessed the impact of containerhips adopting slow steaming approach and concluded that slow steaming has beneficial effects on reducing ship motions, power requirements, fuel consumption and carbon emissions. Although Swire adopts a similar strategy to achieve further fuel savings whichever is possible, it should be borne in mind that slow steaming can only be considered as a short-term strategy to reduce fuel consumption or carbon emissions. In the long term, prolonged slow steaming may place the vessels engine and propellor outside their efficient ranges and therefore it may counteract the benefits. Besides, if the Swire fleet adopts slow steaming as a policy, this will result in the need to add more tonnage to cope with the actual demand and total emissions of the fleet may increase unexpectedly.

Hence Swire has been explicit on her vessels to meet stringent environmental demands since mid-2010s, that is to invest in new vessels and roll out a fleet renewal programme to enhance the scale and scope of the shipping services. This mainly includes constructing effective newbuilding vessels having modern and fuel-efficient design, which is the most direct and sustainable solution in lieu of other vessel optimization methods. As illustrated in Section 2, the represented vessels, except for Containership E, show an attained EEXI lower than the required EEXI values. In fact, more than 80% of the Swire owned vessels have achieved this feat, and our analysis does compound the fact that the vessels can attain A rating for their AER with ease even at high speeds. In terms of EEOI, Swire is confident that the vessels can achieve good ratings if it is going to be part of the statutory compliance, as supported by the AER good achievements. However, because EEOI is dependent on the amount of cargo carried, this will also be reliant on the trade routes of the vessels and market outlook.

Nevertheless, Swire still employs several ships that have attained EEXI more than the requirements, and one example is Containership E. These vessels are unique in their trade and are still valued to Swire despite their design disadvantages. As the vessels are unlikely to comply with slow steaming due to their trade requirements, Swire has embraced different technologies that will aid her entire fleet in achieving better vessel performance, such as applying silicone paint on the vessels, or carrying out design modifications like rudder bulbs. Although these measures may not be sufficient for the less-efficient vessels to meet the compliance goals, the efforts are essential to cut any possible redundant fuel consumption and emissions. In addition, the Swire fleet efficiency team identifies opportunities to improve the vessels EEOI and AER through various data channels, at the same time develop new energy efficiency solutions and modifications that can be implemented across the Shipping or Bulk fleet. It is important to note that Swire is determined not only to meet regulatory requirements for the AER, but also to reduce carbon emissions as much as possible. Swire Shipping and Swire Bulk also have setup a specialized fund at stimulating adoption of energy efficiency technologies.

As the world moves towards 2040, the centrepiece of Swire multi-faceted approach will be for the fleet to transition to new, low/zero-carbon fuels for the vessels. Swire has been seeking possible alternative fuels like biofuels or other possible alternatives, while the replacement will be catered mainly to the less-efficient vessels, which can pinpoint a much more significant improvement in energy efficiency and carbon footprint. Swire has positioned itself at the forefront in pioneering new fuel pathways and piloting innovative technologies to realize this decarbonization goal. Coupled with the efforts of the other shipping forerunners in the maritime industry, Swire is resolute to help drive the systemic change needed to achieve the decarbonization milestones set by IMO.

## References

TEZDOGAN, T.; INCECIK, A.; TURAN, O.; KELLETT, P. (2016), *Assessing the Impact of a Slow Steaming Approach on Reducing the Fuel Consumption of a Containership Advancing in Head Seas*, Transportation Research Procedia 14, pp.1659–1668



# Reliable Hull Performance Analysis using Vessel Technical Index

Prateek Gupta, NTNU, Trondheim/Norway, [prateek.gupta@ntnu.no](mailto:prateek.gupta@ntnu.no)

Sverre Steen, NTNU, Trondheim/Norway

Bingjie Guo, DNV, Høvik/Norway, [bingjie.guo@dnv.com](mailto:bingjie.guo@dnv.com)

Hans Anton Tvette, DNV, Høvik/Norway

## Abstract

*Vessel Technical Index (VTI), originally proposed by DNV, presents a robust and reliable methodology to analyze the hull performance. VTI is calculated based on measured operational data and the hydrodynamic model of a ship. The uncertainty in VTI is not negligible even after adopting several constructive measures, such as using measurement data from advanced sensors, steady-state and extreme weather filtering, etc. Therefore, the current paper analyzes the uncertainty in VTI using Principal Component Analysis (PCA). The prominent factors contributing to the uncertainty in VTI are identified, and solutions are further presented to reduce it for a reliable hull performance analysis.*

## 1. Introduction

The risk associated with decision-making depends on the accuracy of the decision support system, based on which the consequence or feasibility of the decision is evaluated. To mitigate this risk, it is imperative to meticulously manage and enhance the support system's accuracy. In essence, diminishing the uncertainty within the decision support system is paramount, as it enables the formulation of more assured decisions. By analogy, the same applies to the ship performance monitoring methods. Such that low-risk and confident decisions can be made regarding the maintenance schedule of ships, the reliability of ship performance monitoring systems must be improved. Moreover, in the case of ships, this would not only benefit the individual stakeholders like ship owners, operators, etc. but would also be beneficial for the environment by way of a reduction in fuel consumption and greenhouse gas (GHG) emissions.

Ship performance monitoring has been a popular field of research, and it started booming even more in the last decade partly due to the possibility of obtaining propulsion-related data from ships. This advancement led to the development of numerous ship performance monitoring methods. For instance, *Foteinos et al. (2017)* presented a simple method to monitor the performance of a ship by isolating the fouling resistance based on the noon report data. *Carchen et al. (2019)* presented a much more advanced ship performance monitoring system based on a similar approach but using high-frequency in-service data recorded onboard a ship. *Aldous et al. (2015)* argued, based on a statistical analysis, that using high-frequency in-service data helps reduce the uncertainty in ship performance monitoring. However, the noise in high-frequency in-service data still results in a substantial amount of uncertainty in the final results.

In order to limit the influence of noise from in-service data, the ship performance monitoring systems are equipped with data filtering and processing techniques. *ISO 19030 (2016)* proposes to filter the data according to Chauvenet's criterion and a threshold limit applied to a set of variables before carrying out ship performance analysis. *Liu et al. (2020)* presented the ship performance analysis results based on the data filtered according to the acceleration/deceleration of the ship, rate of course change, and primary seaway direction, as well as the difference between speed-through-water and speed-over-ground, and weather conditions. *Guo et al. (2023)* designed an extensive data filtering and processing scheme including a quasi-steady-state filter, a standard deviation-based filter, and a threshold limit applied to a set of variables to reduce the uncertainty from ship performance analysis. However, in all the cases, the final results are still presented with substantial uncertainty. The current work analyzes the results presented by *Guo et al. (2023)* in order to determine the source of this remaining uncertainty and develop solutions to reduce it further.

The Vessel Technical Index (VTI), proposed by DNV (Guo *et al.*, 2021; Tvette *et al.*, 2022; Guo *et al.*, 2023), represents the technical performance of a ship, which is expected to be independent of the environmental and operational conditions. Due to phenomena like marine fouling, the VTI for an individual ship changes over time. The change or variation in VTI over time can, therefore, be used to quantify the change in performance of the ship's hull and propeller. In order to increase the confidence of users on VTI, the uncertainty associated with it must be analyzed and measures must be taken to effectively reduce it to an even lower level. As aforementioned, the current work is based on the results presented by Guo *et al.*, (2023), and the aim here is to analyze the uncertainty in VTI estimates (calculated using the physics-based approach by Guo *et al.*, 2023) using Principal Component Analysis (PCA) and implement some solutions to reduce it. The dataset used here is same as the one presented by Guo *et al.*, (2023), recorded onboard a sea-going ship equipped with advanced sensors for speed-through-water and wave condition measurement.

## 2. Vessel Technical Index (VTI)

By accounting and adjusting for the relevant operational factors and weather effects, VTI isolates the technical condition of a ship, and therefore, it can be used to monitor a ship's technical performance over its lifetime. It can help optimize ship maintenance schedules, properly evaluate the greenhouse gas (GHG) abatement measures, and remove the barriers that are hindering the application of abatement measures. VTI is defined as:

$$VTI = \frac{P_{D-s} - P_{env}}{P_0(V_W, \Delta)} \quad (1)$$

Where  $P_{D-s}$  is the measured ship in-service delivered power, which should be measured at high frequency and averaged to 1 minute to remove the effect of first-order wave force.  $P_{env}$  is the power consumption due to weather, which includes added power due to waves ( $P_{wave}$ ), added power due to wind ( $P_{wind}$ ), and added power due to water temperature ( $P_{temp}$ ). They are, generally, calculated based on the measured weather, by using physics-based methods. However, a data-driven approach for applying the weather load correction is also demonstrated by Guo *et al.* (2023).  $P_0$  is the reference delivered power at the corresponding ship speed-through-water ( $V_W$ ) and displacement ( $\Delta$ ), which is calculated based on the sea trial or model test data. In addition to the weather correction,

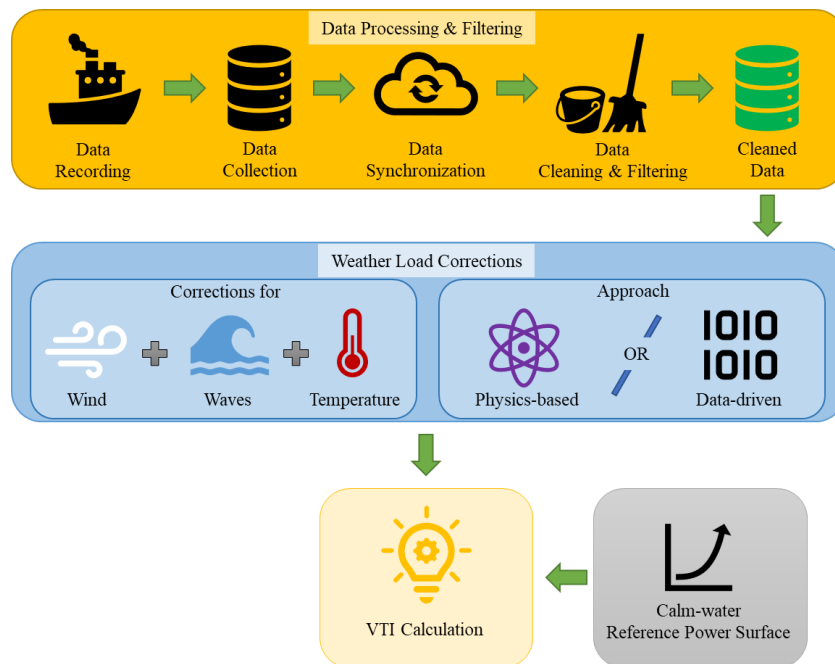


Fig.1: VTI calculation framework, Guo *et al.* (2023)

VTI calculation framework, shown in Fig.1 (originally presented by *Guo et al. (2023)*), also incorporates an extensive data processing and filtering scheme further discussed in Section 4.1.

The procedure for calculating  $P_{wave}$ ,  $P_{wind}$ , and  $P_{temp}$ , using the physics-based approach, is described below.

## 2.1. Added Power due to Waves:

The added power due to waves ( $P_{wave}$ ) can be calculated according to the following equation:

$$P_{wave} = \frac{\bar{R}_{awireg} V_W}{\eta_t} \quad (2)$$

$\bar{R}_{awireg}$  is added resistance in irregular waves,  $V_W$  is ship's speed-through-water, and  $\eta_t$  is the total propulsive efficiency, which is obtained from the self-propulsion model test report. The total propulsive efficiency ( $\eta_t$ ) at different time steps can be obtained by B-spline interpolation on the displacement ( $\Delta$ ) and speed through water  $V_W$ . Since the total propulsive efficiency is obtained for calm water condition, it would not be applicable for the samples with heavy weather conditions, and therefore, they should be dropped in the analysis (as discussed further in Section 4.1). The added resistance due to waves in the irregular sea ( $\bar{R}_{awireg}$ ) is calculated as:

$$\bar{R}_{awireg} = 2 \int_0^{2\pi} \int_0^\infty S(\omega) \frac{R_{AW}(\omega, \theta, V_W)}{\zeta_a^2} D(\theta) d\omega d\theta \quad (3)$$

$S(\omega)$  is ship encounter wave spectrum, and  $D(\theta)$  is wave directional spreading function, and  $\frac{R_{AW}(\omega, \theta, V_W)}{\zeta_a^2}$  is the added wave resistance transfer function, which is calculated here according to the semi-empirical formula derived by *Liu and Papanikolaou (2020)*. This semi-empirical formula has recently been developed based on physical understanding and experimental (model test) data from numerous ships of different sizes and types. It has also been validated extensively in a separate study by *Wang et al. (2021)*.

If the wave spectrum is not directly measured, some standard wave spectrum, with combined or separate wind waves and swell, can be used here. According to *Taskar and Andersen (2021)*, changing the peak enhancement factor in JONSWAP spectrum did not show much influence on the added resistance. Therefore, it is sufficient to use a single wave spectrum for the combination of wind waves and swell for the computation of added resistance in waves. Hence, the Pierson-Moskowitz spectrum (with combined wind waves and swell) is used here. The Pierson-Moskowitz (PM) spectrum can be written as:

$$S_{PM}(\omega) = \frac{5}{16} \cdot H_S^2 \omega_p^4 \cdot \omega^{-5} \exp\left(-\frac{5}{4} \left(\frac{\omega}{\omega_p}\right)^{-4}\right) \quad (4)$$

Where  $\omega_p = 2\pi/T_p$ ,  $T_p$  is peak wave period.  $H_S$  is significant wave height.  $\omega$  is wave frequency.  $D(\theta)$  is the wave directional spreading function which is expressed as, *DNV (2021)*:

$$D(\theta) = \begin{cases} \frac{\Gamma\left(1 + \frac{n}{2}\right)}{\sqrt{\pi}\Gamma\left(\frac{1}{2} + \frac{n}{2}\right)} \cos^n(\theta - \theta_p) & |\theta - \theta_p| \leq \frac{\pi}{2} \\ 0 & \text{otherwise} \end{cases} \quad (5)$$

where  $n$  is the spreading parameter, which is set to be 2.  $\theta_p$  is the primary wave direction.  $\Gamma$  is the Gamma function. More details can be found in DNV's Recommended Practice C205 (DNV, 2021).

## 2.2. Added Power due to Wind

The added power due to wind ( $P_{wind}$ ) can be written as:

$$P_{wind} = \frac{R_{wind} V_W}{\eta_t} \quad (6)$$

Where  $R_{wind}$  is the wind resistance, which can be calculated according to:

$$R_{wind} = \frac{1}{2} C_{DA}(\theta_{rel}) \rho_A V_{wrel}^2 A_{VS} - \frac{1}{2} C_{DA}(0) \rho_A V_G^2 A_{VS} \quad (7)$$

Where  $\rho_A$  is the air density,  $V_{wrel}$  is relative wind speed,  $V_G$  is ship's speed-over-ground,  $A_{VS}$  is the projected transverse area of the ship above the water line,  $C_{DA}(\theta_{rel})$  is the wind resistance coefficient at relative wind direction  $\theta_{rel}$ , and  $C_{DA}(0)$  is the wind resistance coefficient in the head-wind condition. The wind resistance coefficient can be calculated using the regression formula proposed by *Fujiwara et al. (2005)* which is also recommended by *ITTC (2021)*.

## 2.3. Added Power due to Water Temperature:

The estimation of reference power ( $P_0(V_W, \Delta)$ ) is usually based on a temperature of 15°C and water density of 1026 kg/m<sup>3</sup>. To calculate VTI using Eq.(1), the effect of water temperature on the corrected delivered power ( $P_{D-s} - P_{env}$ ) should be corrected according to *ISO 15016 (2015)*. The detailed calculation method can be referred to in *Tvete et al.(2022)*.

## 2.4. Uncertainty in VTI

Both measurement data and empirical models used for correcting environmental loads will bring uncertainty to the final VTI results. Too large uncertainty will have a negative influence on the decisions made by the user. Therefore, minimizing the uncertainty is one of the most critical parts of VTI analysis.

## 3. Principal Component Analysis (PCA)

Principal Component Analysis (PCA), *Jolliffe (2002)*, is an unsupervised machine learning (ML) method used to factorize and reduce the dimensionality of high-dimensional datasets. The dataset or 2-dimensional data matrix ( $X^{m \times n}$ ), with  $m$  rows or samples and  $n$  columns or variables, is factorized into several Principal Components (PCs) as:

$$X^{m \times n} = \sum_{i=1}^A t_i^{m \times 1} \cdot p_i'^{1 \times n} + E_A^{m \times n} = T_A^{m \times A} \cdot P_A'^{A \times n} + E_A^{m \times n} \quad (8)$$

Where  $A$  is the number of PCs extracted from the dataset, also known as model dimensionality;  $t_i$  and  $p_i$  are column vectors representing the scores and loadings, respectively, of the  $i^{th}$  PC;  $T_A$  and  $P_A$  are the score and loading matrices, respectively, comprising  $A$  PCs;  $E_A$  contains the residuals remaining after extracting  $A$  PCs.  $P_A'$  represents the transpose of  $P_A$ . The factorization is generally carried out using one of the two well-known algorithms: Singular Value Decomposition (SVD), *Golub and Reinsch (1970)* and Nonlinear Iterative Partial Least Squares (NIPALS), *Vandeginste et al (1988)*.

The maximum number of PCs that can be obtained from a data matrix is limited by the rank (defined as the maximum number of linearly independent columns or rows) of the matrix itself. However, the number of components (or PCs) to be retained in the model, denoted by the model dimensionality ( $A$ ) in Eq.(8), is determined by the user. The criterion for determining the model dimensionality ( $A$ ) is generally based on the amount of variance carried or explained by the PCs. The PCs are obtained such that the first PC carries the maximum variance from the data matrix, and the succeeding PCs carry as much of the remaining variance as possible, with the amount of carried or explained variance diminishing with the subsequent PCs. Moreover, these PCs are orthogonal to each other. Consequently, in most cases, the last few PCs carry almost negligible variance which is characterized as uncorrelated noise and, therefore, discarded.

### 3.1. Singular Value Decomposition (SVD)

Each PC comprises two elements: its scores and loadings. The scores carry the variance, and the loadings represent the direction of the PC in high-dimensional variable space. The direct (or non-iterative) method to calculate the PCs is Singular Value Decomposition (SVD), *Golub and Reinsch, (1970)*. In SVD, the data matrix is decomposed, using the principles of an eigenvalue problem, as follows:

$$X^{m \times n} = U^{m \times n} \cdot \Sigma^{n \times n} \cdot V'^{n \times n} \quad (9)$$

Where  $U$  contains  $n$  orthonormal eigenvectors of  $X \cdot X'$ . (Orthonormality indicates that  $U \cdot U' = I$ , where  $I$  is the identity matrix.)  $V$  contains  $n$  orthonormal eigenvectors of  $X' \cdot X$ ; and  $\Sigma$  is a diagonal matrix containing the so-called singular values, which are interpreted as the non-negative square roots of the scaled eigenvalues of the covariance matrix of  $X$ . Assuming that  $X$  is mean-centered, the covariance matrix of  $X$  is expressed as  $X' \cdot X / (m - 1)$ . In terms of scores and loadings,  $T_A^{m \times A} = U^{m \times A} \cdot \Sigma^{A \times A}$  and  $P_A^{n \times A} = V^{n \times A}$ .

### 3.2. Correlation Loadings

The correlation loadings, generally represented by  $L$ , are defined as the correlation ( $r$ ) between the standardized (= scaled by its standard deviation.) data variables ( $X$ ) and the standardized PC scores ( $T_{std}$ ). () Assuming that the data matrix ( $X$ ) is already standardized (usual practice before doing PCA), the correlation loadings ( $L$ ) can be expressed as:

$$L = r(X, T_{std}) = \frac{1}{m - 1} X' \cdot U \cdot \Sigma \cdot \sqrt{m - 1} \Sigma^{-1} = \frac{1}{\sqrt{m - 1}} X' \cdot U = \frac{1}{\sqrt{m - 1}} V \cdot \Sigma \quad (10)$$

Thus, the correlation loading vectors are just the loading vectors scaled by the square root of the corresponding eigenvalues.

### 3.3. Explained Variance and Squared Correlation Loadings

The variance extracted or carried by each PC is known as its explained variance, and the cumulative sum of the explained variance for the first  $A$  PCs is the total explained variance of the model. The variance explained by an individual PC can be calculated as the variance in its score vector, which is mathematically equal to the corresponding eigenvalue. The total explained variance ( $\varsigma$ ) is generally presented as a percentage or fraction of the total variance in the original dataset ( $X$ ) as:

$$\varsigma_A = \frac{\sum_{i=1}^A \sigma_i^2}{\sum_{i=1}^n \sigma_i^2} \quad (11)$$

Where  $\sigma_i$  is the  $i^{th}$  element of  $\Sigma$  (diagonal matrix), and  $\sigma_i^2 / (m - 1)$  is the  $i^{th}$  eigenvalue of the covariance matrix of  $X$ . Clearly, if the PCA model is constructed such that it has the maximum



possible number of PCs, i.e.,  $A = n$ , the total explained variance ( $\zeta_A$ ) of the model will become 1. In other words, the PCA model with the maximum possible number of PCs explains the total variance in all the data variables. Considering an individual data variable ( $x_j$ ), the total variance in  $x_j$  will be explained 100% by the set of all possible PCs. Thus, the squared multiple correlation coefficient ( $R^2$ ) or multiple coefficient of determination, *Abdi (2007)*, between the data variable ( $x_j$ ) and the set of all PCs, defined as the fraction of variance in  $x_j$  explained by the set of all PCs, is 1. In the case of orthogonal independent variables (referring to the set of all PCs),  $R^2$  is alternatively defined as the sum of squared correlation coefficients, *Abdi (2007)*, which is same as the sum of squared correlation loadings corresponding to  $x_j$  (by definition in Section 3.2).

$$R_j^2 = 1 \quad \Leftrightarrow \quad \sum_{i=1}^n \{r(x_j, t_{std,i})\}^2 = \sum_{i=1}^n L_{ij}^2 = 1 \quad (11)$$

Where  $t_{std,i}$  represents the standardized scores of  $i^{th}$  PC; and  $L_{ij}$  represents the correlation loading corresponding to  $i^{th}$  PC and  $j^{th}$  data variable ( $x_j$ ). In other words, all the variance in  $x_j$  is unequally distributed over the set of all PCs. Thus, it is more practical to look at the squared correlation loadings instead of just the correlation loadings of PCs to analyze the relationship between different variables, as demonstrated later in Section 5.1.

#### 4. Data Description and Processing

As aforementioned, the current work is an extension of the case study conducted by *Guo et al. (2023)*, and therefore, the same dataset is used here. The data is recorded onboard a sea-going ship with the main parameters presented in Table I. The dataset used here contains 6 moderately long voyages spanning over a duration of about 16 months. The sampling rate of the data is, in general, 1 per minute, however, several individual data samples as well as sections of the time series are missing, more often in the latter part of the time series. Nevertheless, due to the advanced sensors for speed-through-water and wave conditions, the quality of data is believed to be quite good as compared to an ordinary in-service dataset. Out of the 6 recorded voyages, voyages 1, 2, and 5 were carried out in ballast loading conditions, and the rest were carried out in full load conditions.

Table I: Ship main parameters (approximated due to data confidentiality)

Length Between Perpendiculars	225 m
Breadth	32 m
Design Draft	12 m
Design Displacement Volume	76500 m <sup>3</sup>
Ballast Displacement Volume	47000 m <sup>3</sup>
Maximum Continuous Rating (Main Engine)	10 MW @ 89 rpm

Table II presents the list of parameters or variables used for the current analysis. Here, the displacement is manually added as per the reports from the ship's crew, the seawater temperature is obtained from one of the publicly available hindcast or met-ocean data repositories, and everything else is recorded onboard the ship.

Table II: The parameters used for data analysis

	Parameters	Unit
1	Shaft revolutions	rpm
2	Vessel heading	Deg.
3	Wind speed	m/s
4	Wind direction	Deg.
5	Significant wave height	m
6	Primary relative wave direction	Deg.

7	Primary wave period	s
8	Full directional wave spectrum (matrix)	-
9	Speed-over-ground	knot
10	Speed-through-water	knot
11	Shaft power	kW
12	Water depth	m
13	Displacement	m <sup>3</sup>
14	Seawater temperature	°C

#### 4.1. Data Cleaning and Filtering

In addition to typical data cleaning, such as removing out-of-bound or invalid samples, the data is filtered using the following three techniques, to reduce the uncertainty in VTI:

1. Quasi-steady-state (QSS) filter
2. Standard deviation-based filter
3. Physical model-based filter

The first two filters aim to remove noisy, unreliable, and transient samples which may be influenced by the dynamic effects as well as the acceleration, deceleration, or course change maneuvers. Such samples cannot be included in the current analysis as the physics-based model used to calculate VTI does not account for such effects. In other words, the physics-based model used here is only applicable to samples obtained in steady-state, and therefore, the first two filters focus on obtaining only the steady-state samples from the time series. Both these filters use a sliding window which is moved from the start to the end of the time series to identify steady-state samples. The quasi-steady-state filter conducts a Student's *t*-test over the estimated slope of the sliding window, whereas the standard deviation-based filter applies a threshold on the standard deviation of the samples contained in the sliding window. *Guo et al. (2023)* presented a deeper explanation of both these filters. Table III presents the steady-state filtering criteria, comprising these two filters, applied to a set of parameters or variables in order to obtain the samples in steady-state. The size of the sliding window for each variable is defined by the time period given in Table III. Both the quasi-steady-state and standard deviation-based filters are applied to the vessel heading parameter.

Table III: Steady-state filtering criteria for each parameter.

Parameter	Standard Deviation Limit	Time Period [min]
Shaft rpm	Quasi-steady-state (QSS) filter	15
Vessel heading	Quasi-steady-state (QSS) filter	15
	2 deg	30
Water temperature	0.5 °C	60
Relative wind speed	15% mean wind speed (m/s)	30
Relative wind direction	10 deg	60
Significant wave height	0.15 m	30
Primary relative wave direction	10 deg	60
Primary wave period	0.5 s	60
Speed-over-ground	0.1 m/s	30
Speed-through-water	0.1 m/s	30

The third filter, on the other hand, simply applies limits on the weather and operating conditions so that the influence of harsh weather, operating in shallow waters, and variation in the ship's speed is subdued. The physics-based model used to calculate VTI is characterized by wind and wave load corrections, estimated using empirical methods, which are generally known to be inaccurate in harsh weather conditions, more so because of increased ship motions. The shallow water effect, on the other

hand, is unfortunately not accounted for in the VTI calculation framework, due to the unavailability of a reliable methodology. Finally, filtering limits are applied to the speed-through-water and the difference between the speed-through-water and speed-over-ground to subdue the influence of variation in the speed of the ship and the measurement noise in speed-through-water, respectively. Table IV presents the limits applied to various parameters or variables as per the physical model-based filtering scheme.

Table IV: Filtering criteria to remove harsh weather and shallow water effects

Parameter	Limit
Water depth	> 80 m
Speed-through-water	> 11.54 knots & < 15.2 knots
Wind speed	< 7.9 m/s
Relative wind direction (0 & 360 deg. means headwind)	< 70 deg. & (110, 250) deg. & > 290 deg.
Significant wave height	< 3 m
Primary wave direction (0 & 360 deg. means head waves)	< 65 deg. & (115, 245) deg. & > 295 deg.
Difference between speed-through-water and speed-over-ground	< 0.5 knots

## 5. Results

Following the results presented by *Guo et al. (2023)*, the uncertainty in Vessel Technical Index (VTI), estimated for the given dataset, is substantial. In order to obtain reliable results for hull performance analysis using VTI, the obtained uncertainty (or unexplained variance) in VTI is further analyzed in the following sub-section using Principal Component Analysis (PCA). Furthermore, Section 5.2 presents a simple methodology as well as proves its effectiveness in obtaining a better estimate for VTI and reducing its uncertainty. It should be noted that *Guo et al. (2023)* presented two different estimates of the VTI using the physics-based approach, one using the summary wave statistics (i.e., significant wave height, primary wave period, and primary relative wave direction) and Pierson-Moskowitz (PM) spectrum with the standard direction spreading function (further referred as *VTI*), and the other using the measured full directional wave spectrum (further referred as *VTI<sub>Spec</sub>*). The following section presents the results based on both the estimates.

### 5.1. VTI Uncertainty Analysis

The uncertainty in VTI is analyzed here using Principal Component Analysis (PCA). Since PCA is a linear method, some non-linear transformations are introduced based on our domain knowledge to linearize the dataset before calibrating the PCA models, as suggested by *Guo et al. (2023)* for a similar model. Due to the experimentally proven belief that fouling does not grow when the ship is moving, *Malone et al. (1981)*, the VTI is expected to remain constant over a voyage (or a continuous leg during which the ship is moving). The uncertainty in VTI is, therefore, quantified by its variation during a voyage, and in order to analyze it, separate PCA models are created for each voyage. Moreover, since the displacement of the ship roughly remains constant over each voyage for the given dataset, it is not included in the analysis.

As per the results from *Guo et al. (2023)*, the 4<sup>th</sup> voyage presented the highest uncertainty in VTI. Fig.2 shows the squared correlation loadings for the PCA model obtained using the data only from the 4<sup>th</sup> voyage. The x-axis shows the variables used to create the model. As explained in Section 3.3, the squared correlation loadings represent the amount of variance (or uncertainty in the case of *VTI* and *VTI<sub>Spec</sub>*) which is shared (via correlation) between the data variables and Principal Components (PCs). Moreover, the sum of squared correlation loadings for an individual variable over all the PCs is equal to the total variance in that variable, which is 1 if the dataset is standardized as in the current case.

Thus, from Fig.2, it can be concluded that the total variance or uncertainty in  $VTI$  and  $VTI_{Spec}$  is distributed among  $PC-1$ ,  $PC-4$ , and  $PC-2$  in the descending order of shared variance. Out of these,  $PC-1$  shares about 62% and 45% variance with  $VTI$  and  $VTI_{Spec}$ , respectively. The other variables which also share a large amount of variance ( $> 40\%$ ) with  $PC-1$  include significant wave height, primary wave period, and speed-through-water. However, almost negligible shared variance between  $PC-1$  and  $P_{wave}$  indicate unfavourable relative wave direction. Thus, the results indicate that the majority of variance in  $VTI$  and  $VTI_{Spec}$  is correlated or, in this case, caused due to the variation in speed-through-water.

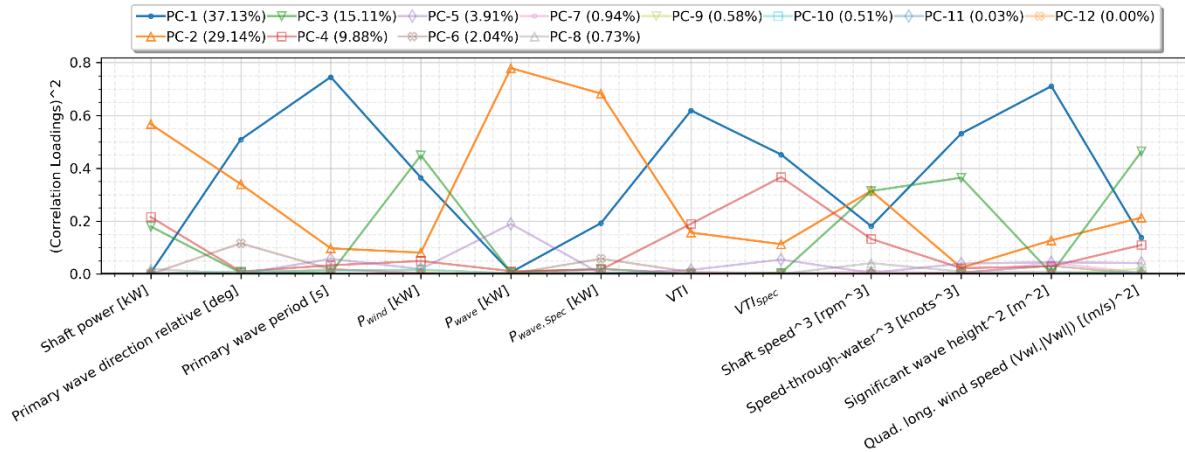


Fig.2: Squared correlation loadings for the 4<sup>th</sup> voyage

Simple cross-plots between the  $VTI$  estimates and speed-through-water, Fig.3, with voyage categories confirm the above results. Fig.3 shows a clear negative correlation between the speed-through-water and  $VTI$  estimates. Since  $VTI$  is simply a ratio of powers corrected to calm water condition (as briefly described in Section 2), both the numerator and denominator are expected to have fundamentally the same or very similar relationship with the speed-through-water. Thus, this correlation between the  $VTI$  and speed-through-water is not really expected. However, there can be several reasons for this correlation ranging from imperfections in the sea trial data to unaccounted weather and dynamic effects.

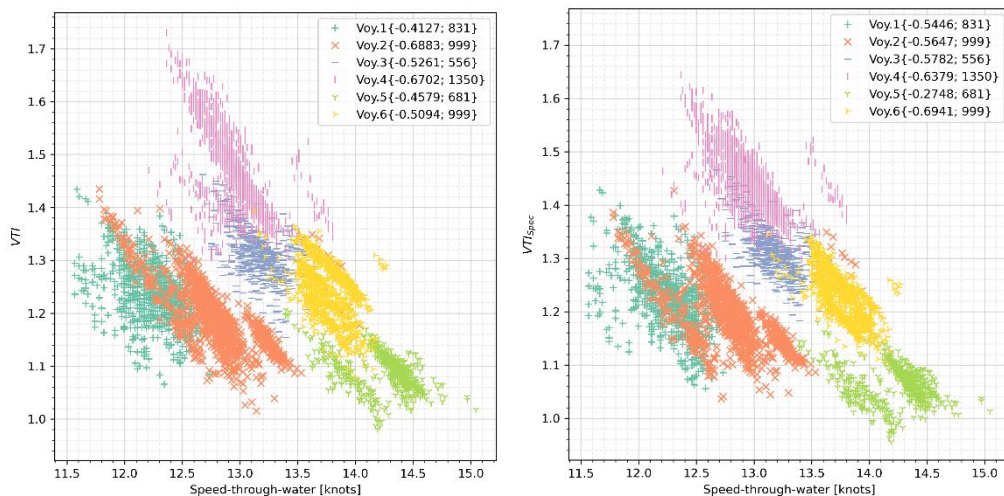


Fig.3: Speed-through-water vs.  $VTI$  estimates with voyage (Voy.) categories. The curly brackets ({} ) in the plot legends show Pearson's correlation coefficient and the number of samples.

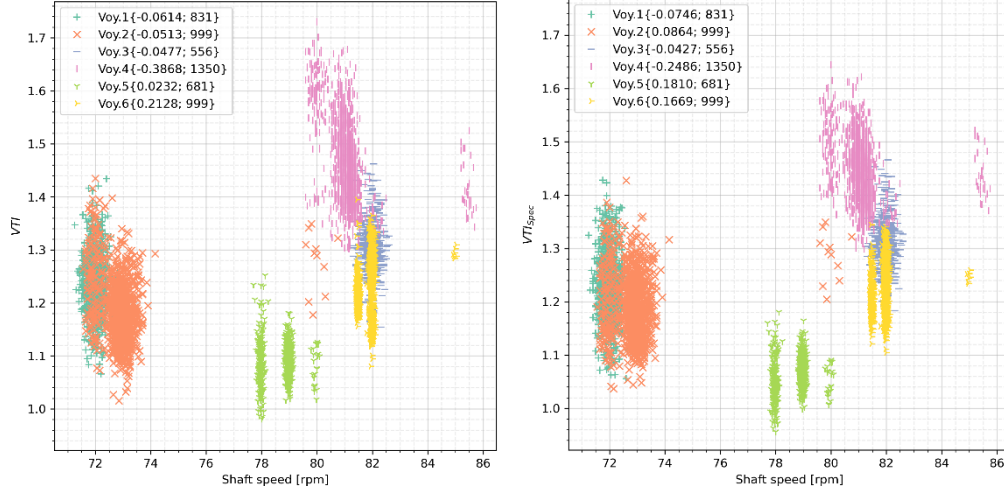


Fig.4: Shaft speed (or rpm) vs. VTI estimates with voyage (*Voy.*) categories. The curly brackets ({} ) in the plot legends show Pearson's correlation coefficient and the number of samples.

The speed-through-water is greatly influenced by the weather and dynamic effects (like instantaneous incident waves, wind gusts, engine dynamics, etc.). So it may be possible that the unexplained correlation, shown in Fig.3, can be attributed to the variations in speed-through-water actually caused due to these effects. Alternatively, it can be said that the environmental or weather load correction ( $P_{env}$ ) may not be sufficient for correcting the measured shaft power to exact calm water condition. Consequently, the effect of unaccounted weather and dynamic effects introduces some noise or uncertainty in VTI which also has some correlation with the speed-through-water, resulting in the correlation shown in Fig.3. Fortunately, it is quite simple to confirm this assertion. Since the only other reason for variation in the speed-through-water is a change in propeller shaft speed (or rpm) for a ship with a single fixed pitch propeller, the absence of such correlation between the shaft speed and VTI would act as definitive proof, as shown in Fig.4.

Fig.4 clearly shows that there is a negligible correlation between the shaft speed and VTI estimates. Moreover, Fig.4 also shows that the formation of separated clusters or clouds for several voyages in Fig.3 is actually due to the change in propeller shaft speed, where each individual cluster belongs to an almost constant shaft speed. Comparing Fig.4 and Fig.3, it is observed that the vertical spread in VTI for a given shaft speed becomes inclined when plotted against the speed-through-water. This is due to the fact that the speed-through-water of the ship reduces if the shaft speed (or rpm) is kept constant and the torque or propeller load is increased gradually due to the effect of weather and system dynamics. Furthermore, a similar but opposite effect should be visible if the VTI is plotted against the shaft power, also shown in Fig.5. The shaft power starts to increase if the rpm is kept constant and the torque is increased gradually. However, the correlation here is not as strong as in the case of speed-through-water due to the fact that the shaft power is less sensitive to the above-mentioned effects.

The VTI calculation framework, Fig.1, which mainly includes correcting the shaft power for environmental load ( $P_{env}$ ) and an elaborate data filtering scheme, intends to estimate VTI such that it is independent of external influences, and ideally, the VTI estimates should lie on a flat horizontal line when plotted against the speed-through-water or shaft power. However, due to a number of reasons, including but not limited to the uncertainty in in-service data, inaccuracies in the environmental load estimation, and inability to correct for dynamic effects (like instantaneous incident waves, wind gusts, engine dynamics, etc.), results in the failure to do so with complete success. Nevertheless, the adopted methodology is still quite effective as per the results presented by *Guo et al. (2023)*. Moreover, since the current work only focuses on a short time series from an individual ship, it cannot be presumed that this trend or correlation, resulting in uncertainty in VTI, would exist in the case of other datasets.



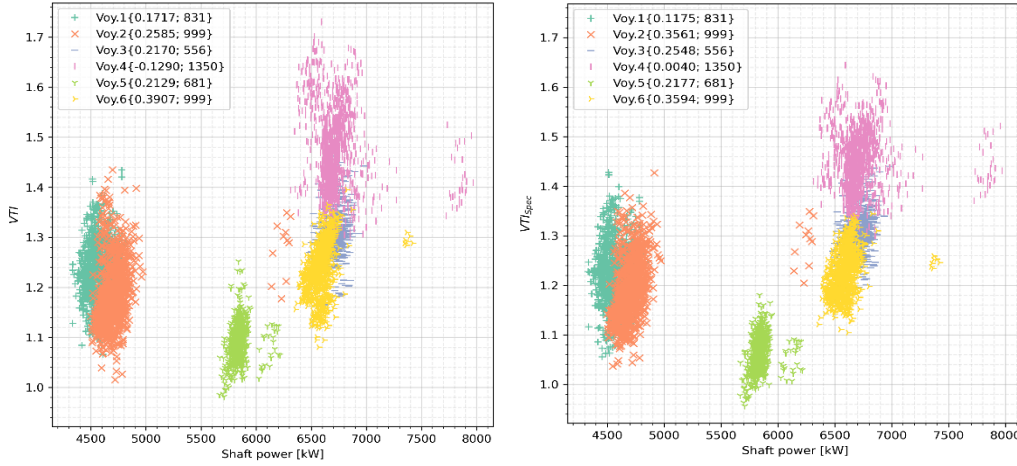


Fig.5: Shaft power vs. VTI estimates with voyage (Voy.) categories. The curly brackets ({} ) in the plot legends show Pearson's correlation coefficient and the number of samples.

## 5.2. VTI Uncertainty Reduction

As per the above discussion, one of the simplest ways to reduce the uncertainty in VTI for the current case is by identifying the most accurate methods for environmental load correction. Possibly the methods suggested by *Guo et al. (2023)* for estimating wind and wave loads as well as the correction for changes in seawater temperature may not be the most accurate, especially when used together. Therefore, further analysis is necessary to identify the most accurate set of methods which can be used to obtain the environmental load correction ( $P_{env}$ ). However, in order to do that a varied group of datasets from several different ships is required so that the effectiveness of such methods can be validated. So it is not feasible to carry out this task in the current work, and therefore, it would be covered in one of the future works. However, it should be kept in mind that, even with the best estimate of  $P_{env}$ , it would not be possible to obtain a single point value for VTI or any other ship performance indicator due to the inherent noise as well as unaccountable dynamic effects (like instantaneous incident waves, wind gusts, engine dynamics, etc.).

Focusing on the current dataset presented in Fig.4, we see that all the vertical clusters corresponding to an individual voyage (having different shaft speeds) do not present much variation with respect to the shaft speed, particularly in the sense that their vertical mean centers would not lie very far away from each other. Thus, it may be appropriate to just pick the most favorable cluster and obtain a better estimate for VTI. The most favorable cluster is the one which has the mildest weather conditions as well as a good enough number of data samples. The measure for mildest weather can be defined based on the ratio of  $P_{env}/P_0$ . The cluster with the lowest mean  $P_{env}/P_0$  would, therefore, be most appropriate to pick. However, the samples with negative  $P_{env}$  must be removed before selecting the most favorable cluster, as these samples may fall below the targeted calm water value (due to insufficient environmental load correction).

Fig.6 shows the best or most favorable clusters for each voyage. Here, the clusters are created simply by dividing the data into discrete bins of shaft speed (rpm), and the clusters with less than 200 samples are not considered. Alternatively, it may be possible to use an advanced clustering method like DBSCAN, *Ester et al. (1996)*, to divide the data into clusters. The mean  $P_{env}/P_0$  for each selected cluster is also reported in the legend of Fig.6. Further, based on the assumption that the samples within each shaft speed cluster reaching the highest speed-through-water would be least affected by the weather and dynamic effects (after having removed the samples with negative  $P_{env}$ ), it would be appropriate to rank or sort the samples in each of these clusters according to descending speed-through-water and only retain a subset of samples with the highest speed-through-water. For selecting the subset of samples, although it would be better to assume a known distribution and use a fixed statistical limit, it is decided to just pick the top 10% samples here for the sake of simplicity (which is actually equivalent to using an empirical distribution).

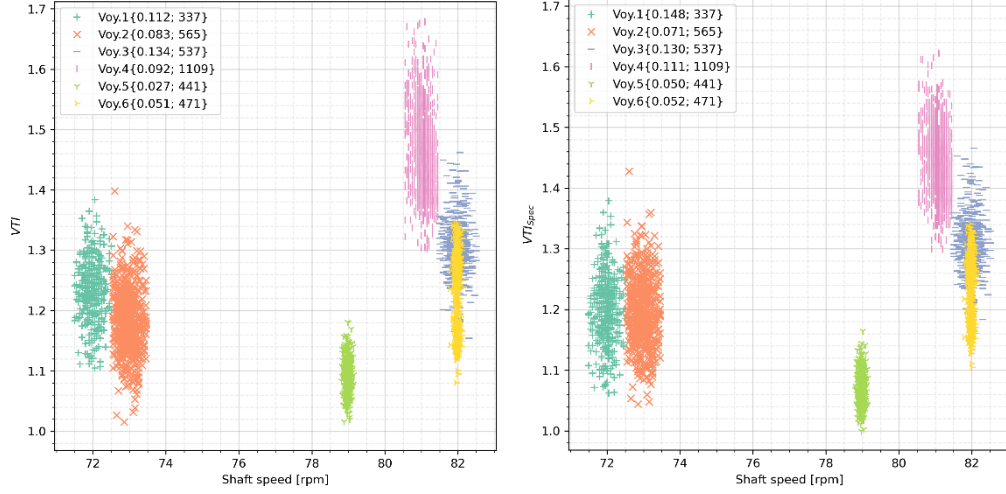


Fig.6: Best clusters for each voyage (Voy.). The curly brackets ({} ) in the plot legends show mean  $P_{env}/P_0$  and the number of samples.

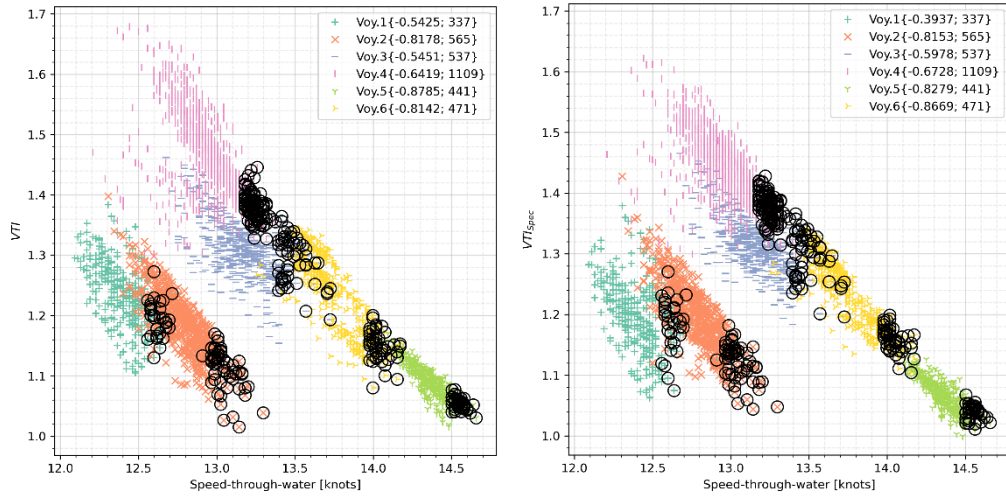


Fig.7: Best clusters for each voyage (Voy.) marked with the top 10% samples having the highest speed-through-water. The marked samples (black circles) are used to calculate a better estimate for VTI. The curly brackets ({} ) in the plot legends show Pearson's correlation coefficient and the number of samples.

Table V: Mean and standard deviation of VTI estimates from *Guo et al. (2023)* and the current work

Voyage	<i>Guo et al. (2023)</i>				<i>Current Work</i>			
	VTI		VTI <sub>Spec</sub>		VTI		VTI <sub>Spec</sub>	
	Mean	Standard Deviation	Mean	Standard Deviation	Mean	Standard Deviation	Mean	Standard Deviation
1	1.24	0.056	1.23	0.061	1.19	0.031	1.18	0.044
2	1.19	0.064	1.19	0.060	1.11	0.034	1.12	0.031
3	1.31	0.045	1.31	0.043	1.29	0.038	1.29	0.040
4	1.47	0.080	1.45	0.056	1.38	0.024	1.38	0.024
5	1.09	0.036	1.06	0.033	1.05	0.010	1.04	0.011
6	1.24	0.052	1.23	0.045	1.15	0.025	1.16	0.020

Fig.7 shows the best clusters marked with the top 10% samples having the highest speed-through-water. The top 10% samples from some of the voyages seem to have a higher level of noise, again,

probably due to the weather and dynamic effects as well as inherent data noise. However, the noisy samples are still within a reasonable range and can be used to quantify VTI further. Figs.8 and 9 show the VTI trends over time calculated using only the top 10% samples.

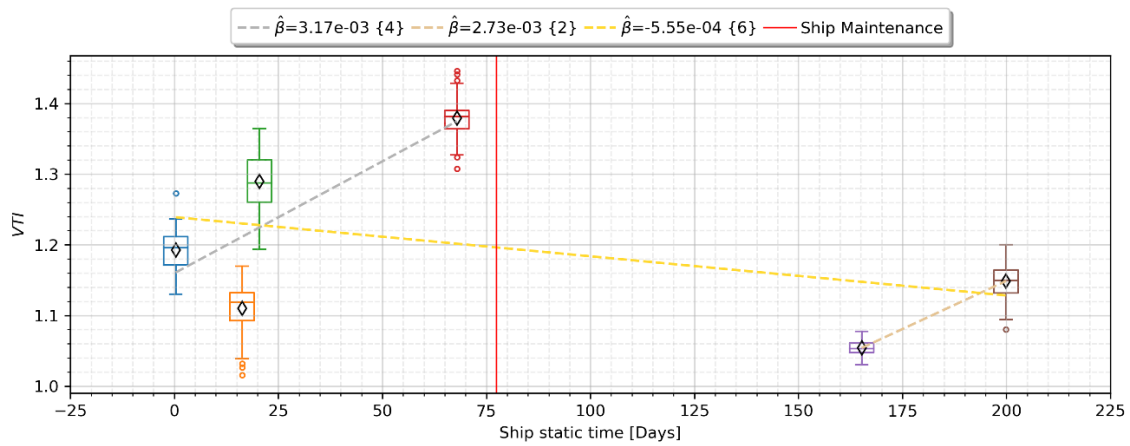


Fig.8: Mean VTI trends over time representing the change in performance of the ship obtained using the top 10% samples from the best clusters. The numbers in curly brackets ({} ) in the plot legend show the number of VTI means used to fit the trend line. The mean of each box plot is marked by a diamond, and the trend lines are fitted on the mean values only.

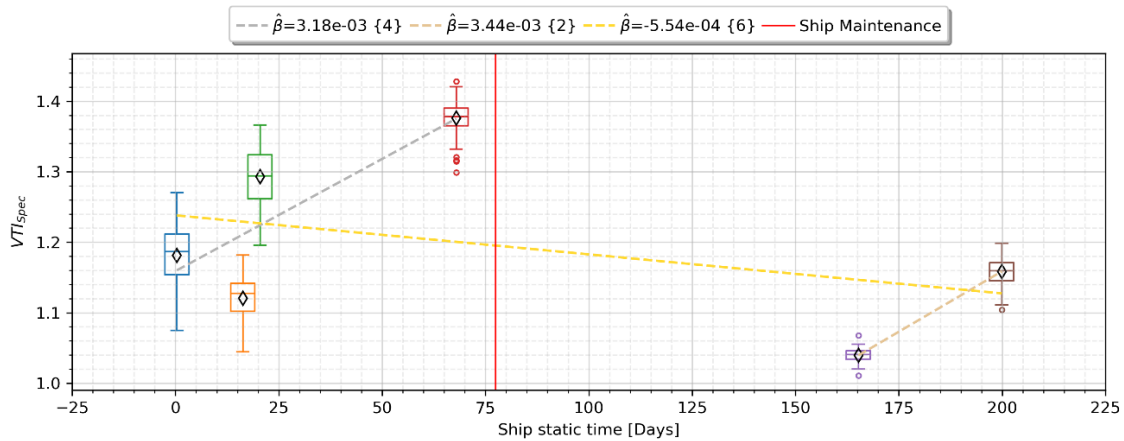


Fig.9: Mean VTI (based on full directional wave spectrum) trends over time representing the change in performance of the ship obtained using the top 10% samples from the best clusters. The numbers in curly brackets ({} ) in the plot legend show the number of VTI means used to fit the trend line. The mean of each box plot is marked by a diamond, and the trend lines are fitted on the mean values only.

Compared to the results presented by *Guo et al. (2023)* also shown in Table V, the mean VTI corresponding to each voyage has reduced due to the use of only a subset of samples with the highest speed-through-water. Additionally, the uncertainty in VTI has reduced substantially proving the effectiveness of the applied methodology. Here, the first voyage, represented by 2 box plots in *Guo et al. (2023)*, is simply reduced to one by removing the samples corresponding to the first box plot. The removal of these samples would not affect the results as the two box plots as well as their means were quite close to each other.

## 6. Conclusion

The analysis presented in the current work shows that the uncertainty in VTI shows a strong correlation with the speed-through-water, but the actual reason for this uncertainty is somewhat surprising. The Vessel Technical Index (VTI) is a simple and intuitive measure of a ship's technical

performance, which is designed to be independent of the environmental and operational conditions. However, even after adopting several constructive measures, such as using measurement data from advanced sensors, steady-state and extreme weather filtering, the uncertainty in VTI remains substantial. The results from the current work indicate that due to inherent noise in in-service data, inaccurate weather corrections, and unaccountable dynamic effects, the VTI varies during a continuous voyage when it is expected to remain constant, resulting in uncertainty. Moreover, the correlation between the speed-through-water and the weather and dynamic effects creates an illusion which would make one believe that the uncertainty in VTI is mainly caused by the variation in speed-through-water.

The current work further presents a simple solution to obtain a better estimate of VTI by isolating a subset of samples independent of the above-mentioned effects. The prescribed strategy substantially reduces the uncertainty in VTI estimates. However, this method could introduce some bias due to limiting the number of samples (10%). More research will be performed to optimize the filtering criteria for steady-state data selection and empirical models for correcting environmental loads in the future to reduce uncertainty.

### Acknowledgments and Funding

This study is partly funded by the research project SFI Smart Maritime - Norwegian Centre for Improved Energy-Efficiency and Reduced Emissions from the Maritime Sector (RCN project number 237917).

### References

- ABDI, H. (2007), *Multiple correlation coefficient*, Encyclopedia of measurement and statistics, pp.648-651
- ALDOUS, L.; SMITH, T.; BUCKNALL, R.; THOMPSON, P. (2015), *Uncertainty analysis in ship performance monitoring*, Ocean Engineering 110, pp.29-38
- CARCHEN, A.; ATLAR, M.; TURKMEN, S.; PAZOUKI, K.; MURPHY, A.J. (2019), *Ship performance monitoring dedicated to biofouling analysis: Development on a small size research catamaran*, Applied Ocean Research 89, pp.224-236
- DNV (2021), *Environmental Conditions and Environmental Loads*, DNV-RP-C205
- ESTER, M.; KRIEGEL, H.-P.; SANDER, J.; XU, X. (1996), *A density-based algorithm for discovering clusters in large spatial databases with noise*, 2<sup>nd</sup> Int. Conf. on Knowledge Discovery and Data Mining, pp.226-231
- FONTEINOS, M.I.; TZANOS, E.I.; KYRTATOS, N.P. (2017), *Ship hull fouling estimation using shipboard measurements, models for resistance components, and shaft torque calculation using engine model*, J. Ship Research 61(02), pp.64-74
- FUJIWARA, T.; UENO, M.; IKEDA, Y. (2005), *A new estimation method of wind forces and moments acting on ships on the basis of physical component models*, J. Jpn. Soc. Nav. Archit. Ocean Eng. 2, pp.243-255
- GOLUB, G.; REINSCH, C. (1970), *Singular value decomposition and least squares solutions*, Numerische Mathematik 14(5), pp.403-420
- GUO, B.; ROGNEBAKKE, O.; TVETE, H.A.; ADAL, C.; STORHAUG, G.; SCHMIDT, M.; BRUSET, T.; PRYTZ, G. (2021), *Setting the Standard for Evaluation of In-Service Technical Ship Performance*, 6<sup>th</sup> HullPIC Conf., Pontignano, [http://data.hullpic.info/HullPIC2021\\_Pontignano.pdf](http://data.hullpic.info/HullPIC2021_Pontignano.pdf)

GUO, B.; GUPTA, P.; STEEN, S.; TVETE, H.A. (2023), *Evaluating vessel technical performance index using physics-based and data-driven approach*, Ocean Eng. 286, 115402

ISO 15016 (2015), *ISO 15016: Ships and Marine Technology — Guidelines for the Assessment of Speed and Power Performance by Analysis of Speed Trial Data*, Int. Standard Org., Geneva

ISO 19030 (2016), *ISO 19030: Ships and marine technology — Measurement of changes in hull and propeller performance*, Int. Standard Org., Geneva

ITTC (2021), *Procedures and guidelines. Preparation, Conduct and Analysis of Speed/Power Trials*. 7.5-04-01-01.1., Revision 06, International Towing Tank Conference

JOLLIFFE, I. (2002), *Principal Component Analysis*, Springer Series in Statistics, Springer

LIU, S.; LOH, M.; LEOW, W.; CHEN, H.; SHANG, B.; PAPANIKOLAOU, A. (2020), *Rational processing of monitored ship voyage data for improved operation*, Applied Ocean Research 104, 102363

LIU, S.; PAPANIKOLAOU, A. (2020), *Regression analysis of experimental data for added resistance in waves of arbitrary heading and development of a semi-empirical formula*, Ocean Eng. 206, 107357

MALONE, J.A.; LITTLE, D.E.; ALLMAN, M. (1981), *Effects of hull foulants and cleaning/coating practices on ship performances and economics*, Trans. Soc. Nav. Archit. Mar. Eng. 88, pp.75-101

TASKAR, B.; ANDERSEN, P. (2021), *Comparison of added resistance methods using digital twin and full-scale data*, Ocean Eng. 229, 108710

TVETE, H.A.; GUO, B.; AGRELL, C.; FERREIRA, C.; ELDEVİK, S.; SCHMIDT, M.; STORHAUG, G. (2022), *Uncertainty Analysis on Vessel Technical Index for Technical Ship Performance*, 15<sup>th</sup> PRADS Symp.

VANDEGINSTE, B.; SIELHORST, C.; GERRITSEN, M. (1988), *NIPALS algorithm for the calculation of the Principal Components of a matrix*, TrAC - Trends in Analytical Chemistry 7(8), pp.286-287

WANG, J.; BIELICKI, S.; KLUWE, F.; ORIHARA, H.; XIN, G.; KUME, K.; et al. (2021), *Validation study on a new semi-empirical method for the prediction of added resistance in waves of arbitrary heading in analyzing ship speed trial results*, Ocean Engineering 240, 109959



# Reduced-Order Modelling for the Preliminary Design of Propellers

Simon Hauschulz, FRIENDSHIP SYSTEMS AG, Potsdam/Germany,

[hauschulz@friendship-systems.com](mailto:hauschulz@friendship-systems.com)

Stefan Harries, FRIENDSHIP SYSTEMS AG, Potsdam/Germany, [harries@friendship-systems.com](mailto:harries@friendship-systems.com)

## Abstract

*The paper addresses reduced-order modelling (ROM), utilizing the proper orthogonal decomposition (POD), for the preliminary design of propellers. The development of a web application is presented which provides both geometry and simulation data. The Wageningen B-Series Propeller web app by FRIENDSHIP SYSTEMS enables the user to easily generate propeller geometry. This paper shows how to enhance the webApp with the results from flow simulations. The first step is to conduct a Design-of-Experiment (DOE), using CAESES and OpenFOAM. The simulation results are taken as input to generate a reduced-order model. Finally, a new web application which can display the output of the ROM, i.e., the pressure distribution on the blade, is presented.*

## 1. Introduction

Propeller design is a complex subject that requires optimization not only of the propeller performance per se, but also of the propeller performance in interaction with a ship's hull. In the preliminary design phase of a ship, simulation data on the hull's wake field is usually not available, which makes the ship-specific design of the propeller impossible. Moreover, there are still many design changes to be made in this phase of the design process which is why it is tried to use as few resources as possible on the design of the propeller. This leads to the use of standard propeller series in the preliminary design phase.

One widely used standard series are the Wageningen B-Series Propellers, also called Wageningen B-Screw Series, that were developed and tested in the Netherlands over several decades. Polynomials for the thrust coefficient ( $K_T$ ) and the torque coefficient ( $K_Q$ ), which were derived from the test results, and the geometrical parameters of the propellers are publicly available, Lammeren (1969), Oosterveld (1975).

Even though a propeller series relieves one of the task of coming up with propeller parameters, the geometry still has to be modeled. In the best case scenario, the model is easily adjustable for different parameters, called parametric design. FRIENDSHIP SYSTEMS published a web application for such a parametric geometry model of the Wageningen B-Series in 2018, see [www.wageningen-b-series-propeller.com](http://www.wageningen-b-series-propeller.com). The web app is powered by CAESES, a CAD tool developed and distributed by FRIENDSHIP SYSTEMS. The application enables users to quickly and easily generate watertight propeller geometries, Harries (2018), Hauschulz (2022).

This paper outlines the use of reduced-order modelling (ROM) for enhancing the existing Wageningen B-Series web application with the pressure distribution on the propeller blade. The ROM is based on OpenFOAM simulations and is created with the software package NAVPACK by NAVASTO. The output of the reduced-order model, i.e., the pressure distribution on the blade, is used in a prototype for a new web application.

## 2. Existing Wageningen B-Series Web App

The existing Wageningen B-Series web application consists of two tools. The Design Tool which just needs a few basic inputs, e.g., diameter, number of blades, expanded area ratio, to generate a Wageningen B-Series Propeller and the Geometry Tool which is intended for users that already have some geometrical parameters for a propeller like pitch, rake and thickness. The prototype of the new web app that provides the propeller geometry and additional simulation data builds partially on the back-end of the Design Tool.

## 2.1. Layout

CAESES provides a default layout for its web applications. The layout consists of a 3D view on the right-hand side, where the geometries are displayed and a sidebar on the left-hand side containing the input and output parameters, Fig.1.

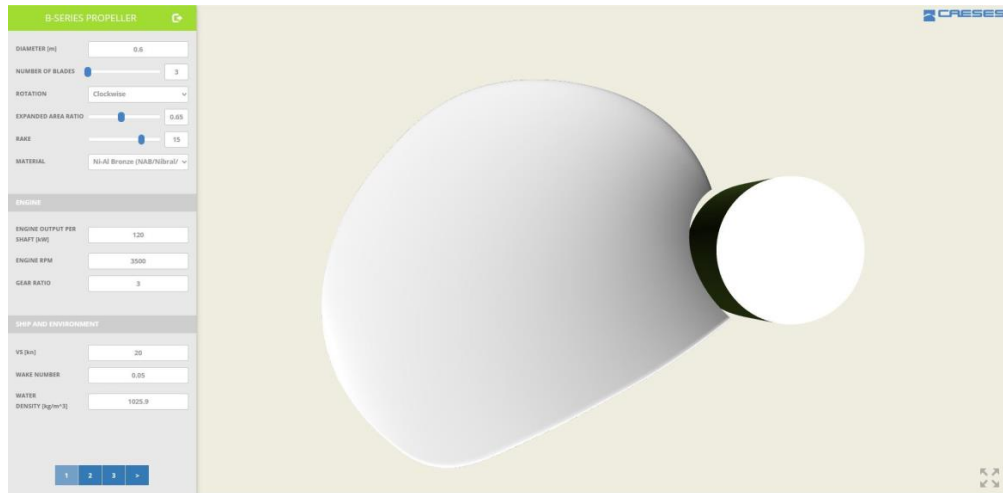


Fig.1: Screenshot of the Existing Wageningen Web Application

The web app creator can choose between a range of components, e.g., sliders, buttons, dropdown menus, but is otherwise largely restricted regarding the design of the web application.

## 2.2. CAESES Back-End

The back-end of the web application is a CAESES project which contains the parametric model of the Wageningen B-Series propeller. The implementation of the geometry is based on the geometrical information provided by *Lammeren (1969)* and *Oosterveld (1975)*. The shape of the propeller blade can be changed by various parameters. The variation of one of these parameters, the expanded area ratio, is shown in Fig.2.



Fig.2: Parametric Wageningen Propeller Model – Variation of EAR

A propeller geometry is generated if the implemented algorithm finds a pitch ratio which is within the bounds of the Wageningen B-Series definition and the resulting torque is as specified by the user. For this, the Wageningen polynomials for  $K_T$  and  $K_Q$  are evaluated and it is checked if the given EAR is larger than a calculated minimum value to avoid cavitation.

### 3. Design of Experiments

In the context of the development of the web application prototype, only Wageningen B-Series propellers with three blades are considered and only three parameters are varied. The expanded area ratio (EAR), the pitch ratio ( $P/D$ ) and the advance coefficient ( $J$ ). The Wageningen B-Series is defined for

$$\begin{aligned} 0.3 &\leq EAR \leq 1.05, \\ 0.5 &\leq P/D \leq 1.4, \\ 0.1 &\leq J \leq 1.5 \end{aligned}$$

and because the parametric model is not robust enough, the parameter space is further limited to

$$\begin{aligned} 0.3 &\leq EAR \leq 0.55, \\ 0.5 &\leq P/D \leq 1.4, \\ 0.1 &\leq J \leq 1.5. \end{aligned}$$

A Sobol sequence is utilized for the initial parameter space exploration and is visualized in Fig.3 with the third dimension, i.e., the expanded area ratio, projected onto a plane.

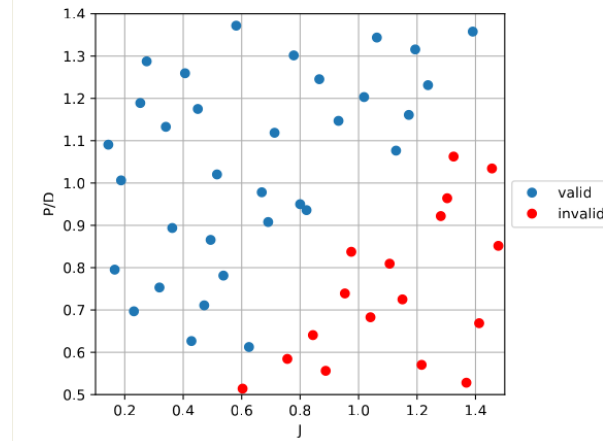


Fig.3: Sobol Samples

All parameter combinations where the thrust coefficient or the torque coefficient is negative are not used for further processing. These invalid designs are coloured red in Fig.3. A comparison between the results of the valid designs and the Wageningen polynomials shows large deviations for  $K_T$  (Fig.4) and  $K_Q$  for high advance coefficient relative to the considered pitch ratio.

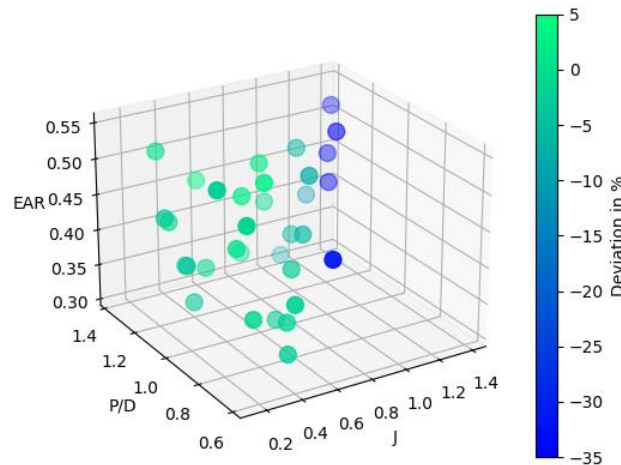


Fig.4: Deviations of  $K_T$  between Wageningen Polynomials and CFD Simulations

To ensure that sufficiently good CFD results are used to build the reduced-order models (ROMs), the parameter space is further restricted.

$$\begin{aligned} 0.3 &\leq EAR \leq 0.55 \\ 0.5 &\leq P/D \leq 1.4 \\ 0.1 &\leq J \leq 0.5 \end{aligned}$$

The valid samples of the initial Sobol sequence inside that parameter space are used for the creation of the ROM. In addition, a uniform sampling with 18 samples is conducted to build another reduced-order model for comparison of the model prediction accuracy. All used samples are shown in Fig.5.

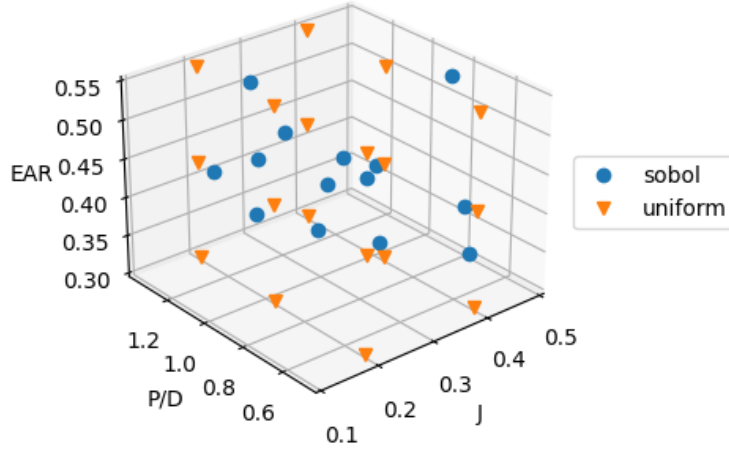


Fig.5: Samples used for the ROMs

#### 4. Reduced-Order Modelling

The aim is to use a reduced-order model to predict the pressure distribution on the propeller blade for any parameter combination given by the web app user. In this paper, the proper-orthogonal decomposition (POD) is utilized to build the ROM and the interpolation (I), i.e., the prediction, is performed with thin plate spline (TPS) regression. The software package NAVPACK from NAVASTO is used, in which the POD+I method is implemented.

##### 4.1. Theory

This subchapter gives a brief introduction to reduced-order modelling with the POD+I method and is based on the explanation in *Karcher (2020)*. For a more detailed introduction to reduced order modelling, see the given reference and the references therein.

Assuming that parameters  $x$  influence a two-dimensional output  $y$ , then the output matrix is

$$y(x) = \begin{bmatrix} y_{11} & \cdots & y_{1b} \\ \vdots & \ddots & \vdots \\ y_{a1} & \cdots & y_{ab} \end{bmatrix} \in R^{a \times b},$$

where  $a$  and  $b$  are the number of discrete sample positions in each direction.

Parameter values  $x$  combined with an output  $y$  are referred to as a snapshot. So,  $x^0$  with  $y^0$  is one snapshot and so on till  $x^m$  with  $y^m$ , where  $m$  is the number of snapshots, e.g., the number of simulations performed.

To find the correlation between snapshots, they are summarized in a matrix  $S$ , the so-called snapshot matrix. To be able to do that, it is necessary that all outputs  $y$  have the same number of sample points

$n_s = a \cdot b$ . The output matrices are summarized by transforming each output matrix into a column vector and then concatenating these vectors. So, the output matrices  $y(x)$  are transformed to

$$y^T = [y_{11} \quad \cdots \quad y_{1b} \quad y_{21} \quad \cdots \quad y_{2b} \quad \cdots \quad y_{a1} \quad \cdots \quad y_{ab}] \in \mathbb{R}^{1 \times n_s}, \quad n_s = a \cdot b.$$

and the snapshot matrix  $S$ , which contains the sample points from all snapshots, is as follows

$$S = \begin{bmatrix} y_{11}^0 & y_{11}^1 & \cdots & y_{11}^m \\ \vdots & \vdots & \ddots & \vdots \\ y_{n_s}^0 & y_{n_s}^1 & \cdots & y_{n_s}^m \end{bmatrix} \in \mathbb{R}^{n_s \times m}.$$

Then  $(S^T S)$  is the correlation matrix of the snapshot matrix and the problem to be solved is the eigenvalue problem

$$(S^T S)V^k = \lambda_k V^k, K = 1, \dots, m,$$

where  $\lambda_k$  is an eigenvalue to the corresponding eigenvector  $V^k$ .

The proper orthogonal decomposition identifies so-called modes  $U$  that can be linearly combined to reconstruct a snapshot, i.e., the output matrix. A mode is defined as

$$U^k = (\sqrt{\lambda_k})^{-1} S V^k \in \mathbb{R}^{n_s}.$$

And a snapshot  $y^i$ , the  $i$ -th column of  $S$ , can be reconstructed with

$$y^i = \sum_{k=1}^m a_k^i U^k, \quad i, k = 1, \dots, m.$$

The coefficients  $a_k^i$  can be calculated with

$$a_k^i = \sqrt{\lambda_k} V_i^k.$$

Since snapshots for evaluated parameter combinations can be reconstructed, the approach of POD+I is to predict snapshots by interpolating the existing coefficients  $a_k^i$ .

## 4.2 Preparation of the Snapshots

As explained in the previous chapter, all snapshots must have the same number of sample points, i.e., mesh points. The unstructured meshes used for the CFD simulations have each different numbers of points, therefore the data fields have different sizes. The solution is to project the data from the unstructured meshes onto a structured mesh. This structured mesh has by construction the same number of points and only the distance between the points changes with the geometry. A comparison between an unstructured mesh used for the CFD simulation and the corresponding structured mesh is shown in Fig.6.

For the projection of the CFD results onto the structured mesh a nearest neighbor algorithm is used which is implemented in NAVPACK.



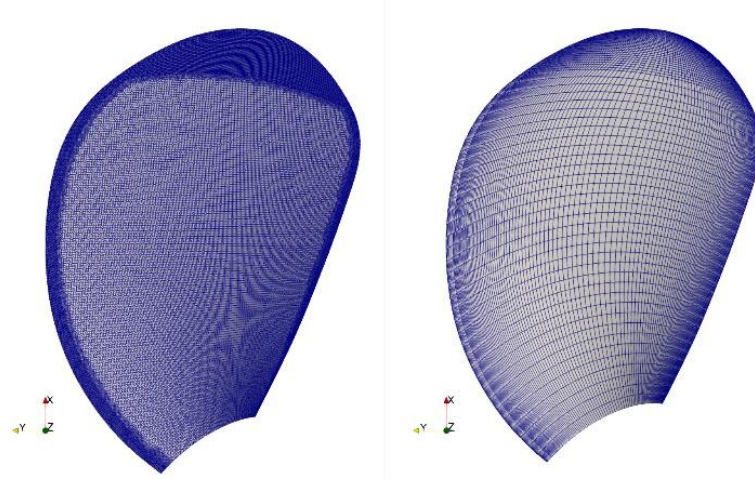


Fig.6: Comparison of Unstructured and Structured Mesh for one Snapshot

### 4.3 Prediction of the ROM

Four different reduced-order models are evaluated. Two models based on the Sobol samples and two models based on the uniform samples. For each sampling method a ROM was built with no mode reduction and one with a mode reduction, that only uses modes with a positive  $R^2$  score. The ROMs were tested for one parameter combination of  $EAR = 0.37$ ,  $P/D = 0.72$  and  $J = 0.26$ . The ROM based on the Sobol samples with mode reduction shows to give the best prediction of the pressure distribution. A comparison between the CFD result and prediction of the reduced-order model is shown in Fig.7 and Fig.8.

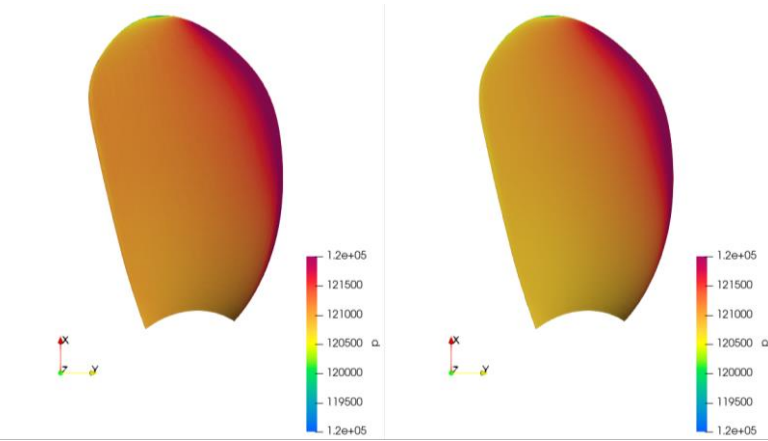


Fig.7: CFD vs. ROM Prediction – Comparing pressure side - Sobol-based with R2 Mode Reduction

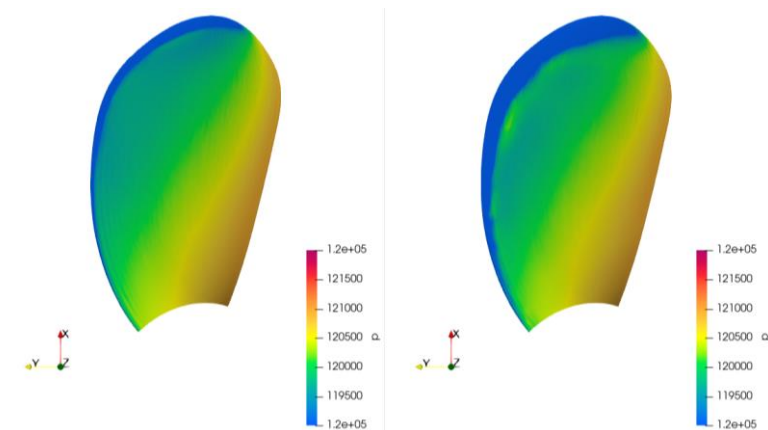


Fig.8: CFD vs. ROM Prediction – Comparing suction side - Sobol-based with R2 Mode Reduction

As can be seen, the prediction of the pressure distribution on the pressure side of the blade comes very close to the simulation. On the suction side of the blade, however, the pressure field deviates strongly in the leading-edge area.

One explanation for this could be that the number of samples is not large enough to sufficiently capture the pressure changes on the blade. Further simulations need to be carried out to clarify this and also other methods to build the reduced-order model should be tested.

## 5. New Wageningen B-Series Web App

The prototype of the web application that combines geometry and simulation data uses a different approach for the layout and not the default CAESES web app layout. The prototype is built using Vue.js, a JavaScript framework for building user interfaces and Vuetify, a library for web components. This new approach enables CAESES users to create more customized web applications. The idea is to still provide predefined components, e.g., sliders, buttons, but also allow the use of own components and other web development frameworks.

### 5.1. Layout

The new layout is specifically designed for this application. Due to the new web app approach, the layout could be completely different for another application. Here, the user inputs are at the top and via the sidebar on the right-hand side, the user can control which output parameters are displayed, Fig.9.

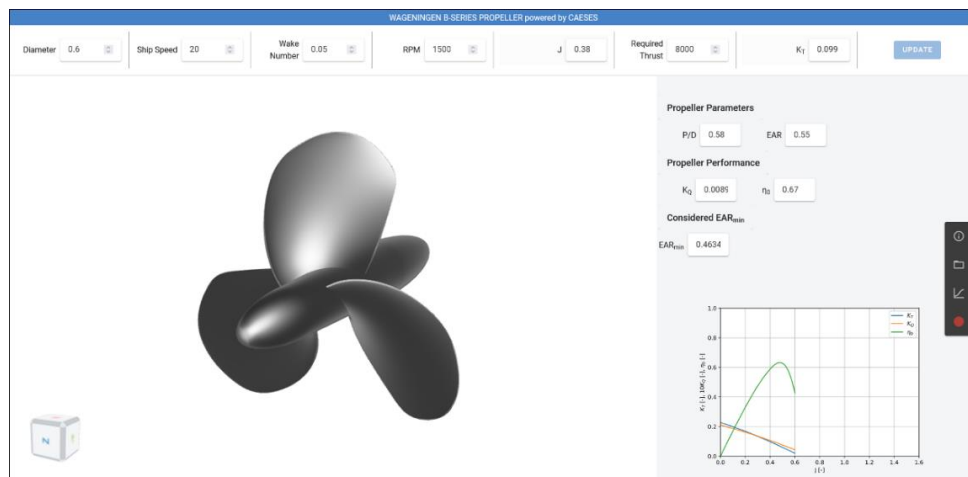


Fig.9: Screenshot of the New Wageningen Web Application



Fig.10: Screenshot of the New Wageningen Web Application – Pressure Distribution Displayed

The output of the reduced-order model, i.e., the pressure distribution on the blade, can also be displayed by clicking on a button on the sidebar. When the pressure distribution gets displayed the geometry shown in the 3D view changes from the complete propeller geometry to only the propeller blade, Fig.10.

## 5.2 CAESES Back-End

The parametric propeller model from the existing Wageningen B-Series web app is still used for the prototype but the algorithm to generate the geometry has changed. In the new web application, the algorithm tries to find a propeller with an expanded area ratio and a pitch ratio which can produce the specified thrust for the given advance coefficient. Like in the existing web app the Wageningen polynomials are evaluated for this. If there exists a parameter combination that fulfils the user inputs and does not violate any constraints, the propeller geometry is generated, and the reduced-order model is evaluated for the parameters. The prediction of the ROM is saved as a VTU-file and then loaded into CAESES where it is sent to the web application.

## 6. Conclusion and Outlook

The paper outlines a way to utilize reduce-order models for the preliminary design of propellers in the form of a web application. Two sampling methods, Sobol and uniform sampling, were used to create different reduced-order models. The ROM based on the Sobol samples and with mode reduction showed to have the best prediction accuracy and the output is used for a web application. That web application is a prototype which demonstrates a new way to create CAESES-powered web apps. This approach is not limited to propeller design and can be used to make sophisticated simulations like CFD and FEM accessible for others.

Further research should be conducted on how to increase the accuracy of the ROM prediction. A better accuracy could be achieved by increasing the number of samples used to create the ROM but also other methods for reduced-order modelling should be tested. When the prediction accuracy is satisfactory, the ROM should be extended to cover all parameter values for which the Wageningen B-Series is defined.

## Acknowledgements

The authors would like to thank Jakob Lohse from NAVASTO for his support in using the software package NAVPACK. Parts of the work presented in this paper were realized within the research and development project DEffProForm, funded by the Federal Ministry for Economic Affairs and Climate Action on the orders of the German Bundestag and PtJ as the conducting agency (FKZ 03SX516C).

## References

- HARRIES, S.; LORENTZ, K.; PALLUCH, J.; PRAEFKE, E. (2018), *Appification of Propeller Modeling and Design via CAESES*, COMPIT Conf., Pavone
- HAUSCHULZ, S.; HARRIES, S.; THIES, F.; von ZADOW, H. (2022), *Web-based Microservices for Fast Modeling and Easy Collaboration*, HIPER Conf., Cortona
- KARCHER, N.; WALLRAFF, M. (2020), *Accelerating CFD solver computation time with reduced-order modeling in a multigrid environment*, Int. J. Numerical Methods in Fluids
- LAMMEREN, W.P.A.; VAN MANEN, J.D.; OOSTERVELD, M.W.C.; VAN OOSSANEN, P. (1969), *The Wageningen B-screw series*, SNAME
- OOSTERVELD, M.W.C., VAN OOSSANEN, P. (1975), *Further Computer-Analyzed Data of the Wageningen B-Screw Series*, International Shipbuilding 22/251

# A Tool to Predict Route-Specific Energy Consumption for Ships with Battery-Supported Propulsion

Christian Emmersberger, Hamburg University of Technology, Hamburg/Germany,  
[christian.emmersberger@tuhh.de](mailto:christian.emmersberger@tuhh.de)

Stefan Krüger, Hamburg University of Technology, Hamburg/Germany, [krüger@tuhh.de](mailto:krüger@tuhh.de)

## Abstract

*This paper describes a tool to predict the power consumption of a ship with battery-supported propulsion on a given route under consideration of (statistically varying) environmental ambient conditions. The tool can be used in conceptual design of ships with such hybrid propulsion systems. It may also be used for decision support in operation. At the heart of the tool is a fast, but flexible manoeuvring simulation tool that allows also inclusion of port manoeuvres. Operational parameters, such as intended speed profiles, are user-specified, while ambient parameters (such as wave height and direction) are statistically varied to reflect realistic long-term conditions on given routes.*

## 1. Introduction

Efforts to reduce costs and emissions in shipping are driving the need for efficiency improvements in ships. A successful efficient ship design depends crucially on the availability of a suitable operational profile. If this is not at hand (e.g. through measured data from similar ships), it has to be estimated. This paper shows an approach for a power and fuel consumption estimation of vessels and is based on a manoeuvring calculation including the propulsion system, the power plant and the engine control. It is possible to assess arbitrary ship routes by setting waypoints on a map. Environmental influences and dynamics like manoeuvring and de- and acceleration are considered. This is particularly important for ships with dynamical manoeuvring behavior in their operation and a broadly spread power demand (e.g. due to channel navigation and harbour manoeuvres). The initial state of ship design dictates the use of only limited information at hand.

Primarily, generating a fitting data basis for the design of the ship's propulsion and energy system is enabled by this method. Better estimations of design parameter, which are particularly dependent on load fluctuation, are possible. This applies to battery charge cycles and thus the battery lifetime, Emmersberger *et al.* (2022a). Moreover, it is suited for analysing specific ship routes and give operational recommendations regarding fuel savings.

The presented method is particularly suitable for ships with a very dynamic sailing profile, where load peaks are relevant to the design. Tillig *et al.* (2019) also presents a fast approach useful in the early design phase to determine the operational profile dependent on the operational area and the occurring environmental loads. In contrast to the presented work, the manoeuvring calculation is performed quasi statically and empirical formulae are used for the hull and rudder forces calculation. As a result, load peaks are not included, and the force calculations only work best for ship hulls applicable on the empirical formulae. Patil *et al.* (2021) uses a motion model combined with a waypoint navigation to calculate the fuel consumption on long overseas voyages. As the manoeuvring is based on the motion model, the approach can hardly be used in the early ship design. In Martelli *et al.* (2014) a 6 DOF numerical model of the ship motion, propulsion system and the system control for the early design is introduced and applied to standard manoeuvres. The hull forces are determined by using regression formulae. The model was supplemented with a guidance and control system and limited environmental influence by Donnarumma *et al.* (2020), but concentrates more on path planning and collision avoidance than generating an operational profile.

## 2. Description of the Calculation Method

Within the ship design environment “E4”, a body force model is implemented for manoeuvring

calculations. It is also used for examining performance of wind (assisted) ships, *Oettle et al. (2023)*, ship in adverse weather conditions, *Krüger et al. (2018)*, or dynamic positioning, *Lübcke et al. (2015)*. It determines the ship's motion from all forces acting on the ship and is based on a model developed by Söding, *Söding (1982)* and *Söding (1984)*. The ship motion is considered in 4 degrees of freedom, where the roll motion is quasi-static and thus decoupled. In particular, the model also takes off-design conditions of the propeller into account, which often occur during dynamic manoeuvres. It is combined with an engines plant model described by *Haack (2006)*. This allows the calculation of standard ship manoeuvres in time domain influenced by the engine limits. This work shows an addition to the standard manoeuvres to estimate the fuel consumption of a ship along a given route.

## 2.1. Force and Moment Calculation

To use the manoeuvring calculation following information need to be provided or can be generated:

- Ship hull form
- Weights and a specific loading condition
- Engine limits and specific fuel consumption
- Resistance curve and hull efficiency elements
- Propeller information

In the ship design environment E4 several methods, like hull form transformation or standard series for resistance and propellers, support the gathering of the required information. Appendix A gives a more detailed description of the manoeuvring model. In the following a brief overview about the calculation basis of the different force modules is given:

- Hull Forces
  - Longitudinal resistance - Resistance curve
  - Transversal forces and moments – Slender-body theory with corrections for the disturbance of the parallel flow at ship ends, missing longitudinal added mass and transversal flow separation
- Wind resistance - Coefficients from Blendermann, *Brix (1993)*
- Added resistance due to waves – Strip code based on potential theory, *Augener (2016)*
- Shallow water
- Propeller forces – KT-KQ Curves and lifting line method for propeller-hull interaction
- Rudder forces in propeller slip stream – Precalculated from a panel code combined with a lifting line approach, *Carstensen (2019)*

## 2.2 Engine Model and Control

The engine is implemented by the engine map and load gradients to meet the load limits and ensure a realistic operation. The system control is divided into the engine and propeller pitch control. The control behaves differently for fixed (FFP) or controllable pitch propeller (CPP) and for constant engine speed or combinator mode. Battery support is not yet integrated in this calculation and is done separately as a post-calculation with the approach described in *Emmersberger et al. (2022b)*.

The engine control is implemented with a PI controller, where the setpoint is the engine torque. The controller input is either the engine speed, the propeller pitch or a combination depending on the propeller type and propulsion mode. In a CPP propulsion system the engine speed is kept constant or a combination of engine speed and propeller pitch, according to the combinator curve, sets the engine torque. If necessary, the permissible engine torque is limited by the engine map and load gradients, whichever allows the least change in torque. The engine speed for the next time step is then determined as a function of the mass moment of inertia of the system (including engine, gearbox, shaft, coupling and propeller).



In addition, the propeller pitch control includes a windmilling and an overload control. The windmilling control temporarily increases the propeller pitch, when the propeller enters the turbine conditions (e.g. when decelerating) to avoid engine overspeed. The overload control reduces the propeller pitch to prevent the propeller torque from exceeding the engine torque limits.

A speed controller has been added to the engine control so that the vessel automatically follows a given velocity. This was done by replacing the former *controller inputs* by the ship speed.

### 2.3. Guidance System

The task of the guidance system is to navigate a route defined by waypoints. The Line of Sight (LOS) Guidance, *Fossen (2011)*, also used in *Breivik et al. (2003)*, *Morearia et al. (2007)* or *Khaled (2010)* is selected for this task. It connects the waypoints with straight lines, which shall resemble the ship's trajectory. The aim of the ship is to converge with this straight line. To do this, a navigation circle is drawn around the ship, so that it intersects with the line between two waypoints, Fig.1. The direction of the vessel to the intersection is determined and is set as the target course. Using this approach, the ship will always find its way back to its trajectory. When a waypoint is reached, the intersection with the next trajectory is chosen.

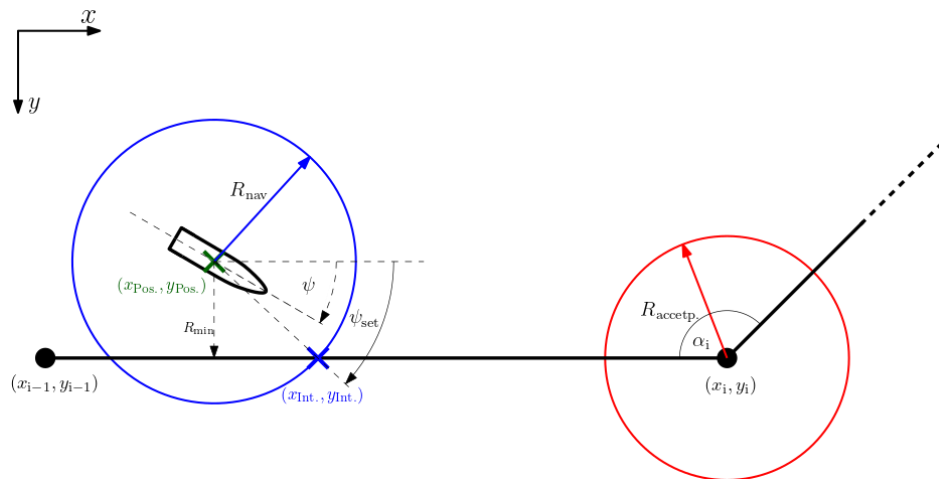


Fig.1: Schematic Depiction of the Line of Sight Concept

To make sure that the radius of the navigation circle intersects with the trajectory, it is chosen by

$$R_{nav} = \max(R_{min} + L_{pp}, 3.2 \cdot L_{pp}), \quad (1)$$

where  $R_{min}$  is the vertical distance between the ship and the trajectory and  $L_{pp}$  is the length between the perpendiculars. The navigation circle is given by

$$(y_{Int} - y_{Pos.})^2 + (x_{Int} - x_{Pos.})^2 = R_{nav}^2, \quad (2)$$

with  $y_{Int.}$  and  $x_{Int.}$  as the point of intersection and  $y_{Pos.}$  and  $x_{Pos.}$  as the ship's position. The intersection point is then found by inserting Eq.(2) into the linear equation of the trajectory

$$y_{Int.} = m \cdot x_{Int.} + b \quad \text{with} \quad (3)$$

$$b = y_i - m \cdot x_i \quad (4)$$

$$m = \frac{y_i - y_{i-1}}{x_i - x_{i-1}}, \quad (5)$$

where  $x_i$  and  $y_i$  stand for the current waypoint and  $x_{i-1}$  and  $y_{i-1}$  for the previous waypoint. The x-coordinate of the intersection  $x_{Int.}$  is found by solving the second order polynomial

$$a_1 \cdot x_{Int.}^2 + a_2 \cdot x_{Int.} + a_3 = 0 \quad \text{with} \quad (6)$$

$$a_1 = m^2 + 1, \quad (7)$$

$$a_2 = 2 \cdot (-m \cdot y_{Pos.} - x_{Pos.} + m \cdot b), \quad (8)$$

$$a_3 = b^2 - 2 \cdot b \cdot y_{Pos.} + y_{Pos.}^2 + x_{Pos.}^2 - R_{nav.}^2, \quad (9)$$

where  $a_1$ ,  $a_2$  and  $a_3$  are the polynomial coefficients. The result, which is closer to the current waypoint, is chosen. The y-coordinate  $y_{Int.}$  can then be found by inserting  $x_{Int.}$  in Eq.(3). The course can now be determined by

$$\psi_{set} = atan2(y_{Int.} - y_{Pos.}, x_{Int.} - x_{Pos.}), \quad (10)$$

where  $\psi_{set}$  is the target value for the course.

The target course is then picked up by the rudder auto pilot, which is implemented as a PI controller. The calculation of the error term of the controller (difference between  $\psi_{set}$  and  $\psi$ ) depends on which quadrants are involved. Suitable control coefficients are found by trial and error. The next waypoint is selected, when the vessel reaches the radius of acceptance  $R_{accept.}$ , Fig.1. This radius depends on the vessel speed and turning angle at the waypoint. The tighter the curve, the larger the radius of acceptance to avoid too much overshoot. The formula of the radius of acceptance is composed of

$$R_{accept.}(v_s) = R_{tact.}(v_s) \cdot (0.7 \cos(\alpha_i) + 1) + v_s \cdot t_{Delay}, \quad (11)$$

with  $R_{tact.}$  as the tactical diameter of a turning circle manoeuvre,  $v_s$  as the ship speed,  $\alpha_i$  as the angle between two trajectories and  $t_{Delay}$  as a delay for the ship's inertia. In Fig.2 a resulting pathway using this guidance system is shown with waypoint coordinates also used by *Khaled (2010)* and *Moreira (2007)* for demonstration purposes.

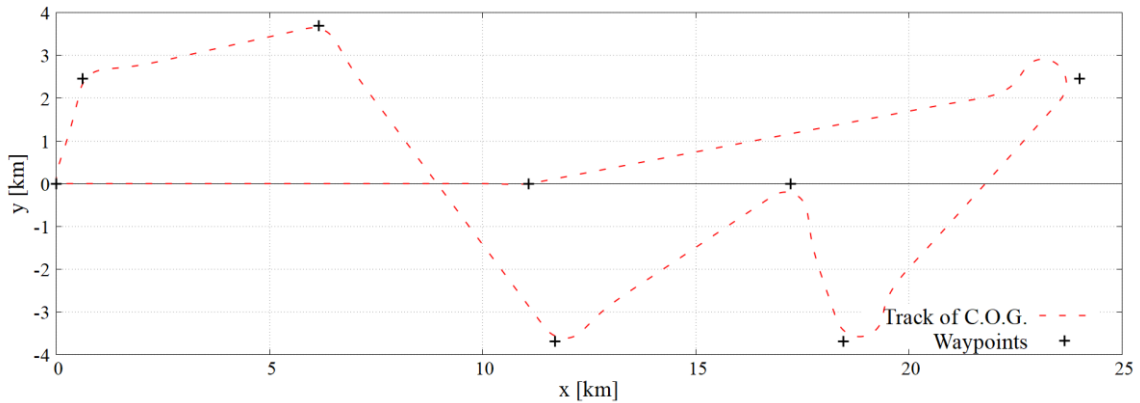


Fig.2: Travelled Path by Using the Described Guidance System

The recreation of a realistic ship route is done by placing the waypoints on a map with the help of the open-source platform Leaflet. After the waypoints are placed, they are retrieved in latitudes and longitudes. These are then converted (using the WGS-84-Ellipsoid) into a flat cartesian coordinate system, which is used from the manoeuvring calculation. The distance between waypoints should be smaller than  $1^\circ$  latitude to ensure comparable bearing between the ship and environmental influences. If the waypoints are placed further away from each other, additional waypoints are inserted.

## 2.4. Port Manoeuvring

Especially port manoeuvring is a highly dynamic event and thus shall be integrated. Therefore, the dynamic positioning calculation, *Lübcke (2019)*, in *E4* is used as a basis. The idea is to assemble the

port maneuver from individual manoeuvre modules, like turning, traversing or slow speed manoeuvring. To avoid a complex control strategy of the propulsion units, the calculation is implemented quasi-statically. For every time step the balance of forces with a given motion is calculated. The motion can be specified by a turning rate or a transversal speed, depending on the manoeuvre module.

## 2.5. Limits

Currently, the applicable propulsion systems are limited to one and twin-screw systems with fixed and controllable pitch propellers. Regarding engines, slow and medium speed engines can be considered. The added resistance in waves is taken as the average from wave drift force calculation in irregular seaway over a short time series and then used in the force balancing. The port manoeuvring is done quasi-statically, so dynamic load peaks are missing.

## 3. Use Case: Montreal-St. Johns

### 3.1. Ship characteristics and Ship Route

To demonstrate the calculation, a ship route between Montreal and St. John's (Newfoundland) is chosen. It is a voyage used by several cargo vessels supplying the island of Newfoundland. The main dimensions in Table I are based on representative characteristics of vessels operating in this region. The waypoints are placed by hand and are derived from the typical pathways. Fig.3 shows the defined waypoints. The river section from Montreal is mostly narrow and has a few bends. After a fifth of the way, the estuary opens up and higher speeds are possible. Due to whale activity some ships restrict themselves to lower velocities to reduce noise in certain areas. Under these premises, the ship speed is specified depending on the waypoint's location, Appendix C, Table III. Furthermore, every waypoint is assigned with environmental variables by using the E.U. Copernicus Marine Service Information, <https://doi.org/10.48670/moi-00022>. To consider the port manoeuvring, the ship behaviour in the harbor is examined by AIS data. In the port of Montreal, the ship starts going backwards for about 900 m and is then turning about 180°, Fig.4a. At arrival at the port of St. John's the procedure is done the other way around by turning 180° and reversing about 500 m, Fig.4b.

Table I: Ship Characteristics

Length	about 192 m
Breadth	about 30
Draft	about 7.4
Displacement	about 15 800 t
Propulsion	2x CPP
Main Engine	2x 8100 kW
Speed	about 22 kn

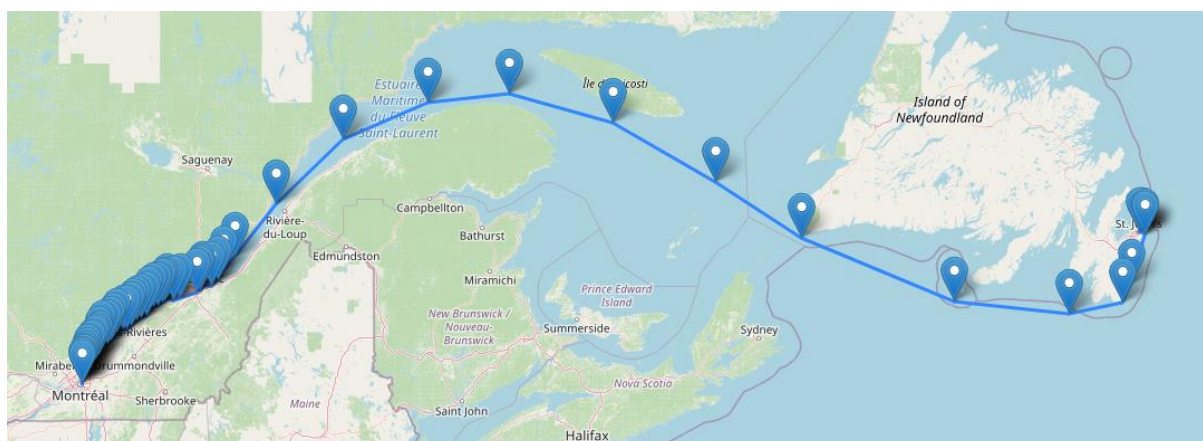


Fig.3: Waypoints of the Ship Route



(a): Montreal



(b): St. John's

Fig.4: Port Manoeuvring Procedure (drawn with CalcMaps)

### 3.2. Results

This section shows exemplary results, that can be withdrawn from the manoeuvring calculation. In case of interest, all manoeuvring and engine related parameters, like rudder angle, engine speed or propeller pitch and many more can be provided and analysed. Looking at the actual calculated pathway of the total voyage, Fig.5, and of the river part, (see Appendix B. Fig.9) show, that the guidance system keeps the ship reliably on track and all waypoints could be reached. The voyage has a duration of 52.82 hours, which fits with the typical travel times. The manoeuvring behaviour is also reflected in the power demand, Fig.6, and the velocity behaviour, Fig.7. The load peaks in the power plot correspond to the acceleration and the manoeuvring around waypoints. Also, the changes in the power demand due to environmental influences can be seen in Fig.6 between minute 1200 and 2600. The total energy demand for the port manoeuvre results in 1621 kWh for Montreal and 1613 kWh for St. John's. Note, that the energy demand is only valid for the used environmental conditions.

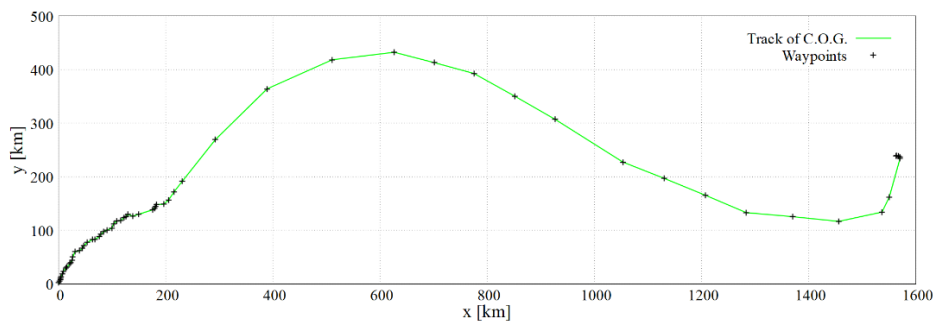


Fig.5: Sailed Route (Travelled Time 52.82 h)

With the conventional setup without battery the fuel consumption results in 89.7 t. Considering battery support using the approach described in *Emmersberger et al. (2022b)*, up to 3.62% fuel can be saved with a 5008.5 kWh battery. Table II shows the difference using a quasi-static or the presented dynamic approach. The consumption, the fuel savings and the operating hours are similarly estimated by both approaches. Whereas the charge cycles are underestimated by 22.1% by the quasi-static calculation.

Table II: Comparison of Dynamic and Quasi-Static Calculation

	Without Battery	Battery with 1050 kWh		
	Fuel Consumption	Fuel Savings	Operating Hours	Charge Cycles
Quasi-static	89.4 t	1.72%	19.53%	1.41
Dynamic	89.7 t	1.67%	19.17%	1.81
Error	0.3%	-2.9%	-1.8%	+22.1%

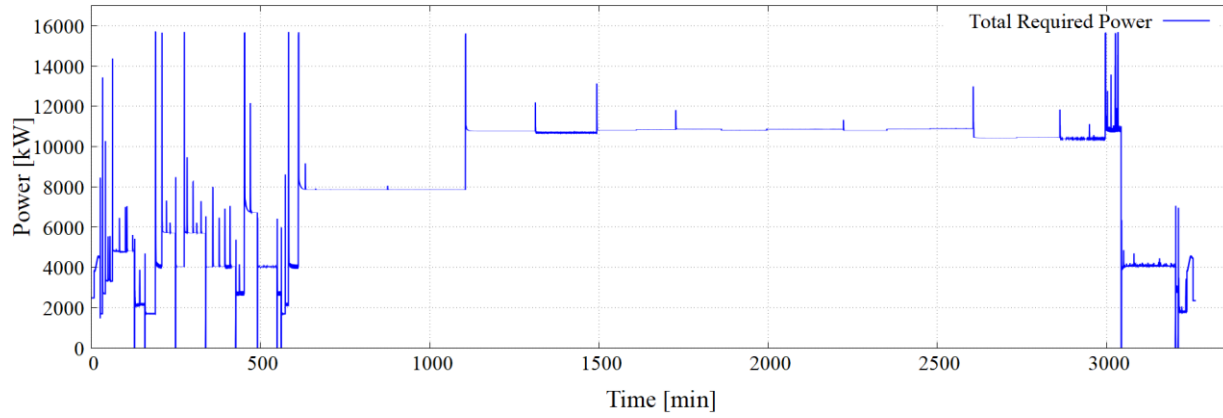


Fig.6: Required Power along the Ship Route

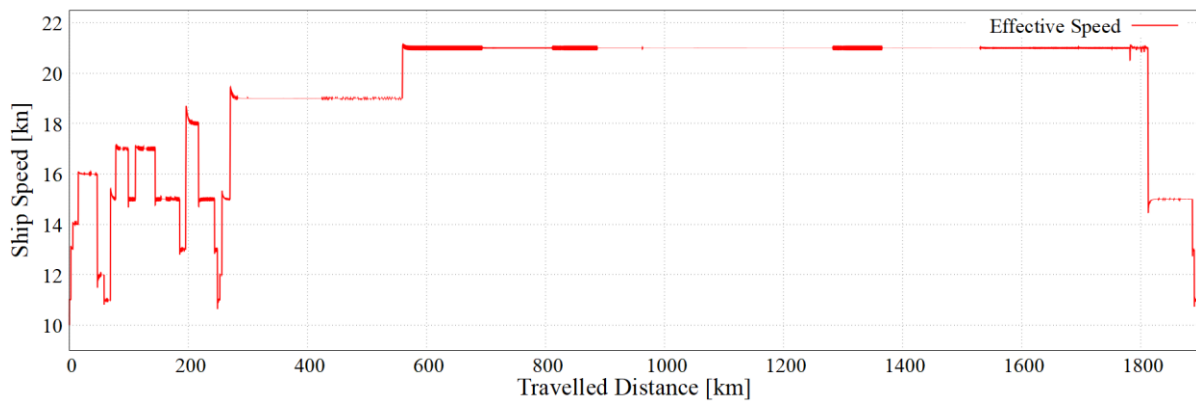


Fig.7: Ship Velocity Along the Route

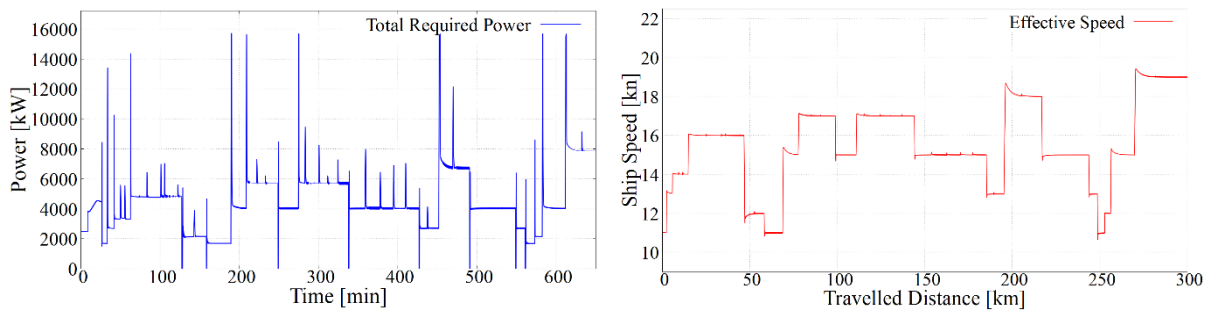


Fig.8: Sailed Route and Waypoint of the River Part

### 3.3. Discussion

The larger load peaks, Figs.6 and 8, are due to acceleration and are dependent on the cruise control and therefore could be adjusted with regard to energy saving by slower acceleration. Otherwise, a battery could be used as ramp support, if the fast acceleration is required. The smaller load peaks are a result from direction change at the waypoints. Also, in those turns the cruise control retains the target speed.

The estimated fuel savings result mainly from the river segment. In the open water the engine can be operated most efficiently without support. During river manoeuvring the second engine can be shut down, due to the backup power the battery provides for acceleration and turning. This leads to a more efficient engine operation. This is confirmed by comparing the histogram of the engine load with and without battery, shown in Appendix B Fig.10. With battery support, the engine load is on average located closer to the engine's optimum at about 85% maximum continuous rating. There was no extensive optimization of the engine-battery configuration conducted in this work, thus other configu-



ration could be tested to increase the energy savings. To save investment costs, it would be possible to install smaller engines, if the top speed is only required for a specific amount of time.

With the information of the power demand in the harbor, an emission free operation can be examined. In this case, it is important to statistically vary the environmental conditions and/or check the needed energy in extreme conditions.

#### 4. Summary and Outlook

A method to estimate the energy consumption of a ship following a specific route defined by waypoints was introduced. It was implemented by extending an existing manoeuvring calculation used in the early design phase for standard manoeuvres. The calculation model covers the hydrodynamic aspects and takes the restrictions from the power plant into account. In addition, port manoeuvring can be considered by assembling individual manoeuvring modules (traversing, turning, ...) depending on the harbour conditions. Also, environmental conditions are applied on the ship model. The ship design environment in which it is implemented, ensures the refinement of the models depending on information at hand in the current design stage.

A case study for a specific ship route has shown the differences between a quasi-static and time-dependent approach. In this specific examination, the battery charge cycles were underestimated by over 20%. The generated sailing profile was used to estimate fuel savings due to battery support, which led to fuel saving of 3.62%. The results are only valid for this specific case, but show that the load fluctuation in highly dynamic ship behaviour influence the design parameters.

Further improvements and possible extension are listed and described below.

- Variable loading conditions - As ships are operated with changing loading and the different resulting floating conditions have an influence on the fuel consumption, this should be statistically considered. For example, like it is done it is done in *Eljardt (2009)* with a quasi-static approach.
- Calculation performance - For a life cycle assessment, the calculation speed is currently a bit slow (10 s for 1 h). But seeing the constant power plateaus in Fig.6, it is possible to increase the calculation steps in parts with less dynamic behaviour without losing accuracy. Above all, the calculation of the additional resistance in swell is quite time-consuming, which is why a pre-calculation and subsequent interpolation of the forces could come into question.
- Environmental loads - Moreover, for more dynamic behaviour of the environmental load, the wind speed and direction can be considered time dependent, as described in *Lübcke (2019)* using a wind spectrum.
- Optimize power demand - The presented tool offers additionally the opportunity to optimize the sailing behaviour regarding the power demand. For example, route segments with shallow water lead to higher consumption at the same ship velocity. Thus, it is beneficial to go slower on shallow water and catch up the lost time in deeper water. The tool could be used to answer which velocities lead to the smallest consumption.
- Control strategies - The cruise and heading control have a significant influence on the required power. Especially, the control behaviour in acceleration and turning should be examined. Furthermore, in the current state the battery support is done in a post calculation. This should be directly integrated into the engine control.
- Life Cycle Assessment - For future work it is planned to automatically run the defined voyage several times with statistically changing environmental influences. Therefore, either specific probability distributions shall be used or databases like the Global Ocean Waves Reanalysis, where a spatio-temporal dependence can be considered.

## References

- AUGENDER, P. (2016), *Computation of Wave Drift Forces for Dynamic Positioning within the Early Design Stage*, PhD Thesis, Hamburg University of Technology
- BREIVIK, M. (2003), *Nonlinear Maneuvering Control of Underactuated Ships*, M.Sc. Thesis, Norwegian University of Engineering Cybernetics, Trondheim
- BRIX, J. (1993), *Maneuvering Technical Manual*, Seehafen Verlag
- CARSTENSEN, B. (2019), *A Method for Rudder Force Calculation in the Design Process Considering Rudder-Propeller-Interaction*, 6<sup>th</sup> Int. Symp. Marine Propulsors
- DONNARUMMA, S.; FIGARI, M.; MARTELLI, M.; ZACCONE, R. (2020). *Simulation of the Guidance and Control Systems for Underactuated Vessels*, Modelling and Simulation for Autonomous Systems
- ELJARDT, G.; GREITSCH, L. (2009), *Operation-Based Ship Design and Evaluation*, 10<sup>th</sup> Int. Marine Design Conf.
- EMMERSBERGER, C.; CARSTENSEN, B.; LUEBCKE, A.; KRUEGER, S. (2022a), *The Necessity of Time-Based Calculations for Dimensioning of Hybrid Power Supply Systems of Ships within the Early Design Stage*, Proc. Inst. of Mech., Part M: J. Eng. for the Maritime Environment (JEME)
- EMMERSBERGER, C.; CARSTENSEN, B.; LUEBCKE, A.; KRUEGER, S. (2022b), *A method for dimensioning hybrid power supply systems of ships within the early design stage*, 15<sup>th</sup> Int. Symp. Practical Design of Ships and other Floating Structures
- FOSSSEN, T.I. (2011), *Handbook of Marine Craft Hydrodynamics and Motion Control*, John Wiley & Sons, p.259
- LAMB, H. (1945), *Hydrodynamics*, New York
- LÜBCKE, A.; AUGENDER, P.; FALKENHORST, A. (2015), *A Fast Method for the Evaluation of the Dynamic Positioning Capability in Time Domain in the Early Design Stage*, 34<sup>th</sup> Int. Conf. on Ocean, Offshore and Arctic Engineering
- LÜBCKE, A. (2019), *Dynamisches Positionieren als Aspekt in der frühen Schiffsentwurfsphase*, PhD Thesis, Hamburg University of Technology
- HAACK, T. (2006), *Simulation des Manövrierhaltens von Schiffen unter besonderer Berücksichtigung der Antriebsanlage*, PhD Thesis, Hamburg University of Technology
- KHALED, N. (2010), *Robust Observers and Controllers for Marine Surface Vessels Undergoing Maneuvering and Course-Keeping Tasks*, PhD Thesis, Wayne State University
- KRUEGER, S.; BILLERBECK H.; LÜBCKE A. (2018), *Safe Maneuvering in Adverse Weather Conditions*, 13<sup>th</sup> Int. Marine Design Conf.
- MARTELLI, M.; VIVIANI, M.; ALTOSOLE, M.; FIGARI, M.; VIGNOLO, S., (2014) *Numerical modelling of propulsion, control and ship motions in 6 degrees of freedom*, Proc. Inst. Mechanical Engineers, Part M: Journal of Engineering for the Maritime Environment 228(4), pp.373-397
- MOREIRA, L.; FOSSSEN, T.I.; GUEDES SOARES, C. (2007), *Path following control system for a tanker ship model*, Ocean Engineering 34, pp.2074-2085

OETTLE, J.; KRUEGER, S. (2023), *A 4 degree of freedom velocity/power prediction program for wind (assisted) vessels*, 42<sup>nd</sup> Int. Conf. Ocean, Offshore and Arctic Engineering

PATIL, P.; SREE, K.P.C.; Vishwanath, N.; Sha, O.; Prakash, S. (2021), *Numerical simulation of ship navigation in rough seas based on ECMWF data*, Brodogradnja 72, pp.19-58

SOEDING, H. (1982), *Prediction of Ship Steering Capabilities: Dedicated to Prof. Grim on the occasion of his 70<sup>th</sup> birthday*, Schiffstechnik 78, pp.3-30

SOEDING, H. (1984), *Bewertung der Manöviereigenschaften im Entwurfsstadium*, Jahrbuch der Schiffbautechnischen Gesellschaft, Vol. 78, pp.179-204

TILLIG, F.; RINGSBERG, J.W. (2019), *A 4DOF simulation model developed for fuel consumption prediction of ships at sea*, Ship and Offshore Structures 14, pp.112-120

VORHOELTER, H. (2011), *Numerische Analyse des Nachstroms und der Propellereffektivität am manövrierenden Schiff*, PhD Thesis, Hamburg University of Technology

## Appendix

### A. Manoeuvring Force Model

The following description can also be found in *Haack (2006)*. The resulting accelerations on the ship are computed by solving the equations

$$X_{Hull} + X_{Rudder} + X_{Propeller} + X_{Seaway} + X_{Wind} = m(\ddot{u} - v\dot{\psi} - x_G\dot{\psi}^2), \quad (12)$$

$$Y_{Hull} + Y_{Rudder} + Y_{Propeller} + Y_{Seaway} + Y_{Wind} = m(\dot{v} - u\dot{\psi} + x_G\dot{\psi}), \quad (13)$$

$$N_{Hull} + N_{Rudder} + N_{Propeller} + N_{Seaway} + N_{Wind} = I_Z\ddot{\psi} + mx_G(\dot{v} + u\dot{\psi}), \quad (14)$$

where  $X$  stands for the longitudinal forces,  $Y$  for the transversal forces and  $N$  for the yaw moments due to the effect specified by the subscript. The velocity and the position are determined by integrating the accelerations.

**Hull forces** - According to the slender body theory, the hull forces are a result of the time rate of change of transverse momentum of the water near the hull. The water close to the hull follows the transverse motion of the ship, whereas the further away from the ship, the influence decreases. The force is then equal to the acceleration of the ‘added mass’, which resembles the water in motion. According to this, the body forces are composed by

$$X_1 = 0, \quad (15)$$

$$Y_1 = \int_{x_{max,\mu}}^L \left( -\frac{\partial}{\partial t} + u \frac{\partial}{\partial x} \right) \mu \cdot (v + x\dot{\psi}) dx, \quad (16)$$

$$K_1 = -mgh + \int_{x_{max,\mu}}^L \left( -\frac{\partial}{\partial t} + u \frac{\partial}{\partial x} \right) z_\mu \mu (v + x\dot{\psi}) dx, \quad (17)$$

$$N_1 = \int_{x_{max,\mu}}^L x \left( -\frac{\partial}{\partial t} + u \frac{\partial}{\partial x} \right) \mu \cdot (v + x\dot{\psi}) dx, \quad (18)$$

with the following denotations:

- $\mu$ : Added mass
- $\int_{x_{max,\mu}}^L dx$ : Integration from the point of maximum added mass to the ship length
- $(v + x\dot{\psi})dx$ : Transverse velocity
- $\left( -\frac{\partial}{\partial t} + u \frac{\partial}{\partial x} \right)$ : Terms for the change of momentum with time and the convective change of momentum due to the longitudinal flow around the hull
- $K_{1,z_\mu}$ : Hydrodynamic roll moment with the vertical point of attack of the added mass

A few corrections have to be made. Regarding the disturbance of the parallel flow due to the flow around the ship ends the two corrections factors

$$k_1 = \sqrt{1 - 0.245\epsilon - 1.68\epsilon^2}, \quad (19)$$

$$k_2 = \sqrt{1 - 0.76\epsilon - 4.41\epsilon^2},$$

with the slenderness  $\epsilon$  two times the draft, are added, Lamb (1945)). The slender body approach doesn't determine the added mass in the x-direction, so the approximation

$$m_x = \frac{2.7\rho \Delta^{\frac{5}{3}}}{L}, \quad (20)$$

takes this into account. After integrating these additions, the force calculation results in the following formulae:

$$X_1 = -m_x \cdot \dot{u}, \quad (21)$$

$$Y_1 = k_1 \int_{x_{max,\mu}}^L \left( -\frac{\partial}{\partial t} + u \frac{\partial}{\partial x} \right) \mu \cdot (k_1 v + k_2 x \dot{\psi}) dx - m_x u \dot{\psi} \quad (22)$$

$$K_1 = -mgh + k_1 + \int_{x_{max,\mu}}^L \left( -\frac{\partial}{\partial t} + u \frac{\partial}{\partial x} \right) z_1 \mu (k_1 v + k_2 x \dot{\psi}) dx \quad (23)$$

$$N_1 = k_2 \int_{x_{max,\mu}}^L x \left( -\frac{\partial}{\partial t} + u \frac{\partial}{\partial x} \right) \mu \cdot (k_1 v + k_2 x \dot{\psi}) dx + m_x uv. \quad (24)$$

Further adjustments are made to consider effects in real fluid. This includes the longitudinal resistance  $R_t$ , where the non-dimensional maneuvering coefficients  $x_{vv}$ ,  $x_{vr}$  and  $x_{rr}$  are accounted for the additional resistance due to oblique flow. Furthermore, the additional forces and moment due to flow separation of the cross flow and the influence of the boundary layer should be taken into account. This leads to additional force components:

$$X_2 = R_t + x_{vv} v_s^2 + x_{vr} v_s \dot{\psi} + x_{rr} \dot{\psi}^2, \quad (25)$$

$$Y_1 = \frac{R_f(v + x_T \dot{\psi})}{u} - 0.5\rho \int_{x_{max,\mu}}^L (v + x\dot{\psi}) |v + x\dot{\psi}| c_D \cdot d \cdot dx \quad (26)$$

$$K_1 = -Y_2(ZCG - 0.65D), \quad (27)$$

$$N_1 = \frac{R_f L^2 \dot{\psi}}{6u} - 0.5\rho \int_{x_{max,\mu}}^L x(v + x\dot{\psi}) |v + x\dot{\psi}| c_D \cdot d \cdot dx, \quad (28)$$

with the following denotations:

- $R_f$ : Frictional resistance
- $\frac{(v+x_T \dot{\psi})}{u}, \frac{L^2 \dot{\psi}}{6u}$ : Influence of the boundary layer
- $c_D$ : Drag coefficient of the transverse flow around a ship section (see Brix (1993) or Lübcke (2019))
- $d, D$ : Local draft and draft above baseline
- $ZCG$ : Center of gravity in z-direction

**Propeller forces** - Propeller forces are determined by KT-KQ curves from model test or standard series. For controllable pitch propeller (CPP) a family of curves is given to account for every pitch angle. When operating in the first quadrant of the open water diagram, the propeller forces can be directly calculated by

$$X_{Prop.} = \rho n^2 D^4 k_t, \quad (29)$$

with  $n$  as the propeller revolutions,  $D$  as the propeller diameter and  $k_t$  as the propeller thrust coefficient from the open water diagram. In specific manoeuvres the propeller is operating in other quadrants, where measurements of the Wageningen B-Series are used for fixed pitch propellers (FPP). For CPPs operating in off-design conditions, different numerical calculations are used. A detailed description can be found in *Haack (2006)*. The wake and thrust deduction are taken from model test or vessels of comparison. In specific manoeuvres (e.g. Crash-Stop) the thrust deduction can deviate, so that in those cases adjustments are made, *Haack (2006)*. Effects on the propeller force due to cross flow are considered as explained in *Vorhölder (2011)*.



**Rudder Forces** - The rudder forces depend on the rudder angle, the inflow and the propeller load. To determine the rudder forces also considering the propeller-rudder interaction a panel method in combination with the lifting line method is used, *Carstensen (2019)*. The forces are calculated beforehand and are then interpolated. The cross flow, when turning or drifting, is influenced by the ship hull and is also considered, *Vorhölter (2011)*.

## B. Results

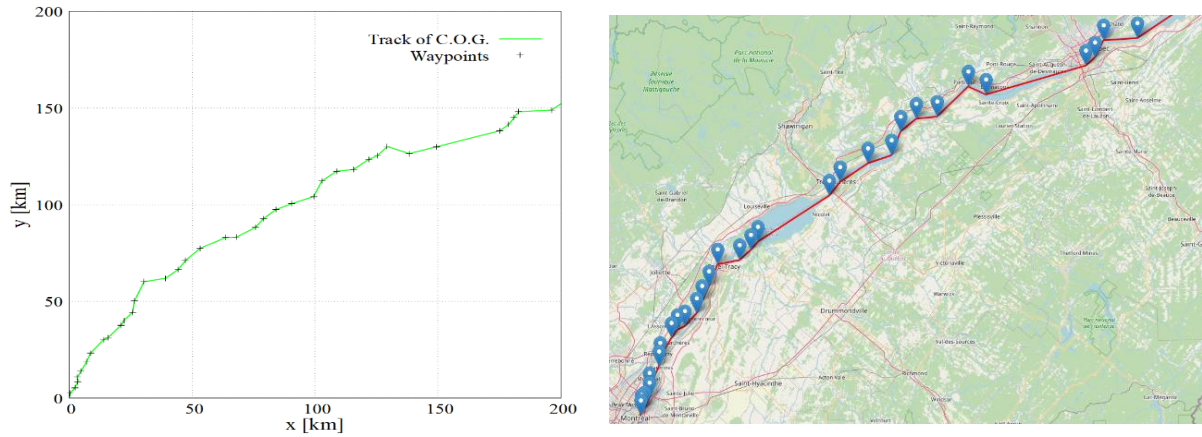


Fig.9: Sailed Route and Waypoints of the River Part

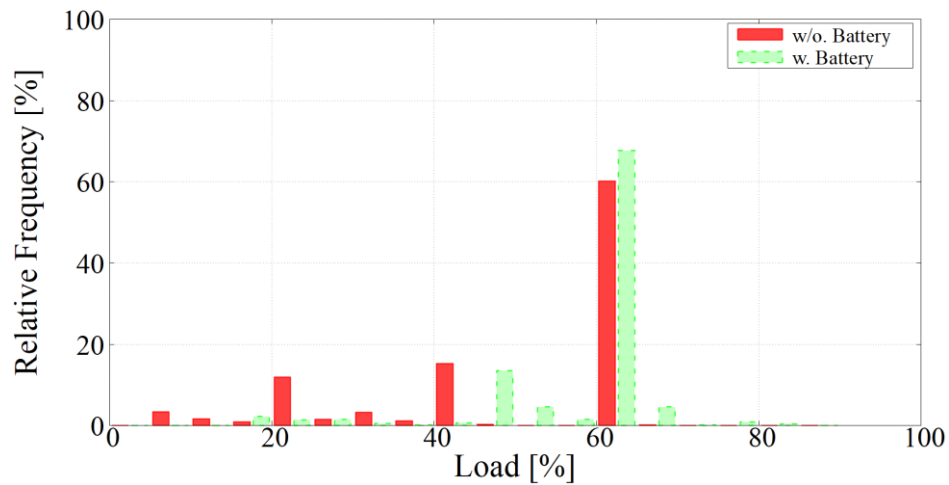


Fig.10: Histogram of the Engine Load With and Without Battery

## C. Ship Route Information

Table III: Waypoints and their Corresponding Target Ship Speed and Environmental Conditions

x [m]	y[m]	Speed [kn]	H <sub>1/3</sub> [m]	$\Psi_{\text{Wave}}$ [°]	T <sub>1/3</sub> [s]	V <sub>Wind</sub> [kn]	$\Psi_{\text{Wind}}$ [°]
435.8105	2493.580	11.00	0	0	0	3	250
2258.678	5355.056	13.00	0	0	0	3	250
3544.768	8468.957	14.00	0	0	0	3	250
3357.284	10833.33	14.00	0	0	0	3	250
4735.980	13784.35	14.00	0	0	0	3	250
6956.246	18591.66	16.00	0	0	0	3	250
8600.177	23165.50	16.00	0	0	0	3	250
13886.93	30108.48	16.00	0	0	0	3	250
15809.03	31267.04	16.00	0	0	0	3	250
21049.33	37695.69	16.00	0	0	0	3	250

22195.64	40020.82	16.00	0	0	0	3	250
25778.62	44420.44	12.00	0	0	0	3	250
26510.51	50222.93	12.00	0	0	0	3	250
30416.52	60156.73	11.00	0	0	0	3	250
39063.07	61915.69	15.00	0	0	0	3	250
44332.13	66446.68	17.00	0	0	0	3	250
47342.59	71202.19	17.00	0	0	0	3	250
53224.89	77444.95	17.00	0	0	0	3	250
63708.04	83053.92	15.00	0	0	0	3	250
67996.50	83213.84	17.00	0	0	0	3	250
75719.96	88233.13	17.00	0	0	0	3	250
79103.01	92886.11	17.00	0	0	0	3	250
84041.71	97473.19	17.00	0	0	0	3	250
90588.09	100584.2	17.00	0	0	0	3	250
99452.08	104222.8	15.00	0	0	0	3	250
102745.3	112270.4	15.00	0	0	0	3	250
108747.2	117316.5	15.00	0	0	0	3	250
115695.7	118265.7	15.00	0	0	0	3	250
121796.6	123464.4	15.00	0	0	0	3	250
125424.5	125406.1	13.00	0	0	0	3	250
129364.8	130072.9	13.00	0	0	0	3	250
138301.5	126443.6	18.00	0	0	0	3	250
149492.0	130018.4	18.00	0	0	0	3	250
175147.8	138267.9	15.00	0	0	0	3	250
178766.1	141485.3	13.00	0	0	0	3	250
180927.9	145002.0	11.00	0	0	0	3	250
182800.5	148102.1	12.00	0	0	0	3	250
196207.9	148987.9	15.00	0	0	0	3	250
205361.2	156773.5	19.00	0	0	0	3	250
215274.5	171528.0	19.00	0	0	0	3	250
231081.5	191895.7	19.00	0	0	0	3	250
292557.1	269279.4	19.00	0	0	0	3	250
389261.8	364153.9	19.00	0	0	0	3	250
510838.9	418413.8	21.00	0.25	105.7	2.13	3.5	254.4
626547.7	432387.6	21.00	2.12	133.15	5.17	1.4	165.9
701106.2	413056.6	21.00	2.46	144.21	5.16	5.26	105.1
775395.5	392719.0	21.00	2.04	145.87	4.75	7.15	139.7
851314.2	350494.3	21.00	3.07	147.92	5.71	7.51	166.5
926653.2	307247.9	21.00	1.96	157.07	4.77	4.8	213.4
1053321.	227433.0	21.00	0.76	144.98	3.21	7.05	167.5
1130432.	197010.6	21.00	0.74	148.6	3.16	4.2	166.8
1207138.	165583.8	21.00	0.43	140.35	2.53	8.39	221.7
1283431.	133173.0	21.00	0.11	102.13	1.63	9.47	227.2
1369912.	125583.2	21.00	0	0	0	9.85	216
1456276.	116757.7	21.00	0.11	32.2	1.63	8.99	211.6
1536846.	134169.6	21.00	0.53	28.16	2.91	11.39	202.2
1550248.	161818.6	21.00	0.28	18.64	2.21	11.39	202.2
1570417.	234175.5	15.00	0.13	357.17	1.25	10.97	185.5
1570042.	237437.5	13.00	0.13	357.17	1.25	10.97	185.5
1567174.	238739.9	11.00	0	0	0	4	185.5
1563428.	239578.1	11.00	0	0	0	4	185.5
1562744.	238966.1	11.00	0	0	0	4	185.5

# Fuel Cell Performance Evaluation under Ship Motions

**Panagiotis Manias**, University of Southampton/UK, [p.manias@soton.ac.uk](mailto:p.manias@soton.ac.uk)

**Dominic Hudson**, University of Southampton/UK, [dominic@soton.ac.uk](mailto:dominic@soton.ac.uk)

**Damon Teagle**, University of Southampton/UK, [daht@soton.ac.uk](mailto:daht@soton.ac.uk)

**Stephen Turnock**, University of Southampton/UK, [s.r.turnock@soton.ac.uk](mailto:s.r.turnock@soton.ac.uk)

## Abstract

*This paper examines the performance of fuel cells under various vessel motions, as they are believed to be a key decarbonisation agent within the marine industry. A series of testing protocols were developed, along with a high-resolution data acquisition system to examine the effect on fuel cell performance under expected sea states. These tests included a wide range of rotational and translational motions in low frequencies, simulating typical wave profiles expected to be encountered while at sea and were carried out on a methanol powered fuel cell, promoted as a battery preserver for marine applications.*

## 1. Introduction:

The current push within the shipping industry to decarbonise all activities by 2050, as set by MEPC 80, IMO (2023), requires significant changes in vessel design. Alternative fuels and consequently powertrains, are considered, relying on a “renewable energies-to-fuel” concept, that would eliminate our dependence on hydrocarbons and their associated Green House Gas emissions.

Fuel cells are believed to be the successor of internal combustion engines in the marine industry, due to the superior efficiency yield they can offer, their rather simple design and their capability of processing zero emission fuels such as pure hydrogen. Although their conception occurred in the late 19<sup>th</sup> century, Bossell (2000), it was only in recent decades that they have been employed either commercially in the automotive industry or in Aerospace, with most examples in the marine industry being auxiliary or supporting equipment, Tronstad *et al.* (2017). Needless to say, there is a long history of internal combustion engines serving as main propulsion engines and enduring ship motions, Molland (2008), but little is known about fuel cells and their response to these. Although most fuel cells need to comply with automotive industry standards, such as the ISO 12405:2 2012, these are in terms of road going behaviour where high frequency and low amplitude motions, meaning vibrations, are expected to be encountered, the exact opposite of what is experienced in ships travelling across the oceans.

As a result, a series of test protocols were developed, along with a high-resolution data acquisition system, to record and process all relevant parameters and results, to show what is the effect on fuel cell performance under expected sea states. These tests included a wide range of rotational and translational motions in low frequencies, simulating typical wave profiles expected to be encountered while at sea, and were carried out on a methanol powered fuel cell, promoted as a battery preserver for marine applications.

## 2. Fuel Cells for Marine applications

Current and most abundant form of energy convertors within the marine industry, are large, reciprocating internal combustion engines, that drive propellers either directly via a shaft or through reduction gearboxes, with some examples in the last decade employing generators for utilizing electric drive operation, Molland (2008) Fossil fuels make up the largest percentage of fuelling methods for the global vessel fleet, however, with the IMO constantly pushing towards the decarbonisation of all maritime activities, alternative fuel propositions are rising with the aim reaching zero or net zero emissions, Smith *et al.* (2021), as well as achieving higher powertrain efficiency to reduce consumption of costly fuels.

Both aims consist the main reason fuel cells are being considered for marine applications since apart from utilising zero emission fuels, fuel cells are inherently more efficient in converting the chemical power embedded within these fuels to electricity than internal combustion engines, Kistner *et al.* (2021), De-Troya *et al.* (2019), McKinlay *et al.* (2021). As a technology, fuel cells were first conceived more than a

century ago. They are electrochemical devices that operate by providing them with a fuel, most common being hydrogen, which reacts with oxygen ions to form water molecules through an ion-conducting electrolyte between the anode and cathode. Due to the ion formation, an electrochemical potential difference is induced within the system, which causes ions to travel through the electrolyte, as they are attracted to their ionic counterparts and form water, *NN (2000), Larminie et al. (2003)*.

Although fuel cells appear to be an ideal candidate for a transition towards a sustainable marine future, fuelled through renewable energy sources, they do come with their own disadvantages. One significant disadvantage is the requirement of a slower alteration of flow to avoid damage of the electrolytic structure, either by water droplet development or thermal damage, *Tang et al. (2010)*. On the contrary, due to the ability of continuously controlling and adjusting the air-fuel mixture entering the combustion chamber, to be combusted within milliseconds, engines can change their power output in response to fluctuating demands almost rapidly, *Khoa and Lim (2022), Taylor (1985)*. essential for coping with manoeuvring conditions and other emergency responses while the ship is underway. As a way to combat this, batteries are proposed to act as dampers against rapid peaks and drops in power demand, were quick discharging and charging can take place respectively, stabilising the fuel cells' power output, *McKinlay et al. (2021,2022), Manias et al. (2022)*.

Quick flow alteration is not the only damaging threat towards fuel cells in need of prevention. Vibration induction through the electrolyte can cause similar effects to its health, as well as negatively impact the flow of fluids within the entire system. So far, any type of certification for ensuring safe operation of fuel cells, is mostly for road applications such as the ISO standards 12405 and 23828, *ISO (2018,2022)*, and the IEC standard IEC 62282, *IEC (2022)*, which emphasize on high frequency and low amplitude motions, expected from the interaction of a vehicle rolling on a road, that would theoretically damage the electrolytes. Table I contains specifications of the standards discussed above.

Table I: Testing standards for fuel cells, *ISO (2018,2022), IEC (2022), Hooper and Marco (2016), SAE(2013)*

Standard	Other standards referencing this specification	Application level	Test frequency range (Hz)	Peak Grms for random PSD	Test duration per axis
<b>SAE J2380</b>	SAND 3123 UL 2580 USABC Procedure 10 (note SAE J2380 based on this standard)	Module and battery (in use for assessment of cells)	10 to 190 Hz	Z Axis profile 1: 1.9 & 0.75 Grms Z Axis profile 2: 1.9 & 0.75 Grms Z Axis profile 3: 1.9 & 0.75 Grms X & Y Axis Profile: 1.5 & 0.4 Grms	Z Axis Profiles 1, 2 and 3 conducted at 1.9 grms for 9 mins each. Z Axis Profiles 1, 2 and 3 conducted at 0.75 Grms for 5 hours and 15 mins each X and Y Axis Profile conducted at 1.5 grms for 10 mins and 48 seconds each X and Y Axis Profile conducted at 0.4 Grms for 38 hours each
<b>ISO 12405:2 2012</b>	None at time of writing	Module, battery (Cells tested to BS62660)	5 to 200 Hz	X axis profile: 0.96 Grms Underfloor Y axis profile: 0.96 Grms	21 hours per axis for 1 sample 15 hours per axis for 2 samples 12 hours per axis for 3 samples

				Z axis profile: 1.44 Grms	
<b>BS62660</b>	ISO 12405 -2	Cells	10 to 2000 Hz	2.83 Grms	8 hours per axis

Apart from the standards that companies must adhere to, for certifying safe operation on road vehicles, separate studies have also been conducted to investigate the effect of vibrations induced in the electrolyte. *El-Emam et al. (2015)* investigated the performance deterioration a PEM stack could have in terms of amplitude and frequency. Other studies investigate the deterioration of the membrane including the anodes and cathodes of a PEM cell as a result of pinhole formations that end up poisoning the electrolyte, *Schmittinger and Vahidi (2008)*. Moreover, vibrations also effect the formation of water molecules in the membrane that can also have a performance effect, *Chen et al. (2009)*. When it comes to studies conducted with regards to the marine environment, the most relevant one is a recent study specific to vibrations induced through a ship's hull. Once again, it was indicated that the influence of ship vibration on the gas transfer characteristics in the PEMFC varies in the direction of the vibration, with the vertical vibration having the most significant influence. Therefore, during actual ship operation and installation, the PEMFC should avoid vibrations perpendicular to the flow channel as much as possible, *Wen et al. (2022)*. Further relevant studies have been completed, during the time experiments were conducted and discussed in this paper, looking at the influence of ship motion on SOFCs, yet these were carried out with a low magnitude of acceleration in mind, typical of what would be expected in large vessels, *Veldhuizen et al. (2023)*.

Consequently, the purpose of this paper is to emphasize on the importance of establishing Fuel Cell testing standards for a wide range of marine applications, which would not only be in terms of inclination but also in terms of rapid, large amplitude accelerations expected from high-speed crafts, to ensure steady and reliable performance from an FC powertrain.

### 3. Experimental Set-Up

The purpose of the experiments discussed in this paper, was to develop a series of testing specific to the motion behaviour expected to find in a vessel travelling across the ocean during rough weather. The motions meant to be replicated have been recorded in the form of angular and linear displacements from a platform floating in the ocean. These motions were then converted into a digital file capable to be processed by the University of Southampton's six degree of freedom "Shaker" platform. Due to magnitude limitations imposed by the machine, the motions were limited in linear displacement while the angular motions were still in maximum displacement. Separate linear motion experiments were also carried out to isolate the influence of lateral acceleration on the fuel cell stack with a maximum acceleration magnitude of 0.6 g. Finally, a combination of both linear and angular motion experiments was carried out which would be the closest representation of motion experienced on board.

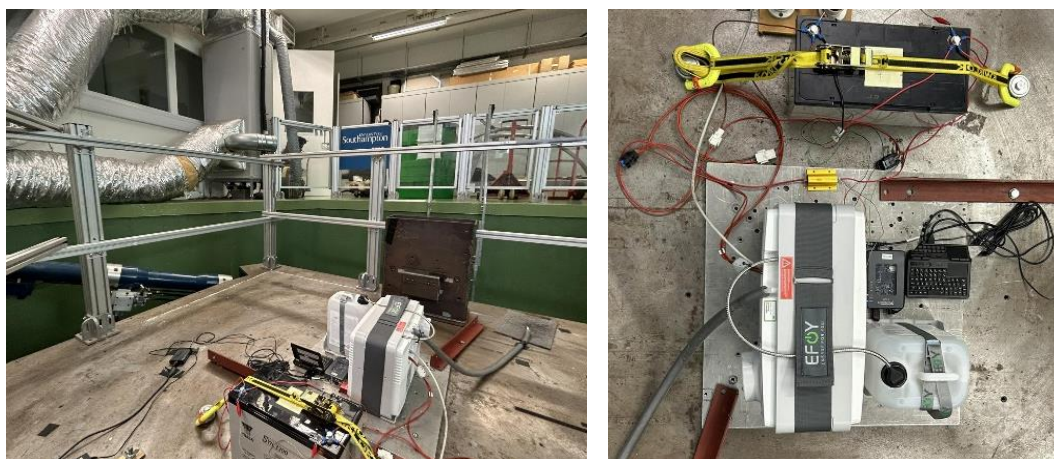


Fig.1: View of fuel cell experiment Set-Up of Shaker (Left) and equipment (Right)



The main plate holding the fuel cell, the data acquisition system and the fuel tank can be seen in Fig.1. This plate was mounted at either the centre of the Shaker's point of rotation or off centred, depending on the type of the experiment taking place. The battery was mounted outside of the main fuel cell holding plate, as the system used to tie it down on the shaker platform, was reinforced due to its heavy mass.

The equipment used to record the charging power output of the fuel cell was mainly comprised by a myRio Module, recording amperage and voltage with the use of a 0.1 Ohm resistor and a potential divider, as well as translational accelerations ( $\text{m/s}^2$ ) in all axes, with an acquisition frequency of 100hz. A secondary IMU was mounted to measure roll, pitch and yaw for the off-centred experiments that took place on the shaker, with all data recorded on a micro-PC.

The equipment used to record the charging power output of the fuel cell was mainly comprised by a myRio Module, recording amperage and voltage with the use of a 0.1 Ohm resistor and a potential divider, as well as translational accelerations ( $\text{m/s}^2$ ) in all axes, with an acquisition frequency of 100 Hz. A secondary IMU was mounted to measure roll, pitch and yaw for the off-centred experiments that took place on the shaker, with all data recorded on a micro-PC.

Finally, the post processing of data collected, involved a significant amount of filtering to remove noises from all the sensors, mainly with fast Fourier transforms, in order to isolate the charging power output of the fuel cell from any “noise” contained within the signal, either through main electrical sources, the battery or micro vibrations induced through the platform.

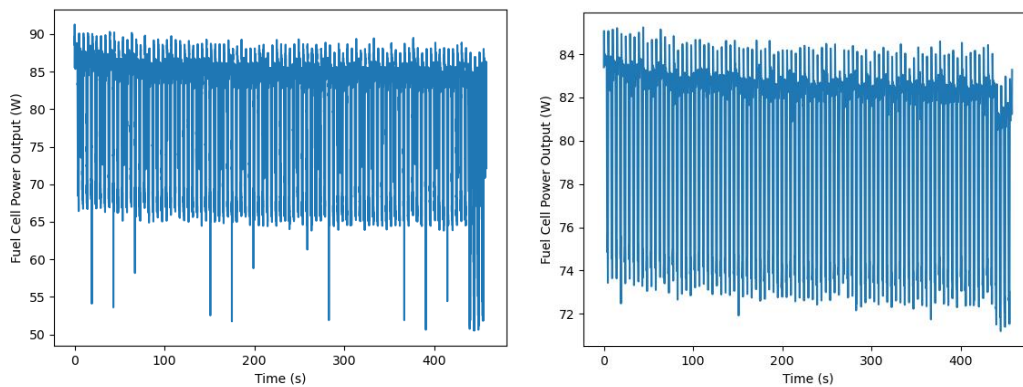


Fig.2: Example of stationary fuel cell charging output unfiltered (left) and filtered (right)

#### 4. Ship Motion Samples

Ship motion experienced on board, is a complicated phenomenon resulting from the influence of waves on the ship's hull, experiencing movement through all six degrees of freedom. These motions can be represented in terms of acceleration either linear or angular can vary greatly from between vessel types, due to the marine industry accommodating many ship designs for the different applications required.

It would be expected from larger ships to provide greater resilience towards accelerations experienced on board, as their inertia is far greater and can overcome that of waves, when compared to significantly smaller high-speed crafts. Nonetheless, for this case study, two samples were taken; one of a model-scale test with regards to a survey vessel out in the open ocean during rough weather, travelling at 16 knots and the other from a high speed craft traveling at 30 kts in the calm waters of the Mediterranean during summer season, Fig.4, both as “extreme” scenarios and possible candidates for fuel cell powertrain employment.

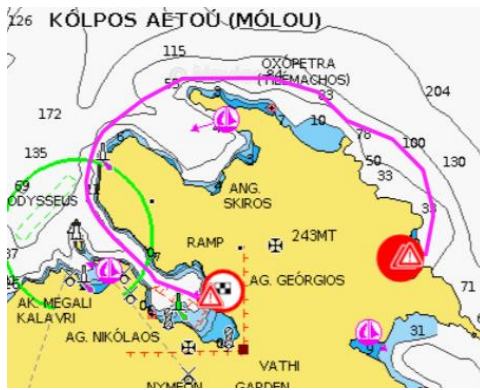


Fig.3: Sample speedboat Course on navigation map, <https://webapp.navionics.com/>

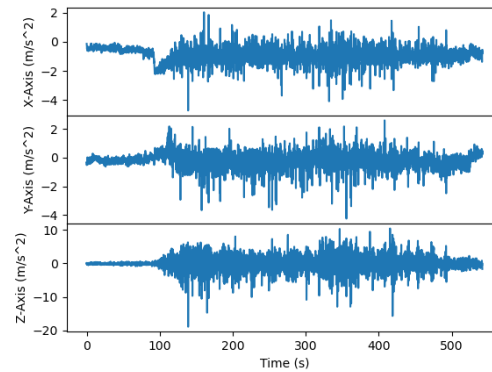


Fig.4: Subsequent vibration experienced

## 5. Fuel Cell Operational Characteristics

The fuel cell used in the experiments, is a typical example of a product marketed for battery preservers on board large recreational boats or motorhomes. This particular fuel cell is a direct methanol fuel cell (DMFC) meaning its primary fuel source is Methanol, which is then internally reformed to hydrogen, with the by-products of this reformation process being water and  $\text{CO}_2$ , *Johee et al. (2015)*. Although this particular fuel cell solution is not zero emission, it still represents an example of this technology in certain marine applications, which does fulfil the international standards expected for portable applications (IEC 62282-5), hence, makes an excellent example for investigating potential issues rising when used in marine applications.

For setting a basis, it was required to record both battery and voltage output of the fuel cell, for an extensive period of time. As such, a 2-hour recording was acquired, whilst the fuel cell was in charging mode and stationary. As observed in Fig.5, the fuel cell in question is designed to have small interruptions during charging mode, to protect the battery and itself from extensive service, which takes place every 15 minutes, while at the same time it slightly discharges the battery to commence with its inner power sustaining operations. It is also clear how in the first hour of testing, there are frequent drops in power, while after the first hour these drops are irregular and further apart. This sample is essential for explaining random drops in power witnessed during the shaker runs, in later figures, to prove whether these occurrences were a result of extreme motion “sickness” or power output irregularities occurring at random.

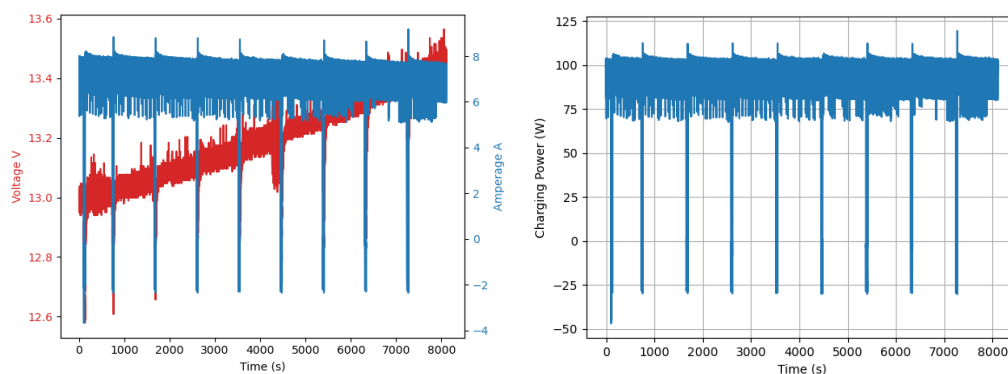


Fig.5: Voltage and amperage of fuel cell against time (left), and charging power output (right)

At the same time, another shorter recording of 300 s is presented, where the fuel cell is stationary and in charging mode, shown in Fig.6. This is used as a comparison for the time extended tests that took place later, simulating rough seas for a survey vessel, with the average time being 150 s. An important thing to note in Fig.6, is that the total average power from the beginning of the recording till the end, is reduced by 0.1%, which is expected due to the battery’s total level of charge rising. Also, within the same figure,

it appears that the charging output signal is in a pulse wave form with a mean variation of 14.7% of the total power output. This percentage of power output variation is significant and must be taken into consideration for when employing a similarly designed fuel cell.

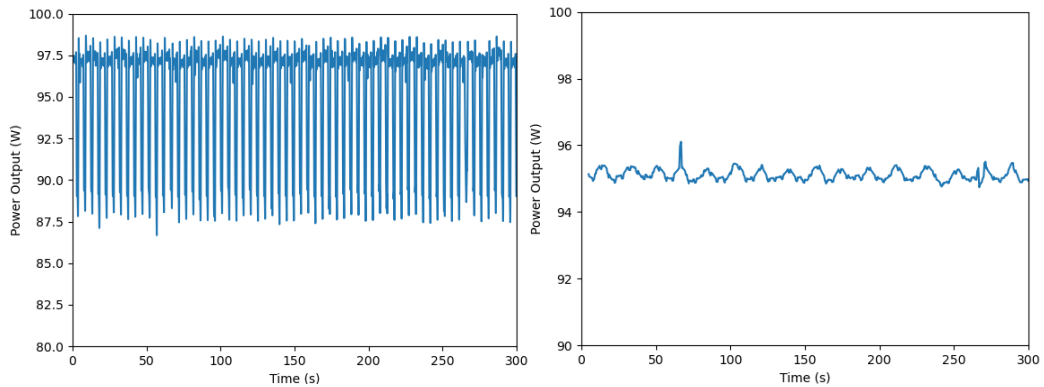


Fig.6: 300s recording of Fuel cell charging, stationary (left) and average output (right)

## 6. Experiments

### 6.1. Initial Testing

The initial testing procedures involved obstruction of the exhaust flow, rapid motion of the methanol fuel tank and simple lift-up tests of the entire assembly, to see the overall short-term reliability of the system in terms of its accessories. As seen in Fig.7, any obstruction of the exhaust flow, possibly due to the collection of water, can lead to partial complete loss of power, depending on the amount of exhaust flow reduction.

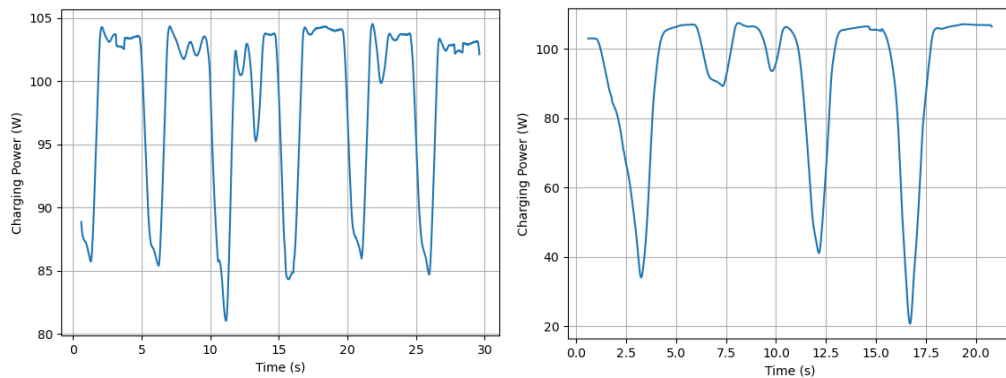


Fig.7: Exhaust pipe partial obstruction occurring in 10 s (left), complete flow obstruction due to water collection (right).

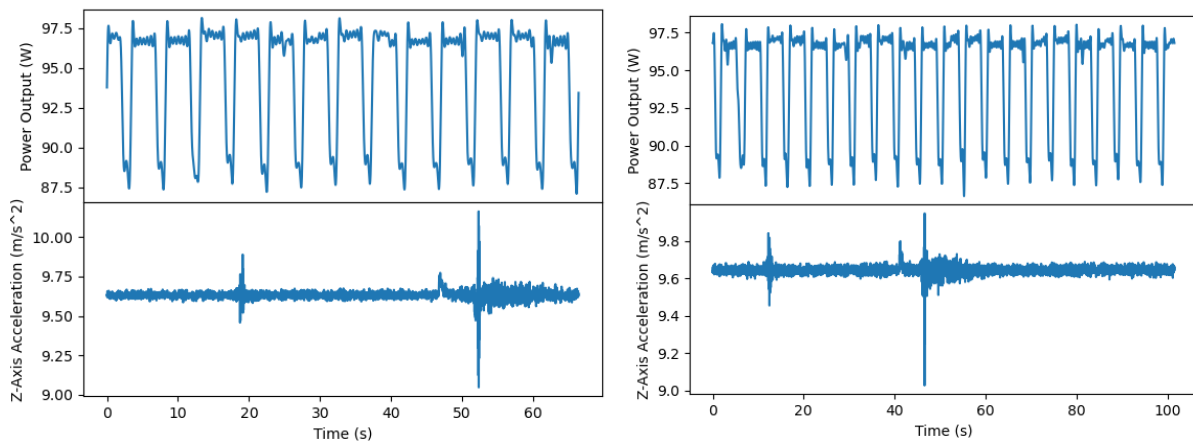


Fig.8: Platform Lift-Up response 1st run (Left) and 2nd run (Right)

When it comes to altering the flow of fuel, it appears that no issues arise by shaking the fuel tank, since this particular fuel cell collects the tank's vapour by vacuuming it with an internal pump. Finally, the entire fuel cell set-up, as observed in Fig.1, was quickly lifted up, in preparation for carrying out the rest of the shaker experiments, shown in Fig.8. Based on Fig.8, the acceleration induced on the fuel cell whilst the shaker platform is being lifted from its resting position to its centre of motion, with  $9.81 \text{ (m/s}^2\text{)}$  being the gravitational potential (g) at this geological point, has no effect on the charging power output, indicating the need for higher magnitude of acceleration motions, through different axes.

## 6.2. Isolated X-Y-Z Axis motion tests

The purpose of these tests was to isolate the axis that appears to have the biggest effect on fuel cell performance. Based on the relevant literature that has been reviewed, it appears that the vertical Z-Axis on fuel cells, is the one that has the most significant effect on fuel cell performance, however, it is still worth exploring this, especially when selecting the appropriate space on which the fuel cells should be mounted on board, where it could be more susceptible to a specific axis acceleration.

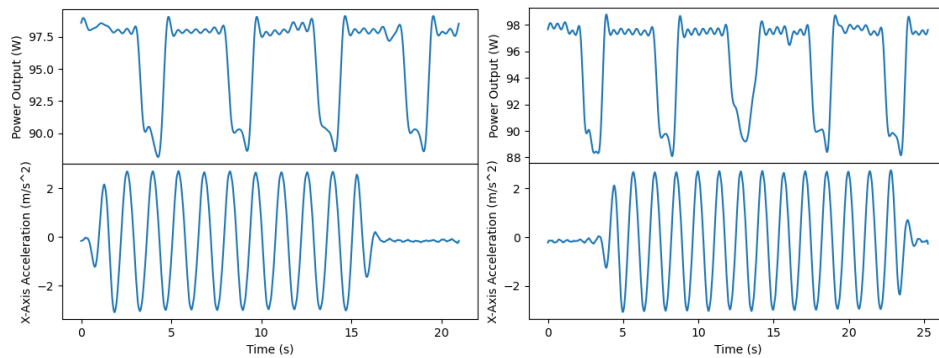


Fig.9: X-Axis 150 mm amplitude and 0.7 Hz motion 1st run (left) and 2nd run (right)

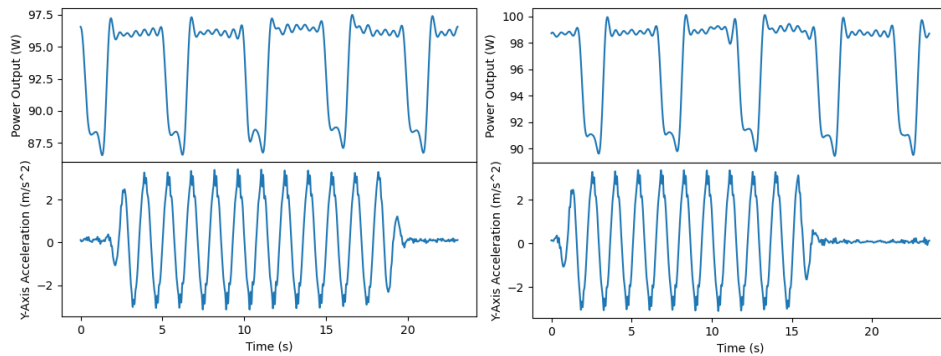


Fig.10: Y-Axis 150mm amplitude and 0.7 Hz motion 1st run (left) and 2nd Run (right)

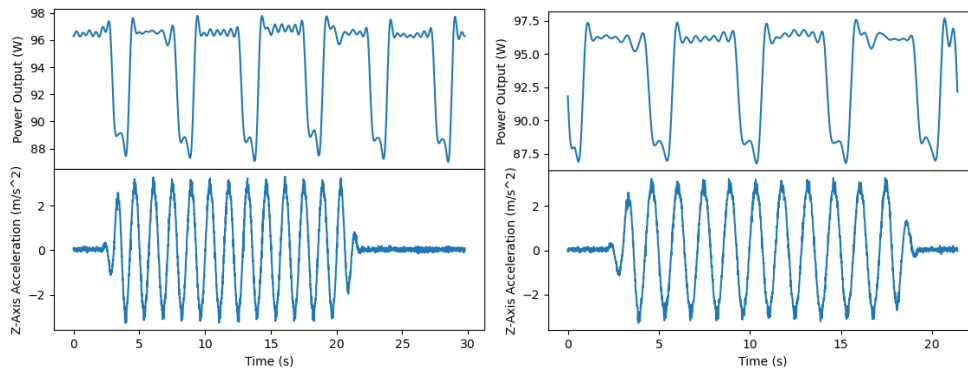


Fig.11: Z-Axis 150 mm amplitude and 0.7 Hz motion 1st run (left) and 2nd run (right)

With a maximum displacement of 30cm and a motion frequency of 0.7 Hz, the maximum magnitude of acceleration experienced in all axes, was  $2 \text{ m/s}^2$  and as can be clearly derived from Figs.9-11, the fuel cell charging power output is not affected. This led to further tests, trying to reach the limit of maximum acceleration that both the shaker platform and the fuel cell unit can sustain, while keeping in mind that the maximum acceleration experienced on board the speedboat, instantaneously reached  $18 \text{ m/s}^2$ . As such, more experiments were carried out, close to the shaker's limit of acceleration, being  $6 \text{ m/s}^2$ , by increasing the motion's displacement and frequency to 48 cm and 1.5 Hz respectively, Figs.12-14.

Considering Figs. 12-14, the maximum acceleration experienced by the fuel cell set up is  $5.5 \text{ m/s}^2$ , yet there is no significant effect on performance apart from the Z-axis displacements. As seen in Figs.14 and 15, one can observe that the fuel cell output is decreasing exactly after the motions initiate and then comes back to its original state, after the motions stop, with the average power output for that time interval being shown in Fig.15. The power drop occurring during the time these extreme motions take place, is in the magnitude of 1-0.5%, hence they can be assumed as negligible.

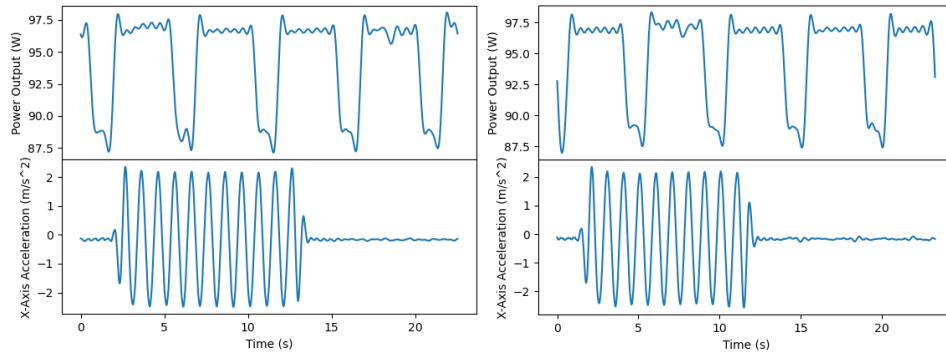


Fig.12: X-Axis 240 mm amplitude and 1 Hz motion, 1st run (left) and 2nd run (right)

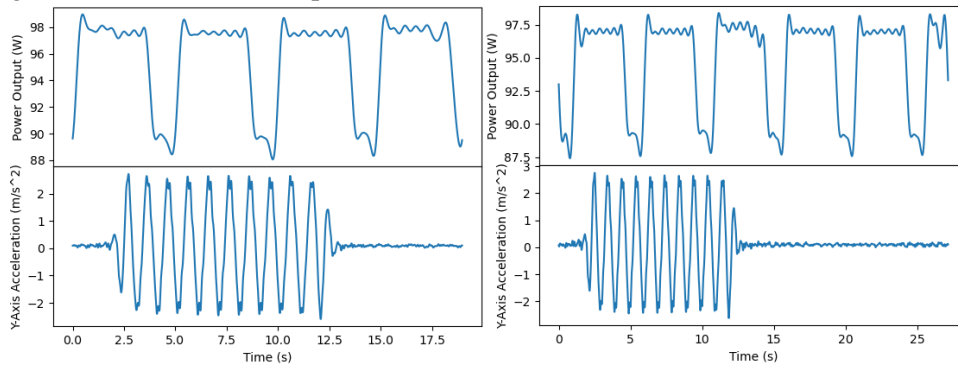


Fig.13: Y-Axis 240mm amplitude and 1 Hz motion, 1st run (left) and 2nd run (right)

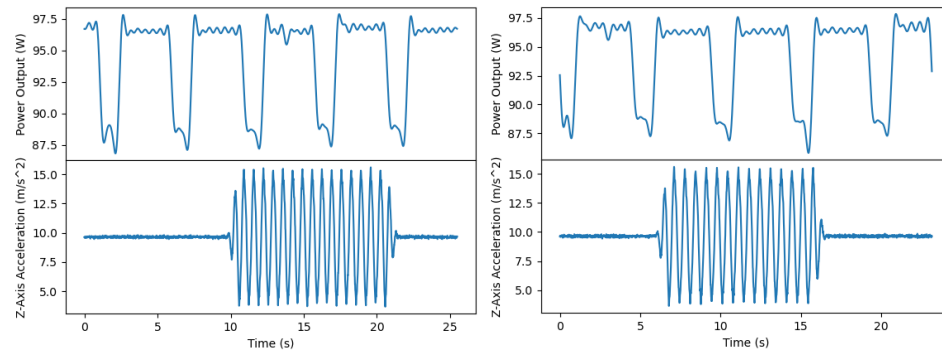


Fig.3: Z-Axis 240mm amplitude and 1.5 Hz motion, 1st run (left) and 2nd run (right)



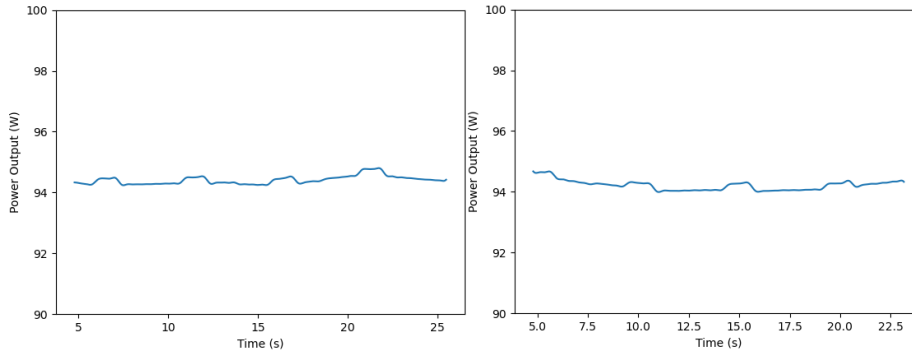


Fig.15: Average Power output with Z-Axis 240 mm amplitude and 1.5 Hz motion, 1st run (left) and 2nd run (right)

### 6.3.Short Linear Acceleration Tests

As a representation of calm weather sailing, the following Figs.16 and 17, are an indication of any implication arising from a sudden encounter of a passing-by wake, to see whether sudden acceleration could theoretically upset the flow of the fuel cell, either instantaneously or with a certain delay. Of course, it makes sense that these tests are carried out only with respect to the Z-Axis, not only because of the results shown in Figs.12-14 but also as it is the expected response from when encountering a wake by a highspeed craft, shown in Fig.3. Fig.16 represents a sudden wake encounter, forcing a  $2 \text{ m/s}^2$  acceleration on the fuel cell's Z-Axis.

There is no effect on the fuel cell's power output at such magnitude of acceleration, Fig.16, and it is also confirmed in Fig.17, where the same approach of sudden motion at 24 cm amplitude and 0.4 Hz frequency, offering higher acceleration, yields the same result.

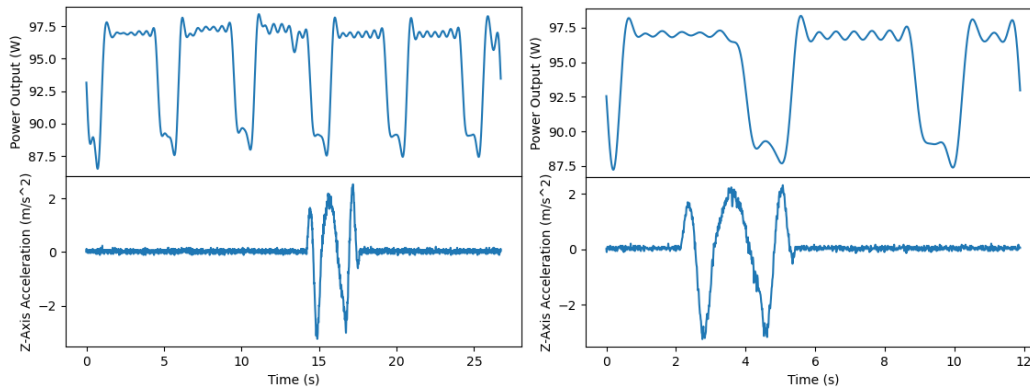


Fig.16: Power output with Z-Axis 200mm amplitude and 0.5 Hz random motion, 1st run (left) and 2nd run (right)

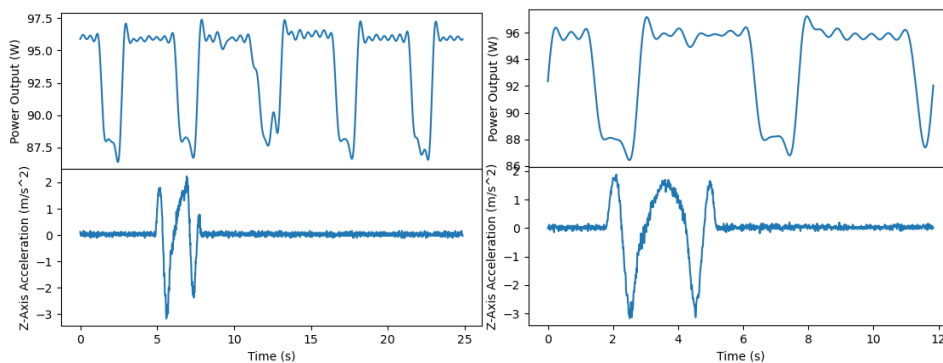


Fig.47: Power output with Z-Axis 240 mm amplitude and 0.4 Hz random motion, 1st run (left) and 2nd run (right)

#### 6.4. Open Sea motion simulation

These tests are based on the initial data sets which are relevant to motions encountered at during strong weather out in the open sea, which were downscaled to meet the shaker platform's displacement limits. Consequently, motions in all 6 degrees of freedom are included which required the use of a second inertia measuring unit to record acceleration of roll, pitch and yaw. Three tests are used as an illustration of the expected acceleration profiles, along with the fuel cell's response, containing different motion profiles.

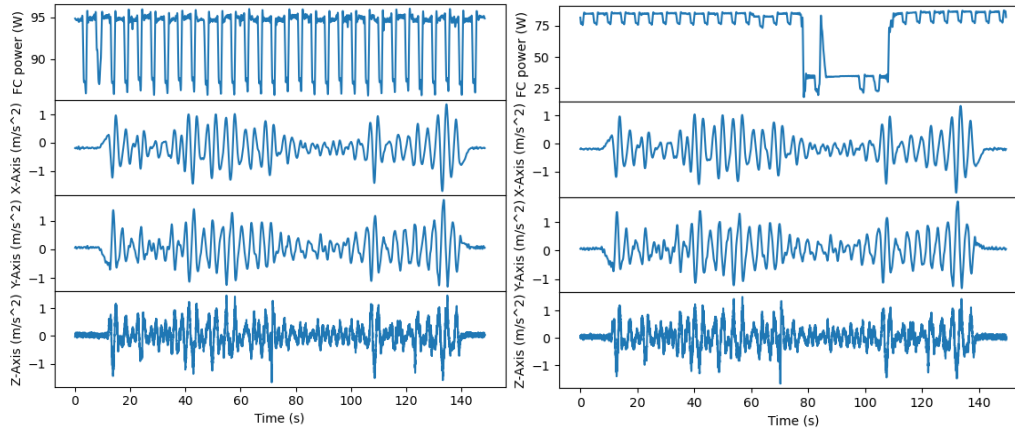


Fig.18: Power output during wave test R8\_490, 1st run (left) and 2nd run (right)

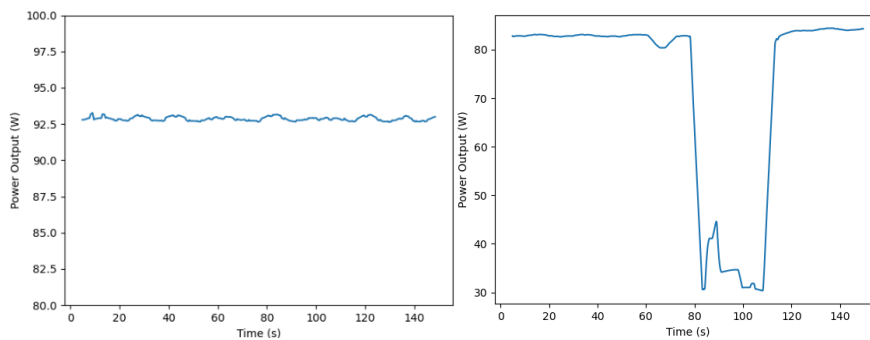


Fig.19: Average Power output during wave test R8\_490, 1st run (left) and 2nd run (right)

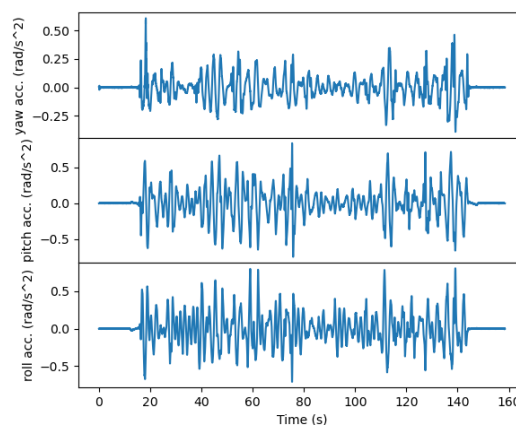


Fig.205: R8-490 test roll, pitch and yaw angular acceleration profile

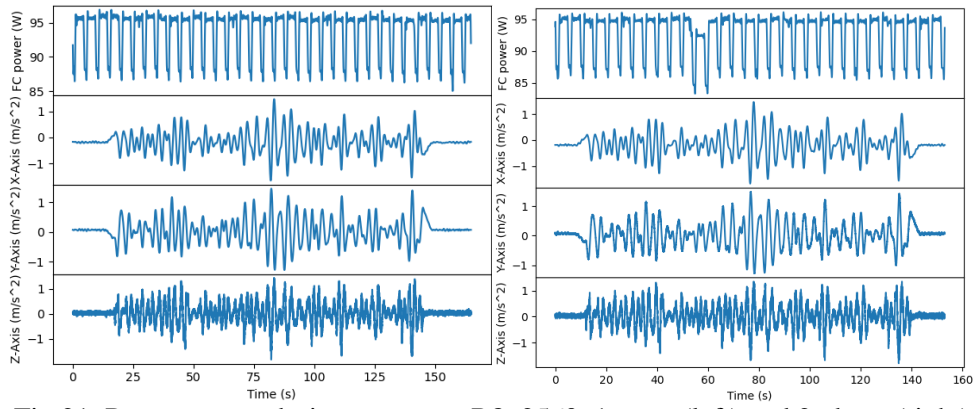


Fig.21: Power output during wave test R8\_2560, 1st run (left) and 2nd run (right)

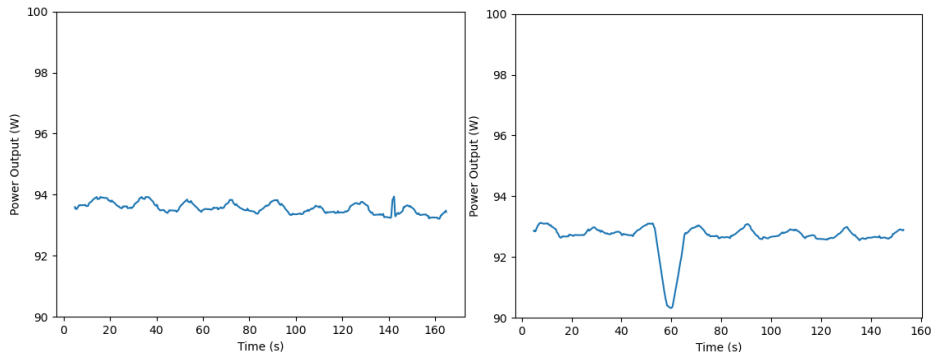


Fig.62: Average Power output during wave test R8\_2560, 1st run (left) and 2nd run (right)

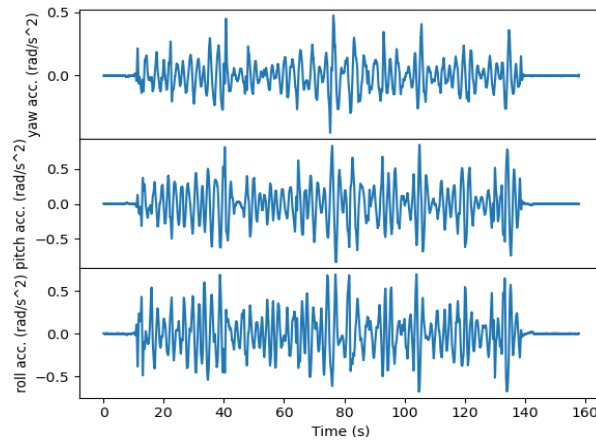


Fig.23: R8-2560 test roll, pitch and yaw angular acceleration profile

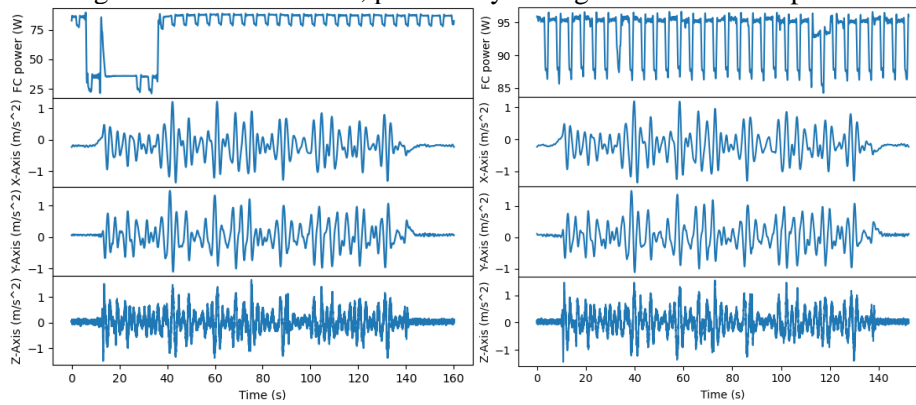


Fig.24: Power output during wave test R8\_3710, 1st run (left) and 2nd run (right)

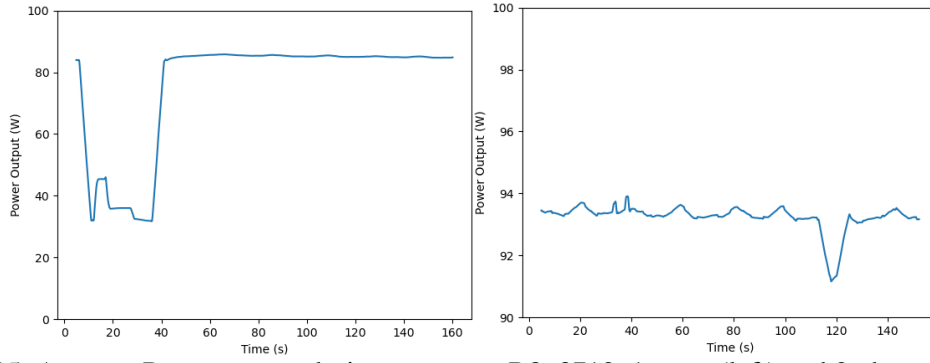


Fig.25: Average Power output during wave test R8\_3710, 1st run (left) and 2nd run (right)

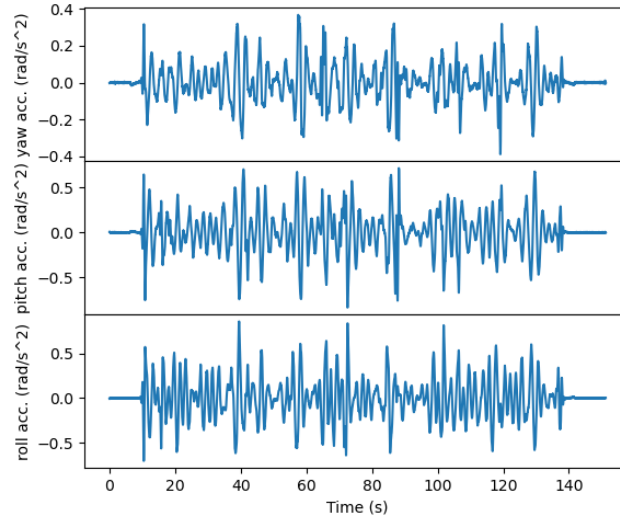


Fig.76: R8-3710 test roll, pitch and yaw angular acceleration profile

Initial simulations of the wave profile experienced on the survey vessel, showed there is no change in the fuel cell's power output, apart from the "routine" shut-down of the fuel cell for battery preservation and inner monitoring. These shutdowns are witnessed in Figs.19 and 25. On the other hand test R8\_2560 showed a repeated decline of the total power output higher than that of steady state (0.1%), which was 0.5%. Although the number is insignificant in terms of the total charge output, it can confirm that there is an effect on fuel cell performance under sustained fuel cell motion.

Moreover, both tests R8\_2560 and R8\_3710 showed a rapid drop of approximately, 3% with respect to the average total power output. Yet, due to the failure of repeating this within a short time domain, they can be considered as part of the expected performance behaviour of this particular fuel cell set-up, observed in Figs.5 and 6. Finally, all R8 tests indicated that linear accelerations can have a higher effect on fuel cell performance than angular accelerations, with test R8\_2560 having the lowest average magnitude of angular acceleration but yielding the highest electrical output degradation.

## 7. Discussion

Considering the testing results presented in the previous section, it seems that the particular fuel cell set up, tested against various ship motions, is quite resilient, yet indeed affected by motion. With accelerations lower than the maximum limit of the testing equipment used, any change witnessed in the fuel cell performance, is a result of its own operational characteristics. Initial figures shown, such as Figs.5 and 6, indicate large fluctuations of the fuel cell's charging output even when stationary, either due to the internal reforming taking place, the inconsistent flow characteristics of the vapour fuel pump, or the formation of water droplets as indicated by the literature review.

Regardless of the motion testing taking place, such a discrepancy in power output should be taken into consideration when developing marine powertrains, but preferably avoided. Although expected for this particular fuel cell, intended to be used as a battery preserver, a supercapacitor or a battery to manage these fluctuations, along with a power management system, should be employed. The utilisation of different design fuel cells which provide “steadier” electrical output would be preferred, yet such a design could be proven to be inherently more sensitive to any motions experienced on board, which constitutes a reason for establishing marine testing standards.

The tests conducted, although slightly more ambitious in terms of the acceleration profiles experienced on board large commercial vessels, they are still nowhere near the ones expected from small, high-speed crafts. Limitations of the testing equipment used in this case, did not allow for achieving the maximum acceleration magnitude recording of  $18 \text{ m/s}^2$  as per the recording collected. Undoubtedly, when considering inter-island links facilitated by highspeed ferries that need to be fully operational across all seasons and weather circumstances, the fuel cells used on board as an agent towards decarbonisation, should be capable of maintaining a steady power output without interruptions. Consequently, further work needs to be conducted as part of establishing standards for the many different types of fuel cells and applications they are meant for, which might require harsher accelerations than what has been tested and published up to this point.

Finally, all tests described in this paper, emphasize on the short-term outcomes of ship motion and not the longer-term reliability concerns that might arise from this exposure. Equipment reliability is crucial whilst sailing in a remote location, hence, it is suggested as part of developing future standards for fuel cell marine powertrains, to examine long term performance degradation as a result of vessel vibrations and motion, depending on the application they are intended for.

## **8. Conclusion**

The purpose of this paper and relevant experimental study was to examine the effects of different types of ship motion upon fuel cell performance. Due to the lack of relevant standards with regards to fuel cells for marine applications, it was deemed important to develop fuel cell performance monitoring equipment as well as relevant motion tests based on data acquired from a large survey vessel and a high-speed craft in different weather conditions.

The fuel cell tested in this case, is promoted as a battery preserver by its manufacturer and this was reflected when a recording of it charging output showed significant fluctuations, as expected for its intended purpose, yet unacceptable for when used as main powering equipment on board vessel. Results from the subsequent testing, showed that the fuel cell’s charging output profile was still within 1% of what was expected to be, whilst stationary, yet there was enough evidence to indicate a relation between motion and fuel cell performance.

Due to the equipment limitations, the full magnitude of the acceleration profiles experienced was unable to be induced upon the fuel cell. Moreover, the testing emphasizes on short term effects caused by the relevant ship motion, which do not necessarily translate to long term reliability. Consequently, future work is recommended on carrying out tests of higher acceleration magnitude for different types of fuel cells, while at the same time repeating these tests or prolonging them to witness any probable causes and modes of failure.

## **Acknowledgements**

This research was conducted as part of the Clean Maritime Demonstration Competition (competition code 2103\_DFT\_CMD\_S1), funded by the Department for Transport and delivered in partnership with Innovate UK.



## References

- BOSSELL, U. (2000), The birth of the Fuel Cell 1835–1845, European Fuel Cell Forum
- CHEN, S.; WANG, X.; ZHU, T.; XIE, X.F. (2019), *Interaction of Vibration and Air Flow-Accelerating Droplet Emission from the Gas Diffusion Layer of Proton Exchange Membrane Fuel Cell*, Int. J. Photoenergy, Vol. 2019
- DE-TROYA, J.J.; ÁLVAREZ, C.; FERNÁNDEZ-GARRIDO, C.; CARRAL, L. (2016), *Analysing the possibilities of using fuel cells in ships*, Int. J. Hydrogen Energy, pp.2853-2866
- EL-EMAM, S.H.; MOUSA, A.A.; AWAD, M.M. (2015), *Effects of stack orientation and vibration on the performance of PEM fuel cell*, Int. J. Energy Research 39/1, pp. 75-83
- HOOPER, J.M.; MARCO, J. (2016), *Defining a Representative Vibration Durability Test for Electric Vehicle (EV) Rechargeable Energy Storage Systems (RESS)*, World Electric Vehicle J. 8/2, pp.327-338
- IEC (2022), *IEC 62282-4-102:2022 RLV "Redline version" Fuel cell technologies*, Int. Electrotechn. Commission, <https://webstore.iec.ch/publication/81113>
- IMO (2023), *2023 IMO Strategy on Reduction of GHG Emissions from Ships*, Int. Mar. Org., London, <https://www.imo.org/en/MediaCentre/PressBriefings/pages/Revised-GHG-reduction-strategy-for-global-shipping-adopted-.aspx>
- ISO (2018), *ISO 12405-4:2018 Electrically propelled road vehicles*, Int. Stand. Org., Geneva, <https://www.iso.org/standard/71407.html>
- ISO (2022), *ISO 23828:2022 Fuel cell road vehicles*, Int. Stand. Org., Geneva, <https://www.iso.org/standard/78416.html>
- JOGHEE, P.; MALIK, J.N.; PYLYPENKO, S.; O'HAYRE, R. (2015), *A review on direct methanol fuel cells–In the perspective of energy and sustainability*, MRS Energy & Sustainability 2, p.E3
- KHOA, N.X.; LIM, O. (2022), *Influence of Combustion Duration on the Performance and Emission Characteristics of a Spark-Ignition Engine Fueled with Pure Methanol and Ethanol*, ACS Omega 7/17, pp.14505-14515, <https://pubs.acs.org/doi/10.1021/acsomega.1c05759>
- KISTNER, L.; SCHUBERT, F.L.; MINKE, C.; BENSMANN, A.; HANKE-RAUSCHENBACH, R. (2021), *Techno-economic and Environmental Comparison of Internal Combustion Engines and Solid Oxide Fuel Cells for Ship Applications*, J. Power Sources 508
- LARMINIE, J.; DICKS, A.; McDONALD, M.S. (2003), *Fuel cell systems explained*, J. Wiley
- MANIAS, P.; McKINLAY, C.J. TURNOCK, S.; HUDSON, D. (2022), *Performance optimisation of solid oxide fuel cells through waste heat recovery systems for marine applications*, Int. Conf. Computer Applications in Shipbuilding (ICCAS), Yokohama
- McKINLAY, C.J.; TURNOCK, S.; HUDSON, D. (2021), *Fuel Cells for Shipping: To meet on board auxiliary demand and reduce emissions*, Energy Reports 7, pp.63-70
- McKINLAY, C.J.; MANIAS, P.; TURNOCK, S.; HUDSON, D. (2022), *Dynamic modelling of ammonia crackers and hydrogen PEM fuel cells for shipping applications*, Int. Conf. Computer Applications in Shipbuilding (ICCAS), Yokohama

MOLLAND, A.F. (2008), *Chapter 6 - Marine engines and auxiliary machinery*, in *The Maritime Engineering Reference Book*, Butterworth-Heinemann, pp.344-482

NN (2000), *Fuel Cell Handbook*. DIANE Publishing

SAE (2013), *SAE J2380: Vibration Testing of Electric Vehicle Batteries*, S. o. A. E. SAE

SCHMITTINGER, W.; VAHIDI, A. (2008), *A review of the main parameters influencing long-term performance and durability of PEM fuel cells*, *J. Power Sources* 180/1, pp.1-14

SMITH, T.; BAREŠIĆ, D.; FAHNESTOCK, J.; GALBRAITH, C.; PERICO, C.V.; ROJON, I.; SHAW, A. (2021), *A strategy for the transition to zero-emission shipping*, Global Maritime Forum, <https://www.globalmaritimeforum.org/publications/a-strategy-for-the-transition-to-zero-emission-shipping>

TANG, Y.; YUAN, W.; PAN, M.; LI, Z.; CHEN, G.; LI, Y. (2010), *Experimental investigation of dynamic performance and transient responses of a kW-class PEM fuel cell stack under various load changes*, *Applied Energy* 87/4, pp.1410-1417, doi: <https://doi.org/10.1016/j.apenergy.2009.08.047>

TAYLOR, C.F. (1985), *Internal Combustion Engine in Theory and Practice, revised, Volume 2: Combustion, Fuels, Materials, Design*, MIT Press

TRONSTAD, T.; ÅSTRAND, H.H.; HAUGOM, G.P.; LANGFELDT, L. (2017), *Study on the use of fuel cells in shipping*, DNV, <https://www.emsa.europa.eu/publications/download/4545/2921/23.html>

VELDHUIZEN, B.; ZERA, E.; VAN BIERT, L.; MODENA, S.; VISSER, K.; ARAVIND, P.V. (2023), *Experimental Evaluation of a Solid Oxide Fuel Cell System Exposed to Inclinations and Accelerations by Ship Motions*, [https://papers.ssrn.com/sol3/papers.cfm?abstract\\_id=4514087](https://papers.ssrn.com/sol3/papers.cfm?abstract_id=4514087)

WEN, X.F.; QIU, Y.; ZHAN, Z.G.; XIAO, L.S. (2022), *Investigation of Ship Vibration Effects on the Gas Distribution and Output Voltage of a Proton Exchange Membrane Fuel Cell*, *ACS Omega* pp.20569-20583

# Towards Zero-Emission Cruise Shipping

**Ivana Melillo**, MSC Cruise Management (UK) Limited, [ivana.melillo@msccm.co.uk](mailto:ivana.melillo@msccm.co.uk)  
**Angela Craciun**, MSC Cruise Management (UK) Limited, [angela.craciun@msccm.co.uk](mailto:angela.craciun@msccm.co.uk);  
**Kenneth Widell**, Wartsila Fi, [kenneth.widell@wartsila.com](mailto:kenneth.widell@wartsila.com)  
**Alexandra Widelund**, Climeon AB, [alexandra.widelund@climeon.com](mailto:alexandra.widelund@climeon.com)  
**Arno Dubois**, Silverstream Technologies, [arno.dubois@silverstream-tech.com](mailto:arno.dubois@silverstream-tech.com)  
**Jan Kelling**, HASYTEC Electronics, [j.kelling@hasytec.com](mailto:j.kelling@hasytec.com)  
**Yildiz Williams**, Lloyd's Register, [Yildiz.Williams@lr.org](mailto:Yildiz.Williams@lr.org);  
**Mia Elg**, Deltamarin, [Mia.Elg@deltamarin.com](mailto:Mia.Elg@deltamarin.com)  
**Veronica Asta**, OPTIMEasy (University of Genoa Spin Off), [veronica.asta@optimeasyway.com](mailto:veronica.asta@optimeasyway.com)

## Abstract

*This paper presents a cruise vessel concept implemented within EU funded project CHEK. Hydrogen is employed as marine fuel in combination with various modern technologies comprising ultrasound antifouling, hull air lubrication, waste heat recovery and cruise itinerary optimization planning tool. The design aims to achieve reductions of at least 50% in energy demand, 99% in greenhouse gas emissions, and 95% in black carbon emissions. The preliminary results demonstrate the potential of these technologies for the future generations of cruise ships. They also provide fundamental input to a digital tool for vessel design and operations under development within the project.*

## 1. Introduction

The global maritime shipping industry is committed to a complete and immediate decarbonization of international shipping and transport. To achieve net zero will require a complete transition away from fossil fuels, meaning the heavy fuel oil and marine diesel must be replaced with fuels that are derived from renewable sources. At present, the production of renewable fuels has not reached the scale required and most remain prohibitively expensive. The full engagement of energy providers, governments, and other public and private entities is required to ensure that the right infrastructure exists on land, and that renewable fuels become available at scale all around the world.

Cruising is a technically complex and energy intensive sector. Various pathways to decarbonization, spanning ship design, energy efficiency, new technology and fuels are being assessed. A single solution has not yet emerged, and achieving net zero will require a combination of different technologies and fuels.

Such combination of innovative technologies working in symbiosis is presented in the Meraviglia class cruise vessel concept implemented within EU funded project CHEK, which aims to achieve reductions of at least 50% in energy demand, 99% in greenhouse gas emissions, and 95% in black carbon emissions. Rather than “stacking” the technologies onto existing vessel design, a unique Future-Proof Vessel (FPV) Design Platform is being developed to ensure maximized symbiosis between the novel technologies proposed and taking into consideration the vessels’ real operational profile. The energy saving target in the vessel concepts developed in project CHEK is compared to a vessel of similar dimensions that is fulfilling EEDI Phase 2 requirements.

The technologies tested and/or simulated to minimise emissions and maximize energy efficiency of the cruise vessel, include Hydrogen engine, Air lubrication system, Ultrasound antifouling system, Ship hull design, Fuel flexible gas engine incl. over-the-air software updates, Hybrid energy management, Waste heat recovery, Waste to power, Automated vessel routing/sailing and Cruise itinerary optimisation tool.

In the next Chapters are depicted five of the above technologies with results simulated by the Digital Master, being complemented by a review of the operational profile and existing infrastructure.

## 2. Technologies description

Technologies described in this paper are: Hydrogen engine, Waste heat recovery system, Ultrasound antifouling system, Hull air lubrication system and Cruise itinerary optimisation tool.

### 2.1. Hydrogen Engine

For the conceptual cruise ship design, engines running on hydrogen were selected as one of the key technologies to reach the overall goal of a 99% reduction in greenhouse gas emissions and a 95% reduction in black carbon emissions.

Building upon earlier R&D activities within Wärtsilä, a thorough review of relevant literature and research papers, the CHEK work on creating a hydrogen engine concept started with the creation of a set of engine requirements. Key aspects taken in consideration were safe and reliable operation, attainable power output and the possibility to run on 100% hydrogen to enable near zero emissions.

#### 2.1.1 Hydrogen engine specification and main components

The four-stroke lean-burn natural gas engine used in the present experiments has been built from the beginning to the end into a single cylinder engine, Table I. The engine speed is 750 rpm, typical for 50 Hz genset applications. The engine is optimized to deliver about 600 kW/cylinder. Only pure hydrogen is used as a main fuel.

Table I: Engine specification

Engine type	W31SGSCE (spark-ignited four-stroke medium bore single cylinder gas engine)
Cylinder bore	310 mm
Stroke	430 mm
Number of valves	2 inlet and 2 exhaust valves
Nominal power	600 kW (LNG fueled)
Speed	750 rpm
Turbo charger	Simulated by using compressed air
Loading	Generator

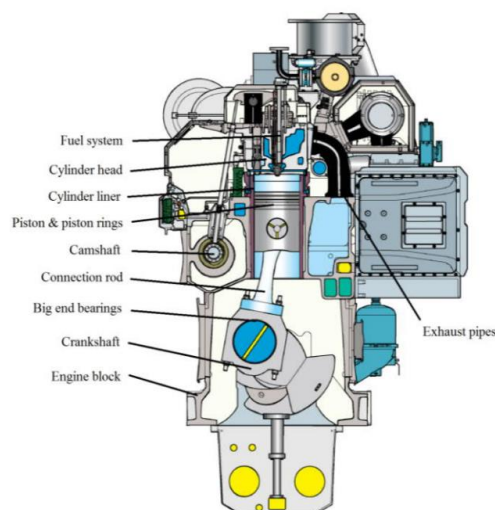


Fig.1: Engine main components

Most of the main components are the same for single cylinder (SCE) and multicylinder (MCE) as seen in Fig.1. The engine block is made in one piece of nodular cast iron and designed to absorb internal forces from the running engine. The oil sump is mounted below the engine block. Camshaft

is forged in one piece and connected to the engine block via the main bearing. The connecting rod is forged with alloy steel and connects the piston to the crankshaft. Piston is made from steel and moves up and down inside the cylinder liner. Cylinder head is the top piece of the engine made of cast iron. It contains intake and exhaust valves, exhaust gas pipe to exhaust system, cooling water and fuel pipe connections. The camshaft is driven by the crankshaft via a gear train to activate the intake and exhaust valves by the step-less valve mechanism.

The fuel system consists of two individual combustion chambers, the pre-combustion chamber (PCC) and the main chamber (MC) with separated gas fuel supplies. The aim is to produce a near stoichiometric air-fuel mixture inside PCC, while keeping the MC mixture lean.

The purpose of the lean gas combustion is to reduce NO<sub>x</sub> emissions, and the specific fuel consumption. Upon spark ignition the PCC pressure increases rapidly, forcing the burning PCC charge into the MC in the form of jet flames. These ignite the charge, allowing stable and efficient combustion under lean conditions. The exhaust manifold pipe is connected to the cylinder head. The pipe is made of heat resistant nodular cast iron alloy and the whole exhaust system is enclosed in an insulating box.

### 2.1.2 Hydrogen engine testing

Following the definition of the engine requirements, the team moved on to conduct a first probing test campaign in 2021 (Fig.2). Again, particular focus was put on safety. A very visible laboratory safety measure was to equip the engine with an “extraction hood” to ensure any possible hydrogen leak would not lead to a situation in which the lower explosion limit would be exceeded.

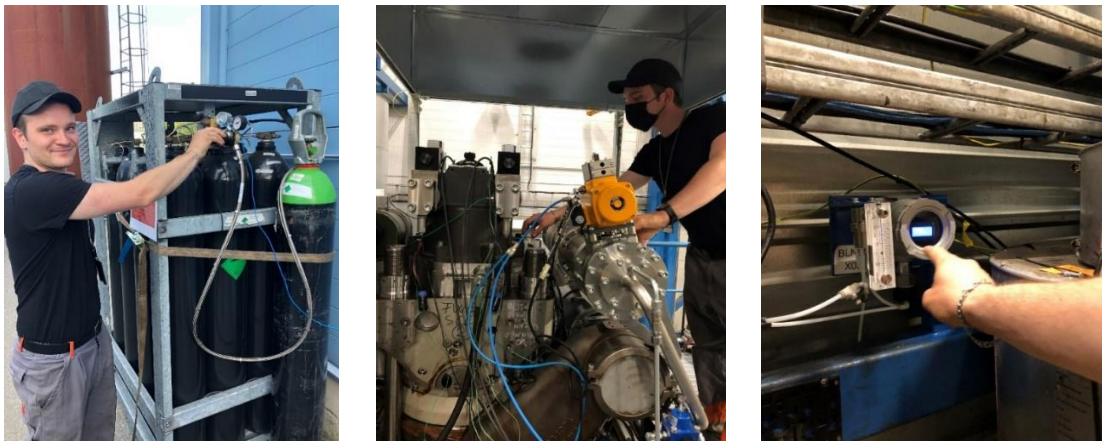


Fig.2: Impression of first CHEK hydrogen engine test campaign (Wärtsilä)

Following the first engine test campaign, several development and test cycles followed for both engine hardware and control software. Modified components included:

- Fuel supply system (piping, pressure regulator)
- Cylinder head
- Piston top & compression ratio
- Turbocharger
- Control system

Construction of the final prototype engine was completed by fitting one of Wärtsilä's laboratory test engines with modified components and control software, after which another intensive measurement campaign followed. The final test campaign was witnessed by representatives from Lloyd' Register, MSC Cruise, and University of Vaasa. The targets set on output, emissions, and efficiency in the project were met, making this step of the hydrogen engine concept development a success.



## 2.2. Waste Heat Recovery system (WHR)

Climeon's main goal in the CHEK project is to develop and test a future proof waste-heat-recovery prototype based upon existing Organic Rankine Cycle (ORC)-technology which is optimised to generate electricity from the available waste heat in the CHEK vessel. A digital model of the product to be integrated in the digital twin of the future vessel platform shall also be developed. The prototype is being tested in-lab, based upon engine parameters and real-life operations conditions and the results from the test shall be used to further optimise the digital model of the ORC. The ORC generated electricity shall contribute to lower the energy demand and greenhouse gas emissions from the respective vessel by reducing the running time of the ship's engines producing electricity to cover the hotel load and onboard electricity need.

### 2.2.1 Description of the technology

The Organic Rankine Cycle is a thermodynamic cycle which converts heat into electricity by using the temperature difference between a hot and cold source. It can be applied to the waste heat recovery process to generate clean energy from low temperature waste heat. For the marine application standard sources of waste heat are jacket cooling, HT-cooling, scavenge air cooling and surplus heat from exhaust. But other waste heat sources can also be used. The cold source is normally the sea water.

The ORC WHR system functions as a closed loop steam turbine system but uses an organic fluid instead of water as working media. The organic fluid has a boiling point lower than water, which enables the ORC system to successfully generate electricity from waste heat with a temperature less than 100 Deg C. The working media selected is non-flammable, non-toxic and has minimal GWP (Global Warming Potential) and ODP (Ozone Depletion Potential).

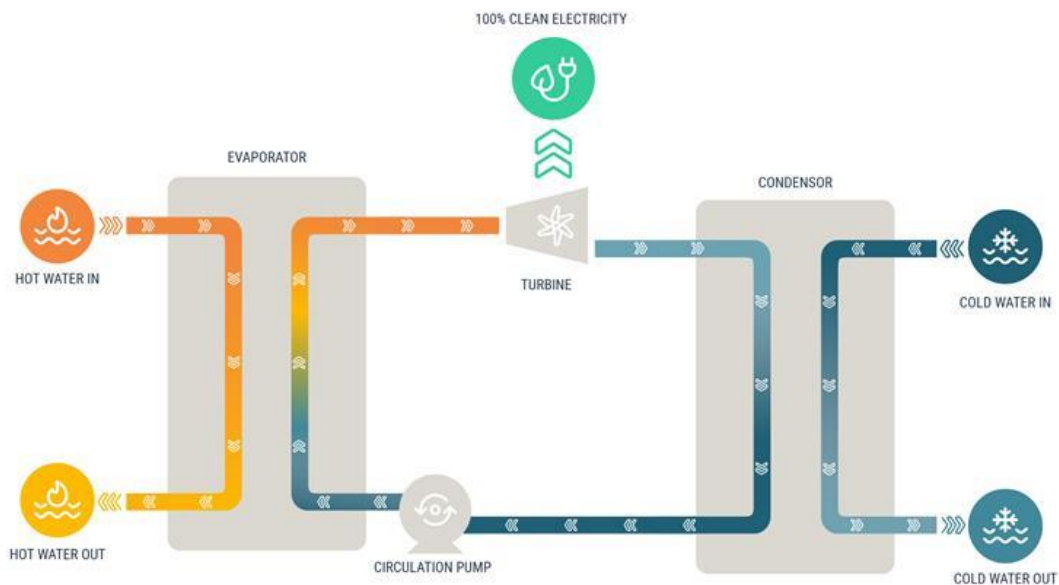


Fig.3: ORC WHR system process

The prototype for the CHEK cruise ship is developed upon the product Climeon HeatPower 300 Marine. And lab tests are performed on that product. For the testing of CHEK cruise ship real life data, the hot source temperatures serving as input to the ORC WHR are based upon the HT-cooling water boosted with surplus steam. The temperatures of the cold source are selected to be within the temperature range of the sea water in which the cruise ship is selected to operate.



Fig.4: Climeon ORC-WHR product HeatPower 300

### 2.2.2 ORC Waste Heat Recovery on ships

A ship's max. available thermal energy in the waste heat and max. ORC WHR power output based on engine type and circuit design, define how much electricity that could be produced when the ship operates in optimal conditions. However, to define the total, real-life ship-specific energy savings the vessel's operational profile must be assessed to determine what impact this will have on the availability of thermal energy.

A vessel's determined itinerary and operation, as well as the weather conditions, affect the engine load and speed. In turn, these affect the available thermal energy and, therefore, the output of on-board waste heat to power system. Further, when using seawater as a cold-water source for an ORC WHR system, the temperature of the seawater also impacts the net power output, as shown in Fig 5.

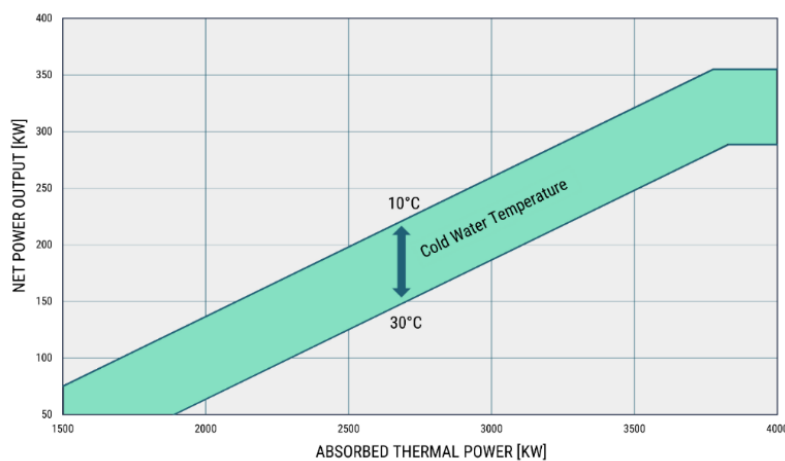


Fig.5: Power output from HeatPower 300 at different absorbed thermal powers and sea water temperatures

Fig.5 shows how seawater temperature and absorbed thermal power impact the net power output of Climeon's ORC WHR product HeatPower 300 Marine. The hot water temperature is set to a fixed value within the normal range of engine cooling water temperatures and the cold water (seawater) temperatures varies between 10 and 30°C. As the graph shows, when available thermal energy exceeds 3500 kW and the seawater temperature reaches 10°C, HeatPower 300 Marine can deliver a maximum power output of 355kW.

### 2.2.3 Preliminary results

Since the operational profile and integration of the ORC in the vessel have such an impact on energy savings for an ORC WHR system, the power output and total energy savings from the CHEK optimized ORC WHR system is simulated in the Digital master of the vessel, and results are presented in chapter 3 of this paper. However, final results will be provided from the Digital Twin simulations in which the ORC model and the available waste heat streams from the machinery and engines are updated based upon the real-life test results.

### 2.3. Ultrasound antifouling system

The innovative Ultrasound Antifouling Technology “Dynamic Biofilm Protection Intelligent®” prevents biofouling and marine growth in various marine applications, such as propellers, pod drives, bow/stern thrusters, sea water cooling systems and freshwater generators. Systems and coatings which release biocides and/or heavy metals into the oceans can be replaced in an environmentally friendly and sustainable way.

A non-toxic and environmentally friendly alternative for biofouling prevention is the use of acoustic waves in the ultrasound frequencies ( $>20$  kHz). Such a biofouling prevention system usually consists of a signal generator, a power amplifier and an array of piezoelectric transducers which excite the solid structure. The acoustic waves induce stresses and displacements along the hull. The magnitude of vibration depends on various parameters including the material, its properties and thickness, the applied frequency as well as the input power. After the initial excitation, we typically see compressional and shear waves in the solid. The oscillators of a compressional wave vibrate in the direction of propagation whereas those of shear waves vibrate perpendicularly to it. Compressional waves travel at higher propagation speeds.

#### 2.3.1 Description of the HASYTEC Dynamic Biofilm Protection Intelligent

The DBPi-System (or any other HASYTEC system) consists of three components. The modular control unit (MCU), the ultrasound transducers and the cables for power supply, which include alarm and connection of the transducer with the MCU.



Fig.6: An example of installed MCU on board of Cruise Ship



Fig.7: Application of coating after transducer gluing (example from sea chest installation)

Currently up to eight transducers can be connected per control unit, which consume a maximum power of 20-30 W each. The electronics are powered by an internal power supply unit that supports 115VAC and 230VAC. It provides sufficient power even at higher ambient temperatures up to +70°C so that there is no loss of ultrasound performance. Together with the ultrasonic generators and the mainboard for control and monitoring, the MCU is placed in a die-cast aluminium alloy housing which has IP66 protection class. The built-in plug connection allows for easy installation and replacement of defective components.

The DBPi is a plug & play device which, after start-up, automatically finds and sets the optimal frequencies for each connected ultrasonic transducer within its macro environment. Several sensors monitor temperature, current, voltage and output power. Active monitoring of temperature, current, voltage and output power detects a deterioration in the operating range of the respective transducer when environmental conditions change and enable adaption so that the transducers can operate in its optimal range. As the system should ideally run 24/7, this gives the opportunity to react quickly to errors and keep downtime as low as possible.

The installation concept of the system was vessel-specific and differed for the various applications treated.

### 2.3.2 Preliminary results

When a vessel moves through water at a certain speed, the propulsion system must generate an appropriate amount of thrust to overcome the resistance associated with the movement. The total resistance is a combination of several factors concerning friction, as well as weather and sea conditions. The most significant part of the friction, accounting for up 90% of the total resistance, is the frictional drag of a vessel's hull, Schultz (2007). Thus, the roughness of the hull directly affects the total resistance of a vessel in water.

To maintain the desired speed, an appropriate increase in the thrust needs to be delivered, thereby leading to higher fuel consumption and costs.

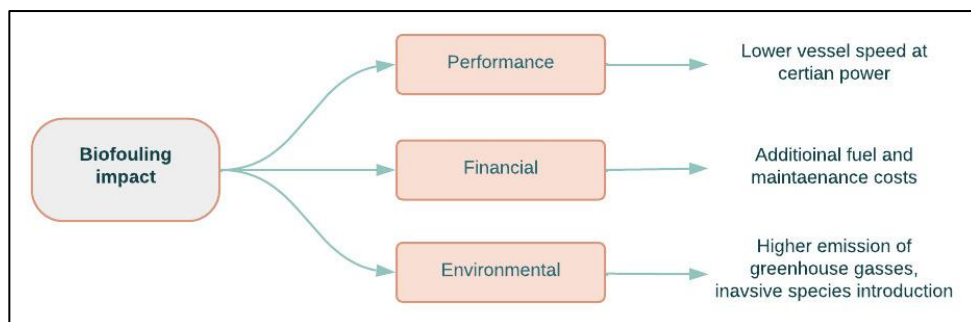


Fig.9: Impact of Biofouling

Hull roughness needs to be considered as it significantly impacts the resistance. Computer Fluid Dynamics (CFD) modelling of increased roughness within the scope of CHEK estimated that there is

a ~ 10% increase of effective power (the power needed to move a ship through water at a certain speed), when the hull was covered by light slime (using the Naval Ship Technical Manual - NSTM).



Fig.8: Hull patches coating on Cruise Ship

The impact on hull and propeller condition and the standard deterioration of the surfaces due to fouling and deposits and related possible energy savings derived from the ultrasound antifouling prototypes installed on the CHEK cruise is currently being evaluated by monitoring the case vessel with regular underwater inspections. Results from these real-life demo voyages will eventually feed into the Digital Twin simulations, enabling to evaluate and show the potential of ultrasound antifouling systems to achieve significant reductions in energy demand, in greenhouse gas and in black carbon emissions.

## 2.4. Air Lubrication system

Further drag reduction, and associated energy saving, is realised through the installation of an air lubrication system (ALS). The Silverstream® System, as developed and commercialised by Silverstream Technologies, is a unique hull air lubrication system deploying a bubble carpet along a ship's flat bottom through fluid shearing. When the ALS is engaged, the vessel's frictional drag reduces, which manifests itself through a reduction of the shaft power and an increase of the vessel speed. The ALS is a fuel agnostic energy saving solution, realising energy savings independently of the chosen fuel type, and can be implemented on newbuild vessels as well as retrofitted during a regular drydock period.

The system consists of three main components and a control and automation system. First, there are the oil-free positive displacement screw compressors, dimensioned for each specific vessel (class) and operational profile, delivering the air required for lubrication. Second, a system of piping and valves allows for the air to be delivered to third and final component, the patented Air Release Units (ARUs). The ARUs are placed along the flat of bottom line at the front of the ship and introduce air into the water through an open water interface inside each unit and a physical phenomenon called the Kelvin-Helmholtz instability, allowing for efficient generation of a high-quality bubble carpet. The airflow is governed by the control and automation system and is aimed to ensure bubble carpet stability and optimal drag reduction as a function of the ship's speed and draught (as based on extensive experimental full-scale testing in HSVA's HYKAT cavitation tunnel). The performance of the ALS has been independently verified by various third parties, showing average net savings between 5 and 10%.



Within project CHEK, Silverstream provided the future customer with a considered business case, detailing the technical and economic viability of ALS for both candidate vessels. The business case outlines three key areas: the design, the operation, and the installation of the ALS. The first part outlines the design and configuration of the system such that it has minimal impact on the arrangement of the vessel. The designed system for the cruise ship consists of 8 compressors, 16 ARUs in the conventional 1-to-2 layout. Such design work further includes determination of the ARU arrangement and structural integration, insight into the compressor functionality, selection, and positioning (through an exploratory visit of a Meraviglia Cruise Ship), outline of piping network and valve specification, diagrams of the electrical system, HVAC modifications, electrical connectivity, and discussion of the control and monitoring system (automation). The second part defines and estimates the system performance considering the most likely operational profile of the vessel, providing data for the development of the digital twin on the predicted performance of the ALS (as will be discussed next). The third and final part ensures the design of the system is feasible such that it could be installed within an agreed timeframe by a competent shipyard. An indicative project schedule for the realisation, development, and installation of ALS for the ship, including information on installation and commissioning activities, brings all together with a system cost analysis and risk register, before insight into Silverstream's performance verification protocols provides feedback to the performance estimation.

For the project, the performance of the ALS has been estimated based on Silverstream's established procedure as a function of the ship's flat of bottom area, percentage of lubrication achieved (vessel specific as established by ARU arrangement), the lubrication effectiveness, and the energy needed to achieve the lubrication. Once the system is commissioned, a range of methods can be used to demonstrate the achievement of the predicted savings, as Silverstream has realised in the past through independent verification. The methods range from full (traditional) sea trials for one or more engine settings, to longer term measurements of data during in-service activity. Each of the methods is based on the simple principle of turning the ALS on and off and comparing the achieved vessel performance. The predicted savings, as to be used in further calculations and digital twin development, for the cruise ship, for both laden and ballast cases across the speed range were provided to the digital twin development team. The savings provide an overview of the gross savings and the power consumption of the compressors required to achieve the mentioned gross savings. Within the digital twin, the gross savings can directly be applied as a deduction to the vessel's power consumption, while the compressor power is to be included in the hotel load. The implementation of the savings made by ALS stress the fuel agnostic character of the technology as the savings are realised through a direct reduction of the power consumption of the vessel.

## **2.5. Cruise itinerary optimisation tool**

A cruise itinerary is a timetable that specifies a sequence of ports that the ship must call to perform a cruise. Aside from the specific vessel, and its nautical capabilities, cruise itineraries have three characteristics: (1) the ports that the ship will visit, (2) time constraints specifying port arrival and departure times, and (3) general geographical area all the ports included in the itinerary are located in.

### **2.5.1. Cruise Itinerary Optimisation Problem**

Given,

- a ship pre-assigned to a particular basin,
- the list of the available ports of that basin
- and a duration and a starting port,

during the itinerary design process are selected the ports that the ship has to visit together with the arrival and the departure time of the ship at/from each port. Also, the % of tourists to embark at each selected port can be defined. The latter required to include in the decisional process the touristic

attractiveness, the revenue and the costs. Environmental impact centres around emissions, particularly the CII indicator, influenced by ship characteristics, fuel types, and sailing speeds. Tourist attractiveness is gauged through appealing and accessibility. Revenues include ticket sales, shore excursions, on-board services and beverage. Costs encompass fuel, port charges, and food expenses.

### **2.5.2 Cruise Itinerary Optimisation Tool (CIOT)**

The Cruise Itinerary Optimisation Tool (CIOT) includes the main aspects of the explained Cruise Itinerary Optimisation Problem mathematically modelled with a specific optimization approach, which allows to obtain as output the solution.

The high-level design of the tool includes the data derived from MSC systems and databases, a computation layer which allow to transform the general data collected by the MSC systems into the specific data and data format required by the optimization approach. This computation layer is the results of an intense phase of work and analysis to understand the best way to mathematically model and represent all the several aspects which have to be taken into consideration when defining an itinerary. Then, the optimisation approach is fed by input data from a dedicated database which collects the information in the right format and computation from the previous layer. Finally, a user interface allows the operators to insert the scenario data, to run the optimization tool and to obtain the results.

The CIOT allows to solve different problems that combine three main decisions: the selection of the ports of call; the definition of the ports of call sequence; the definition of the ports of call timings.

The system has three main modes, plus an intermediate mode, yielding a total of four problems, with:

- Mode1, given all the ports in the itinerary and their sequence, timings are optimised;
- Mode2, given all the ports in the itinerary, both sequence and timings are optimised;
- Mode2/3, only some ports are given, leaving the tool free to select the remaining ports to insert in the itinerary and optimizing both sequence and times;
- Mode3, the tool is free to select all the ports in the itinerary (except the port of embarkation and disembarkation which is given), optimizing both sequence and timings.

With this configuration, we are dealing with a multi-objective approach obtaining as output a set of efficient solutions. In this case, the user can compare and choose the best itinerary within the efficient set of those which respect the requirements with the possibility of including in the reasoning also non mathematically modelled details and aspects.

Further, it is allowed to run the system in two other ways:

- 1) Minimizing the emission impact while constraining a minimum level of operative margin to reach;
- 2) Maximizing the operative margin while constraining a maximum level for the emission impact.

Both these configurations represent a single objective approach (i.e. emission impact minimization when 1), profit maximization when 2)) providing as output the optimal solution found.

### **2.5.3 Preliminary Results**

This section reports an analysis in which the CIOT has been used to compare the results terms of CII of an already performed MSC itinerary and the optimized ones. The CII (Carbon Intensity Indicator) is a measure of how efficiently a ship transports goods or passengers and is given in grams of CO<sub>2</sub> emitted per cargo-carrying capacity and nautical mile.

The used CII formula is the following:

$$CII = \frac{CO2 \text{ Emission}}{\text{Ship Gross Tonnage} * \text{Sailed Distance}}$$

Firstly, the optimisation system has been directed (i.e., constrained) to obtain a desired itinerary. This has been possible thanks to Mode1, mode that allows to fix the ports and the sequence, optimising only the timings. The obtained CII is 9.16, which belongs to the CII class D, Fig.11.

Day	% Embark	Port	Technical arrival	Commercial arrival	Commercial departure	Technical departure	Stop Duration
1	70%	Valencia	-	19:00	19:15	10:00	-
2	0%	Barcelona	08:15	08:30	18:30	18:45	10:00
3	0%	Marseille	08:45	09:00	18:00	18:15	09:00
4	0%	Genova	10:45	11:00	20:30	20:45	09:30
5	20%	Livorno	07:45	08:00	17:30	17:45	09:30
6	10%	Napoli	12:45	13:00	19:30	19:45	06:30
7	-	At sea	At sea	At sea	At sea	At sea	At sea
8	-	Valencia	08:45	09:00	-	-	-
Total stay							54:30:00
Total miles							1643
From	To	Speed	Index	Value	CII Class	Fuel	Demand (ton)
Valencia	Barcelona	15.0	CII	9.16	D	HSFO	802.5
Barcelona	Marseille	16.0	CO2	2583.38		MGO	26.08
Marseille	Genova	15.0	SOx	7.88			
Genova	Livorno	9.0	NOx	40.38			
Livorno	Napoli	17.0	CH4	0.04		Active Hours (navigation)	43
Napoli	Valencia	19.75	PM10	6.68		Active Hours (port)	54
	Avg	15.29	PM25	6.15			
			CO	2.01	Index	Value	
			Carbon output	0.19	% Occupancy LB	1.0	
			ACIC	27.62	% Occupancy Total	1.0	
			Tot cons / ALBD	26.96	Nights	7	
			Tot CO2 / ALBD	84.05	ALB	4391	
			Tot cons / miles	0.5	ALBD	30737	
			CO2 / miles	1.57			

Fig.11: Solution obtained with Mode1

Day	% Embark	Port	Technical arrival	Commercial arrival	Commercial departure	Technical departure	Stop Duration
1	100%	Valencia	-	19:00	19:15	08:30	-
2	At sea	At sea	At sea	At sea	At sea	At sea	At sea
3	0%	Napoli	09:15	09:30	16:30	16:45	07:00
4	0%	Livorno	12:15	12:30	19:30	19:45	07:00
5	0%	Genova	09:15	09:30	16:30	16:45	07:00
6	0%	Marseille	10:45	11:00	18:00	18:15	07:00
7	0%	Barcelona	09:45	10:00	17:00	17:15	07:00
8	-	Valencia	10:15	10:30	-	-	-
Total stay							43:30:00
Total miles							1681
From	To	Speed	Index	Value	CII Class	Fuel	Demand (ton)
Valencia	Napoli	19.75	CII	8.79	C	HSFO	790.79
Napoli	Livorno	16.5	CO2	2536.12		MGO	22.71
Livorno	Genova	9.0	SOx	7.76			
Genova	Marseille	14.0	NOx	39.64		Index	Value
Marseille	Barcelona	14.0	CH4	0.04		Active Hours (navigation)	49
Barcelona	Valencia	11.0	PM10	6.54		Active Hours (port)	47
	Avg	14.04	PM25	6.02			
			CO	1.98	Index	Value	
			Carbon output	0.19	% Occupancy LB	1.0	
			ACIC	26.5	% Occupancy Total	1.0	
			Tot cons / ALBD	26.47	Nights	7	
			Tot CO2 / ALBD	82.51	ALB	4391	
			Tot cons / miles	0.48	ALBD	30737	
			CO2 / miles	1.51			

Fig.12: Solution obtained with Mode2

Day	% Embark	Port	Technical arrival	Commercial arrival	Commercial departure	Technical departure	Stop Duration
1	0%	Valencia	-	19:00	19:15	08:30	-
2	70%	Barcelona	09:15	09:30	16:30	16:45	07:00
3	0%	Marseille	08:15	08:30	16:00	16:15	07:30
4	0%	Livorno	09:15	09:30	16:30	16:45	07:00
5	0%	Napoli	12:45	13:00	20:00	20:15	07:00
6	30%	Civitavecchia	08:45	09:00	16:00	16:15	07:00
7	At sea	At sea	At sea	At sea	At sea	At sea	At sea
8	-	Valencia	10:15	10:30	-	-	-
Total stay							44:00:00
Total miles							1633
From	To	Speed	Index	Value	CII Class	Fuel	Demand (ton)
Valencia	Barcelona	14.0	CII	7.8	B	HSFO	677.36
Barcelona	Marseille	14.0	CO2	2184.63		MGO	23.29
Marseille	Livorno	16.0	SOx	6.65			
Livorno	Napoli	16.0	NOx	34.15		Index	Value
Napoli	Civitavecchia	16.0	CH4	0.03		Active Hours (navigation)	52
Civitavecchia	Valencia	14.5	PM10	5.66		Active Hours (port)	45
	Avg	15.08	PM25	5.21			
			CO	1.7	Index	Value	
			Carbon output	0.16	% Occupancy LB	1.0	
			ACIC	23.5	% Occupancy Total	1.0	
			Tot cons / ALBD	22.79	Nights	7	
			Tot CO2 / ALBD	71.08	ALB	4391	
			Tot cons / miles	0.43	ALBD	30737	
			CO2 / miles	1.34			

Fig.13: Solution obtained with Mode2/3

Then, relaxing the model with Mode2 (in which only the ports are selected, and the sequence and timings are optimised), the CII obtained is 8.79, which belongs to the CII class C, Fig.12.

In this step, the CII improvement has been about 4.2%.

Moreover, the modality for defining new itineraries (Mode2/3) has been used discarding 2 out of the 6 ports of the real itinerary to see if in attempt to improve the environmental impact the tool would select different ports. The CII obtained is 7.8, which belongs to the CII class B (Figure 13). The CII improved by around 17.4% from initial CII of 9.16.

Switching from mode 1 to mode 2 and finally to mode 2/3, although the objective was to minimise the CII, the operating margin also improved. Hence, for this test, increasing the degree of freedom of the tool yields better values in terms of both CII and operating margin.

In the project, a pilot of Cruise Itinerary Optimisation Tool has been defined, developed and tested. The system includes all the main elements to be taken into consideration for the cruise itinerary planning, definition and evaluation and is focused on the minimisation of the environmental impact. Attractiveness and Profitability are also included for the business sustainability of the obtained results

from the tool. The system can be used as Decision Support System for the Cruise Itinerary Planning Process thanks to the possibilities to be used for planning, simulating, evaluating and performing several scenario analysis.

### 3. Future-proof vessel design platform - Digital master

For enabling the CHEK ambitious targets regarding energy efficiency and emission reductions in real life projects, a digital design process is developed which can encompass complex interactions between the ship, her systems and external forces. The digital design modelling is performed in several generations, enabling feedback from actual operations once the ship measurement data is available. These together form a digital thread for the ship and the developed methods are a central part of a future-proof vessel design platform, applicable for any ship.

The Future-proof ship design platform and the related digital modelling does not consist of one single program but it is rather a combination of several “layers” of simulations and analysis, Fig.14. It is a flexible approach towards various ship types and various levels of detail in the project.

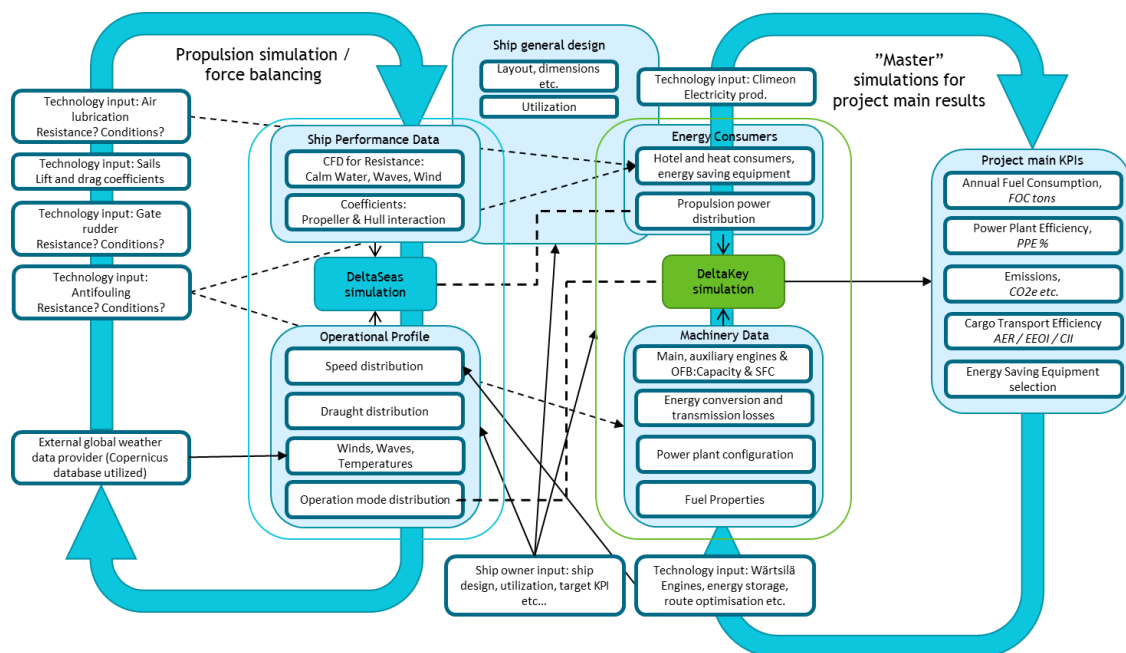


Fig.14: Digital modelling related factors illustrated

The digital modelling generations in CHEK are divided into three: Digital prototype, Digital Master and Digital Twin. The digital modelling and the methodology in project CHEK are discussed in more detail in another HIPER 2023 conference paper that illustrates CHEK results: “Development in CII performance of a bulk carrier, transitioning from today’s state of the art to net-zero design”. The digital model generations are also presented in a conference publication by *Hinz et al. (2023)*.

The current results are obtained from the Digital Master stage, where data from a reference cruise ship has been utilized regarding typical electricity and heat consumers as baseline, but a new, digital hull, has been generated for the vessel and the ship propulsion power is simulated including realistic weather loads. The method is explained in more detail by *Krishnan et al. (2023)*. The input data regarding technologies originates typically from reference data obtained from CHEK partners.

The energy saving target in the vessel concepts developed in project CHEK is compared to a vessel of similar dimensions that is fulfilling EEDI Phase 2 requirements. The attained EEDI value is calculated for the CHEK vessels and a relative difference between these two is calculated. The same relative difference that is gotten in this comparison is, then, utilized to establish a baseline fuel consumption and emission production for the vessel. The results are compared against this baseline.

Nevertheless, for clarity, we present the energy efficiency improvements separately for this EEDI-related baseline comparison and the results obtained with the digital modelling. The EEDI-baseline comparison is illustrated in Fig.15.

EEDI phase II target	10.24
Attained EEDI value	9.07
The difference, target vs attained, %	28.12 %
CHEK fuel savings goal, cruiser	50 %
Remaining energy gap to close	21.88 %
CHEK emissions savings goal	99 %
Remaining emissions gap to close	70.88 %

Fig.15: Cruise ship EEDI Phase 2 baseline and attained EEDI value (gCO<sub>2</sub>/nm/GT) and the resulting fuel and energy saving according to project CHEK definitions

Table II: Digital master stage simulation results of CHEK cruise vessel including short explanation of the cases

Simulation case	Explanation	Fuel cons. change %	CO <sub>2</sub> emissions change
New benchmark	New operating profile and hull form (compared to digital prototype)	REF	REF
Fouling	New benchmark + 5 % fouling margin on propulsion power (estimated based on visual inspections)	1,8%	1,8%
Batteries	New benchmark + 5 MWh battery with spinning reserve function and peak shaving	-0,1%	-0,1%
Shore Power	New benchmark + Shore power available in all ports	-12,6%	-12,6%
ORCs	New benchmark + 2 x 300 kWe heat to power modules installed in the system	-1,9%	-1,9%
ALS	New benchmark + Air lubrication. 5 % constant propulsion power savings at sea assumed	-1,8%	-1,8%
Heat10	New benchmark + 10 % reduction of the boiler consumption due to usage of energy saving devices in the HVAC systems	-2,7%	-2,7%
Hotel5	New benchmark + 5 % reduction in hotel power due to usage of HVAC energy saving devices in the HVAC systems.	-2,7%	-2,7%
46TSDF	New benchmark + existing engines replaced with TSDF version in LFO mode	-2,3%	-2,3%
CHEK combo	All of the above energy saving measures combined except “Hotel5”	-19,1%	-18,9%
Hydrogen combo	All of the above energy saving measures combined except “Hotel5” + Hydrogen as primary fuel used. No confirmed hydrogen operated engine data was utilized, but same combustion efficiency was assumed both for hydrogen and diesel variations.	-23,5%	-98,2%

The energy simulation results are presented in Table II. Both individual technologies and a combination of them is presented. Nevertheless, even in the “single technology” related results we can already observe a significant impact of the various ship energy system components working in



synergy. For instance, the available waste heat for the machinery and, thus, machinery efficiency, is a driver for the Organic Rankine Cycle process.

From the results obtained so far in the project we can conclude that the “EEDI comparison” indicates already considerable improvements (28,12%) in the energy efficiency in the CHEK design without considering the energy saving technologies. Furthermore, the technology mix simulated indicates additional 19,1% energy saving and further savings to be gained if hull fouling could be eliminated. Overall, the project goals seem to be achievable, but further work is still required.

The modelling work continues with the “Digital twin” stage, where the model will be enhanced with additional benchmark operational data measured from a reference ship. Also, conclusions will be drawn from the onboard tests performed with the ultrasound fouling reduction technology. In addition to this, the model factors and components will be updated with data from the recently performed lab tests or reference results measured from similar ships regarding majority of the CHEK technologies, such as Waste heat recovery and air lubrication.

#### 4. Operational profile and existing infrastructure

During CHEK project, a review of the operational profile and existing infrastructure for Meraviglia cruise ship has been undertaken. Based on the list of ports of call for the current and future operational profile of the ship, current port infrastructure has been reviewed in the following fields and gaps have been identified as summarised below:

- **Onshore power supply / Cold ironing:** This method is a shore connection, or shore-to ship power providing shoreside electrical. During cold ironing, the ship turns off its engines while berthed at a port and plugs into an onshore power source. This is only effective if the electric produced from renewable and sustainable sources. The onshore power source is still in the developmental phase for a number of ports with a few exceptions over some ports providing such service to ships that are berthed during their operation. However, there are no ports that accommodate cold ironing for the cruise ship which is disappointing and demonstrates that the gap in this infrastructure is big.
- **Bunkering:** LNG as an alternative fuel for ships is increasingly adopted as a strategy for environmental compliance, either sailing or at port. With an immediate significant impact on emission reduction like Sulphur Oxides emissions (SOx), Particulate Matter (PM), and also of Nitrogen Oxides (NOx) the motivations for the use of LNG as fuel in maritime transport are today highly favoured by a relevant multi-layered regulatory frame. Although it is still considered as a transitional fuel due to its being a fossil fuel, it is also worth noting that bio- or synthetic LNG would only be considered effective if the production is from renewable and sustainable sources.

A growing number of proponents of Hydrogen (H<sub>2</sub>) suggest it may enable a zero-GHG energy pathway as a marine fuel and commodity or cargo. H<sub>2</sub> is non-toxic, colourless and odourless. It is less dense than air, is not a greenhouse gas and will not trap heat in the atmosphere. However, it has a significant flammability range and low ignition energy. H<sub>2</sub> bunkering infrastructure in ports are in discussions by international organizations and bunker market players.

Our research shown that the LNG & H<sub>2</sub> bunkering facilities are only available in few ports. Some ports hold the infrastructure to facilitate LNG bunkering and some has taken initiatives to provide LNG bunkering in the coming years.

H<sub>2</sub> as a fuel consideration is still in the early days and the research has identified that none of the ports has any bunkering infrastructure in place, however a few ports have taken earlier initiatives to accommodate such facility and have plans for H<sub>2</sub> bunkering infrastructure in the years to come. It's worth to note that H<sub>2</sub> infrastructure and logistic are unlikely to be ready within the next six years for these vessels to operate smoothly.

- **Port Green Incentives:** These are incentive programs initiated by multiple ports on major shipping routes to collaborate and create benefits for both ports, ships owners/operators and the environment. By being compliant towards the set environmental standards ship owners/operators not only receive recognition by the maritime industry, but are also entitled to various financial, operational, and promotional gains.

There are a number of incentive programs initiated by multiple ports on major shipping routes to collaborate and create benefits for both ports and ships owners/operators. The aim of installing energy saving devices in the future ship design is to reduce fuel consumption and thereby reducing emissions from ships. Research was conducted on the port green incentives provided by each port which concluded that between 5 to 15% of port dues may be reduced depending on the amount of greenhouse gas emissions reductions. These can be a significant savings for the cruise ship in its operation.

## 5. Conclusions

This study presented a set of technologies tested and/or simulated to minimise emissions and maximize energy efficiency of a cruise vessel concept as part of CHEK Project.

From the results obtained so far, we can conclude that the “EEDI comparison” indicates already considerable improvements in the energy efficiency in the CHEK design without considering the energy saving technologies. The technology mix simulated indicates further energy savings.

Making the project goals achievable, further review of the operational profile and existing infrastructure for Meraviglia cruise ship has been performed. Overall, gaps are identified in the existing port infrastructure therefore, for smooth operation in the near future, improvements should be made especially around cold ironing and both LNG and H<sub>2</sub> bunkering (from renewable and sustainable sources) for the relevant ports.

## Acknowledgements

The research presented in the paper was conducted under EU Horizon 2020 project deCarbonising sHipping by Enabling Key (CHEK – Contract No. 955286).

## References

- BUCCI, V. (2022), *Strategies for ship decarbonization, technical measure for reducing Energy Efficiency Existing Ship Index*, University of Trieste
- CHEN, J. M.; NIJKAMP, P. (2018), *Itinerary planning: Modelling cruise lines’ lengths of stay in ports*, Int. J. Hospitality Management 73, pp.55-63
- CHEN, J.M.; PETRICK, J. F.; PAPATHANASSIS, A.; LI, X. (2019), *A meta-analysis of the direct economic impacts of cruise tourism on port communities*, Tourism Management Perspectives 31, pp.209-218
- CONNOLLY, D.; DUBOIS, A. (2022), *Status of Air Lubrication Technology*, 14<sup>th</sup> Symp. High-Performance Marine Vehicles (HIPER)
- CUSANO, M.I.; FERRARI, C.; TEI, A. (2017), *Port hierarchy and concentration: Insights from the Mediterranean cruise market*, Int. J. Tourism Research 19(2), pp.235–245
- DEMIREL, Y.K.; SONG, S.; TURAN, O.; INCECIK, A. (2019), *Practical added resistance diagrams to predict fouling impact on ship performance*, Ocean Eng. 186, 106112

DUBOIS, A. (2022), *Hull Air Lubrication: A Practical, Proven Energy Saving Solution*, RINA Scaling Decarbonisation Solutions: Reducing Emissions by 2030, Rotterdam

EHRGOTT, M. (2005), *Multicriteria optimization*, Springer

EHRGOTT, M. (2006), *A discussion of scalarization techniques for multiple objective integer programming*, Annals of Operations Research 147, pp.343-360

ERRIU, M.; BLUS, C.; SZMUKLER-MONCLER, S.; BUOGO, S.; LEVI, R.; BARBATO, G.; MADONNARIPA, D.; DENOTTI, G.; PIRAS, V.; ORRU, G. (2014), *Microbial biofilm modulation by ultrasound: Current concepts and controversies*, Ultrasonics Sonochemistry, 21(1), 15–22

HINZ, T.; MAZERSKI, G.; KRISHNAN, A.; MOLCHANOV, B.; ELG, M.; WEJBERG, V. (2023), *Digital Twin for Evaluation of Emission Reduction by Novel Technologies*, COMPIT Conf., Drübeck

KRISHNAN, A.; HINZ, T.; MAZERSKI, G. (2023), *Bulk carrier with rigid sails – combined effects of realistic weather conditions*, Int. Symp. Hydrodynamics in Ship Design Safety, Manoeuvring and Operation, Poland

KRISHNAN, A.; HINZ, T.; MAZERSKI, G. (2023), *Bulk carrier with rigid sails – combined effects of realistic weather conditions*, Int. Symp. Hydrodynamics in Ship Design Safety, Manoeuvring and Operation, Poland

LINDHOLDT, A.; DAM-JOHANSEN, K.; OLSEN, S.; YEBRA, D.; KIIL, S. (2015), *Effects of biofouling development on drag forces of hull coatings for ocean-going ships: a review*, J. Coatings Technology and Research 12, pp.415-444

MANCINI, S.; STECCA, G. (2015), *A large neighbourhood search based matheuristic for the tourist cruises itinerary planning*, Computers & Industrial Engineering 122, pp.140–148

MSC CRUISES, *Sustainability Report 2022*, MSC Cruises

RODRIGUEA, J.P.; NOTTEBOOMB, T. (2013), *The geography of cruises: Itineraries, not destinations*, Applied Geography 38, pp.31–42

SATTA, G.; PAROLA, F.; PENCO, L.; PERSICO, L. (2015), *Word of mouth and satisfaction in cruise port destinations*, Tour. Geogr. 17 (1), pp.54–75

SCHULTZ, M.P. (2007), *Effects of coating roughness and biofouling on ship resistance and powering*, Biofouling 23 (5), pp.331–341

SILBERSCHMIDT, N.; TASKER, D.; PAPPAS, T.; JOHANNESSON, J. (2016), *Silverstream® System –Air Lubrication Performance Verification and Design Development*, 10<sup>th</sup> Symp. High-Performance Marine Vehicles (HIPER)

SILBERSCHMIDT, N.; PAPPAS, T.; CONNOLLY, D.; DE FREITAS, L. (2018), *‘Full Scale Performance Measurement and Analysis of the Silverstream Air Lubrication System’*, Full Scale Ship Performance – RINA Conf.

WANG, Y.; JUNG, K.A.; YEO, G.T.; CHOU, C.C. (2014), *Selecting a cruise port of call location using the fuzzy-AHP method: A case study in East Asia*, Tourism Management 42, pp.262-270

# Development in CII Performance of a Bulk Carrier, Transitioning from Today's State of the Art to Net-Zero Design

**Annika Sandberg**, Deltamarin Ltd, Helsinki/Finland, [annika.sandberg@deltamarin.com](mailto:annika.sandberg@deltamarin.com)

**Mia Elg**, Deltamarin Ltd, Helsinki/Finland, [mia.elg@deltamarin.com](mailto:mia.elg@deltamarin.com)

**Bogdan Molchanov**, Deltamarin Ltd, Helsinki/Finland, [bogdan.molchanov@deltamarin.com](mailto:bogdan.molchanov@deltamarin.com)

**Arun Krishnan**, Deltamarin Ltd, Helsinki/Finland, [arun.krishnan@deltamarin.com](mailto:arun.krishnan@deltamarin.com)

**Ville Wejberg**, Deltamarin Ltd, Helsinki/Finland, [ville.wejberg@deltamarin.com](mailto:ville.wejberg@deltamarin.com)

## Abstract

*This paper will present the improvement in environmental performance of a kamsarmax size bulk carrier in the framework of an EU funded project CHEK. In addition to an efficient design, various modern technologies will be integrated in the design, such as sails to capture wind energy, hull air lubrication, gate rudder and waste heat recovery systems. The project aims to achieve 99% reductions in green house gas emissions and up to 50 % energy savings. This study focuses especially on presenting how the design and technologies work in synergy impacting the rating of the carbon intensity index.*

## 1. Introduction

Shipping decarbonization is one of the most important focus areas of the industry at present. The carbon footprint and, in general, ship emission footprint is caused by a combination of the ship design and technology mix, the way the ship is operated, and the fuels utilized. Since all these factors are interrelated, also the ship design and analysis methods should consider the relevant aspects both at the start of a new ship design process, as well as in planning a conversion to an existing ship. This conference paper presents a case example of reducing ship environmental impact in the framework of an EU-funded project CHEK.

### 1.1. Introduction to CHEK

Project CHEK is a three-year project, which aims to develop solutions for decarbonizing long-distance shipping. The aim of the project is to disrupt the way the ships are both designed and operated. In project CHEK the focus of the development work is in two case vessels – a wind energy optimized bulk carrier and a hydrogen powered cruise ship. Both case vessels will be equipped with an interdisciplinary combination of innovative technologies which are working in symbiosis for achieving the project ambitious targets. The goal of project CHEK is to reduce greenhouse gas emissions by 99%, achieve 40-50% energy savings and reduce black carbon emissions by over 95% compared to a typical existing, EEDI phase 2 compliant reference vessels.

The leading principle in project CHEK is that the new technologies are not just stacked on existing ship design, but a unique “Future-proof vessel (FPV) design platform” is developed and utilized for maximizing the symbiosis between the proposed novel technologies, the relevant design aspects, and realistic operational profiles from reference vessels. The FPV platform will also be used to expand the learnings from the two case vessels towards global fleet.

The FPV platform consists of various layers of digital modelling, which is also realized in several generations, improving the accuracy at each revision. Some of the CHEK technologies are also demonstrated onboard existing ships. This paper focuses on the bulk carrier case vessel of project CHEK and reports some of the most relevant results from the current generation of digital modelling highlighting the interrelations between variables. The focus is in documenting the advancements in the project in terms of energy savings and improvements in carbon intensity.

## 1.2. Carbon Intensity Index

Carbon Intensity Index is a metric that link the CO<sub>2</sub> emissions to the amount of cargo carried over the traveled distance. The CII must be calculated annually, and ships will receive a CII rating, depending on the result. The rating determines the ship's energy efficiency and is given in grams of CO<sub>2</sub> emitted per cargo capacity and nautical mile. Ratings range from A to E with A being the best. The goal is for a ship to achieve rating C or better. If a ship is rated D for three ensuing years, or E for one year, it must submit a corrective action plan to show how rating C or better will be achieved, *IMO (2022)*

To ensure compliance with regulations and IMO's strategy towards decarbonization the attained CII must be annually documented and authenticated against the required CII, that becomes progressively more stringent every year, *IMO (2022)*. The first year of the attained CII verification will be in year 2024 for the operation in year 2023, *DNV (2023)*.

## 2. Methodology

### 2.1. Digital modelling in project CHEK

#### 2.1.1. Overview to digital modelling methodology in CHEK

In project CHEK the ship digital modelling, as basis for FPV design platform is based on modelling the CHEK case vessels in three different modelling "generations": Digital prototype, Digital master, and Digital twin. These different modelling generations for together the digital thread in the project and they are divided evenly in the project timeline. This publication presents the obtained results from the digital master phase.

In the digital prototype stage, the CHEK vessel model energy consumption was largely based on historical operation data measured from the reference vessels. In the digital master stage both the CHEK cruise ship and bulk carrier are based on a new hull design, and only parts of the ship hotel and heat consumption rely on reference ship data as source. In the digital Twin stage, the modelling methods will be further improved, and the implemented technology data will be backed by either in-lab measurements or measurements from ship real-life demonstrations. Overall, the purpose of model development on a digital thread is to begin from rough, conceptual models and bring more details to them along the project development. There is a clear analogy to a typical ship design project and its timelines in the project CHEK. The project CHEK digital thread and the first stage modelling is described by *Hinz et al. (2023)*.

In order to produce a scalable platform for modelling any type of ship on various level of detail, Deltamarin has continued to develop in project CHEK the necessary digital design tools, which are not stacked into one single program, but it is rather a flexible coupling of various dimensions of modelling. Fig.1 illustrates the main composition in the digital design tools.

The first dimension, DeltaWay includes the hull and volume model of the ship, including the ship arrangement. In general, the ship dimension data can be combined to various databases regarding materials, equipment and their costs and this information is utilized in ship projects often for cost modelling and various project planning. In project CHEK the DeltaWay-dimension is revolving mainly around the case ship hull development and performing the necessary naval architectural analysis, such as stability assessment or structural calculations and layout generation regarding the studied technologies, where it is relevant.

The second dimension, DeltaSeas combines the digital hull to a digital representation of ship external forces, the "digital seas". The result is a realistic propulsion profile, including the impact of wind and waves to the ship, and various other relevant factors regarding propulsion equipment and hull condition. The weather modelling is essential in generating ship designs that have sails. In project CHEK two



WindWing sails are installed onboard existing bulk carrier and the resulting performance is compared to the digital modelling results in the CHEK Digital Twin modelling stage. The necessary force balancing algorithms are developed in project CHEK and implemented at the Digital Twin stage, but already the Digital Master model includes obtaining weather data along the ship route and modelling the wind and wave impact. The modelling method is explained more detailed by *Krishnan et al (2023)*.

The third digital model dimension, DeltaKey builds upon the two earlier “layers” and adds a digital representation of the equipment and the main energy flows within the ship. DeltaKey is a system level energy model, and it’s further developed in project CHEK especially regarding the technologies studied and certain essential interactions between them and the ship. Next section explains a bit further the energy modelling approach in project CHEK, since it is the central part of producing the main results and functional integration of the CHEK technologies.

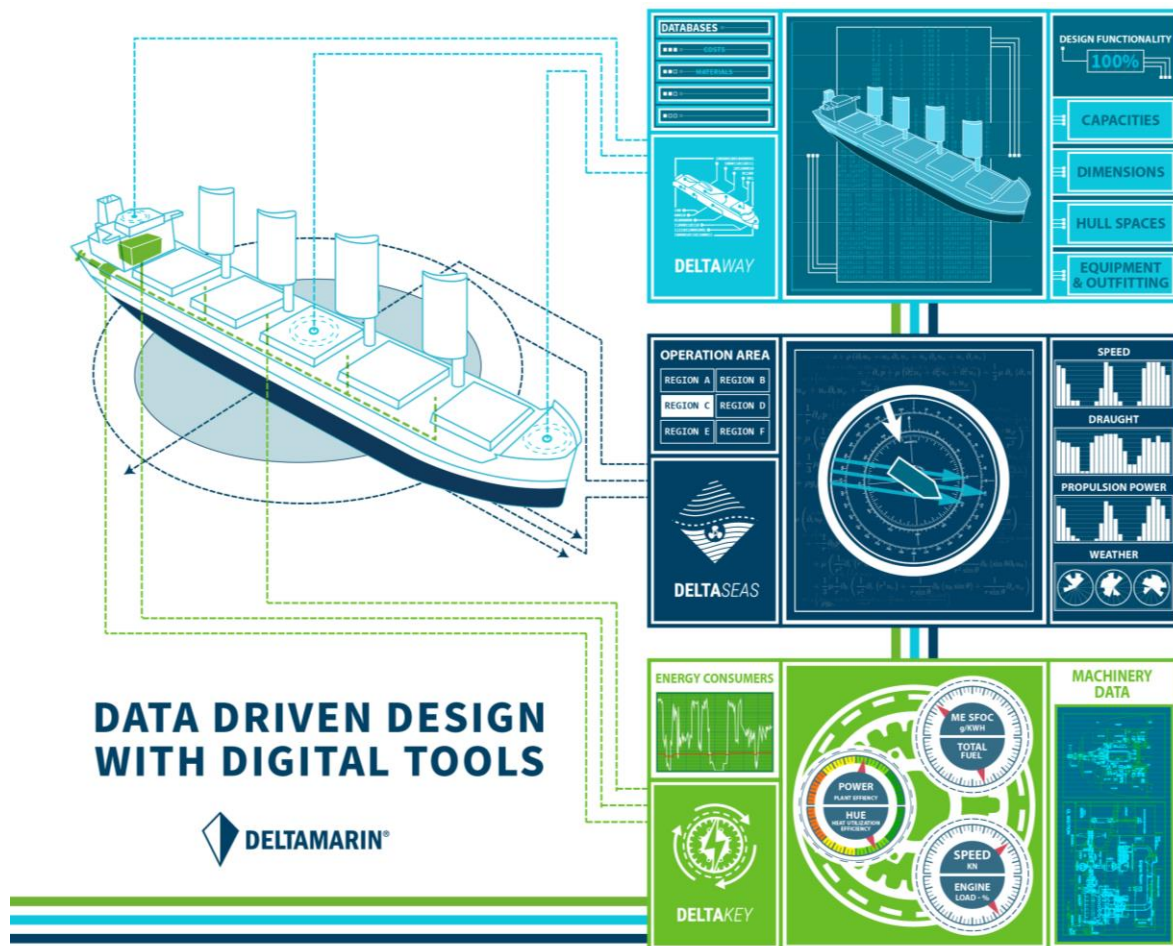


Fig.1: Digital modelling tools overview

### 2.1.2. DeltaKey energy modelling in project CHEK

DeltaKey is a system level energy model, which is configured in Matlab and Simulink environments. The basic setup of the model is a quasi-static energy balance calculation on a fixed time step. Various dynamic processes and energy storages can be applied according to the need. The model development dates over a decade back in history. It started as dynamic, multi-domain simulation model development involving also Simscape environment, configured for the typical ship energy domains, as described in a conference publication by *Elg et al. (2014)*. The current form of the model was driven by practical requirements from the ship project development, aiming for having a flexible, scalable model that can be adapted to any type of machinery, adding new components fast. Fig.2 illustrates snapshots from the Simulink environment from the boiler and main machinery configuration part of the model.

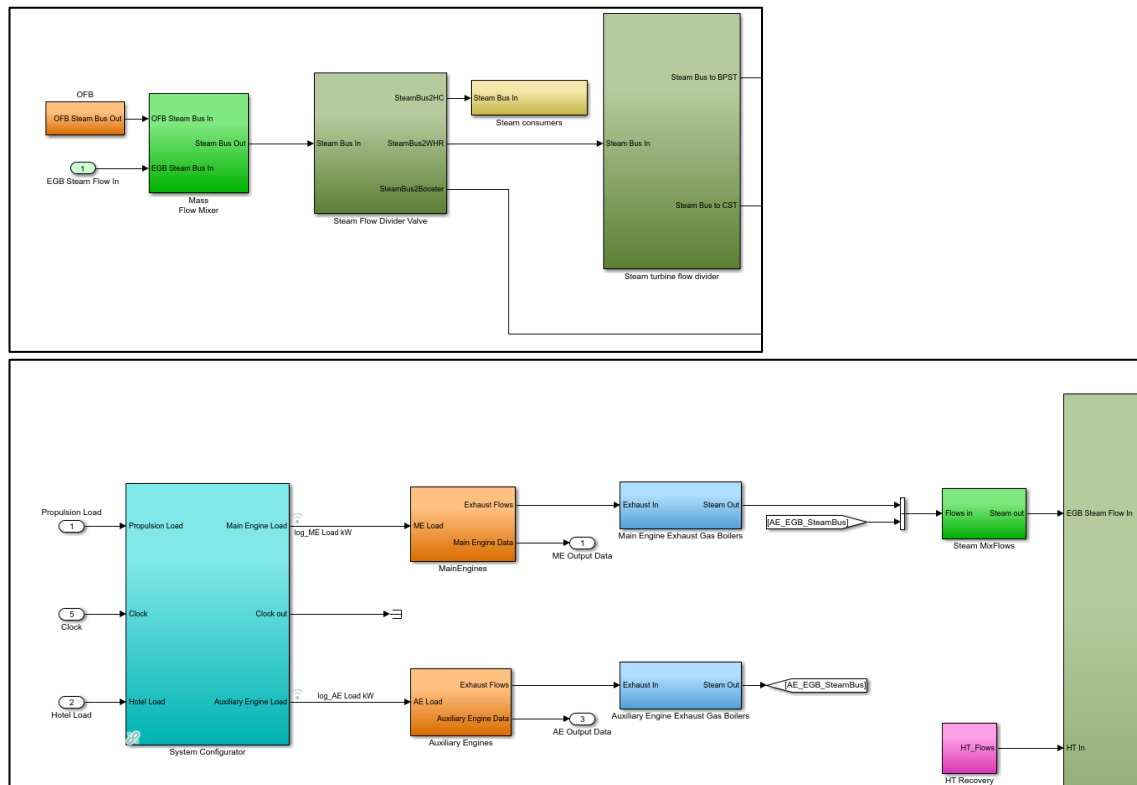


Fig.2: DeltaKey energy model snapshots

Fig.3 lists the typical groups which are always case by case configured in the model. The necessary input for the energy model is the ship operational profile, the machinery configuration, fuel data and the ship energy consumption. Various other equipment, such as batteries, energy saving devices etc. will also have to be configured, if they are included in the modelled system.

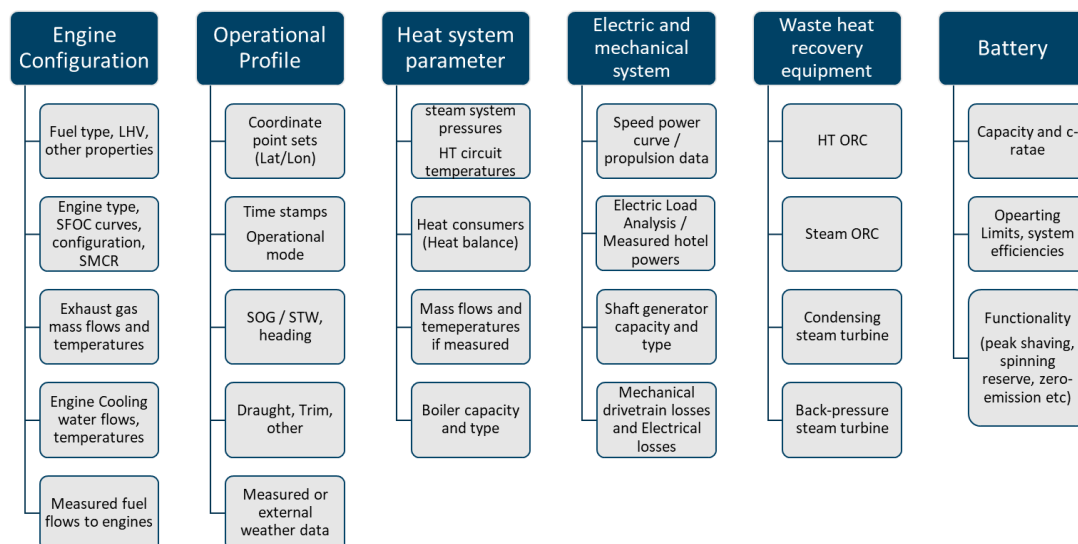


Fig.3: DeltaKey typical configuration input

The propulsion power can be inserted in the energy model in form of simplified speed-power curves including relevant marginals, or once available, such in the case of CHEK, the propulsion power is produced by DeltaSeas. The typical output of an energy model is the energy distribution within the ship, and various key performance indicators (KPI) as illustrated in Fig.4. In addition to demonstrating the various ship KPIs, the energy model is a good platform for various design improvement studies.

Lately, the DeltaKey model was utilized for a multi-objective optimization task. The case description can be found in a publication by *Elg et al. (2022)*.

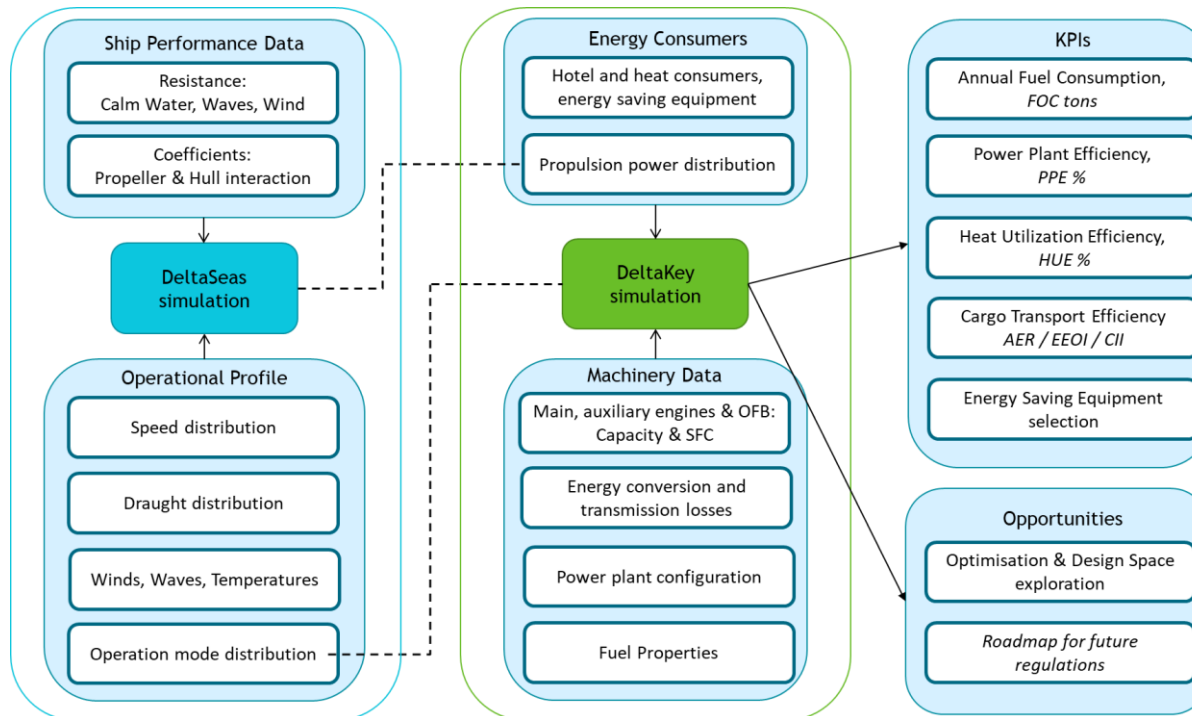


Fig.4: Overview of DeltaSeas and DeltaKey connection and the typical output of the model

## 2.2 General design data

A Kamsarmax sized bulk carrier was used as a reference hull for this project. Kamsarmax bulkers have standardized basic parameters with rather similar hull forms. Nevertheless, during the generation of the baseline hull for the project CHEK, improvement potential between 2.2% to 5.5% in propulsion power were recorded by *Krishnan et al. (2023)*. The ship design for this particular bulk carrier has been developed by Deltamarin and the basic particulars of it are presented in Table I.

Table I: Basic particulars of Kamsarmax bulk carrier in project CHEK from *Krishnan et al. (2023)*.

Length overall (LOA)	229.00 m
Length between perpendiculars (LPP)	225.06 m
Breadth	32.26 m
Deadweight and draft	80900 MT at 14.475 m
Laden- service speed and shaft power	14 knots at 80% MCR

## 2.3. Operating profile and weather data

Six different routes have been selected as realistic samples of operations for this size of bulk carrier. These routes are based upon information provided by the ship charterer and are presented in Table II. In order to account for weather variability, based on the vessel's position and assumed time the wind and wave parameters are gathered from a weather database. The main databases are provided by the European Commission initiative called Copernicus that aggregates data provided by European meteorological institutes. Further information regarding operating profile and weather data is presented in a conference publication by *Krishnan et al. (2023)*.

Table II: Routes from *Krishnan et al. (2023)*

	Departure	Arrival	Via	Length
<b>A</b>	Brazil	China	Cape of Good Hope	11220 nm
<b>B</b>	China	Australia (Newcastle)		4812 nm
<b>C</b>	Australia (Newcastle)	Brazil	Cape Horn	7243 nm
<b>D</b>	Australia (Newcastle)	Brazil		3646 nm
<b>E</b>	Rotterdam	Baltimore		3646 nm
<b>F</b>	Baltimore	Brazil		5002 nm

Hotel and heat power demands are modelled according to the operating mode of the vessel. The operation mode distribution is presented in Fig.5 and the details are outlined in sections below. The sea water temperature is modelled at a constant 25°C until better inputs are available to the model. The sea water in this case mainly influences in the ship heat balance and the waste heat recovery related technology.

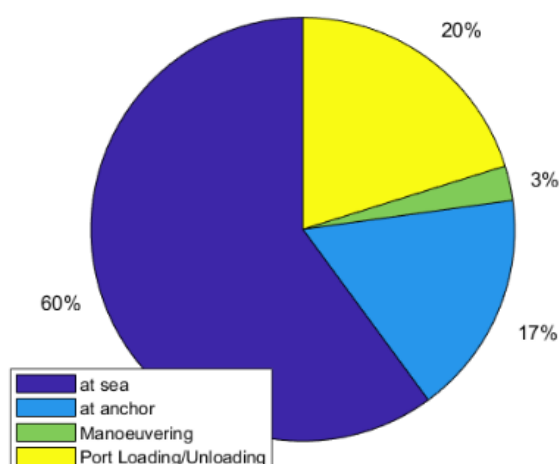


Fig.5: Operation mode distribution in the bulk carrier model

## 2.4. Key machinery components

### 2.4.1. Fuel type used and fuel properties

Following fuel types and parameters have been used in the simulations. Heavy fuel oil (HFO) is considered as main fuel type for cases with 2-stroke engine. Marine diesel oil (MDO) or liquified biogas (LBG) are assumed as primary fuel type for cases with 4-stroke engine. Fuel properties assumed for energy modelling are shown in the table below. The CHEK project emission targets for the bulk carrier are defined on a “well to wake” basis. During the time for preparing this publication, the fuel carbon factors were not established in a satisfactory manner. Therefore, this publication focuses mainly on the fuel saving impact and the tank-to-wake direct carbon emissions. We also provide an estimation of the potential impact of reducing ship carbon emissions by also applying for the LBG fuel a simplified factor of “0” regarding the well-to-wake emissions, without focusing on the diesel fuel well-to-wake factors or methane slip. The work towards state-of-the-art emission footprint calculation is continued in the future publications regarding ship life cycle analysis and the digital twin simulations.

Energy source	Table III: Fuel properties		
	LHV, MJ/kg	Density (kg/m <sup>3</sup> )	Carbon factor
HFO	40 200	0.991	3.114
MDO	42 700	0.920	3.206
LBG (Tank to Wake)	49 700	0.450	2.750
LBG (Well to Wake)	49 700	0.450	0

#### 2.4.2. Machinery configuration

There are three different propulsion configurations used in the simulations. For simulations with 2-stroke engine the MAN engine 5S60ME-C8.5 PL-EGB (8800 kW) was used. Wärtsilä's W8V31 engine (5200 kW) was employed when a 4-stroke engine was used and MDO was considered as the primary fuel. Conversely, Wärtsilä's W8V31DF engine (4800 kW) was chosen for applications where a 4-stroke engine was utilized, and LBG assumed as the primary fuel.

The 2-stroke engine configuration with fixed-pitch propeller represents a typical baseline machinery for the bulk carrier. Fig.6 illustrates a fuel-flexible 4-stroke engine machinery with shaft generators mounted on gearbox and a controllable-pitch propeller (CPP). During the simulations for digital master stage of the project, the simulation model did not yet include the combined optimization of the propeller loading and engine efficiency. The digital twin stage will include this aspect and also include the CPP efficiency. For the simulations for digital master, a fixed loss of 1% was included for the shaftline and 2% additional losses due to the gearbox in the 4-stroke machinery.

For cases with 4-stroke engines the powerplant will have 1 auxiliary engine installed. The auxiliary engine is Wärtsilä's 6L20DF engine (960 kW, 1000 RPM). Due to the usage of shaft generators at sea and a relatively small share of annual energy consumed in ports, the auxiliary engine will have a somewhat small impact on the total energy efficiency. For cases simulated with 2-stroke engine the electricity is generated with three Yanmar gensets (3 x 500 kW, 900 RPM). No shaft generator is considered for simulations with 2-stroke engine.

In all machinery configurations the exhaust gas heat is recovered from the main engines, but not from the auxiliary engines. In the 4-stroke configuration also the engine high temperature cooling water is assumed to be available for selected ship heat consumers and the heat-to-power conversion.

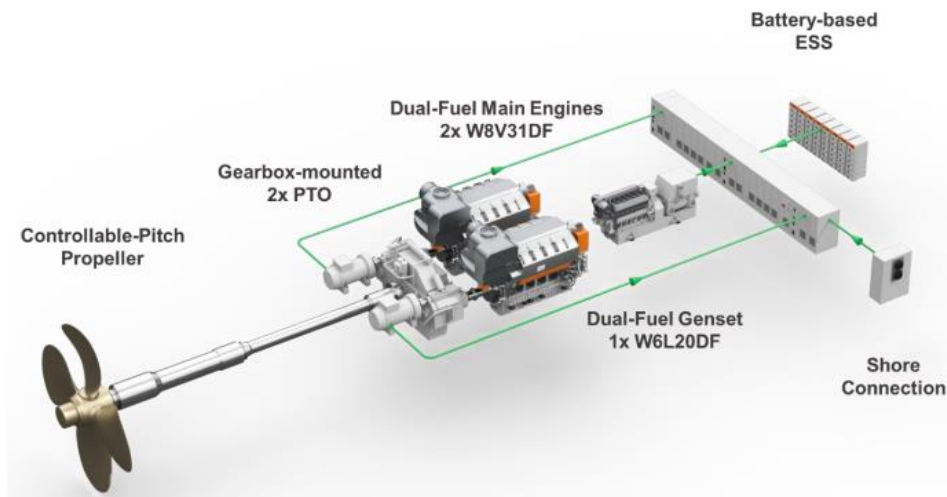


Fig.6: 4-stroke fuel flexible engine configuration including batteries and shore power



## 2.5. Power demand

The power demand for various speeds is shown in Table IV, for design draft with a 15% sea margin included. Losses in energy between engine and consumers are not included.

Table IV: Power demand (kW) for design draft for various speeds

Speed	11kn	14kn	16kn
Power	1756 kW	3266 kW	4860 kW

For the differences between the hotel load consumers, a set of reference electrical load analyses (ELA) for Kamsarmax bulker concepts with 2-stroke and 4-stroke machinery have been analyzed and the differences are presented in Fig.7.

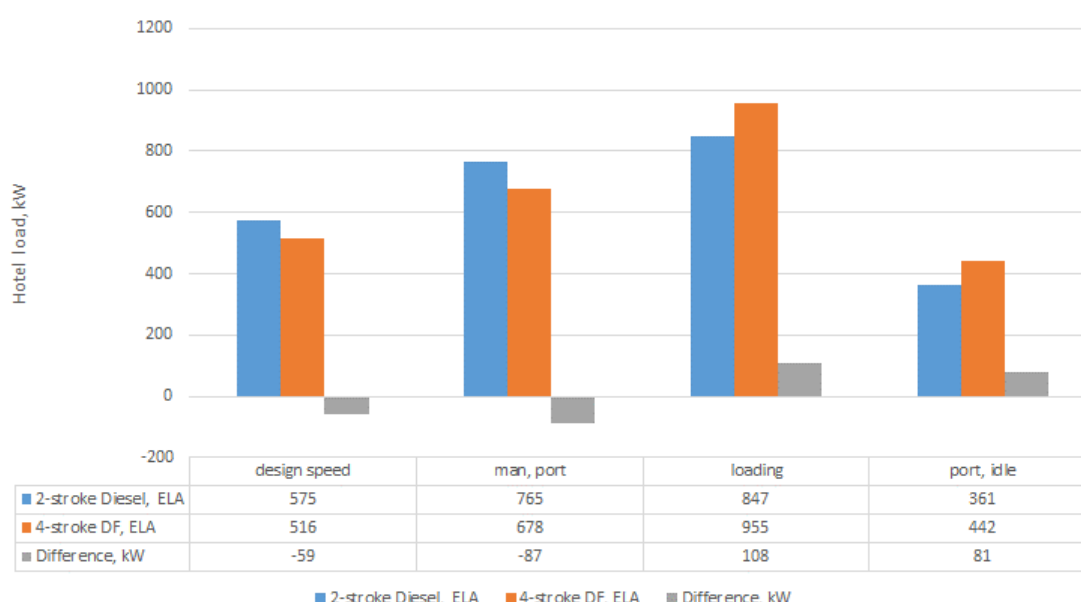


Fig.7: Indicative differences in hotel load with a 2-stroke and 4-stroke DF machinery

The heat balance of the vessel will undergo significant changes when the ship transitions from HFO to LBG fuel. The main difference will come from the tank heating requirements, where a lot of heat is required for keeping warm the fuel storage tanks to keep them pumpable and avoid wax formation. In addition, fuel supply lines will not require as much heating for the separators.

VLSFO Version						
Temperature	AT SEA			IN PORT		
	-10	25	35	-10	25	35
Steam consumers	632	392	264	594	360	175
HT consumers	247	19	17	248	37	33
<b>SUM, kW</b>	<b>879</b>	<b>411</b>	<b>281</b>	<b>842</b>	<b>397</b>	<b>208</b>

LBG Version + Optional savings						
Temperature	AT SEA			IN PORT		
	-10	25	35	-10	25	35
Steam consumers	359	64	40	357	60	40
HT consumers	237	9	7	309	62	38
<b>SUM, kW</b>	<b>596</b>	<b>73</b>	<b>47</b>	<b>666</b>	<b>122</b>	<b>78</b>
<b>Improvement relative to VLSFO</b>	<b>-32 %</b>	<b>-82 %</b>	<b>-83 %</b>	<b>-21 %</b>	<b>-69 %</b>	<b>-62 %</b>

Fig.8: Heat balance comparison between VLSFO and LBG-fueled bulker

To optimize the heat system further, heat consumers that require lower grade heat such as space heating, potable water heating and preheating of AC air have been assigned to engine high temperature (HT) cooling water rather than steam. Fig.8 illustrates the heat balance comparison between the main fuels, based on preliminary heat balance for the vessel as a function of the environmental temperature.

## **2.6. Energy saving devices**

### **2.6.1. Shore power**

Even docked ships consume energy, as several of the ship functions are still operating. For example, ventilation, heating/cooling, pumps, and control systems to name a few. When in port the generators are running resulting in air emissions that drive the warming of the climate. Instead of letting the generators on board make the electricity, this can come from shore power. The reduction potential is from 50% to 100% in port for the electrical motors on board, <https://glomeep.imo.org/technology/shore-power/>.

In the energy model shore power is assumed as either available in all ports or not available at all. In the simulation cases where shore power is applied it is assumed that shore power is available in all ports with a power of 1500 kW.

### **2.6.2. Organic Rankine cycle (ORC)**

ORC units are a low-temperature heat engine, that convert heat into electricity. The electricity produced from the waste heat reduces loads on the main engines and thereby fuel consumption as well as emissions.

The working principle of ORC is similar to a traditional Rankine cycle. where pressurized water is evaporated and expanded through a steam turbine. The main difference compared to the Rankine cycle is that ORC uses an organic fluid as working fluid instead of water. A more detailed description of the ORCs working process is discussed in another HIPER 2023 conference paper “Towards zero-emission cruise shipping”.

In this case 2 x Climeon’s HP150 product are “installed” onboard since the performance model of the CHEK optimized prototype based upon the HeatPower 300 unit was not available during the creation of the Digital Master stage models. Nevertheless, the performance figures for the ORCs were received from Climeon. The ORCs are connected to a separate waste heat recovery loop, which collects energy both from the engine’s HT cooling water as well as exhaust heat through a steam booster.

### **2.6.3 Batteries**

In the simulation model the battery’s main functionality is to enable higher engine load points, closer to 90-95% instead of the traditional 60% load before additional engine kicks in. The battery acts as a spinning reserve, compensating for short term load spikes. It is assumed that main engines are allowed to run at 100%, supplying power to the propulsion shaft and shaft generators when the battery is installed. Without batteries, shaft generators are disabled when main engines reach 90% load and auxiliary generators take over.

### **2.6.4 Air Lubrication System (ALS)**

Air Lubrication Systems can save up to 10% net fuel consumption and emissions. An Air Lubrication System reduces frictional resistance of the hull by creating a carpet of microbubbles. The system works in all sea conditions, is not weather dependent and does not have a negative impact on the normal operational profile, <https://www.wartsila.com/marine/products/propulsors-and-gears/energy-saving-technology/air-lubrication-system>.

Air lubrication was modelled according to preliminary estimates of gross power savings as a result of the drag reduction achieved and electrical power demand needed to run the system, provided by the company Silverstream Technologies for the Silverstream® System, during project CHEK. In the current model generation, the air lubrication system is considered by using a percentage reduction in final shaft power demand, while the electrical load will be included in the vessel's hotel load.

### 2.6.5. Sails

Fixed sails can use the wind to replace some of the required propulsion power onboard. Savings are naturally highly dependent on the wind conditions in which the ship operates, <https://glomeep.imo.org/technology/fixed-sails-or-wings/>.

Two sails that assist the propulsion, are considered in the energy simulation. The particulars of the sails were provided by BAR Technologies. The span and chord of the sail is 37.5m and 20m respectively. Air density is considered as 1.225 kg/m<sup>3</sup>. A more detailed description over the wind power effect on the bulker's propulsion power demand is recorded by *Krishnan et al. (2023)* in another conference paper. To accurately predict the savings of sails a 4DOF analysis of the ship must be done as well as conducting a force balancing optimization routine to determine the yaw, heel moments, thrust and leeway of the ship. The more accurate propulsion model, as well as updated sail model based on feedback from onboard demonstration will be a part of the next generation of the digital model. BAR Technologies have already produced highly sophisticated 6DOF model, including the weather routing, which was used to design their WindWings.

### 2.6.6 Gate rudder

A gate rudder provides additional thrust and enhanced maneuverability to the ship. This leads to a reduced fuel consumption and to ability of maintaining a set course. The reduction in fuel consumption depends on the vessel type, its operational profile as well as the reference propeller and rudder, <https://www.wartsila.com/marine/products/propulsors-and-gears/energy-saving-technology/gate-rudder-tm>. In simulations where gate rudder is applied, at this stage of the project without yet having the gate rudder simulation results as input, 8% constant propulsion power savings are assumed. Simulation results are derived based on this assumption.

## 2.7. Simulation matrix

Table V lists the simulated cases as a part of the “Digital master” model generation in project CHEK

Table V: Simulation matrix, all results are compared to benchmark cases

Case #1	<b>2S New Benchmark</b>	2-stroke benchmark, no additional energy-saving improvements.
Case #2	2S fouling	2-stroke benchmark + 20% increase in propulsion power due to fouling
Case #3	<b>4S New Benchmark</b>	New benchmark with the 4-stroke configuration (incl. shaft generator)
Case #4	Shore Power	4-stroke benchmark + shore power (1500 kW) available in all ports
Case #5	ORCs	4-stroke benchmark + 2 x 150 kW waste heat to power modules installed in the system

Case #6	ALS	4-stroke benchmark + air lubrication savings estimated by Silverstream Technologies
Case #7	Sails	4-stroke benchmark + 2 sails provided from BAR technologies
Case #8	Gate Rudder	4-stroke benchmark + 8% constant propulsion power savings.
Case #9	4S LBG	4-stroke benchmark + LBG as primary fuel.
Case #10	CHEK Combo	All the above energy savings measures combined except gate rudder and including battery as spinning reserve.
Case #11	LBG Combo (TtW)	All the above energy savings measures combined except gate rudder. Also battery included. LBG as main fuel. Results presented on Tank-to-Wake basis.
Case #12	LBG Combo (WtW)	All the above energy savings measures combined except gate rudder. Also battery included. LBG as main fuel. Results presented on Well-to-Wake basis.

### 3. Results

In this section a summary of the results is presented, reflecting the digital master stage of project CHEK.

#### 3.1 Energy model results and discussion

Tables VI (a and b) presents the energy model results in greater detail. In all scenarios a clean hull is assumed except in case “2s fouling”, there a 20% increase in propulsion power is considered to quantify the effect of hull fouling. The CO<sub>2</sub> emission reduction goal in project CHEK for the bulk carrier is defined as “well-to-wake” basis. Therefore, the results for the bio gas fuel are presented both with well-to-wake and tank-to-wake basis.

Table VI a: Simulation results for each scenario

Name	2S New Benchmark	2S Fouling	4S New Benchmark	Shore Power	ORCs	ALS
Amount of months	12	12	12	12	12	12
Main Engine fuel, t	4026	4740	4561	4561	4312	4170
Main engine pilot fuel, t	0	0	0	0	0	0
Auxiliary engine fuel, t	896	896	390	135	390	390
Auxiliary engine pilot fuel, t	0	0	0	0	0	0
Oil-fired boiler fuel, t	186	212	54	54	54	54
Cold Iron MWh	0	0	0	1179	0	0
<b>Total fuel cons, MWh</b>	<b>57107</b>	<b>65383</b>	<b>59363</b>	<b>56338</b>	<b>56412</b>	<b>54734</b>
PP efficiency avg. %	47,6 %	48,4 %	44,5 %	44,8 %	46,8 %	45,4 %
AE load, avg %	48,5 %	48,5 %	55,1 %	36,7 %	55,1 %	55,1 %
ME load, avg %	49,0 %	58,4 %	45,8 %	45,8 %	78,0 %	77,4 %
ME total run-hours	5266	5266	10470	10470	6193	5933
AEs total run-hours	16022	16022	3494	1730	3494	3494
SG total run-hours	0	0	5266	5266	5266	5266
Prop MWh	22468	26784	22468	22468	22468	19550
Hotel MWh	3669	3669	3656	3656	3656	4999
CO <sub>2</sub> Emissions, tons	15905	18210	16040	15228	15248	14794

Table VI b: Simulation results for each scenario

Name	Sails	Gate Rudder	4S LBG	CHEK Combo	LBG Combo (TtW)	LBG Combo (WtW) <sup>a</sup>
Amount of months	12	12	12	12	12	12
Main Engine fuel, t	3864	4124	3729	3540	2942	2942
Main engine pilot fuel, t	0	0	183	0	117	117
Auxiliary engine fuel, t	390	390	331	135	113	113
Auxiliary engine pilot fuel, t	0	0	16	0	9	9
Oil-fired boiler fuel, t	54	54	47	54	47	47
Cold Iron MWh	0	0	0	1179	1179	1179
<b>Total fuel cons, MWh</b>	<b>51104</b>	<b>54185</b>	<b>58938</b>	<b>44227</b>	<b>44225</b>	<b>44225</b>
PP efficiency avg. %	45,3 %	45,4 %	44,8 %	46,1 %	46,1 %	46,1 %
AE load, avg %	55,1 %	55,1 %	54,7 %	36,7 %	36,7 %	36,7 %
ME load, avg %	71,3 %	77,0 %	48,9 %	66,7 %	70,5 %	70,5 %
ME total run-hours	5919	5897	10532	5721	5882	5882
AEs total run-hours	3494	3494	3590	1730	1730	1730
SG total run-hours	5266	5266	5170	5266	5266	5266
Prop MWh	19182	20670	22468	16264	16264	16264
Hotel MWh	3656	3656	3656	4999	4999	4999
CO <sub>2</sub> Emissions, tons	13813	14646	11931	11954	8932	401

Overall, the results indicate that already a combination of various energy saving technologies that can be integrated in the ship design can make a huge improvement. The hull efficiency improvement results were not a part of this comparison, and also the impacts of weather routing were not included in these results, but still the combined effects of several improvements could reach improvements at the range of 20-30% in energy, and the carbon emissions on a well-to-wake basis approach zero with the bio-gas concepts. Also the attained EEDI of the CHEK bulk carrier without energy saving devices is 8.55% below the reference figure, EEDI phase 2 requirement.

In the presented results the ship operational profile included only 60% of the time operation at sea and the operation profile itself at sea was rather restricted at this stage. For technologies such as sails, the operational profile is in a key role when assessing the profitability since the benefits are reached when the ship is sailing. Nevertheless, according the current modelling generation results the daily fuel saving was approximately 3.2 tons per each day sailing sea. The simulation model development in project CHEK still continues regarding the sails with more accurate modelling, but also getting real measurement data from the installed BAR Technologies WindWings by Yara Marine. The current feedback from sail manufacturer and developer is that the WindWings reduce the energy consumption by 1.5 tons per WindWing per day, which is close to the current model generation results on this specific operation profile.

One of the guiding principles of project CHEK is to search for combined effects of various improvements working in symbiosis. From the results we can observe that namely single technology upgrades can make a considerable impact, such as the sails. Shore power connection on both ends, and in all ports can save up to 5% of total energy consumption and thereby reduce CO<sub>2</sub> emissions significantly. One downside to consider is that shore power might become a higher cost than fuel.

Nevertheless, there are numerous interconnections between the equipment onboard reaching all the way to the entire design and the ship cargo carrying capacity. This paper focuses on the holistic impact of technologies on the ship energy level, and even with the sails we can observe that even though the impact of the technology is mainly regarding the reduced propulsion power, also the engine utilization is changing, leading to larger total saving than what could be observed from the propulsion power simulations alone. In the illustrated 4-stroke engine configuration the average engine loading is increased, the average power plant efficiency lifted and the total engine running hours considerably reduced.

The holistic effect of technologies is even larger when examining results with the ORC. The simulation with ORC improves the energy consumption with almost 5%. Nevertheless, the pure power production with the ORC covers less than 3% of the ship energy requirements. In this case, the electricity production of the ORCs is able to reduce the ship electrical load, which would typically be provided by the shaft generators, switching the engine configuration from two engines on a relatively low load to one



main engine on a relatively good load. The result is a better average power conversion efficiency from fuel to power, leading to lower fuel consumption.

### 3.2 CII results and conclusions

The results for CII are presented in Fig.9. The CII calculation is based on MEPC 78 decisions (commenced in June 2022). The reduction of the reference line is assumed to be 2,625% between the years 2026 and 2030 to meet the goals set by IMO (a 40% reduction in carbon intensity from a Tank-to-Wake perspective), and 2% per year until year 2040. The alternative “CHEK combo” will stay compliant with CII rules in their current form until year 2040 and beyond, staying in superior rating most of its lifetime. Also, a combination of various energy saving methods produces almost equal reduction in the CII than fuel change to gas, once calculating only the tank-to-wake emissions based on the current rules.

With the new revised IMO strategy at MEPC 80 it is important to note that in the near future, the CII scope is expected to expand from the Tank-to-Wake perspective to consider the ship’s emissions from the Well-to-Wake, in other words, lifecycle perspective. This expansion will likely involve stricter requirements, driven by the global commitment to be achieving net-zero emissions by or around year 2050.

When developing new designs, it is important to simulate the impact of the design variations in the current rule framework, such as the CII. Nevertheless, the rules will be developed in the future for enabling the goals of shipping decarbonization, which might include adjusting the baselines and introducing various correction factors. Therefore, for being able to adjust for stricter rules and emission limits, it is important to view both absolute reductions in fuel consumption and the ship emissions and simulate the ship along her realistic operational profiles. This approach gives the tools for ship owners and operators to choose a strategically wise combination of design features and technologies for their ships from the start and preparing for certain upgrades in the future, once they are required by the rules and enabled by the clean fuel infrastructure, for instance.

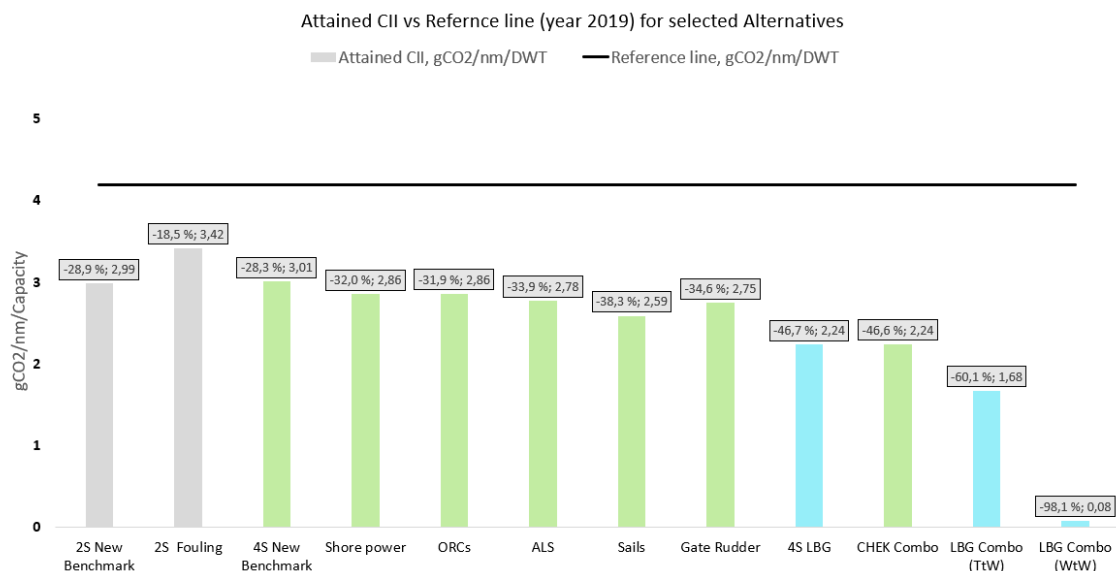


Fig.9: Attained CII performance vs required CII for all simulations

### 4. Conclusions

This study presented a set of results from project CHEK regarding the impact that various technologies and their combination can make to a bulk carrier energy efficiency and carbon emissions on a typical route. Even when simulating the impact of individual changes made to the ship, certain surprising

observations could be made regarding the energy and fuel consumption, due to the various interconnections between ship energy system components.

Once several energy saving applications are combined into the ship design, the total energy saving against the baseline is less than the sum of the saving figures from each individual change. The reason for this is also the numerous interconnections between processes, which are present also when simulating individual changes. For instance, the sails reduce alone the ship engine loads considerably, which results in less waste heat available for the ORCs. Modelling the simultaneous impact of various technologies, even on a rough level regarding some of the technologies, gives valuable insight into projected environmental performance of the ship.

These results provided a small outlook into the benefits and necessity to evaluate various technologies and design choices not only from the naval architectural point of view, but also from energy system perspective, assessing the holistic impact of various technologies operating simultaneously on a realistic operational profile. Once the project CHEK is concluded, we can take some learnings from the accuracy of the early stage digital modelling results compared to models supported by latest measurements from laboratory tests or ship onboard measurements.

### Acknowledgements

The research presented in the paper was conducted under EU Horizon 2020 project deCarbonising sHipping by Enabling Key (CHEK – Contract No. 955286).

### References

- DNV (2023), *CII – Carbon Intensity Indicator*, <https://www.dnv.com/maritime/insights/topics/CII-carbon-intensity-indicator/index.html>
- ELG, M.; KORVOLA, T.; MOLCHANOV, B.; TRAN, L.; LAPPALAINEN, J. (2022), *Improving ship sustainability by re-using engineering simulators in multi-objective optimization*, Int. J. Maritime Eng. 164
- ELG, M.; QUACH, S.; KINNUNEN, A.; ZOU, G.; TAMMI, K. (2014), *Improvements in Machinery Design of a Bulk Carrier by Utilising Multi-Domain Energy Flow Simulation*, 13<sup>th</sup> COMPIT Conf., Redworth
- HINZ, T.; MAZERSKI, G.; KRISHNAN, A.; MOLCHANOV, B.; ELG, M.; WEJBERG, V. (2023), *Digital Twin for Evaluation of Emission Reduction by Novel Technologies*, 22<sup>nd</sup> COMPIT Conf., Drübeck
- IMO (2022), *Rules on ship carbon intensity and rating system into force*, Int. Mar. Org., London, <https://www.imo.org/en/MediaCentre/PressBriefings/pages/CII-and-EEXI-entry-into-force.aspx>
- KRISHNAN, A.; HINZ, T.; MAZERSKI, G. (2023), *Bulk carrier with rigid sails – combined effects of realistic weather conditions*, Int. Symp. Hydrodynamics in Ship Design Safety, Manoeuvring and Operation, Poland
- MAZERSKI, G.; KRISHNAN, A.; HINZ, T. (2022), *D6.4 Meraviglia and Kamsarmax hull design 3D models*, D6.4, p.44

# Smart ShaPoLi Solution for EEXI Compliance

Erik van Ballegooijen, VAF Instruments, Dordrecht/The Netherlands, [evballegooijen@vaf.nl](mailto:evballegooijen@vaf.nl)

## Abstract

*For further reduction of greenhouse gases by sea going vessels, the IMO EEXI regulations have come into force per 1<sup>st</sup> of January 2023. One of the possibilities to comply with the EEXI regulations is to reduce and limit the ships propulsion shaft power via a ShaPoLi solution as per IMO resolution MEPC.335(76). This paper describes the development and working principle of a smart ShaPoLi solution based on manual (power) control. As will be discussed, the manual control ShaPoLi has advantages over an automatic (power) control ShaPoLi from vessel safety, technical, and commercial point of view.*

## 1. Introduction IMO EEXI regulations

In order to further reduce the green house gas emissions by sea going vessels, the IMO has released EEXI regulations. These EEXI regulations shall apply to all vessels of 400 GT and above which are engaged in international voyages. In this, EEXI stands for Energy Efficiency Existing Ship Index, and is in short a calculation method to determine the maximum engine / propulsion power of an individual vessel, with which it's CO<sub>2</sub> emissions are within given limits. This has to be calculated for each individual vessel and requires class approval via submitting an "EEXI Technical File". More information on how to calculate the EEXI of an individual vessel can be found in IMO's resolution MEPC.350(78) "Guidelines on the method of calculation of the attained Energy Efficiency Existing Ship Index (EEXI)".

In addition to the IMO's MEPC.350(78) guidelines on the calculation of the individual vessels EEXI, the IMO has also released other EEXI related resolutions. One, the MEPC.351(78) "Guidelines on survey and certification of the attained energy efficiency existing ship index (EEXI)", is providing more information on the procedures for the survey and certification of the EEXI of the individual vessel.

The other related IMO resolution is the MEPC.335(76) "Guidelines on the shaft / engine power limitation system to comply with the EEXI requirements and use of a power reserve". This resolution is providing (technical) guidelines on how to actually limit the engine / propulsion power on board of a vessel, and how to use such a system in practice. For the "smart ShaPoLi solution" as discussed in this paper, the MEPC.335(76) resolution has been leading.

### 1.1. IMO MEPC.335(76)

To provide some technical and operational guidelines for a system to limit the vessels engine / propulsion power in order to operate the vessel EEXI compliant, the IMO has released the above mentioned MEPC.335(76) resolution. In this resolution 2 basic technical solutions are provided for limiting the engine / propulsion power. On one hand this can be done by directly limiting the engine power itself via a so called Engine Power Limitation system or EPL. This EPL is limiting the engine power via either mechanical ways (like blocking/limiting fuel rack), or electronically via adding a limit in the engines software.

On the other hand an engine / propulsion power limitation can be achieved by limiting the power to the propeller or Shaft Power, the so called Shaft Power Limitation (ShaPoLi) solution. The basic idea of this ShaPoLi solution is to measure the shaft power to the propeller via a shaft power meter, and provide a feedback loop to limit therewith the engine power and CO<sub>2</sub> emissions.

In the MEPC.335(76) both the EPL and the ShaPoLi solutions are described in some technical detail. In addition, this resolution provides information on:

- How to use the engine power reserve by unlimiting the shaft / engine power limitation
- The belonging Onboard Management Manual (OMM) for ShaPoLi / EPL systems
- How to demonstrate the compliance of the ShaPoLi / EPL system

The discussion in this paper will mainly focus on the development of the ShaPoLi part of the MEPC.335(76) resolution.

## 1.2. Technical requirements for a ShaPoLi solution provided by IMO MEPC.335(76)

From the MEPC.335(76) resolution the following list of technical and operational requirements can be derived for a ShaPoLi system (copied or freely translated from the original resolution).

**Definition of a ShaPoLi:** *Overridable Shaft Power Limitation* (ShaPoLi) system means a verified and approved system for the limitation of the maximum shaft power by technical means that can only be overridden by the ship's master or the officer in charge of navigational watch (OICNW) for the purpose of securing the safety of a ship or saving life at sea.

**The ShaPoLi system should consist of the following main arrangements:**

1. Sensors for measuring the torque and rotational speed delivered to the propeller(s) of the ship. The system includes the amplifier and the analogue to the digital converter
2. A data recording and processing device for tracking and calculation of the data
3. A control unit for calculation and limitation of the power transmitted by the shaft to the propeller(s)

**General ShaPoLi system requirements:**

- It should be non-permanent (overridable) but should require the deliberate action of the ship's master or OICNW to enable the use of unlimited shaft / engine power (power reserve) of the ship. For systems that use a Password/PIN to control access to the power reserve override, attention should be paid to ensure that the necessary Password/PIN is always available when override is required.
- For a ShaPoLi system for the electronically controlled engine, the control unit should inform the ship's master or OICNW clearly and conspicuously when the ship's shaft / engine power exceeds the limited shaft / engine power as stated in the Onboard Management Manual (OMM) for ShaPoLi or in any case of system malfunction.
- The ShaPoLi system (or each subsystem) should be tamper-proof.
- The ShaPoLi system for the electronically controlled engine should indicate the following data during operation: shaft rotational speed, shaft torque and shaft power (and total shaft power in case of multiple shaft arrangements) to be recorded constantly in unlimiting mode
- Where technically possible and feasible, the ShaPoLi system should be controlled from the ships' bridge and not require attendance in the machinery space by ship's personnel.

The above list of requirements from the MEPC.335(76) are a combination of high level procedural requirements combined with some detailed technical choices or indications. For the development of the in this paper discussed “smart” ShaPoLi solution, the following points played an important role.

First of all, the ShaPoLi solution should be overridable. This has to do with the safety aspect of the vessel. In cases where the safety of a vessel is at risk, for instance in heavy weather conditions, it is necessary to be able to use the full engine power, and therewith to go over the EEXI power limit. But in these conditions, there must be provided a kind of operational barrier to go over the EEXI power limit. The MEPC.335(76) in this respect already mentions a possible detailed technical solution as a

power limit barrier, the “Password/PIN”, to control access to the engine power reserve. This is indicating towards the direction of an engine power limitation by technical means.

Secondly the ShaPoLi should, according the MEPC.335(76), have “a control unit for calculation and limitation of the power transmitted by the shaft to the propeller(s)”. Also this is indicating towards the direction of an engine power limitation by technical means, i.e. the control unit. But as will be discussed further on in this paper, the smart part of the ShaPoLi solution is in the technical choice of the control unit being a manual control of engine power by the crew on the bridge, instead of an automatic control.

## 2. Technical layout choices for the ShaPoLi solution

Given the above discussed MEPC.335(76) provided technical requirements for a ShaPoLi solution, the first straight forward technical ShaPoLi layout might look like in Fig.1, and can be described by limiting the engine power via “automatic control”. As can be recognised, the three MEPC.335(76) required components are present (shaft power meter, data recording and processing device, and a control unit for engine power limitation), next to the power override control functionality on the bridge.

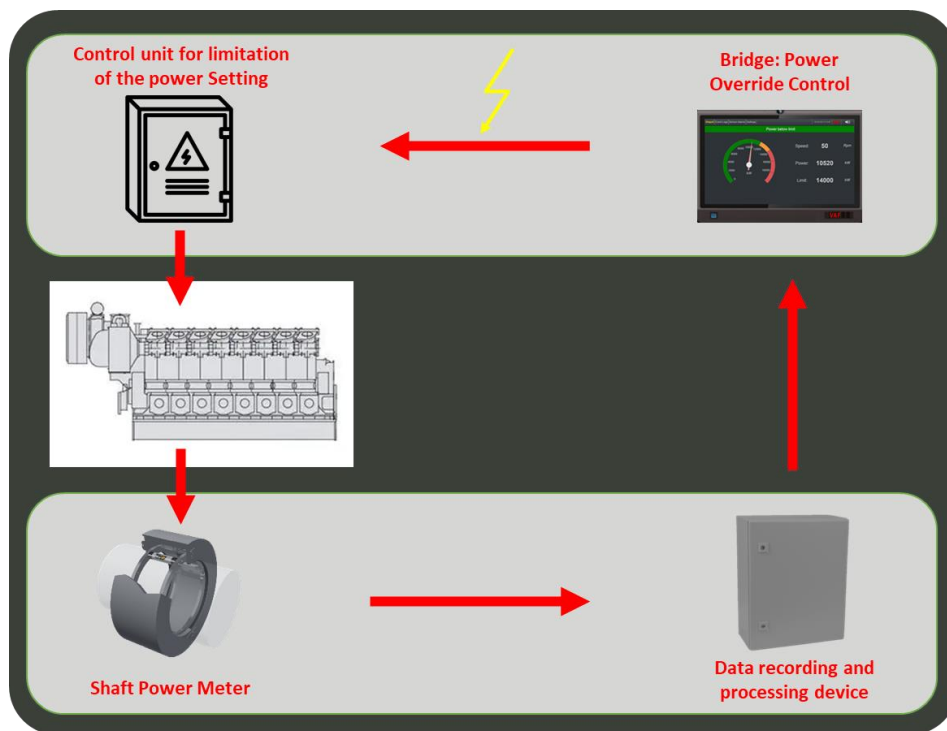


Fig.1: “Automatic control” ShaPoLi

The above solution of automatic control of the engine power limitation requires an electronic direct connection to the engine power settings. This has an effect on vessels safety, and also uniformity and cost price of such a ShaPoLi solution. As an alternative to the automatic control ShaPoLi, a “manual control” ShaPoLi is an option. In the next paragraphs both solutions are discussed in more detail.

### 2.1. Automatic control power limitation

The fact that for an automatic control ShaPoLi solution a direct electronic coupling is needed between the ShaPoLi control unit, and the engine controls has several technical, safety and commercial aspects.

First of all, since there is a direct electronic coupling to the engine controls, the ShaPoLi interfacing will be engine maker and type specific. This requires technical integration of the signals per engine maker and type. This introduces engine dependent variations of ShaPoLi solutions. In addition, this requires coordination and information exchange between the ShaPoLi supplier and the engine



manufacturer for each individual vessel. It can be imagined that this is time consuming, labour intensive and error prone. In addition, the on board installation requires additional effort as well.

Next to this, since the automatic control ShaPoLi is hard wired in the primary vessel propulsion controls, this calls for an extra layer of technical safety, and stability of the integrated ShaPoLi solution. As such the automatic control ShaPoLi has to fulfil strict classification rules and safety requirements as it is part of the primary vessel propulsion control system.

Third point of attention concerning the automatic control ShaPoLi is related to safety. For an automatic control ShaPoLi the engine power is electronically limited. In case of emergency this limitation should be able to be removed quickly. Preferably the engine power reserve (available power above EEXI power limit) should be able to be made available instantly by the crew if the need is there. In case of an automatic control ShaPoLi solution, the release of the engine power reserve could be arranged via, like the MEPC.335(76) is proposing, a PASSWORD or PIN code. This imposes a safety risk in cases where the PASSWORD or PIN code is lost or typed in wrong, typically in distressed situations since vessel safety is at risk.

Last point to mention is that the engine maker, type and vessel specific automatic control ShaPoLi solution has thus many variants. From technical and commercial point of view, standardisation of the ShaPoLi solution is preferred. All these variants therewith also have a negative impact on the commercial side of a ShaPoLi solution.

## **2.2. Manual control power limitation**

Based on the above discussed technical, safety and commercial aspects of the automatic control ShaPoLi, VAF Instruments has developed a smart ShaPoLi solution called the “manual control” version. Since for the discussed automatic control ShaPoLi, the interfacing to the engine maker, type, and specific engine controls, is an important limiting factor (from safety, technical, and commercial point of view), VAF Instruments thought of a technical solution to overcome this hurdle. The solution lies in replacing the automatic electronic engine power limitation control, by the already present manual engine power control by the crew (for instance via the engine control lever on the bridge). Fig.2 shows this manual control ShaPoLi solution schematically, where the control unit of the automatic control is replaced by manual control by the crew via already present bridge engine control lever.

Since for the manual control ShaPoLi the crew is in between, there is still the need to create a certain barrier before (deliberately) going over the EEXI power limit. This barrier is created in 2 ways by the manual control ShaPoLi solution. One, via providing an audible and visual alarm on the bridge by the ShaPoLi Bridge Panel PC (SBP-3), and two via the automatic logging in the ShaPoLi system of the events where the vessel is going over the EEXI power limit. In this way the crew is alarmed in case of going over the EEXI power limit, and the crew is aware that all these events are automatically logged, which event logs can be verified by for instance Port State Control (PSC).

The manual control ShaPoLi has several technical, safety and commercial advantages over the automatic control ShaPoLi. From technical point of view, it does not require any technical/electronic interfacing with the vessels engine control system. This reduces significantly the ShaPoLi engineering and installation efforts. Since it is not in the vessel primary propulsion control loop, therewith the technical part of the manual control ShaPoLi solution has to fulfil less strict classification rules and technical requirements compared to the automatic control ShaPoLi.

From safety point of view the manual control ShaPoLi solution has advantages above the automatic control ShaPoLi and EPL solutions. Since it does not electronically or physically limits the engine power (like is done with for instance a PASSWORD, PIN code, or fuel rack limitation bolt), the crew has instantly available the engine power reserve above the EEXI limit. In vessel safety critical situations, where the power reserve is needed (like severe weather conditions, saving lives at sea, or piracy), this instant availability of the power reserve is a very important advantage.

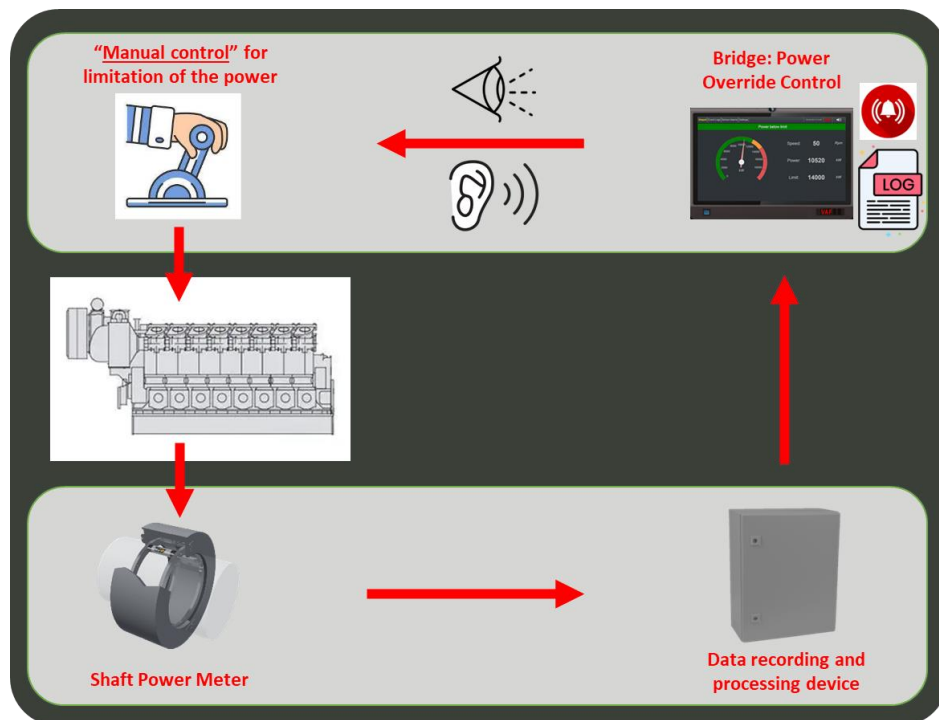


Fig.2: "Manual control" ShaPoLi

In addition, this opens the opportunity of standardisation of the ShaPoLi solution, to a so called one size fits all ShaPoLi, which is engine maker and type independent. This in itself is also beneficial for the crew since they can operate the same ShaPoLi solution on all vessels they are sailing with, independent of the various vessel engines. Further on, the standardised manual control ShaPoLi solution can be pre installed on a vessel in a very early stage of the project, as it is a kind of stand-alone solution with limited vessel specific interfacing to be engineered up front.

This standardisation of the manual control ShaPoLi solution also provides commercial benefits, as no engineering and interfacing is required with the engine controls, resulting in shorter preparation and installation times. In addition, standardisation has a positive cost effect on a manual control ShaPoLi solution.

Further on the manual control ShaPoLi solution can handle all type of propulsion lines like single and twin screw, fixed pitch propellers (FPP) and controllible pitch propellers (CPP), 2 engines on 1 shaft line, and possible PTO/PTI. Herewith a ShaPoLi solution has a wide variety of applications in various propulsion line configurations.

### 3. Regulatory steps for approval manual control ShaPoLi

The MEPC.335(76) resolution is providing some technical details on how a ShaPoLi solution could look like. As discussed before, the MEPC.335(76) is describing a control unit to control the engine power. The technical solution of such a control unit can be either by automatically (electronically) limiting the engine power, or manually (via the already present engine bridge controls). VAF Instruments has chosen the manual control ShaPoLi as the technical solution.

In order to reach approval of the manual control ShaPoLi, VAF Instruments has held discussions with many stakeholders in the maritime business, who are involved in the general regulations, acceptance, approval, and use of ShaPoLi solutions.

From IACS side (the International Association of Classification Societies) a working group was established to develop guidelines in response to the Resolutions MEPC.333(76), MEPC.334 (76), and

MEPC.335 (76) relating to EEXI. Part of the work done by the IACS working group is to provide more technical details on the MEPC proposed EPL and ShaPoLi solutions. As a result, the IACS workgroup released a recommendation, IACS Rec. 172 “EEXI Implementation Guidelines”. In Paragraph 6.6 the manual control ShaPoLi is described as an accepted ShaPoLi solution, Fig.3.

**No.  
172**  
(cont)

**6.6 Onboard Management Manual (OMM)**

- Regarding Resolution MEPC.335(76), section 2.1.1.3 “a control unit for calculation and limitation of the power transmitted by the shaft to the propeller(s)” : If this control is independent from the engine automation the following shall be satisfied:
  - Override of limitation is indicated by giving an alarm on the bridge, clearly informing the ship's master or OICNW:
    - In case of exceedance, the ship's master or OICNW to manually reduce the power within the limit;
    - In case of deliberate use of power reserve, data recording to commence automatically;
  - Data recording device as defined in section 2.1.1.2.

The OMM should clearly define this confirmation of the alarm as the deliberate action in agreement with requirement in chapter 2.2.1.

Fig.3: IACS Recommendation No. 172 “EEXI Implementation Guidelines”

Important to notice in this recommendation is that: 1) the control unit for limitation of the power to the propeller can be independent from the engine automation, and 2) that in case of exceeding the EEXI power limit, the ship's master or OICNW can manually reduce the engine power. Herewith the VAF Instruments manual control ShaPoLi solution is accepted as a technical solution to comply with EEXI power limitation.

#### 4. Manual control ShaPoLi system layout

In parallel to the regulatory acceptance and approval process of the manual control ShaPoLi solution, VAF Instruments developed the technical solution itself. In principle the solution exists of 3 parts as prescribed by the MEPC 335(76) EEXI regulations, Fig.4:

1. VAF T- or TT-sense torque meter for measuring shaft power (optional a 3<sup>rd</sup> party torque meter can be connected to the VAF ShaPoLi data logging box SDB-3);
2. VAF ShaPoLi Data Logging Box (SDB-3);
3. VAF ShaPoLi Bridge Panel PC (SBP-3).

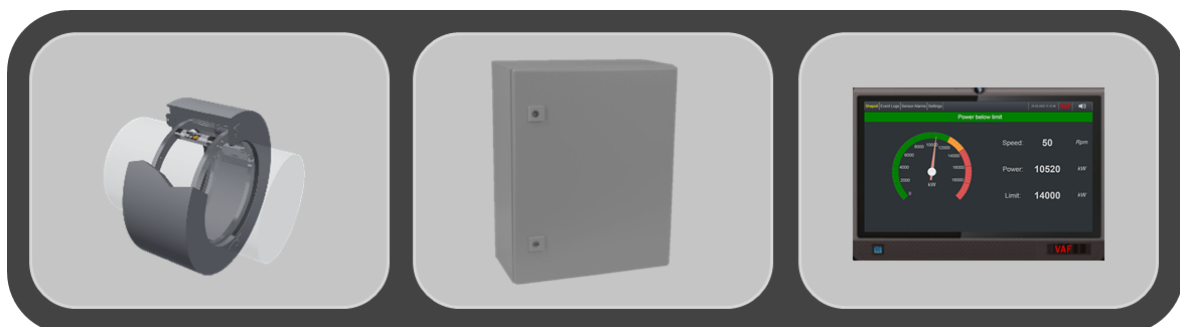


Fig.4: VAF Instruments manual control ShaPoLi solution components

Based on information provided by IACS, a ShaPoLi solution should be type approved. For the components of the VAF Instruments ShaPoLi, and the total ShaPoLi solution, all class requested type approval tests were performed like EMC, vibration, humidity, but also functional tests. This resulted in

the VAF Instruments ShaPoLi solution to receive a DNV type approval certificate TAA0000363, making it the first type approved manual control ShaPoLi solution in the market. Later on the VAF ShaPoLi solution also received type approvals from other class societies.

#### **4.1. VAF Instruments T- or TT-Sense shaft power meter**

The VAF Instruments T-sense (or TT-Sense) optical shaft power measuring system is mounted on the propeller shaft. When a shaft is subject to torque this will result in a small strain at the shaft surface. A LED and an extremely accurate optical cell can detect these small movements of the surface. The measured values are transferred continuously from the rotating shaft to the stator part through a wireless data connection. Power transmission from the stator to the rotating shaft is performed by means of induction. The Shaft -Power and -RPM signals are connected to the VAF ShaPoLi Data Logging Box SDB-3. The VAF T-Sense torque sensor is type approved by major classification societies.

#### **4.2. ShaPoLi Data Logging Box SDB-3**

The VAF ShaPoLi Data Logging Box (SDB-3), is a data recording and processing device, which will handle data from a ships shaft power/torque meter (VAF Instruments T-Sense, or 3<sup>rd</sup> party shaft power meter) and the external GPS signals. The SDB-3 is showing the measured shaft power, providing audible and visual alarming when propulsion power is above the EEXI power limit, and receives crew input commands, via the ShaPoLi Bridge Panel PC (SBP-3) on the bridge.

In addition, the SDB-3 is maintaining a database storage of the recorded conditions, Event Logs, when the vessel has sailed with actual propulsion power being above the EEXI power limit. In addition the SDB-3 logs possible malfunctioning of the system and sensors, i.e. in case of signal losses. The SDB-3 consists of a processor unit, a power supply, and various input/output PCB's for the I/O of the to be connected sensors and the Bridge Panel PC.

The processor unit runs dedicated ShaPoLi software that handles the sensor data input, records & processes it, and makes the data available to the Bridge Panel PC (SBP-3). Connections between the SDB-3 in the Engine Room (ER) or Engine Control Room (ECR), and the ShaPoLi Bridge Panel PC on the bridge, is via ethernet. Preferably the existing ship's network is used for this.

#### **4.3. ShaPoLi Bridge Panel PC SBP-3**

To visualize the actual measured shaft power data, and to provide a visual and audible alarm in case the shaft power is above the EEXI power limit, the ShaPoLi Bridge Panel PC (SBP-3) is located on the bridge. Via the touch screen of the SBP-3, the crew can also provide input to the ShaPoLi system. The SBP-3 is connected to the SDB-3 via an ethernet connection.

As this SBP-3 on the bridge is the interfacing of the ShaPoLi solution with the crew, on the SBP-3 various information is shown like actual power and RPM information, EEXI power limit, power reserve, alarm conditions, and recorded Event Logs of engine power above EEXI power limit events. These Event Logs can also be checked later on by for instance PSC. Next the SBP-3 allows for the crew to provide feedback to the ShaPoLi system like accepting an EEXI alarm and providing additional reasons for making use of the power reserve, which information is logged along in the Event Logs.

The ShaPoLi Bridge Panel PC SBP-3 has 5 submenu's: ShaPoLi, Event Logs, Alarms, Signals and Settings. By touching the relevant tab, the specific menu will be displayed. The ShaPoLi Home menu and the Event Log menu will be described in more detail.

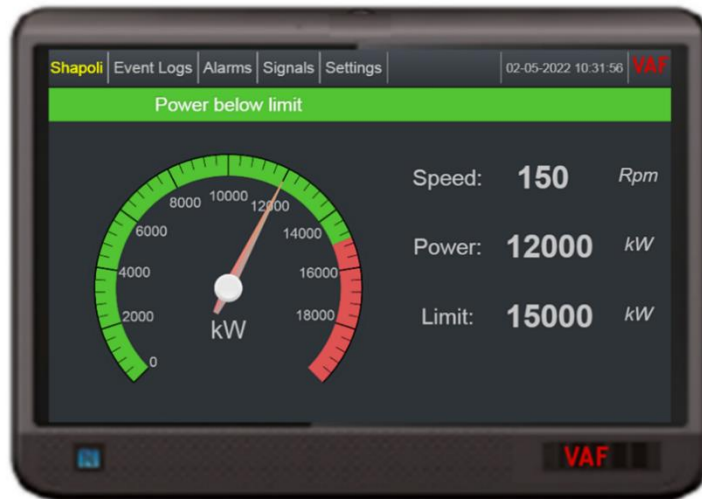


Fig.5: VAF Instruments ShaPoLi Bridge Panel PC SBP-3

#### 4.3.1. SBP-3 ShaPoLi Home menu

By touching the ShaPoLi tab in the top left corner the ShaPoLi home screen will appear. The ShaPoLi home screen is showing all important actual information regarding Shaft Power Limitation. The actual shaft power indicator is visualized on the left. On the right the actual Shaft Speed, actual Shaft Power and the EEXI Power limit are indicated. A **green** ShaPoLi bar shows that the actual shaft power is below the EEXI limit, and no other alarms are present.

The green bar in the ShaPoLi home screen will change to **red** when one of the following alarms occur:

- Power is over the EEXI Shaft Power Limit
- MODBUS communication failure
- NMEA communication failure
- ANALOGUE communication failure
- Missing ShaPoLi settings
- I/O communication failure

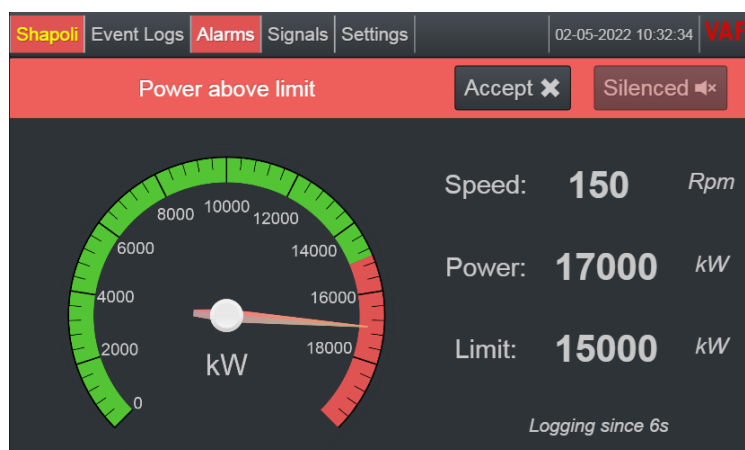


Fig.6: SBP-3, power exceeding EEXI limit alarm screen

The message in the red bar depends on the alarm. In case of an alarm, for instance when going over the EEXI power limit, the tabs “ShaPoLi” and “Alarms” will be colored red and will blink, the speaker in the ShaPoLi Bridge Panel PC will be activated providing an audible alarm, and the SDB-3 software starts logging this event immediately. These alarms can be silenced and/or accepted by the crew on the SBP-3 touch screen.



### 4.3.2 SBP-3 Event Logs menu

In the submenu Event Logs all the Logging events are listed. For example, when the actual shaft power is exceeding the EEXI power limit, the event will be listed in this Event Logs menu. The crew can Verify an event by touching the ‘Verify event’ button. In this submenu the Start time and End time will be shown. The crew can choose a reason why the power reserve is used. The following pre-set reasons can be chosen as are defined in the MEPC.335(76):

- Weather or ice-conditions
- Saving a life at sea
- Pirate avoidance
- Maintenance
- Other (please fill in free text)

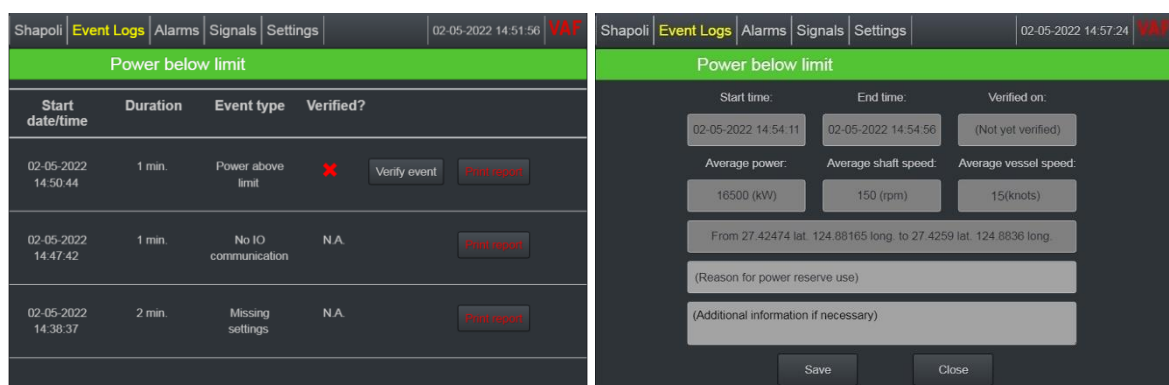


Fig.7: ShaPoLi Event Log to be verified & Event Log visualization

When the event is verified by selecting a reason, the red cross (✗) turns into a green checkmark (✓). Besides the “Power above the EEXI Shaft Power Limit” event the other mentioned alarm events will also be logged in the Event Log menu.

### 5. VAF Instruments ShaPoLi pilot vessel OLYMPIA.GR

As a next step the VAF Instruments developed manual control ShaPoLi solution was installed and tested on a pilot vessel. For this the Greek owned shipping company M/MARITIME offered their vessel MV OLYMPIA.GR to install and field test this ShaPoLi solution. The vessel OLYMPIA.GR is a 2018 build bulk carrier.



Fig.8: M/MARITIME vessel OLYMPIA.GR, pilot vessel for VAF Instruments ShaPoLi solution

On this vessel the VAF Instruments T-Sense shaft power meter, ShaPoLi data logging box SDB-3, and Bridge Panel PC SBP-3 were installed. The straightforward easy installation and trial of this first VAF Instruments ShaPoLi solution, supported in the further acceptance and approval of this type of manual control ShaPoLi solutions. Herewith the advantages of a manual control ShaPoLi solution where proven in practice.

## 6. Future advantages of the manual control ShaPoLi solution

In general, the primary purpose of a ShaPoLi solution is to limit the vessels emissions of greenhouse gases, particularly CO<sub>2</sub>, via the limitation of the vessels propulsion power.

But since a VAF Instruments ShaPoLi solution consists of a T-Sense shaft power meter, and an SDB-3 data collection box, the high frequent shaft power meter data logged by the SDB-3 together with GPS location and SOG, can also serve as valuable input for ship propulsion performance analysis. For this the propulsion data collected by the SDB-3 can also be send by the SDB-3 to the VAF Instruments IVY cloud dashboard solution (see Figure 9). Once this high frequent data is in the IVY cloud (basic) analysis can be done on the propulsion performance of the vessel.

In the VAF Instruments IVY cloud solution all kind of dashboards, graphs, KPI's and reports are generated like:

- Speed (SOG) – Power curves
- RPM – Power curves
- Vessel voyage analysis (route, SOG, RPM, Engine Power, etc.)
- Voyage reports (duration, distance sailed, average SOG, average Engine Power / RPM, etc.)

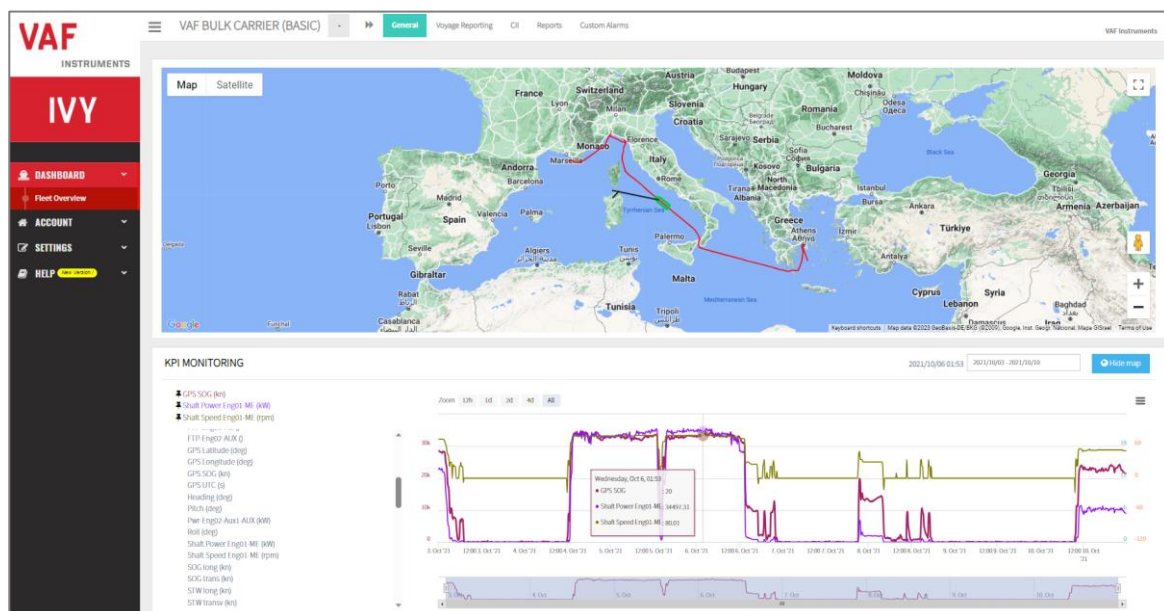


Fig.9: VAF Instruments IVY cloud high frequent data dashboard

The performance team of a ship owner or manager gets from the information presented in the IVY cloud dashboards a detailed insight in the performance of the vessel and how to further improve its operations. As via the ShaPoLi solution basic propulsion performance information is gathered as high frequent data, in a later stage data from additional sensors could be coupled, like for instance fuel flow meters to also monitor the fuel use of the vessel.

The collection of this propulsion related high frequent data also supports in improving the vessels fuel consumption, CO<sub>2</sub> emissions, and therewith improving CII rating, reduction of EU ETS taxes, etc. As

such, installation of the ShaPoLi solution in combination with the VAF Instruments IVY cloud solution opens up numerous opportunities to improve the vessels performance beyond the (minimum) EEXI compliance.

## **References**

IMO Resolution MEPC.335(76), 17 June 2021, *Guidelines on the shaft / engine power limitation system to comply with the EEXI requirements and use of a power reserve*

IMO Resolution MPEC.350(78), 2022, *Guidelines on the method of calculation of the Attained Energy Efficiency Existing Ship Index (EEXI)*

IMO Resolution MPEC.351(78), 2022, *Guidelines on survey and certification of the Attained Energy Efficiency Existing Ship Index (EEXI)*

IACS Recommendation No. 172, June 2022, *EEXI Implementation guidelines*

DNV Type Approval TAA0000363, 5 September 2022, *ShaPoLi Data Logging Box SDB-3, ShaPoLi Bridge Panel PC SBP-3*

# Learnings from a Biofuel Trial

Emir Ejder, DFDS, Istanbul/Turkey, [emiejde@dfds.com](mailto:emiejde@dfds.com)

Frederik Hammer Berthelsen, DFDS, Copenhagen/Denmark, [frber@dfds.com](mailto:frber@dfds.com)

## Abstract

*The maritime industry is shifting away from traditional marine fuels and turning to environmentally friendly alternatives to reduce Greenhouse Gas Emissions (GHG). Biofuels are one of the alternative marine fuels and often suggested as an essential fuel type in the future. Within the scope of the study, feedback was received from company vessel where biofuel (B100) was used. The purpose of analysing the crew's experiences and vessels fuel consumption figures was to validate that biofuel is technically and operationally feasible. The data obtained indicate that biofuels have the potential to assist in meeting emission reduction objectives.*

## 1. Introduction

Maritime transport is a sector that accounts for a significant portion of global trade and is a critical element for economic growth. However, as carbon emissions are of increasing concern in this field, innovative solutions are needed for environmental sustainability and climate change mitigation. In recent years, alternative fuels for emission reduction have attracted a great deal of attention and play an important role in the evolution of the maritime industry towards a sustainable future. Fuels such as hydrogen, ammonia, methanol and liquefied natural gas (LNG) are just some of the options being explored to replace fossil fuels and reduce the industry's carbon footprint, *Ejder and Arslanoğlu (2022), Harahap et al. (2023)*.

Among these alternative fuels, biofuels have significant potential during the transition to sustainable shipping. Biofuels are renewable energy sources produced from biological sources such as vegetable oils, animal fats and waste products. Unlike fossil fuels, biofuels have the potential to maintain the carbon balance in the atmosphere because plants absorb carbon dioxide from the atmosphere as they grow. This means that emissions from the combustion of biofuels can be offset by the amount of carbon absorbed during growth, *Jamil (2023)*. The most common types of biofuels are biodiesel and bioethanol. These fuels can replace or blend with fossil fuels, especially in the transport sector. The sustainability of biofuels may vary depending on the raw material used, the production method and the application area. Especially second and third generation biofuels have the potential to reduce environmental impacts as they are produced from more sustainable sources such as waste products and algae, *Hsieh and Felby (2017), Neupane (2023)*.

The advantages of biofuels for their use in the marine industry are primarily that they can lead to significant reductions in greenhouse gas emissions, are derived from a renewable source and are compatible with existing engine technologies, *Islam Rony et al. (2023)*. However, biofuels also have some disadvantages. Sustainability concerns, energy density and storage issues can sometimes complicate the use of these fuels, especially depending on the production processes, raw material sources and the regions where they are used. Therefore, it seems that biofuels can play a critical role in the short and medium term in achieving emission reduction targets in the maritime sector.

DFDS feels the responsibility of being one of Europe's leading maritime transport and logistics companies. Since its establishment, it has adapted to the ever-changing dynamics and challenges of the industry and continues to lead the sector with innovative solutions. The main challenges in maritime transport are increasing fuel costs, compliance with international maritime standards, pressure to reduce carbon emissions and fluctuations in global trade. In addition, increasing environmental regulations and sustainability expectations require the industry to take steps to increase energy efficiency and reduce its environmental footprint.

The company's biofuel trial onboard Acacia Seaways reflects this commitment. This vessel currently uses Ultra Low Sulphur Fuel Oil (ULSFO) and has no scrubber system, making the cost difference between ULSFO and biofuel less pronounced compared to Heavy Fuel Oil (HFO). This economic difference provides a better incentive to switch to biofuel, even though additional costs are still necessary.

The trial on Acacia Seaways focussed on the use of biofuel in the main engines, while the auxiliary engines and boiler were run on MGO (Marine Gas Oil). This approach allowed an in-depth analysis of the biofuel's performance, emission reduction capability and applicability in practical marine operations. Previous tests by engine manufacturers have confirmed that biofuel can be successfully used in similar engines and can be easily integrated into existing systems.

The biofuel used in the trial is B100 FAME, which stands for Fatty Acid Methyl Esters. B100 stands for 100% biofuel composition. It is a pure biofuel product that does not contain any mixture of conventional fuels. The feedstock for this biofuel is second generation, derived from waste products such as used cooking oil, animal fat or forestry waste. This approach is in line with sustainability goals by utilising renewable resources and reducing dependence on virgin materials.

Sustainability in the maritime sector is becoming more and more prominent. DFDS' trials with biofuels reflect the industry's efforts in this direction. Biofuels stand out as an alternative with the potential to reduce maritime carbon emissions in the short term, but more comprehensive solutions and approaches need to be developed in the long term. With its steps in this field, DFDS has gained experience with biofuel which can be used in the future for further biofuel initiatives. These efforts are part of the industry's steps towards fulfilling its environmental responsibilities and remind us that there is still much work to be done on this journey.

## **2. Initial work**

The use of biofuels in the maritime sector requires a very detailed preparation process. DFDS followed a step-by-step approach in realising this transformation. In March 2022, the project was initiated and technical and operational planning, as well as the necessary approvals and procurement processes of biofuel were planned. Just a few months later, in August 2022, the Lithuanian flag state approved the Acacia Seaways vessel to conduct trials with biofuel B100.

In October 2022, the Acacia Seaways vessel took the step of switching from ULSFO to biofuel and made its first voyage on biofuel. This trial period lasted until December 2022, during which the last refuelling of biofuel took place. However, in January 2023, after the last voyage on biofuel, the ship returned to operations on ULSFO fuel. This process clearly shows how a switch to biofuel require serious preparation and planning.

### **2.1. Practical learnings**

Effective planning and coordination were crucial to transition to biofuel successfully. This involved establishing a timeline, coordinating with fuel suppliers, discussing with the crew and ensuring the availability of necessary resources. Before the trial, extensive compatibility tests were performed to confirm the suitability of the biofuel with the vessel's fuel system. Tank cleanliness was also assessed, and necessary cleaning procedures were conducted to avoid contamination or compatibility issues. Additionally, the settling tanks were emptied to a minimum level before refilling them with biofuel to prevent adverse effects from fuel mixing. During the first two to three days of the trial, the fuel filters underwent 2-3 rounds of cleaning to maintain their efficiency. Furthermore, an additional cleaning process was carried out for the separators to ensure their optimum operation. Continuous fuel system monitoring was vital to detect and address fuel leaks promptly. Regular checks and maintenance procedures were established to ensure the integrity of the fuel system throughout the trial. Optimizing the fuel system involved closing the heating system traces. Only the drainage and leak systems were slightly opened,



facilitating optimal operation conditions, and minimizing potential issues. Biofuel operation conditions were like Marine Gas Oil (MGO), with some key considerations. The pour point of biofuel,  $\sim 12^{\circ}\text{C}$ , required precautions to prevent fuel gelling at lower temperatures. FAME demonstrated good combustion abilities; however, it was found to be sensitive to water content, which can lead to microbial growth. When the fuel is consumed continuously, and with a steady flow, the risk of microbial growth is reduced. However, it is essential to implement proper measures for moisture control to mitigate effectively. FAME can be used in blends with other fuels or as pure FAME, providing flexibility in utilizing biofuels in various proportions.

### 3. Analysis

During the trial, Acacia Seaways used a total of 2,145 tons of biofuel. This amount reflects the volume of fuel to meet the ship's operational energy needs without deviating from its usual operation in the trial period. Bunkering operations and energy consumption data provide critical information on the scale and scope of biofuel utilisation, which is essential for sustainability assessments.

Analyses using Well-to-Wake (WtW) and Tank-to-Wake (TtW) calculation methods have shown significant reductions in  $\text{CO}_2$  emissions. On a Well-to-Wake basis a reduction of 5,297 tons of  $\text{CO}_2$  equivalent was achieved, when the entire life cycle of the biofuel was considered. This means a WtW  $\text{CO}_2\text{e}$  reduction of 82%. On a Tank-to-Wake basis the biofuel trial contributes to a reduction of 5,918 tons of  $\text{CO}_2$  emissions. In the Tank-to-Wake calculations biofuel B100 is defined as a zero-emission fuel and the TtW  $\text{CO}_2$  reduction is therefore 100%. This explains the higher Tank-to-Wake savings than Well-to-Wake.

When the energy content of biofuel is compared to ULSFO, it is observed that biofuel consumption is approximately 14% higher to achieve the equivalent energy output. This is based on test samples of the ULSFO fuel in the period before the biofuel trial and samples of the biofuel during the trial. Here it was shown that the ULSFO had an average energy content of 42.5 MJ/kg and the biofuel had an energy content of 37.2 MJ/kg. This clearly demonstrates that while biofuel offers environmental benefits such as a reduced carbon footprint, it requires higher volumetric requirements to balance energy levels. It was therefore included in the Well-to-Wake calculations that 14% more fuel is needed when operating on B100 instead of ULSFO. The energy content of different fuel types is therefore very important when assessing the environmental impact of switching between fuel types.

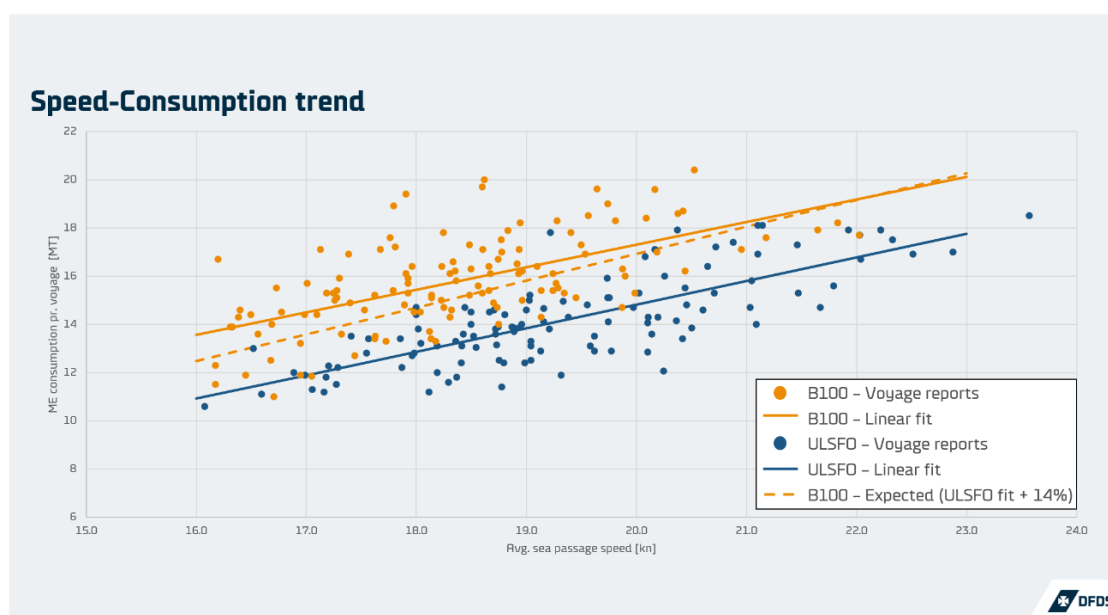


Fig.1: Speed-consumption trend for biofuel B100 trial and the pre-trail period on ULSFO

Fig.1 shows the speed-consumption trend during the biofuel trial compared to the pre-trial period. The trendlines are showing around 14% more consumption when running on biofuel B100 which supports the measured difference in energy content.

During the biofuel trial Acacia Seaways travelled 5% slower on average compared with the three months before the trial. This reduction in speed had therefore an impact on fuel consumption, where the main engine consumption only showed an 11% increase in average fuel consumption per voyage during the trial. If the average speed had been the same in the two periods and seasonality effects are neglected, it would have been expected to see an increase in main engine consumption of 14% according to the difference in energy content. The trial was done in October to December whereas the pre-trial period was July to September which would therefore lead to seasonality effects. Fig.2 shows the consumption and speed per voyage. The consumption goes up and the reduction in speed is also seen but not as clear as the difference in consumption.

During the biofuel trial, a 6% reduction in Marine Gas Oil (MGO) consumption for auxiliary engines and boilers was observed, which is due to the lower heating requirements of biofuel compared to ULSFO. When studying the total consumption, Acacia Seaways consumed 10% more fuel per voyage during the biofuel deployment compared to the pre-trial period. This is therefore taking into account the 11% increase in main engine consumption and 6% reduction in consumption on auxiliary engines and boiler.

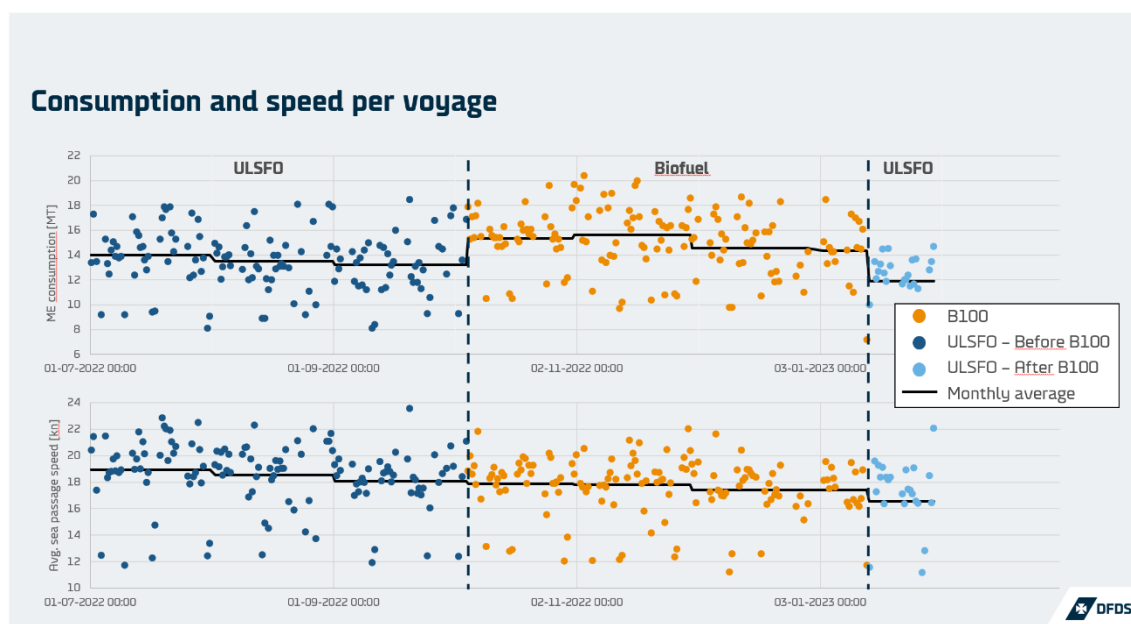


Fig.2: Consumption and speed per voyage over time during the biofuel B100 trial, pre-trial period and post-trial period

#### 4. Discussion

Acacia Seaways' biofuel experience provides an important analytical insight into the effectiveness of sustainable energy sources in the maritime sector. This experience provides valuable data not only on the current state of biofuel technology, but also on its potential future applications.

The recorded reductions in CO2 emissions were supported by Well-to-Wake (WtW) and Tank-to-Wake (TtW) calculations, suggesting a potential role for biofuels in short-term carbon mitigation strategies. However, emerging challenges, such as relatively lower energy content, may limit the large-scale adoption of biofuels e.g. by more often bunkering and it might limit the availability of biofuel. Comparisons with ULSFO based on both measuring the energy content from fuel samples and comparison of the fuel consumption on Acacia Seaways confirm that

biofuels have a higher consumption requirement to achieve equivalent energy coverage. This means that the operational costs will increase more than just when comparing fuel prices, which makes the energy content essential in the business case as well as when assessing the environmental impact. This energy content difference raises questions as to whether biofuels can compete economically with ULSFO or other conventional fuels. But future regulation such as EU ETS will drive this change to green fuels and can potentially lead to that biofuel can compete with conventional fuels.

Operational challenges are another factor affecting the adaptation and implementation of biofuel technology. Findings such as the reduction in heating requirements for the fuel system point to operational dynamics that need to be considered during biofuel integration. However, the reductions in fuel consumption in auxiliary engines and boilers suggest that biofuels may have some operational advantages. Such advantages could be critical for a more widespread acceptance of biofuels in the marine industry. However, more extensive studies are needed to fully evaluate these potential advantages and determine how to optimise them in real world applications.

#### **4.1. Regulatory reporting**

For the 2022 regulatory reporting the CO<sub>2</sub> reduction of operating on biofuel could not be considered for the IMO DCS reporting for DFDS. But after MEPC 80 CO<sub>2</sub> reduction due to biofuel is now considered when sustainability certificates are available according to MEPC.1/Circ.905. The emission factor used will be the Well-to-Wake emissions expressed from the sustainability certificate (expressed as gCO<sub>2</sub>eq/MJ) multiplied by the energy content (lower calorific value expressed as MJ/g). This means that biofuel thereby can have an impact on CII but not as a zero-emission fuel. This means that Well-to-Wake emission factors will be used for biofuel going forward even though Tank-to-Wake emission factors are used for the conventional fuels. This is the solution until operationalization of a well-to-wake GHG methodology through the LCA Guidelines by IMO according to MEPC.1/Circ.905.

Based on CII calculated for 2022 (even though CII was not into force) the three months of biofuel trial would lead to a 22% reduction in CII if biofuel CO<sub>2</sub> was calculated according to MEPC.1/Circ.905 compared to how biofuel was considered for 2022 regulatory reporting. For Acacia Seaways this would mean an improvement from D to B in CII score for 2022.

For EU MRV reporting for 2022 biofuel B100 was considered zero-emission. Thereby biofuel will also have an impact on EU ETS.

#### **5. Conclusion**

The results of the trial with biofuel B100 FAME on Acacia Seaways demonstrate the potential of sustainable energy sources in the maritime sector. The trial was completed without significant operational or technical problems, allowing biofuels to be considered as a reliable and efficient energy source. The capacity of the sustainability certified second generation biofuel to significantly reduce CO<sub>2</sub> emissions is remarkable at a time when sustainable energy solutions are an urgent need.

The recognition of biofuel B100 as a zero-emission fuel in EU/UK MRV and IMO DCS reporting opens up new opportunities and incentives to limit carbon emissions in the maritime sector. The emission reductions recorded during the trial provide an important example of how sustainability can be turned into a commercial advantage in the maritime sector when this is recognised in regulatory reporting.

The knowledge gained from this experience will help shape future research and implementation strategies by providing valuable insights into the integration of biofuels into the maritime industry. In this context, the commercialisation of biofuel operation will allow the maritime

industry to not only fulfil its environmental responsibilities, but also deliver tangible CO<sub>2</sub> reductions to customers. This process represents a critical step in the industry's progress towards a sustainable future.

## References

EJDER, E.; ARSLANOĞLU, Y. (2022), *Evaluation of ammonia fueled engine for a bulk carrier in marine decarbonization pathways*, J. Cleaner Production 379, <https://doi.org/10.1016/j.jclepro.2022.134688>

HARAHAP, F.; NURDIAWATI, A.; CONTI, D.; LEDUC, S.; URBAN, F. (2023), *Renewable marine fuel production for decarbonised maritime shipping: Pathways, policy measures and transition dynamics*, J. Cleaner Production 415, <https://doi.org/10.1016/j.jclepro.2023.137906>

HSIEH, C.-W.C.; FELBY, C. (2017), *Biofuels for the marine shipping sector An overview and analysis of sector infrastructure, fuel technologies and regulations*, IEA Bioenergy, <https://www.ieabioenergy.com/wp-content/uploads/2018/02/Marine-biofuel-report-final-Oct-2017.pdf>

ISLAM RONY, Z.; MOFIJUR, M.; HASAN, M.M.; RASUL, M.G.; JAHIRUL, M.I.; FORRUQUE AHMED, S.; KALAM, M.A.; ANJUM BADRUDDIN, I.; YUNUS KHAN, T.M.; SHOW, P.L. (2023), *Alternative fuels to reduce greenhouse gas emissions from marine transport and promote UN sustainable development goals*, Fuel 338, <https://doi.org/10.1016/j.fuel.2022.127220>

JAMIL, F. (2023), *A Review on Biodiesel Production, Analysis, and Emission Characteristics from Non-Edible Feedstocks*, ChemistrySelect 8(31), e202300800

NEUPANE, D. (2023), *Biofuels from Renewable Sources, a Potential Option for Biodiesel Production*, Bioengineering 10(1), <https://doi.org/10.3390/bioengineering10010029>

# Combine and Conquer for Smart Hull Management

Helle Vines Ertsås, Jotun, Sandefjord/Norway, [helle.v.ertsas@jotun.no](mailto:helle.v.ertsas@jotun.no)  
Morten Sten Johansen, Jotun, Sandefjord/Norway, [morten.sten.johansen@jotun.com](mailto:morten.sten.johansen@jotun.com)

## Abstract

*This paper describes Jotun's Hull Skating Solutions (HSS), which use proactive hull cleaning to combat early-stage fouling to maintain an always clean hull. The Hull Skating Solutions consist of five key elements: (1) SeaQuantum Skate coating capable of enduring repeated mechanical contact with the proactive cleaning brush without erosion of the coating; (2) Proactive condition monitoring utilizing big data to trigger condition-based cleaning events and for performance monitoring based on ISO 19030; (3) HullSkater robot for in-water inspection and proactive hull cleaning; (4) Service support in application and remote control of the Hull Skater operation; (5) Performance-based contracts ("clean hull guarantee"). The paper describes the key elements of HSS and first in-service experience.*

## 1. Introduction

The accumulation of fouling over time leads to a significant drop in performance and an increase in the vessel's fuel consumption and environmental footprint, Fig.1, *GIA (2021)*. To counter this, ship operators use hull coatings with anti-fouling properties. However, these coatings will not always deliver optimal anti-fouling protection due to changing operational profiles or the operation being so challenging that fouling pressures exceeding coating tolerance.

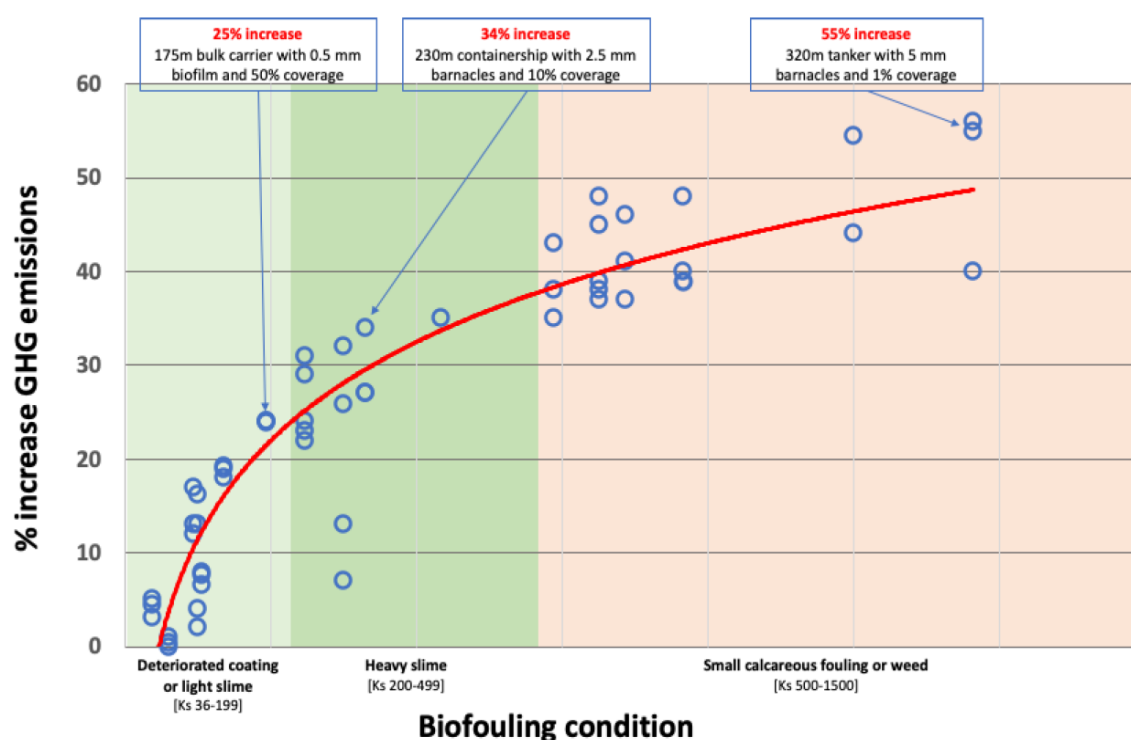


Fig.1: Effect of biofouling on Greenhouse Gas (GHG) emissions, *GIA (2021)*

Various circumstances can prove challenging for hull performance, especially if speed, periods of inactivity and water temperature lie outside the coating's tolerance. For example, bulk carriers, tankers, and general cargo ships can spend long periods in ports being loaded and unloaded. Some of them may also be prevented from berthing for long periods due to neap tides. In such cases, shallow water and temperate environments can lead to accelerated fouling. Many shipowners must deal with these challenging operations on a regular basis.



According to the IMO's 4<sup>th</sup> GHG emissions study, *IMO (2020)*, International shipping emitted around 919m tons of CO<sub>2</sub> and 21m tons of other GHGs in 2018 (incl. methane, NO<sub>x</sub>, SO<sub>x</sub>). According to the same study, 9% of consumption and emissions were caused by biofouling, resulting in a total annual reduction potential of 83m tons of CO<sub>2</sub> and around 2m tons of other GHGs. The share of consumption and emissions caused by biofouling corresponds with findings from other studies including the Clean Shipping Coalition submission to the 63<sup>rd</sup> IMO Marine Environment Protection Committee meeting, *CSC (2015)*.

For ships with greater biofouling pressure, the share of additional fuel consumption caused by biofouling is likely to greatly exceed the 9% average for all ships. The improvement potential is therefore considerable.

Aside from cleaning during dry-dockings, hulls and propellers may be cleaned occasionally in water while in service. This is normally done as reactive cleaning when significant performance loss due to heavy fouling becomes evident. Today, performance monitoring software tools allow detecting varying degrees of fouling based on the degrading ship's performance, triggering cleaning in response. However, at this stage fouling is already a major problem.

Traditional cleaning is done manually by divers. This approach, still in common use, has become increasingly under scrutiny. Diving teams may be good at clearing the fouling from the hull but there are problems. Firstly, it is a labor intensive and costly process. If there are not enough divers available, the time needed can be difficult for ship operators to fit into schedules and may lead to off-hire time for ships. Moreover, manual cleaning often leads to the coating becoming damaged, Fig.2 (right) and with even worse fouling after a very short time. The effect on the environment is also an issue as the cleaning process may result in aquatic invasive species and/or eroded coating materials being deposited into the water column, Fig.2 (left), with detrimental effect on local ecosystems. In response, port authorities have become increasingly restrictive on in-water cleaning, making following IMO's biofouling guidelines difficult to follow. Finally, and perhaps most importantly, in some situations manual cleaning with divers place the divers at risk. Injuries and deaths are reported each year.

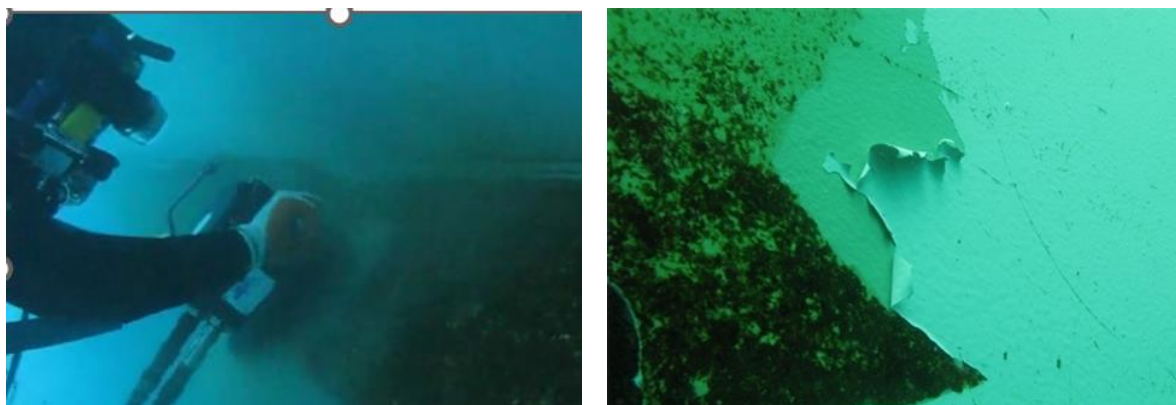


Fig.2: Traditional cleaning releasing fouling and paint particles (left); resultant paint damage (right)

Robotic cleaning (with autonomous or remotely controlled robots) is another way to clean hulls and there are a range of solutions of varying maturity emerging, *Bertram (2021)*. Most of the more recently developed robots allow the capture of the removed coating and biofouling for proper disposal in port. However, the common denominator for most cleaning technologies in use today is that they are used reactively – they are designed for and applied when the fouling has already become a problem.

## 2. Proactive cleaning and the Jotun Hull Skating Solution

To combat fouling and address the concerns of port authorities regarding release of invasive species, Jotun has adopted proactive cleaning through its Hull Skating Solutions, <https://www.jotun.com/ww->

[en/industries/solutions-and-brands/hull-skating-solutions/overview](https://www.jotun.com/en/industries/solutions-and-brands/hull-skating-solutions/overview). Proactive cleaning, sometimes also referred to as grooming, has been increasingly advocated, e.g. *Hunsucker et al. (2018)*, *Swain et al. (2020)*. Jotun has been active in promoting a corresponding standard for in-water cleaning, *Oftedahl and Skarbø (2021)*, *Oftedahl et al. (2022)*, *Skarbø (2022)*.

Biofouling progresses in several stages:

- Stage 1 (USN FR 0 to 10): Settlement of individual bacteria
- Stage 2 (USN FR 20): Biofilm / slime
- Stage 3 (USN FR 30): Algae and single-cell organisms
- Stage 4 (USN FR 40 and up): Macro-fouling (tubeworms, barnacles, etc.)

In the above list, USN FR refers to the US Navy Fouling Rating scale, *US Navy (2006)*.

In Jotun's Guideline for Proactive Cleaning of Hull Areas in Port & at Anchorage, *Oftedahl and Enström (2020)*, Annex 1, proactive cleaning is defined as the proactive removal of fouling at earlier stages, well before it reaches macro-fouling. Proactive cleaning is achieved by cleaning the hull regularly before macro-fouling takes hold, typically at the slime stage. Fouling is therefore removed before it significantly affects hull performance and before there is biofouling waste to be captured. Fouling at such an early stage can be removed by small shear forces, without damage to or erosion of the coating.

## 2.1. Solution elements

Jotun's Hull Skating Solutions (HSS) combine five elements, Fig.3, addressing technical, operational and commercial issues:



Fig.3: The five elements in the Hull Skating Solutions

- **High performance coating** – Jotun's 'SeaQuantum Skate' coating was developed specifically to optimize performance in combination with the robotic cleaning technology of the HullSkater robot. The coating based on silyl acrylate can endure repeated mechanical contact with the proactive cleaning brushes without erosion.
- **Proactive condition monitoring** – This is an essential component of predictive hull maintenance, enabling the HullSkater to operate when needed. Jotun's in-house data scientists and marine biologists have developed an algorithm predicting when fouling start to occur on the vessel's hull. This enables the Skate Operator to appropriately time the deployment of the system. As part of the monitoring, vessel performance is analyzed and document using the ISO 19030 standard for hull and propeller performance, *ISO (2016)*.
- **Inspection and proactive cleaning** – The HullSkater is the first robotic device purposely designed for proactive cleaning, Fig.4. It has high inspection and cleaning capacity and removes fouling without damaging the anti-fouling coating. The HullSkater is always kept onboard in a portable station, Fig.5, with launch and recovery ramp. This means that it is always available and can be used when the ship is in harbour or at anchor. It is launched and retrieved by the ship's crew, Fig.6.

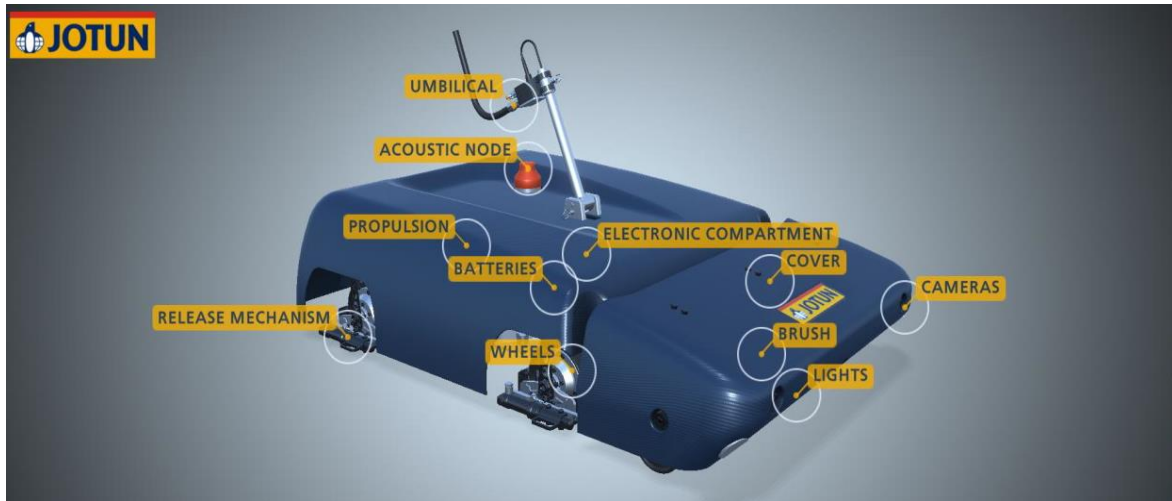


Fig.4: HullSkater robot



Fig.5: HullSkater in docking station



Fig.6: HullSkater being launched

- High-end technical service** – HSS includes highly skilled coating advisors who ensure correct coating application of the high-performance coating, including a comprehensive regime for measuring and documenting the quality of the application process. Every HSS delivery is supported by a certified project manager, overseeing the application process, and ensuring smooth instalment and set-up of the robotics. Once the HullSkater is launched, it is remotely operated by dedicated Skate Operators from Jotun, Fig.7, working by the “follow the sun” principle with operating hubs in all time zones, enabling 24/7 support.

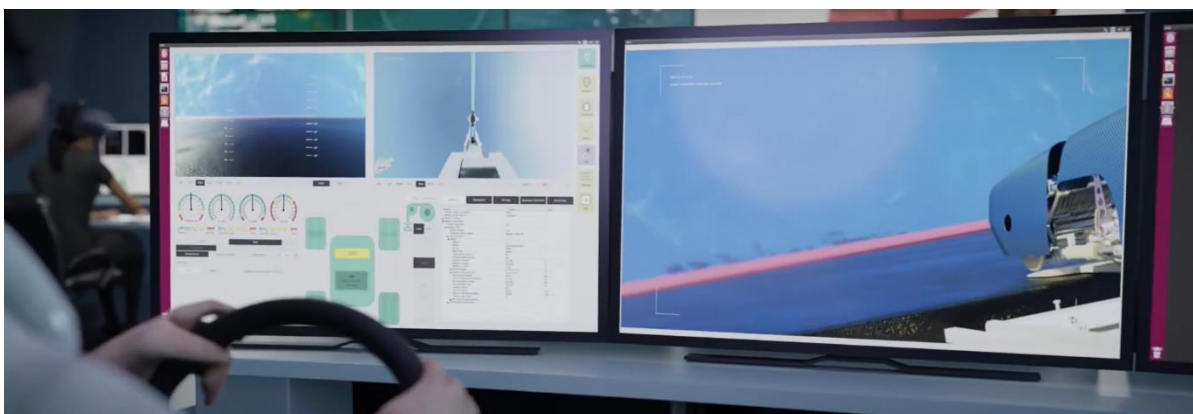


Fig.7: Remote control of HullSkater

- Performance and service level guarantees** – The confidence in Jotun’s Hull Skating Solutions allows us to offer performance and service level guarantees fitting the needs of the most challenging operations.

## 2.2. How it works

Jotun Hull Skating Solutions is installed on the vessel at the new build or dry dock yard and remains on board and in operation all through the drydocking cycle, Fig.8.

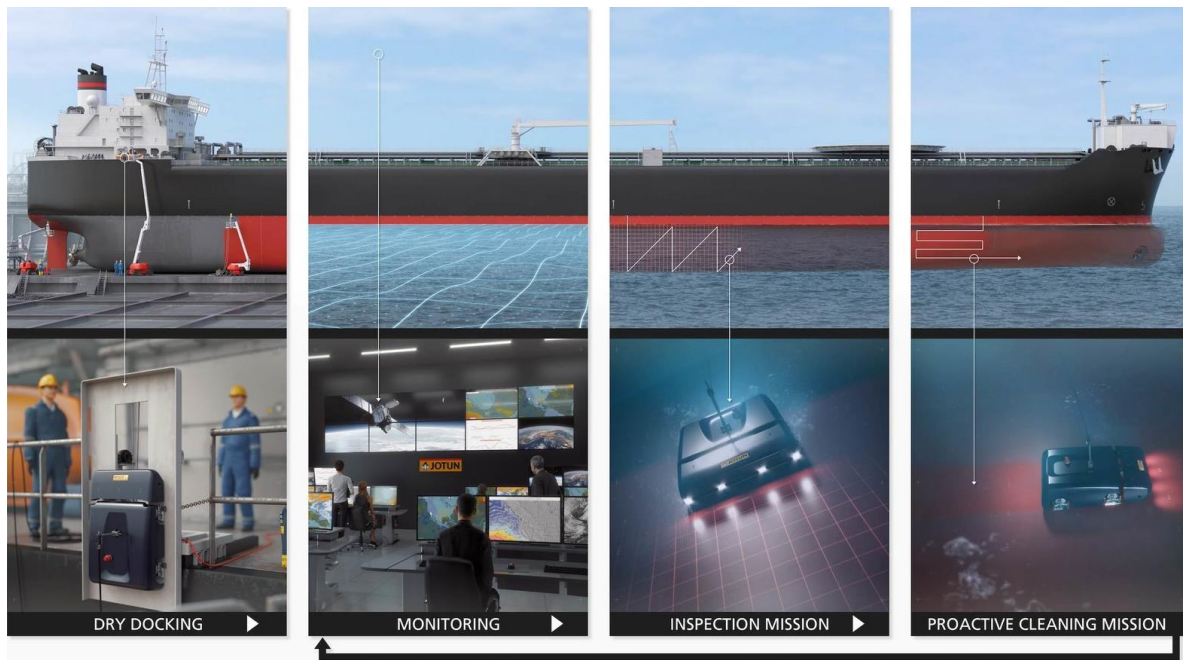


Fig.8: How it works

- **Drydocking** – During drydocking, the painting process is supervised by a certified Jotun Project Manager, who also is responsible for the installation of the HullSkater and the Skate Station.
- **Monitoring** – In addition to the performance monitoring following ISO 19030, advanced machine learning algorithms are used to predict the probability of fouling based on operational areas and ship operational parameters, and to identify when the Skater needs to be deployed for an inspection and potentially proactive cleaning mission.
- **Inspection Mission** – When alerted by the fouling prediction algorithm, the Jotun Skate Operator contacts the ship to schedule an inspection mission, Fig.9. The Jotun HullSkater can be operated in port or at anchor, as long as there is sufficient 4G coverage for communication.
- **Proactive Cleaning Mission** – During the inspection mission, if light fouling is detected, the Skate Operator initiates proactive cleaning. If time does not allow a proactive cleaning mission, then the Jotun Skate Operator agrees with the ship when the next opportunity will be.

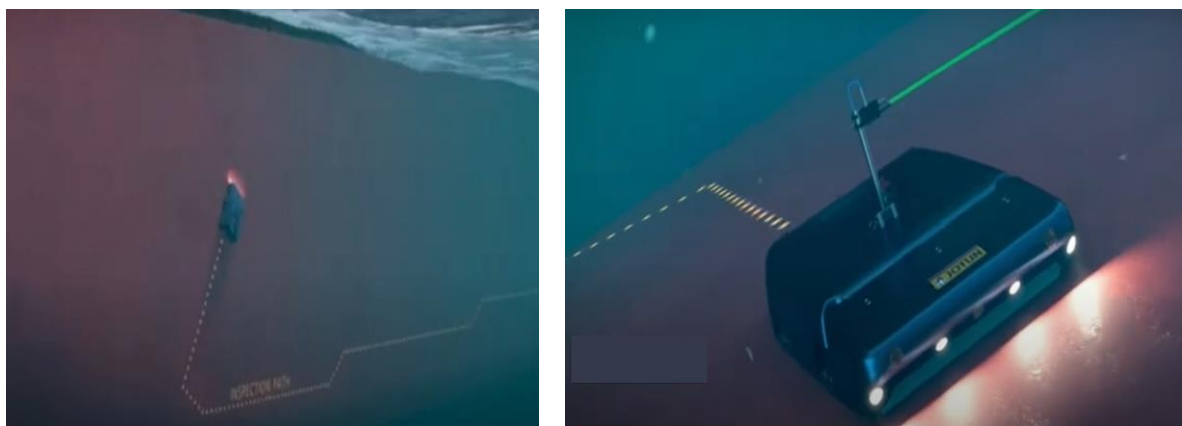


Fig.9: Initial inspection follows prescribed path to examine the hull condition



### 3. In-service experience

In 2016, Jotun approached Wallenius Wilhelmsen to pilot-test the system onboard one of its vessels. In 2017, Wallenius Wilhelmsen gave Jotun's HSS team access to the "Talisman", Fig.10, a 38500 DWT RoRo carrier built in 2000.



Fig.10: First application case: "Talisman" of Wallenius Wilhelmsen

The project team applied antifouling test patches on the hull, installed the unit on board, and trained crew members on maintenance, deployment, retrieval, and storage of the unit.

Over the last years, several vessels have been made "Skater ready" by applying SeaQuantum Skate antifouling coating and marking the hull with no-skate zones, and the HullSkater have been installed as part of the *final verification* of the solution. *Final verification* means verifying the solution technically, operationally and commercially, and documenting performance of the vessels involved.

The multi-year pilot test with Wallenius Wilhelmsen and other shipowners, provided the project team with valuable insight on what worked – and what didn't. Following a number of tests at different ports, Jotun has been working to establish agreements with some ports which require documentation of a clean underwater hull prior to the port call. Regulatory compliance, securing access to ports through documentation of a clean hull, have become even more important over the last years. The cost of being rejected from port can be huge, and an onboard solution for documentation of hull condition can mitigate this risk.

Jotun have also developed a guideline for ports to assess and accredit in-water robotic cleaning, *Ofstedahl and Enström (2020)*. This guideline will eventually be replaced by the ISO standard on proactive cleaning, which the Clean Hull Initiative (CHI) have initiated (*Skarbø, 2022*).

### 4. Conclusion

Hull Skating Solutions offers an innovative hull management approach to address both energy efficiency keeping the CII (Carbon Intensity Indicator) low, Fig.11, and biofouling management to minimize transport of invasive species. Preliminary results from performance monitoring of the vessels involved in the final verification of Hull Skating Solutions confirms GIA findings in Fig.11.



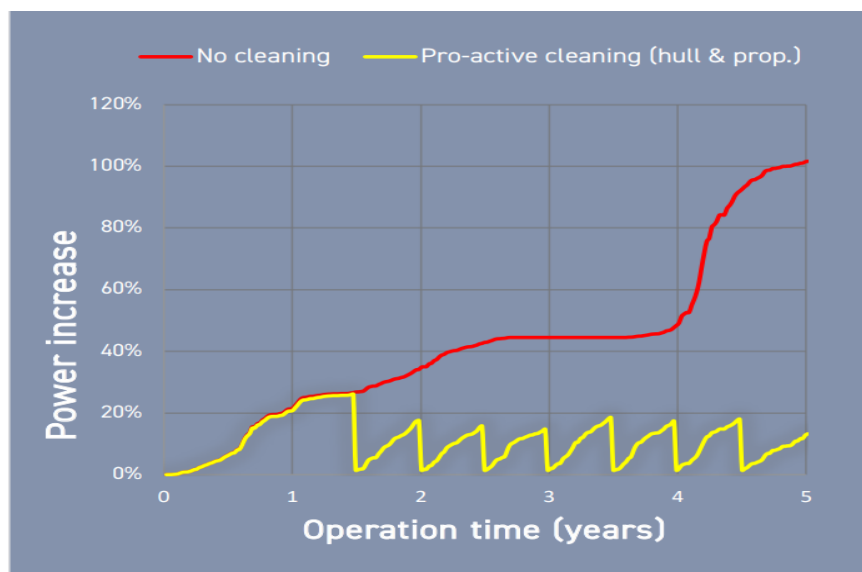


Fig.11: Effect of proactive cleaning (yellow curve) on fuel and emission reduction, GIA (2022)

## Acknowledgements

Developing the Hull Skating Solutions would not have been possible without world-class partners, which we gratefully acknowledge. Thanks go to the many colleagues at Kongsberg, Semcon, DNV, Telenor, DNB / EksFin, Wallenius Wilhelmsen and our other customer partners joining the exiting journey of this groundbreaking innovation.

## References

BERTRAM, V. (2021), *Robotic Hull Cleaning – State of the Art and Roadmap*, 13<sup>th</sup> HIPER Symp., Tullamore, pp.37-44,

CSC (2015), *A transparent and reliable hull and propeller performance standard*, Clean Shipping Coalition submission to MEPC 63, IMO, London, [https://bellona.no/assets/sites/3/2015/06/fil\\_MEPC\\_63-4-8\\_-\\_A\\_transparent\\_and\\_reliable\\_hull\\_and\\_propeller\\_performance\\_standard\\_CSC1.pdf](https://bellona.no/assets/sites/3/2015/06/fil_MEPC_63-4-8_-_A_transparent_and_reliable_hull_and_propeller_performance_standard_CSC1.pdf)

GIA (2021), *Impact of Ships' Biofouling on Greenhouse Gas Emissions*, Global Industry Alliance for Marine Biosafety, IMO, London, <https://wwwcdn.imo.org/localresources/en/MediaCentre/Documents/Biofouling%20report.pdf>

GIA (2022), *Analysing the Impact of Marine Biofouling on the Energy Efficiency of Ships and the GHG Abatement Potential of Biofouling Management Measures*, GloFouling Partnerships Project Coordination Unit, Int. Maritime Org., London, [https://www.glofouling.imo.org/\\_files/ugd/34a7be02bd986766d44728b85228c3ec9b95ee.pdf](https://www.glofouling.imo.org/_files/ugd/34a7be02bd986766d44728b85228c3ec9b95ee.pdf)

HUNSUCKER, K.; BRAGA, C.; ERGODAN, C.; GARDNER, H.; HEARIN, J.; RALSTON, E.; GEOFFREY SWAIN, G.; TRIBOU, M.; WASSICK, A. (2018), *The Advantages of Proactive In-Water Hull Grooming from a Biologist's Perspective*, 3<sup>rd</sup> HullPIC Conf., Redworth, pp.210-222, [http://data.hullpic.info/hullpic2018\\_redworth.pdf](http://data.hullpic.info/hullpic2018_redworth.pdf)

IMO (2020), *4th IMO GHG Study – Final Report*, IMO, London, <https://wwwcdn.imo.org/localresources/en/OurWork/Environment/Documents/Fourth%20IMO%20GHG%20Study%202020%20-%20Full%20report%20and%20annexes.pdf>

ISO (2016), *ISO 19030 - Ships and marine technology – Measurement of changes in hull and propeller performance*, Part 2, ISO, Geneva

OFTEDAHL, G.A.; ENSTRÖM, A. (2020), *Proactive Cleaning and the Jotun Hull Skating Solution*, 1<sup>st</sup> PortPIC Conf., Hamburg, pp.66-78, [file:///D:/PortPIC2020\\_Hamburg.pdf](file:///D:/PortPIC2020_Hamburg.pdf)

OFTEDAHL, G.A.; SKARBØ, R.C. (2021), *A Way Forward for In-water Proactive Cleaning*, 3<sup>rd</sup> PortPIC Conf., Hamburg, pp.67-75, [http://data.hullpic.info/PortPIC2021\\_Pontignano.pdf](http://data.hullpic.info/PortPIC2021_Pontignano.pdf)

OFTEDAHL, G.A.; SKARBØ, R.; JOHANSEN, M.S.; ERTSÅS, H.V.; OEPSTAD, C. (2022), *A Way Forward for In-water Proactive Cleaning*, 3<sup>rd</sup> PortPIC Conf., Hamburg, pp.67-75, [http://data.hullpic.info/PortPIC2022\\_Hamburg.pdf](http://data.hullpic.info/PortPIC2022_Hamburg.pdf)

SKARBØ, R. (2022), *The Clean Hull Initiative One Year Later: Towards an ISO Standard on Proactive Hull Cleaning*, 3<sup>rd</sup> PortPIC Conf., Hamburg, pp.150-154, [http://data.hullpic.info/PortPIC2022\\_Hamburg.pdf](http://data.hullpic.info/PortPIC2022_Hamburg.pdf)

SWAIN, G.; TRIBOU, M.; GARDNER, H.; HUNSUCKER, K. (2020), *In-Water Grooming of Fouling Control Coatings: From Research to Reality*, 1<sup>st</sup> PortPIC Conf., Hamburg, pp.29-37, [http://data.hullpic.info/PortPIC2020\\_Hamburg.pdf](http://data.hullpic.info/PortPIC2020_Hamburg.pdf)

US NAVY (2006), *Naval Ships' Technical Manual Chapter 081 – Waterborne Underwater Hull Cleaning Of Navy Ships*, <https://maritime.org/doc/nstm/ch081.pdf>

# A Case Study: Combined Effect of a Silicone-Based Low Friction Coating and a Weld Seam Fairing Solution

**Philippos Sfiris**, Hempel A/S, Athens/Greece, [phsf@hempel.com](mailto:phsf@hempel.com)  
**Yigit Kemal Demirel**, Hempel A/S, Barcelona/Spain, [ykd@hempel.com](mailto:ykd@hempel.com)  
**Andrea Farkas**, Hempel A/S, Zagreb/Croatia, [afar@hempel.com](mailto:afar@hempel.com)  
**Sofia Pagoni**, Hempel A/S, Athens/Greece, [sop@hempel.com](mailto:sop@hempel.com)

## Abstract

*This paper presents a ship-specific study that evaluates the potential combined effect of Hempaguard X7, a silicone-based low-friction coating, and SeamFlow, an innovative weld seam fairing solution. Utilizing Hempel's framework for evaluating energy efficiency measures, the study assesses a specific scenario involving the application of Hempaguard X7 and SeamFlow, comparing the findings with a conventional approach using a self-polishing coating system. The ship-specific analyses explore the efficiency gains achieved through this technology combination, encompassing effects on required power, total fuel consumption, and variations in the Carbon Intensity Indicator (CII) rating over a 5-year docking cycle. The findings demonstrate that the application of Hempaguard X7 and SeamFlow can lead to substantial fuel savings and reduction in emissions.*

## 1. Introduction

A moderate scenario of global trade growth at 1-2% per annum will necessitate significant fleet development in the coming decades. Considering the limited supply of alternative fuels in the 2020s, a substantial gap exists in meeting the demand until zero-carbon ships become available. According to a recent analysis by *Stopford (2022)*, this gap is expected to be primarily filled by existing vessels and new vessels entering the market, which will continue to rely on diesel technology. These vessels are projected to dominate the fleet composition for the next decade, until more advanced ships utilizing technologies such as LNG, dual fuel, and electric propulsion are introduced. The same analysis also indicates that these ships are expected to account for 50% of shipping emissions from 2020 to 2050.

Therefore, the decarbonization challenge is, to a large extent, a challenge concerning what the shipping industry can do with its existing fleet for the next decade. Shipping must meet its short-term emissions reduction requirements through operational measures and technical upgrades using currently available energy efficiency technologies. Silicone-based and other advanced antifouling coating systems represent one of the most mature technological upgrades capable of providing immediate improvements in ship energy efficiency, *ABS (2021)* and *IMO (2023)*. There are several other options, however, that should be taken into consideration in combination with selecting the right coating system, including, but not limited to, installing energy saving devices to reduce friction and/or improve propeller efficiency, increasing the frequency of dry dockings, adopting a proactive hull cleaning policy, use of biofuels in the fuel mix. In this context, Hempel's innovative silicone-based low friction coating, Hempaguard X7, and novel weld seam fairing solution, SeamFlow, offer promising avenues for enhancing energy efficiency. Notably, these technologies present a unique advantage in that they enhance energy efficiency without imposing any additional operational burdens or energy consumption during routine ship operations, while also demonstrating resilience against potential biofouling issues.

The vital question for ship owners and operators remains: "How can we make informed decisions in selecting the most suitable measures to enhance energy efficiency?" Addressing this question necessitates ship-specific investigations due to the multitude of influencing factors. Given the multitude of factors involved, it becomes crucial to assess energy efficiency measures in a structured and ship-specific manner, empowering ship owners and operators to make well-informed decisions. This market demand calls for a comprehensive evaluation of such options, considering not only regulatory compliance but also operational, techno-economic and environmental perspectives. In response to this need, Hempel has introduced a framework that evaluates emissions reduction pathways from distinct

angles before any ship-specific investment is made. The outcome is a ship-specific report, offering transparency and clarity on the expected impact of various scenarios considered by the shipowner or operator, as reported by *Sfiris et al. (2023)*.

This paper focuses on showcasing the potential benefits of Hempaguard X7, a silicone-based low friction coating, when used in conjunction with SeamFlow, an innovative weld seam fairing solution. To achieve this objective, we leverage Hempel's framework to provide a comprehensive assessment of the impact and implications of adopting this novel technology bundle on a specific ship over a 5-year docking cycle. It is important to note that this paper reports a subset of results from the larger investigation, in line with the scope and objectives defined for this study. We selected the same ship and case study used by *GEF-UNDP-IMO (2022)* and *Sfiris et al. (2023)*. Through this ship-specific analysis, we will uncover insights into the efficiency gains, reduction in total fuel consumption and favorable CII ratings achievable with the application of Hempaguard X7 and SeamFlow, and compare the findings with the traditional scenario of selecting a conventional self-polishing coating (SPC).

## 2. Methodology

### 2.1 Case study

We selected the same ship and case study used by *GEF-UNDP-IMO (2022)* and *Sfiris et al. (2023)*. The present case study involves the adoption of a silicone-based low friction paint, Hempaguard X7, and an innovative welding seam fairing solution, SeamFlow. The combined effects of this technology bundle on the ship's required power, total fuel consumption, CII rating variations over a 5-year docking cycle are demonstrated. The results are then compared with the traditional scenario of selecting a conventional self-polishing coating (SPC) with a responsive cleaning approach. This traditional approach was originally presented in *GEF-UNDP-IMO (2022)* and the further analysis were carried out by *Sfiris et al. (2023)*. Table I displays the principal particulars and selected scenarios for the target vessel.

Table I: The principal particulars and selected comparative scenarios of the target vessel, adapted from *GEF-UNDP-IMO (2022)* and *Sfiris et al. (2023)*

Vessel type	Bulk carrier
Deadweight	40,000 t
Length	179 m
Breadth	28 m
Design draft	10.6 m
Wetted surface area	7,350 m <sup>2</sup>
Speed	14 knots
Fuel consumption (clean - SPC)	20.4 t/day
Operating region	Mediterranean region
Operation period	5 years
Comparative scenarios	Baseline scenario: SPC + responsive cleaning* Present scenario: Hempaguard X7 + SeamFlow

\*This scenario refers to the 'Scenario 2' of *Sfiris et al. (2023)* and 'Hull & propeller cleaning' scenario of *GEF-UNDP-IMO (2022)*.

### 2.2 Technologies adopted

#### 2.2.1 Hempaguard X7

Hempaguard is a highly innovative and advanced marine coating solution developed by Hempel. It is specifically designed as an eco-friendly fouling control coating for the underwater hulls of ships and vessels and incorporates cutting-edge technology to enhance fuel efficiency, reduce maintenance costs, and minimize the environmental impact associated with traditional antifouling coatings. Key features and benefits of Hempaguard include:

- **Fouling Release Mechanism:** Hempaguard utilizes a unique fouling release mechanism, where the surface of the coating is designed to be extremely smooth. This makes it difficult for marine organisms, such as algae and barnacles, to adhere to the hull. As a result, when the vessel is in motion, these organisms are more likely to be naturally detached from the hull, reducing drag and improving fuel efficiency.
- **Hydrogel Layer:** One of the defining features of Hempaguard is its incorporation of a hydrogel layer. This layer, when activated by water, creates a water-like boundary that marine organisms find inhospitable for attachment. In addition, the hydrogel helps to control the biocide release to the surface.
- **Low Biocide Content:** Unlike traditional antifouling coatings that rely heavily on biocides (chemical substances that deter or inhibit the growth of marine organisms), Hempaguard utilizes a minimal amount of biocides. This approach reduces the release of potentially harmful substances into the marine environment, aligning with more environmentally conscious practices.
- **Fuel Efficiency:** The fouling resistance and smoother hull provided by Hempaguard contribute to improved hydrodynamics. This reduction in drag leads to better fuel efficiency and lower fuel consumption for vessels using this coating.
- **Extended Dry-Docking Intervals:** The fouling resistance of Hempaguard can lead to longer periods between required dry-docking and maintenance, reducing operational downtime and maintenance costs for shipowners and operators.
- **Operational flexibility:** Hempaguard is designed to perform effectively across a range of vessel speeds, from slow to high speeds. Moreover, its biocide release rates escalate with rising temperatures, guaranteeing peak efficiency even when confronting rigorous hard-fouling challenges.

Overall, Hempaguard is a prime example of environmentally conscious innovation in the marine industry that fuses antifouling and fouling release technologies by biocidal activation of a hydrogel-layer. This means that Hempaguard offers unprecedented fouling control performance while minimizing the biocide release to the environment. Taking together, the limited amount of biocide utilized in Hempaguard, to efficiently prevent biofouling and the significantly improved fuel-efficiency even after prolonged operation times, makes Hempaguard the most efficient and environmentally friendly fouling control coatings available today. Fig.1 illustrates the condition of a ship's hull surface coated with Hempaguard.

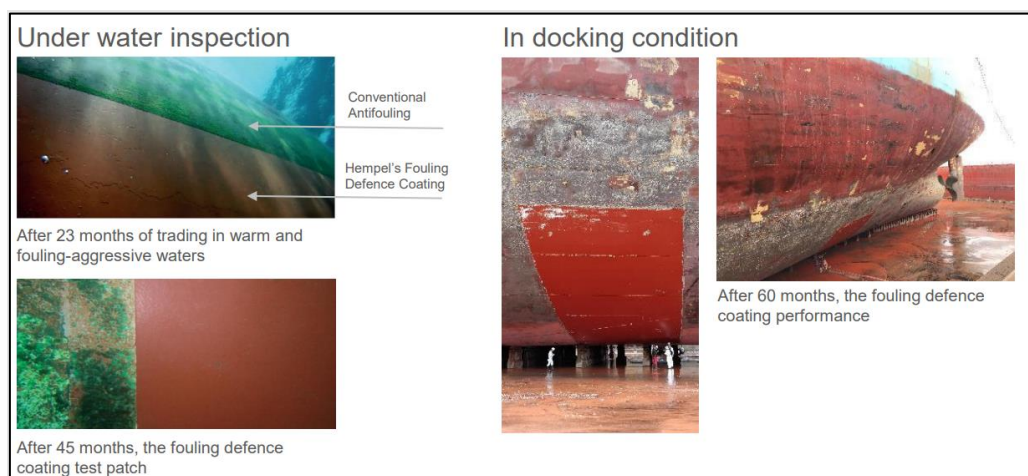


Fig.1: The surface condition of a ship hull coated with/without Hempaguard

The enhanced fuel efficiency can be attributed to i) an immediate power gain after the application due to smoothness compared to SPCs, and ii) a slow rate of degradation caused by mechanical deterioration of the coating, biofouling accumulation, and aging.



For this case study, the latter factor is assumed to result in a 1.4% speed loss over a 5-year period. This represents the guaranteed maximum average speed loss of a vessel with the Hempaguard X7 coating system, as per ISO 19030. The speed loss value is translated into an evenly distributed yearly increase in power.

The study by *Bertelsen and Meseguer Yebra (n.d.)* has reported an immediate power gain ranging from 6% to 8% when compared to conventional antifouling coatings. This insight is drawn from a compilation of various studies, elaborated upon in the same report. In addition, silicone-based topcoats are reported to consistently decrease the frictional resistance compared to SPC type paints, as shown by *Candries and Atlar (2005)*, *Schultz (2004)*, *Demirel (2015)*.

In the context of our specific case study, instead of relying solely on the findings mentioned above, we have opted to employ the results derived from towing tank experiments of flat plates performed by *FORCE (2007)*. This choice offers a more tailored approach to our investigation. By utilizing these results, we calculated the ship-specific immediate power gain at the vessel's design speed. This method enables a more precise alignment of the outcomes with the specific characteristics of our case study.

First, the roughness functions for the silicone-based low friction coating in the as-applied condition were determined using the towed plate method developed by *Granville (1987)*. Once the roughness functions and their corresponding behaviors were experimentally established, the effect of this specific surface condition on the ship's frictional resistance was computed. This was achieved through the application of the similarity law scaling procedure proposed by *Granville (1958)*, a method widely accepted and utilized in the literature, e.g. *Schultz (2004)*, *Schultz (2007)*, *Demirel et al. (2017)*, *Song et al. (2021)*. Consequently, the coating- and ship-specific roughness allowance value, represented by  $\Delta C_F$ , was calculated. Subsequently, the roughness allowance value for Hempaguard X7 was used to calculate the decrease in total resistance and power requirements for the vessel as compared to its configuration with a conventional SPC system. The procedure is summarized and illustrated in Fig.2.

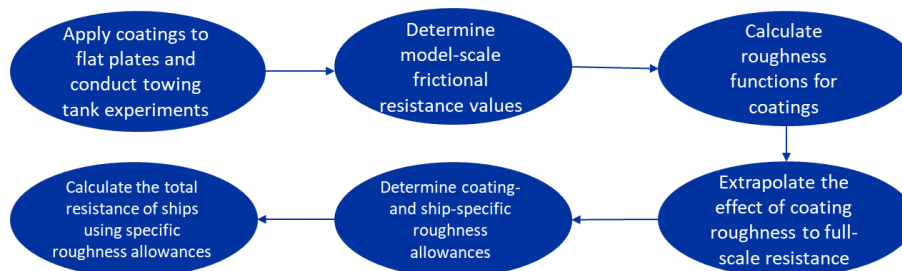


Fig.2: The procedure for calculating the effect of coating roughness on ship resistance

### 2.2.2 SeamFlow

SeamFlow represents a complete system of coating, application tools and dedicated service which improves drag characteristics of marine vessel by fairing welding seams, Fig.3. The concept has been patented by Hempel AS in 2018.

Since most of ships are welded structures, welding seams protrude from the hull causing the increase in total resistance which leads to an increase in fuel consumption, *Ciortan and Bertram (2014)*. Welding seams typically protrude 3-9 mm from the hull and smoothing the welding seams by grinding is expensive and long operation, which is risky to ship structure. The reduction of weld seam height directly causes the reduction in drag, which is demonstrated in several studies, *Ciortan and Bertram (2014)*, *Wang (2018)*. It is thus well established that weld seams transverse to the sailing direction are contributing significantly to the total resistance of ships. Therefore, it is intuitive that fairing out the weld seams leads to a hydrodynamically smoother surface, which will then reduce the impact of the weld seams on the total resistance of ships. Hempel's concept for solving this problem includes application of special modified epoxy on welding seams using the special equipment, tools and dedicated services. Thus, welding seams along the ship hull are faired and in that way the drag

coefficient of welding seam is reduced from 60% up to 80%, *FORCE (2017)*. The concept has been documented using three different approaches: CFD modelling, *FORCE (2021)*, rotor studies as well as towing tank experiments, *FORCE (2017)*.

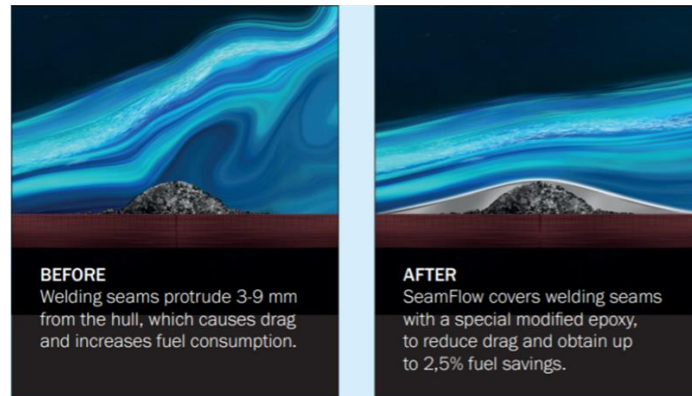


Fig.3: The main idea of SeamFlow

It is important to acknowledge the potential variability in the number of weld seams as well as their height due to factors such as shipyard capabilities and structural designs. As these specific details were not available for this case study, the total number of weld seams and their height are assumed. These assumptions play a critical role in further analysis, influencing the insights derived from this paper. This study operates within the bounds of these assumptions, and it is important to acknowledge their potential impact on the outcomes and conclusions presented in this paper.

In the present scenario, we assumed a setup with weld seams spaced 5 m apart and an initial weld height of 3 mm. These parameters are based on common figures for North European shipyards, as reported by *Ciortan and Bertram (2014)*. We also adopted their assumption that 10% of the welds exhibit poor welding quality with a height of 7 mm. It is important to note that the distance between weld seams is reduced in the fore and aft parts of the ship due to its complex shape.

The SeamFlow performance gain calculator is employed to assess the reduction in a ship's total resistance resulting from the application of SeamFlow, Fig.4. This calculator is an in-house developed Python tool specifically designed for calculating ship-specific reductions in total resistance attributed to SeamFlow application. It draws its foundation from the theory of 'drag of surface imperfections' elucidated in *Hoerner (1965)*, with the reduction in the drag coefficient of welding seams determined through towing tank experiments conducted on flat plates by *FORCE (2017)*.

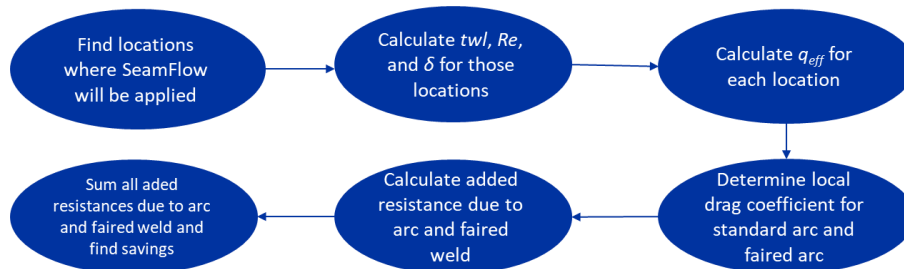


Fig.4: The flowchart of the SeamFlow performance gain calculator

The input for the SeamFlow performance gain calculator includes the IMO number (or ship principal particulars), welding seam heights, and the distances between welding seams. In cases where the exact locations of welding seams and their lengths are known, this information can also be inputted directly. Alternatively, if such details are unavailable, the SeamFlow performance gain calculator can predict the locations and lengths of transverse welding seams ( $twl$ ) based on the known distance between them and the ship's principal particulars.

Subsequently, the calculator proceeds to calculate the relevant parameters such as Reynolds numbers ( $Re$ ), boundary layer thicknesses ( $\delta$ ), and effective dynamic pressures ( $q_{eff}$ ) at specific locations. With this information, it computes drag coefficients and added resistances for both standard and faired welding seams. The final step of the calculation involves aggregating all added resistances to determine the savings achieved through the application of SeamFlow.

### 2.3 Details of scenarios and assumptions

The baseline scenario is directly taken from *Sfiris et al. (2023)*, with the same assumptions being utilized. The analysis considers the ship under study entering dry-dock and the adoption of the listed energy efficiency measures.

Table II: The analyzed scenarios and assumptions used

Scenario	Hull coating	Hull related measures	Propeller related measures	Assumptions used
Baseline scenario	SPC AF coating	Hull cleaning after 3 & 4 years	Propeller cleaning after 3 & 4 years	Assumption 1** Assumption 2** Assumption 3** Assumption 4** Assumption 5** Assumption 8
Present scenario	Hempaguard X7	SeamFlow (for 38 weld seams in total, with 4 poorly welded)	Propeller polishing, twice a year	Assumption 9 Assumption 10

\*\*See *GEF-UNDP-IMO (2022)* for the description of the assumptions.

Table III: The details of the assumptions used for the present study

Assumptions	Description
Assumption 8	<ol style="list-style-type: none"> <li>The bulk carrier enters drydock at the end of 2023 and leaves the dry-dock on 1st January 2024.</li> <li>The bulk carrier was assumed to be coated with an SPC in the previous docking cycle, and it entered the dry-dock with biofouling growth and mechanical degradation of the coating. The impact from ageing is ignored.</li> <li>Spot blasting (40%) was conducted before the application of the SPC in the current dry-dock.</li> <li>The hull comprises a total of 38 weld seams, out of which 4 are poorly welded. Poor weld quality is defined by a weld height of 7mm, whereas high-quality welds have a height of 3mm.</li> <li>The total resistance of the ship was estimated using the widely recognized Holtrop and Mennen method (Holtrop and Mennen, 1982). Subsequently, the propeller load, advance coefficient, torque coefficient, propeller's operational rate and brake power were computed.</li> <li>The increase in power due to the aging of the ship, <math>\Delta P_{B\_aging}</math> is disregarded for both the current and previous docking cycle.</li> </ol>
Assumption 9	<ol style="list-style-type: none"> <li>The bulk carrier enters drydock at the end of 2023 and leaves the dry-dock on 1st January 2024.</li> <li>The bulk carrier was assumed to be coated with an SPC in the previous docking cycle, and it entered the dry-dock with biofouling growth and mechanical degradation of the coating. The impact from ageing is ignored.</li> <li>Full blasting was conducted before the application of Hempaguard X7 and SeamFlow in the current dry-dock.</li> <li>The hull comprises a total of 38 weld seams, out of which 4 are poorly welded. Poor weld quality is defined by a weld height of 7mm, whereas high-quality welds have a height of 3mm.</li> <li>The reduction in total resistance and the resulting total resistance of the ship, which was equipped with the Hempaguard X7 coating system and SeamFlow, were calculated in accordance with Section 2.2. Following this, the propeller load, advance coefficient, torque coefficient, propeller's operational rate, and brake power were computed. The immediate power gain achieved after the application of Hempaguard X7 and SeamFlow, in comparison to SPC, was determined to be 7.82%.</li> <li>Considering the points above, the decrease in the ship's required power (at the same speed) due to the full blasting and adoption of Hempaguard X7 and SeamFlow was estimated to be 10.32% (2.5% + 7.82%) compared to the required power of the ship that underwent spot blasting and was coated with SPC, corresponding to baseline scenario.</li> <li>The increase in power due to the aging of the ship, <math>\Delta P_{B\_aging}</math> is disregarded for the previous docking cycle.</li> </ol>
Assumption 10	The increase in power over time, attributed to mechanical deterioration of the coating, fouling accumulation, and aging is assumed to result in a 1.4% speed loss over a 5-year period. This represents the guaranteed maximum average speed loss of a vessel with the Hempaguard X7 coating system, as per ISO 19030. The speed loss value is translated into an evenly distributed yearly increase in power.

Table II shows the assumptions used for the analyzed scenarios, and Table III shows the details of the assumptions used for the present study.

### 3. Results

#### 3.1 Required power change

Fig.5 shows the changes in the required power of the bulk carrier to maintain the 14 kn design speed. The changes in the required engine power for the baseline scenario are directly taken from *GEF-UNDP-IMO (2022)*. The required engine power for the present scenarios has been calculated based on the information provided in Section 2. The negative value at Year 0 is attributed to the immediate power gain observed after the full blasting process and application of Hempaguard X7 and SeamFlow.

The different scenarios analyzed in the study show varying effects on the required power for ship operation. The baseline scenario demonstrates immediate drops in power requirements upon the application of cleaning measures. At the end of the docking cycle (Year 5), the power increase value for this scenario is 19% (*GEF-UNDP-IMO, 2022*). Notably, the present scenario outperforms the baseline scenario, thanks to the combined benefits of an initial power gain after dry-docking and a slow deterioration over time. However, focusing solely on the required power values may be misleading when comparing different options, as the primary difference lies in the total fuel consumed during the docking cycle. Therefore, a comprehensive assessment considering overall fuel consumption is crucial for making informed decisions.

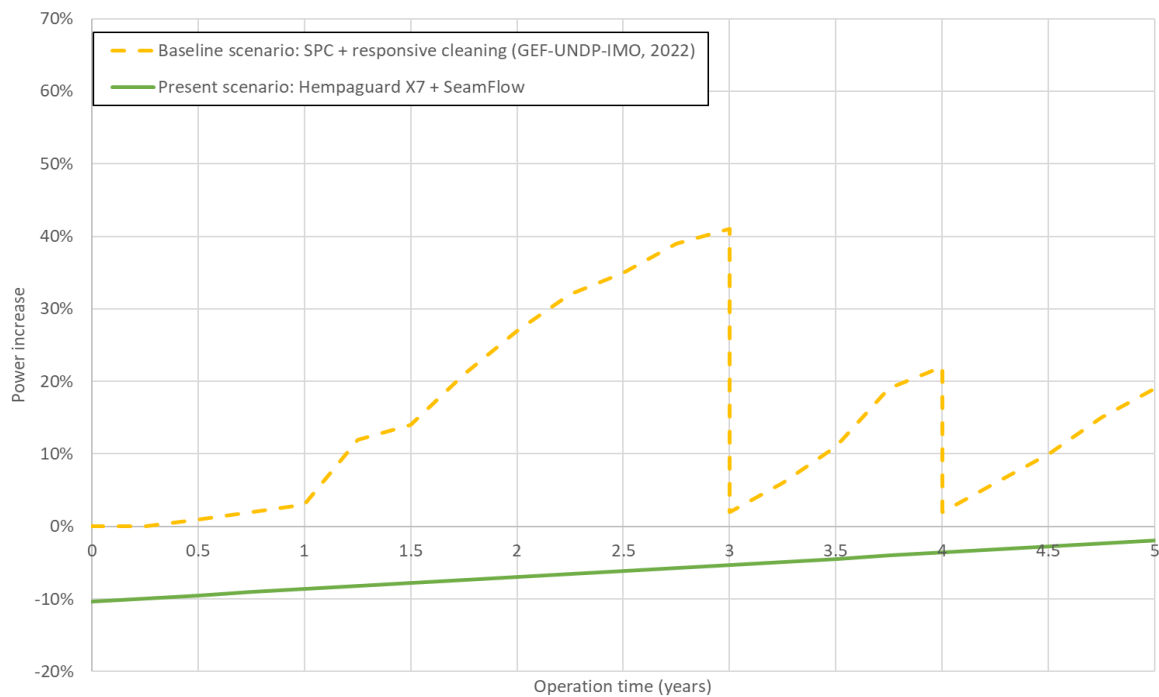


Fig.5: Variations in required power of bulk carrier under the analyzed scenarios over 5-year operation

#### 3.2 Cumulative fuel consumption

Fig.6 presents a comparison of the cumulative fuel consumption of the bulk carrier under the analyzed scenarios. The cumulative fuel consumption values for the baseline scenario is directly taken from *GEF-UNDP-IMO (2022)*. The cumulative fuel consumption for the present scenario, has been calculated based on the information provided in Section 2.

As the operation time extends, the variations in cumulative fuel consumption between the scenarios become more distinct. The results from the original report indicate that the baseline scenario results in

a total fuel consumption of ~42,000 tons, *GEF-UNDP-IMO (2022)*. The results from the present study emphasize the significant potential for fuel savings by adopting a silicone-based low friction coating and weld seam fairing solution, as the total fuel consumption can be decreased to below ~34,200 tons. These findings underscore the impact energy efficiency measures can have in optimizing fuel efficiency for bulk carriers and highlight the substantial fuel-saving benefits of adopting Hempaguard X7 and SeamFlow.

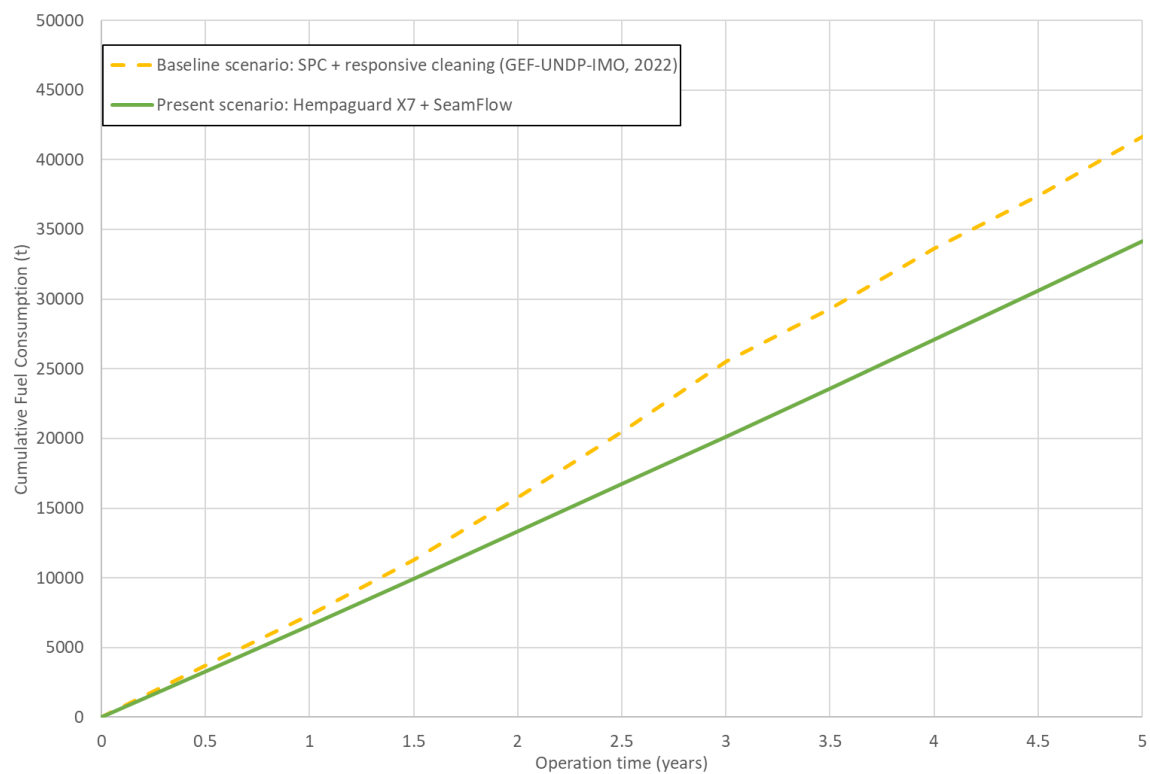


Fig.6: Cumulated fuel consumption of bulk carrier under analyzed scenarios over 5-year operation

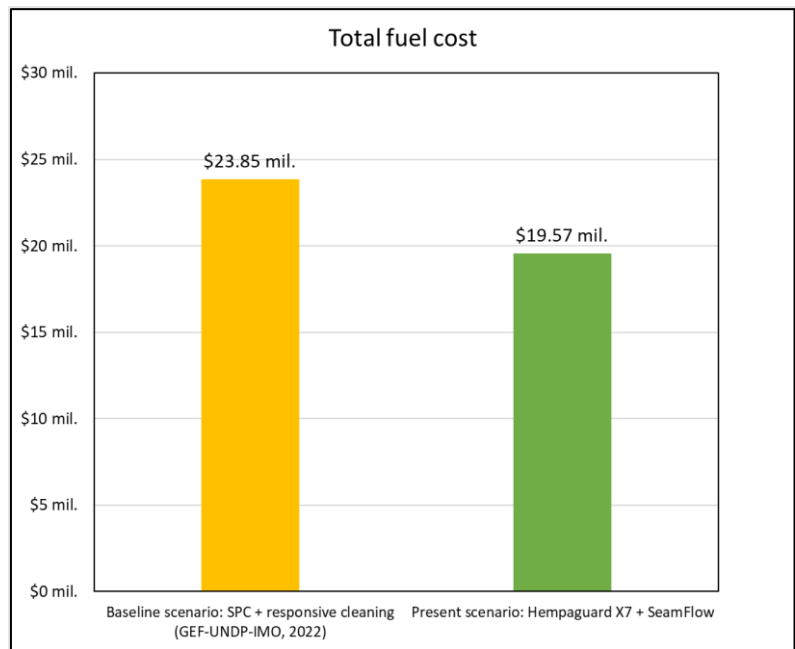


Fig.7: Total fuel cost of bulk carrier under the analyzed scenarios over 5-year operation

The total fuel costs for the 5-year operation of the bulk carrier were estimated based on predicted fuel consumption under different scenarios. Fig.7 illustrates the total fuel cost of the bulk carrier across the



scenarios, with calculations based on a fuel price of 572.5 USD per metric ton of Heavy Fuel Oil. The findings indicate that the total fuel cost over the 5-year operation can reach ~\$23.85 million and under the baseline scenario, *GEF-UNDP-IMO* (2022). Adopting a silicone-based low friction coating and weld seam fairing solution can further decrease the total fuel cost to ~\$19.57 million.

### 3.3 Carbon Intensity Indicator (CII)

The CII (Carbon Intensity Indicator) is a measure for a ship's energy efficiency and is given in grams of CO<sub>2</sub> emitted per cargo-carrying capacity and nautical mile, *DNV* (2023). Since the nautical miles of the ship operated in this cycle and the attained CII of the previous year before the dry-dock are unknown, we relied on a set of assumptions to derive a representative CII value and demonstrate the impact of each scenario on the CII rating. The following assumptions, identical to those used by *Sfiris et al.* (2023), were employed:

- The ship enters drydock at the end of 2023 and leaves the dry-dock on 1<sup>st</sup> January 2024 so that the effect of each scenario would fully impact the CII of 2024 onwards.
- Required annual operational CII,  $CII_{required}$ , in 2024 is the attained CII of the 'ideal ship'. This 'ideal ship' is assumed to be coated with SPC and remain unaffected by any biofouling accumulation, coating degradation, or aging in 2024. In simpler terms, the sum of  $\Delta P_{B\_fouling}$ ,  $\Delta P_{B\_mechanical}$ , and  $\Delta P_{B\_aging}$  is considered to be zero for the 'ideal ship' in 2024.
- The reduction factors for Phase 3 (2027 – 2030) have not yet been announced. A 3% reduction was assumed for this specific period.

By using the assumptions above, we can directly see the effect of each scenario on the CII starting from the 1<sup>st</sup> year compared to an 'ideal ship' that is operating without any increase in the required power. The details of CII can be seen in *IMO* (2021*b,c,d,e*). The theoretical CII of the 'ideal ship' is calculated to be 6.056 in 2024. The effect of each option on the CII value was then calculated for each year as shown in Table IV.

Table IV: The CII values of the ship under different scenarios

	2024	2025	2026	2027	2028
Baseline scenario: SPC + responsive cleaning	6.12 (C)	7 (E)	8.09 (E)	6.74 (E)	6.69 (E)
Present scenario: Hempaguard X7 + SeamFlow	5.48 (B)	5.58 (C)	5.69 (C)	5.79 (C)	5.89 (D)

The CII analysis across the different scenarios reveals important insights into energy efficiency, environmental impact, as well as critical compliance consideration. According to IMO regulations, a vessel that receives three consecutive "D" ratings or a single "E" rating in a given year is mandated to develop and present a corrective action plan, outlining the strategies to attain a CII index of "C" or higher. This underscores the significance of adhering to the established efficiency standards. Furthermore, as stipulated by the IMO, there is a proactive encouragement for administrations, port authorities, and relevant stakeholders to offer incentives to ships that achieve "A" or "B" ratings, fostering an environment of enhanced energy efficiency and sustainability within the maritime industry.

The present scenario consistently demonstrates favorable CII values for each year, starting at 5.48 g of CO<sub>2</sub> emitted per cargo-carrying capacity and nautical mile in 2024 (B rating). The values gradually increase to 5.58 (C) in 2025, 5.69 (C) in 2026, 5.79 (C) in 2027, and finally reaches 5.89 (D) in 2028. These CII values for the present scenario show the considerable emission reduction potential that the shipping industry can achieve today with these technologies. On the other hand, baseline scenario exhibits higher CII values with consecutive E ratings, indicating non-compliance with the regulatory threshold, relatively lower energy efficiency and higher environmental impact over multiple years. Ships operating under the baseline scenario will need to implement additional measures to improve energy efficiency and reduce their CII ratings to align with the regulations set by the IMO. These findings underscore the significance of selecting measures that prioritize energy efficiency and reduce carbon emissions while ensuring compliance with the established energy efficiency standards.

#### 4. Conclusions and discussion

In the context of the maritime industry's urgent need for energy efficiency improvements, this paper presents a ship-specific study that evaluates the combined effects of Hempaguard X7, a silicone-based low-friction coating, and SeamFlow, an innovative weld seam fairing solution. Leveraging Hempel's comprehensive framework for assessing energy efficiency measures, we conducted a detailed analysis of a scenario on a bulk carrier vessel over a 5-year docking cycle. The findings highlight the following key insights:

Immediate Power Gain and Energy-Saving Potential: The immediate power gain attributed to the integration of Hempaguard X7 and SeamFlow is analogous to the power gain achieved through other Energy Saving Devices (ESDs), such as Mewis Ducts and Pre-Swirl Fins. This synergy between the two technologies contributes significantly to reducing the ship's resistance and enhancing energy efficiency. An often overlooked aspect, the distinction between full blasting and spot blasting during dry-docking significantly influences the power gain. Our analysis highlights that full blasting, as employed in conjunction with the adoption of Hempaguard X7 and SeamFlow, creates a smoother hull, thereby resulting in substantial power savings that extend beyond the initial post-docking period.

Enduring Performance and Operational Continuity: Hempaguard X7's prolonged operational effectiveness, characterized by its slow degradation rate (max average speed loss of 1.4%) and immediate power gain due to X7 and SeamFlow, positions this technology combination as a potent energy efficiency solution.

Environmental Impact and Sustainability: The study's focus on energy efficiency aligns harmoniously with the maritime industry's broader commitment to environmental sustainability. By contributing to reduced fuel consumption and subsequent carbon emissions, the combined technologies of Hempaguard X7 and SeamFlow align with global efforts to minimize the sector's ecological footprint. This engagement with sustainable practices resonates with ongoing industry trends and regulatory aspirations for a greener maritime future.

Operational Integration and Ease of Adoption: The integration of Hempaguard X7 and SeamFlow showcases not only their energy efficiency benefits but also their seamless integration into regular ship operations. Unlike some other energy-saving solutions that might demand significant operational changes or additional energy inputs, these technologies enhance performance without disrupting established practices. This integration underscores their practical appeal to shipowners and operators looking for streamlined and effective energy-saving measures.

Unlocking Economic Resilience: The economic aspect of this study merits special attention. Although we do not provide a comprehensive Total Cost of Ownership (TCO) analysis, it is essential to underscore that while the initial investment in Hempaguard X7 and SeamFlow is a necessary consideration, their rapid payback period resulting from substantial fuel efficiency gains is a crucial factor to take into account. This economic resilience renders the adoption of these technologies not only environmentally responsible but also financially prudent. It is important to note that while TCO typically encompasses various costs associated with technology adoption, such as upfront investment cost, maintenance and operational expenses, the dominant parameters influencing TCO in this context are fuel consumption and savings, which this paper primarily addresses.

Moreover, the study's methodological rigor, incorporating towing tank experiments and established theoretical frameworks, establishes a robust approach for evaluating energy efficiency measures, particularly tailored to real-world maritime scenarios.

In conclusion, Hempaguard X7 and SeamFlow significantly advance maritime energy efficiency and environmental responsibility. This study enriches the ongoing dialogue on carbon emissions reduction and provides practical insights aligned with industry objectives to optimize fuel consumption and compliance.

## References

- ABS (2021), *Sustainability Trends: Tankers*, American Bureau of Shipping, Houston
- BERTELSEN, M.R.; MESEGUER YEBRA, D. (n.d), *HEMPAGUARD - Evidence of performance gains*, HEMPEL, <https://www.hempel.com/-/media/Files/Global/PDF/Resource-centre---Marine/Technical-papers/Hempaguard---Performance-and-evidence.pdf>
- CANDRIES, M.; ATLAR, M. (2005), *Experimental investigation of the turbulent boundary layer of sur-faces coated with marine antifoulings*, J. Fluids Eng. 127 (2), pp.219–232
- CIORTAN, C.; BERTRAM, V. (2014), *RANSE Simulations for the Effect of Welds on Ship Resistance*, Numerical Towing Tank Symposium (NuTTS), Marstrand
- DEMIREL, Y.K.; UZUN, D.; ZHANG, Y.; FANG, H.-C.; DAY, A.H.; TURAN, O. (2017), *Effect of barnacle fouling on ship resistance and powering*, Biofouling 33(10), pp.819–834
- DEMIREL, Y.K. (2015), *Modelling the roughness effects of marine coatings and biofouling on ship frictional resistance*, PhD thesis, University of Strathclyde, DOI: 10.48730/4b6n-9153
- DNV (2023), *CII – Carbon Intensity Indicator*, <https://www.dnv.com/maritime/insights/topics/CII-carbon-intensity-indicator/index.html>
- FORCE Technology (2007), *Skin friction of fouling control coatings*, FORCE 107-2411, FORCE Technology, Lyngby
- FORCE Technology (2017), *Resistance of welding seams on a flat plate Model Tests*, FORCE 117-31663, FORCE Technology, Lyngby
- FORCE Technology (2021), *CFD based welding seam drag evaluation*, FORCE 121-22954-1C, FORCE Technology, Lyngby
- GEF-UNDP-IMO (2022), *Analysing the Impact of Marine Biofouling on the Energy Efficiency of Ships and the GHG Abatement Potential of Biofouling Management Measures*, GloFouling Partnerships and GIA for Marine Biosafety, Int. Mar. Org., London, <https://www.glofouling.imo.org/files/ugd/34a7be02bd986766d44728b85228c3ec9b95ee.pdf>
- GRANVILLE, P. S. (1987), *Three indirect methods for the drag characterization of arbitrarily rough surfaces on flat plates*. J Ship Res. 31, pp.70–77
- GRANVILLE, P. S. (1958), *The frictional resistance and turbulent boundary layer of rough surfaces*. J Ship Res. 2, pp.52–74
- HOERNER, S.F. (1965), *FLUID-DYNAMIC DRAG, theoretical, experimental and statistical information*. Hoerner Fluid Dynamics
- HOLTROP, J.; MENNEN, G. (1982), *An approximate power prediction method*, International Ship-building Progress, 29(335), pp.166–170
- IMO (2023), *Report on the study on the readiness and availability of low- and zero-carbon ship technology and marine fuels*, MEPC 80/INF.10, Int. Mar. Org., London, <https://wwwcdn.imo.org/localresources/en/MediaCentre/WhatsNew/Documents/MEPC80.INF10.pdf>

IMO (2021a), *2021 Guidelines on operational carbon intensity indicators and the calculation methods (CII Guidelines, G1)*, Int. Mar. Org., London, [https://wwwcdn.imo.org/localresources/en/OurWork/Environment/Documents/Air%20pollution/MEPC.336\(76\).pdf](https://wwwcdn.imo.org/localresources/en/OurWork/Environment/Documents/Air%20pollution/MEPC.336(76).pdf)

IMO (2021b), *2021 Guidelines on the reference lines for use with operational carbon intensity indicators (CII reference lines guidelines, G2)*, Int. Mar. Org., London, [https://wwwcdn.imo.org/localresources/en/OurWork/Environment/Documents/Air%20pollution/MEPC.337\(76\).pdf](https://wwwcdn.imo.org/localresources/en/OurWork/Environment/Documents/Air%20pollution/MEPC.337(76).pdf)

IMO (2021c), *2021 Guidelines on the operational carbon intensity reduction factors relative to reference lines (CII reduction factors guidelines, G3)*, Int. Mar. Org., London, [https://wwwcdn.imo.org/localresources/en/OurWork/Environment/Documents/Air%20pollution/MEPC.338\(76\).pdf](https://wwwcdn.imo.org/localresources/en/OurWork/Environment/Documents/Air%20pollution/MEPC.338(76).pdf)

IMO (2021d), *2021 Guidelines on the operational carbon intensity rating of ships (CII rating guidelines, G4)*, Int. Mar. Org., London, [https://wwwcdn.imo.org/localresources/en/OurWork/Environment/Documents/Air%20pollution/MEPC.339\(76\).pdf](https://wwwcdn.imo.org/localresources/en/OurWork/Environment/Documents/Air%20pollution/MEPC.339(76).pdf)

SCHULTZ, M.P. (2004), *Frictional resistance of antifouling coating systems*, J. Fluids Eng. 126, pp.1039–1047

SCHULTZ, M.P. (2007), *Effects of coating roughness and biofouling on ship resistance and powering*, Biofouling 23, pp.331–341

SFIRIS, P.; DEMIREL, Y.K.; AVLONITIS, V.; PAGONI, S. (2023), *Navigating Energy Efficiency Dilemmas in the CII Era*, 8<sup>th</sup> Hull Performance & Insight Conference (HullPIC), Pontignano, [http://data.hullpic.info/HullPIC2023\\_Pontignano.pdf](http://data.hullpic.info/HullPIC2023_Pontignano.pdf)

SONG, S.; DAI, S.; DEMIREL, Y.K.; ATLAR, M.; DAY, S.; TURAN, O. (2021), *Experimental and theoretical study of the effect of hull roughness on ship resistance*. J. Ship Res. 65(1), pp.62–71

STOPFORD, M. (2022), *Shipping's Era of Change*, MarEcon, <https://forums.capitallink.com/shipping/2022german/files/stopford.pdf>

WANG, X.; OLSEN, S. M.; ANDRES MARTINEZ, E.; OLSEN, K. N.; KIIL, S. (2018), *Drag resistance of ship hulls: Effects of surface roughness of newly applied fouling control coatings, coating water absorption, and welding seams*, J. Coatings Technology and Research 15, pp.657–669

# **Biomimetics for Maritime Applications – En Route to Decarbonization until 2050**

**Elisabeth Banken**, Fraunhofer CML, Hamburg/ Germany, [elisabeth.banken@cml.fraunhofer.de](mailto:elisabeth.banken@cml.fraunhofer.de)  
**Vincent E. Schneider**, Fraunhofer CML, Hamburg/Germany, [vincent.schneider@cml.fraunhofer.de](mailto:vincent.schneider@cml.fraunhofer.de)  
**Johannes Oeffner**, Fraunhofer CML, Hamburg,/Germany, [johannes.oeffner@cml.fraunhofer.de](mailto:johannes.oeffner@cml.fraunhofer.de)

## **Abstract**

*Bio-inspired solutions for maritime applications are plentiful and can support the goal of significantly reducing the emissions produced by ships. This paper highlights many innovative and future-oriented biomimetic solutions with the potential to actively support the switch to greener technologies, thereby complying with current and future legislation protecting the marine environment and mitigate further progress of climate change. The paper focusses on biomimetic ideas to improve fuel consumption, support climate neutrality, optimize digitalization approaches. It in particular focusses on connect existing strategies in nature with suitable applications for maritime technologies with the intent to promote and inspire continuous research in biomimetic solutions.*

## **1. Introduction**

On the way to climate neutrality until 2050 under the recently strengthened IMO regulations, the maritime industry is facing great challenges in reducing associated GHG emissions and drastically improve its overall climate footprint. Further pressure to change is also exerted through national decarbonization targets (e.g., EU Green Deal) or environmental protection acts (e.g., EU Marine Strategy Framework Directive, UN Sustainable Development Goals) and the general public. Here, the awareness for sustainability and interest in proper use and care of marine environments have skyrocketed in recent years. Furthermore, many companies, especially the big players, set their own net zero emissions targets.

Many of the existing issues with emission reduction within the maritime industry can be addressed using biomimetic approaches and integrating innovative bio-inspired solutions. Biomimetic design has already proven its feasibility and advantage through examples like drag-reducing ship coatings inspired by shark skin or the salvinia plant, rotors and propulsion systems inspired by whale fins and even satellite imaging technology for ocean observation and monitoring based on the compound of the mantis shrimp.

These innovative solutions will be presented in the following, starting with concepts for logistics and digitalization and moving over bio-inspired hydrodynamic as well as machinery and propulsion systems over to other important biomimetic GHG reducing features.

## **2. Bio-inspired Solutions for Logistics and Digitalization**

For the last few decades, the maritime industry has been transforming, moving towards digitalisation of transportation processes, shipyard 4.0 and intelligent devices to streamline operations, optimize resource utilization and thus, improve the sector's overall footprint. From virtual system design of ships to digital twins across the whole life cycle, more intelligent and connected shipping solutions are being developed and implemented throughout the industry.

Digital twins in particular present the opportunity to test not only surrounding conditions and innovative ship designs before implementing real-life prototypes and experiments but can also determine the effectiveness of bio-inspired solutions and evaluate their economic and environmental potential compared to conventional technologies. Thus, digital technologies such as artificial intelligence, especially based on machine learning, and computer-based modelling and simulation have evolved rapidly in recent years, DNV (2022).



One application for digital solutions for shipping logistics with the potential to optimize resource management is the route planning of ships. Difficult travel conditions such as harsh weather or large waves cause the ship to consume more fuel to get to their target than with a quiet sea. Therefore, algorithms have been developed, capable of using real-time AIS data to calculate the route with the highest fuel efficiency and thus least quantity of emissions. Weather routing tools take weather measurements and predictions into account enabling energy efficient routing by means of bypassing bad weather and/or making use of tail wind. Many bio-inspired algorithms exist that are used for path optimization, routing, and navigation. They are usually part of evolutionary algorithms which have been inspired by natural techniques, processes, and behaviours to spontaneously find the best routes for vehicles, *Poudel et al. (2023)*. Biomimetic algorithms are usually inspired by swarm intelligence from animals such as ants, bees, or fish and are multi- or behaviour-based mimicking neural networks. These types of algorithms have demonstrated overall better performance, especially regarding their convergence rate and are therefore a favoured tool to be implemented, *Darwish (2018)*, *Yi et al. (2021)*, *Jinquiang et al. (2021)*.

Swarm technology applied to multiple individual vessels (underwater and/or surface vehicles) has been gaining much attention within recent years as it widens the field of applications and activities to be performed, which are otherwise not possible with single ships. Thus, in order to achieve proper and safe communication as well as control among cooperating vessels, swarm intelligence inspired by animals such as ants or bees is applied, *Kim et al. (2021)*. Autonomous control also reduces human error and simplifies the interaction and control of multiple independent vehicles, *Lazarowska (2015)*. Especially, use cases involving underwater or water quality monitoring are discussed, as it enables the observation and measurement of abiotic conditions or algal bloom covering a large area using a fleet of ROVs, *Darlis et al. (2023)*.

Growing autonomy of ships and entire fleets can significantly decrease the operational costs, *Kretschmann et al. (2017)*, as well as reduce human error and resulting accidents, *Borkowski et al. (2021)*. To allow for safe and reliable autonomy, lots of data in terms of real-time tracking and additional technology such as sensors are required to observe the surrounding, process acquired information and produce an appropriate action of the ship. Furthermore, reliable systems allowing for autonomous navigation though heavy traffic are required but systems with sufficient functionalities have not yet been developed. As the processing and implementation of data is rather complex and available technology limited, provisions to appropriately respond to spontaneous deviations are necessary. In addition, surrounding ships and obstacles may not behave in the predicted manner, demanding a way of immediately reacting to and preventing collisions with other ships, harbour infrastructure or other obstructions in the ship's path. Some bio-inspired models and algorithms have been developed for the control, navigation and path planning of vessels, some even have provisions for collision prevention, *Borkowski et al. (2021)*.

Many flying insects demonstrate great real-time tracking abilities. Dragonflies for example can pursue and catch prey regardless of turbulent environments with distracting stimuli. They have specialized neurons called small target motion detector neurons, which are very sensitive to target contrast and translate into an efficient and highly adaptable visual processing system, *Bagheri et al. (2017)*. Based on this mechanism, algorithms for navigation and trajectory planning have been established in robotics applications, *Philippides et al. (2011)*, *Ma et al. (2009)*, *Ni et al. (2020)*.

Furthermore, locusts are specialists in avoiding collisions as they can recognize approaching obstacles even in low-contrast conditions or textured backgrounds in motion. This ability stems from their lobula giant movement detector neurons, enabling them to adapt their mid-flight movement to alter their trajectory and avoid the collision once such an alert is triggered. Other sectors have already profited and successfully implemented bio-inspired anti-collision and tracking algorithms and technologies in for example smart vehicles, *Yue et al. (2006)*, *Keil et al. (2018)*, *Colonnier et al. (2019)*, *Bagheri et al. (2017)*.

Lastly, remote sensing offers a great opportunity to observe earth and gather data, especially with

respect to environmental changes over time. Satellite technology and observation tools are rapidly maturing, continuously improving the acquisition and transmission of AIS data on ships. Yet, conventional optical systems have been known to suffer dynamic illumination conditions or solar glare, *Yilmaz et al. (2017)*.

In nature, compound eyes are widely spread amongst insects and describe spherical visual arrangements of numerous cone-shaped sensing units called ommatidia, which observe with high sensitivities, a variety of dimensions, and accept light from narrow angles, *Deng et al. (2016)*, *Gonzalez-Bellido et al. (2011)*. The lobster's eyes in particular have a favourable wide field of view and sufficient focusing energies to create a sharp and detailed picture. Technical adaptations of the compound eye have been shown to outcompete conventional systems and have already been implemented as satellite payloads in form of an X-ray telescope with great all-sky and sun-monitoring capabilities, *Hudec and Remisova (2017)*, *Hudec et al. (2006)*, *Tamagawa et al. (2020)*, *Zhao et al. (2017)*, *Yuan et al. (2018)*.

### **3. Bio-inspired Solutions for Hydrodynamic-Improving Strategies**

Natural evolution has encountered and solved several problems faced by waterborne transport such as reducing drag and maintaining clean surfaces by either cleaning or growth prevention. In the following respective biomimetic concepts are discussed.

#### **3.1. Drag-reducing Coatings and Surface Properties**

While in technical applications, most commonly the smoothness of a surface is correlated with drag reduction, in nature specially solutions with rough, structured surfaces stand out as examples for drag reduction. One of the most prominent and well-researched biomimetic approaches are the drag reducing properties of shark skin. Its skin is covered with grooved placoid scales, creating streamwise oriented canals which channel the flow and reduce tangential flow. The scales in shortfin mako shark (*Isurus paucus*) range from 0.2 to 0.5 mm with grooves of 100 µm width, *Pu et al. (2016)*, *Yu et al. (2020)*. Technical applications of such structures are called riblets, Fig.1A, for which small-scale experiments of artificial canals with differing geometric properties showed drag reduction of 4 -d 13%. The authors note the lack of larger scales of these experiments, which are only feasible using computational fluid dynamics (CFD), *Abdulbari et al. (2015)*. Geometrically categorizing the riblets and applying them on bow and aft section of a container vessel with subsequent CFD simulation showed a reduction in drag of 3.9%, *Ibrahim et al. (2018)*. Hydrodynamic experiments comparing riblets and shark skin showed that the friction reducing effect of riblets is with 7% however only half of what the natural model achieves, *Oeffner and Lauder (2021)*.

Noteworthy are also the findings regarding the hypothesized drag reduction of dolphin skin which was famously reported as the Gray's Paradox, *Gray (1936)*. 70 years later, *Fish (2006)*, reviewed the work performed and states that although dolphins show very low drag overall, its reason is most likely reduced flow separation and subsequently minimized drag due to an overall turbulent boundary layer. Furthermore, drag in dolphin skin is kept low primarily due to streamlining of the body and appendages by behavioural mechanisms, *Yu et al. (2020)*.

Another animal known for its swimming capabilities is the penguin, which is inspiration for active air lubrication using microbubbles, Fig.1B. *Bannasch (1995)* proposed that special feathers around a penguin's beak induce a turbulent boundary layer delaying flow separation over the penguins body, for which model experiments showed a significant drag reduction, *Parfitt and Vincent (2005)*. Reports of the bubbles emerging from the plumage at high-speed align with laboratory experiments of microbubbles yielding a drag reduction – a concept that finds application in ship development, *Davenport et al. (2011)* and has successfully been implemented by a number of companies that distribute active air lubrication systems for ships (e.g. Silverstream) form continuous release of air bubbles another drag reducing system relying on air are the leaves of the salvinia plant (*salvinia molesta*). These plants combine geometric hair-like structures, Fig.1C, on their surfaces with selective chemical coating and intricate 3D-hierarchical morphological structures to achieve air retention,

creating a slip-condition at their surface. The structures protruding their surface are of differing geometry, but have superhydrophobic surface properties with a hydrophilic tip in common, *Tricinci et al. (2023)*. While the complexity of the structure and its technical abstraction are requiring intricate manufacturing techniques a significant drag reduction can be shown with long air retention times, *Kim et al. (2022)*. Interestingly, similar structures as in shark skin and lotus leaves are proposed for rice leaves and butterfly wings. Both bear a similar superhydrophobic surface such as salvinia leaves, *Fig.1D*. Rice leaves exhibit hierarchical micropapillae with an epicuticular wax layer and longitudinal grooves, which create a superhydrophobic and low adhesion surface that direct waters flow. *Bixler and Bhushan (2012,2913)* draw a comparison with geometrically similar structures of shark skin and realise a drag reduction of a coated rice leaf of 26%.

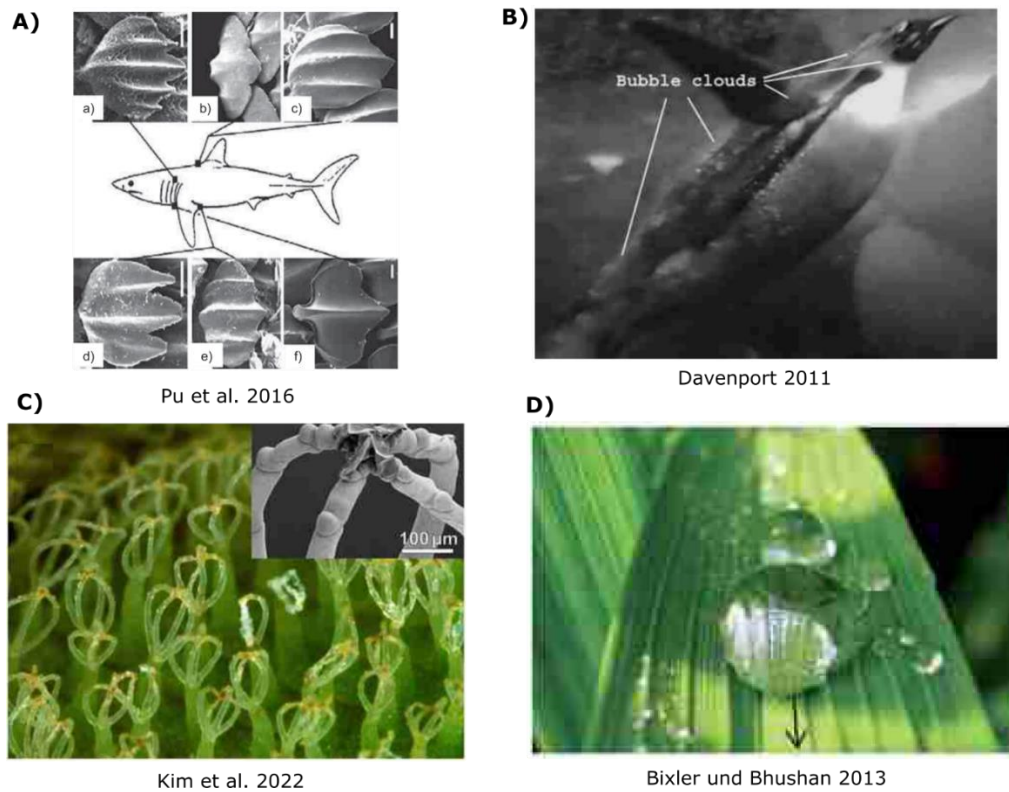


Fig.1: Examples of drag reducing biological mechanisms

### 3.2. Self-cleaning Surfaces and Anti-fouling

The aforementioned organisms that achieve drag reduction using superhydrophobic surfaces are also of interest for self-cleaning and anti-fouling applications, most prominently the lotus leaf, *Fig.2A*. The leaves feature superhydrophobic and low adhesion micropapillae, which are arranged in a hierarchical fashion featuring microbumps which are covered with low surface energy waxy structures, *Bixler and Bhushan (2013)*. While the structures found in lotus leaf are mainly a superhydrophobic surface, for which group other biological examples such as rice leaf, cicada wings and butterfly wings can be named, another self-cleaning mechanism is based on hydrophilic and oleophobic surfaces. For the latter, the shell of a snail consists of an aragonite layer covered with a protein layer, which has a rough structure of line grooves and micro-grooves from 0.5 mm down to 10  $\mu\text{m}$  in dimension. This structure with high regularity is hypothesized to catch water droplets and therefore leading to the repellence of oil, *Nishimoto and Bhushan (2013)*.

Another example is well-known in biomimetics for its dry adhesion, but also shows great self-cleaning capabilities. The feet of geckos are covered with well-aligned fine microscopic hairs called setae. These setae are approximately 100  $\mu\text{m}$  in length and 5  $\mu\text{m}$  in width, carrying each hundreds of smaller nanoscale spatulae. With these spatulae gecko feet and their opposing surface generate van der Waals

forces that are strong enough to allow geckos to climb walls and hang upside down. To achieve this efficient adhesion, geckos need to maintain clean feet, while maintaining the adhesion force. Contact mechanical models showed that energetic disequilibrium leads to the self-cleaning when walking for a few steps on a clean surface. Self-cleaning is proposed to be dependent largely on spatula and particle size, *Liu and Jiang (2012)*.

While self-cleaning is mainly referred to removing non-living particles, huge amounts of drag on vessels can be generated by organisms living in the hull, generally described as biofouling. Since all animals living in water encounter the same environmental conditions, species such as shark show remarkable anti-fouling capabilities, but also the aforementioned lotus leaf is discussed to be very resistant to anti-fouling, *Sullivan and O'Callaghan (2020)*. An approach very close to application are the also aforementioned leaves of salvinia plants, which have been abstracted into an air retaining foil which has been applied to ship hulls, *Barthlott et al. (2010)*, *Oeffner (2020)*.

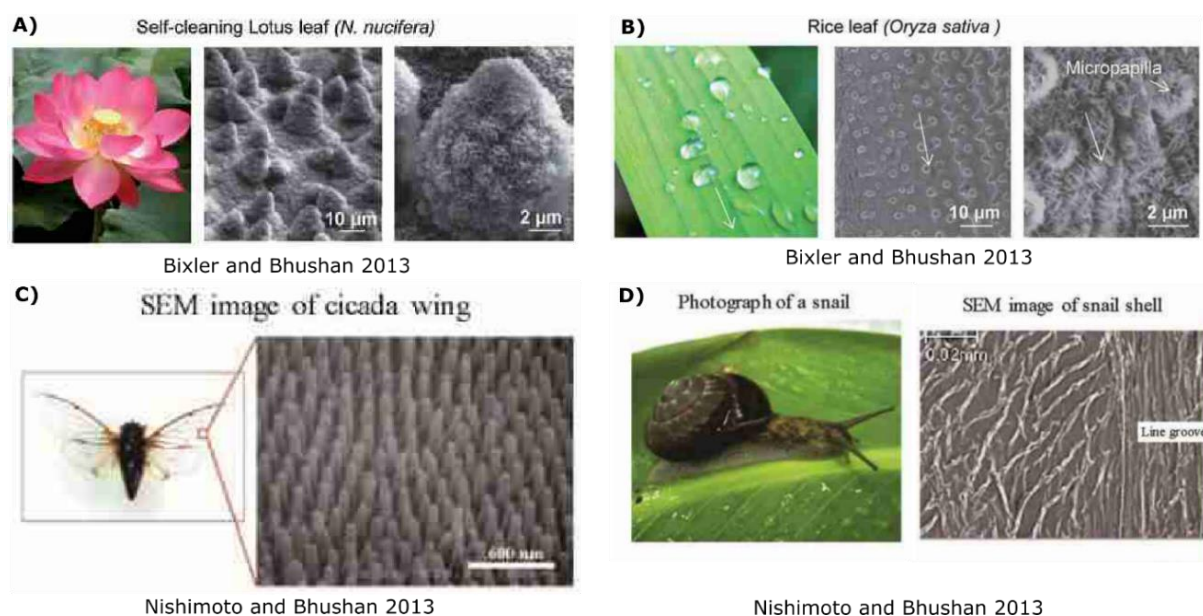


Fig.2: Examples of self-cleaning and anti-fouling in nature

## 4. Bio-Inspired Solutions for Machinery and Propulsion System Improvements

### 4.1. Examples for Small and Large Maritime Vessels

A myriad of bio-inspired propulsion systems exists, which are primarily based on technical adaptations of various fish and mammal fins. *Lamas et al. (2011)* for example successfully built a flexible undulating surface mimicking the motion of fish fins together with a mechanical transmission via crankshaft, Fig.3A, for the propulsion of a small catamaran. Another commercially available example is the FinX thruster inspired by the wave pattern of dolphins' caudal fins with a high amplitude at a low frequency and uses a custom undulating elastomer membrane shown in Fig.3B to propel boats forward, *FinX (2023)*. While concepts like these present promising results in terms of propulsion efficiency, they mainly apply to small ships and boats used for recreational purposes or underwater robotics.

A solution for bigger vessels such as ROPAX ferries or bulk carriers used for short sea applications has been proposed by *Belibassakis et al. (2021)*, who developed a bio-inspired wing to extract wave energy and generate sufficient thrust to propel the vessel forward. The respective prototype is depicted in Fig.3C. A similar approach made by the O-foil© concept has not proven to be successful yet.

Wavefoil are commercially available retractable bow foils with a mechanism to retract/deploy the foils in and out of the ship hull. When deployed, the foils are close to horizontal and fixed relative to the ship. The foils dampen the ship motions in waves and convert the relative vertical motion between the



water and the foils into propulsive thrust. Fuel savings are obtained since the foils simultaneously reduce motions and the associated added resistance in waves and provide auxiliary thrust. Depending on factors like wave conditions, ship dimensions and ship speed, fuel savings of around 8% can be achieved, *Hagen (2018)*.

Commonly proposed alternative propulsion options for ships include fuel cells and batteries. In polymer electrolyte membrane fuel cells, bipolar plates are typically responsible for the transport of reactants, heat, and electrons, and can inhibit flooding as well as improve cell function at high currents. Due to the associated costs of bipolar plates, alternative solutions are being investigated. One of which are bio-inspired designs taking inspiration from the fluid management structures found in plant leaves, animal blood vessels or lungs. Among others, *Chadwick et al. (2022)* developed a fuel cell with similar passive unidirectional water wicking geometries to improve fuel cell performance with promising results for further analysis, *Chadwick et al. (2022)*, *Ibrahim-Rassoul et al. (2019)*.

Other bio-inspired energy storage systems besides fuel cells exist that take inspiration by the highly porous interconnected structures and composite architecture found in bones, *Shin et al. (2020)*, or the structure of fish gills and their function of transferring different oxygen compounds, *Wu et al. (2021)*.

For large ships and vessel for deep sea transport in need of large amounts of power, the availability of bio-inspired solutions is very limited. Nevertheless, some examples and adjacent ideas can be found in literature. Large shipping vessels commonly use propellers to generate sufficient thrust to propel a ship forward working against the tide and hull resistance. The largest impact on the performance efficiency is the shape of the propeller, which over the years has been optimized for maximum thrust, torque and efficiency. Nevertheless, researchers and ship operators continuously look for improvements boost efficiency further. One such examples is the propeller design proposed by *Arifin et al. (2022)* with tubercle structures added on the leading edge inspired by the humpback whales' fins. As already successfully implemented for wind turbines, *Fish et al. (20211)*, *Ng et al. (2017)*, the proposed propeller design achieves noise and cavitation reduction but suffers from pressure loss and subsequently lower torque, *Arifin et al. (2022)*, *Stark and Shi (2021a,b)*.

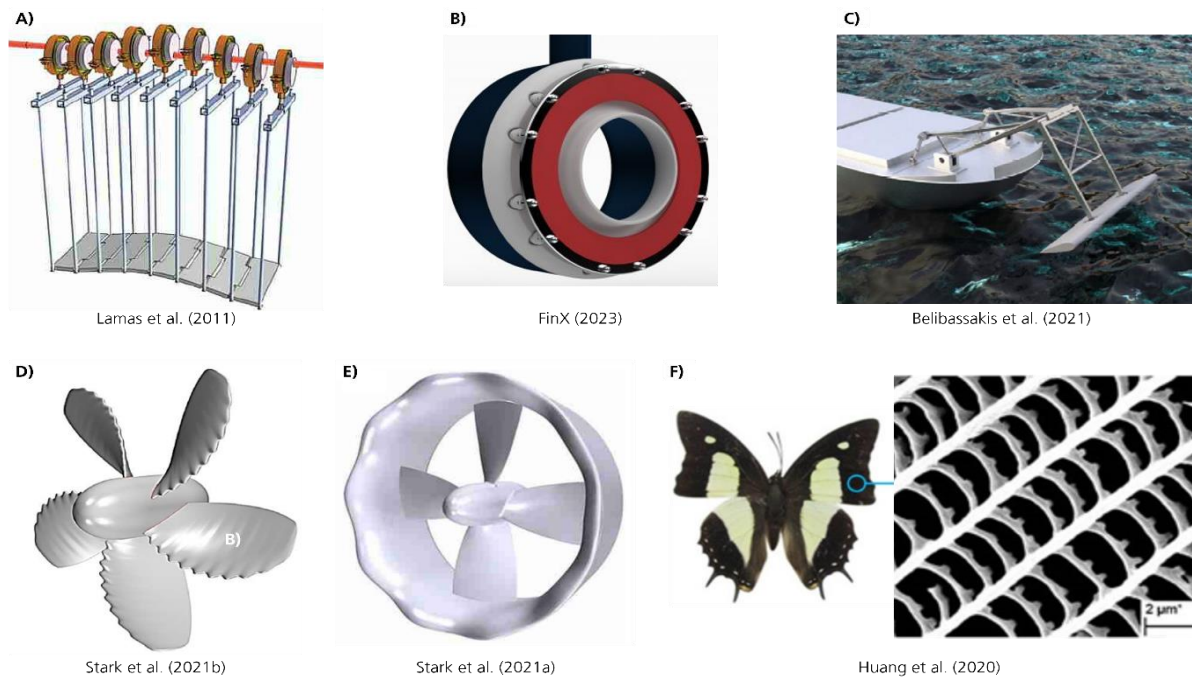


Fig.3: Bio-inspired propulsion mechanisms

Another frequently discussed and already tested concepts to decrease a ship's fuel consumption is using on-board auxiliary wind and solar power to aid propulsion. Especially solar technology holds great



potential for biomimetic improvement. Thus, biological compounds as well as nanostructures have been investigated and partially translated into working prototypes, *Romero et al. (2017)*, *Huang et al. (2020)*, *Yoon et al. (2021)*, *Chen et al. (2011)*. As an example, some species of butterflies appear to have black wings but, contrary to popular belief, this is due to close to 100% absorption of sunlight and only very little reflection thanks to a specialized, rather than a black, pigment. The special structure consists of a mesh-like surface equipped with ridges and holes, Fig.3F, which was mimicked by *Huang et al. (2020)* and adapted for the use in solar panels. The bio-inspired solar panel achieved a reduction in reflection to less than 5%, subsequently achieving 66% higher current in a short-circuit. A secondary example still under investigation is presented by the oriental hornets, which are even thought to convert sunlight into electrical energy using a specific pigment in their cuticle to harvest solar energy. They prefer working in the sun, where the brown coloured sections of their cuticles covered in tiny creases can trap radiation, which is then absorbed inside the cuticle, *Plotkin et al. (2010)*.

## **4.2. Alternative solutions indirectly supporting decarbonization**

Besides the bio-inspired solutions presented above, others exist that can indirectly be used to create environmental benefits for the maritime industry. Those include efficiency improvements for energy generation systems and post-emission treatments as applied to conventional fuel types using scrubbers.

### **4.2.1. Energy Generation**

Similar to wind and solar power, other alternative power systems are under development with the goal to reduce the emissions of maritime transport. One of which is cold ironing or shore power, where ships are equipped with all-electric drives and on-board batteries, allowing vessels to drive and navigate completely electrically. Batteries are charged using electricity provided at the ports and store sufficient quantities of power for the respective journey. Since no fuels are burned in the process of converting electricity to motion, emissions are considerably lower. Nevertheless, the emission of cold ironing strongly depends on the onshore energy mix and energy carriers used to generate the respective electricity. Thus, when relying on fossil fuels for the generation of electricity, the emission reduction of shore power stays absent. Therefore, using sustainable and green technologies for power generation are vital, *Abu Bakar et al. (2023)*, *Qi et al. (2020)*.

Nature also deals with a variety of processes to produce and convert different types of energy. As previously demonstrated through the example of butterfly wing inspired solar panel structures, solar radiation offers great potential for biomimetic application. Other examples for generating solar energy using bio-inspired concepts are solar collectors adopting a sunflower-like organization of mirrors to harvest the greatest amount of radiation.

Other bio-inspired concepts can be used to boost the efficiency of energy production systems and convert mechanical work into electricity. The ocean is a powerful tool with high-power waves generated by the tides and lunar cycle. Ocean waves have long been discovered as a great way to generate sustainable energy by converting them into electricity. Inspiration for wave-like motion can be found abundantly in nature. A bioinspired concept of a wave energy converter is the centipede wave energy converter, which consists of a ribbon of buoys harvesting the waves' energy while resembling the body segments and legs of a centipede. A tubular backbone houses the generators, which are driven by the buoys moving up and down, *Zhang and Aggidis (2018)*. Another approach to recover energy from waves is presented in form of a foldable wing for underwater robots, drawing inspiration from flying fish. This foldable wing exhibits great increase of area when opened, allowing for a large energy capturing surface, *Chen et al. (2023)*.

### **4.2.2. Post-Emission Options**

Due to the limited availability of alternative, low-emission fuels and an inadequate infrastructure to supply sufficient resources throughout international harbours, the emission reduction of the maritime industry is largely dependent on supplementary on-board carbon capture and storage capabilities, *DNV*

(2022). It is also a valid option to reduce the emissions of existing ships, where retrofitting to accommodate alternative fuels is too costly.

The idea of carbon capture takes inspiration from nature as plants use sunlight, water, and carbon dioxide during the day, in order to produce energy. During that process, the carbon dioxide is reduced to carbon monoxide before it can be converted into energy. Likewise, researchers have created an electrochemical CO<sub>2</sub> reduction process using metal nanocatalysts, capable of reducing CO<sub>2</sub> into specific carbon products more efficiently, which can then be fed into the production process of chemicals, *Zhang et al. (2020)*.

## 5. Other Bio-Inspired Concepts with Application to Maritime Technologies

Thanks to the diversity of biological examples in nature, a myriad of other bio-inspired concepts and solutions exist that present beneficial for the maritime industry. Those include solutions for robotics, autonomous vehicles, sensing as well as localisation and navigation systems and light weight construction.

In contrast to propulsion systems for large ships and commercial vessels, autonomous underwater vehicles (AUV) can profit from their smaller size and general hydrodynamic geometry. Thus, multiple bio-inspired concepts have been proposed and implemented to propel and drive smaller AUVs underwater, *Paley and Wereley (2021)*. *Liu and Curet (2018)* for example developed an undulating single fin propulsion system for AUVs mimicking the fin of the knifefish resulting in higher efficiencies and superior manoeuvrability compared to propeller-driven vehicles. Others have used the tail fin of tuna fish and its side-to-side movement as inspiration for underwater robotics, *Costa et al. (2018)*. Showing great potential for AUV as well are penguins with their low-drag body shape. For Adélie penguins swimming at 2.2 m/s in an unrestrained environment drag coefficient of 0.0368 was determined, being significantly lower than that of a comparable spindle body (drag coefficient of 0.03), *Culik et al. (1994)*. A pressure tolerant vehicle was designed and developed to market readiness by the company EvoLogics to carry underwater acoustic communication technology and taking advantage of the low drag and high manoeuvrability of the penguin body form, *Schmidt et al. (2011)*. Further studies into efficient vehicle shapes shown positive effects on long distance travelling inspired by manta ray and squids, as well as high manoeuvrability and cross flow stability inspired by box fish and sea turtles, *Hoffmann and Kesel (2019)*.

Another interesting area where bio-inspired concepts are of interest is adhering to rough and uneven surfaces under flow conditions as well as gripping objects of unknown geometry. For the former cling fish have developed a uniquely shaped dorsal fin that allows them to adhere to rough and uneven surface due to a combination of friction and suction. These adhesion devices can be used to attach to overgrown underwater structures to perform inspections or as a gripper for the soft manipulation of fragile objects, *Sandoval et al. (2019)*. Another approach for purely gripping is inspired by the tail of sea horses, which sport great flexibility but curiously do not have a circular cross section. Their tail is of segmented architecture with a square cross section, allowing greater deformation without damage while returning to their original form when removing the load, *Porter et al. (2015)*. These properties inspired a seahorse-tail inspired manipulator using soft robotics, *Marzougui et al. (2022)*. As mentioned above, localisation and navigation are of great importance within the maritime sector. Thus, much effort has been put into developing very precise and reliable systems for underwater applications. One of these systems is inspired by seal whiskers with which pinnipeds not only feel objects but also track hydrodynamic trails. *Alvarado et al. (2013)*, *Hanke et al. (2010)* developed underwater whiskers adapted from seals in an attempt to overcome the prevalent limitations of current movement and obstacle localization systems such as GPS, IMUs, acoustic or sonar systems. The sensor makes use of deflection measurements of single hairs in order to determine and locate objects in the vicinity, *Alvarado et al. (2013)*.

Similar to the whisker's inspired sensors, others have been developed for localisation and navigation purposes based on other biological features. A prominent example is the development of active sonar,

where wave signals are emitted into all directions, which bounce off surrounding animals and obstacles. The reflected signal wave received back delivers information on the distance of any obstructions. This technology was developed on the basis of marine mammal echolocation, who use it for navigation, localisation and general intraspecific communication, *Jiang et al. (2018)*.

Lastly, the knifefish mentioned above is not only often mimicked for its swimming gate but also has the ability to use electrolocation to locate objects as it is slightly electric. It uses specialized organelles to recognize external charges across an electric field. Their electroreceptors are highly sensitive and can detect even small amplitude changes which indicate distortion of field lines and therefore an obstacle. A similar system has been adapted using a simple electrical circuit setup and proven functional, *Truong et al. (2015)*.

These only indicate a handful of applications in the maritime industry that do not directly apply to emission savings but still might have a positive effect on the industry.

## 6. Conclusion

This paper summarizes available and innovative bio-inspired concepts to promote the sustainability of the maritime industry, especially for maritime transport and shipping. Biomimetics and bio-inspired solutions help bring innovation in a broad spectrum of areas, such as logistics, the optimization of hydrodynamics of maritime vessel with respect to drag reduction, self-cleaning and anti-fouling. Furthermore, new and innovative vessel designs for large and small vehicles can be derived from nature and finally, underwater manipulation as well as localisation and sonar imaging can be further developed introducing biomimetic concepts. Other fields that might benefit from bio-inspired concepts and designs within the maritime sector are robotics and material sciences, recreational sporting equipment (wetsuits and surfboards), as well as sensors, *Blasiak et al. (2022)*.

While most of the proposed concepts and technologies remain within the research and development stage, the increasing pressure to act and find solutions to reduce the shipping industry's carbon footprint and thus mitigate climate change creates a positive boost for innovative and forward-thinking technologies like biomimetic solutions. Especially topics such as active air lubrication using microbubbles or bow foils are in an advanced stage and are deployed at full scales. For smaller vehicles, the integration of innovative approaches is easier, as shown by EvoLogics with their PinGuin AUV, which is a full-scale AUV capable of 5 m/s swimming speed with high manoeuvrability.

The technical development process of our current transport vehicles, such as ships, has always been influenced by nature. This involves the most obvious characteristics such as streamlined ship shapes, sails or propeller fins. Observing nature has given inventors ideas ever since. As the economic, political and environmental pressure rises to make transport modes more energy and environmental efficient research and development could benefit from intensifying biological inspired approaches as evolution has produced the most efficient and sustainable ways of using and coexisting with nature. Thus, future developments incorporating biomimetics and bio-inspired solutions should continue to foster new ideas and promote new and creative solutions to Maritimes most urging issues.

## References

- ABDULBARI, H.A.; MAHAMMED, H.D.; HASSAN, Z.B.Y. (2015), *Bio-Inspired Passive Drag Reduction Techniques: A Review*, Chem. Bio. Eng. Reviews 2/3, pp.185–203
- ABU BAKAR, N.N.; BAZMOHAMMADI, N.; VASQUEZ, J.C.; GUERRERO, J.M. (2023), *Electrification of onshore power systems in maritime transportation towards decarbonization of ports: A review of the cold ironing technology*, Renewable and Sustainable Energy Reviews 178, p.113243
- ALVARADO, P.V.; SUBRAMANIAM, V.; TRIANTAFYLLOU, M. (2013), *Performance analysis and characterization of bio-inspired whisker sensors for underwater applications*, Int. Conf. Intelligent

Robots and Systems, pp.5956–5961

ARIFIN, M.D.; FELAYATI, F.M.; MUHAMMAD, A.H. (2022), *Flow Separation Evaluation on Tubercle Ship Propeller*, CFD Letters 14/4, pp.43–50

BAGHERI, Z.M.; WIEDERMAN, S.D.; CAZZOLATO, B.S.; GRAINGER, S.; O'CARROLL, D.C. (2017), *Performance of an insect-inspired target tracker in natural conditions*, Bioinspiration & Biomimetics 12/2, p.25006

BANNASCH, R. (1995), *Hydrodynamics of penguins - An experimental approach*, The Penguins; Ecology and Management, pp.141–176

BARTHLOTT, W.; SCHIMMEL, T.; WIERSCH, S.; KOCH, K.; BREDE, M.; BARCZEWSKI, M.; WALHEIM, S.; WEIS, A.; KALTENMAIER, A.; LEDER, A.; BOHN, H.F. (2010), *The salvinia paradox: superhydrophobic surfaces with hydrophilic pins for air retention under water*, Advanced Materials 22/21, pp.2325–2328

BELIBASSAKIS, K.; VERMEIDEN, J.; TOWNSEND, N. (2021), *Combined performance of innovative biomimetic ship propulsion system in waves with Dual Fuel ship engine and application to short-sea shipping*, 31<sup>st</sup> Int. Ocean and Polar Eng. Conf.

BIXLER, G.D.; BHUSHAN, B. (2012), *Bioinspired rice leaf and butterfly wing surface structures combining shark skin and lotus effects*, Soft Matter 8/44, p.11271

BIXLER, G.D.; BHUSHAN, B. (2013), *Fluid drag reduction and efficient self-cleaning with rice leaf and butterfly wing bioinspired surfaces*, Nanoscale 5/17, pp.7685–7710

BLASIAK, R.; JOUFFRAY, J.B.; AMON, D.J.; MOBERG, F.; CLAUDET, J.; SØGAARD JØRGENSEN, P.; PRANINDITA, A.; WABNITZ, C.C.C.; ÖSTERBLUM, H. (2022), *A forgotten element of the blue economy: marine biomimetics and inspiration from the deep sea*, PNAS nexus 1/4

BORKOWSKI, P.; PIETRZYKOWSKI, Z.; MAGAJ, J. (2021), *The Algorithm of Determining an Anti-Collision Manoeuvre Trajectory Based on the Interpolation of Ship's State Vector*, Sensors 21/16

CHADWICK, E.A.; SHRESTHA, P.; PARMAR, H.B.; BAZYLAK, A.; SCHULZ, V. (2022), *Biomimetic Microchannels for the Passive Management of Water in PEM Fuel Cells*, ECS Meeting Abstracts MA2022-02/40, p.1455

CHEN, J.Y.; CHANG, W.L.; HUANG, C.K.; SUN, K.W. (2011), *Biomimetic nanostructured antireflection coating and its application on crystalline silicon solar cells*, Optics express 19/15, pp.14411–14419

CHEN, W.; LU, Y.; LI, S.; GAO, F. (2023), *A bio-inspired foldable-wing wave energy converter for ocean robots*, Applied Energy 334, p.120696

COLONNIER, F.; RAMIREZ-MARTINEZ, S.; VIOLLET, S.; RUFFIER, F. (2019), *A bio-inspired sighted robot chases like a hoverfly*, Bioinspiration & Biomimetics 14/3, p. 36002

COSTA, D.; PALMIERI, G.; PALPACELLI, M.-C.; PANEBIANCO, L.; SCARADOZZI, D. (2018), *Design of a Bio-Inspired Autonomous Underwater Robot*, J. Intelligent & Robotic Systems 91/2, pp.181–192

CULIK, B.M.; BANNASCH, R.; WILSON, R.P. (1994), *External devices on penguins: how important is shape?*, Marine Biology 118/3, pp.353–357

- DARLIS, D.; JAYA, I.; PRIANDANA, K.; NOVITA, Y.; RACHMAT, A. (2023), *State-of-the-Art of the Swarm Ship Technology for Alga Bloom Rapid Monitoring*, Int. J. Advanced Computer Science and Applications 14/3, pp.572–576
- DARWISH, A. (2018), *Bio-inspired computing: Algorithms review, deep analysis, and the scope of applications.*, Future Computing and Informatics J. 3/2, pp.231–246
- DAVENPORT, J.; HUGHES, R.N.; SHORTEN, M.; LARSEN, P.S. (2011), *Drag reduction by air release promotes fast ascent in jumping emperor penguins—a novel hypothesis*, Marine Ecology Progress Series 430, pp.171–182
- DENG, Z.; CHEN, F.; YANG, Q.; BIAN, H.; DU, G.; YONG, J.; SHAN, C.; HOU, X. (2016), *Dragonfly-Eye-Inspired Artificial Compound Eyes with Sophisticated Imaging*, Advanced Functional Materials 26/12, pp.1995–2001
- DNV (2022), *Maritime Forecast to 2050*, Energy Transition Outlook 2022, DNV, Hovik
- FINX (2023), *Towards another future, powered by nature*, <https://finxmotors.com/en/accueil-english/>
- FISH, F.E. (2006), *The myth and reality of Gray's paradox: implication of dolphin drag reduction for technology*, Bioinspiration & Biomimetics 1/2, pp.17–25
- FISH, F.E.; WEBER, P.W.; MURRAY, M.M.; HOWLE, L.E. (2011), *The tubercles on humpback whales' flippers: application of bio-inspired technology*, Integrative and Comparative Biology 51/1, pp.203–213
- GONZALEZ-BELLIDO, P.T.; WARDILL, T.J.; JUUSOLA, M. (2011), *Compound eyes and retinal information processing in miniature dipteran species match their specific ecological demands*, Proc. National Academy of Sciences of the United States of America 108/10, pp.4224–4229
- GRAY, J. (1936), *Studies in Animal Locomotion*, J. Experimental Biology 13/2, pp.170–180
- HAGEN, B.V. (2018), *Influence of a Wavefoil on the Wave Pattern Resistance of a Ship*, NTNU, Trondheim
- HANKE, W.; WITTE, M.; MIERSCH, L.; BREDE, M.; OEFFNER, J.; MICHAEL, M.; HANKE, F.; LEDER, A.; DEHNHARDT, G. (2010), *Harbor seal vibrissa morphology suppresses vortex-induced vibrations*, J. Experimental Biology 213/Pt 15, pp.2665–2672
- HOFFMANN, F.; KESEL, A.B. (2019), *Biologically inspired optimization of underwater vehicles hull geometries and fin propulsion*, IEEE OCEANS, Marseille
- HUANG, Z.; SHI, X.; WANG, G.; LEUKKUNEN, P.; HUTTULA, M.; CAO, W. (2020), *Antireflective design of Si-based photovoltaics via biomimicking structures on black butterfly scales*, Solar Energy 204, pp.738–747
- HUDEC, R.; REMISOVA, K. (2017), *Application of biomimetics in X-ray optics*, Contrib. Astron. Obs. Skalnaté Pleso/47, pp.67–75
- HUDEC, R.; SVEDA, L.; PÍNA, L.; INNEMAN, A.; SEMENCOVA, V.; SKULINOVA, M. (2006), *LOBSTER: new space x-ray telescopes*. Int. Conf. Space Opt.
- IBRAHIM, M.D.; AMRAN, S.N.A.; YUNOS, Y.S.; RAHMAN, M.R.A.; MOHTAR, M.Z.; WONG, L.K.; ZULKHARNAIN, A. (2018), *The Study of Drag Reduction on Ships Inspired by Simplified Shark Skin Imitation*, Applied Bionics and Biomechanics 2018, p.7854321



- IBRAHIM-RASSOUL, N.; SI-AHMED, E.-K.; SERIR, A.; KESSI, A.; LEGRAND, J.; DJILALI, N. (2019), *Investigation of Two-Phase Flow in a Hydrophobic Fuel-Cell Micro-Channel*, *Energies* 12/11, p.2061
- JIANG, J.; WANG, X.; DUAN, F.; LI, C.; FU, X.; HUANG, T.; BU, L.; MA, L.; SUN, Z. (2018), *Bio-Inspired Covert Active Sonar Strategy*, *Sensors* 18/8
- JINQIANG, H.; HUSHENG, W.; RENJUN, Z.; RAFIK, M.; XUANWU, Z. (2021), *Self-organized search-attack mission planning for UAV swarm based on wolf pack hunting behavior*, *J. Systems Engineering and Electronics* 32/6, pp.1463–1476
- KEIL, M.S.; ROCA-MORENO, E.; RODRIGUEZ-VAZQUEZ, A. (2018), *A neural model of the locust visual system for detection of object approaches with real-world scenes*, *Quantitative Biology*, <https://arxiv.org/pdf/1801.08108.pdf>
- KIM, M.; YOO, S.; JEONG, H.E.; KWAK, M.K. (2022), *Fabrication of Salvinia-inspired surfaces for hydrodynamic drag reduction by capillary-force-induced clustering*, *Nature Communications* 13/1, p.5181
- KIM, S.R.; JO, H.J.; KIM, J.H.; PARK, J.Y. (2021), *Formation Control of Swarming Vessels Using a Virtual Matrix Approach and ISOT Guidance Algorithm*, *Processes* 9/9, p.1581
- KRETSCHMANN, L.; BURMEISTER, H.C.; JAHN, C. (2017), *Analyzing the economic benefit of unmanned autonomous ships: An exploratory cost-comparison between an autonomous and a conventional bulk carrier*, *Research in Transportation Business & Management* 25, pp.76–86
- LAMAS, M.; RODRÍGUEZ, J.; RODRÍGUEZ, C.; GONZÁLEZ, P. (2011), *Three-dimensional CFD analysis to study the thrust and efficiency of a biologically-inspired marine propulsor*, *Polish Maritime Research* 18/1
- LAZAROWSKA, A. (2015), *Swarm Intelligence Approach to Safe Ship Control*, *Polish Maritime Research* 22/4, pp.34–40
- LIU, H.; CURET, O. (2018), *Swimming performance of a bio-inspired robotic vessel with undulating fin propulsion*, *Bioinspiration & Biomimetics* 13/5, p.56006
- LIU, K.; JIANG, L. (2012), *Bio-Inspired Self-Cleaning Surfaces*, *Annual Review of Materials Research* 42/1, pp.231–263
- MA, Z.; KRINGS, A.W.; HIROMOTO, R.E. (2009), *Dragonfly as a model for UAV/MAV flight and communication controls*, *IEEE Aerospace Conf.*, pp.1–8
- MARZOUGUI, D.; ADRIAENS, D.; WYFFELS, F. (2022), *Evolutionary co-optimisation of robot morphology and control: toward a seahorse-tail inspired robotic manipulator*, *SEB Annual Conf.*
- NG, B.F.; NEW, T.H.D.; PALACIOS, R. (2017), *Bio-inspired Leading-Edge Tubercles to Improve Fatigue Life in Horizontal Axis Wind Turbine Blades*, *35th Wind Energy Symp.*
- NI, J.; WANG, X.; TANG, M.; CAO, W.; SHI, P.; YANG, S.X. (2020), *An Improved Real-Time Path Planning Method Based on Dragonfly Algorithm for Heterogeneous Multi-Robot System*, *IEEE Access* 8, pp.140558–140568
- NISHIMOTO, S.; BHUSHAN, B. (2013), *Bioinspired self-cleaning surfaces with superhydrophobicity, superoleophobicity, and superhydrophilicity*, *RSC Adv* 3/3, pp.671–690

- OEFFNER, J. (2020), *Reducing Friction with Passive Air Lubrication: Initial Experimental Results and the Numerical Validation Concept of AIRCOAT*, 12<sup>th</sup> HIPER Symp., pp.405–417
- PALEY, D.A.; WERELEY, N.M. (2021), *Bioinspired Sensing, Actuation, and Control in Underwater Soft Robotic Systems*, Springer
- PARFITT, A.R.; VINCENT, J.F.V. (2005), *Drag reduction in a swimming humboldt penguin, Spheniscus humboldti, when the boundary layer is turbulent*, J. Bionic Engineering 2/2, pp.57–62.
- PHILIPPIDES, A.; STEADMAN, N.; DEWAR, A.; WALKER, C.; GRAHAM, P. (2011), *Insect-inspired visual navigation for flying robots*, Springer
- PLOTKIN, M.; HOD, I.; ZABAN, A.; BODEN, S.A.; BAGNALL, D.M.; GALUSHKO, D.; BERGMAN, D.J. (2010), *Solar energy harvesting in the epicuticle of the oriental hornet (Vespa orientalis)*, Die Naturwissenschaften 97/12, pp.1067–1076
- PORTER, M.M.; ADRIAENS, D.; HATTON, R.L.; MEYERS, M.A.; MCKITTRICK, J. (2015), *Why the seahorse tail is square*, Science 349/6243, aaa6683
- POUDEL, S.; ARAFAT, M.Y.; MOH, S. (2023), *Bio-Inspired Optimization-Based Path Planning Algorithms in Unmanned Aerial Vehicles: A Survey*, Sensors 23/6
- PU, X.; LI, G.; LIU, Y. (2016), *Progress and Perspective of Studies on Biomimetic Shark Skin Drag Reduction*, Chem. Bio. Eng. Reviews 3/1, pp.26–40
- QI, J.; WANG, S.; PENG, C. (2020), *Shore power management for maritime transportation: Status and perspectives*, Maritime Transport Research 1, p.100004
- ROMERO, E.; NOVODEREZHNIKIN, V.I.; VAN GRONDELLE, R. (2017), *Quantum design of photosynthesis for bio-inspired solar-energy conversion*, Nature 543/7645, pp.355–365
- SANDOVAL, J.A.; JADHAV, S.; QUAN, H.; DEHEYN, D.D.; TOLLEY, M.T. (2019), *Reversible adhesion to rough surfaces both in and out of water, inspired by the clingfish suction disc*, Bioinspiration & Biomimetics 14/6, p.66016
- SCHMIDT, T.; GELZE, J.; LEHR, H.; MISCHNICK, D.; OLENEW, E.; PRERADOVIC, O.; KORNER, G.; KORNER, H.-M.; THIEDE, C.; KRUGER, S.; HUTH, H.; BANNASCH, R.; KEBKAL, A.; YAKOVLEV, S. (2011), *A pressure-tolerant AUV for deep sea applications [in:] OCEANS'11 MTS/IEEE KONA: IEEE*, pp.1–4.
- SHIN, K.H.; PARK, S.K.; NAKHANIVEJ, P.; WANG, Y.; LIU, P.; BAK, S.M.; CHOI, M.S.; MITLIN, D.; PARK, H.S. (2020), *Biomimetic composite architecture achieves ultrahigh rate capability and cycling life of sodium ion battery cathodes*, Applied Physics Reviews 7/4.
- STARK, C.; SHI, W. (2021a), *Hydroacoustic and hydrodynamic investigation of bio-inspired leading-edge tubercles on marine-ducted thrusters*, Royal Society Open Science 8/9, p.210402
- STARK, C.; SHI, W. (2021b), *The Influence of Leading-Edge Tubercles on the Sheet Cavitation Development of a Benchmark Marine Propeller*, 40<sup>th</sup> Int. Conf. Ocean, ASME
- SULLIVAN, T.; O'CALLAGHAN, I. (2020), *Recent Developments in Biomimetic Antifouling Materials: A Review*, Biomimetics 5/4, p.58
- TAMAGAWA, T.; UCHIYAMA, K.; OTSUBO, R.; YUASA, T.; ZHOU, Y.; MIHARA, T.; EZOE, Y.; NUMAZAWA, M.; ISHI, D.; FUKUSHIMA, A.; SUZUKI, H.; UCHINO, T.; SAKUTA, S.;

ISHIKAWA, K.; ENOTO, T.; SAKAMOTO, T. (2020), *Multiplexing lobster-eye optics: a concept for wide-field X-ray monitoring*, J. Astron. Telesc. Instrum. Syst./6(2)

TRICINCI, O.; PIGNATELLI, F.; MATTOLI, V. (2023), *3D Micropatterned Functional Surface Inspired by Salvinia Molesta via Direct Laser Lithography for Air Retention and Drag Reduction*,=, Advanced Functional Materials, p.2206946

TRUONG, N.; SHOUKRY, Y.; SRIVASTAVA, M. (2015), *Bio-inspired underwater electrolocation through adaptive system identification*, American Control Conf., pp.4473–4478.

WU, X.; MIAO, H.; YIN, M.; HU, R.; WANG, F.; ZHANG, H.; XIA, L.; ZHANG, C.; YUAN, J. (2021), *Biomimetic construction of bifunctional perovskite oxygen catalyst for zinc-air batteries*, Electrochimica Acta 399, p.139407

YI, X.; ZHU, A.; YANG, S.X. (2021), *MPPTM: A Bio-Inspired Approach for Online Path Planning and High-Accuracy Tracking of UAVs*, Frontiers in Neurorobotics 15, p.798428

YILMAZ, Ö.; AOUF, N.; CHECA, E.; MAJEWSKI, L.; SANCHEZ-GESTIDO, M. (2017), *Thermal Analysis of Space Debris for Infrared Based Active Debris Removal*, Proc. IMechE Part G: J. Aerospace Eng. 20(10), pp.1–13

YOON, J.; HOU, Y.; KNOEPFEL, A.M.; YANG, D.; YE, T.; ZHENG, L.; YENNAWAR, N.; SANGHADASA, M.; PRIYA, S.; WANG, K. (2021), *Bio-inspired strategies for next-generation perovskite solar mobile power sources*, Chemical Society Reviews 50/23, pp.12915–12984

YU, C.; LIU, M.; ZHANG, C.; YAN, H.; ZHANG, M.; WU, Q.; LIU, M.; JIANG, L. (2020), *Bio-inspired drag reduction: From nature organisms to artificial functional surfaces*, Giant 2, p.100017

YUAN, W.; ZHANG, C.; LING, Z.; ZHAO, D.; WANG, W.; CHEN, Y.; LU, F.; ZHANG, S.-N.; CUI, W. (2018), *Einstein Probe: a lobster-eye telescope for monitoring the X-ray sky*, 43<sup>rd</sup> COSPAR Scientific Assembly, p.76

YUE, S.; RIND, F.C.; KEIL, M.S.; CUADRI, J.; STAFFORD, R. (2006), *A bio-inspired visual collision detection mechanism for cars: Optimisation of a model of a locust neuron to a novel environment*, Neurocomputing 69/13-15, pp.1591–1598

ZHANG, H.; AGGIDIS, G.A. (2018), *Nature rules hidden in the biomimetic wave energy converters*, Renewable and Sustainable Energy Reviews 97, pp.28–37.

ZHANG, X.; WANG, Y.; GU, M.; WANG, M.; ZHANG, Z.; PAN, W.; JIANG, Z.; ZHENG, H.; LUCERO, M.; WANG, H.; STERBINSKY, G.E.; MA, Q.; WANG, Y.-G.; FENG, Z.; LI, J.; DAI, H.; LIANG, Y. (2020), *Molecular engineering of dispersed nickel phthalocyanines on carbon nanotubes for selective CO<sub>2</sub> reduction*, Nature Energy 5/9, pp.684–692

ZHAO, P.; LI, B.; SHI, W.; WANG, W.; ZHANG, K.; YAN, Z.; YANG, M.; ZUO, X. (2017), *The model research of satellite space laser communication based on compound eye array*, 14<sup>th</sup> Int. Bhurban Conf. on Applied Sciences & Technology (IBCAST), pp.722–726

# Comparison of Full-scale Flettner Rotor Performance Prediction Methods with Sea Trial Data

**Stavros Kontos**, RISE, SSPA Maritime Centre, Gothenburg/Sweden, [Stavros.Kontos@ri.se](mailto:Stavros.Kontos@ri.se)  
**Da-Qing Li**, RISE, SSPA Maritime Centre, Gothenburg/Sweden, [Da-Qing.Li@ri.se](mailto:Da-Qing.Li@ri.se)  
**Chiara Wielgosz**, RISE, SSPA Maritime Centre, Gothenburg/Sweden, [Chiara.Wielgosz@ri.se](mailto:Chiara.Wielgosz@ri.se)  
**Laura Marimon Giovannetti**, RISE, SSPA Maritime Centre, Gothenburg/Sweden, [Laura.MarimonGiovannetti@ri.se](mailto:Laura.MarimonGiovannetti@ri.se)  
**Frederik Gerhardt**, RISE, SSPA Maritime Centre, Gothenburg/Sweden, [Frederik.Gerhardt@ri.se](mailto:Frederik.Gerhardt@ri.se)  
**Sofia Werner**, RISE, SSPA Maritime Centre, Gothenburg/Sweden, [Sofia.Werner@ri.se](mailto:Sofia.Werner@ri.se)  
**Ville Paakkari**, Norsepower, Helsinki/Finland, [Ville.Paakkari@norsepower.com](mailto:Ville.Paakkari@norsepower.com)

## Abstract

*Following IMO's request to reduce green-house gas emissions from shipping, wind assisted propulsion has emerged as a feasible solution. Flettner rotor sails are one of the several technical solutions that have the potential to reduce GHG emissions. Predictions of the power saving potential of wind assistance solutions are important for the acceptance of these new technologies and their market take-up. Such predictions can be carried out at various levels of accuracy and based on different approaches. The industry has not yet converged towards a standard approach. Any validation of performance prediction methods is therefore an important contribution. In 2019 the Scandlines hybrid-ferry "Copenhagen" was retrofitted with a Flettner rotor. Sea trial measurements were carried out within the EU Interreg project WASP to confirm the power saving. These measurements, conducted by the ship owners and one of the authors, present a unique opportunity to validate predictions of the rotor performance. In this study we assess the performance of several prediction methods, ranging from simple generic models to the full-scale 3D CFD simulations. The comparison with the sea trial reveals some interesting effects that may have a large impact on the selection of prediction methods.*

## 1. Introduction

Following IMO's request to reduce green-house gas emissions from shipping (IMO (2017)), wind propulsion has emerged as a feasible solution. The number of cargo vessels equipped with wind assistance technology is still low but rapidly increasing. Flettner rotors are, so far, the most common type with several manufacturers active on the market, but there are also other types like rigid wings, soft sails and suction wings.

The emission reduction that a wind assistance technology can offer is typically predicted at the design stage using numerical or experimental tools. Since the wind propulsion industry is fairly new, at least on a larger commercial scale, the community has not converged towards a standard procedure for power saving predictions. Currently, a Specialist Committee under International Towing Tank Conference, (ITTC) is working on new guidelines for expressing the performance indicators, Werner (2023a), and prediction methods, Werner (2023b). IMO has published guidelines for the inclusion of wind into the EEDI calculation, which is in principle a basic power saving prediction, IMO (2021).

Traditionally, Velocity Prediction Programs (VPP) have been used to assess the performance of sailing vessels. VPPs compute the equilibrium of aerodynamic and hydrodynamic forces for a given wind condition while attempting to optimize for ship speed, Larsson (1990). Most often 4-DOF (surge, sway, heel and yaw) are considered, and an iterative method is used to reach the equilibrium solution. Extensions to these models can maintain a constant speed and optimize for minimum power consumption when motor sailing. Modern approaches use optimization algorithms like e.g., SLSQP, Olsson (2020), Garenaux et al. (2020), or the Nelder-Mead simplex algorithm, Tillig and Ringsberg (2019).

Many unknowns remain on how to accurately predict the performance of wind propulsion technologies.

Although full scale experiments are both rare and in-accurate, it is important to compare them with predictions, to increase the knowledge on prediction methods fidelity. Different attempts are reported in the literature for the validation of power prediction methods. Recently published full-scale campaigns for wind assisted ships have mainly been based on long-term monitoring data, such as for m/v Viking Grace, *Paakkari (2019)* and for m/v Maersk Pelican, *Paakkari (2020)*. An advantage of this type of data is that it reflects the variety of weather conditions and operational profile that the ship encounters, as well as the real operability factors like idling time due to maintenance, weather routing, and crew skills. A challenge of using long-term monitoring data to detect even moderate power savings is the large scatter of such data, combined with the difficulty of finding a comparable reference period with all other conditions, except the wind propulsion installation, unchanged. The main disadvantage is, however, the long period of time that such campaign requires. This is both costly and impractical in a commercial context and for EEDI verification.

Another strategy for performance verification of wind propulsion is to carry out short, dedicated tests over a few hours, compare the ship's speed and power when the wind device is turned on and off, and carefully record the environmental conditions. This methodology is reported for m/v E-Ship 1, *Schmidt (2013)*, and for m/v Fehn Pollux, *Vahs (2019)*, but showing only one selected (favourable) condition with no explanation on how to extrapolate this to a useful KPI.

In this paper we compare power saving prediction models against sea trial measurements for a limited number of wind conditions. The full-scale data used in this comparison have earlier been reported in *Werner et al. (2021)*. Additionally, we combine the sea trial results, the power prediction model and a voyage simulation to derive the most representative power saving potential for the ship. CFD simulations are used to try to understand possible reasons for the observed differences.

## 2. Test case

The RoPax ferry m/v Copenhagen (L=156.45m, B=24.6m, IMO 9587867) operates on the route Gedser-Rostock. She is equipped with a 5 m x 30 m Norsepower rotor sail with an end plate. The rotor technology is described in detail in *Paakkari (2020)*. The rotor is positioned longitudinally around mid-ship, 22.62 m above design water line. The rotation speed of the rotor is set automatically by its control system based on the measured apparent wind speed. The anemometer is positioned in the top of the signal mast over the bridge. The vessel is driven by two Azimuth thrusters and a centre propeller with controllable pitch.



Fig.1: m/v Copenhagen with a Norsepower rotor

## 3. Rotor force modelling challenges

Often the rotor force modelling of power prediction models relies heavily on aerodynamic data acquired with CFD computations or wind tunnel testing. However, these methods assume that the rotor experiences the free stream velocity and neglect any effect that hull and superstructure of a ship introduce.



To assess the performance of the rotor sail, dedicated sea trials of a few hours' duration were carried out in March 2020, *Werner et al. (2022)*. This work revealed that, overall, the predicted performance agreed well with the measured, but there are some interesting differences. This observation cannot be generalized for different vessels, however. The authors suspect that one reason for the deviation is the effect of the disturbance of the ship's superstructure and freeboard on the air flow experienced by the wind propulsion devices. This is a strong motivation for supplementing the performance results (computational or experimental) with deeper analysis using CFD.

Fig.2 illustrates lift and drag coefficients of a single rotor as function of the rotor spin ratio  $SR$ ,

$$SR = \frac{n \pi D}{U_{\infty}} \quad (1)$$

where  $n, D$  are the rpm and diameter of the rotor and  $U_{\infty}$  is the freestream velocity. The figure compares experimental data, *Vahs (2019)*, to SSPA's URANSE calculations and other sources from the literature. As can be seen SSPA calculations and manufacturer data agree reasonably well, with SSPA predicting higher lift and higher drag at spin ratios below 4. The most likely reason for this is that the SSPA-URANSE calculations were conducted at full-scale Reynolds numbers  $\mathcal{O}(10^6)$  whereas manufacturer data are i.a. based on wind tunnel data at  $Re \mathcal{O}(10^4 - 10^5)$ . As discussed by *Li et al. (2012)* the difference in Reynolds numbers affects aerodynamic lift slightly and drag forces significantly. The comparison in Fig.2 illustrates that there can be a large spread between datasets from different sources and highlights the importance of complementing experimental and computational results with full scale data.

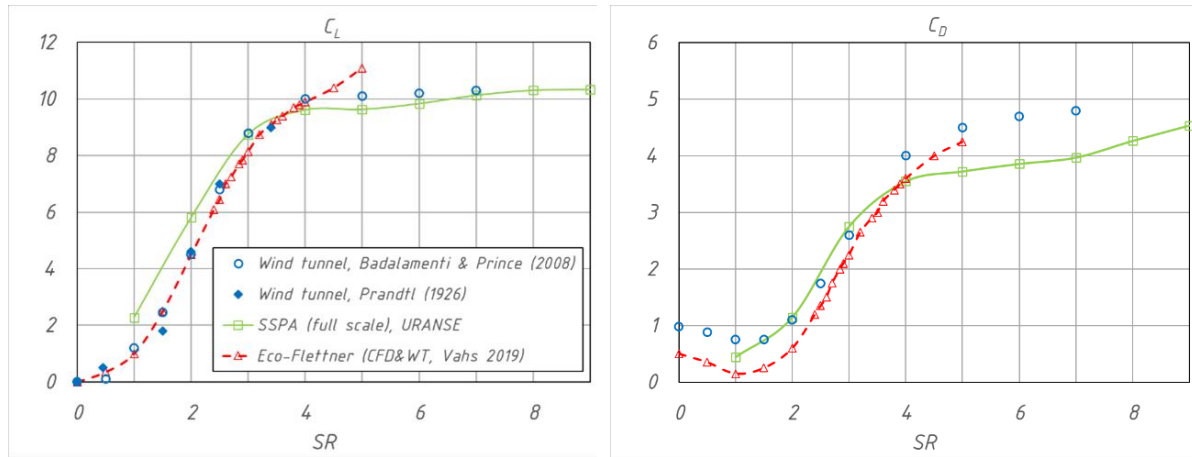


Fig.2: Lift and drag coefficients for standalone Flettner rotor as function of spin ratio  $SR$

#### 4. CFD study of hull-rotor interaction

The performance of a Flettner rotor standalone is significantly different from its performance onboard a vessel, due to a mutual interaction effect between rotor and ship hull. On the one hand, the presence of ship hull and superstructure creates a large disturbance to the flow approaching the hull and rotor because of the blockage effect. The flow arriving at rotor position can be slowed down but it can also be speeded up at some part of rotor height, depending on the wind direction and the extent of blockage effect. Compared with the far field, the apparent wind direction above deck is also modified due to the blockage effect of ship. Therefore, rotor performance is influenced by this change of inflow. On the other hand, the rotation motion of rotor modifies the flow around and alters the pressure field around the ship hull. This results in a somewhat different aerodynamic loading on the hull and superstructure.

One of the reasons for the difference between the predicted performance and the sea trial results can be lack of proper modelling of the interaction effects between hull and rotor. From our experience and the open literature, the interaction effect plays an important role on the rotor performance onboard. Since

the sea trial is conducted in limited conditions, it is interesting to know if the interaction effect is constant or varies with different conditions. For example, Jones et al. (2019) and Garenaux et al. (2020) observed the hull-rotor interaction effects are largest in beam reach conditions and are dependent on spin ratios of rotor. What about influence of wind speed, wind angles, freeboard height and placement of rotor on ship? The following CFD studies explore some of the effects.

#### 4.1. Simplified test case – Box hull

A simplified case is studied to achieve general preliminary results of the influence of the hull on the performance of a Flettner rotor. The well-known KVLCC2 (KRISO Very Large Crude Carrier) ship is represented by a box with the general dimensions of the tanker in ballast conditions: length  $L = 317.48$  m, breadth  $B = 58$  m and freeboard  $f = 20$  m. A generic Flettner rotor with Aspect Ratio ( $AR$ ) = 6 and diameter  $D = 5$  m, with an endplate of diameter  $D_{ep} = 10$  m of thickness  $t_{ep} = 0.1$  m, is positioned on the simplified hull in the centerline amidship. A fully developed Atmospheric Boundary Layer (ABL) profile is used for the velocity profile. The ABL is described by a power law  $U_{ABL} = U_{ref} \left( \frac{z}{z_{ref}} \right)^\alpha$  with the exponent  $\alpha$  equal to 1/7 as suggested by the International Towing Tank Conference (2014). The reference height  $z_{ref}$  is set at 10 m, while the reference speed  $U_{ref}$  is one of the variables of the study. An Apparent Wind Angle ( $AWA$ ) of  $90^\circ$  is used for all the cases, while the reference velocity  $U_{ref}$ , spin ratio  $SR$  and  $RPM$  of the Flettner rotor have been varied. The variation was systematic, generating three different studies, summarized in Table :

- *RPM* study: the *RPM* of the Flettner rotor is kept constant to 180 rpm, while the reference velocity  $U_{ref}$  is varied between 5, 10, 15, and 20 m/s.
- $U_{ref}$  study: the reference speed is kept constant at 10 m/s while the *RPM* of the Flettner rotor is varied to obtain different flow regimes characterized by *SR* values 1,3,5, and 7.
- *SR* study: the *SR* of 5, coinciding with the *SR* of the case with  $U_{ref} = 10$  m/s and  $RPM = 180$ , is kept constant between the different reference velocities of 5, 15, and 20 m/s varying correspondingly the *RPM* of the Flettner rotor.

Table I: Summary of the simulated cases

Study	$U_{ref}$ [m/s]	<i>RPM</i> [deg/min]	<i>SR</i> [-]	Time-step [s]
<i>RPM</i> study	5	180	9	0.005
	10	180	5	0.005
	15	180	3	0.005
	20	180	2	0.005
$U_{ref}$ study	10	45	1	0.019
	10	120	3	0.007
	10	250	7	0.003
<i>SR</i> study	5	90	5	0.009
	15	270	5	0.003
	20	360	5	0.002

It is important to comment on the *RPM* values chosen for each study. The *RPM* value for the *RPM* study is a common reference operational rotational speed, the values chosen for the  $U_{ref}$  study are realistic for the operational conditions of a Flettner rotor, while the *RPM* values calculated for the *SR* study do not represent a realistic setup but are examined since considered academically justified. The choice of a simplified geometry is driven by the possibility to save cells not having to mesh the complicated geometries of the bow and stern considering that the Flettner rotor is positioned at amidship, where the cross section is fundamentally rectangular, therefore well depicted by the chosen simplified geometry, and the wind direction is perpendicular to the geometry, excluding any flow

variation due to interaction upwind with the hull superstructures. However, there are other limitations present in this test case, a grid density and time-step studies have yet to be carried out, but a grid density and time-step value commonly used in industrial applications have been used; a URANS approach might not be considered the most accurate to simulate a flow over a step, basically this test case, but the results are accepted as preliminary. Moreover, a better understanding of setting the ABL in the CFD simulations is needed, but it is considered that all the cases are set identically, hence the general behavior of the Flettner rotor within the different tested cases is assumed comparable.

#### 4.1.1. Set-up

The Unsteady Reynolds-Averaged Navier-Stokes (URANS) equations are solved with the commercial code Star CCM+ 2206 (17.04.007). The equations are solved using a finite volume discretization with a collocated variable arrangement and a pressure-based approach. The coupling between momentum and continuity equations is achieved via the SIMPLE algorithm. The Shear-Stress Transport (SST)  $k-\omega$  turbulence model is used. Convection, diffusivity, and temporal discretization schemes are second-order accurate for all the transport equations. The time-step for each case is set in function of the *RPM* of the rotor to obtain a rotation of  $5^\circ$  per time-step, Table I; and the simulations are run for a total time of 120 s. The Newtonian fluid air at  $15^\circ\text{C}$ , with corresponding density  $\rho = 1.225 \text{ kg/m}^3$  and dynamic viscosity  $\mu = 1.802 \times 10^{-5} \text{ kg/ms}$ , is simulated in a rectangular prism computational domain. The domain spans in the X and Y directions from  $-3L$  to  $3.5L$  and in the Z-direction from zero to  $3L$ , with the zero of the coordinate system coinciding with the center bottom of the simplified hull. The following boundary conditions are set: velocity inlet (purple) with fully developed ABL is prescribed at  $-X$ ,  $-Y$ ,  $+X$ , and top boundaries, while the  $+Y$  boundary (green) is set as pressure outlet and the bottom of the domain, the simplified hull, and the rotor and endplate are set as no-slip walls (orange). A visualization of the domain and corresponding boundary conditions is shown in Fig.3. A structured grid with circa 18.5M cells density is generated, with custom prism layers created on the wall surfaces to obtain a  $y^+$  value higher than 50, enabling the use of wall functions. On the wall surfaces, specific surface cell sizes are set to achieve surface cells of  $2\%D$  on the rotor and endplate surfaces, and of  $10\%D$  on the box hull. Additionally, an isotropic volume refinement of  $20\%D$  cells is created around the hull and rotor, visible in Fig.3. The box refinement is centered with the coordinate system center and has the following dimensions: a length of  $80D$ , a width of  $20D$  and a height of  $12D$ .

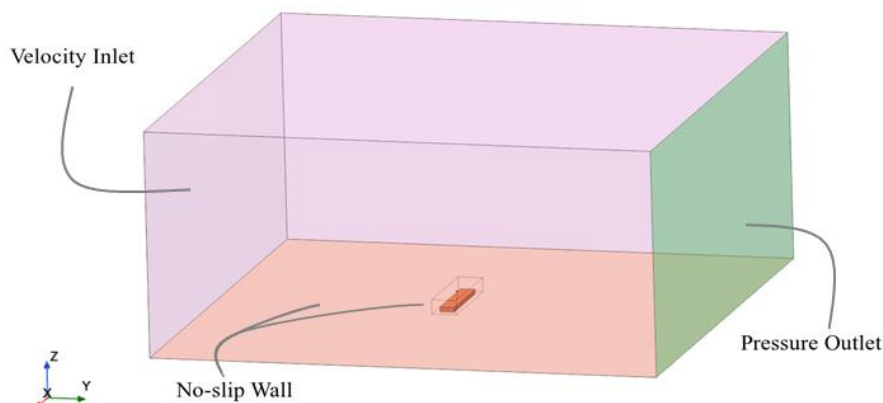


Fig.3: Domain and boundary conditions of the simplified hull test case

#### 4.1.2. Results

The preliminary results of the numerical simulations of the simplified hull are showed below. In Fig.4, the thrust coefficient  $C_X$  and the side force coefficient  $C_Y$  are showed versus the spin ratio with the data organized in function of the three different studies. Note that for this analysis the  $C_X$  correspond to the lift coefficient and the  $C_Y$  to the drag coefficient since the  $AWA = 90^\circ$ . Additionally, the thrust and side force curves obtained by CFD calculations of a generic standalone Flettner rotor are added to show the effect of the presence of the hull on the performance of the WPU (Wind Propulsion Unit). From these

plots, it is visible how the thrust coefficient is further affected by the presence of the hull compared to the side force coefficient. Moreover, the performance of the rotor is only dependent on the spin ratio value, independently of the  $RPM$  and  $U_{ref}$  of the specific case. A clear loss in performance is detectable for lower values of  $SR$ , with increasing thrust for increasing  $SR$  until a plateau is reached. The lowest value simulated is  $SR = 1$  and looking at the flow visualization for this case, Fig.5, it is visible how almost the entire surface of the Flettner rotor is covered by vortices. The reason for this behavior is the characteristic of the flow at such low  $SR$ , in this case caused by a low  $RPM$  of the rotor that does not permit the fluid to adhere to the surface of the WPU allowing a high level of vorticity.

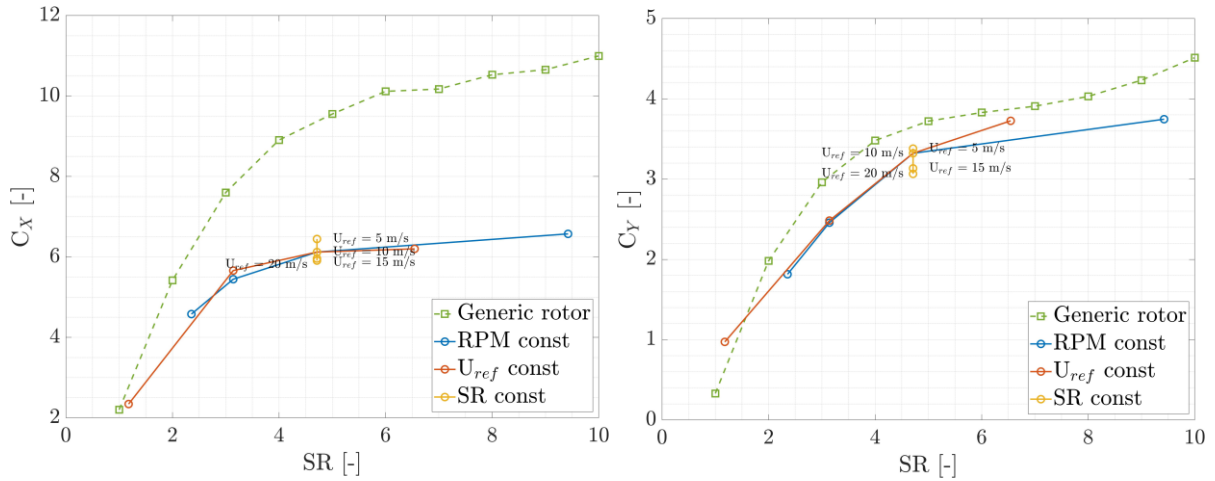


Fig.4: Standalone generic rotor compared to rotor on simplified box shaped hull

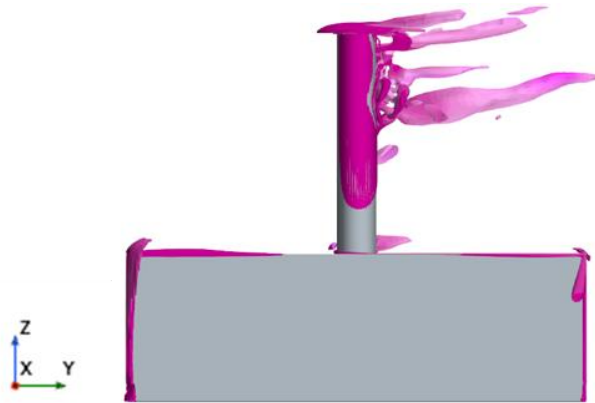


Fig.5: Simplified box shaped hull with  $SR = 1$ . At  $AWA = 90^\circ$

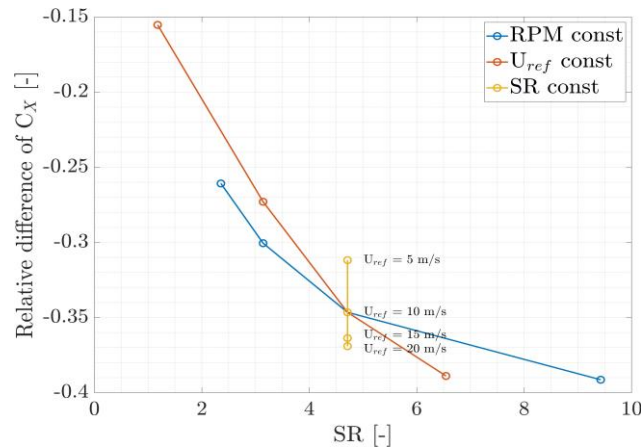


Fig.6: Relative difference of thrust coefficient  $C_x$  between the generic rotor on the boxed shaped hull and the generic standalone rotor

When looking at the relative difference of the thrust coefficient between rotor on the hull and generic rotor (relative difference of  $C_X = (C_{X \text{ rotor on hull}} - C_{X \text{ generic rotor}})/C_{X \text{ generic rotor}}$ ) in Fig.6, it is visible how with increasing  $SR$  the effect of the presence of hull is worsening the rotor performance.

In Fig.7, a YZ plane cutting the rotor in half, shows where the flow is accelerated and decelerated with respect to the magnitude of the far field velocity. The four images below are for the *RPM* study case, where the rotor *RPM* is kept constant to 180 and the reference speed is varied. It is interesting to notice how the recirculation bubble upstream, generated by the presence of the hull, does not change visibly between all the  $U_{ref}$ , while the flow just following the rotor is more impacted, the accelerated flow area reduces with increasing reference speed.

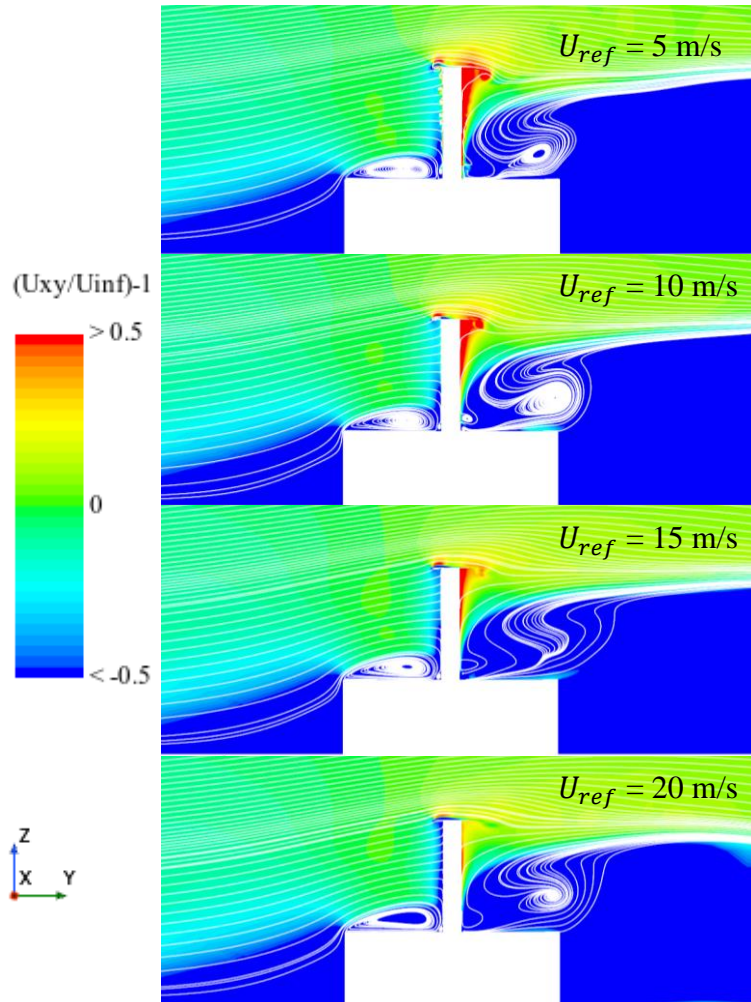


Fig.7: Simplified box shaped hull for the RPM study case

#### 4.2. The ferry Copenhagen

The sea trialed ferry Copenhagen was numerically simulated in four wind conditions that correspond to the ship operated in a reference condition at a true wind speed TWS=10 m/s and a ship speed of 16 knots. The ship main dimensions are given in section 2 and the wind conditions shown in Table II, where the suffix “\_10” means that the wind is defined at 10-meter height over sea.



Table II: Wind conditions and rotor operational conditions

Case No	AWS_10	AWA_10	SR
	[m/s]	[°]	[-]
1	17.3	20	2.3
2	14.2	43	2.8
3	11.6	57	3.4
4	6.2	86	5.9

#### 4.2.1. CFD setup

The computations for the ferry have similar setups to what are used for the Box-hull case, hence, only the differences are highlighted below. The computational domain is a rectangular box with the ship located in the center bottom of the domain. The origin of the coordinate system is defined at the intersection between the aft-perpendicular line and the baseline of the ship, with positive x direction towards bow and positive y direction towards port side of the ship. The domain spans in the X and Y directions from  $-3.5L$  to  $3.5L$  and in the Z-direction from zero to  $2.5L$ , where  $L$  is the perpendicular length of the ship. Polyhedral meshes were used. A different mesh is created for each wind condition due to difference in Reynolds ( $Re$ ) numbers from case to case. The non-dimensional wall distance  $y^+$  to the body surface is set to be approximately 55 or above. Additionally, an isotropic volume refinement of  $20\%D$  cells is created around the hull and rotor. The mesh count is about 20 million cells. The air density and kinematic viscosity were the same as in the sea trial at  $4^\circ\text{C}$ . No-slip wall Boundary Condition (BC) is applied on rotor, hull surface, and water surface. Velocity Inlet (including ABL profile) and Pressure Outlet BC are applied on different side of domain depending on the wind direction.

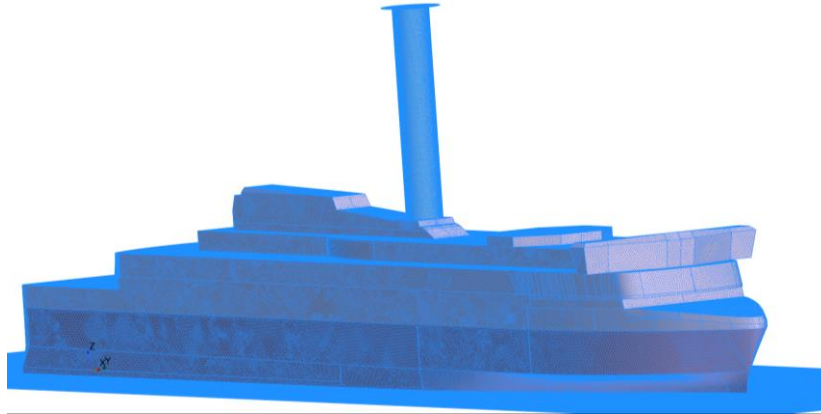


Fig.8: Surface mesh on hull and rotor surface of m/v Copenhagen

#### 4.2.2. Results

##### 4.2.2.1. Influence of hull

Let's first look at a one-way interaction effect. More specifically, the influence of hull on the wind profile above deck at the rotor installation location from the CFD results at the four wind conditions. Fig.9 presents the flow field scenarios at a transversal plane cutting through the fluid domain at the location where the rotor would have been installed. The simulations were made for the hull without rotor. The 2D streamlines ( $U_y$  and  $U_z$  velocity component) give us an idea how the flow changes from the left (entering the domain) to the right (exiting the domain) on this vertical cutting plane. The ship is positioned with the bow facing the viewer (though the ship geometry is not shown here). The contour plot of the change of the horizontal velocity (vector sum of  $U_x$  and  $U_y$ ) from its far field value shows how the horizontal magnitude varies on the cutting plane. The magnitude  $U_{xy}$  has been normalized by the far field wind speed at the same height. Therefore, a positive  $U_{xy}$  means an increased horizontal

flow speed whereas a negative  $U_{xy}$  means a decreased flow speed, as compared with the corresponding magnitude at far field. Common to all cases are the occurrence of a horseshoe vortex at the left corner of the hull due to the blockage of atmospheric boundary layer flow near water surface and a large separation bubble at the right corner of the hull. The strength of the vortices seems to increase with the increase of wind angle for the computed cases. Separation occurs on deck as the flow passes over the freeboard. Flow separates also behind various step-like superstructure. The extent of separation is largely dependent on apparent wind angle.

As seen in Fig.9, starting at low apparent wind angles (AWA\_10), from  $20^\circ$  to  $43^\circ$  even at  $57^\circ$ , the red area of the  $U_{xy}$  contours represents a region with speed higher than the freestream. Furthermore, a convex form of the streamlines is formed above the deck, suggesting that the speed increase is the highest in this region. The increase of flow speed  $U_{xy}$  in this region will make a positive and favorable contribution to the force generation on rotors. Namely, a rotor can possibly generate a higher force onboard ship than the case with rotor standalone! Immediately above the deck and below the convex streamlines, there is one or a few small blue areas that result from the vortex formation and flow separation behind the rotor support (a step-like structure). In this area the flow becomes much slower than freestream and the lift generation is deteriorated, compared to the rotor in standalone situation. Contrary to the first three wind angles, the last case at AWA\_10= $86^\circ$  is close to a beam reach angle, the flow pattern becomes very different. The large blue area to the right indicates massive flow separation on the port side. This is not surprising because the largest blockage effect and flow separation take place in beam reach conditions. The streamlines above the deck height all have an ascending form from left to right, instead of a convex form. It means that the speed increase is still relatively slow, as confirmed by the color scale of  $U_{xy}$  above the deck.

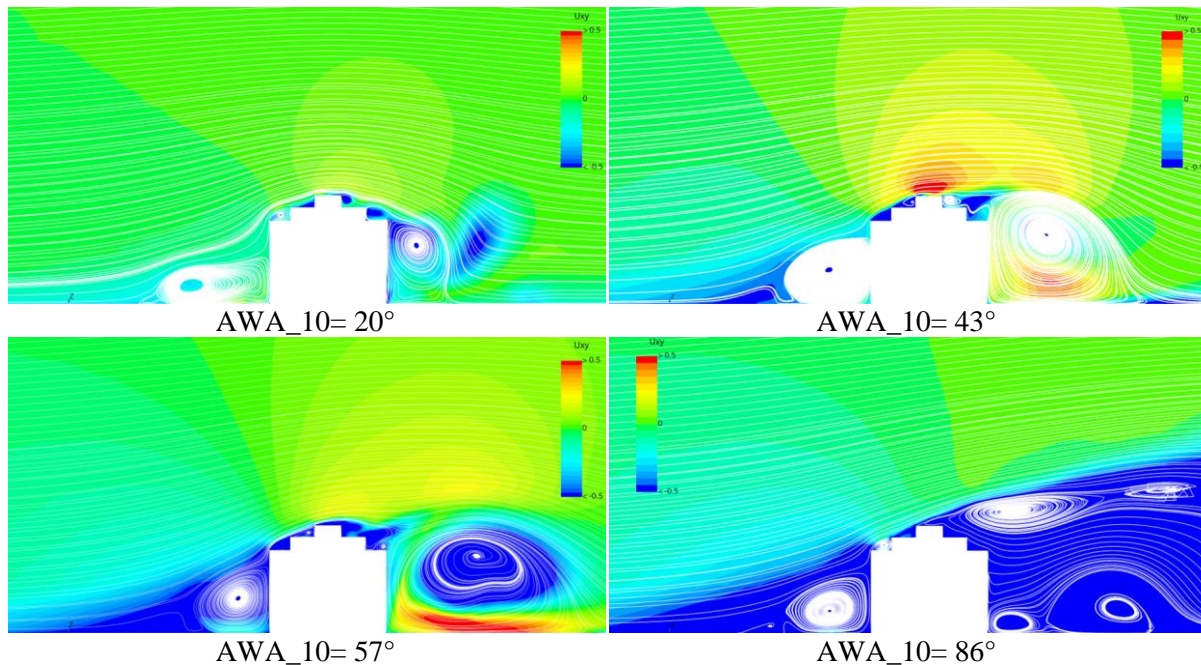


Fig.9: Air flow (from left) passing over the hull at four different wind angles at a transversal plane cutting the rotor install location. The 2D streamlines are drawn with  $U_y$  and  $U_z$  velocity component. The contour plots are made of  $U_{xy}$ .  $U_{xy}$  is the difference between the local and the far field horizontal velocity magnitude (vector sum of  $U_x$  and  $U_y$ ), normalized by the corresponding magnitude at the same height in far field.  $U_{xy} < 0$  means that the flow is slower and  $U_{xy} > 0$  the flow is faster than the far field apparent wind at the same height.

Some quantitative data is plotted in Fig.10, to illustrate what has just been discussed. The figure to the left shows the change of AWA profile at the rotor axis location, the figure to the right shows the change of the normalized  $U_{xy}$  at the same location. The image of ship hull and rotor was added to the plot to visualize the extent of flow disturbances relative the rotor-height. The increase of  $AWA_{local}$  in upwind

conditions ( $AWA_{10}=20^\circ, 43^\circ$  and  $57^\circ$ ) would result in a somewhat higher thrust when the rotor force is projected to ship's moving direction. Special attention is paid to the speed change for the case  $AWA_{10}=86^\circ$ , where the flow over almost the entire rotor-height is still slower than the free stream due to the severe blockage effect on the freeboard at starboard side. The recovery of flow speed starts only from a height taller than rotor height. It means that the rotor works in an unfavorable inflow condition (mainly reduced speed but also slightly reduced apparent wind angle) as compared with the upwind cases, as well as compared with the rotor standalone condition. As seen in Fig.9 and Fig.10, the wind angle and the height of freeboard are two parameters that influence the flow passage over the hull-rotor configuration. The formation of deck can also have an effect on the extent of separation.

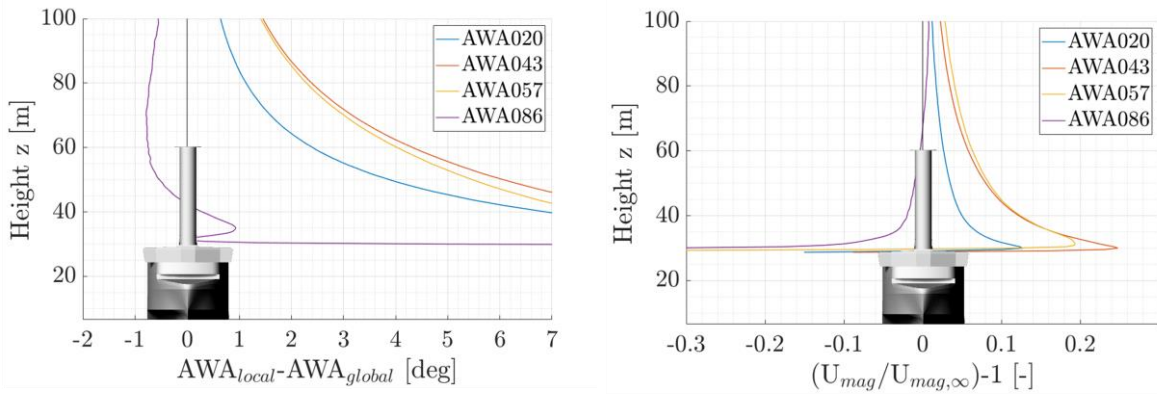


Fig.10: Left: change of AWA. Right: change of magnitude of the horizontal velocity (normalized). From RANS simulation of hull without rotor (Gray hull and rotor is added for reference)

The above analysis addresses only the one-way interaction, i.e., the disturbance of ship hull on the incoming flow to rotor, it is not the true picture of the mutual interaction between rotor and hull. Nevertheless, it provides useful information for rotor suppliers and ship operators on what flow disturbance an installed rotor is likely to meet with, where to place the rotor and possibly the lowest installation height for maximizing rotor performance onboard.

#### 4.2.2.2. Interaction effects

The performance of rotor onboard a ship can be affected by the hull-rotor interaction both favorably and unfavorably, depending on the AWA, SR, freeboard height and deck contour, as well as the placement of rotors.

First, let's look at the positive and negative effects with regard to the pressure coefficient ( $C_p$ ) distribution on the rotor surface of two configurations: one with the rotor standalone on a very large flat plate (representing the open sea), and the other configuration with the rotor operating onboard of the ferry Copenhagen. The comparison is made for the same wind conditions as before. Same meshing strategy and numerical setup have been applied for the case with rotor standalone. The result is shown in Fig.11, where the rotor standalone case is placed on the left (at the same height as the rotor height onboard) in each plot. For the rotor onboard cases, pressure distribution on part of the ship superstructure is also visible in the figure. The dark blue area of  $C_p$  means strong under-pressure and a high-lift generation area compared to other colored areas. It is seen in Fig.11, common to all cases, less lift is generated on the lower part of rotor because of interaction between two sets of boundary layer flows at the junction, one developed on the rotor surface and the other developed on the horizontal wall. For the rotor onboard configuration, the force generation on the lower part of rotor is further affected by the disturbed flow from the rotor supporting base at the root and the transverse flow arising from the freeboard side. The pressure distribution on the rest (mid and upper) part of rotor is different at different AWA. At the two upwind conditions,  $AWA_{10}=20^\circ$  and  $43^\circ$ , the overall blue area on the rotor onboard configuration is larger than the rotor standalone case, showing a positive interaction effect that a higher lift is generated along the rest part of rotor. This is mainly caused by the locally increased flow speed ( $U_{xy}$ , see Fig.10) along the rotor height due to hull influence. We see here that the positive

effect takes a dominance at these two angles. Looking at the two higher angles,  $AWA_{10}=57^\circ$  and  $86^\circ$ , the overall blue area on rotor becomes less than the rotor standalone case, showing a *negative* interaction effect that less lift force is generated. The negative effect seems to be dominant. Note that from low to high wind angle, the spin ratio SR of rotor is increasing, that is why the blue area on rotor grows progressively with increasing AWA for the rotor standalone configuration.

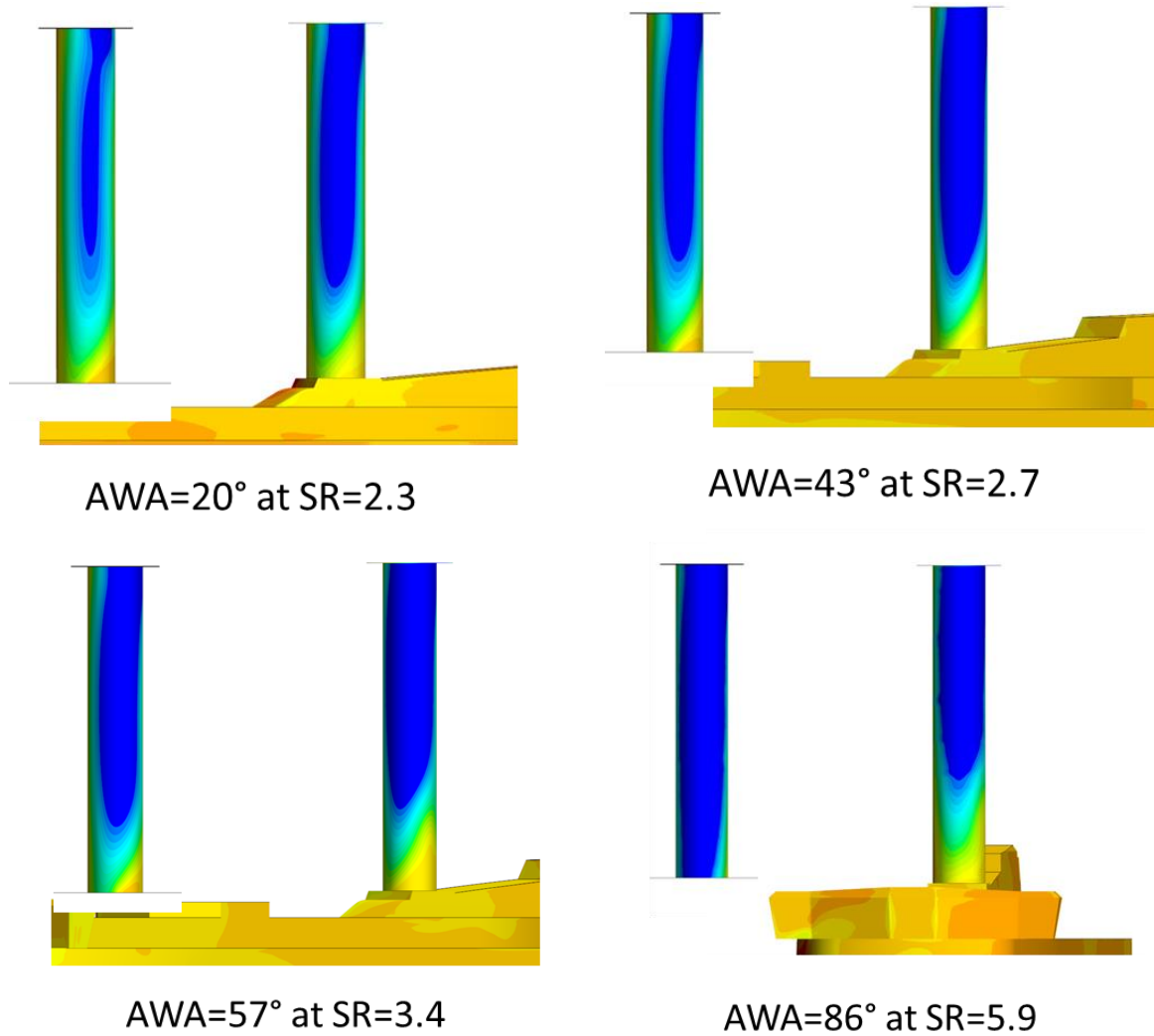


Fig.11: Pressure distribution (contour plot of  $C_p$ ) on rotor surface for two configurations

The interaction effect in the beam reach region ( $AWA_{10}=86^\circ$ ) appears to be most severe for two reasons. First, the large stagnation area of freeboard slows down the approaching flow substantially not only on the hull side but also to a height beyond and above the deck height (refer to  $U_{xy}$  profile in Fig.10 at this condition), causing a severe speed loss on the lower part of rotor. Second, the rotor spins at a high SR at this condition. The higher the SR, the larger the rotor-induced flow field hence a stronger impact on flow around the hull and in rotor wake. A rotor operating at high SR is prone to separate too, meaning a stronger interaction between the rotor boundary and the horseshoe vortex at the root. These two effects result in a much less lift generation on the lower part of rotor, as visualized by the cyan and yellow colors in Fig.11.

Next, the change of thrust coefficient ( $\Delta C_x$ ) between the rotor onboard and the rotor standalone configuration are presented in Fig.12, as a function of SR and AWA (some additional computations were supplied for this figure). The change ( $\Delta C_x$ ) is a measure of interaction effect on thrust. As can be seen in Fig.12, for upwind conditions at spin ratios lower than 3,  $\Delta C_x$  is positive, indicating a favorable interaction effect (higher thrust) for rotor onboard a ship. The change of  $C_x$  in Fig.12 reflects the similar behavior as observed on the pressure distribution in Fig.11. With the increase of SR and the increase of



AWA, we see that  $C_x$  becomes substantially lower than the rotor standalone case. The performance loss with increasing  $SR$  at  $AWA=90^\circ$  for the Box-hull case (Fig.6) showed a very similar character as observed here for Copenhagen. The general trend observed in the present study is quite similar to that reported by *Garenaux et al. (2021)*.

The following features of interaction effects can be summarized from the study:

1. There are both positive and negative interaction effects with respect to the performance of the rotor compared to a rotor standalone case. The main beneficial effect is the increase of wind speed above the ship deck. It is counteracted by a loss of suction on the lower part of the rotor.
2. The interaction effect is influenced by AWA. With increase of AWA from upwind to beam reach angle, the interaction effect becomes stronger, and the negative effect takes over and becomes dominant.
3. The interaction effect is influenced by  $SR$ , the higher the  $SR$ , the stronger the effect. If  $SR$  is constant, any change made to  $AWS$  and  $RPM$  has no effect on rotor performance.
4. The height of freeboard, the deck profile, the form/shape of supportive base to rotor, and the superstructure around rotor all influence the development of boundary layer on deck and have an influence on flow passing the lower part of the rotor and the lift generation on that part.

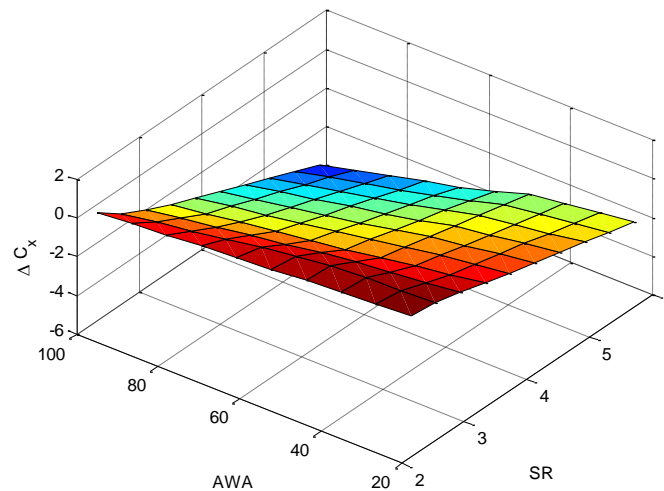


Fig.12: The change of thrust ( $\Delta C_x$ ) between a rotor onboard case and a rotor standalone case, as function of spin ratio ( $SR$ ) and apparent wind angle ( $AWA$ ).

The flow field for the rotor installed onboard the ferry is also studied for the four wind conditions in Table II. The flow pattern at the vertical plane cutting through the rotor axis is presented in Fig.13. The same plotting style as used for Fig.9 has been used here. An obvious difference from Fig.9 is the large red area next to the right side (downstream) of rotor. The rotor is rotating in anti-clockwise direction if viewing it from above. The rotor induces a rotational flow field around it, therefore, on the cutting plane this induced flow on the right side has the same direction as the relative ship velocity (both pointing in the negative direction of  $x$ -axis). The superimposition of the two velocity components leads to a  $U_{xy}$  greater than free stream. The induced flow on the left side of rotor is opposite to the relative ship velocity, therefore it cancels out part of ship speed and decreases somewhat the magnitude of  $U_{xy}$ . This is why we see large red area at right side and a narrow blue area at left side next to the rotor. Compared with Fig.9, the horseshoe vortex at left corner starboard side and the separation bubble on leeward side of ship have similar characters as those in Fig.9. They differ slightly in size and height, except for  $AWA_{10}=86^\circ$  case that shows an elongated separation bubble on the leeward side. A visible difference is observed at leeward-side junction corner of the rotor, where a blue area (instead of red) occurs. This is a consequence of interaction between two boundary-layer flows at the junction of rotor and rotor-support that alters the formation and transport of the horseshoe vortex.



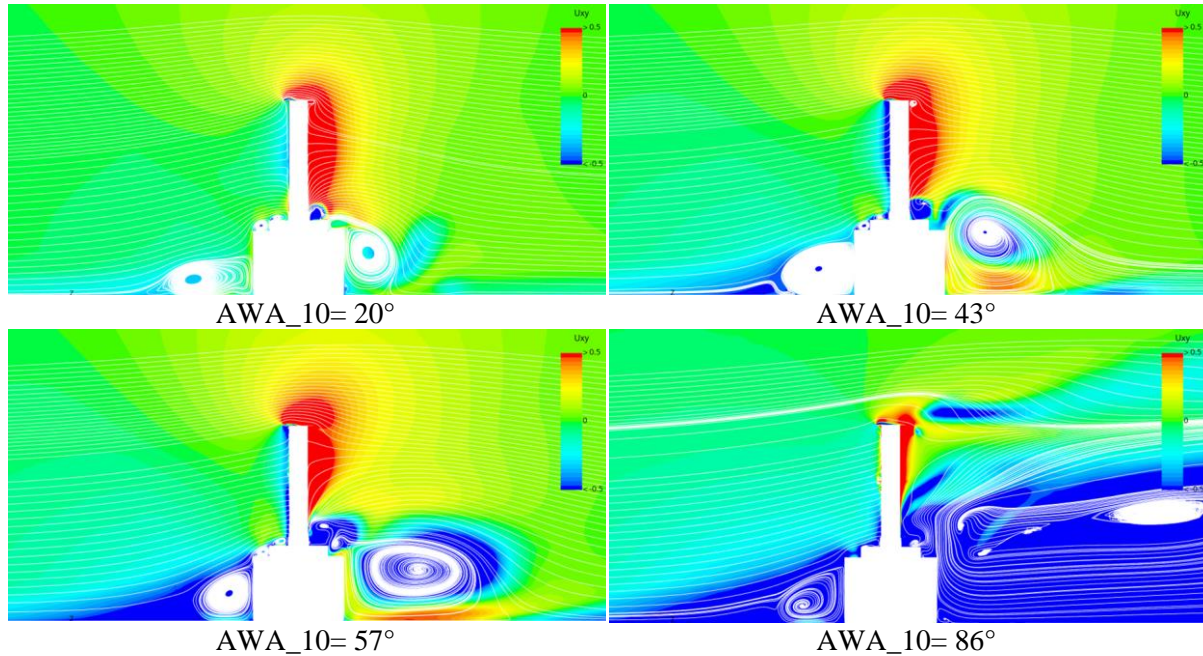


Fig.13: Flow pattern at four different AWA angles for the rotor onboard case, same plotting style as Fig.9.

#### 4.2.2.3. RANS vs. hybrid RANS-LES method

Are the large separations in the close beam-reach wind conditions realistic? Could it be caused by the limitation of RANS method in modeling flow separation in extreme case as such? It is known that RANS methods have difficulty in predicting flow with massive separation behind blunt bodies, therefore, we suspect that the RANS method might have over-predicted the interaction effect for wind in the beam-reach conditions. We performed a set of simulations with a very fine mesh (62 million cells) and employed a latest hybrid RANS-LES method in STAR-CCM+ for the rotor-hull configuration. The method is called Scale-Resolving Hybrid (SRH) method and belongs to the category of Hybrid Temporal LES (HTLES) models. The model uses a filter kernel that includes both space (LES) and time (URANS) components. It establishes a continuous connection between URANS and LES models by controlling the energy partition between the resolved and modeled scales, therefore it is able to resolve a wider spectrum of turbulence scales than a RANS method.

The results of hybrid RANS-LES simulations are preliminary, but the accumulated time signals appear to be long enough to collect averaged forces. The changes of force coefficients  $\Delta C_x$  predicted by the hybrid and RANS method are somewhat different. At the two upwind conditions, the difference in  $\Delta C_x$  between the two methods is small to moderate. The difference in  $\Delta C_x$  grows larger as the AWA increases and enters in the beam-reach region. A large difference in  $\Delta C_x$  is noted at the highest angle (AWA\_10=86°). Recall that  $\Delta C_x$  is a measure of interaction effect on thrust, it means that the interaction effect predicted by the RANS-LES method is significantly weaker than the RANS method. The results of the hybrid method support our suspicion on the overprediction of interaction effect by the RANS method, yet it's too early to draw a conclusion based on the limited study here.

The vortex structure representing the resolved turbulence length-scales are presented in Fig.14 for the case at AWA\_10=86°. Not surprisingly, we see much more details on the small structure vortices predicted by the hybrid RANS-LES, in contrast to only the large-scale vortices by RANS (left figure). Interesting to point out is the very strong horseshoe vortex at the rotor root predicted by the RANS, the extent of which seems to be over-predicted compared with the RANS-LES method. This might give an explanation why RANS resulted in a lower force at this condition.

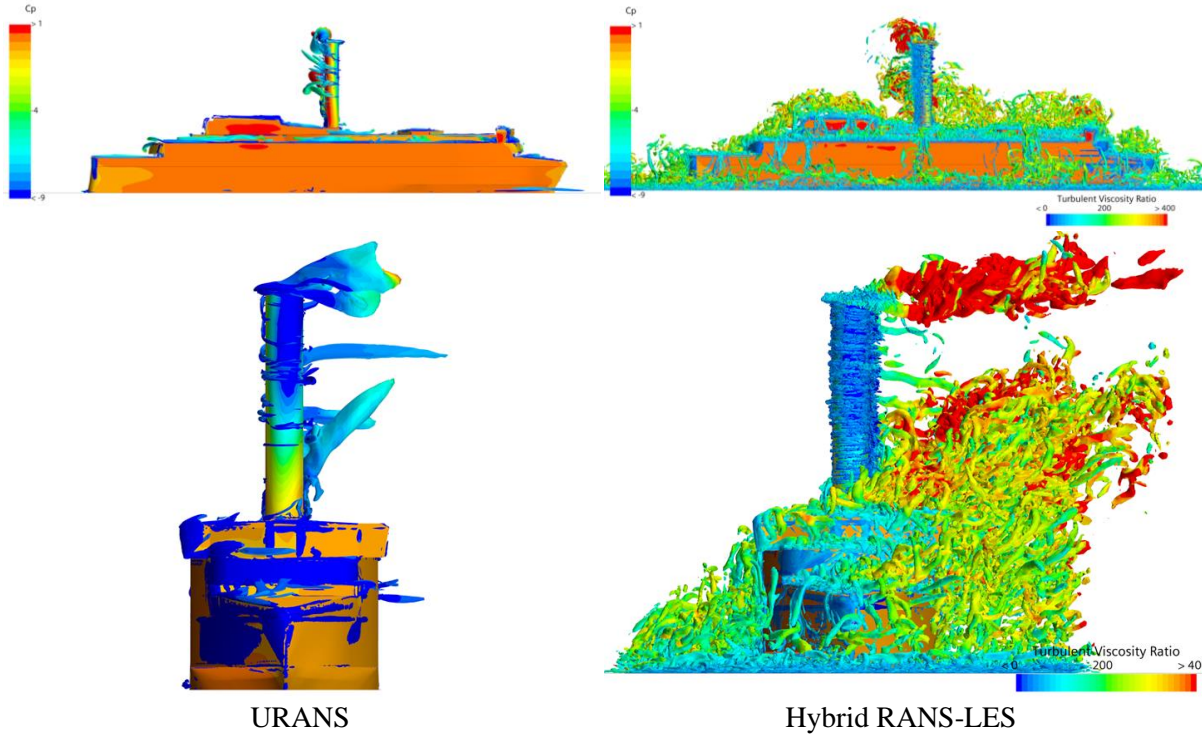


Fig.14: Vortex structure predicted by URANS and hybrid RANS-LES at AWA\_10= 86° condition

## 5. Power prediction models

During the various stages of the design process, different fidelity models are needed. A specialist committee under ITTC in collaboration with some of the authors of this paper are developing Recommended Procedures and Guidelines for predicting the power savings of wind powered ships. The different power prediction models are classified in levels based on their fidelity. We will cover the three levels of increasing fidelity models below, and we will compare their performance with the sea trial results.

### 5.1. Power prediction model – Level I (1 DOF, EEDI type)

*IMO (2021)* published an updated guideline for calculating the effect of “innovative energy efficiency technologies”, such as wind assistance technologies, on EEDI. The first level serves as a simplified, non-conservative approach for getting a first estimate of possible power savings that should not be used for decision making. The power savings for this level are calculated as

$$\Delta P = \frac{F_x \cdot V_s}{\eta_D} - P_{in} \quad (2)$$

where  $F_x$  is the aerodynamic force from the wind propulsion device in the x-direction [N],  $V_s$  is the ship speed [m/s],  $\eta_D$  is the propulsive efficiency [-] and  $P_{in}$  is the power consumption of the device [W].

### 5.2. Power prediction model – Level II (4 DOF)

Level II models can according to the ITTC draft Guidelines provide early business case assessment support. Most physical effects are accounted for, but at a level of fidelity and computational effort that allows for assessment of several design configurations.

RISE uses the tool Seaman Winds which includes a PPP (Performance Prediction Program). It can be used for finding the maximum ship speed for a purely sailing ship, or the lowest power for a constant

speed of a motor-sailing ship, while enforcing force equilibrium in surge, sway roll and yaw. The optimization is achieved using a sequential least squares quadratic programming algorithm (SLSQP) that belongs in the family of gradient based algorithms. The PPP relies on a modular setup of static force modules to compute the force residuals in the 4 DOF at every iteration of the optimization algorithm. The most relevant for this work are the hull and rudder hydrodynamics and the rotor aerodynamics.

The modeling of the hydrodynamic related forces is listed below:

- Calm water resistance is estimated from the SSPA/RISE database of model test results. Alternatively, it can be modelled based on generic methods as in *Holtrop Mennen (1982)*.
- The propulsive efficiency is modelled using propeller open water curves and propulsive factors from towing tank tests of the actual vessel or from the SSPA/RISE database.
- Added resistance in waves is estimated using the SSPA/RISE database or modelled with a modified STAWAVE-2, *ITTC (2021)*, empirical method and spectral superposition theory.
- Manoeuvring and rudder forces are modelled as polynomials with hydrodynamic coefficients and velocities of the ship through water. The coefficients are obtained with regression analysis of virtual captive tests (VCT) of the full-scale ship or from the SSPA/RISE database of manoeuvring model tests. For more details about the VCT method, see *Alexandersson et al. (2017)*.
- Hydrostatic forces are based on hydrostatic data for the specific loading condition.

Rotor sails are modeled using generic lift and drag curves that have been derived using CFD, Fig.2, for the usual rotor aspect ratios available on today's market, see *Li et al (2012)*. When the rotor thrust is negative, it is assumed that the rotor is turned off. In head wind, the rotor is assumed to give an added resistance defined as:

$$R_{\text{rotor}} = C_{D \text{ rotor}} \frac{1}{2} \rho_{\text{air}} \cdot H \cdot D \cdot AWS_x^2$$

where  $\rho_{\text{air}}$  is the air density [ $kg/m^3$ ],  $H, D$  is the rotor height and diameter [ $m$ ] and  $AWS_x^2$  is the apparent wind speed in the x-direction in [ $m/s$ ]. The rotational speed of the rotor and the power required to operate it are based on information from the rotor provider.

To provide an intermediate fidelity level between I and II, the PPP can be reduced to 1 DOF while maintaining the same force modelling modules. For completeness, this 1 DOF model is included in the comparison and will be referred to as "1 DOF with propeller" in the discussion.

### 5.3. Power prediction model – Level III (4 DOF, hull interaction)

Level III is a higher fidelity approach that, according to the ITTC draft Guidelines, can lead to a performance contract. For most applications this is the final level. In this level the modelling is extended to include the influence of the ship superstructure on the rotor performance. This is accomplished by using CFD simulations of the hull and rotor together. The simulations are carried out for a range of wind angles and for various spin ratios. The difference between the rotor-on-hull force and the force from a single standalone rotor is extracted ( $\Delta C_x, \Delta C_y$ ). These coefficients vary in a regular manner with AWA and SR, Fig.12, but to less degree on wind speed (see section 4.1). In the performance prediction program,  $\Delta C_x$  and  $\Delta C_y$  can be extracted in any condition by surface interpolation, and the actual  $C_x$  can be calculated based on  $\Delta C_x$  and  $\Delta C_y$  and the standalone rotor model.

### 5.4. Power prediction model – Level III (4 DOF, correlated to sea trial)

In order to produce a model for the final route assessment, the model is correlated to the sea trial results by modifying the correction of  $C_x$  and  $C_y$  as a function of AWA and SR. This is a way of including unknown effects, for the final power saving potential calculation.

### 5.5. Power prediction model from the rotor provider – with hull interaction and rotor performance from full scale installation)

The EEDI framework described in MEPC Circ.896 mentions that the hull-sail and sail-sail interactions should be accounted for when assessing the aerodynamic thrust force  $F_x$ .

To achieve this, the performance prediction tools from Norsepower developed to match the requirements set by EEDI calculation guidelines were deployed. These tools combine the full-scale performance measurements, conducted on Norsepower installations, and the disturbance field caused by the ship's hull using superposition. The preliminary version of the full-scale lift and drag curves was earlier published in *Dupuy et al. (2023)*.

The aerodynamic forces are converted to power savings according to method described above.

## 6. Voyage simulation

To predict the power savings of a ship fitted with a Wind Propulsion System (WPS) on a given route RISE uses the inhouse tool Seaman Winds. The tool combines the output of the power prediction models described above, with weather statistics along the route and performs a Monte Carlo simulation to calculate statistics of the power and energy savings. The algorithm is described in detail in *Olsson et al. (2020)*. A brief description will be given below.

The selected route is divided in legs. For each leg a discrete joint weather distribution is defined based on the hourly wind data. These leg-wise distributions are uncorrelated. A Monte Carlo (MC) simulation follows.

In every iteration of the MC simulation and for every leg of the route:

- Compute the average azimuth and distance that the ship travels on this leg.
- Draw a sample weather condition from the discrete, joint weather distribution. The sample is randomly chosen based on its probability of occurrence, i.e. a weather condition with 2% probability of occurring has a 2% probability of being sampled.
- Use the ship performance polar curves computed with the PPP to evaluate the performance under the specific weather conditions.
- Use the results of each leg of this MC iteration to calculate an aggregate result for the whole route.

Finally, combine the aggregate route results from all MC iterations into a single cumulative performance distribution. The assumptions made in the voyage simulations are:

- Fixed ship speed ( $V_s = 16$  knots)
- Air density  $1.24 \text{ kg/m}^3$  all year around.
- The main engine is assumed to always deliver enough power and torque to reach the in-tended speed, i.e. no involuntary speed reductions.
- Engine efficiency variation with load not accounted for.
- Voluntary speed reductions are not accounted for.
- Hull fouling is not accounted for.

In this study the weather statistics used are from the ERA5 reanalysis dataset available at Copernicus Climate Data Store, *Hersbach et al. (2023)*. For comparison, the wind statistics from the EEDI Global Weather matrix IMO (2021) are also included. The EEDI matrix is constructed to represent the wind on the major world-wide trade routes.

## 7. Sea trial

A sea trial was performed on March 6-7, 2021, with m/v Copenhagen for the purpose of evaluating the performance of the rotor. The test procedure, data collection and measurements have been described in detail in earlier papers, *Werner (2021,2022)*. A short summary is given here.

Eight short speed runs were conducted, alternating between rotor switched on and rotor switched off. The speed, power and wind were measured. The power-saving from the rotor is derived by translating the measured speed and power differences to a single power saving for a given nominal ship speed and reference wind speed using the ships speed-power curve, as shown in Fig.15. Finally, the power savings are normalised to a given nominal wind speed and ship speed. This is done using a new ITTC procedure, which will be published in 2024.

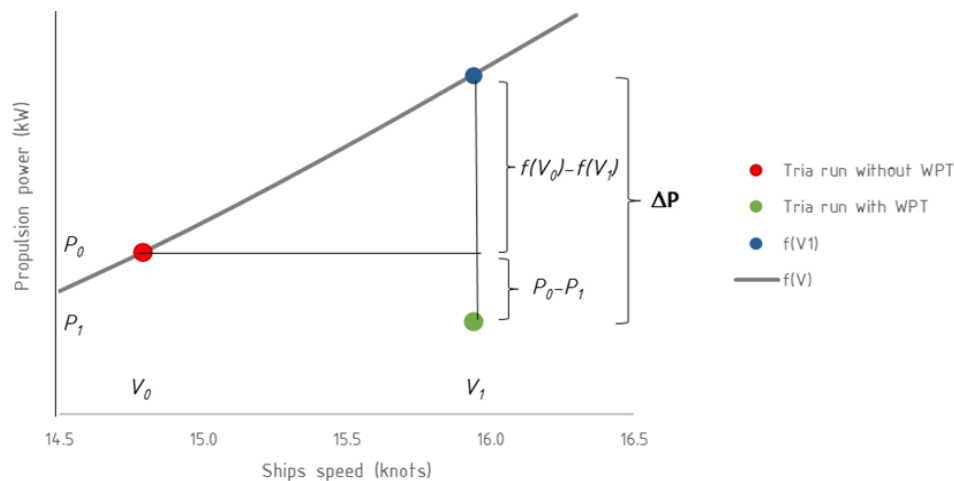


Fig.15: Extracting the sea trial power difference due to the rotor using the ship's speed-power curve

### 7.1 Sea trial uncertainty assessment

Here follows an estimate of the uncertainty of the derived power difference, following ITTC 7.5-02-01-01 (Type A). The authors do not claim it to be a complete uncertainty assessment, but an indication of the magnitude of the larger error sources. One large uncertainty stem from the standard deviation of the speed log (see Table ), which was retrieved at low frequency (1 min). However, comparing with a prediction based on GPS speed shows that the uncertainty is probably less than the standard deviation indicates.

Table III: Speed trial uncertainty assessment.

Variable	Comment, source of uncertainty	Uncertainty of variable (Type A)
Heading	Standard deviation of time signal	1°
STW	Standard deviation of time signal	0.25 kts
STW	Comparing with analysis based on SOG	0.1 kts
power	Standard deviation of time signal	90 kW
AWA	Standard deviation of time signal Disturbance of hull	5°
AWS	Standard deviation of time signal Disturbance of hull Atmospheric boundary layer difference from 1/7 power law	2 m/s
	Assumptions in the normalization method. Assessed by varying the input.	50 kW



The anemometer also affects the evaluation uncertainty. The fluctuation of the natural wind is high and therefore, higher frequency logging would have been preferred. The most problematic is the disturbance caused by the hull, which is very difficult to assess. It is difficult to measure the “true” apparent wind experienced by the rotor, since all possible locations to place an anemometer is disturbed by the hull or the rotor. In the uncertainty assessment the disturbance is estimated to be 2 m/s. The resulting total uncertainty is plotted as error bars in the plots below.

## 8. Performance prediction results

In this chapter the three different fidelity levels of power prediction models are compared to the sea trial data. The sea trial data have been normalised to the nominal ship speed  $V_s = 16$  kn and  $TWS = 10$  m/s. The results of the model correlated to the sea trial are used for a voyage simulation on the route Gedser-Rostock.

### 8.1. Comparison of sea trial and power prediction models

In Fig.16, we compare the two Level I models (EEDI type with fixed  $\eta_D = 0.66$  and 1 DOF with propeller model) with the sea trial data. The plotted error bars correspond to the uncertainty analysis from subsection 7.1.  $\eta_D = 0.66$  is the propulsive efficiency for the ship without rotor from the model test report. When including a propeller model the effect of increased efficiency when off-loading the propeller is accounted for. Therefore, the power saving gain is larger.

Compared to the sea trial points, the 1 DOF propeller model overpredicts the savings for  $TWA > 80^\circ$ . The fixed  $\eta_D$  1 DOF model coincidentally matches well the sea trial data for  $TWA > 100^\circ$  but underpredicts the savings for smaller wind angles.

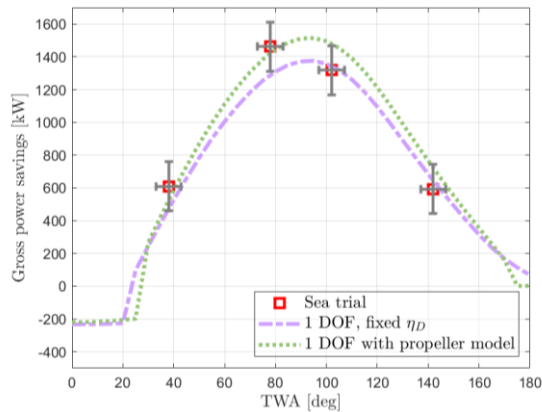


Fig.16: Gross power savings. Power prediction model – Level I

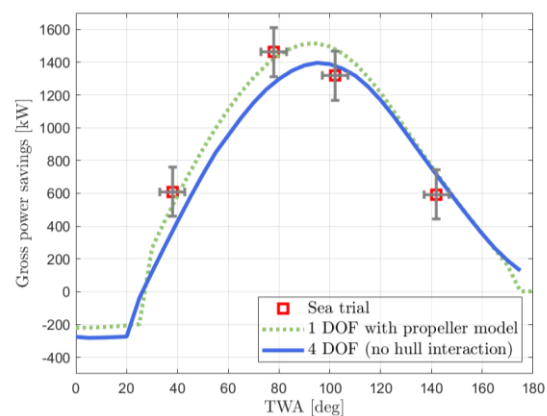


Fig. 17: Gross power savings. Power prediction models – Level I & Level II

In Fig.17, the 4 DOF Level II model (without hull interaction) is included. The side force of the rotor and the included effects of drift and heel reduce the power savings compared to the 1 DOF propeller model. This effect is mainly for  $TWA < 100^\circ$ , where the side force has an adverse effect. However, the power savings are still underpredicted for  $TWA < 100^\circ$ .

Fig.18 compares the two 4 DOF level III models. The model that utilizes CFD simulations is plotted only for the range of TWA where the CFD simulations were available. It performs reasonably well for the largest range of TWA but it underpredicts the savings for  $TWA > 130^\circ$ . Fig.18 also includes the 4 DOF level III model that is correlated to the sea trial results using a specially developed analysis method.

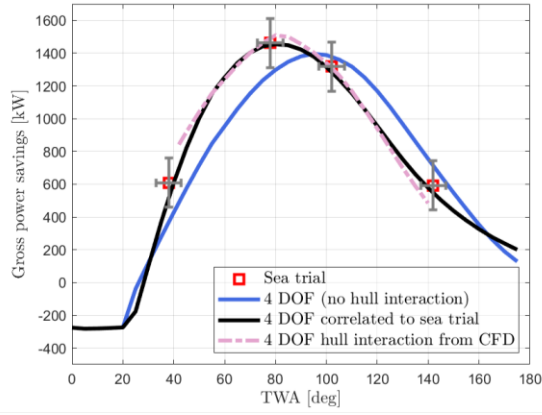


Fig.18: Gross power savings. 4 DOF models compared

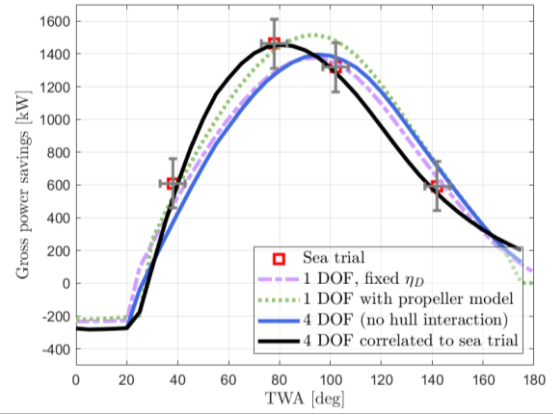


Fig. 18: Gross power savings. All power prediction model levels compared

Fig.19 includes the 4 DOF level III model that takes into account the influence of the wake of the hull by correlating the model to the sea trial results using a specially developed analysis method.

Fig.20 shows the power prediction model from the rotor provider that takes into account hull interaction and rotor performance from the full-scale installation. The model matches the sea trial data well.

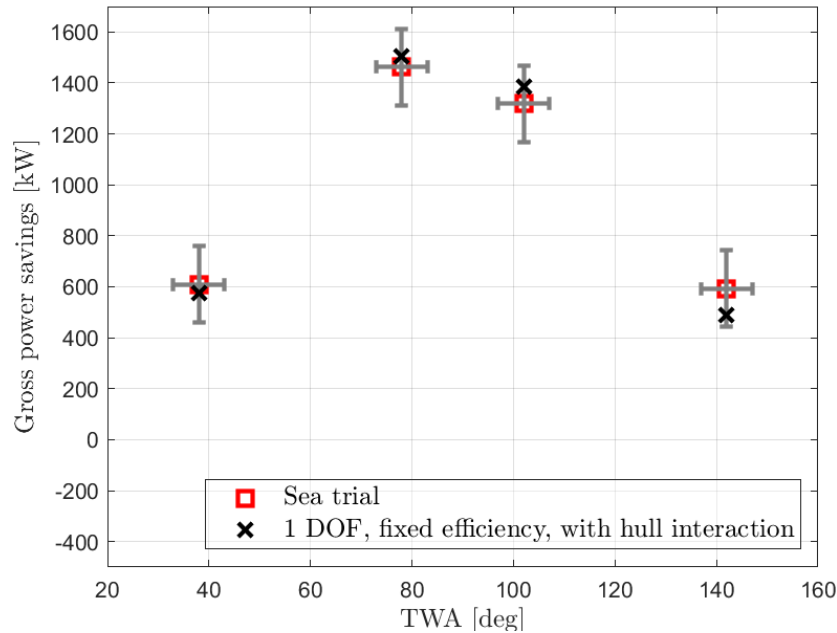


Fig.20: Power prediction model from the rotor provider – with hull interaction and rotor performance from full scale installation

## 8.2. Predicted power saving potential on the Gedser-Rostock route

The Level III model as correlated to the sea trial results was used as an input for the route simulation. The route was simulated using weather statistics from two sources, the Copernicus Climate Data Store and the EEDI weather matrix. The power savings based on the two sources are presented in Table IV.

Table IV: Power savings potential when considering only the sea legs and with 100% operability

	Copernicus weather statistics	EEDI weather statistics
Power saving [kW]	380	320

The Copernicus weather statistics provide the measured weather on the exact route over the full year of 2019. The EEDI weather matrix is an attempt of having a generalized weather that can be applied to any route as a baseline comparison. Fig.21 shows heat maps of the joint probability distribution of the two weather sources. The prevailing winds on the Gedser-Rostock route, as captured by the Copernicus weather data, are towards the beam. The generalized EEDI weather matrix includes high probability of wind against the bow, which leads to decreased power savings compared to Copernicus. The negative values on the 2.5-percentile correspond to the days where head wind is encountered, and the rotor adds an additional drag.

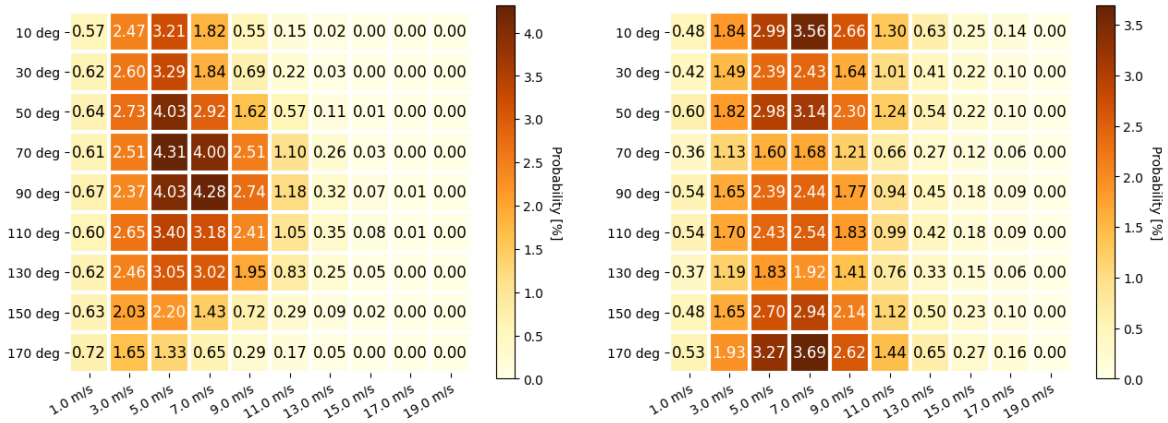


Fig.21: Weather joint probabilities of TWS and TWA relative to the route heading. Copernicus on the left (outbound). EEDI on the right.

Fig.22 shows the power saving results that are gathered in Table IV. Probability density function and cumulative probability of the required power with and without WPS are also plotted.

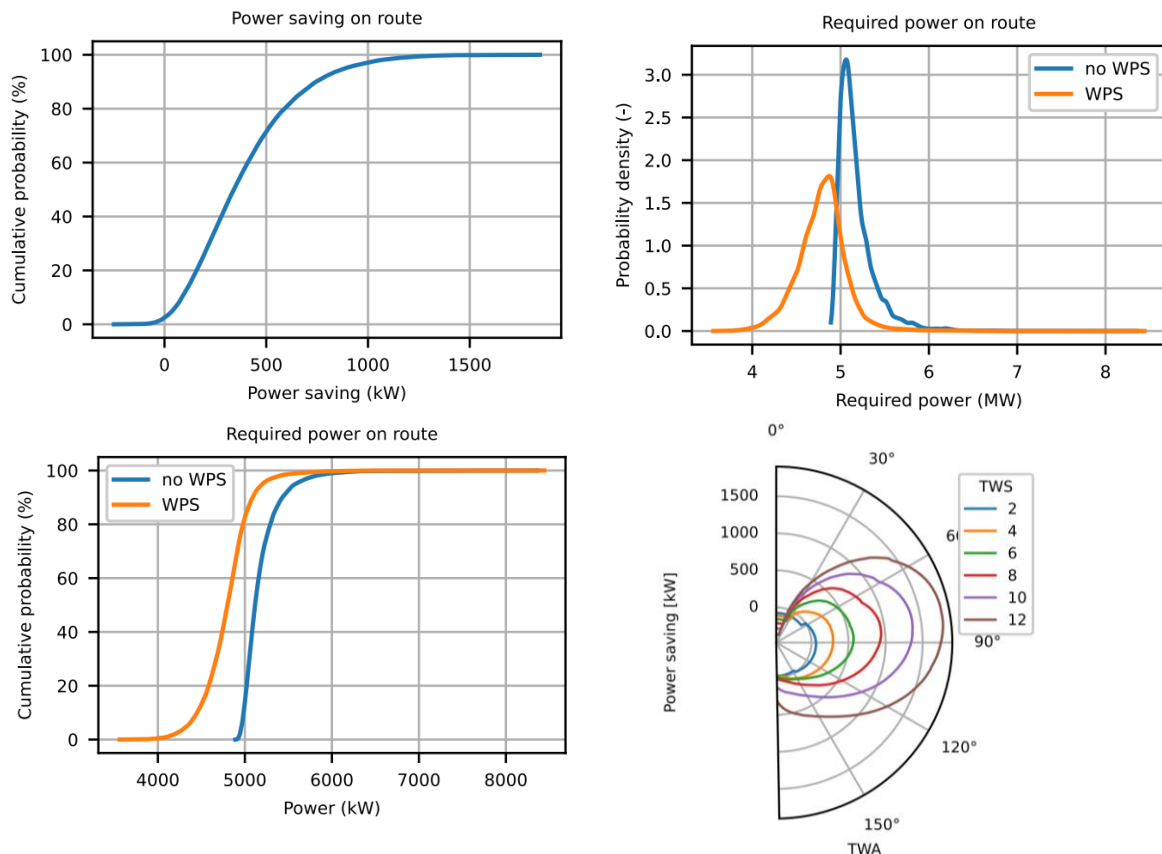


Fig.22: Power saving statistics from the route simulation using Copernicus data. Polars from the Level III power prediction model on the bottom right.

## 9. Conclusions

The purpose of this work is to compare different fidelity power prediction models with sea trial measurements and comment on their performance. Furthermore, CFD simulations are utilised to understand the underlying physics that cause power prediction models to deviate from the full-scale data.

All three different levels of power prediction models performed reasonably well for their intended purpose. Level I was sufficient to provide an early estimate of power savings. Level II includes most of the important physics and is suitable for early business case assessment support. Level III includes additional physical effects (rotor-hull interaction) and matched well with the sea trial data.

Including or excluding the various physical effects in the prediction can have a significant effect on the predicted power saving. For example, using a propeller model results in higher power saving prediction compared to using a fixed propulsion efficiency. Including leeway (4DOF) gives lower power savings mainly in upwind conditions. Including hull aerodynamic interaction gives (for this case) higher savings in the upwind. For present case, the different effects happen to cancel each other in such a way, that the simplest methods possible works better than the middle level models. This is of course not always true and therefore, the highest Level is recommended for the highest fidelity level.

Conclusions on rotor-hull interaction:

1. Rotor-hull interaction cannot be ignored. The interaction influences the performance and the operation of rotor onboard ship.
2. The interaction effect seems to be mainly governed by the apparent wind angle and spin ratio, apart from the freeboard and deck shape.
3. There are both positive and negative interaction effects with respect to the performance of the rotor compared to standalone case. The main beneficial one is the increase of wind speed over the hull, this is however counteracted by a loss of suction in the lower part of the rotor.
4. The formation of deck contour (flat or convex) can affect the extent of flow separation on deck and the transport of the horseshoe vortex originated from the root of rotor.
5. Comparison with sea trials indicates that the trends of interaction effects predicted with CFD can be useful for improving the predictions. However, the flow physics on the rotor-hull interaction is very complicated, especially for wind in the beam-reach conditions where the hull blockage effect and flow separation are the most severe ones. The widely used URANS methods seem to overpredict the interaction effects in beam-reach conditions. An advanced hybrid RANS-LES method explored in the present study shows a potential to improve the prediction. Further investigations on the various CFD methods currently used by the industry and their reliability and limitations to predict rotor-hull interaction are required. Sea trials, like the one described in this paper, present a unique and valuable way to validate CFD predictions and assess their credibility.

The overall conclusion is that there are still large uncertainties and unknowns in all prediction methods as well as in full scale measurements. Only by combining them can we increase the knowledge and accuracy of predictions.

## Acknowledgements

The computations and data handling of the simplified test case were enabled by resources provided by the National Academic Infrastructure for Supercomputing in Sweden (NAISS) and the Swedish National Infrastructure for Computing (SNIC) at the PDC Center for High Performance Computing, KTH Royal Institute of Technology, partially funded by the Swedish Research Council through grant agreements no. 2022-06725 and no. 2018-05973. The financial support from SSPA's intern funding organization (Utdelningsnämnderna för Hugo Hammars fond för sjöfartsteknisk forskning) is gratefully acknowledged for part of this work within project HHS 299 "Full scale validation of Flettner rotor performance onboard a ship".

## References

- ALEXANDERSSON, M.; KORKMAZ, K.B.; MAZZA, G. (2017), *Virtual Captive Tests with a destroyer hull form*, 20<sup>th</sup> Numerical Towing Tank Symposium (NuTTS), Wageningen
- DUPUY, M.; LETOURNEL, L.; PAAKKARI, V.; RONGERE, F. (2023), *Weather Routing Benefit for Different Wind Propulsion Systems*, 6<sup>th</sup> Int. Conf. Innovation in High Performance Sailing Yachts and Wind-Assisted Ships
- GARENAUX, M.; SCHOT, J.J.A.; EGGERS, R. (2020), *Numerical analysis of Flettner rotors performances on the MARIN Hybrid Transition Coaster*, HIPER Conf., Cortona
- GARENAUX, M.; SCHOT, J.J.A. (2021), *Flettner rotors performance and interaction effects on the MARIN Hybrid Transition Coaster*, RINA Int. Conf. Wind Propulsion
- HERSBACH, H.; BELL, B.; BERRISFORD, P.; BIAVATI, G.; HORÁNYI, A.; MUÑOZ SABATER, J.; NICOLAS, J.; PEUBEY, C.; RADU, R.; ROZUM, I.; SCHEPERS, D.; SIMMONS, A.; SOCI, C.; DEE, D.; THÉPAUT, J.N. (2023). *ERA5 hourly data on single levels from 1940 to present*, Copernicus Climate Change Service (C3S) Climate Data Store (CDS), DOI: 10.24381/cds.adbb2d47
- HOLTROP, J.; MENNEN, G.G.J. (1982), *An approximate power prediction method*, Int. Shipbuilding Progress 29
- IMO (2017), *Strategic plan for the organization for the six-year period 2018 to 2023*, Int. Mar. Org., London
- IMO (2021), *2021 Guidance On Treatment Of Innovative Energy Efficiency Technologies For Calculation And Verification Of The Attained EEDI And EEXI*, MEPC.1-Circ.896, Int. Mar. Org., London
- ITTC (2014), *Analysis of Speed/Power Trial Data*, <https://itc.info/media/4210/75-04-01-012.pdf>
- JONES, L.; PRINCE, M.; HUDSON, D.; COCKS, J. (2019), *Predicted fuel-savings for a Flettner rotor assisted tanker using computational fluid dynamics*, RINA Int. Conf. Wind Propulsion
- LARSSON, L. (1990), *Scientific Methods in Yacht Design*, Annual Review of Fluid Mech. 22, pp.349-385
- LI, D.Q.; ANDERSEN, M.L.; ALLENSTRÖM, B., (2012), *Performance and vortex formation of Flettner rotors at high Reynolds numbers*, 29<sup>th</sup> Symp. Naval Hydrodynamics
- OLSSON, F.; GIOVANNETTI, L.; WERNER, S.; FINNSGÅRD, C. (2020), *A Performance Depowering Investigation for Wind Powered Cargo Ships Along a Route*, J. Sailing Technology 5, pp.47–60, doi:10.5957/jst/2020.3.1.47
- PAAKKARI, V. (2019), *Performance verification of a recent rotor sail installation*, RINA Wind Propulsion, London
- PAAKKARI, V.; HURFORD, A.; CRADDOCK, C. (2020), *Rotor sail GHG reduction potential, modelling and sea trial validation*, 5<sup>th</sup> Int. Conf. Innovation in High Performance Sailing Yachts and Sail-Assisted Ship Propulsion, Gothenburg
- SCHMIDT, A.; VAHS, M. (2013), *Entwicklung eines innovativen Schiffsantriebes gekennzeichnet durch den Einsatz von Magnus-Rotoren zur Windenergienutzung in Kombination mit einem hierauf abgestimmten Antriebspropeller*, Final report for the development project promoted under the Az. 25741 -24/0 by the German Bundesstiftung Umwelt



TILLIG, F.; RINGSBERG, J.W. (2019), *A 4 DOF simulation model developed for fuel consumption prediction of ships at sea*, Ships and Offshore Structures 14(S1), pp.112-120

VAHS, M., (2019), *Retrofitting of Flettner rotors – results from sea trials of the general cargo ship “Fehn Pollux”*, Int. Conf. Wind Propulsion, London

WERNER, S.; NISBET, J.; OLSSON, F. (2022), *Sea Trial Methodology for Wind Assisted Ships*, 7<sup>th</sup> Hull Performance & Insight Conference (HullPIC), Tullamore

WERNER, S.; GERHARDT, F.; KONTOS, S. (2023), *Key Performance Indicators for Wind-Powered Ships*, RINA Wind Propulsion, London

WERNER, S.; GERHARDT, F.; ALTERSKJAER, A. (2023), *Performance Indicators for Wind Powered Ships: Towards an Industry Standard*, 8<sup>th</sup> Hull Performance & Insight Conf., Pontignano

# AI-enabled Democratizing of CFD Data for Decarbonization of Shipping

Sven-Eric Salecker, Jakob Lohse, NAVASTO, Berlin/Germany, [jakob.lohse@navasto.de](mailto:jakob.lohse@navasto.de)

## Abstract

*A novel approach to the utilization of CFD data is discussed. The paper presents an overview of the use of artificial intelligence in producing stand-alone machine learning models from complex numerical simulations and considers possible applications of these models related to the decarbonization of shipping. These models may be accessed by both simulation experts and non-experts alike to instantly predict all potential design space solutions. This will democratize simulation results for embedded applications such as Digital Twins. It will help to increase the accuracy and confidence in each system component and therefore in the overall system representation.*

## 1. Introduction

Various numerical Computer Aided Engineering (CAE) methods are used in modern ship design. To determine and optimize the operational efficiency of ships, Computational Fluid Dynamics (CFD) simulations are a common tool. The focus of these simulations is usually on the ship's hull with its appendages, propulsion, and rudder system. While the results are shared in the required forms such as geometry files and design tables between those involved in the development, further use of the simulation data is uncommon. Considering the Carbon Intensity Indicator (CII) requirements, a more collaborative approach that allows the entire ship and each subsystem to be simulated and optimized may be beneficial. Such a virtual system representation, commonly referred to as a Digital Twin (DT), can be used during the design phase of the vessel and throughout its lifecycle, and can even be adapted with later modifications such as Wind Assisted Ship Propulsion (WASP) or enriched with sensor data to optimize routing and analyze the operational profile. It is important that each "model is accurate enough to capture the relevant dynamics of the ship", Pedersen *et al.* (2019).

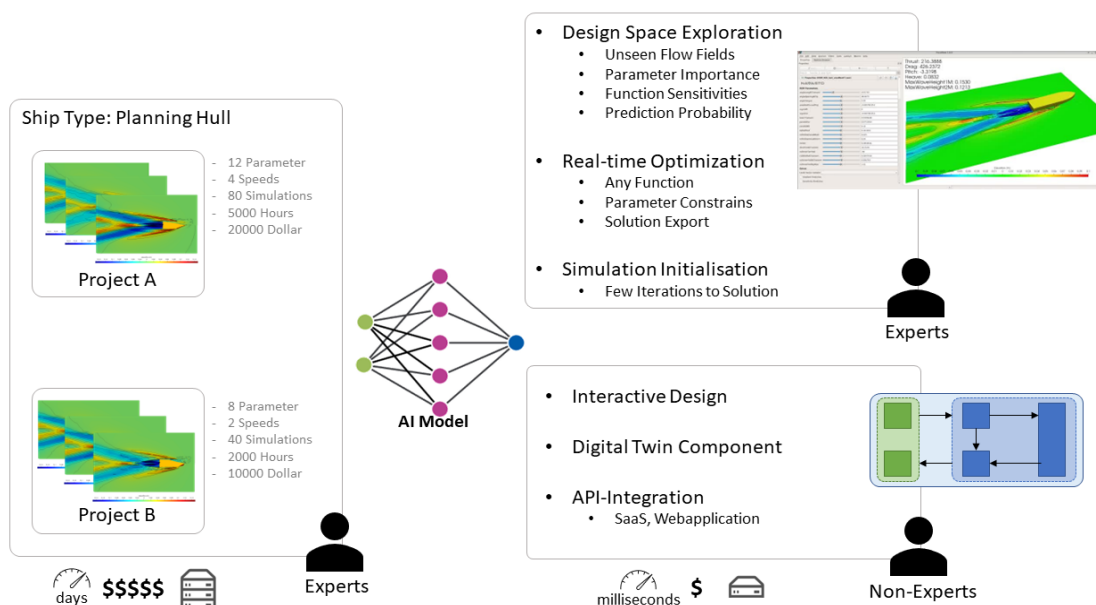


Fig.1: Offline model creation (left) and Online model application (right) phase of AI-model for the scope of various simulation user. While an offline phase by CFD experts is still necessary for data creation the online phase and is a new concept made available using AI-models

While some subsystems are adequately represented by mathematical models, others, especially complex fluid dynamic systems, can be easily under- or overestimated, reducing confidence in the full DT. Recent advances in Artificial Intelligence (AI) make it possible to convert CFD simulation data from

current or previous projects into a stand-alone Machine Learning (ML) model that can predict accurate solutions with the same quantity as a full simulation, but up to 100,000 times faster. These AI models can be accessed and controlled by simply changing the defining geometric and environmental parameters. This can be done through a Graphical User Interface (GUI) as well as within an embedded application such as a DT component. In addition, further information can be derived from the model as it contains the relationships and dependencies of all parameters and geometries to the flow results and can therefore provide an optimized state immediately. Thus, as illustrated in Fig.1, after the so-called offline phase in which the simulation data is generated by simulation experts, it is possible for other users in subsequent online phases to access data that was previously hardly accessible to them, and this in a time frame of a few milliseconds that is useful for the respective application.

## **2. AI-Model**

Classical CFD workflows culminate in a flow result, which can be utilized to resolve a design issue. Scalar values can be computed from the data to evaluate specific key functions, and simulation experts can visually examine the flow features, such as the wake. The AI-model approach builds up on the said data and uses multiple results as training data, with the model's quality determined by the data. It decomposes distinctive flow characteristics from each solution, along with their respective contributions to said characteristics as well as the influence of each parameter. This information is then used to compose a new solution that incorporates a comprehensive flow field. Various techniques such as Proper Orthogonal Decomposition (POD-I), *Karcher (2022)* or Graph Neural Networks (GNN), *Battaglia et al. (2018)*, can be employed for decomposition and composition. As the time and computational resources required to for this work can be allocated before the model's application, this phase is commonly referred to as the offline phase, *Salmoiraghi et al. (2016)*. The phase in which the model's predictions are required in real-time on personal computers is thus termed the online phase. Control of the model's composition should be either parametrically or shape-centric, depending on the data's nature and the subsequent application of the AI-model.

### **2.1. Parametric Approach**

Today, most Computer Aided Engineering (CAE) utilize some form of parametric data. These parameters can be either geometric or boundary based. Geometric parameters define the shape of the object being investigated, such as the ship fixed main dimensions or its position within the coordinate system, such as depth or trim angle. Boundary parameters describe the environment that affecting that object, such as ship speed or inflow angle. In a parametric approach, those explicitly available parameters that fully describe the problem are correlated with the desired output (e.g. the flow fields) using machine learning techniques such as the aforementioned POD-I.

### **2.2. Shape Centric Approach**

When consistent geometric input parameters are not available or when investigating new unparameterized shapes, a shape-centric approach can use the solutions and geometries of the training data to compose new prediction based on a geometry input. This enables the training of a generic model on multiple not completely coherent data sets, making it possible to reuse legacy data. The geometry input could be the bare ship hull or a vessel's superstructure. In a shape-centric approach, the deep learning models, such as GNN, can learn the relevant features directly from the geometry.

### **2.3. Response Model**

The term 'response model' refers to a system and its output response when provided with a specific set of input parameters. Fig.2 compares different methods of such a model and their attributes for receiving a response. The analytical function, AI-model and CFD simulation response model methods are compared based on three categories: input and output capabilities, response time and response uncertainty.

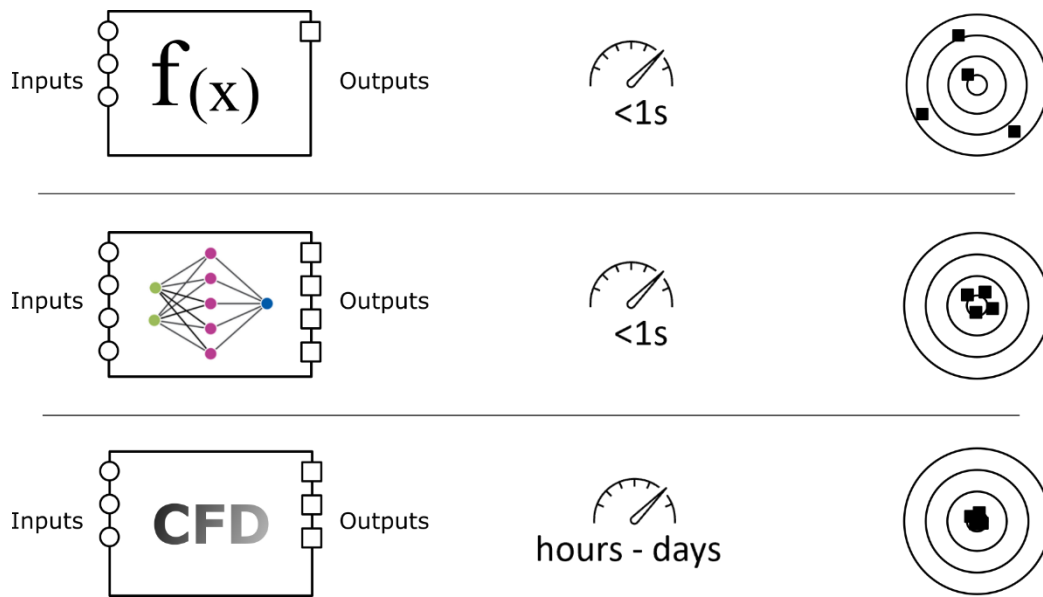


Fig.2: Comparison matrix of different methods used for model response (left), computation time (mid) and uncertainty (right) for heuristic model (top), AI-model (mid), CFD simulation (bottom)

The heuristic response model can process scalar values as inputs and generate scalar values as outputs, via basic formulas, interpolations, or lookup tables. While this approach is the fastest one, it may lead to uncertainties as it often oversimplifies systems. Utilizing a CFD simulation – or more accurately, a CFD workflow - as a response model, offers several benefits. It enables the utilization of extensive input parameters, such as ship hull, resulting in a greater number of more complex output responses. For instance, the flow field or integrated scalar values can be generated with almost no uncertainty if the CFD simulation is validated with in respect to the inputs. Nonetheless, obtaining this response takes several hours to days, rendering it impractical for Digital Twin (DT) applications. The use of an AI-model can process all input parameters from the training data, along with additional parameters, such as scalar CFD outputs or artificial parameters detected within the AI-model itself. Regarding outputs, the AI-model can return traditional CFD outputs, such as scalar values and flow fields, as well as unique responses, including sensitivities within the training data or parameter importance to the given function objects. The AI-model provides these responses quickly and with comparable low uncertainty to the CFD response. It is accessible within a dedicated file container and can be employed in various applications.

### 3. Applications

Typically, an AI-model is a dedicated file container that can be integrated into various applications to facilitate interaction. Although this interaction is evident to users with simulation experience, a new approach is to democratize the work of the CFD department to other units in the same organization or even external units by allowing interaction for users without simulation knowledge. This chapter details various applications tailored to different user groups.

#### 3.1. Simulation Expert Applications

The first instances of AI-models were initially used in conventional post-processing tools utilized by CFD professionals for carrying out design studies. This is possible because the AI-model can be analyzed in a way comparable to a single CFD result. Although it is recommended that certain individuals within an organization to possess AI proficiency, the advantage of this approach is that specialized expertise is not a strict requirement for engaging with the AI-model. Understanding of fluid mechanics is sufficient.

### 3.1.1. Design Space Exploration

While traditional studies require analyzing multiple CFD results to identify differences, interaction with the AI-model allows simultaneous analysis of all designs within a design domain, breaking with the iteration paradigm. Design space exploration is a prevalent application, wherein varied flow characteristics can be evaluated across the entire design domain. Fig.3 showcases a commonly used open-source post-processing tool with a slider panel to adjust geometric or boundary parameters to new values. Here, the example pertains a design study on planing hull by *Ahmed* (2022). For each parameter adjustment a new flow result will be shown instantly.

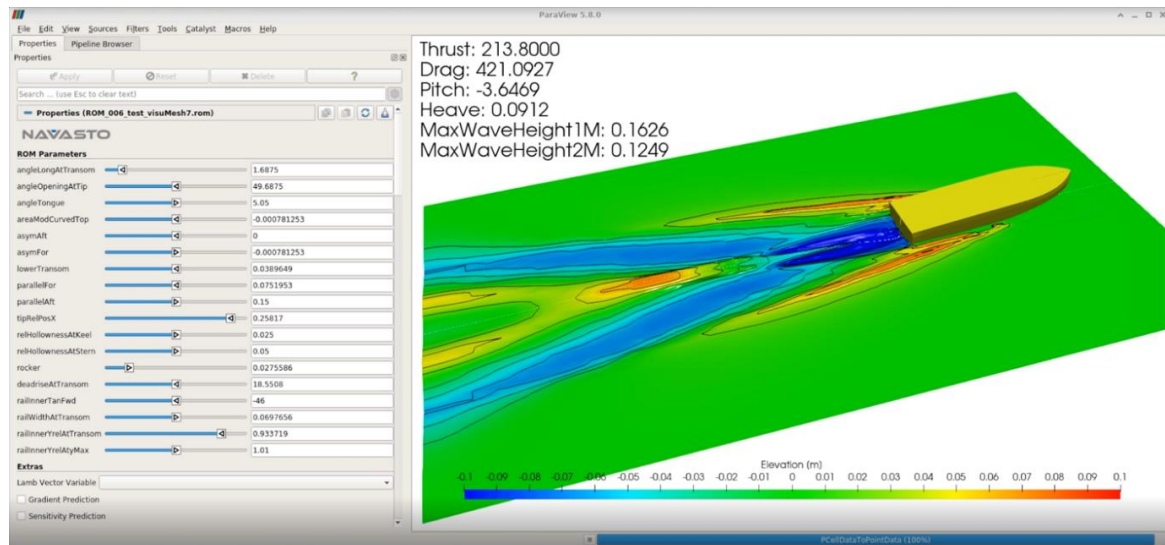


Fig.3: Parametric input panel and visualization view to interact with AI-model and get real-time response of flow field and key performance indicators (via ParaView® Plugin). Data source: FRIENDSHIP SYSTEMS (Thrust for half model, drag for full model)

### 3.1.2. Design Optimization

As the AI-model recognizes the importance of each parameter to a function object in relation to other snapshots, it facilitates further exploration through sensitivities with respect to the shape under investigation or the relevant performance indicators. Fig.4 illustrates the correlation between the input parameter to an objective function, in this case ‘Thrust’, that the model was trained on. These can be provided as parameter importance or as surface sensitivities. In this case, visualizing how a surface alteration (inward or outward) affects the scalar output.

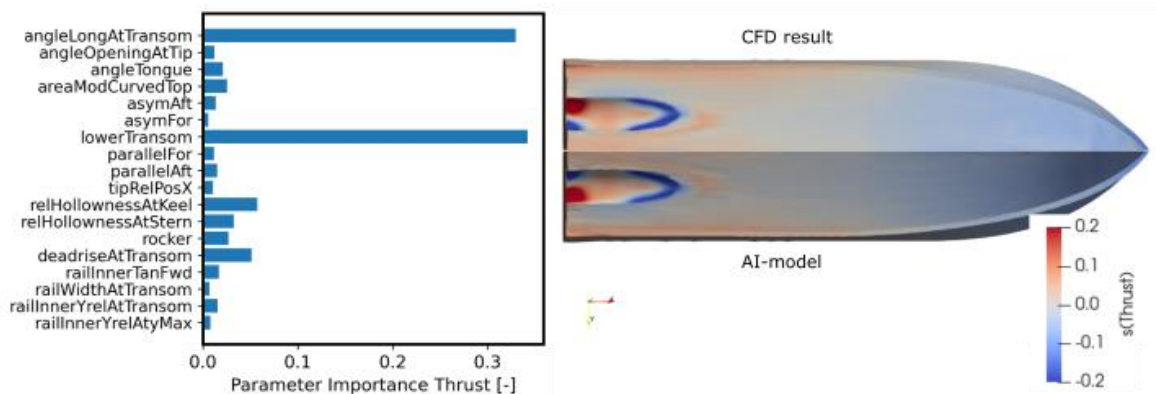


Fig.4: Parameter importance (left) and surface sensitivity regarding the thrust as an objective(right) (blue regions: push inward to lower required thrust, red regions: pull outward for lower thrust). Data source: FRIENDSHIP SYSTEMS



Because the AI-model has access to all pertinent information, including surrogates for each response output response, real-time optimizations within the design domain, including multi-objective and multi-constraint optimizations, are possible. The optimized result will be computed within seconds to minutes and can be visualized in the post-processing tool show in Fig.3.

### 3.2. Design Engineer Applications

As the production of CFD results is costly and requires expertise and HPC infrastructure, democratizing its use to a broader audience is an ongoing objective. Currently, this is only partially feasible by combining the scalar responses into a highly specialized application that delivers answers very specific questions, such as ship trim assistants, giving to correct trim angle for a vessel's operation point, *Hansen and Freund (2010)*. The democratization of data, which enables the user to choose how and which data to access, has the potential to enhance the speed, accuracy, and certainty of design predictions.

#### 3.2.1. Interactive Design

When multiple branches of engineering are involved in the same domain but with different objectives the shape of an object may differ, and it must be adjusted for each design iteration. Based on the design paradigm, i.e., form-follows-function or function-follows-form, object shapes are interchanged and validated in a time-consuming process. A prominent example of this is the design department and the aerodynamics department in the automotive industry. The sailing industry faces an equal process for new sailing shapes when changes occur. In Fig.5 illustrates a comparison between the CFD simulation and the AI-model based on an input geometry. An accurate response was generated utilizing a 3D sailing plan and a sailing condition.

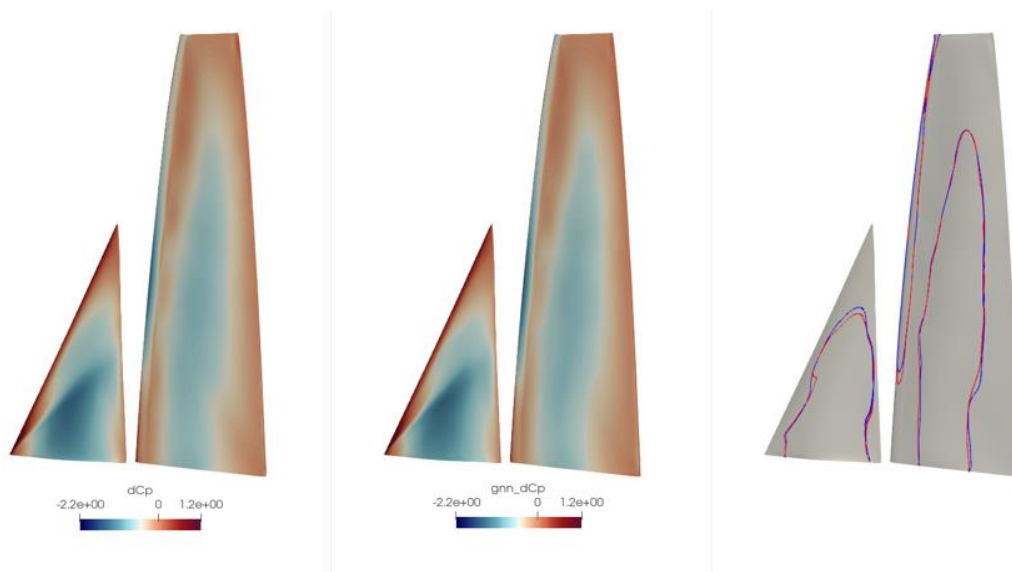


Fig.5: Comparison of sailing configuration: unseen validation data (left), AI-model prediction (middle), pressure coefficient isosurfaces (right). Source: undisclosed America's Cup Team

In an interactive setting the aerodynamic AI-model would provide basic metrics, such as lift-to-drag ratio, enabling the design engineer to assess the aerodynamic performance of their modifications. know how his changes perform aerodynamically. This could significantly increase the number of evaluated designs, since the iterative paradigm has been resolved.

#### 3.2.2. Embedded Applications

In holistic system approaches such as Model Based System Engineering (MBSE), which are necessary to construct valid digital twins, each system must be considered for its accurate responses to various input ranges. This approach could facilitate more detailed system control and optimization, and it could

also lay the foundation for model-based class approval, as described in *Astrup and Cabos (2017)*, or implied by *Pedersen et al. (2019)* for the verification of autonomous vessels through simulation-based testing. The components of a digital twin, which describe flow-based results originating from CFD results via AI-models, have the potential to replace function-based assumptions and provide more accurate results. This can be achieved without the digital twin operator being a CFD expert. Moreover, it is possible to calibrate the model by comparing flow values within the flow field to real-world sensor data. Alternatively, the digital twin can respond to a given inflow parameter by adopting a specific state.

#### 4. Use Cases: Wind Assisted Ship Propulsion

A prevalent method for assessing vessels equipped with WASP systems involves using Performance Prediction Programs (PPP), which are adapted from the Velocity Prediction Programs (VPP) utilized in sailing sports. The aim of PPPs is to equalize all forces and moments acting on a vessel to achieve equilibrium for a specific condition. This is achieved by dividing the problem into progressively smaller isolated models, such as hydrodynamics and aerodynamics and then further into hull hydrodynamics and rudder hydrodynamics, aerodynamic resistance, and side forces of the overwater hull and superstructure. This allows the use of analytical functions or simplified assumptions without the necessity for a computationally complex and expensive simulation. Some models, like the WASP model, include the findings of aerodynamic studies in the format of a fitted response surface, *Vilanova et al. (2021)*. Incorporating AI-models for diverse models or sub-models could potentially enhance the generalization and accuracy of these PPPs.

##### 4.1. Generic Model of Hydrodynamics in Oblique Flow

The current Performance Prediction Programs (PPP) do not account for resistance adjustments due to heel or pitch, as noted by *Vilanova et al. (2021)*, or the oblique flow through the leeway angle despite studies by *Wang and Wan (2015)* suggesting that additional resistance may be reasonable. To account for these factors, a hydrodynamic AI-Model trained on CFD sailing conditions could accurately predict forces and moments within the PPP routine. A generic AI-Model would be required to train on various ship hulls for a generic PPP. It could take the hull geometry as an input, if available, Fig.6.

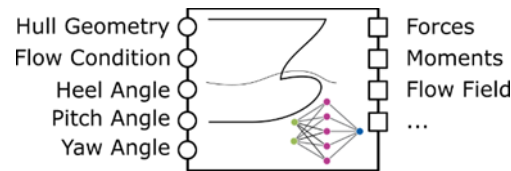


Fig.6: Hydrodynamic AI-model for sailing hull condition

As maintaining course stability poses a significant challenge in wind-assisted propulsion, linking the components could enable the transfer of hull wake to a potential AI-model of the rudder, facilitating examination of various rudder types, Fig.7. This would yield a more accurate comprehension of the magnitude of drag generated for the purpose of stabilizing the vessel's sailing course, countering the yaw moment. A generalized AI-model of the rudder is one option, but it is also possible that the designer and manufacturer of the rudder could provide a model.

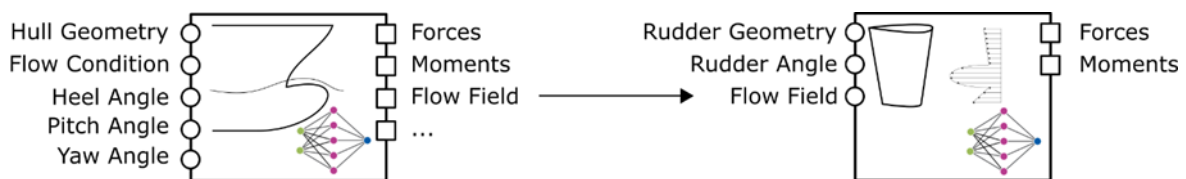


Fig.7: Ensemble of hydrodynamic AI-model for oblique hydrodynamic resistance + hydrodynamic AI-model for rudder system coupled together to share information (downwards)

Since the hydrodynamic AI-model has information about the entire flow field, the latter can be extracted

at any point and provided as input information to the next AI-model, if the model has been trained on such an input information. Fig.8 shows the extracted wake field from a hydrodynamic bare hull simulation is shown.

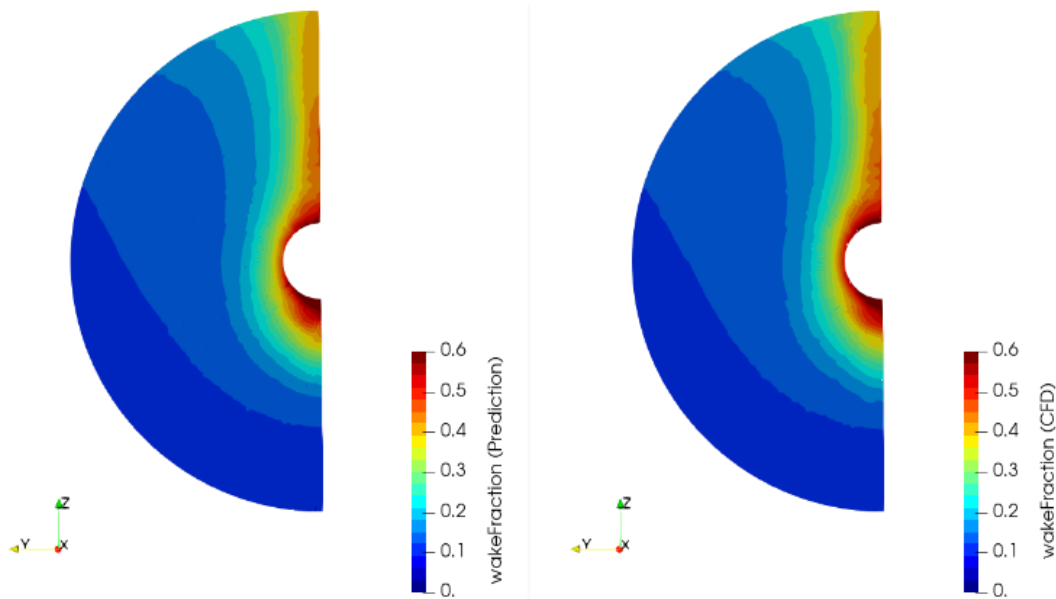


Fig.8: Comparison of wake field from bare hull simulation, hydrodynamic AI-model (left) and ground truth (right). Source: FRIENDSHIP SYSTEMS

#### 4.2. Generic Model of Aerodynamic Wind Loads

Recent numerical studies have demonstrated the influence of the aerodynamic wind loads on various superstructure types and loading conditions including the pronounced flow separation on deck of complex ship superstructures, *Moctar et al. (2023)*. These studies indicate differences of up to 25% in longitudinal forces across different loading scenarios for container vessels, as well as notable lateral forces. Due to the nature of the unsteady flow and complex geometry of ship superstructure, studies evaluating added resistance models are uncommon and a generalized quasi-analytical model cannot be derived. A universal AI-model could provide qualified predictions for the added resistance and the working conditions on the deck for WASP systems, incorporating different superstructures, inflow angles, ship and wind speeds, and atmospheric boundary layers, Fig.9.

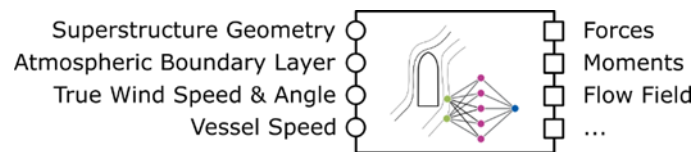


Fig.9: Aerodynamic AI-model for superstructure resistance

#### 4.3. Models for retrofitted WASP systems

Retrofitting WASP systems may be an option to meet CII requirements. Which type of system, how many and where on deck depends on many factors. From an aerodynamic point of view, it is a matter of reducing the power required on the vessel's routes. Key factors are the aerodynamic forces generated by each sail system at each position on deck, the spacing between multiple systems, the angle of attack and the chamber. Current WASP models in PPPs use aerodynamic loads from databases of lift and drag coefficients normally obtained in free flow conditions. The interaction effects in current PPPs are often not considered, although in some cases aerodynamic coefficients can change by up to 20% for Flettner rotors, *Vilanova et al. (2021)*. Incorporating the interaction into account could lead to a significant change in power saving polars and therefore route optimization results.

### 4.3.1. Ship-Sail Interaction

With obstacles such as masts, cranes, and deckhouses as well as the boundary layer on the deck, it is difficult to make any assumptions about inflow velocity for this area due to recirculation zone described by *Sherry et al. (2009)*. By coupling the AI-models together, as illustrated in Fig.10, it is possible to accurately describe the forces created by the WASP system on a given deck layout.

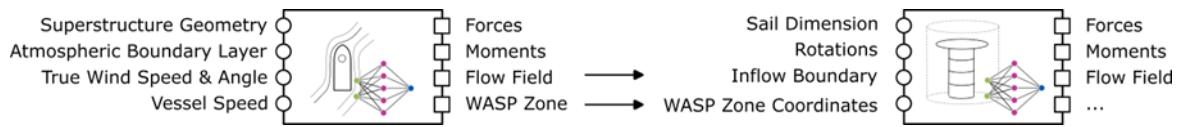


Fig.10: Ensemble of aerodynamic AI-model for superstructure resistance inclusive operation zone for WASP system + aerodynamic AI-model for sailing system coupled together to share information (downwards)

### 4.3.2. Sail-Sail Interaction

Sail systems are not only influenced by the deck layout but also by other upstream sail systems, each of which has a wake field. In a multi-sail system layout, it would be possible to consider the resulting wake field of one sail system as an inflow boundary for the second sail system, Fig.11.

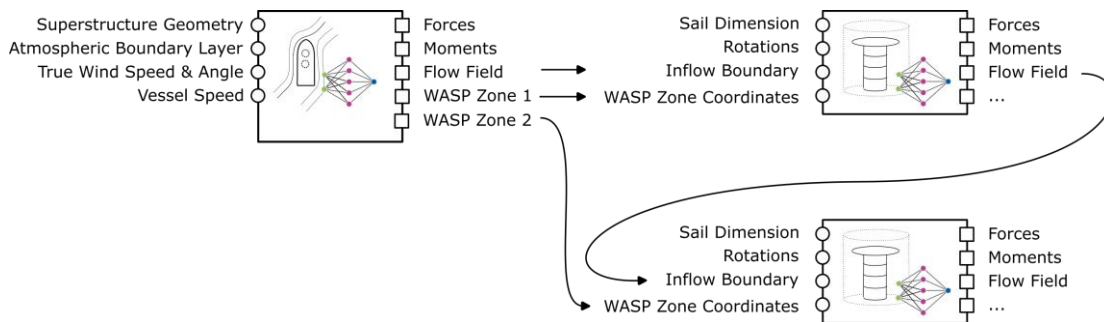


Fig.11: Ensemble of aerodynamic AI-model for superstructure resistance inclusive operation zone for two WASP systems + aerodynamic two AI-models for sailing systems coupled together to share information (downwards)

## 4.4. Modular OSP-PPP

The collaborative development of coupled AI-models, which share downstream flow results, would benefit when the manufacturer's *Intellectual Property Rights* (IPR) are considered. The Open Simulation Platform (OSP), [www.opensimulationplatform.com](http://www.opensimulationplatform.com), provides an ecosystem for all stakeholders to share simulation models. Secured and trusted components could be made available, allowing for modular exchange, such as with WASP systems at a particular position on deck or the rudder loads. This would enable the discovery of optimal solution for every vessel and its loading condition, common routes, and operational profile, while overall requiring less computational effort. By feeding in sensor data, such as from LiDAR on the atmospheric boundary layer, instant answers could be obtained on how to trim your sails to wind twist for optimal performance. This could also play a part in autonomous shipping where such decisions need to be made during transit.

## 5. Conclusion and outlook

An overview of AI-models is presented including the types of inputs and outputs that can be facilitated to during their generation. These include geometric parameters such as scalar values, boundary parameters such as ship velocity or a velocity distribution across an inflow plane, and surfaces like a ship hull or a sailing 3D plan. Furthermore, a comparison was made to demonstrate the advantages of using an AI-model as a response model has advantages over various response models when used online.

The application of the AI-model has been shown to be equally valuable to both simulation experts and design engineers alike. The former can gain more detailed insights into the evaluated system and perform accurate optimizations in real-time breaking the iterative working concept. The latter can use the model in interactive or embedded form receive a qualified response without the requiring expert simulation knowledge.

It has been described how these embedded applications could bring more prediction accuracy to Performance Prediction Programs (PPP). They could replace various sub-models and even allow for the linking of complete wake fields for ship-sail or sail-sail interactions. Additionally, a collaboration between different design units has been exhibited.

In conclusion, AI-models offer a transformative approach to system evaluation and optimization, democratizing the capabilities once restricted to simulation experts and making them accessible to design engineers. The versatility in accommodating various input types - ranging from geometric parameters to complex boundary conditions - establishes the efficacy and adaptability of AI-based response models. Not only do these models enhance real-time analytics and system understanding, but they also play a pivotal role in improving the accuracy of PPPs and facilitating inter-disciplinary collaboration. Therefore, the deployment of AI-models stands as a promising frontier for future research and application in systems design and performance optimization.

### Acknowledgements

The authors would like to express gratitude to FRIENDSHIP SYSTEMS AG for their valuable assistance with contemporary CFD use cases.

### References

AHMED, O. (2022), *Speeding-Up Simulation Driven Design for High-Speed Planing Boat*, Master Thesis, École Centrale de Nantes

AHMED, O.; HARRIES, S.; LOHSE, J.; SALECKER, S.E. (2023), *Parametric Modeling, CFD Simulations, DoE and Machine Learning for the Design of a Planing Boat*, Conf. Computer Applications and Information Technology in the Maritime Industries (COMPIT), pp.176-192

ASTRUP, O.C.; CABOS, C. (2017), *A Model Based Approval Process for Basic Hull Design*, 18<sup>th</sup> Int. Conf. Computer Applications in Shipbuilding (ICCAS), pp.410-419

BATTAGLIA, P.W.; HAMRICK, J.B.; BAPST, V.; SANCHEZ-GONZALEZ, A.; ZAMBALDI, V.; MALINOWSKI, M.; TACCHETTI, A.; RAPOSO, D.; SANTORO, A.; FAULKNER, R.; GULCEHRE, C.; SONG, F.; BALLARD, A.; GILMER, J.; DAHL, G.; VASWANI, A.; ALLEN, K.; NASH, C.; LANGSTON, V.; DYER, C.; HEESS, N.; WIERSTRA, D.; KOHLI, P.; BOTVINICK, M.; VINIYALS, O.; LI, Y.; PASCANU, R. (2018), *Relational inductive biases, deep learning, and graph networks*, <https://arxiv.org/abs/1806.01261>

HANSEN, H.; FREUND M. (2010), *Assistance Tools for Operational Fuel Efficiency*, 9<sup>th</sup> Conf. Computer Applications and Information Technology in the Maritime Industries (COMPIT), pp.356-366

KARCHER, N. (2022), *POD-Based Model-Order Reduction for Discontinuous Parameters*, Fluids Special Issue Aerodynamics of Road Vehicles and Trains, pp.1-18

MOCTAR, O.; LANTERMANN, U; SHIGUNOV, V.; SCHELLIN, T.E. (2023), *Experimental and numerical investigations of the effects of the ship superstructure on wind-induced loads for benchmarking*, Physics of Fluids



PEDERSEN, T.A.; GLOMSRUD, J.A.; HAUGEN, O.I. (2019), *Towards Simulation-based Verification of Autonomous Navigation Systems*, 2<sup>nd</sup> Int. Seminar on Safety and Security of Autonomous Vessels (ISSAV), pp.1-13

SALMOIRAGHI, F.; BALLARIN, F.; CORSI, G.; MOLA, A.; TEZZELE, M.; ROZZA, G. (2016), *Advances in geometrical parametrization and reduced order models and methods for computational fluid dynamics problems in applied sciences and engineering: overview and perspectives*, VII European Congress on Computational Methods in Applied Sciences and Engineering, pp.1013-1031

SHERRY, M.; JACONO, D.L.; SHERIDAN, J.; MATHIS, R.; MARUSIC, I. (2009), *Flow Separation characteristics of forward facing step immersed in a turbulent boundary layer*, Int. Symp. Turbulence and Shear Flow Phenomena, pp.1325-1330

VILANOVA, M.R.; HANSEN, H.; BINGHAM, H.B. (2021), *Performance Prediction Program for Wind-Assisted Cargo Ships*, J. Sailing Technology, pp.91-117

WANG, J.; WAN, D. (2015), *Numerical Simulation of an Oblique Towed Ship by naoe-FOAM-SJTU Solver*, Int. Ocean and Polar Engineering Conf., pp.432-438

# Methanol as a Marine Fuel: Techno-Economic Considerations

Ivan Stojanovic, Lloyd's Register, Hamburg/Germany, [ivan.stojanovic@lr.org](mailto:ivan.stojanovic@lr.org)

## Abstract

*The use of methanol as a marine fuel has gained significant attention in recent years due to its potential to address environmental and sustainability concerns in the shipping industry and allow the shipowners and operators to achieve EU and IMO targets. This study presents the current market trends, regulatory landscape and techno-economic analysis of methanol as marine fuel. The potential benefits and challenges associated with the widespread interest in methanol as a marine fuel are evaluated, considering factors such as technology readiness, emissions reduction potential and commercial viability. Considerations shipowners and operators need to take into account when transitioning to methanol as a fuel are discussed. The impact on the fuel emissions and CO2 tax, such as EU-ETS and FuelEU is investigated, quantifying the emissions and costs for the MR tanker.*

## 1. Introduction

When ordering the vessel today, the Ship Owners are challenged with selecting the right fuel option. Typical vessel life-span is around 20-years and the risk of the asset becoming stranded or too expensive to operate increases as the emissions regulations become more stringent. Different considerations should be made when selecting the fuel option: technical maturity and safety, rules and regulations, fuel storage and handling requirements, impact on the vessel range, supply availability and bunkering infrastructure, emissions life cycle, crew training and ultimately commercial feasibility.

Green methanol as a marine fuel has gained momentum across shipping as one of the future fuels that could potentially offer substantial reductions in CO2 intensity. Engine technology for this fuel option has matured and methanol engines have already been deployed and in operation on a number of vessels. Still, the supply of bio-methanol and e-methanol is limited, and current costs of production are not able to justify the techno-economic case for choosing this option. However, EU already adopted Fit for 55, a set of policies that will incentivise emitters trading in Europe to find alternative solutions and decrease their emissions by at least 55% by 2030, or pay to comply. Simultaneously, IMO is working on the set of emissions measures, soon to be adopted. With increasingly rigorous emissions penalties, and decreasing cost of methanol production, this alternative fuel may become a viable option for the Ship Owners and Charterers.

### 1.1. Market Trends and Methanol Production Pathways

Methanol is a low-flashpoint liquid fuel, which can be burned in the Internal Combustion Engines, or utilised in the Fuel Cells. It offers reduced emissions profile, including lower sulphur oxides, nitrogen oxides and particulate matter comparing to fuel oil. Additionally, if produced using sustainable feedstock, methanol has the potential to substantially reduce the vessels emissions profile.

Currently, there are 29 methanol fuelled vessels in operation and over 200 on order, with 15 planned retrofits. The vessel segments with methanol propulsion option on order are: Containerships, Bulk carriers, Oil & Chemical Tankers, Ferries, <https://www.clarksons.net/>.

Methanol-fuelled vessels on order are dual fuel, meaning they can operate on conventional fuel and switch to green methanol, once the emissions regulations tighten and the cost of fuels drops to commercially viable levels. The interest for this fuel keeps growing, with large shipping companies like A.P. Moller Maersk signing a number of commercial agreements with methanol producers, securing supply of green methanol for their fleet, <https://www.maersk.com/news/articles/2023/09/08/equinor-and-maersk-partner-to-supply-first-methanol-enabled-container-vessel>.

Methanol can be produced through various processes, including those for fossil-based and green methanol (bio- or e-). Currently, most of the produced methanol comes from natural gas as feedstock (grey methanol).

Grey methanol is produced using Steam Methane Reforming (SMR) process, where natural gas reacts with steam at high temperatures and pressures to produce hydrogen gas and carbon monoxide. These gases are then catalytically converted to methanol. Brown methanol is produced from coal using gasification process. These pathways have no environmental benefits.

There is an increasing number of green methanol production projects with sustainable feedstock. Bio methanol is produced using Biomass Gasification process, using biomass as feedstock, such as wood, agricultural residues or municipal waste, which are gasified to produce syngas. This syngas, containing hydrogen and carbon monoxide, is then converted into methanol using similar processes as in grey methanol production. E-methanol is produced using green hydrogen (produced via electrolysis using renewable electricity) and it can also be integrated with Direct Air Capture (DAC), to achieve carbon neutrality.

Each approach has its advantages and disadvantages in terms of cost, environmental impact, and scalability, and the choice of production method often depends on factors such as feedstock availability, cost and location, and energy source. E-methanol has higher emissions reduction potential. The challenges to produce e-methanol are: high cost and limited production capacity of DAC and limited global electrolyser production capacity, <https://www.zerocarbonshipping.com/>.

To estimate the emissions reduction potential and commercial feasibility of methanol, two pathways were selected for this study. First production pathway is bio-methanol produced from the forest residue as the feedstock. The second pathway is e-methanol produced from renewable hydrogen (from electrolysis using renewable electricity) and CO<sub>2</sub> coming from DAC.

Different fuels are assigned different emission factors, taking into account both the fuel production process (Well-to-Tank) and utilisation in the energy converter on the vessel (Tank-to-Wake). Well-to-Tank and Tank-to-Wake emissions factors for the fuel pathways selected in this study are defined in the Annex II of the FuelEU Maritime Directive and Annex III of Directive (EU) 2018/2001.

Bio-methanol produced from forest residue offers up to 80% of emissions reduction, while e-methanol offers up to 97% reduction. Impact of the emissions costs to bio- and e-methanol, comparing to fuel oil, will be presented in Chapter 5.

## 2. Technical Considerations

In 2015, Swedish Ferry operator Stena, retrofitted one of its RoPax vessels, Stena Germanica, allowing the vessel to run on both diesel and methanol fuels. Additionally, number of methanol carriers have been operating using their cargo as a fuel, with more vessels across different segments with methanol dual engines on order.

Methanol dual fuel engines are technically mature and available for both newbuilds and retrofits. Methanol is used as a main fuel, while 5% diesel is used as pilot fuel. Major engine makers are offering these engines:

1. MAN 2-Stroke ME-LGIM;
2. Wärtsilä 32 medium-speed;
3. ABC medium-speed DZD;
4. HiMSEN 4-stroke H32DF-LM (to be delivered);
5. WinGD X-DF-M (to be delivered).

The integral parts of the methanol system are:

1. Main dual fuel propulsion engine;
2. Methanol bunker tanks;
3. Cofferdams;
4. Bunkering skid;
5. Fuel Preparation Room (fuel pumps, Fuel Valve Train);
6. Inert Gas System (Nitrogen);
7. Transfer system from Fuel Preparation Room to the Fuel Valve Train;
8. Transfer system from Fuel Valve Train to main engine;
9. Airlock space;
10. Ventilation system in fuel preparation and fuel handling spaces;
11. Gas and vapour detection system;
12. Firefighting equipment.

There are several different options for methanol fuel tanks:

1. Integral tank: it is a part of the ship's hull, taking the same loads as the hull;
2. Independent tanks: self-supporting tanks which are not the part of the ship's hull;
3. Portable tank: independent tank, which can be connected and disconnected from the ship systems and removed from the ship.

There is a requirement that the methanol bunker tanks are protected by the cofferdams, which impacts the fuel storage capacity, however alternative arrangements are also possible. Fuel tank considerations are discussed in the below Section.

### 3. Rules and Regulations

To provide an international standard for ships using methyl/ethyl alcohol as fuel, IMO adopted the Interim Guidelines for the Safety of Ships Using Methyl/Ethyl Alcohol as Fuel, *IMO (2020)*. Interim Guidelines use the goal-based approach to provide specifications for the arrangement, installation, control and monitoring of machinery, equipment and systems for ships operating on methyl/ethyl alcohol as fuel, in order to minimise the risk to crew, ship and the environment.

Interim Guidelines suggest that the cofferdams are required to provide the protection against the fuel leakage into hazardous zones and toxic, flammable vapours between the fuel tank and other areas. Alternative design considerations can also be considered. The Guidelines also allow for the Alternative Design, provided that equivalent safety is achieved using risk-based approach:

“Appliances and arrangements of methyl/ethyl alcohol fuel systems may deviate from those set out in these Interim Guidelines, provided such appliances and arrangements meet the intent of the goal and functional requirements concerned and provide an equivalent level of safety to the relevant sections.”

Due to methanol's lower calorific value (LCV) of 19.9 MJ/kg, which is roughly half of VLSFO, there is a compromise between the vessel range, bunkering frequency or cargo capacity. To achieve more space for the bunker tanks (without cofferdams), Alternative Design approach potentially allows for the methanol tanks to be positioned below the waterline, in the double hull lower ballast tanks, provided equivalent safety is achieved. When alternative tank design is considered, draft, trim and stability criteria need to be satisfied using adjacent ballast tanks. Inspection, maintenance and repair procedures also need to be considered. The construction challenges of alternative tank arrangements remain.

For methanol retrofit projects, existing HFO tanks can be converted to methanol tanks, but special zinc silicate coatings must be applied as methanol is corrosive. Methanol is lighter than the fuel oil, so the number and size of the fuel storage tanks is determined based on the available weight to achieve the same vessel displacement. MDO/MGO tanks remain, due to operational flexibility, pilot fuel requirement and redundancy (Safe Return to Port).

#### 4. Emissions Regulations

With current and upcoming emissions regulations on both regional and global level, green methanol has the potential to reduce emissions penalties, due to lower Well-to-Wake emissions.

As a part of Fit for 55 package, the European Union introduced a set of emissions regulations to reduce greenhouse gas emissions from ships operating in EEA waters and incentivise the use of low carbon future fuels. Emissions scope include CO<sub>2</sub>, CH<sub>4</sub> and N<sub>2</sub>O emissions.

The European Union's Emissions Trading System (ETS) for the maritime industry represents a Cap-and-Trade market-based approach, strategically aimed at holding accountable polluting vessels engaged in trade within Europe. Scheduled to take effect in 2024, the EU-ETS for shipping will impose charges on high-emission vessels for their operational CO<sub>2</sub> emissions, specifically those incurred during voyages to and between European ports.

For the purposes of this study, it is assumed that the vessel in scope will be making port calls from international to EEA ports. As a result, this vessel will be subject to a 50% levy on CO<sub>2</sub> emissions on the Tank-To-Wake (TtW) basis, with a 100% charge for emissions generated during the time spent in and between EU ports. Impact of EU-ETS costs is examined in Chapter 5.

FuelEU is also an integral component of the European Union's "Fit for 55" initiative. It is regulatory mandate requiring vessels with a gross tonnage exceeding 5,000 to gradually reduce emissions from operations, based on the energy consumed on Well-to-Wake (WtW) basis. Commencing on January 1, 2025, the reduction benchmarks are established as follows: 2% reduction by 2025, 6% by 2030, 14.5% by 2035, 31% by 2040, 62% by 2045, culminating in 80% reduction target by 2050.

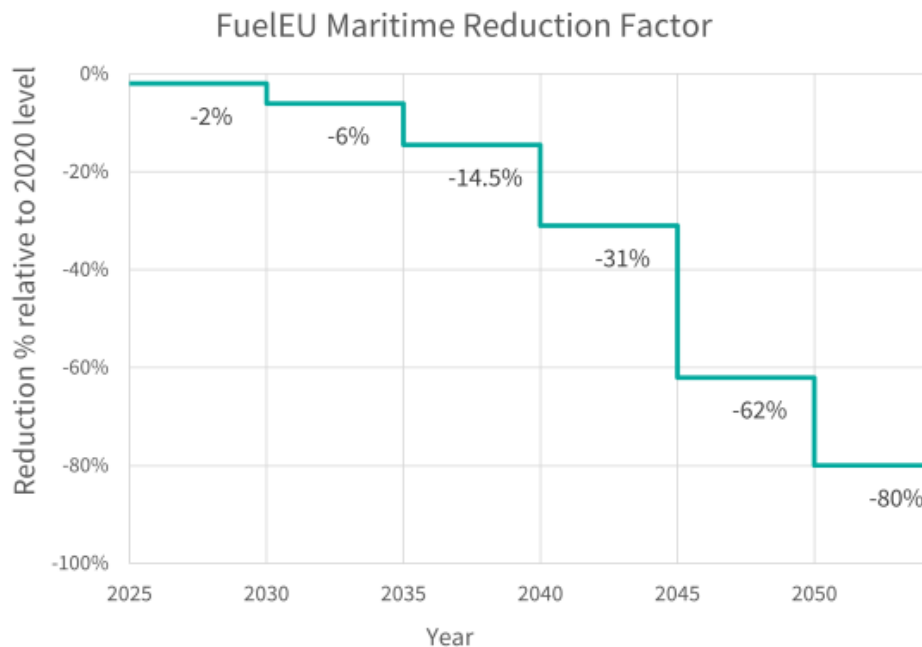


Fig.1 : FuelEU Maritime emission reduction targets

Similar to EU-ETS, the vessel calling EEA ports from non-EEA ports will be penalised for 50% of the energy used in that voyage, and voyages within EEA will be penalised for all the energy used in those voyages.

Additionally, the FuelEU Directive will reward the consumers of low carbon renewable fuels of non-biological origin (RFNBOs), with emissions reduction factor of 2, for the RFNBO fuel uptake between 1 January 2025 and 31 December 2033. This is designed to promote the uptake of synthetic fuels such



as e-diesel, e-methanol, e-LNG, e-hydrogen. Reward factor for using Wind Assisted Propulsion is also included in the Directive, but out of scope in this study.

On the global level, International Maritime Organization (IMO) members have adopted the Revised Strategy on Reduction of GHG Emissions from Ships, increasing the reduction targets to reduce emissions from shipping operations, <https://www.lr.org/en/services/classification-certification/fit-for-55/fueleu-regulation/>. Levels of the revised ambition are:

- Further improvement in energy efficiency through EEDI requirements;
- Reduction of CO<sub>2</sub> emissions per transport work by at least 40% by 2030, 70% by 2040, and Net-zero GHG emissions by or around 2050, comparing to 2008;
- Uptake of zero or near zero emissions technologies and fuels to increase to at least 5% by 2030.

IMO indicated that the mid-term GHG reduction measures will be adopted, including both technical measures (fuel standards) and emissions pricing mechanism. These measures are expected to be adopted and approved by 2027, with entry into force in 2028. In its Life Cycle Assessment Guidelines (LCA) guidelines, the IMO proposed that the GHG intensity of marine fuels will be measured on a Well-to-Wake basis, including both Well-to-Tank and Tank-to-Wake emissions. Commercial impact of these measures is also presented in Chapter 5.

## 5. Total Cost of Ownership

This Chapter presents the techno-economic analysis for the MR tanker using methanol as fuel, trading on a fixed route between Europe and USA, illustrating the commercial impact of different fuel options. Emissions penalties, fuel costs and additional CAPEX are compared for bio-methanol, e-methanol and fuel oil. EU-ETS costs, FuelEU penalties are estimated for the vessel, given its exposure to EEA.

An increasing number of organizations within the shipping sector are advocating for the implementation of carbon pricing mechanisms on the IMO level. There have been multiple proposals for carbon pricing submitted to the IMO, ranging between USD 56 to USD 300. European Central Bank assumes that the carbon pricing will reach to EUR 140 per tonne of CO<sub>2</sub> by 2030, *IMO (2023)*. In addition, for the period between 2030 to 2050, UK'S Department of Energy and Climate Change assumes that the EU-ETS price could reach the average level of around EUR 200. Based on these projections, below Figure shows the assumed EU-ETS price projections for this study. The impact of the potential Global carbon tax is also included in this study.

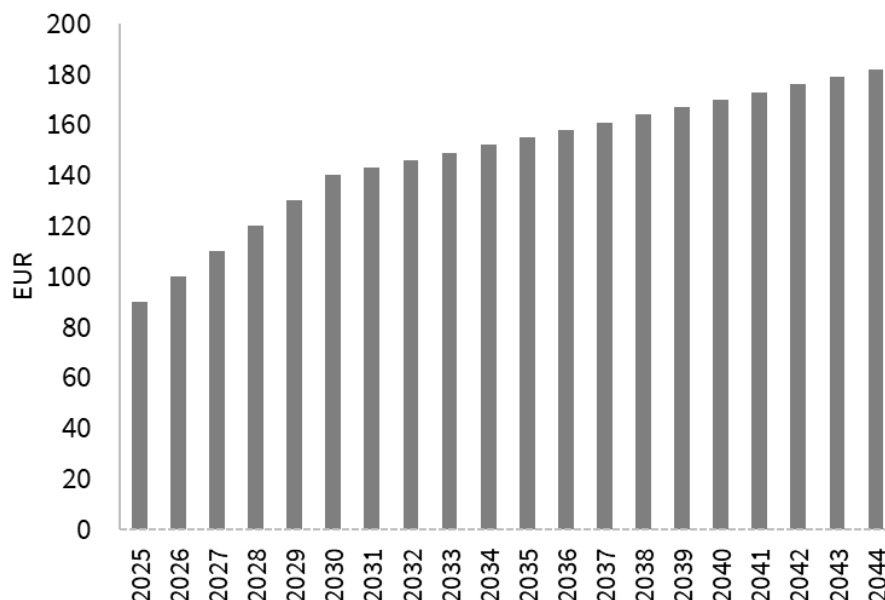


Fig.2: EU-ETS price projections

Fig.2 presents the estimated EU-ETS prices throughout the vessel life-cycle. The price for TtW emissions starts at EUR 90 in 2025 and increases gradually to EUR 180.

Fig.3 shows the Global CO<sub>2</sub> prices assumed in this study, suggesting the penalties on Well-to-Wake (WtW) basis and global adoption from 2028, starting at USD 100 and increasing gradually to USD 180.

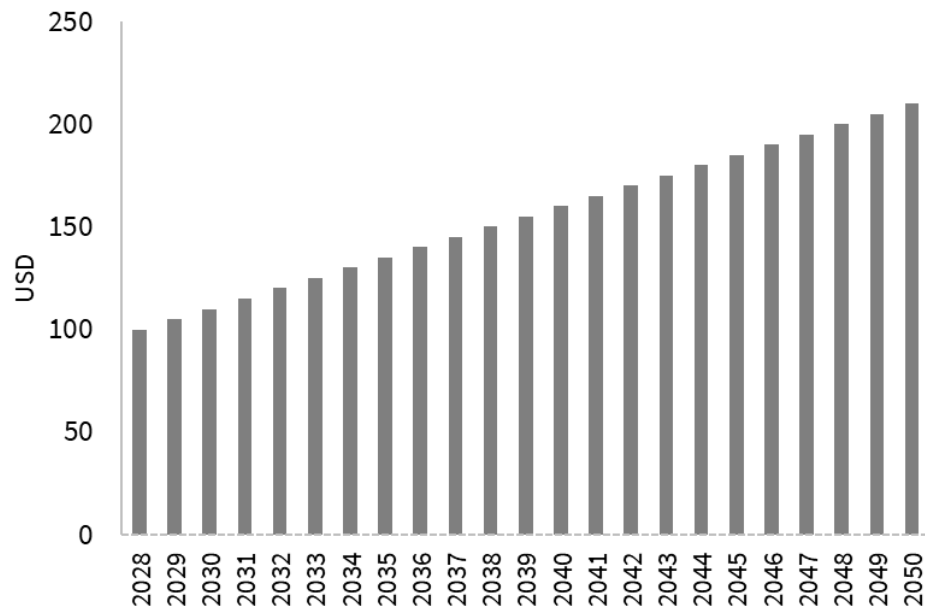


Fig.3: Global carbon price projections

Fuel prices are also taken into consideration in this study, to model the impact of the fuel costs throughout the vessel life cycle. Methanol Institute price projections were taken for bio- and e-methanol, as shown on Fig.4. It is assumed that the prices of new fuels will decrease with economy of scale and maturation of the production processes. Higher range of methanol prices is included, due to the current uncertainty how the supply chain of green methanol will develop in the future.

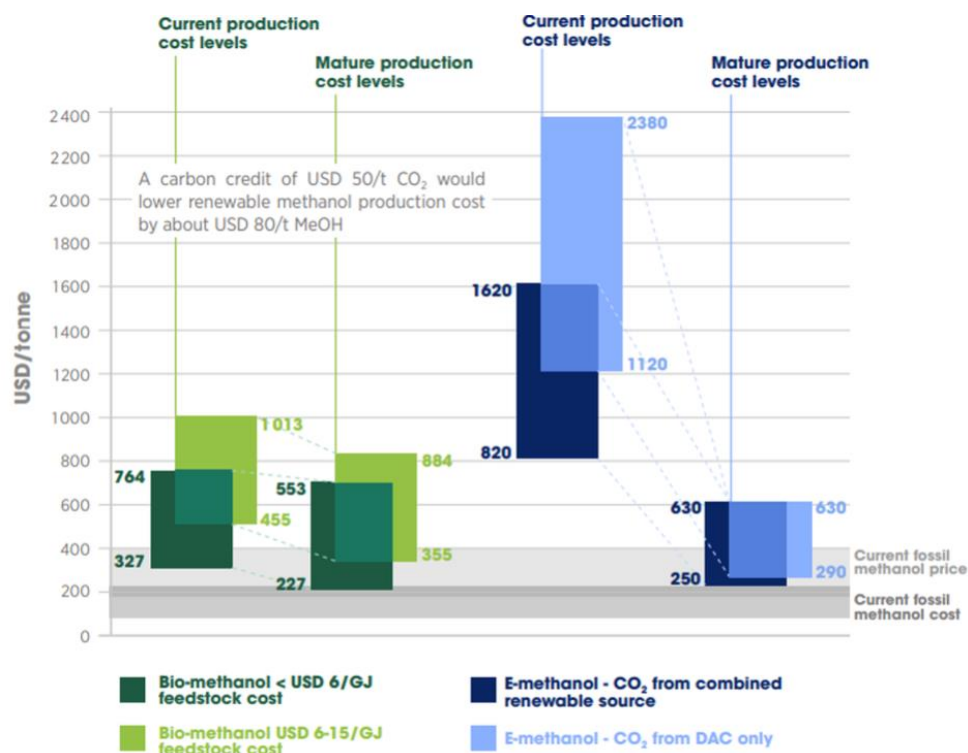


Fig.1: Bio-methanol and e-methanol prices, UK (2023)

The current VLSFO bunker price, <https://shipandbunker.com/prices>, was taken to make a price outlook for the future, assuming it will continue to increase with annual inflation of 3%. Fig.5 shows the fuel prices assumed in this study.

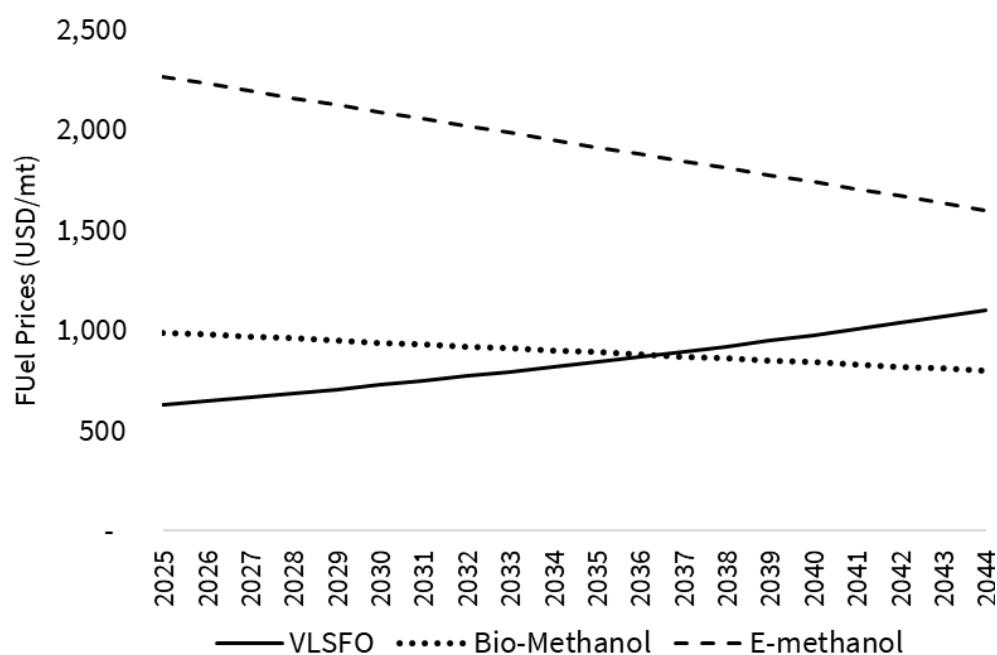


Fig.2: Fuel price projections

MR tanker of 50,000DWT is selected for Total Cost of Ownership (TCO) analysis, to compare how commercially attractive bio-methanol and e-methanol fuel options are comparing to fuel oil. It is assumed that his vessel is trading between Europe and USA and spends 70% of time in transit and 30% in port and anchorage. Table I presents vessel assumptions used for the TCO analysis.

Table I: Vessel assumptions

Vessel Type	MR tanker
Vessel DWT	50,000
Service speed	12-13kn
Main Engine Average Fuel Consumption	20 MT/day
Auxiliary Engine Average Fuel Consumption	3 MT/day
Vessel life cycle	20 years (2025-2045)

It is assumed that the bio- and e-methanol are introduced gradually into vessel operations, as the production capacity increases and cost decrease. Annual fuel quantity for bio- and e-methanol is calculated as the amount required annually in order to reduce overall emissions and achieve the FuelEU compliance balance and avoid FuelEU penalties, as shown in Table II.

Table II: Fuel selection profile, percentage of fuels consumed (fuel switching, no fuel blending)

Fuel	2025-2029	2030-2034	2035-2039	2040-2044
VLSFO (%)	100			
Bio-methanol vs VLSFO (%)	5/95	10/90	20/80	40/60
E-methanol vs VLSFO (%)	3/97	8/92	16/84	33/67

CAPEX values are also included in the study. CAPEX required for the methanol propulsion system are projected based on the MAN's estimates for LR1 tanker, *MAN (2018)*. In this case, additional CAPEX required for the methanol systems (in addition to diesel propulsion option) is estimated as USD 3 million. However, these costs will vary depending on the commercial agreements between the ship owner and engine maker, shipyard. Additional maintenance costs and crew training costs were not considered in this study.

Note that the impact on the vessel cargo capacity, range and potential increase in charter rates have not been included in this study, and these factors will have an impact to the methanol business case.

Fig.6 shows the fuel costs and emissions costs for different fuel scenarios, comparing the methanol options with the conventional fuel throughout the vessel life cycle.

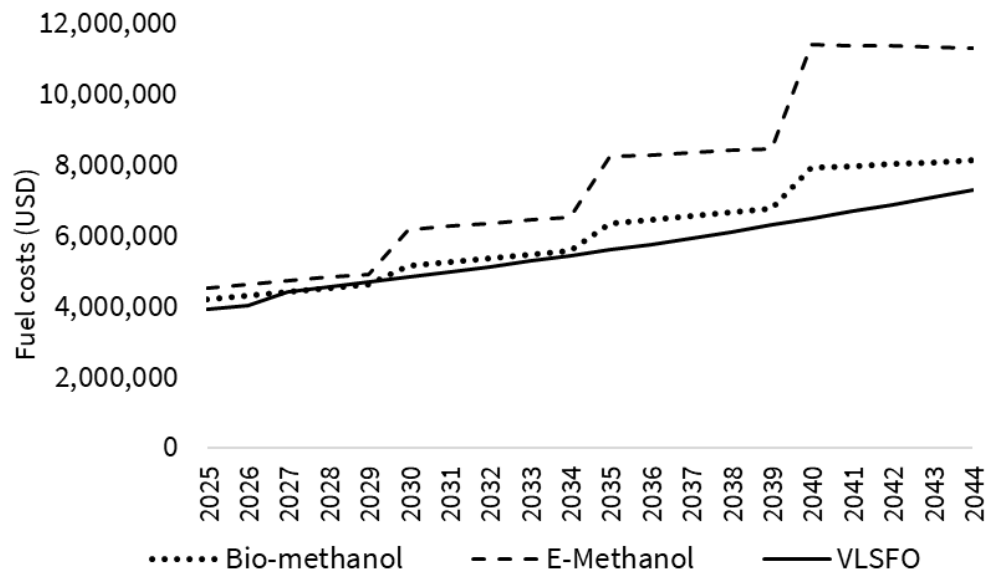


Fig.3: Fuel costs

We can observe that the fuel costs for methanol options are higher throughout the vessel life cycle, due to high initial prices of both bio- and e-methanol and lower LCV (thus more fuel is required to achieve the same power). Therefore, for methanol options to become commercially attractive, emissions costs need to be lower than the difference in the fuel costs.

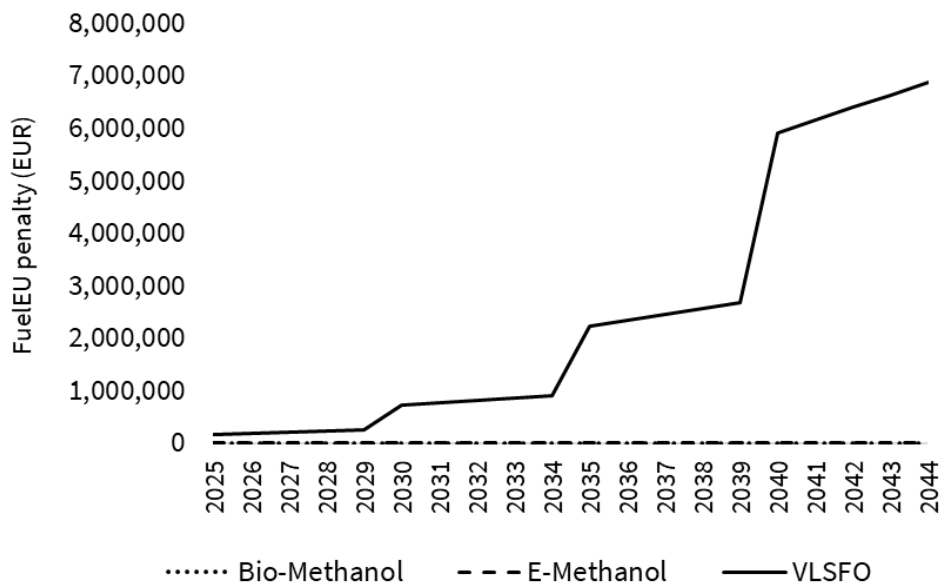


Fig.4: FuelEU penalties

Fig.7 shows that FuelEU penalty for both methanol options is zero, assuming the fuel uptakes in Table II are providing compliance with FuelEU target, and therefore no penalties will be induced.

Fig.8 compares EU-ETS costs for the fuel options. We can observe that the EU-ETS costs are lower for methanol options than VLSFO. Phase-in factor of 70% has been applied in 2025 for the EU-ETS costs (thus the increase from 2025 to 2026).

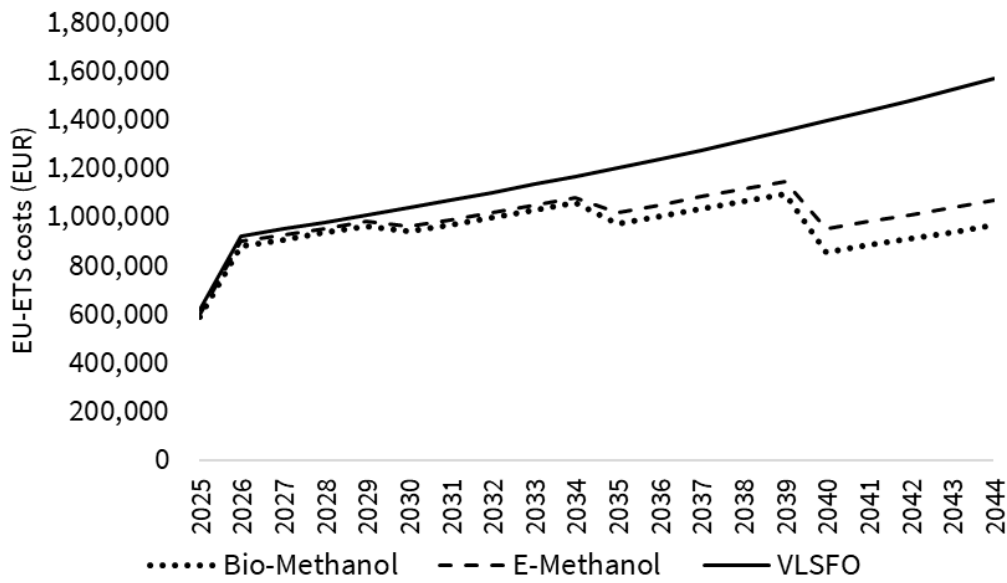


Fig.5: EU-ETS costs

Assuming the adoption of the Global carbon tax from 2028, Fig.9 shows the projected costs for the selected fuel options.

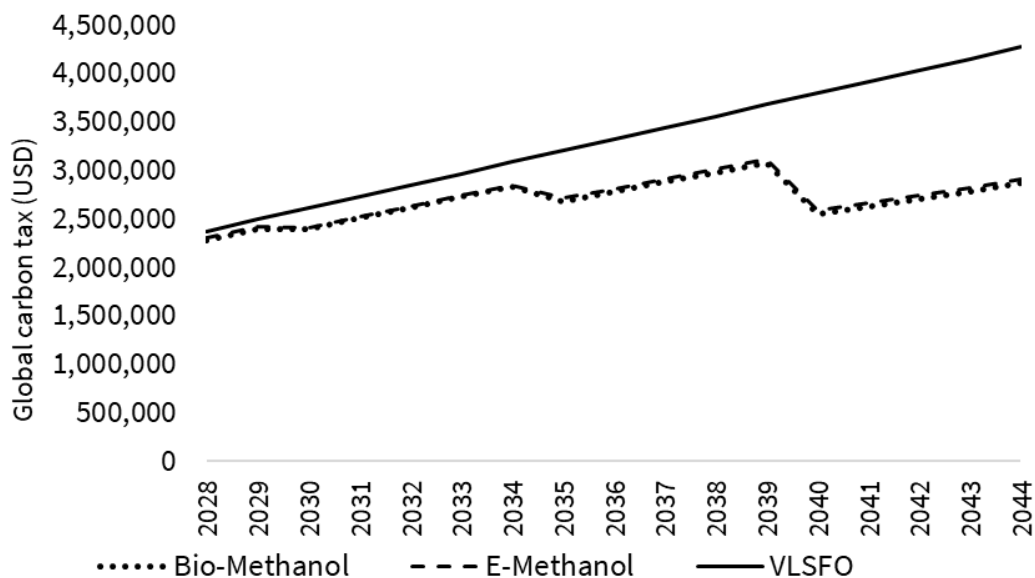


Fig.6: Global carbon tax costs

Similar trend is observed, where methanol fuel options have lower Global carbon costs, due to lower WtW emissions. Slight difference between bio-methanol and e-methanol costs exist due to difference in the annual fuel uptakes of these fuels (as shown in Table II).

Finally, Figs.10 and 11 present Total Cost of Ownership. Fig.10 chart assumes only EU-ETS and FuelEU taxes, together with the fuel costs, while Fig.11 assumes the adoption of the Global carbon tax and simultaneous removal of the EU-ETS tax.



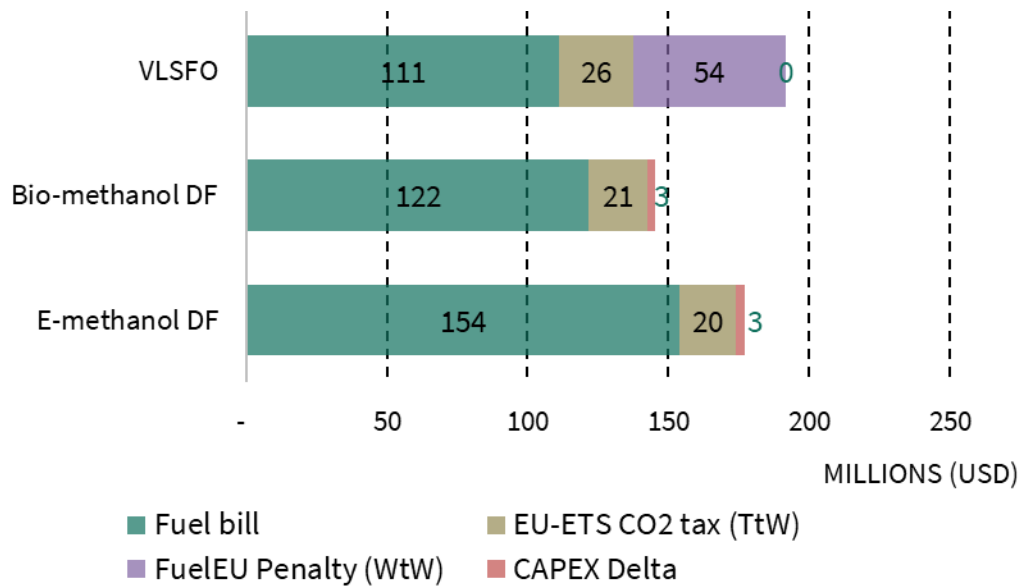


Fig.7: Total Cost of Ownership, including only European emissions taxes

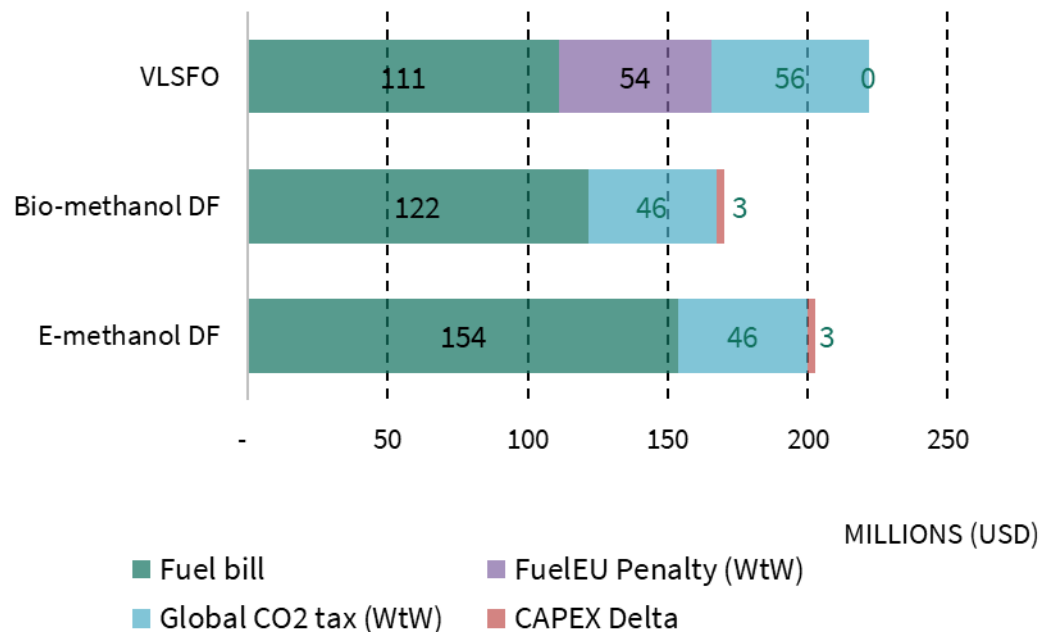


Fig.8: Total Cost of Ownership, including Global tax, excluding EU-ETS

From the TCO charts, we can observe that on the Total Cost of Ownership basis, the methanol fuel options are more beneficial comparing to VLSFO. Even though the fuel costs are higher, the emissions costs become a deciding factor. The main sensitivities of the TCO are: fuel prices projections, emissions taxes outlook and price levels, and the time the vessel is exposed to European ports.

## 6. Conclusions

This study covers high-level considerations of methanol as marine fuel, including technical aspect, emissions regulations and commercial analysis for this alternative fuel option.

Methanol engine technology is mature and commercially available, with vessels already sailing with methanol engines. Furthermore, there is a growing number of vessels on order with dual-fuel methanol engines, potentially enabling the transition from conventional to green fuels.

In the context of emissions regulations, the tightening regulatory landscape is a pivotal factor. The EU-ETS and FuelEU Directives have already been adopted, sending a strong signal that transition to green fuels is necessary for both compliance and commercial reasons. Additionally, the prospect of a Global carbon tax exists, adding further incentive to the start switching to green fuels.

However, despite the promising potential of green methanol, the challenges still remain. Limited supply availability and bunkering infrastructure, and high costs of production are currently limiting factors for wider adoption of bio- and e-methanol (for globally trading vessels), and there is still uncertainty how this will develop in the future.

Total Cost of Ownership analysis provides an insight that green methanol fuel options have the potential to be commercially competitive with conventional fuel, particularly as the emissions targets become more rigorous and the cost of compliance increases.

## References

IMO (2020), *Interim guidelines for the safety of ships using methyl/ethyl alcohol as fuel*, Int. Mar. Org., London

IMO (2023), *Guidelines on life cycle GHG intensity of marine fuels (LCA Guidelines)*, Int. Mar. Org., London, <https://www.imo.org/en/OurWork/Environment/Pages/Lifecycle-GHG---carbon-intensity-guidelines.aspx>

MAN (2018), *Costs and benefits: Alternative fuels for an LR1 product tanker*, MAN, Copenhagen, <https://www.man-es.com/docs/default-source/document-sync/costs-and-benefits-alternative-fuels-for-an-lr1-product-tanker-key-results-from-a-dnv-gl-and-energy-solutions-joint-study-eng.pdf>

UK (2023), *Guidance on Estimating Carbon Values Beyond 2050: An Interim Approach*, UK's Department of Energy and Climate Change

# Applying Fouling Detection with ROV and AI and Big Data Analysis for EEXI/CII Fleet Optimization

Michael Stein, Vesselity Maritime Analytics, Rostock/Germany, [stein@vesselity.de](mailto:stein@vesselity.de)

## Abstract

*A clean ship hull is defined by studies to be the optimal, most cost-effective way of meeting EEXI/CII regulations, with saving potential of up to 7% fuel without retrofitting. Such gains, however, require knowledge and data of the ship hull. With in-water surveys being conducted every 2.5 years in the past, this knowledge was scarce to non-existing for ship owners and operators. The most recent rise, of mobile, handheld micro-ROV systems have the potential of changing the way hull inspections are conducted. In combination with marine fouling AI detection, the roughness of a ship's hull can be calculated and optimal cleaning and coating decision can be derived. With regard to latest EEXI/CII regulations, micro ROV systems provide a valuable tool for continuous hull monitoring for marine fouling detection and management. This paper describes the combination of micro-ROV systems and customized deep convolutional neural networks for EEXI/CII fleet optimization in an introductory analysis.*

## 1. Introduction

Water covers about 71% of this world's surface, Capocci *et al.* (2017), resulting in ~90% of the global trade being conducted or linked to the shipping industry. In 2016 still only 5% of the oceans were stated to be explored, Capocci *et al.* (2017), which only increased to ~20% in 2020, Nippon Foundation (2020). This increase of knowledge is to a large extent based on emerging underwater robotics and technology, McLean *et al.* (2018), that promoted comprehensive exploration of oceans previously out of reach to the human eye, McLean *et al.* (2018). The general absence of knowledge in deep sea exploration is also reflected in the commercial shipping industry. Under normal operative circumstances ship hulls and propulsion systems are inspected once every 2.5 years for the sake of mandatory intermediary classification of its seaworthiness. Every 5 years, the ship is lifted out of the water for a mandatory detailed dry dock inspection, often followed by hull cleaning and coating actions. Within these 2.5 year cycles knowledge of the status and condition of the ship hull and propulsion is scarce to non-existing. Divers used to be the only mean to receive underwater information if any given infrastructure, while their costly operation and their demand for safety measurements led them to become a service of necessity rather than a service of precaution. This implies, that 90% of the global trade is being conducted by ships that are operated and chartered with close to no know knowledge about the hull status for over ~900 days in a row and actual marine fouling measurements being only able to conducted manually once every ~1.800 days.

This paper argues that similar to oceanic cartography, the maritime hull status mapping is faced with huge potential for optimization through the use of emerging technologies. The author argues that this potential is mainly based on the ROV and artificial intelligence (AI) technology, moreover in the combination of both. This paper introduces the operation of ROVs towards ship management and hull performance optimization and its combination with artificial intelligence in form of deep convolutional neural networks (DCNN).

## 2. Methodology

The studying of innovative approaches and new operations in academic research is initially accompanied by a certain scarcity of existing literature. This situation requires a structured framing of the research topic with existing sources and an application of suitable research methodologies. The methodology chosen for this paper is a mixed-method approach of both qualitative and quantitative analysis with a grounded theory approach resulting in introductory frameworks as a basis for future research.

The qualitative approach of the mixed method evaluation is based on a three-fold literature review. First, existing sources framing the topic of micro ROV operations in the maritime industry are reviewed. This review excluded any contributions of large working class ROVs of the oil and gas sector as well as technical demonstration papers of ROV prototyping, hence only focussing on the application of commercially available micro-ROV hardware in maritime applications. Second, the application of AI more specific deep convolutional neural networks for underwater image recognition are reviewed. Third, the recently entered into force regulations of EEXI/CII are reviewed.

The quantitative approach of this paper underlies in a structured global ROV market analysis including a summary of the market data forecast till 2030. In order to acknowledge the quite new micro ROV sector as part of the well-situated working class ROV sector, both are evaluated and visualized. Since market data on that regard is scarce and to the best of the author's knowledge not scientifically proven in any study, this approach reflects only an initial attempt at providing quantitative insights.

The underlying theoretical approach of this paper's mixed method methodology follows grounded theory, *Glaser and Strauss (1967)*. Grounded theory is applied by studies focussing on new phenomena or innovative approaches with scarce underlying literature therefore chosen to be suitable for this paper. In a very brief summary, the theory describes the framing of a research topic by triangulation of already existing knowledge of connected topics to allow for initial but structured evaluations of any new phenomena.

The conclusion and visualization of this paper's research is conducted by conceptual frameworks as a solid basis for future research. Conceptual frameworks provide a widely accepted academic tool that furthermore allow for a visualization of insights. Since the topic of ROV-based EEXI/CII optimization assisted by AI is defined by the author to be an applied topic, the aim of this contribution is to balance both the scientific rigor and the economic relevance when discussing this paper's results. This paper aims at achieving this aspect by the choice of the above-mentioned methods.

### 3. Literature analysis

#### 3.1. Micro-ROV operations

A first systematic overview of general ROV operations has been provided by *Capocci et al. (2017)*. A structure that is applied but restructured for the literature review of this paper displayed in Table I. Regarding marine science, data of industrial ROVs represent one of the most substantial data sources of the oceans, *Macreadie et al. (2018)*. Examples are the application of historical ROV data to characterize reefs within oil and gas infrastructure, *Thompson et al. (2018)*, or the operation of ROV systems in seafloor mapping, *Lambertini et al. (2022)*. With regard to disaster response, ROVs delivered scientific insights following the Tokoku earthquake and tsunami disaster in Japan, *Murphy et al. (2011)*, *Osumi (2014)*. In 2015, a micro ROV inspected the Costa Concordia wreck for documentation, *Allotta et al. (2015)*. Underwater archology benefits from micro ROV systems as diving buddy, *Capocci et al. (2017)*, for documentation and surface recognition as well as planning and supporting of underwater sites, *Bruno et al. (2015)*. Especially for archaeological sites of a limited size, micro ROV systems offer a great benefit for a fast and mobile operation for documentation and 3D mapping. The aspect of military operations includes the use of unmanned vehicles such as ROV systems. *Keranen et al. (2012)* described the ROV detection capabilities of unexploded ordnance (UXO) in seaport operations. Recent contributions describe ROV systems for electromagnetic detection, *Schultz et al. (2021)*, an UXO detection for offshore sites, *Shmatkov and Antonov (2021)*. Micro-ROVs will provide a value-adding component of visual confirmation on potential UXO findings. Given their high manoeuvrability and low financial risk, micro-ROV systems offer great advantage in the evaluation of UXO. Ship and Port security is defined since 2002 by the International Ship and Port Facility Security (ISPS) Code as part of the Safety of Life at Sea (SOLAS) convention. UAV and ROV in general have been evaluated towards their potential for ISPS assistance by *Stein (2018)*. The contribution reveals that ROV operations play a role in major ISPS operation categories of monitoring, inspecting and management, by either assisting human operations or replacing them with remote

operation. Industrial inspection reflect a rather applied field with currently limited scientific literature. However, the aspect of ROV based ship hull inspection was introduced by *Nicinski (1983)* using a magnetic vehicle attached to the hull. These systems, however, can only operate on clean surfaces, making it non-operable on hulls with marine fouling when magnetic wheels cannot attach. Non-magnetic ROV systems have later been tested on ship hull inspection in by *Lynn and Bohlander (1999)*.

Table I: Micro ROV operation framework, based on *Capocci et al. (2017)*

Marine Science	Disaster Response	Underwater Archeology	Military Operations	Security	Industrial Inspection	
					off shore	near shore
oceanography	oil spill detection	retrieving of artifacts	UXO identification	contraband detection	wind farm inspection	port inspection ship inspection
reef research	maritime accidents	documentation	Surveillance		pipeline inspection	bridge inspection tank inspection
water quality assessment	search & rescue	dive buddy			oil platform inspection	aquaculture inspection
wildlife research	ghost net detection					hazardous environment inspection

### 3.2. EEXI/CII

Global marine traffic is based on simple slow-moving Diesel engines with predominantly two stroke engines, burning fuel of significantly worse quality compared to other modes of transportation, *Wharton (1991)*. This convenience, however, comes with an impact on global greenhouse gas emissions. According to estimations, the shipping sector produces 3.3% of the global CO<sub>2</sub> emissions, an equivalent of 1,046 million tonnes annually, *IMO (2009)*. While NO<sub>x</sub> and SO<sub>x</sub> emissions caused by commercial ships increased by about 40% from 2000 to 2020, *Kamil et al. (2020)*, annual CO<sub>2</sub> emissions were forecasted to increase by up to 250% by 2050 if unregulated, *Prastowo et al. (2020)*. To reduce these forecasts, the UN proposed a g-CO<sub>2</sub>/ton mile by design index in 2015. In 2023 this index went into force by the international maritime organization (IMO) as Annex VI of MARPOL known as the EEXI (Energy Efficiency for Existing Ships) index. Its goal is a short term reduction of greenhouse gas emissions by 40% till 2030 compared to 2008 base values (see *Rutherford et al., 2020*). According to *Polemis et al. (2023)* this marks the first time that an international regulation enforces a speed limit for ships, although being indirect. Together with EEXI comes CII (Carbon Intensity Index) described as “metric that evaluates GHG emissions concerning the volume of freight and miles traveled”, *Polemis et al. (2023)*. The index categories A-E determine the ship’s carbon intensity rating, whereas a value exceeding the determined norm value of a specific ship class will lead to its decommission. Only 30% of existing ships conform to the IMO’s criteria according to *Clarksons (2021)*. They further state that 40% of tankers and 25% of bulk carriers will exceed their defined EEXI levels by far, thus requiring tremendous operative measures to comply, *Polemis et al. (2023)*. The IMO proposes a set of emission reduction measurements, however the lack of economic assistance for ship owners and the rather vague GHG reduction impacts on the actual EEXI lead most likely to a challenge in the market for vessel operators to actual comply with the new rules. *Lindstad and Bø (2018)* evaluated EEDI-compliant technologies for GHG emissions under a variety of actual operational scenarios and ranked those. According to them, the most cost-effective approach for meeting the standards is a clean hull in combination with an internal combustion engine. In fact, cleaning the ship hull has previously been identified to save ~7% fuel through reduced water resistance by *Adland et al. (2018)*. In order to determine, whether a hull is clean enough or requires cleaning, measurements are required for decision assistance. Among the most promising technologies to determine and analyse the smoothness of a ship’s hull, this paper introduces the combination of micro-ROV systems and AI that will be introduced in the following chapters.



### 3.3. Introduction of AI in underwater operations

Artificial intelligence (AI) can be described as the part of modern computer science with predominant interest in most recent times. Aspect of deep learning and deep convolutional neural networks (DCNN) offer applicable scenarios for ROV systems with an underlying potential for disruption of the maritime industry, *Meng et al. (2018)*. Especially the emergence micro-ROVs solving the problem of underwater data collection, *Liu and Fang (2020)*. Modern computer languages such as python and tensorflow with their libraries and powerful deep models (*Islam et al. 2020*) as well as increasing computational power boost developments in AI application. Receiving high quality data for AI training was stated to be a challenging task in the past, *O'Byrne et al. (2018)*, but with the widespan availability of micro-ROV systems, this obstacle was removed to a large extent. However, underwater images provide certain obstacles with regard to image recognition in form of optical distortion artefacts, absence of background patterns, *O'Byrne et al. (2018)*, changes in light, or motion blur. According to *Islam et al. (2020)* applications of terrestrial data-based neural network models are inapplicable for underwater image recognition, while the absence of existing underwater DCNN literature limits existing networks to only performing simple tasks. Examples are provided by *O'Byrne et al. (2018)* for marine structures, *Islam et al. (2020)* and *Liu and Fang (2020)* for diver and fish recognition, *Chin et al (2021)* for kelp and oyster recognition and *Bloomfield et al. (2021)* for fouling classification. All of these contribution are limited to test pictures in either experimental designs or under very clear underwater visibility conditions using well-structured and centered images for training. The absence of training data on marine fouling on merchant vessels limits the training data to real-world ROV inspection videos under real and non- experimental conditions.

### 4. Introduction of the micro ROV class

Underwater drones were predominantly developed by the Navy with systems like CURV I–III before the technology was adopted by the oil and gas industry in the 1980s, *Capocci et al. (2017)*. This paper applied the terminology ROV (remotely operated vehicles) otherwise referred to as UUV (underwater unmanned vehicles). All systems described and evaluated in this paper are operated via cable connection to the surface. The area of AUVs (autonomous underwater vehicles) is acknowledged but disregarded for reasons of research limitation.

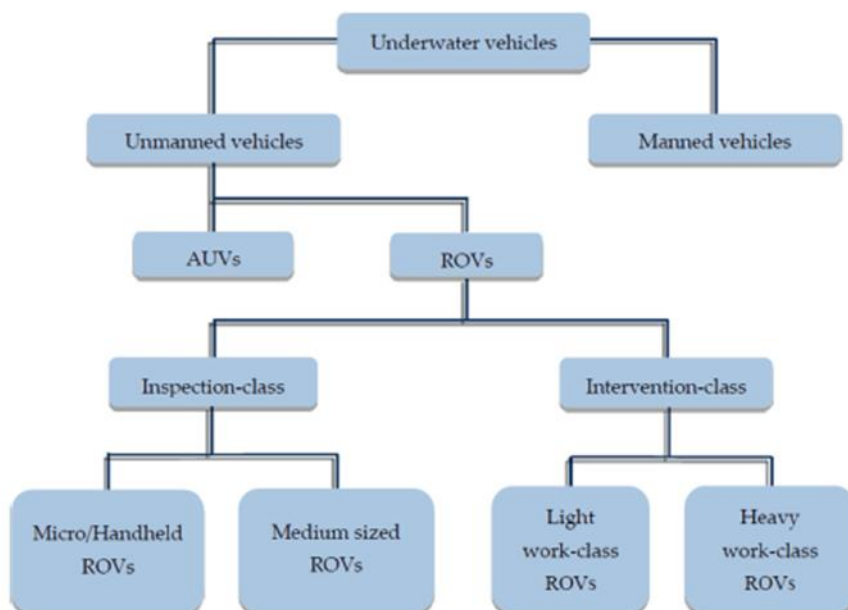


Fig.1: Underwater vehicle classification matrix, *Capocci et al. (2017)*

In the contribution from the aviation sector, *Sprague (2004)* state a reduction of up to 5 times the weight of the pilot in redundant safety equipment when unmanned a commercial plane. These numbers shall

visualize the reduction in size and costs of conventional airplanes compared to unmanned aerial systems. Although these scales cannot be transferred one to one to the ROV sector, they do display a shift from former large, expensive hardware with redundant systems to a smaller, modern and commonly available technology. On the ROV side, the smaller, lighter and less expensive inspection class has emerged from the predominant intervention class of the oil and gas sector as displayed in Fig.1. Intervention class ROV weight up to 5.000 kg, *Capocci et al. (2017)*, require launch and recovery systems and come with an investment of several hundred thousands of dollars and more. The inspection class with focus on micro-ROV system on the other hand operates systems of ~10 kg that can be operated single handed and at investment costs on average of 10.000\$ as shown later in this chapter.

The light weight of the micro ROV hardware offers a high degree of mobility allowing flexible operations. *Capocci et al. (2017)* argue that whilst the early micro-ROVs were limited in bandwidth due to copper fibre cables, recent hardware allows bandwidth of 500–1000 Mb/s over distances up to 500 m. On the trade-off side, micro-ROVs are predominantly reduced to video and manoeuvring systems limiting their operation to inspection services only. However, as the next chapters reveal, the operational potential of this lightweight ROV systems for the maritime industry are considerable.

According to IMCA (2015), 700 intervention class ROV systems were in operation in 2015 of which 550 systems belonged to the intervention class. An introductory market analysis on micro ROV systems and their market entry reveals a number of 22 micro-ROV systems below 25.000\$ costs having entered the market in the past decade since 2012. A global number of 12 manufactures mostly founded in the past two decades since 2001 launched these micro-ROV systems.

Fig.2 displays the micro-ROV systems by market entry date as well as costs and operational depth. According to the results of the analysis, the SeaOtter-1 was the first micro-ROV system commonly available in 1994. The SeaOtter-1 was upgraded to a version 2 in 2007 still predating all other ROV systems found. On average, 2017/2018 reflects the date of the micro-ROV market launch whereas in 2020 the largest number of new micro-ROV systems have entered the market in one year. Fig.2 reveals two cluster of investment costs of the revealed micro-ROV systems. The more expensive cluster has an average cost of 17.900\$ while the cheaper cluster has an average of 4.100\$ investment costs. The overall cost average of 10.000\$ is only covered by approximately 4 micro-ROV systems. Based on the fact sheets of the systems, the ROVs range between 50-305m (165-1.000 feet) in operational depth. The upper limit can be explained by the material used, mostly being plastic an aluminium.

A sum of 12 manufactures of micro-ROVs has been identified as shown in Table II. China is the predominant origin with 5 manufactures. In terms of operability, some ROV systems cannot be regarded because of their weight of 20 kg and more, which makes it almost impossible to launch and retrieve them without winches or cranes. Also some systems require a source of electricity, resulting in operative challenges in remote areas such as port facilities.

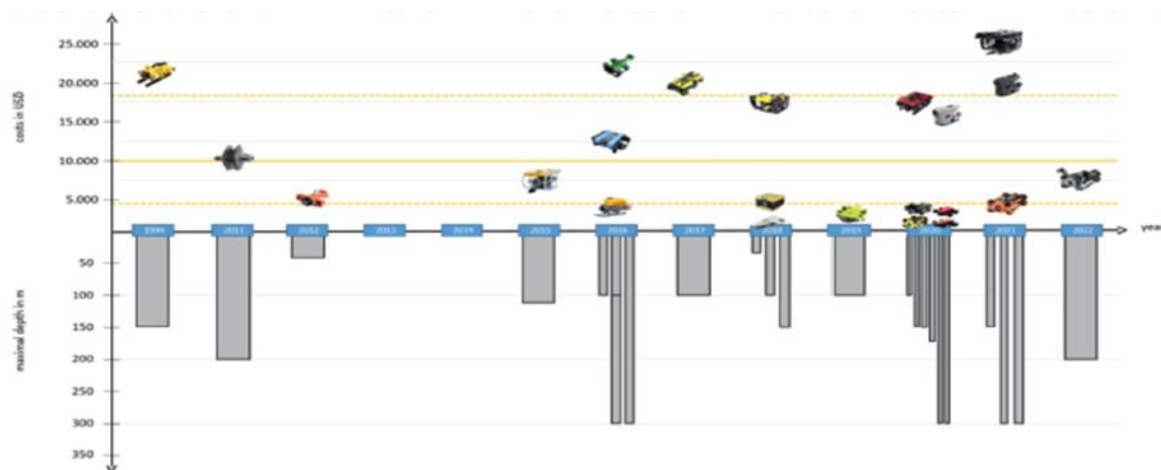


Fig.2: Micro-ROV market entry/cost/depth matrix

Table II: Micro-ROV details

Manufacturer	Year	Country	ROV	start	kg	Depth	Cost
Aquabotix	2011	Australia	Hydroview	2012	16	45	5.500
Aquabotix	2011	Australia	Endura 300	2016	7	305	17-25.000
Blue Robotics	2014	USA	BlueROV2	2016	12	100-305*	10-15.000*
Blueye Robotics	2015	Norway	Blueye Pro	2020	9	305	15.000
Blueye Robotics	2015	Norway	Blueye X3	2021	9	305	20.000
CCROV	2015	China	CCROV	2018	5	100	4.500
Chasing Innovation	2016	China	M2	2020	5	100	2.700
Chasing Innovation	2016	China	M2 Pro	2021	6	150	4.000
Chasing Innovation	2016	China	M2 Max	2022	8	200	7.500
Deep Trekker Inc.	2010	Canada	Pivot	2021	16	305	25.000
Deep Trekker Inc.	2010	Canada	DTG-2 (3)	2011	8		
Geneinno	2013	China	T1	(2019)		200	11.000
Geneinno	2013	China	T1 Pro	2020	4	150	3.000
Gnom ROV	2001	Russia	GNOM	2020	4	175	4.700
Gnom ROV	2001	Russia	Standard	2015	18	120	7.500
Gnom ROV	2001	Russia	GNOM		11		
Gnom ROV	2001	Russia	Baby	2016		100	4.000
JW Fishers	1968	USA	GNOM Pro	2018	35	150	17.000
MarineNav Ltd.	2005	Canada	SeaOtter-1(-2)	1994	20		
MarineNav Ltd.	2005	Canada	Oceanus	(2007)		150	21.000
MarineNav Ltd.	2005	Canada	Mini		37		
MarineNav Ltd.	2005	Canada	Oceanus	2017	22	100	20.400
MarineNav Ltd.	2005	Canada	Hybrid	2020		305	17.000
Powervision	2009	China	power Ray	2018	4	30	950
QYSEA	2016	China	Fifish V6	2019	4	100	1.500
QYSEA	2016	China	Fifish V6		5		
QYSEA	2016	China	Plus	2020		150	3.000

\*variable frame material

## 4.2 Market analysis of the ROV sector

The quantitative evaluation of this paper is based on a market analysis of the offshore and the micro ROV market. A structured market report analysis of leading data providers has been conducted via online research in April 2023. In total 15 reports provided market data and forecast whereas 11 reports contain data of the intervention class and 4 reports contain data of the inspection class. All reports included global ROV market values between 2021 and 2023 as well as a market forecast based on the compound annual growth rate (CAGR). Using the CAGR formula, missing values of the reports were calculated assuming linear growth rates for the period 2022–2030. During the evaluation, a high deviation between the different market predictions were identified. In order to enhance the market data validity, the third quartile was applied, resulting in 11 reports being accepted. One report only provided CAGR predictions without the annual value rate of the market, so it was included in the CAGR evaluation but not in the annual value calculation. After the third quartile application, the mean value of each year was calculated from the offshore ROV market data. Of the four inspection-class market reports no huge value deviation was identified, resulting in the choice of mean values without quartile exclusion. Table III reveals almost similar CAGR growth rates for the intervention class and for the inspection class till 2030 with 8.21% and 8.09%. In terms of total market value, the intervention class market is approximately 5 times larger than the inspection class, potentially explained by the huge difference in ROV costs.

Table II: Global ROV market analysis

	Year	2022	2023	2024	2025	2026	2027	2028	2029	2030	CAGR
Intervention class	N	10	10	10	10	10	10	10	10	10	11
	Average (Mil \$)	2.800	3.047	3.323	3.626	3.960	4.328	4.733	5.179	5.635	8,21
	Delta (Mil \$)	752	870	1.008	1.173	1.368	1.597	1.867	2.185	2.582	2,48
Inspection class ROV	N	4	4	4	4	4	4	4	4	4	4
	Average (Mil \$)	420	451	485	522	562	605	653	706	763	8,09
	Delta (Mil \$)	168	170	174	177	183	190	200	212	228	3,34

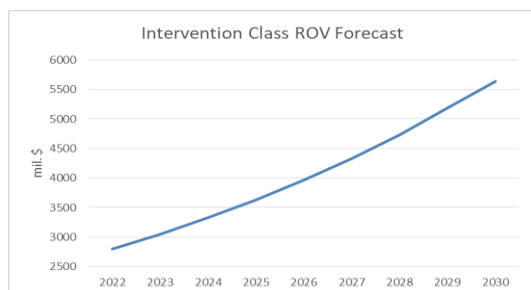


Fig.3: Intervention class market forecast

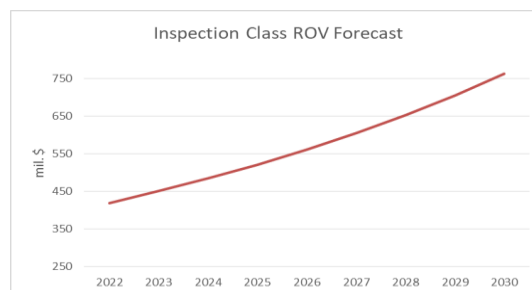


Fig.4: Inspection class market forecast

## 5. Introduction of a customized marine fouling detection AI

According to *Lindstad and Bø (2018)* the most cost-effective approach for meeting EEXI/CII standards is a clean hull. Optimal in-water hull cleaning can save up to 7% fuel according to market studies of *Adland et al. (2018)*. Such gains, however, require knowledge and data of the ship hull. With in-water surveys being conducted every 2.5 years in the past, this knowledge was scarce to non-existing for ship owners and operators. AI application for underwater image recognition in the past were not suitable for multi-object semantic segmentation according to *O'Byrne et al. (2018)*.

This paper introduces a new design of a deep convolutional neural network for multi-object semantic segmentation of marine fouling data to close this gap. The underlying objective of semantic segmentation lies in the classification of each pixel of an image. Pre classified categories are searched for in the image to, finally, predicting a result map containing “semantic” information, *Liu and Fang (2020)*. The segmentation separates the image into individual portions for computer-based image analysis and understanding, *Meng et al. (2018)*. The challenge underwater, however, lies in changing light conditions, motion-background blur and the absence of clear foreground and background characteristics, causing underwater image segmentation to lag behind land-based methods, *Meng et al. (2018)*.

By operating an encoder-decoder model with custom architecture, multi-object semantic segmentation of marine fouling on hulls was achieved despite challenging underwater conditions. An early stage of the AI design promising operative results of the neural network were obtained. According to *Lui and Fang (2020)* the mean intersection over union (MIoU) is introduced as cross-combination ratio to quantify a convolutional neural network's identification accuracy. Prior precision measurements failed taking into account the specific accuracy of the image segmentation itself hence are found to be inferior to the MIoU. A comparison of the initial network output compared to existing contributions revealed a high MIoU of .85 and conventional precision values of .95. Figs.5 to 7 display test scenarios where the AI evaluated realistic ROV inspection footage. Fig.5 shows an example with good visible conditions and a clear foreground. Fig.6 tested the AI, which was trained on ship hulls with marine fouling, on a clean ship hull with a quay wall covered in fouling. Notable is that the identification of the fouling was significant without confusion of the actual ground. Fig.7 tested a scenario against the light with high visibility resulting in background blur of the ship covered with heavy fouling. These promising results of the network are underlined by its high values in MIoU compared to similar contributions as revealed in Table IV.

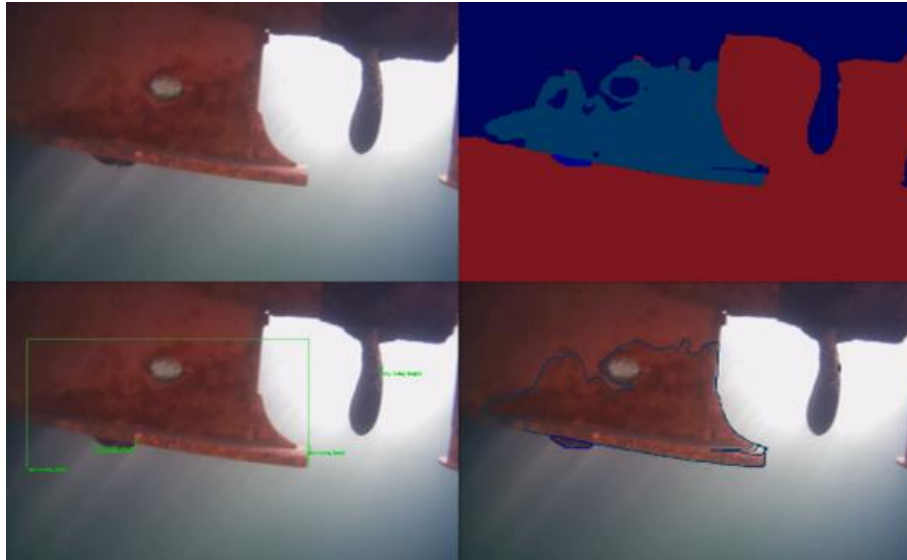


Fig.5: Ship example

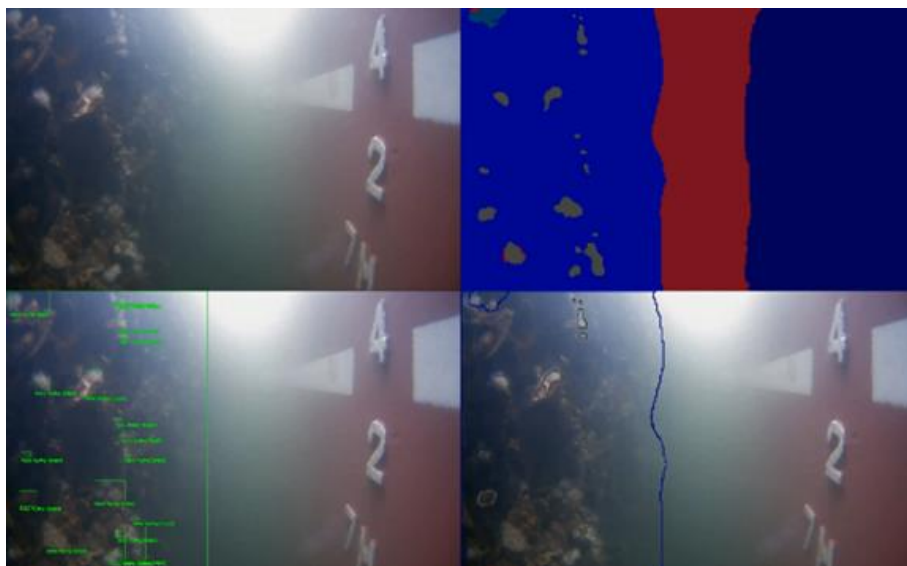


Fig.6: Ship and port wall comparison low visibility, against light

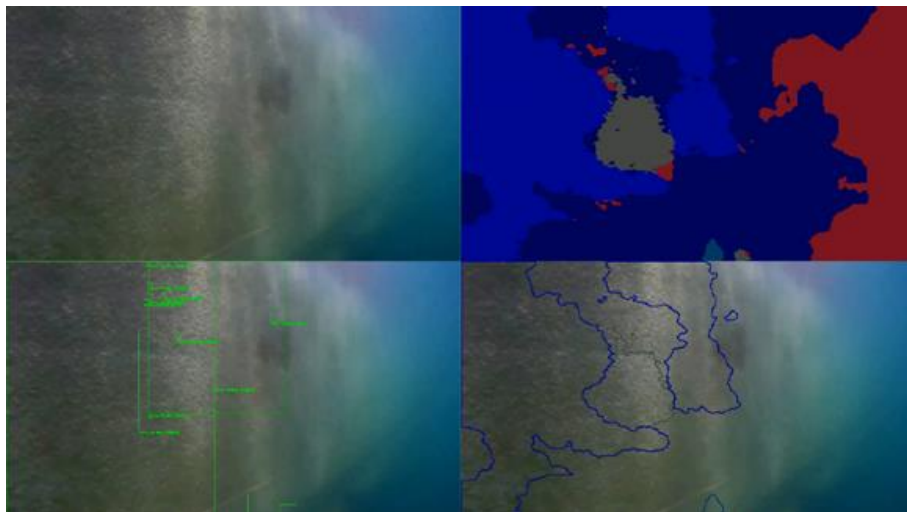


Fig.7: Heavy fouling example, high visibility, against light; Top left original; top right output; bottom left and right operation examples

Table IV: DCNN precision results and label data quantity

Source	Precision	MIoU	data
<i>Bloomfield et al (2021)</i>	0.7960	-	10.263
<i>Islan et al. (2020)</i>	0.8697	0.8414	1.525
<i>O'Byrne et al. (2018)</i>	0.9400	0.8700	2.500
<i>Liu &amp; Fang (2020)</i>	-	0.6465	2.237
<b>Our approach</b>	<b>0.9500</b>	<b>0.8500</b>	<b>1.128</b>

Table V: Influence on different encoders on the model precision

Encoder format	MIoU*	data
PSPNet	.45	1.128
Simple Unet	.51	
Unet with Resnet50 encoder	.54	
SUIMNet with RSB encoder	.73	
<b>SUIMNet with VGG encoder</b>	<b>.85</b>	

Our network approach exceeds all existing contributions of underwater semantic image segmentation in terms of precision and ranks second in terms of MIoU, albeit having the smallest amount of training data of 1.128 images. As revealed in Table V, the correct choice of the encoder format has a huge effect on the networks MIoU with a SUIMNet /VGG encoder obtaining the highest results among the training data. Further evaluations are necessary in order to test the outcome for robustness. However, precautions against overfitting were taken when training the network indicating the strength of the initial results.

## 5.2. Introduction of a EEXI optimization approach

Applying a custom deep neural network to underwater imagery can be an effective way to identify different classes of biofouling on ship hulls. By training the neural network on a dataset of labeled images of biofouling, the system can learn to recognize and classify various types of marine organisms and other debris that accumulate on the hull. This can help ship owners and operators to better understand the extent and type of biofouling on their vessels, which in turn can inform decisions about hull cleaning and maintenance schedules. Additionally, using automated image analysis can be more efficient and accurate than manual inspection methods, making it a valuable tool for marine industry professionals to only name one example of AI and ROV combinations.

The objective is to create a framework for ship owners, charterers, and port operators to assess marine fouling based on ROV data evaluated by a DNCC and its implication in emissions using ship voyage data of the location (AIS) and the voyage fuel consumption (MRV) data in a later step. Both AIS and MRV data are publically available that makes a comparison on a ship-based case study possible.

## References

ADLAND, R.; CARIOU, P.; JIA, H.; WOLFF, F.C. (2018), *The energy efficiency effects of periodic ship hull cleaning*, J. Cleaner Production 178, pp.1-13



- ALLOTTA, B.; BRANDINI, L.; CASAGLI, N.; COSTANZI, R.; MUGNAI, F.; MONNI, N.; NATALINI, M.; RIDOLFI, A. (2015), *Development of Nemo ROV for the Inspection of the Costa Concordia Wreck*, J. Engineering for the Maritime Environment 231/1, pp.3–18
- BRUNO, F.; MUZZUPAPPA, M.; LAGUDI, A.; GALLO, A.; SPADAFORA, F.; RITACCO, G.; ANGILICA, A.; BARBIERI, L.; DI LECCE, N.; SAVIOZZI, G.; LASCHI, C.; GUIDA, R.; DI STEFANO, G. (2015), *A ROV for supporting the planned maintenance in underwater archaeological sites*, OCEANS'15, Genova, pp.1-7
- BLOOMFIELD, N.J.; WEI, S.; WOODHAM, B.A.; WILKINSON, P.; ROBINSON, A.P. (2021), *Automating the assessment of biofouling in images using expert agreement as a gold standard*, Scientific reports 11.1, pp.1-10
- CAPOCCI, R.; DOOLY, G.; OMERDIĆ, E.; COLEMAN, J.; NEWE, T.; TOAL, D. (2017), *Inspection class remotely operated vehicles—A review*, J. Marine Science and Engineering 5(1)
- CLARKSONS (2021), *Review: Disruption Upside & Surging ClarkSea...*, Clarksons Research, <https://insights.clarksons.net/2021-review-disruption-upside-surging-clarksea/>
- CHIN, C.S.; SI, J.; CLARE, A.S.; MA, M. (2017), *Intelligent image recognition system for marine fouling using Softmax transfer learning and deep convolutional neural networks*, Complexity
- GLASER, B.; STRAUSS, A. (1967), *Grounded theory: The discovery of grounded theory*, Sociology: The Journal of the British Sociological Association 12, pp.27–49
- IMCA (2015), *IMCA World-Wide ROV Personnel and Vehicle Statistics for 2014*, Int. Marine Contractors Association, Richmond
- IMO (2009), *Second IMO Greenhouse Gas Study*, Buhaug et al., Int. Mar. Org., London
- IMO (2022), *Guidelines on the Method of Calculation of the Attained Energy Efficiency Existing Ship Index (EEXI)*, Res. MEPC.350(78), Int. Mar. Org., London, [https://wwwcdn.imo.org/localresources/en/OurWork/Environment/Documents/Air%20pollution/MEPC.350\(78\).pdf](https://wwwcdn.imo.org/localresources/en/OurWork/Environment/Documents/Air%20pollution/MEPC.350(78).pdf)
- ISLAM, M.J.; EDGE, C.; XIAO, Y.; LUO, P.; MEHTAZ, M.; MORSE, C.; ENAN, S.S.; SATTAR, J. (2020), *Semantic segmentation of underwater imagery: Dataset and benchmark*, Int. Conf. Intelligent Robots and Systems (IROS), pp.1769-1776
- JIAN, M.; LIU, X.; LUO, H.; LU, X.; YU, H.; DONG, J. (2021), *Underwater image processing and analysis: A review*, Signal Processing: Image Communication 91, 116088
- JONES, D.O.B. (2009), *Using existing industrial remotely operated vehicles for deep-sea science*, Zool. Scripta 38, pp.41–47
- KAMIL, M.; MUSLIM, M.; SAAT, A.M. (2020), *Effective control of SOx and NOx release to the atmosphere from emissions of ship propulsion engines*, Advancement in Emerging Technologies and Engineering Applications: Lecture Notes in Mechanical Engineering; Springer
- KERANEN, J.; SCHULTZ, G.; BASSANI, C.; SEGAL, S.; KINNAMAN, B. (2012), *Remotely-Operated Vehicle applications in port and harbor site characterization: Payloads, platforms, sensors, and operations*, OCEANS'12, pp.1-9
- LINDSTAD, E.; BØ, T.I. (2018), *Potential Power Setups, Fuels and Hull Designs Capable of Satisfying Future EEDI Requirements*, Transportation Research Part D: Transport and Environment 63, pp.276–290

LIU, F.; FANG, M. (2020), *Semantic segmentation of underwater images based on improved Deeplab*, J. Marine Science and Engineering 8(3)

LAMBERTINI, A.; MENGHINI, M.; CIMINI, J.; ODETTI, A.; BRUZZONE, G.; BIBULI, M.; MANDANICI, E.; VITTUARI, L.; CASTALDI, P.; CACCIA, M.; DE MARCHI, L. (2022). Underwater Drone Architecture for Marine Digital Twin: Lessons Learned from SUSHI DROP Project, Sensors, 22(3), <https://www.mdpi.com/1424-8220/22/3/744>

LYNN, D.C.; BOHLANDER, G.S. (1999), *Performing ship hull inspections using a remotely operated vehicle*, OCEANS'99, Vol. 2, pp.555-562

MACREADIE, P.I.; McLEAN, D.L.; THOMSON, P.G.; PARTRIDGE, J.C.; JONES, D.O.B.; GATES, A.; BENFIELD, M.C.; COLLIN, S.P.; BOOTH, D.J.; SMITH, L.L.; TECHERA, E.; SKROPETA, D.; HORTON, T.; PATTIARATCHI, C.; BOND, T.; FOWLER, A.M. (2018), *Eyes in the sea: unlocking the mysteries of the ocean using industrial, remotely operated vehicles (ROVs)*, Sci. Total Environ. 634, pp.1077–1091

McLEAN, D.L.; MACREADIE, P.; WHITE, D.J.; THOMSON, P.G.; FOWLER, A.; GATES, A.R.; BENFIELD, M.; HORTON, T.; SKROPETA, D.; BOND, T.; BOOTH, D.J.; TECHERA, E.; PATTIARATCHI, C.; COLLIN, S.P.; JONES, D.O.B.; SMITH, L.; PARTRIDGE, J.C. (2018), *Understanding the global scientific value of industry ROV data, to quantify marine ecology and guide offshore decommissioning strategies*, Offshore Technology Conf. Asia, Kuala Lumpur

MENG, L.; HIRAYAMA, T.; OYANAGI, S. (2018), *Underwater-drone with panoramic camera for automatic fish recognition based on deep learning*, IEEE Access 6, pp.17880-17886

MURPHY, R.R.; DREGER, K.L.; NEWSOME, S.; RODOCKER, J.; STEIMLE, E.; KIMURA, T., ... KON, K. (2011), *Use of remotely operated marine vehicles at Minamisanriku and Rikuzentakata Japan for disaster recovery*, IEEE Int. Symp. Safety, Security, and Rescue Robotics, pp.19-25

NICINSKI, S. (1983), *Development of a remotely operated ship hull inspection vehicle*, OCEANS'83, pp.583-587

NIPPON FOUNDATION (2023), *GEBCO Seabed 2030 Project. Nearly a Fifth of World's Ocean Floor Now Mapped*, [https://www.gebco.net/documents/seabed2030\\_brochure.pdf](https://www.gebco.net/documents/seabed2030_brochure.pdf)

O'BYRNE, M.; PAKRASHI, V.; SCHOEFS, F.; GHOSH, B. (2018), *Semantic segmentation of underwater imagery using deep networks trained on synthetic imagery*, J. Marine Science and Eng. 6(3)

OSUMI, H. (2014), *Application of Robot Technologies to the Disaster Sites*, Lessons learned from the Great East Japan Earthquake Disaster: Report of the JSME Research Committee on the Great East Japan Earthquake Disaster, Japan Society of Mechanical Engineers, pp. 58-73

PRASTOWO, H.; PITANA, T.; KUSUMA, H. (2020), *Activity-Based Fuel Oil Consumption Estimation for Calculating Energy Efficiency Operational Indicator (EEOI) in an Indonesian Merchant Ship*, Earth Environ. Sci.

POLEMIS, D.; BOVIATIS, M.; CHATZINIKOLAOU, S. (2023), *Assessing the Sustainability of the Most Prominent Type of Marine Diesel Engines under the Implementation of the EEXI and CII Regulations*, Clean Technologies 5(3), pp.1044-1066

RUTHERFORD, D.; MAO, X.; COMER, B. (2020), *Potential CO2 Reductions Under the Energy Efficiency Existing Ships Index*, International Council on Clean Transportation

SCHULTZ, G.; MILLER, J.; KERANEN, J.; SHUBITIDZE, F. (2021), *ROV-based 3D controlled source electromagnetics for UXO detection and classification*, Symp. Application of Geophysics to Engineering and Environmental Problems 2021, pp.346-346

SPRAGUE, K.L. (2004), *Civilian applications and policy implications of commercial unmanned aerial vehicles*, PhD thesis, Massachusetts Institute of Technology

SHMATKOV, A.A.; ANTONOV, N.A. (2021), *Experience in Application of a Specialized ROV for The Detection of UXOs when Performing Offshore Site Surveys*, Engineering and Mining Geophysics 2021, pp.1-6

STEIN, M. (2018), *Integrating unmanned vehicles in port security operations: an introductory analysis and first applicable frameworks*, Oceans Yearbook 32, pp.556-583

THOMSON, P.G.; FOWLER, A.M.; DAVIS, A.R.; PATTIARATCHI, C.B.; BOOTH, D.J. (2018), *Some Old movies become classics – a case study determining the scientific value of ROV inspection footage on a platform on Australia's North West Shelf*, Front. Mar. Sci. 5:471. doi: 10.3389/fmars.2018.00471

WHARTON, A.J. (1991), *Diesel Engines*, Butterworth-Heinemann

# Techno-economic Vessel Design Method for Assessing Alternative Fuels & Power Architectures

Kenneth Goh, Knud E. Hansen, Perth/Australia, [KEG@knudehansen.com](mailto:KEG@knudehansen.com)

## Abstract

*This paper presents a calculation methodology for determining the effect of carbon neutral alternative fuels, such as ammonia and hydrogen on the vessel design and operational economics. The methodology encompasses the primary requirements of the fuel including storage, handling, processing, waste, emissions and cost. These requirements will have an effect on the design of the vessel, for example the overall dimensions or arrangement of the vessel layout, which in turn will affect the vessel build cost.*

## 1. Introduction

The move towards viable fossil fuel alternative fuels presents many challenges for the shipping industry. Propulsion suppliers must grapple with the fuels that are less energy dense, have different combustion properties and difficult storage requirements. For ship designers, these alternative fuels require vessels to be larger but also presents opportunities for vessel layouts to be optimised for more efficient operations.

The present study focuses on three such alternative fuels methanol, ammonia and hydrogen. Some of these alternative fuels can be used in different types of engines and this efficacy also needs to be assessed. Further complicating the matter is that some fuels are converted into other fuels before use or feedstocks are carried with the fuel being produced on board the vessel.

The study will focus on the vast majority of merchant vessels, over 90% of sailing tonnage, that are powered by 2-stroke slow speed engines directly coupled to lowly loaded propellers. This configuration is generally accepted as being the most efficient powering arrangement for a ship which operates the majority of its time at sea at greater than 50% propulsion power.

The current standard carbon-based marine fuels can be divided into residual HFO, distillate MGO, blended MDO and gases such as methane or its liquified state LNG. When these fuels are combusted in engines to power ships, large quantities of carbon dioxide (CO<sub>2</sub>) gases are emitted, exacerbating the greenhouse effect of the earth's atmosphere and increase the temperature of the climate. Alternative fuels are needed to eliminate or greatly reduce CO<sub>2</sub> emissions from shipping.

## 2. Alternative Fuels

### 2.1. Methanol

With a chemical formulation of CH<sub>3</sub>OH, methanol as a fuel is not carbon free and combustion in an engine produces CO<sub>2</sub>. However, the production methods proposed using biomass or CO<sub>2</sub> can offset the emissions produced when used as a fuel.

The energy density of methanol is about 19.9 MJ/kg. While methanol derived from such renewable sources can be considered carbon-neutral in terms of the carbon cycle, it's crucial to consider the entire lifecycle and production process to assess its overall environmental impact.

### 2.2. Ammonia

With a chemical formulation of NH<sub>3</sub>, ammonia as a fuel is totally carbon free. Ammonia is currently widely used as a refrigerant, in fertiliser production and for many other industrial purposes. Ammonia production and logistics is highly mature although scaling up production in an environmentally friendly

way is challenging since all manufacturing processes require hydrogen as a feedstock, which itself is energy intensive to produce. The energy density of ammonia is about 21.8 MJ/kg.

## 2.3. Hydrogen

With a chemical formulation of  $H_2$ , hydrogen as a fuel is totally carbon free. It is widely used for many industrial purposes, including production of ammonia as described below. The gravimetric energy density of hydrogen at 120 MJ/kg is very high compared to other fuels. However, the very low physical density of hydrogen gas of 0.09 kg/m<sup>3</sup> makes storage and transportation of hydrogen difficult. Therefore, storage of hydrogen as either a compressed gas or as a liquid is used.

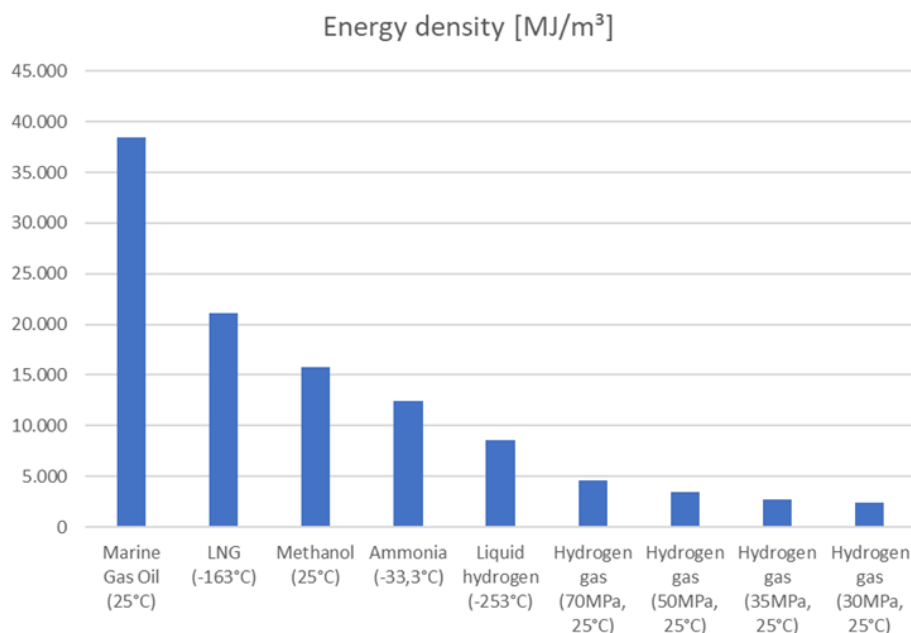


Fig.1: Volumetric energy density of marine fuels

## 3. Fuel Production

### 3.1. Fuel Oil Production Baseline

When considering the viability of a marine fuel the entire chain from extraction, production and logistics of transport and storage must be considered, even before the fuel is bunkered. This analysis should consider not only the financial cost but also the energy required, and the emissions produced. This is commonly referred to as a well-to-wake analysis.

For example, for current fossil fuels the accepted industry cost of producing fuel oils like Marine Diesel Oil (MDO) is about 10 USD/GJ, or about 0.40 EUR/litre. The energy ratio required is about 1.2 units to produce 1.0 unit of MDO or about 47 MJ/kg. It should be noted that with many fuels, more energy is required to produce the fuel than the energy contained in the actual fuel produced. The process of extracting and distilling fossil fuels also produces large quantities of carbon emissions.

### 3.2. Methanol Production

Green methanol is considered a sustainable and low-carbon alternative to conventional methanol, which is typically produced from fossil fuels. The production of methanol using biomass feedstock offsets the CO<sub>2</sub> emitted during combustion as the growth of the feedstock absorbs CO<sub>2</sub> from the environment. Suitable renewable biomass feedstock includes wood chips, grasses, algae and crop and food waste. E-methanol is produced from renewable electricity and captured CO<sub>2</sub>.

### **3.3. Ammonia Production**

#### **3.3.1. Ammonia from Methane Reforming**

Brown ammonia made from natural gas via the Steam Methane Reforming (SMR) and the Haber-Bosch process takes about 50 MJ/kg ammonia. This is much less than for MDO, but ammonia only has half the energy density at 22 MJ/kg. The energy ratio required is therefore about 2.3 which is more than for MDO at 1.2.

Blue ammonia is also made by natural gas and SMR, however more methane is used to reduce the CO<sub>2</sub> created. The Carbon Capture Storage (CCS) process reduces carbon emissions by 60-70% but requires additional energy for the SMR and CCS. This increases the total energy required to produce the ammonia to 54 MJ/kg and increases the energy ratio to 2.5.

#### **3.3.2. Ammonia from Electrolysis**

The SMR process is considered 'brown' due the carbon fuel feedstock required and carbon emissions produced. Producing green ammonia via PEM electrolysis uses electrical energy instead of heating. The electrolyser required to produce the hydrogen feedstock needs about 36 MJ for every kilogram of ammonia produced.

Adding the energy required by the Haber-Bosch process gives a total of 45 MJ/kg. The energy ratio required for green ammonia therefore about 2.1, which is less than the energy required by SMR. If the electrolyser can be powered by renewable power such as wind or solar, then the process can be considered totally 'green' since no carbon is emitted in the process.

### **3.4. Hydrogen Production**

#### **3.4.1. Hydrogen from Electrolysis**

For production of hydrogen, we have already discussed the PEM electrolyser required to produce hydrogen feedstock for ammonia production. Since hydrogen has much lower physical density compared to ammonia, a much greater amount of energy is required to produce the same mass of hydrogen. Current electrolyzers need about 190 MJ/kg to produce hydrogen while future electrolyzers currently in testing will reduce the energy required to about 150 MJ/kg. As described above, compressing or liquefying hydrogen will require an additional 20 MJ/kg or 35 MJ/kg respectively. The energy ratio is therefore 1.42 for compressed 500 bar hydrogen and 1.54 for LH<sub>2</sub> given the energy density of hydrogen is 120 MJ/kg.

#### **3.4.2. Hydrogen from Ammonia**

The low volumetric energy density of hydrogen and the difficulty of storage sufficient fuel has led to a number of other hydrogen strategies. Storage of ammonia fuel with on-board conversion to hydrogen via a cracking process has been proposed. The power required for this process is at best 40 MJ/kg. The hydrogen can then be used in either internal combustion engines or fuel cells.

#### **3.4.3. Hydrogen from Solid Carriers**

There is significant research and development into using solids and nano-structures for physisorption an/or chemisorption for storage of hydrogen. A wide range of materials and techniques are being explored. One such approach is using boron nitride hex as the storage medium and ball-milling to bind the hydrogen. In another process by Hyrea, fuel bricks call Solid Hydrogen Cells (SHC) are created directly in the electrolysis process for storage and transport. The SHCs on the vessel are processed using seawater with a catalyst to produce hydrogen. Although these processes are still in development, it is important that the calculation model is able to encompass such processes.



## **4. Alternative Fuel Storage**

### **4.1 General**

The design and location of fuel storage bunkers on vessels have typically been a combination of physical requirements for example HFO fuel needed constant heating and LNG tanks needing to withstand high pressures or having thick insulation tanks and rule requirements such as needing voids around fuel tanks and not locating fuel tanks forward of the collision bulkhead.

The high volumetric energy density of carbon-based fuels has generally allowed ship designers a high degree of freedom in arranging the ships fuel bunker tanks. Typically, in a merchant vessel only about 1.0% to 3.0% of the hull volume is required for fuel tanks depending on the range and speed required. The fuel mass fraction of about 2% to 5% of the vessel displacement is low enough that longitudinal location of the fuel tanks to balance the vessel as fuel is consumed is rarely a primary consideration in the arrangement of the vessel. By comparison, a typical commercial airliner requires a fuel mass fraction of between 30% to 40% with balance during consumption a crucial consideration.

### **4.2. Methanol Storage**

Methanol can be stored as a liquid at ambient temperatures. When fuel tanks are integrated into the ship structure void spaces separating the tanks from other spaces and the hull shell are required. The density of liquid methanol is about 0.79 kg/L. This results in a volumetric energy density of about 15.7 MJ/L. Therefore, the storage space required for methanol is about 2.5 to 3 times when compared to MDO fuel.

### **4.3. Ammonia Storage**

For storage as a liquid at atmospheric pressure ammonia needs to be kept at  $-33^{\circ}\text{C}$  requiring insulated fuel tanks. When fuel tanks are integrated into the ship structure void spaces separating the tanks from other spaces and the hull shell are required. Ammonia is also highly toxic as a gas. The density of liquid ammonia is about 0.68 kg/L. This results in a volumetric energy density of about 14.8 MJ/L. Therefore, the storage space required for ammonia is about 3 to 4 times when compared to MDO fuel.

### **4.4. Compressed Hydrogen Storage**

Hydrogen gas is compressed up to 700 bar for automotive fuel applications in carbon fibre wrapped tanks. However, 500 bar is likely the economic limit of the larger tanks required for the marine industry. Compressed hydrogen at 500 bar has an energy density of about 3.6 MJ/L which is only a tenth of MDO. The need for unitary tanks able to withstand the 500 bar pressure will reduce the storage by a half again. Therefore about 20-30 times the space is required to store hydrogen compressed to 500 bar compare to MDO fuel. The energy required to compress hydrogen to an over-pressure of 600 bar for bunkering is about 20 MJ/kg.

### **4.5. Liquid Hydrogen Storage**

Liquid Hydrogen (LH2) at atmospheric temperature requires liquefaction down to  $-253^{\circ}\text{C}$  requiring special materials and heavy insulation for the fuel tanks. LH2 has a low physical density of 0.07 kg/L, which is about twice that of compressed hydrogen. The energy density of LH2 is therefore about 8.5 MJ/L which is about a fifth compared to MDO. With thick tank insulation required, it is expected that the required storage volume required will be about 6-10 times of that required by MDO fuel. The energy required for liquefaction of hydrogen gas to LH2 is about 35 MJ/kg.

## 5. Alternative Fuel Engines

### 5.1. Internal Combustion Engines

Methanol can be used in current diesel engines with relatively minor changes to the fuel injection systems. With an auto-ignition temperature methanol at 470°C a small amount of about 5% diesel pilot fuel, is required for methanol combustion. The liquid methanol requires gasification prior to engine injection which is a relatively simple process that can utilise waste heat from the engine.

Although testing of ammonia fuelled engines is just beginning, it is expected that diesel engines with relatively minor changes to the fuel injection systems can be used. With a higher auto-ignition temperature of 650°C, the amount of diesel pilot fuel for stable combustion is expected to be greater than the 5% required for methane and methanol engines. The NO<sub>x</sub> emissions from the combustion process can use existing catalytic reactor technology designed for fossil fuel emissions.

The liquid ammonia requires gasification prior to engine injection which is a relatively simple process that can utilise waste heat from the engine or the heat from the air conditioning systems which will also reduce the vessel's electrical load. Ammonia is highly toxic as a gas and will require extensive new safety measures to be implemented, such as double-wall fuel piping, gas detection and breathing equipment.

Hydrogen can be used with conventional Internal Combustion Engines (ICE) with modifications to fuel injection, timing and emission control systems. Note however, there has been little impetus from marine engine makers to develop hydrogen fuelled engines due to the difficulty of fuel storage. Testing of hydrogen engines has been on-going in the automotive industry. The efficiency of hydrogen engines is potentially higher than similar engines using fuel oils with a thermal efficiency of over 40% demonstrated on small high-speed engines.

The Specific Fuel Consumption (SFC) of alternative fuelled internal combustion engines is a direct factor of the fuels mass energy density. Therefore, the SFC for methanol and ammonia fuelled engines will be about twice that of fuel oil engines since the energy density is about half. The overall thermal efficiency of large 2-stroke marine reciprocating engines remains unchanged at about 45-50%. Heat recovery systems from the engine exhaust and cooling systems can increase the effective thermal efficiency of these engines to about 50-55%.

For electrical power generation the 4-stroke marine reciprocating engines used will have thermal efficiencies of about 40-45% with the fuel mass energy density used for calculating SFC. Electrical power generation has the additional losses of the generator which reduces the electrical power efficiency to 38-43% of the fuel energy.

The size of weight of engines and their supporting systems is a major consideration for the design of the ships. For a typical merchant vessel with an aft engine room, the designer is always trying to reduce the length of the engine room to maximise the cargo volume in the hull.

Alternative fuelled ICEs will have very similar supporting systems as current fuel oil vessels. There will be little change to the cooling, lubrication, compressed air and exhaust systems. The main differences will be with the fuel processing and fuel handling systems. These changes are not expected to be significant in terms of size, weight or energy consumption.

Current merchant vessels using residual fuels like HFO require energy to heat and purify the fuel before use by the engine. This process also generates considerable waste sludge, that must be burnt by an on-board incinerator or stored for offloading to port facilities. The purity of bunkered alternative fuels will be much higher, with little or no on-board purification required. The heating requirements for alternative fuels will also be less than that of HFO and could also be used to lower the energy requirements of air conditioning systems in the case of cryogenic fuels such as ammonia and LH<sub>2</sub>.

## **5.2. Fuel Cells**

Unlike other alternative fuels, hydrogen can also be used in Proton Exchange Membrane (PEM) fuel cells that combine hydrogen and oxygen in the air to directly produce electricity. Along with the fuel cells, the propulsion system requires power converters and electric motors. The efficiency of PEM are typically about 55-60%.

Significant progress is being made in the reduction of size of commercially available PEM fuel cells. *Nedstack*, a manufacturer of marine fuel cell systems has reduced the size of its 500 kWe fuel cell from a 20 ft container to 10 m<sup>3</sup> and the weight from 11 tons down to 2 tons.

Fuel cells are mechanically much simpler than ICEs and require fewer supporting systems. For example, fuel cells have no moving parts, so lubrication systems are only required for the propulsion shafting. Compressed air for engine starting is also not required. The ventilation and combustion air requirements are about 50% compared to ICEs requirements and the exhaust system is much smaller, only having to move 6% of the volume and 10% of the mass compared to the exhaust of an ICE. The exhaust is pure water vapour that could be condensed for use on the vessel, saving further energy.

Vessels using alternative fuels in ICEs will also need dual fuel systems, since diesel pilot fuel is still required for the running of the engines. This adds additional complexity, cost and work for the crew which are absent when using fuel cells.

The gasification process of LH2 could also significantly lower the energy requirements of air conditioning systems, which is a heavy electrical consumer particularly on ferry, cruise and accommodation vessels.

## **6. Techno-Economic Model**

### **6.1. Technical Model**

The technical model developed combines information from the industry and the KEH design database to arrive at accurate estimates for vessels principal particulars including dimensions, capacities, weights, powering, and electrical loads.

### **6.2. Navigation Model**

The speed and resistance from model testing of the hull and sail rig was translated from the polar plots of wind speed and direction into a spreadsheet.

Global wind and wave data was sourced from the European Centre for Medium-range Weather Forecast (ECMWF). The vessel course was plotted and divided into 16 legs. From the wind and wave data the sea margin for the added resistance in waves is estimated. Effective power is then calculated and shaft power based on typical propulsion efficiencies for various types of vessels and propulsors.

Although the current navigation model is represented by a single time 'snap-shot', testing with a model in which the weather progresses with the voyage did not produce significantly different results.

### **6.3. Energy Model**

Although a complete well-to-wake energy analysis is required to determine how 'green' any mode of transport is, there are multiple production and logistical variables that will be difficult to quantify. Therefore the energy model considers on the fuel cost and fuel consumed.

Vessel propulsion, power consumption and engine efficiency are modelled. Other losses in the power transmission system, for example gearboxes or converters, are also added where applicable. These are

used to calculate the fuel consumption and the amount of fuel needed to be bunkered. The fuel tank size is then calculated based on the fuel properties and the type of fuel tank. Once the space required for the fuel tank is known, this may require the vessel to be lengthened with follow-on consequences for the steel weight and vessel cost.

#### 6.4. Cost Model

Empirical formulars, based on academia and market information are then used to estimate both capital and operational costs. The regression based cost models are used to calculate new building costs based on steel and equipment weights, block coefficient, installed power and machinery type.

Note that real world shipbuilding cost can be highly variable due to market supply and demand, Government incentives and other investment capital. The cost model is adjusted for annual inflation to correct formulas based on older market information.

The cost for alternative fuels is rapidly changing as demand sand global supply chains adjust. Alternative fuel costs used in the present study are based on market expectations for the near-term period of 2025 to 2030.

Fuel	Cost (USD per ton)	Cost (USD per GJ)
MDO	1,000	25
Green methanol	2,000	100
Green ammonia	1,500	68
Green hydrogen (LH2)	5,000	25
Solid hydrogen carrier		

Fig.2: Cost of marine fuels

Note that green hydrogen is expected to be competitive with fossil fuels with 10 years. This also considers the difficultly and additional costs of transporting and storing low temperature cryogenic fuels.

Other operational costs such as manning, maintenance and port fees are also added.

The final comparative metric given is the Required Freight Rate (RFR), that is the actual cost of transporting the cargo per ton.

### 7. Alternative Fuel Power Architectures

#### 7.1. HFO 2-stroke Engine Baseline

This is the baseline design which represents a Handymax bulk carrier with a deadweight of 50,000 tons. Handymax vessels are the most numerous bulk carrier type with over 3,700 vessels in the global fleet. The vessel uses HFO fuel and is powered by a 2-stroke engine.

#### 7.2. Methanol 2-stroke Engine Variant

This design variant is the most similar to the baseline vessel. The vessel uses methanol fuel but otherwise is the same as the baseline.

#### 7.3. Ammonia 2-stroke Engine Variant

This design variant uses ammonia fuel but otherwise is the same as the baseline.

#### **7.4. Compressed Hydrogen 2-stroke Engine Variant**

This design variant uses compressed Hydrogen fuel but otherwise is the same as the baseline.

#### **7.5. Liquid Hydrogen 2-stroke Engine Variant**

This design variant uses liquid Hydrogen fuel but otherwise is the same as the baseline.

#### **7.6. Compressed Hydrogen Fuel Cell Variant**

This design variant uses compressed Hydrogen fuel and PEM fuel cell propulsion system.

#### **7.7. Liquid Hydrogen Fuel Cell Variant**

This design variant uses liquid Hydrogen fuel and PEM fuel cell propulsion system.

#### **7.8. Ammonia to Hydrogen Fuel Cell Variant**

This design variant uses ammonia fuel with on-board conversion to hydrogen and PEM fuel cell propulsion system.

#### **7.9. Solid Fuel to Hydrogen Fuel Cell Variant**

This design variant uses a solid hydrogen carrier fuel with on-board conversion to hydrogen and PEM fuel cell propulsion system.

### **8. Conclusion**

This study develops a method to analyse various fuel and propulsion architectures.

There are obviously many factors such as location of resources, feedstock and CO<sub>2</sub> storage, the cost of power, storage and transport logistics that will affect the cost and energy chain. These factors are relatively minor compared to the production and processing of the fuels. The intention of this study is “not to go down every rabbit hole” chasing energy losses, but to provide an overall energy picture to clarify overall efficiencies and how the fuel storage and processing requirements affect the design of ships.

There are many ways to arrange engine rooms and fuel tanks and the model cannot be expected to encompass all possible design solutions. The main purpose of this type of the model is to give an understanding of the relative size of the main systems and their logical location relative to each other in a two-dimensional mapping.

The model produces economic results in which the transport efficiency of each fuel and engine architecture can be directly compared.

### **References**

BROWN, T. (2017), *Round-trip Efficiency of Ammonia as a Renewable Energy Transportation Media*, Ammonia Energy Association, <https://www.ammoniaenergy.org/articles/round-trip-efficiency-of-ammonia-as-a-renewable-energy-transportation-media/>

GAO, W.; FU, Z.; LI, Y.; LI, Y.; ZOU, J. (2022), *Hydrogen-fuel-internal-combustion-engines*, Scholarly Community Encyclopedia, <https://encyclopedia.pub/entry/31794>

GARDINER, M. (2009), *Energy requirements for hydrogen gas compression and liquefaction as related to vehicle storage needs*, Department of Energy USA

LANGMI, H.W. (2022), *Hydrogen Storage*, in *Electrochemical Power Sources: Fundamentals, Systems & Applications*, pp.455-486

NN (1996), *Modern Wind Ships – Phase 1*, Knud E. Hansen A/S, <https://www.osti.gov/etdeweb/servlets/purl/515478>

NN (2022), *Ammonia as a Marine Fuel*, Maersk Mc-Kinney Moeller Centre

ROSANDER, M.; BLOCH, J.O.V. (2000), *Modern Wind Ships – Phase 2*, Knud E Hansen A/S, <https://www2.mst.dk/udgiv/publications/2000/87-7944-019-3/pdf/87-7944-020-7.pdf>

THOMAS, G.; PARKS, G. (2006), *Potential Roles of Ammonia in a Hydrogen Economy – Vehicular Study*, Department of Energy USA



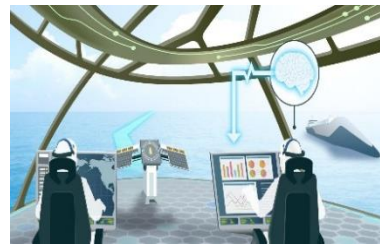
## Index by Authors

Albert	19	Marzi	108
Altenbach	135	Mayorga	32
Asta	218	Melillo	218
Atallah	127	Migeotte	19
Banken	285	Molchanov	234
Barsotti	75	Oeffner	285
Belibassakis	86	Öster	86
Berthelsen	259	Paakkari	299
Bertram	6,41,53,116	Pagoni	273
Carrera Viñas	80	Pang	155
Carugno	19	Perez Fernandez	62
Craciun	218	Pinkert	141
Demirel	273	Plowman	41
Dhyani	155	Salecker	322
Dubois	218	Sandberg	234
Ejder	259	Schneider	285
Elg	218,234	Schomberg	127
Emmersberger	189	Schreiner	108
Ertsås	265	Steen	166
Farkas	273	Sfiris	273
Föste	108	Stein	343
Früchtenicht	32	Stenzel	108
Gaspar	41	Stojanovic	332
Gerhardt	299	Stübing	108
Gerland	127	Teagle	203
Giovannetti	299	Turnock	203
Goh	355	Tvete	166
Guo	166	Van Ballegooijen	248
Gupta	166	Vonach	80
Hansen	116	Von Zadow	19
Harries	19,181	Wejberg	234
Hauschulz	181	Werner	299
Hildebrandt	19	Wesnigk	101
Hochkirch	116	Widell	218
Hollenbach	116	Widelund	218
Hudson	203	Wielgosz	101,299
Johansen	265	Williams	218
Kelling	32,218		
Kontos	299		
Krishnan	234		
Krüger	189		
Li	299		
Liarokapis	86		
Lohse	322		
Manias	203		
Marioth	101		

**16<sup>th</sup> Symposium on  
High-Performance Marine Vehicles – “Technologies for the Ship of the Future”**



**Drübeck / Germany, 10-12 June 2024**



**Topics:** ultra-efficient & zero-emission ships / EEXI & CII issues / alternative fuels / electric ships  
advanced designs & retrofits / shipyard 4.0 / future materials / future use of oceans / blue economy /  
intelligent & connected ships / future antifouling / biomimetic marine technologies

**Organiser:** Volker Bertram ([volker@vb-conferences.com](mailto:volker@vb-conferences.com))

**Advisory Committee:**

Catherine Austin	I-tech	Andrea Coraddu	TU Delft	Richard Marioth	Idealship
Ulrich Bernhardt	DNV	Robert Dane	Ocius	Kohei Matsuo	NMRI
Carlo Bertorello	Naples University	Thomas De Nucci	USCG Academy	Ivana Melillo	MCS
Carsten Bullemer	Maritime Data Systems	Stefan Harries	Friendship Systems	Geir Axel Oftedahl	Semcon
Emilio Campana	CNR	Thomas Hildebrandt	Numeca	Pierre Sames	DNV
Roy Campe	CMB	Jan Kelling	Hasytec	Noah Silberschmidt	Silverstream Technologies
		Jiulun Liu	Wuhan Univ Technology	Teus van Beek	Wärtsilä

**Venue:** The conference will be held at the Kloster Bernried in Bernried/Germany

**Format:** Papers to the above topics are invited and will be selected by a selection committee.  
Proceedings will be electronic pdf version in colour.

**Deadlines:** anytime Optional “early warning” of interest to submit paper  
01.2.2024 First round of abstract selection (1/3 of available slots)  
**01.3.2024 Second round of abstract selection (remaining 2/3 of slots)**  
25.5.2024 Payment due for authors  
30.5.2024 Final papers due (50 € surcharge for late submission)

**Fees:** **700 € / 350 €** regular / PhD student – early registration (by 15.4.2024)  
**800 € / 400 €** regular / PhD student – late registration

Fees are subject to VAT.

Fees include proceedings, lunches and coffee breaks, and conference dinner.

Fees apply also to authors.

**Sponsors:** Tutech Innovation, Hasytec, Idealship – further to be announced

**Media Partner:** Hansa, Royal Institution of Naval Architects

**Information:** [volker@vb-conferences.com](mailto:volker@vb-conferences.com)